frontiers | Research Topics

Immunity in the development of anti-cancer drug resistance

Edited by
Heng Sun, Haitao Wang, Xuebing Li and Ya Meng

Published in
Frontiers in Pharmacology
Frontiers in Oncology
Frontiers in Cell and Developmental Biology

ISSN 1664-8714
ISBN 978-2-83251-190-9
DOI 10.3389/978-2-83251-190-9

About Frontiers

Frontiers is more than just an open access publisher of scholarly articles: it is a pioneering approach to the world of academia, radically improving the way scholarly research is managed. The grand vision of Frontiers is a world where all people have an equal opportunity to seek, share and generate knowledge. Frontiers provides immediate and permanent online open access to all its publications, but this alone is not enough to realize our grand goals.

Frontiers journal series

The Frontiers journal series is a multi-tier and interdisciplinary set of open-access, online journals, promising a paradigm shift from the current review, selection and dissemination processes in academic publishing. All Frontiers journals are driven by researchers for researchers; therefore, they constitute a service to the scholarly community. At the same time, the *Frontiers journal series* operates on a revolutionary invention, the tiered publishing system, initially addressing specific communities of scholars, and gradually climbing up to broader public understanding, thus serving the interests of the lay society, too.

Dedication to quality

Each Frontiers article is a landmark of the highest quality, thanks to genuinely collaborative interactions between authors and review editors, who include some of the world's best academicians. Research must be certified by peers before entering a stream of knowledge that may eventually reach the public - and shape society; therefore, Frontiers only applies the most rigorous and unbiased reviews. Frontiers revolutionizes research publishing by freely delivering the most outstanding research, evaluated with no bias from both the academic and social point of view. By applying the most advanced information technologies, Frontiers is catapulting scholarly publishing into a new generation.

What are Frontiers Research Topics?

Frontiers Research Topics are very popular trademarks of the *Frontiers journals series*: they are collections of at least ten articles, all centered on a particular subject. With their unique mix of varied contributions from Original Research to Review Articles, Frontiers Research Topics unify the most influential researchers, the latest key findings and historical advances in a hot research area.

Find out more on how to host your own Frontiers Research Topic or contribute to one as an author by contacting the Frontiers editorial office: frontiersin.org/about/contact

Immunity in the development of anti-cancer drug resistance

Topic editors

Heng Sun — University of Macau, China

Haitao Wang — Center for Cancer Research, National Cancer Institute (NIH), United States

Xuebing Li — Tianjin Medical University General Hospital, China

Ya Meng — Zhuhai Precision Medical Center, Zhuhai People's Hospital, China

Topic coordinator

Xinwei Wu — National Institutes of Health (NIH), United States

Citation

Sun, H., Wang, H., Li, X., Meng, Y., eds. (2023). *Immunity in the development of anti-cancer drug resistance*. Lausanne: Frontiers Media SA.

doi: 10.3389/978-2-83251-190-9

Table of contents

frontiers | Frontiers in Pharmacology

TYPE Editorial
PUBLISHED 16 December 2022
DOI 10.3389/fphar.2022.1120037

OPEN ACCESS

EDITED AND REVIEWED BY
Dianwen Ju,
Fudan University, China

*CORRESPONDENCE
Ya Meng,
mengya_85@163.com
Haitao Wang,
haitao.wang@nih.gov
Xuebing Li,
xbli@tmu.edu.cn
Xinwei Wu,
xinwei.wu@nih.gov
Heng Sun,
HengSun@um.edu.mo

SPECIALTY SECTION
This article was submitted to Pharmacology of Anti-Cancer Drugs, a section of the journal Frontiers in Pharmacology

RECEIVED 09 December 2022
ACCEPTED 12 December 2022
PUBLISHED 16 December 2022

CITATION
Meng Y, Wang H, Li X, Wu X and Sun H (2022), Editorial: Immunity in the development of anti-cancer drug resistance.
Front. Pharmacol. 13:1120037.
doi: 10.3389/fphar.2022.1120037

Editorial: Immunity in the development of anti-cancer drug resistance

Ya Meng[1]*, Haitao Wang[2]*, Xuebing Li[3]*, Xinwei Wu[2]* and Heng Sun[4,5,6]*

[1]Guangdong Provincial Key Laboratory of Tumor Interventional Diagnosis and Treatment, Zhuhai People's Hospital, Zhuhai Hospital Affiliated With Jinan University, Zhuhai, China, [2]Thoracic Surgery Branch, Center for Cancer Research, National Cancer Institute (NCI), Bethesda, MD, United States, [3]Tianjin Key Laboratory of Lung Cancer Metastasis and Tumor Microenvironment, Tianjin Lung Cancer Institute, Department of Lung Cancer Surgery, Tianjin Medical University General Hospital, Tianjin, China, [4]Cancer Center, Faculty of Health Sciences, University of Macau, Macau, Macau SAR, China, [5]MOE Frontiers Science Center for Precision Oncology, University of Macau, Macau, Macau SAR, China, [6]Zhuhai Research Institute, University of Macau, Zhuhai, Macau SAR, China

KEYWORDS

cancer therapy, drug resistance, immunity, precision oncology, tumor microenvironment

Editorial on the Research Topic
Immunity in the development of anti-cancer drug resistance

Development of resistance is the leading cause for cancer therapy failure (Vasan et al., 2019). Drug resistance could be innately generated before or during tumorigenesis; or acquired in response to cancer treatment. Multiple factors could affect the development of anti-cancer drug resistance, such as the mutation spectrum, cross-talks, and networks among pivotal signaling pathways of the cancer cells, as well as the tumor macro- and micro-environment, in which immunity is of the utmost importance (Wang et al., 2019). Actually, immunity itself serves as the first barrier against cancer initiation, and also works as the first "drug" to kill the cancer cells. In this Research Topic, we discussed the interplay between cancer and immunity, especially focusing on how cancer cells and immune cells affect each other during carcinogenesis and in the development of anti-cancer drug resistance.

It is well accepted that cancers are attributed to occurrence and accumulation of mutations, and the resulting abnormal activity and/or function of oncogenes and tumor suppressors. In addition to enhanced proliferation, survival, and anti-apoptosis capacities of cancer cells, the dysfunction of oncogenes and tumor suppressors is involved in the modulation of cancer immunity, which in turn protects cancer cells from immune surveillance and elimination. For example, Muthalagu et al. (2020) reported in pancreatic ductal adenocarcinoma (PDAC), activation of oncogenes Myc and KRAS could block the infiltration of NK cells *via* repressing type I interferon pathway, thus strengthen survival capacity to PDAC cells. In this Research Topic, Luo et al. reported that the KRAS-associated genes score correlated with the infiltration of several types of immune cells, including NK cells,

memory CD4 T cells, plasma cells, and mast cells and might thus serve as a promising signature to distinguish the prognosis, molecular and immune characteristics of colon cancer patients. Besides, Hu et al. identified ST8SIA1, which plays an oncogenic role in triple-negative breast cancer (TNBC) (Nguyen et al., 2018), gliomas (Ohkawa et al., 2021), and other cancers, as a novel immune-related biomarker in clear-cell renal cell carcinoma (ccRCC). ST8SIA1 expression levels were negatively correlated with tumor purity and positively associated with infiltrated immune cells and expression of immune checkpoint genes. In addition, Xing et al. reviewed the recent findings of FBXW7, especially its tumor suppressive roles in multiple types of cancers, through regulating different immune cells for immune evasion and cancer development. Taken together, certain oncogenes and/or tumor suppressors not only play significant roles in initiating and fueling tumorigenesis, but also profoundly contribute to shaping the cancer immunity.

Aside from the influence of oncogenes and tumor suppressors, critical signaling pathways have been uncovered to control the drug sensitivities of cancer cells, such as the cancer cell dormancy regulated by Rb1-E2F signaling (Knudsen et al., 2019), epithelial to mesenchymal transition (EMT) induced by TGF-beta signaling (Katsuno et al., 2019), and so on. In this Research Topic, Zhu et al. investigated the roles of oxidative stress (OxS)-related genes in anti-cancer drugs sensitivity of lung adenocarcinoma (LUAD), and found a four OxS gene signature is correlated with the tumor mutation burden, tumor associated immune cell infiltration, and the expression of immune checkpoint molecules, which may contribute to individualized immunotherapeutic strategies for LUAD. Moreover, Feng et al. found that the peroxisome proliferator-activated receptor (PPAR) signaling pathway, related to fatty acid biosynthesis, might be a potential sorafenib resistance pathway in hepatocellular carcinoma (HCC) *via* regulating stemness of cancer cells. And in gastric cancer, Zhang et al. discovered that an EMT and immunity-related gene signature could be utilized as a biomarker to assess prognosis and guide precise treatment. Besides, epigenetic regulation such as DNA/RNA/histone modification, also broadly and deeply affects drug sensitivity. In this Research Topic, Meijing et al. identified three types of m6A methylation modification patterns are significantly different in immune infiltration in stomach adenocarcinoma (STAD). Further analysis by the researchers indicated that the m6A modification pattern may be a critical factor leading to inhibitory changes and heterogeneity in tumor micro-environment.

Anti-cancer drugs treatment not only targets the cancer cells but also reshapes the tumor macro-and micro-environment, which correspondingly affects the therapeutic efficacy of cancer patients. In this Research Topic, Tian et al. reviewed the critical roles of tumor micro-environment and immune escape in tumor occurrence, metastasis and anti-cancer drug resistance after sorafenib treatment in HCC patients. The relevant mechanisms focused on hypoxia, tumor-associated immune-suppressive cells, and immunosuppressive molecules. Moreover, Liu et al. found that macrophages and neutrophils are highly infiltrated, while $CD8^+$ T cells are decreased in a sorafenib-resistant mouse HCC model. The authors identified nalidixic acid as a promising antagonist for sorafenib-resistant HCC treatment. In addition, Yang et al. investigated the roles of neutrophils in bladder cancer and established a neutrophil-based prognostic model incorporating five neutrophil-related genes, which may contribute to individualized prognostic prediction and clinical decision-making. Besides immune cells, inflammatory factors such as a series of cytokines and chemokines strongly modulate the responses of cancer cells to drugs. Wu et al. addressed the recent research progresses on regulating inflammatory factors for an intentional controlling anti-cancer response with immune checkpoint inhibitors. Indeed, the cross-talk between cancer cells and immune cells within the microenvironment, and the interplay between *in situ* cancers and the systematic immunity deserve more in-depth and detailed investigation in future, to further solve the mystery of anti-cancer drug resistance and shed light on the identification of novel and more effective drugs.

In recent years, cancer immunotherapies, including Chimeric Antigen Receptor (CAR) T cell and Immune Checkpoint Blockage (ICB) therapies, have achieved great success, though many knotty problems remain to be solved. Furthermore, with our deepening and broadening understanding of the roles and mechanisms of immunity in the development of anti-cancer drug resistance, more attention and effort will be paid to attacking the resistant cells from an immunomodulatory perspective in the near future, which we hope will eventually benefit cancer patients.

Author contributions

All authors listed have made a substantial, direct, and intellectual contribution to the work and approved it for publication.

Funding

This work was supported by the National Natural Science Foundation of China (82003450, 81602587, and 82273019), Macao Science and Technology Development Fund (FDCT) grants (0006/2021/AGJ and 0065/2021/A), the Key Project of Cancer Foundation of China (CFC2020kyxm003), the Tianjin Key Medical Discipline (Specialty) Construction Project (TJYXZDXK-061B), General Project of Tianjin Lung Cancer Institute (TJLCMS2021-03).

Acknowledgments

I would like to express my sincere thanks to the guest editorial team and all the reviewers who participated in the

handling of this Research Topic. At the same time, I would like to thank all the authors who contributed to this Research Topic.

Conflict of interest

The authors declare that the research was conducted in the absence of any commercial or financial relationships that could be construed as a potential conflict of interest.

Publisher's note

References

Katsuno, Y., Meyer, D. S., Zhang, Z., Shokat, K. M., Akhurst, R. J., Miyazono, K., et al. (2019). Chronic TGF-beta exposure drives stabilized EMT, tumor stemness, and cancer drug resistance with vulnerability to bitopic mTOR inhibition. *Sci. Signal* 12 (570), eaau8544. doi:10.1126/scisignal.aau8544

Knudsen, E. S., Pruitt, S. C., Hershberger, P. A., Witkiewicz, A. K., and Goodrich, D. W. (2019). Cell cycle and beyond: Exploiting new RB1 controlled mechanisms for cancer therapy. *Trends Cancer* 5 (5), 308–324. doi:10.1016/j.trecan.2019.03.005

Muthalagu, N., Monteverde, T., Raffo-Iraolagoitia, X., Wiesheu, R., Whyte, D., Hedley, A., et al. (2020). Repression of the type I interferon pathway underlies MYC- and KRAS-dependent evasion of NK and B cells in pancreatic ductal adenocarcinoma. *Cancer Discov.* 10 (6), 872–887. doi:10.1158/2159-8290.CD-19-0620

Nguyen, K., Yan, Y., Yuan, B., Dasgupta, A., Sun, J., Mu, H., et al. (2018). ST8SIA1 regulates tumor growth and metastasis in TNBC by activating the FAK-AKT-mTOR signaling pathway. *Mol. Cancer Ther.* 17 (12), 2689–2701. doi:10.1158/1535-7163.MCT-18-0399

Ohkawa, Y., Zhang, P., Momota, H., Kato, A., Hashimoto, N., Ohmi, Y., et al. (2021). Lack of GD3 synthase (St8sia1) attenuates malignant properties of gliomas in genetically engineered mouse model. *Cancer Sci.* 112 (9), 3756–3768. doi:10.1111/cas.15032

Vasan, N., Baselga, J., and Hyman, D. M. (2019). A view on drug resistance in cancer. *Nature* 575 (7782), 299–309. doi:10.1038/s41586-019-1730-1

Wang, X., Zhang, H., and Chen, X. (2019). Drug resistance and combating drug resistance in cancer. *Cancer Drug Resist* 2 (2), 141–160. doi:10.20517/cdr.2019.10

frontiers | Frontiers in Pharmacology

ORIGINAL RESEARCH
published: 14 June 2022
doi: 10.3389/fphar.2022.899725

A KRAS-Associated Signature for Prognostic, Immune and Chemical Anti-Cancer Drug-Response Prediction in Colon Cancer

Kangjia Luo[1†], Yanni Song[2†], Zilong Guan[1†], Suwen Ou[1], Jinhua Ye[1], Songlin Ran[1], Hufei Wang[1], Yangbao Tao[1], Zijian Gong[1,3], Tianyi Ma[1], Yinghu Jin[1], Rui Huang[1], Feng Gao[4]* and Shan Yu[5]**

[1]Department of Colorectal Surgery, The Second Affiliated Hospital of Harbin Medical University, Harbin, China, [2]Department of Breast Surgery, Harbin Medical University Cancer Hospital, Harbin, China, [3]Department of General Surgery, The People's Hospital of Duerbert Mongolian Autonomous County, Harbin, China, [4]Department of Gastrointestinal Surgery, The Affiliated Hospital of Medical School of Ningbo University, Ningbo, China, [5]Department of Pathology, The Second Affiliated Hospital of Harbin Medical University, Harbin, China

OPEN ACCESS

Edited by:
Heng Sun,
University of Macau, China

Reviewed by:
Aiping Zhang,
University of Macau, China
Jingbo Zhou,
University of Macau, China

***Correspondence:**
Rui Huang
huangrui2019@163.com
Feng Gao
gf9777@126.com
Shan Yu
yushan@hrbmu.edu.cn.

[†]These authors have contributed equally to this work

Specialty section:
This article was submitted to Pharmacology of Anti-Cancer Drugs, a section of the journal Frontiers in Pharmacology

Received: 19 March 2022
Accepted: 26 May 2022
Published: 14 June 2022

Citation:
Luo K, Song Y, Guan Z, Ou S, Ye J, Ran S, Wang H, Tao Y, Gong Z, Ma T, Jin Y, Huang R, Gao F and Yu S (2022) A KRAS-Associated Signature for Prognostic, Immune and Chemical Anti-Cancer Drug-Response Prediction in Colon Cancer. Front. Pharmacol. 13:899725. doi: 10.3389/fphar.2022.899725

Background: KRAS mutation, one of the most important biological processes in colorectal cancer, leads to poor prognosis in patients. Although studies on KRAS have concentrated for a long time, there are currently no ideal drugs against KRAS mutations.

Methods: Different expression analysis and weighted gene coexpression network analysis was conducted to select candidate genes. Log-rank tests and Cox regression picked out the prognostic genes to build a KRAS-related gene prognostic score (KRGPS). A nomogram based on KRGPS was built to predict survival of clinical patients. Comprehensive analysis showed the prognosis, immune microenvironment and response to immune therapy and chemotherapy in KRGPS subgroups.

Results: We collected a KRGPS from the set of two genes GJB6 and NTNG1, with low-KRGSP patients having better progression-free survival (PFS). Low KRGPS is correlated with high infiltration of activated NK cells, plasma cells and activated memory CD4 T cells and that these cells benefit more from immune checkpoint inhibitor therapy. However, high KRGPS is associated with high infiltration of activated mast cells, pathways of immune dysregulation and a high ratio of TP53 and KRAS mutations. KRGPS subgroups are also sensitive to chemotherapy differently. A nomogram, established based on the KRGPS and pathological stage, predict 3- and 5-years PFS well.

Conclusions: The KRAS-associated score acts as a promising signature to distinguish prognosis, molecular and immune characteristics, and benefits from immune and chemical therapy. These KRAS-associated genes could be promising targets for drug design.

Keywords: KRAS mutation, colorectal cancer, prognostic signature, immune microenvironment, immune/chemotherapy

INTRODUCTION

In recent years, the incidence and mortality of colorectal cancer (CRC) have gradually increased, particularly in individuals under 50 years of age. Due to new advances in early diagnosis and treatment strategies, the death rate of CRC has dropped. Nevertheless, it still constitutes the third leading cause of cancer-related death around the world (Miller et al., 2019). Many oncogenes, which play a pivotal role in promoting cancer progression, have been reported to be steadily active in cancer due to genetic alterations. Mutations in the RAS family (KRAS, NRAS, and HRAS) are well-known drivers of CRC, and KRAS mutations are available in CRC patients at the highest frequency among them (Vogelstein et al., 1988; Kim et al., 2020). The presentation of KRAS mutations from CRCs is associated with a worse prognosis than non-KRAS oncogenic ones (Hayama et al., 2019; Wiesweg et al., 2019).

KRAS is activated at the membrane downstream of the epidermal growth factor receptor (EGFR) family, allowing signal transmission from the cell surface to the nucleus and managing many crucial cellular processes (Markman et al., 2010). Studies have highlighted that mutations in KRAS accelerate tumorigenesis (Schwitalla et al., 2013) and critically drive resistance to rapamycin (Hung et al., 2010), MEK inhibition (Haigis et al., 2008), and dietary restriction of serine and glycine (Maddocks et al., 2017). Indeed, KRAS mutation permanently promotes over 10 tumorigenic signaling cascades, especially the mitogen-activated protein kinase (MAPK) pathway and phosphoinositide 3-kinase (PI3K) pathway (Thein et al., 2021). Despite more than 3 decades of research efforts, there are still no effective inhibitors against KRAS for routine clinical practice, prompting the concept that RAS may be undruggable (Papke and Der, 2017). In 2019, there was a breakthrough in which two inhibitors, MRTX849 and AMG 510, successfully targeted KRAS (G12C) mutations in colon adenocarcinomas[1] (Hallin et al., 2020). However, the duration of response for most patients is still not satisfying, with a median progression-free survival of only 6.3 months shown by the most recent clinical trial data (including 42 patients with colorectal cancer) (Hong et al., 2020). We have not identified ideal targets for the development of drugs against KRAS until today, and more information about KRAS is needed.

Researchers always try to display the landscape of CRC focusing on a specific gene or signaling pathway and ignoring the synergistic effects of others. As a result, drugs based on these findings always show great deficiency in patients. The combination of drugs targeting different motifs has shown great advantages according to the outcome of clinical trials, which is more than a single plus of them (Al-Attar and Madihally, 2020; Rudzińska et al., 2021). Thus, we hypothesized that the KRAS-associated signature gene set may be an ideal target to counterbalance the burden of KRAS mutations. In this study, we identified genes affected by KRAS mutations and established a two-gene signature, which is a robust prognostic biomarker and a potential target for drug design.

[1]Author Anonymous (2019). AMG 510 First to Inhibit "Undruggable" KRAS Cancer Discov. 9(8), 988–989. doi:10.1158/2159-8290.CD-NB2019-073

MATERIALS AND METHODS

Data Source

Gene expression data and corresponding clinical features of colon adenocarcinomas were downloaded from TCGA for training (https://portal.gdc.cancer.gov/). The profile of gene expression (GSE39582), including 574 samples and matched clinical information, was downloaded from the GEO website for validation (https://www.ncbi.nlm.nih.gov/geo/). Gene IDs were transformed by "clusterProfiler" (Yu et al., 2012), and samples were removed with survival times shorter than 1 month.

Identification of Differentially Expressed Genes

The KRAS mutation was defined as the presence of missense mutation sites including putative driver and unknown significance. To obtain DEGs between subgroups of colon cancer patients with or without KRAS mutations in the TCGA cohort, the R package "edgeR" was used as the standard comparison model (McCarthy et al., 2012). Sequencing expression was normalized through "TMM", and the DEG threshold was set at $|\log2\ FC| \geq 0.585$ and $p < 0.05$.

Identification of Hub Genes

The R package "WGCNA" was used to identify hub genes of DEGs. A soft threshold of 4 was obtained with a RsquaredCut at 0.9. Based on a power of 4, we calculated module eigengenes blockwise from all DEGs in one step. Finally, 7 modules were distinguished by setting the merging threshold function at 0.25. The edges between genes of significantly related modules were used to construct the network with weight >0.2 in Cytoscape (v3.8.2).

Construction of the KRAS-Related Gene Prognostic Score

The R package "survival" was used to evaluate correlations between the hub gene expression levels and the progression-free survival (PFS) of CRC patients. Genes with p value <0.05 were identified. Based on the PFS-related genes (pseudogenes were dropped), Lasso regression was conducted 500 times according to the manual of the R package "glmnet", and a set of genes that contributed to significant PFS was collected. KRGPS was calculated as the formula:

$$KRGPI = \sum_{i=1}^{n} (Exp_i * Coe_i)$$

"n" represents the number of genes in the model, Exp_i represents the expression of $gene_i$ and Coe_i represents the regression coefficient of $gene_i$ determined by multivariate Cox regression.

Construction of Nomogram

Univariate and multivariate Cox regression was used to determine whether the KRGPS was independent of the clinical characteristics (including age, sex, pathological stage) of patients.

Based on the KRGPS and pathological stage, a nomogram was constructed to predict the 3- and 5-PFS. The calibration curves and C-index were used to discriminate the nomogram predicted status and the true survival.

Analysis of Molecular and Immune Characteristics

To analyze the landscape of gene mutations, information was obtained from the TCGA database, and the quantity and quality of gene mutations were analyzed by the R package "Maftools". Pieces of information between mRNA and TF and miRNA were obtained from chEA3 (https://maayanlab.cloud/chea3/#top), TargetScanHuman 8.0 (http://www.targetscan.org/vert_80/) and miRDB (http://mirdb.org/). Gene set enrichment analysis (GSEA) was used to probe the signaling pathways on which the differentially expressed genes were concentrated. To evaluate the infiltration of immune cells, CIBERSORT. R (available online at HTTPS://cibersort.stanford.edu/) was conducted according to the expression data of samples. The distribution of immune cells was compared between KRGPS subgroups through the Wilcoxon test. Levels of 33 immune checkpoints were also evaluated in KRGPS subgroups.

Forecasts of Immunotherapeutic and Chemotherapeutic Response

The Tumor Immune Dysfunction and Exclusion (TIDE) algorithm was managed (online at HTTP://tide.dfci.harvard.edu/) to predict clinical responses to immune checkpoint inhibitors as reported (Jiang et al., 2018; Fu et al., 2020). The R package "pRRophetic" was used to estimate the chemotherapeutic response of each patient based on the levels of transcripts.

Cell Culture, RNA Extraction and Quantitative Real-Time PCR

Human colon cancer cell lines SW620, HCT116 and HT29 were cultured in RPMI-1640 medium (Gibco, United States) supplemented with 10% fetal bovine serum (FBS, Biological Industries, United States) in a humidified 5% CO_2 atmosphere at 37 C. All cell lines were purchased from American Tissue Culture Collection (ATCC).

Total RNAs of cells were extracted by TRIzol reagent (Invitrogen, United States) and was reversely transcribed to cDNA via PrimeScript™ RT Master Mix (Takara, Japan). Quantitive real-time PCR was performed by using PowerUp™ SYBR™ Green Master Mix (Applied Biosystems, United States) before loading in StepOne™ Real-Time PCR System (Applied Biosystems). Each reaction was tested in quadruplicate. ACTB was used as the internal reference and the $2^{(-\Delta\Delta Ct)}$ method was used for evaluating the relative mRNA levels. The sequences of primers were listed below:

Human NTNG1: Forward: 5′- GAGCATCCCTTGTGAGCT GT -3′, Reverse: 5′- TGAGGACTTTGGTGGAAGCC -3′;

Human GJB6: Forward: 5′- ACACTTTCATCGGGGGTGTC -3′, Reverse: 5′- GCAGTGTGTTGCAGACGAAG -3′;

Human ACTB: Forward: 5′- GATTCCTATGTGGGCGAC GA -3′, Reverse: 5′- AGGTCTCAAACATGATCTGGGT -3′.

IHC Staining

30 formalin-fixed, paraffin-embedded (FFPE) tissues were obtained from the Department of Colorectal Surgery, Second Affiliated Hospital of Harbin Medical University. Sections of FFPE tissue (5 um thick) were obtained and deparaffinized with xylene and rehydrated using standard procedures. Tissue sections were incubated with anti-GJB6 (ab200866, Abcam) antibody (1:50) for 3 h at room temperature. Washed again with PBS, the slides were incubated with goat anti-rabbit IgG-HRP for 1 h. At last, slides were treated with 3,3′-diaminobenzidine and counterstained with hematoxylin. The staining intensity of GJB6 immunoreactivity was evaluated by two pathologists respectively.

DNA Extraction and Sanger Sequencing

DNA was extracted from eight 5 μm FFPE tissues using the Tiangen DNA FFPE Tissue Kit (Tiangen, China) according to the manufacturer's protocol. To investigate the mutational status of codons 12 and 13, exon 2 of the KRAS gene was amplified with a specific primer: Forward: 5′-ATTACGATACACGTCTGCAGT CAACTG-3′, Reverse: 5′-CAATTTAAACCCACCTATA ATGGT-3'. PCR products were purified and sequenced at 3730XL (ABI, United States). The sequence data were analyzed using the SnapGene (Version 6.02).

Statistical Analysis

All statistical analyses were performed using R software (Version: 4.0.4) and Python (Version: 3.8.8). The Wilcoxon test was performed to compare variables between two groups. p value <0.05 was considered significant.

RESULTS

KRAS Mutations in CRC Patients

CRC treatment decisions have been based on histological considerations for a long time (National Health Commission of the People's Republic of China, 2020), while novel insights into tumor biology and genetic alterations have rapidly changed the process of therapeutic decisions. KRAS, according to TCGA, is the fourth mutation gene in colon adenocarcinomas (CAs) at a frequency of 37%, with missense as the leading mutation type (**Supplementary Figure S1A**). Compared with unaltered CAs, KRAS-mutated CAs suffered from shorter disease-free survival and progression-free survival times (**Supplementary Figures S1B,C**). Then, we conducted our exploration to seek details about KARAS mutations (**Figure 1**).

Hub DEGs Related to KRAS Mutation

Depending on the status of KRAS mutation, the samples of colon adenocarcinomas were divided into two subgroups. A total of 1,045 DEGs ($|logFC| > 0.585$ and p-value < 0.05) were obtained,

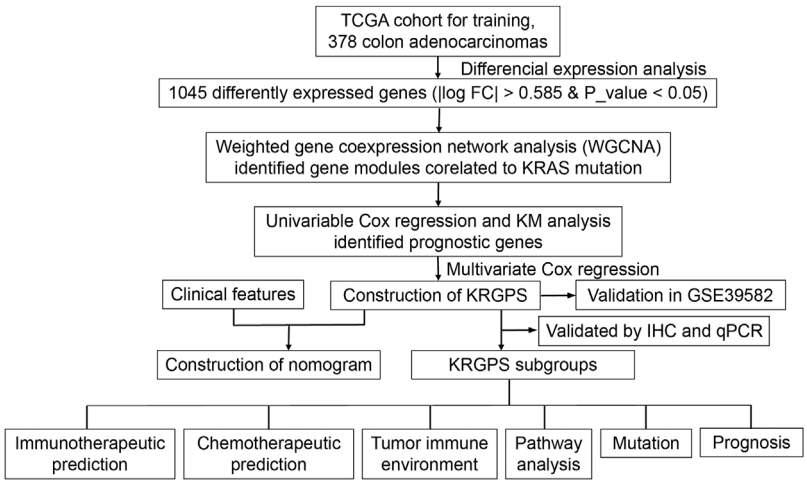

FIGURE 1 | Flow chart overview of the schedule performed to construct a prognostic gene model of colon adenocarcinoma.

of which 700 genes were upregulated and 345 were downregulated in the KRAS mutation group compared with the KRAS-unaltered group (**Figure 2A**). Weighted gene coexpression network analysis (WGCNA) was conducted on these DEGs to obtain the hub genes. With a correlation coefficient greater than 0.9, the optimal soft-thresholding power was 4 in terms of the scale-free network (**Supplementary Figure S2**). Based on the optimal power, the DEGs were apportioned into 7 modules through average linkage hierarchical clustering (**Figure 2B** and **Supplementary Figure S3A**). As shown by the Pearson correlation coefficient between a module and sample character, brown and black modules were positively related to KRAS mutation status, while blue, yellow and green modules were negatively related (**Figure 2C**). Gene network of these modules is shown in **Figure 2D**. KEGG and GO analyses based on these genes are displayed in **Supplementary Figures S3B,C**. Negative regulation of megakaryocyte differentiation, antimicrobial humoral response, humoral immune response mediated by circulating immunoglobulin and lymphocyte chemotaxis were core immune processes, on which these genes were concentrated (**Supplementary Figure S3D**).

Identification of Prognostic Signatures and Construction of a Nomogram

To determine the prognostic genes, univariate Cox regression and K-M analysis were performed. With $p < 0.05$, 5 genes were regarded as progression-free survival (PFS)-related (**Figures 3A,B**, **Supplementary Figures S4A–C**), based on which multivariate Cox regression was conducted before we obtained a set of 2 prognostic genes. As shown in **Supplementary Figure S5A**, missense mutations were most prevalent in these genes, and their total mutation rates were no more than 4%. For the regulatory network of biomarker genes, there were 2 transcription factors (TFs) and 5 miRNAs interacting with both genes (**Supplementary Figure S5B**). Next, we evaluated the levels of biomarker genes in colon cancer and normal colon epithelium cell lines. The outcomes of qPCR displayed that GJB6 was expressed in HT-29 cells with wild-type KRAS, while we could hardly detect the levels of it in HCT-116 and SW-620, which is KRAS mutated (**Figure 3C**). Nor did we detect the expression of NTNG1 in these cell lines (data were not shown). We further evaluated the levels of GJB6 in 30 CRC patients. KRAS mutation at G12/13 site was detected by Sanger sequencing, and 6 of them were KRAS mutated at the site of G12 in exon2 (**Supplementary Table S1**). To confirm the state of the gene, their levels of GJB6 were evaluated by IHC. Results showed that 7 of 24 were GJB6-positive in KRAS-wild samples, while 1 of 6 samples was positive in KRAS-mutation (**Figure 3D**).

A KRGPS, with the formula KRGPS = expression of GJB6 * (0.454) + expression of NTNG1 * (1.02), was calculated for prognostic prediction. Samples were separated into low- or high-KRGPS subgroups by the median score. The Kaplan–Meier plot suggested that patients in different KRGPS groups had significantly separated PFS with high KRGPS corresponding to terrible status (**Figure 3F**). Interestingly, high KRGPS also predicted worse progression-free survival of patients in GSE39582 and shorter overall survival (**Figure 3G** and **Supplementary Figure S4D**).

Then, we investigated whether the gene-derived risk score was an independent biomarker concerning clinical signatures. Univariate Cox regression analysis showed that KRGPS, as well as pathologic stage, was significantly associated with the prognosis of CRC patients (**Figure 4A**). Multivariate Cox regression analysis validated KRGPS as an independent prognostic factor adjusted for other clinical signatures (**Figure 4A**). Based on KRGPS and pathologic stage, a nomogram was constructed to predict the prognosis of CRC patients at 3 and 5 years (**Figure 4B**). Calibration plots indicated that the nomogram had a good performance and was therefore an ideal model (**Figure 4C**). The C-index of the nomogram indicated a better prognostic value than the pathological stage, which is

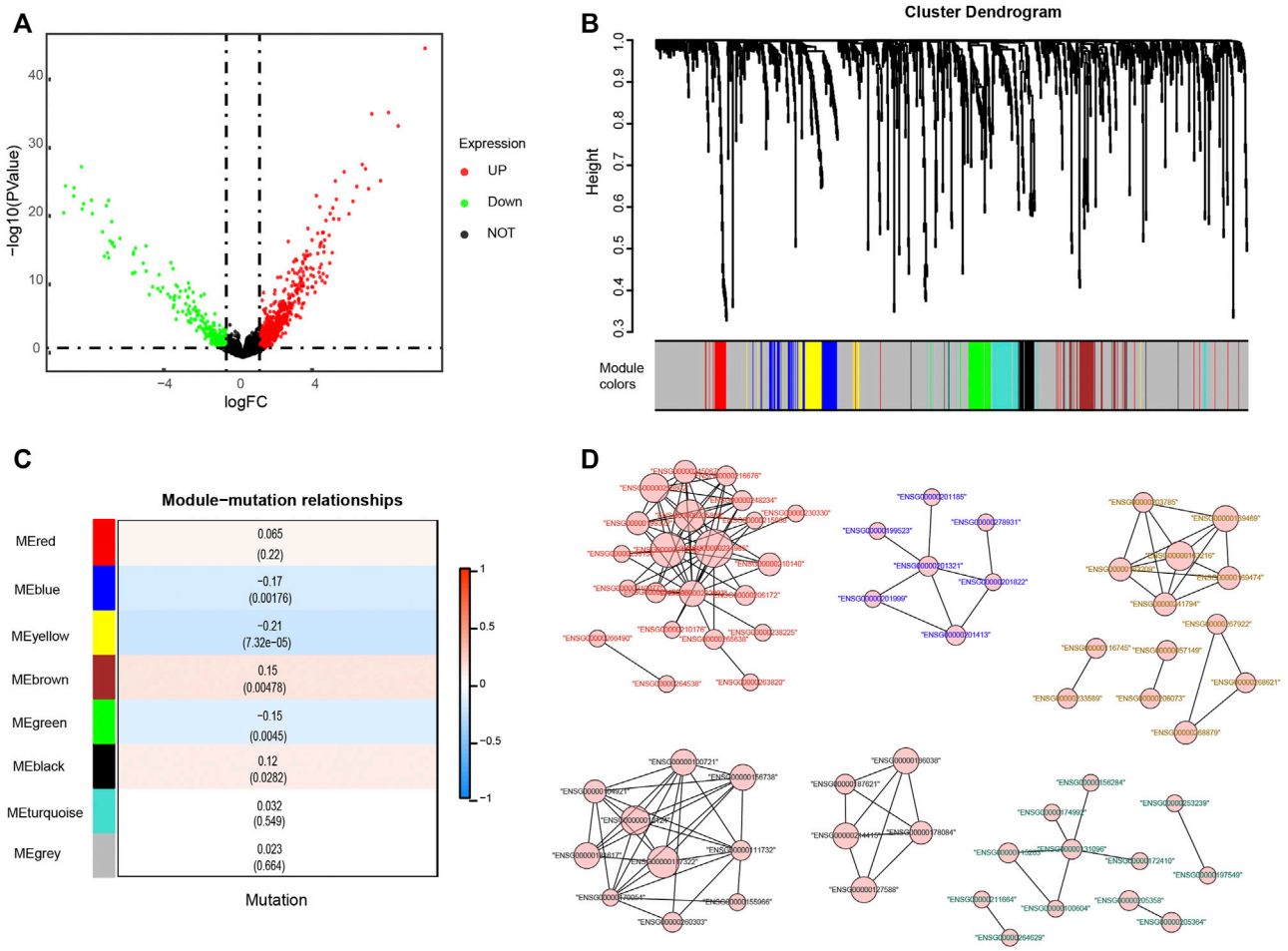

FIGURE 2 | Identification of genes related to KRAS mutations. **(A)** Differentially expressed genes (DEGs) of KRAS mutation subgroups with a cut-off at $p < 0.05$ and $|\log_2 FC| > 0.585$ **(B)** Weighted gene coexpression network analysis (WGCNA) of KRAS mutation-related genes with a soft threshold $\beta = 4$ **(C)** Spearman correlation analysis of gene modules and KRAS mutations. **(D)** The gene network of KRAS-related genes. The color of the labels and the shape of gene nodes indicate the affiliation of genes.

recommended as the gold standard for clinical decisions over time (**Figure 4D**).

Molecular Characteristics of Different KRGPS Subgroups

Somatic mutations were also evaluated in subgroups of KRGPS with the heading mutated genes APC, TP53, TNN and KRAS in both subgroups (**Figure 5A**). Mutations in FAT4, DNAH5 and ZFHX4 were more common in the KRGPS-low subgroup, although USH2A, RYR2 and PCLO were more common in the KRGPS-high subgroup (**Figure 5A**). Fisher's exact test showed that the mutation status of TTN, PIK3CA, MUC16, SYNE1, RYR2, PCLO and USH2A were correlated to KRGPS in statistics (**Supplementary Table S2**). Additionally, the TMB of the KRGPS-low subgroup was lower than that of the KRGPS-high subgroup (**Supplementary Figure S6A**).

The results of GO analysis by GSEA showed that spliceosomal tri-snRNP complex assembly, integrator complex, spliceosomal snRNP assembly, keratinization and cornification were heading functions enriched in low-KRGPS subgroups, while the gene sets of the high-KRGPS subgroups were mainly enriched in functions of detection of molecules of bacterial origin, platelet-derived growth factor binding, insulin-like growth factor receptor binding, midbrain dopaminergic neuron differentiation and low-density lipoprotein particle binding (**Figure 5B**). KEGG analysis revealed enrichment of malaria, the PI3K-Akt signaling pathway, cytokine–cytokine receptor interaction and the AGE-RAGE signaling pathway in diabetic complications in the KRGPS-high group but pancreatic secretion in the KRGPS-low group (**Supplementary Figure S6B**).

Immune Landscape in Different KRGPS Subgroups

As the GO analysis showed, the KRGPS-related genes were associated with the immune response. A total of 22 types of infiltrating immune cells were evaluated among samples through

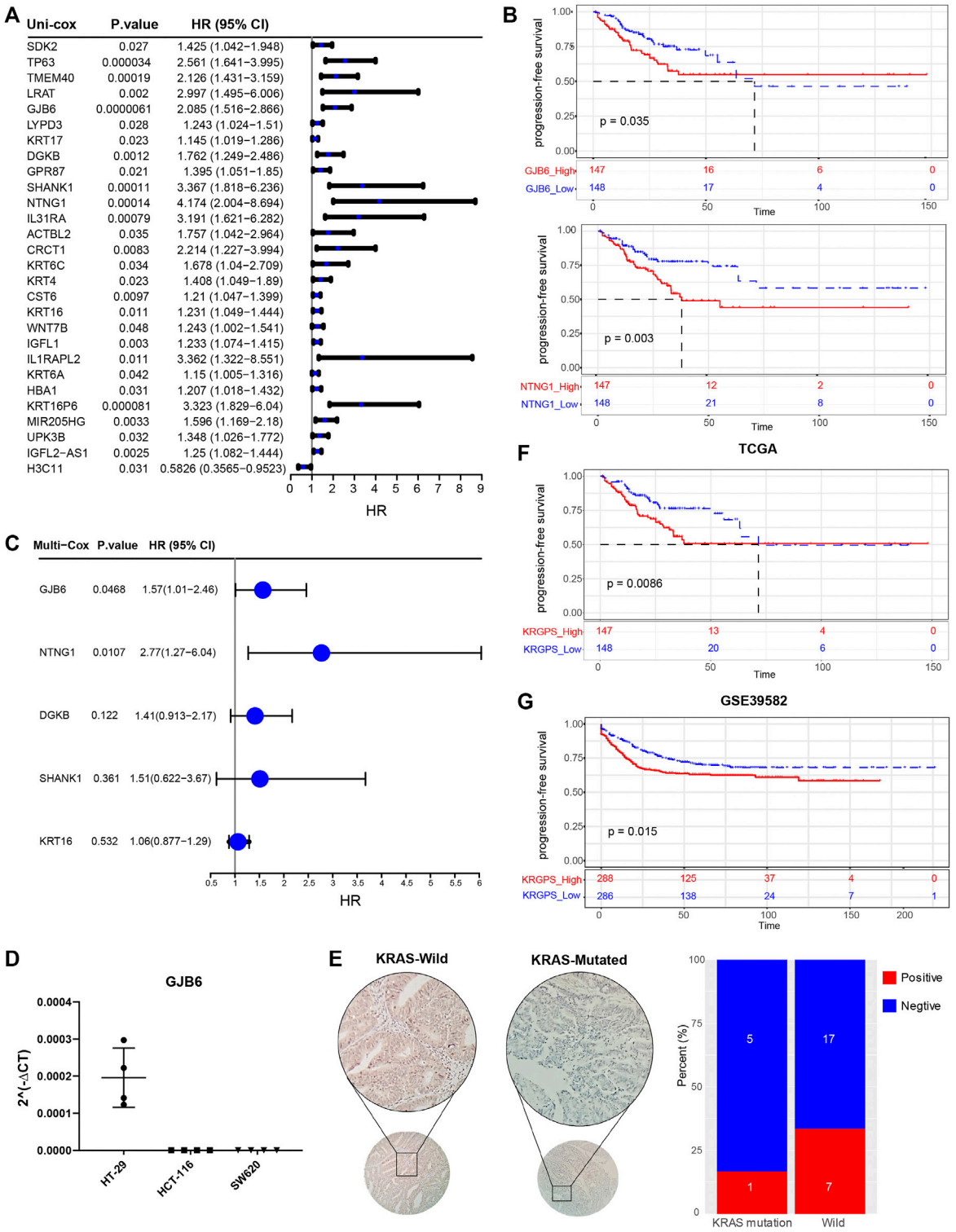

FIGURE 3 | Identification of prognostic signatures. **(A)** Univariate Cox analysis of 28 KRAS-related genes with $p < 0.05$. **(B)** Kaplan–Meier survival analysis of NTNG1 and GJB6 in TCGA cohort ($p < 0.05$) **(C)** Multivariate Cox regression analysis of 5 prognostic genes determined by Kaplan–Meier survival analysis. **(D)** RT-PCR validation of GJB6 in different COAD cell lines. HT-29 was KRAS-wild while HCT-116 (G13) and SW620 (G12) were KRAS-mutated **(E)** Representive IHC results of GJB6 in CRC patients with KRAS mutated or not. Scale, 200x. Percent of GJB6 positive samples in KRAS-mutated and wild patients. **(F)** Kaplan–Meier survival analysis of KRGPS in the TCGA cohort (Log-rank test) **(G)** Validation of KRGPS in the GEO cohort by Kaplan–Meier survival analysis (Log-rank test).

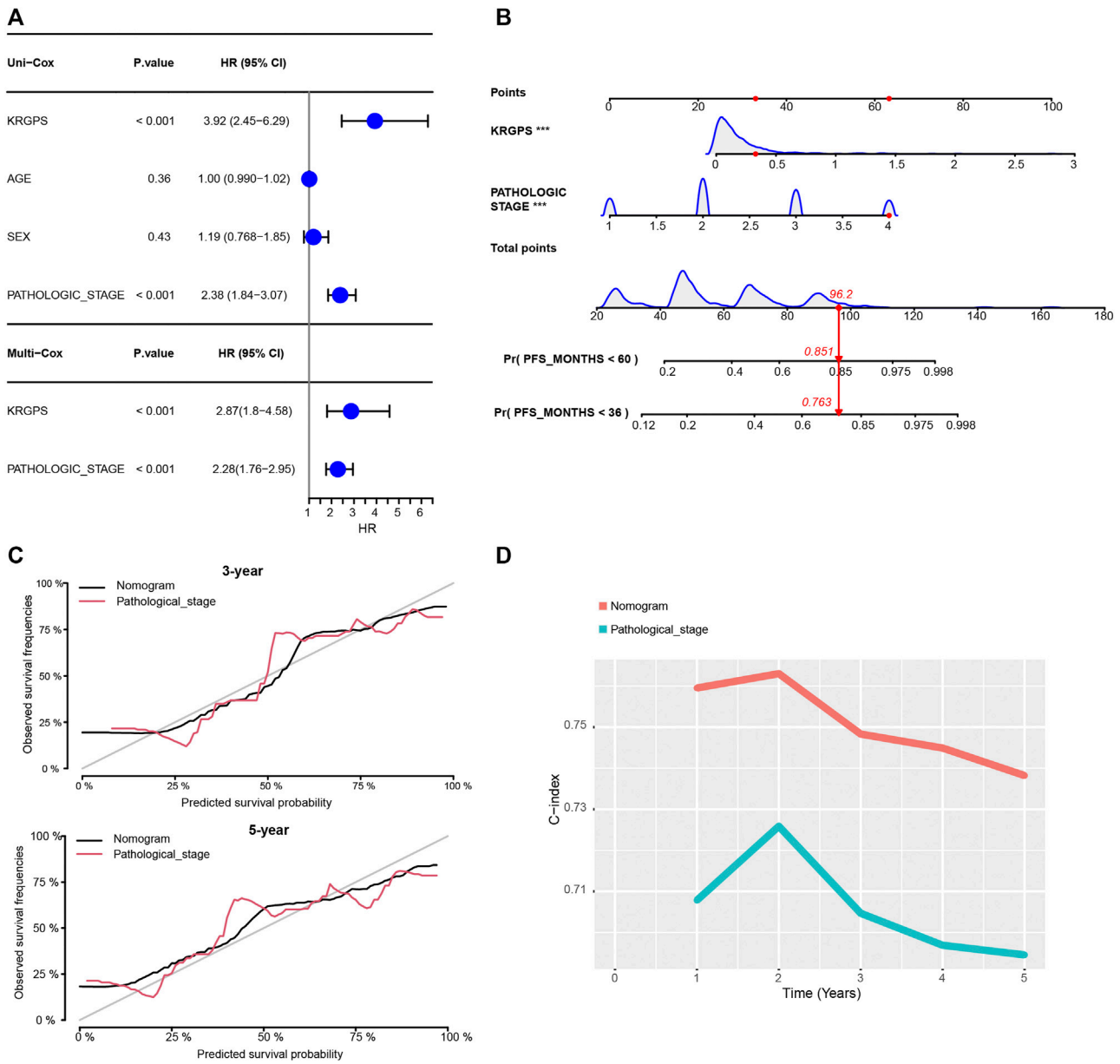

FIGURE 4 | Construction of the nomogram. **(A)** Univariate and multivariate Cox regression of clinical signatures and KRGPS. **(B)** The nomogram was constructed based on the independent prognostic factors evaluated by multivariate Cox regression **(C)** The calibration plots for the internal validation of the nomogram predicting 3-years and 5-years PFS. **(D)** C-index of the nomogram and pathological stage predicting PFS in different years.

CIBERSORT. The clinicopathological characteristics of different KRGPS subgroups related to the immune landscape are presented in **Figure 6A**. Plasma cells, activated NK cells and activated memory CD4 T cells were enriched in the low-KRGPS group, while activated mast cells were concentrated in the high-KRGPS group (**Figure 6B**). We also observed the relevance between KRGPS and 33 immune checkpoints, of which 20 genes were significantly decreased in the low-KRGPS group compared with the high-KRGPS group (**Supplementary Figure S7**). The antitumoral immune microenvironment may contribute to the good prognosis of patients in the low-KRGPS subgroup.

Prediction of Immune and Chemical Therapy in KRGPS Subgroups

TIDE was used to assess the potential clinical efficacy of immunotherapy in different KRGPS subgroups. In this study, the low-KRGPS subgroup corresponding to low dysfunction scores implied that KRGPS-low patients could benefit more from immune checkpoint inhibitor (ICI) therapy than KRGPS-high patients, although the T cell exclusion scores showed no significant differences between the KRGPS subgroup (**Figure 7A**). Next, we investigated the response to

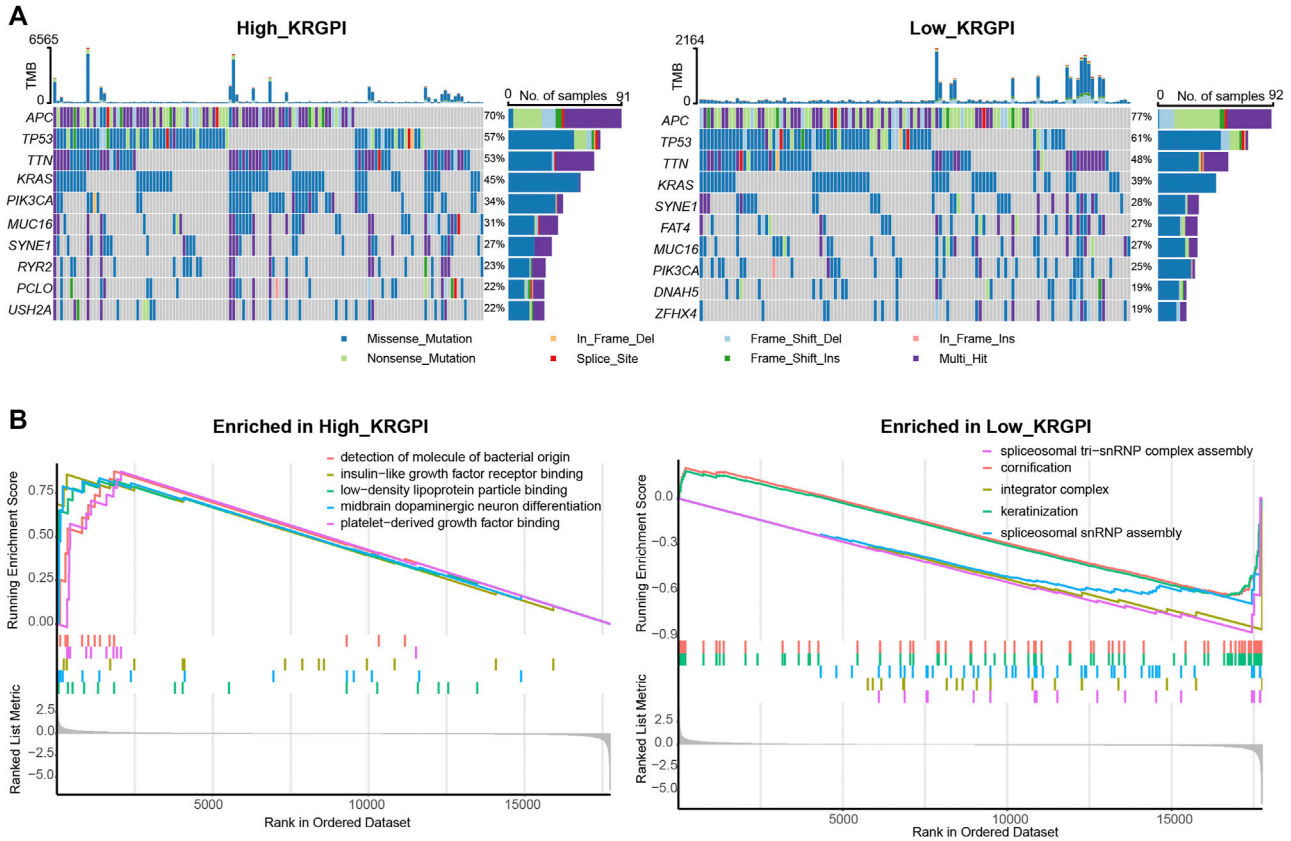

FIGURE 5 | Molecular characteristics of KRGPS subgroups. **(A)** Top 10 mutated genes in KRGPS subgroups. **(B)** Top 5 pathways enriched in different KRGPS subgroups by GO analysis ($p < 0.05$).

chemotherapy of patients in KRGPS subgroups. A total of 34 drugs displayed significant differences in the estimated IC50 of patients in separated KRGPS subgroups (**Figure 7B**).

DISCUSSION

CRC leads to a large number of cancer-related mortalities around the world, and KARAS mutations contribute to a poor prognosis and resistance to receptor tyrosine kinase (RTK) inhibitors and monoclonal antibodies against epidermal growth factor receptor (EGFR) (cetuximab and panitumumab), for example, in CRC patients (Karapetis et al., 2008). More importantly, drugs targeting KRAS directly or indirectly have not been satisfied until today (Zhu et al., 2021). Under this circumstance, more details about KRAS mutations are required, which should be a powerful foundation for drug design.

In our study, WGCNA was first used to recognize the modules of genes correlated to KRAS mutations. Survival analysis indicated a set of four genes that forecast the prognosis of patients efficiently. Based on these genes, we established a KRGPS to predict CRC prognosis and separated patients with CRC into two subgroups, with low-KRGPS patients having a better prognosis. KRGPS was made up of two genes, namely, GJB6 and NTNG1. Results of qPCR suggested that the levels of GJB6 were distinguished according to the status of KRAS-mutation, though we didn't detect the signals of NTNG1 in colon cancer cell lines. In CRC patients, the GJB6 levels were further evaluated by IHC, as well as the KRAS status by Sanger sequencing. More GJB6 were detected in KRAS-wild patients compared with KRAS-mutated, which validated the findings in colon cell lines. Research had announced that the levels of GJB6 were also decreased during the development of cancers, including gastric cancer, gliomas and head and neck cancer (Ozawa et al., 2007; Sentani et al., 2010; Artesi et al., 2015). For NTNG1, as reported, hypermethylated regions were frequently detected in cancers, implying its potential function for CRC resistance and why there was no detection of this gene (Andrew et al., 2017).

Despite the evolution of intrinsic molecules in tumor cells, the development of cancer has been regarded as a process that leads from cancer immunosurveillance to tumor escape (Dunn et al., 2002). According to the model of immunosurveillance, the clinical manifestation of cancer is dual: 1) neoplastic cell variants with limited immunogenicity are detected by the immune system, and 2) neoplastic cells actively restrain tumor-targeting immune reactions (Pietrocola et al., 2017). Increased immunosuppressive cells, decreased immunoreactive cells and increased expression of immune checkpoints in immune cells and tumors always come along with cancers, especially in

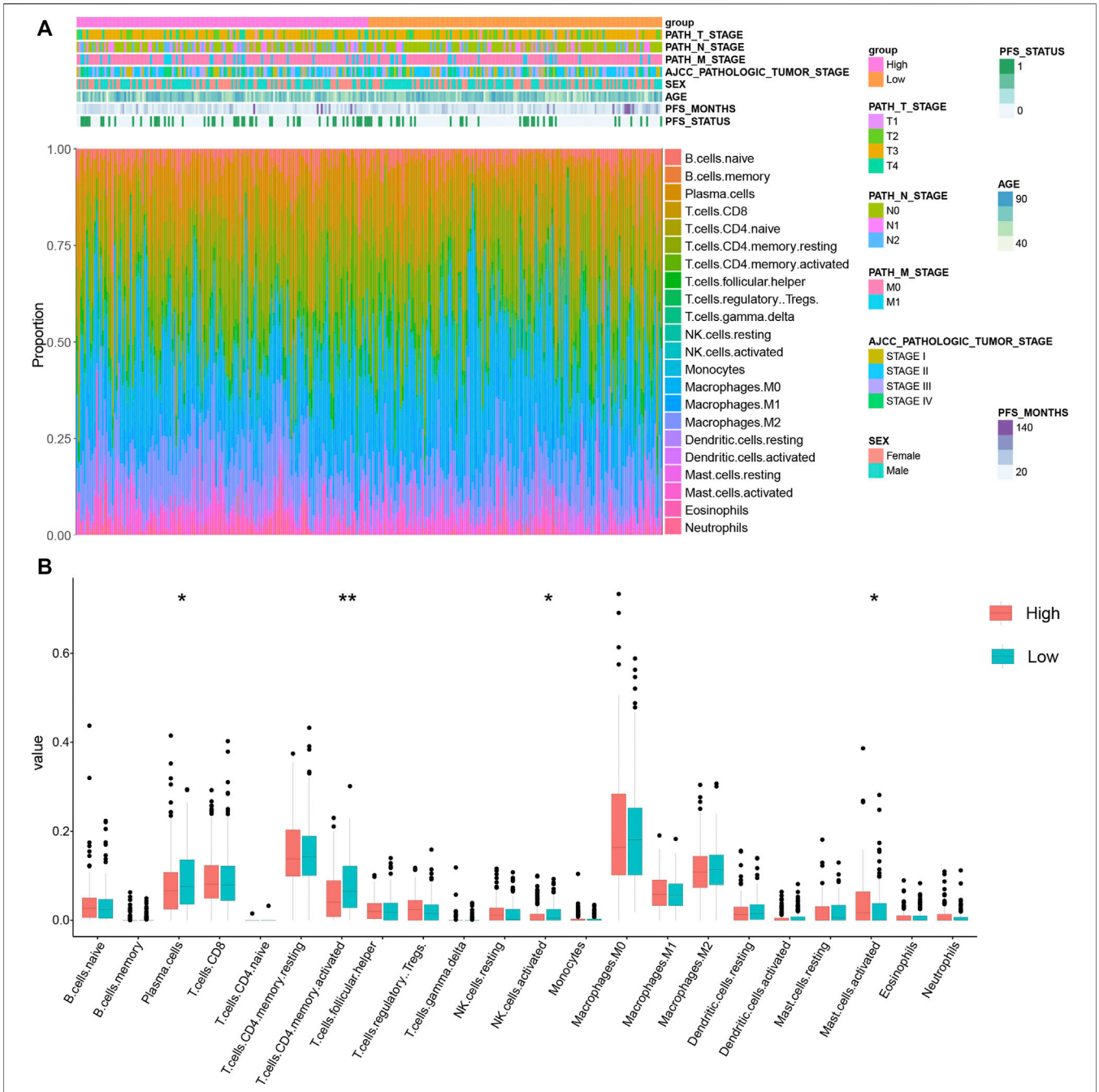

FIGURE 6 | The distribution of infiltrating immune cells in KRGPS subgroups. **(A)** The landscape of the tumor immune environment and clinical features of patients. **(B)** Levels of 22 infiltrated immune cells in KRGPS subgroups by Cibersort. *$p < 0.05$, **$p < 0.01$, ***$p < 0.001$, ****$p < 0.0001$.

advanced patients. In our study, as functional enrichment progressed, genes of WGCNA modules that correlated firmly with KRAS mutations took part in many immune processes. GO analysis revealed that functions, such as regulation of macrophage differentiation, B cell receptor signaling pathway, and regulation of humoral immune response, clustered in patients in the KRGPS subgroup. Next, we compared the distribution of immune cells of subgroups. The enrichment of plasma cells, activated NK cells and activated CD4 memory T cells and the decreased activated mast cells may account for the better survival of low-KRGPS patients. On the other hand, the levels of 18 immune checkpoints were significantly inhibited in the low-KRGPS subgroup, in favor of immune activation. Collectively, KRGPS is a biomarker of active immunity.

Studies on gene mutations also provide insight into the nature of the KRGPS subgroups. A lower incidence of KRAS mutations was

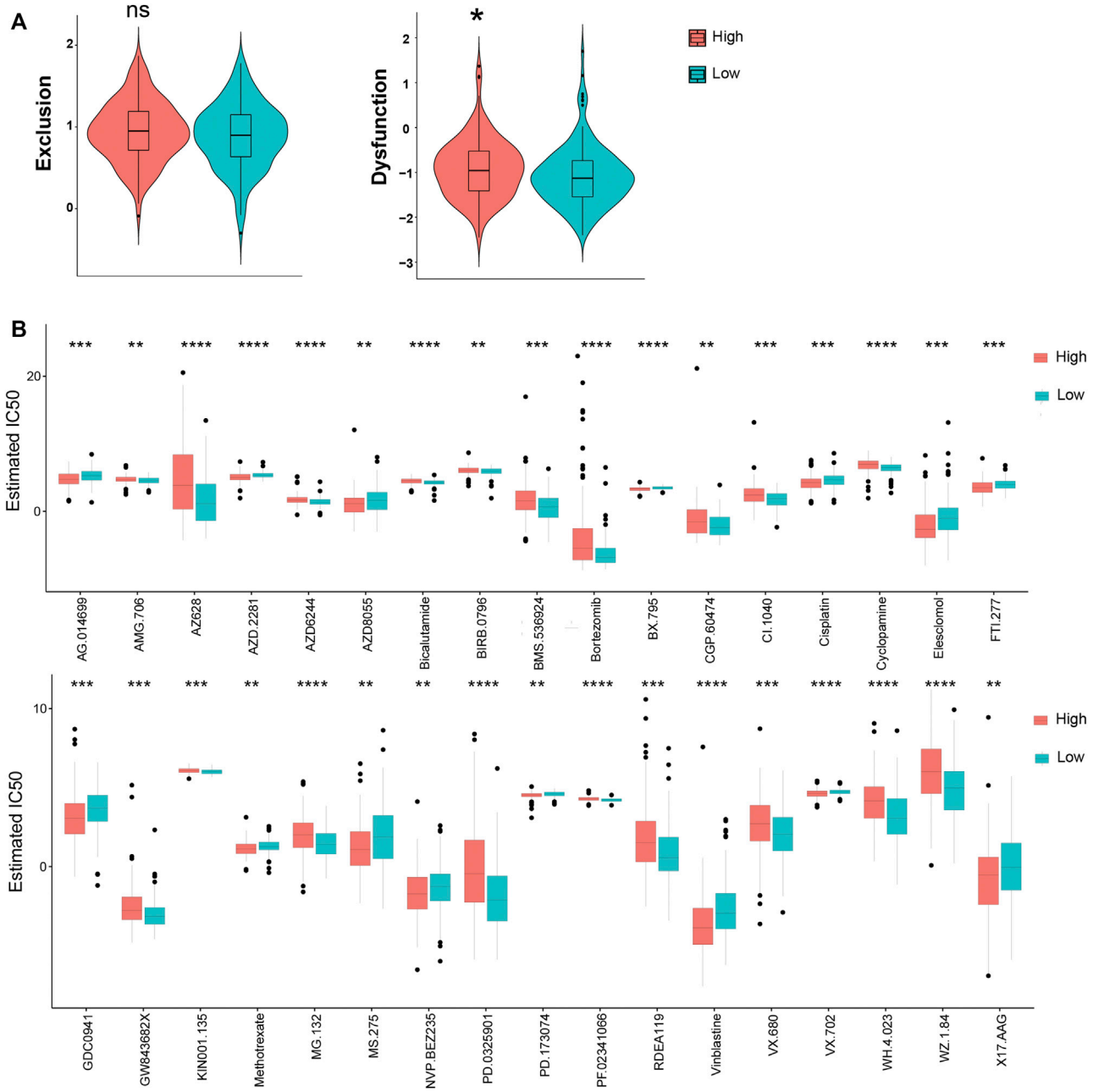

FIGURE 7 | The prognostic value of KRGPS in patients receiving immune and chemical therapy. **(A)** Exclusion and dysfunction scores of samples in KRGPS subgroups. **(B)** Chemotherapeutic responses of high- and low-KRGPS patients. *adj.p < 0.05, **adj.p < 0.01, ***adj.p < 0.001, ****adj.p < 0.0001.

located in the low-KRGPS group than in the high-KRGPS group, showing the largest difference in mutations between groups. Moreover, there was a higher rate of TP53 mutation in the high-KRGPS group. TP53 mutation, as reported, determines many biological behaviors of CRC, such as lymphatic and vascular invasion, chemoresistance, and the prognosis of patients (Russo et al., 2005; Iacopetta et al., 2006; Li et al., 2015). In this way, KRGPS-low patients with high KRAS and TP53 mutations had worse survival than KRGPS-high patients, in agreement with our survival outcomes. Tumor mutational burden (TMB), a summary of gene mutations, is positively related to the response of patients receiving immune therapy (Schrock et al., 2019). Our study showed that low-KRGPS patients have low TMB scores, implying a lower likelihood of low-KRGPS patients benefiting from immune checkpoint inhibitors (ICIs).

The tumor immune dysfunction and exclusion (TIDE) module can estimate multiple published transcriptomic biomarkers to predict patient response, which identifies factors that undergo two mechanisms of immune escape: the induction of T cell dysfunction in tumors with high infiltration of cytotoxic

T lymphocytes (CTLs) and T cell exclusion in tumors with low CTL levels (Jiang et al., 2018). Low KRGPS, consisting of low T cell dysfunction, may predict a favorable response to ICIs. In contrast, KRGPS predicts the opposite response of ICIs depending on TMB and TIDE. Further studies are calling for, although Liu announced that TIDE predicted the response of ICIs more accurately than other biomarkers, such as mutation load. Chemotherapy is widely used in cancer therapy, and high-KRGPS patients with colon cancer were significantly sensitive to 15 chemotherapeutic agents but blunt to 19 drugs compared with low-KRGPS patients.

In routine clinical guidelines, the pathologic stage is a pivotal prognostic joint of CRC patients. However, it could not fully reflect the biological heterogeneity of patients, as patients with the same pathologic stage lead to absolutely separate outcomes. Currently, the combination of gene markers and clinical signatures is widely used to predict the prognosis of patients. We constructed a nomogram based on the KRGPS derived from genes related to KRAS mutation and pathologic stage to predict patient outcomes, which shows a better efficiency of prediction.

This study still had several limitations. First, our study universally analyzed KRAS mutations, ignoring the separation among molecular subtypes. Mysteries on specific KRAS mutations are waiting for exploration. Moreover, on account of the retrospective data from public databases, case selection bias may cover up some problems. A randomized controlled trial may unravel more information about KRAS mutation.

CONCLUSION

Overall, for the first time, this study identifies a two-gene signature associated with KRAS mutations that can independently predict the prognosis of patients with CRC. Gene-derived KRGPS also helps to distinguish immune and molecular features, although further explorations are needed to clarify more details. These two genes, NTNG1 and GJB6, could be potential targets for drug design.

DATA AVAILABILITY STATEMENT

The datasets presented in this study can be found in online repositories. The names of the repository/repositories and accession number(s) can be found in the article/ **Supplementary Material**.

ETHICS STATEMENT

The studies involving human participants were reviewed and approved by Research Ethics Committee Second Affiliated Hospital of Harbin Medical University. The ethics committee waived the requirement of written informed consent for participation.

AUTHOR CONTRIBUTIONS

KL, YS and ZG designed the experiment. HW, JY, SR and SO dealt and analyzed the data. YT, ZG, TM and YJ draw the figures. KL and SY wrote the article. FG and RH directed the experiment and revised the manuscripts. All authors read and approved the final manuscript.

FUNDING

Ministry of Education Chunhui Project Cooperative Research Project (No. HLJ2019010 to Yanni S). Heilongjiang Natural Science Foundation of China (No. LH 2020H120 to Yanni S). Haiyan Research Fund of Harbin Medical University Cancer Hospital (No. JJZD 2020–04 to Yanni S). National Natural Science Foundation of China (No.81872034 to Rui H). Chen Xiao-ping Foundation For The Development Of Science and Technology of Hubei Province (No. CXPJJH12000002-2020025 to Rui H). Wu Jieping Medical Foundation (No. 320.6750.18492 to Feng Gao).

SUPPLEMENTARY MATERIAL

The Supplementary Material for this article can be found online at: https://www.frontiersin.org/articles/10.3389/fphar.2022.899725/full#supplementary-material

REFERENCES

Al-Attar, T., and Madihally, S. V. (2020). Recent Advances in the Combination Delivery of Drug for Leukemia and Other Cancers. *Expert Opin. Drug Deliv.* 17 (2), 213–223. doi:10.1080/17425247.2020.1715938

Andrew, A. S., Baron, J. A., Butterly, L. F., Suriawinata, A. A., Tsongalis, G. J., Robinson, C. M., et al. (2017). Hyper-Methylated Loci Persisting from Sessile Serrated Polyps to Serrated Cancers. *Int. J. Mol. Sci.* 18 (3), 535. doi:10.3390/ijms18030535

Artesi, M., Kroonen, J., Bredel, M., Nguyen-Khac, M., Deprez, M., Schoysman, L., et al. (2015). Connexin 30 Expression Inhibits Growth of Human Malignant Gliomas but Protects Them against Radiation Therapy. *Neuro Oncol.* 17 (3), 392–406. doi:10.1093/neuonc/nou215

Dunn, G. P., Bruce, A. T., Ikeda, H., Old, L. J., and Schreiber, R. D. (2002). Cancer Immunoediting: from Immunosurveillance to Tumor Escape. *Nat. Immunol.* 3 (11), 991–998. doi:10.1038/ni1102-991

Fu, J., Li, K., Zhang, W., Wan, C., Zhang, J., Jiang, P., et al. (2020). Large-scale Public Data Reuse to Model Immunotherapy Response and Resistance. *Genome Med.* 12 (1), 21. doi:10.1186/s13073-020-0721-z

Haigis, K. M., Kendall, K. R., Wang, Y., Cheung, A., Haigis, M. C., Glickman, J. N., et al. (2008). Differential Effects of Oncogenic K-Ras and N-Ras on Proliferation, Differentiation and Tumor Progression in the Colon. *Nat. Genet.* 40 (5), 600–608. doi:10.1038/ng.115

Hallin, J., Engstrom, L. D., Hargis, L., Calinisan, A., Aranda, R., Briere, D. M., et al. (2020). The KRASG12C Inhibitor MRTX849 Provides Insight toward Therapeutic Susceptibility of KRAS-Mutant Cancers in Mouse Models and Patients. *Cancer Discov.* 10 (1), 54–71. doi:10.1158/2159-8290.CD-19-1167

Hayama, T., Hashiguchi, Y., Okamoto, K., Okada, Y., Ono, K., Shimada, R., et al. (2019). G12V and G12C Mutations in the Gene KRAS Are Associated with a Poorer Prognosis in Primary Colorectal Cancer. *Int. J. Colorectal Dis.* 34 (8), 1491–1496. doi:10.1007/s00384-019-03344-9

Hong, D. S., Fakih, M. G., Strickler, J. H., Desai, J., Durm, G. A., Shapiro, G. I., et al. (2020). KRASG12C Inhibition with Sotorasib in Advanced Solid Tumors. *N. Engl. J. Med.* 383 (13), 1207–1217. doi:10.1056/NEJMoa1917239

Hung, K. E., Maricevich, M. A., Richard, L. G., Chen, W. Y., Richardson, M. P., Kunin, A., et al. (2010). Development of a Mouse Model for Sporadic and Metastatic Colon Tumors and its Use in Assessing Drug Treatment. *Proc. Natl. Acad. Sci. U. S. A.* 107 (4), 1565–1570. doi:10.1073/pnas.0908682107

Iacopetta, B., Russo, A., Bazan, V., Dardanoni, G., Gebbia, N., Soussi, T., et al. (2006). Functional Categories of TP53 Mutation in Colorectal Cancer: Results of an International Collaborative Study. *Ann. Oncol.* 17 (5), 842–847. doi:10.1093/annonc/mdl035

Jiang, P., Gu, S., Pan, D., Fu, J., Sahu, A., Hu, X., et al. (2018). Signatures of T Cell Dysfunction and Exclusion Predict Cancer Immunotherapy Response. *Nat. Med.* 24 (10), 1550–1558. doi:10.1038/s41591-018-0136-1

Karapetis, C. S., Khambata-Ford, S., Jonker, D. J., O'Callaghan, C. J., Tu, D., Tebbutt, N. C., et al. (2008). K-ras Mutations and Benefit from Cetuximab in Advanced Colorectal Cancer. *N. Engl. J. Med.* 359 (17), 1757–1765. doi:10.1056/NEJMoa0804385

Kim, D., Xue, J. Y., and Lito, P. (2020). Targeting KRAS(G12C): From Inhibitory Mechanism to Modulation of Antitumor Effects in Patients. *Cell.* 183 (4), 850–859. doi:10.1016/j.cell.2020.09.044

Li, X. L., Zhou, J., Chen, Z. R., and Chng, W. J. (2015). P53 Mutations in Colorectal Cancer - Molecular Pathogenesis and Pharmacological Reactivation. *World J. Gastroenterol.* 21 (1), 84–93. doi:10.3748/wjg.v21.i1.84

Maddocks, O. D. K., Athineos, D., Cheung, E. C., Lee, P., Zhang, T., van den Broek, N. J. F., et al. (2017). Modulating the Therapeutic Response of Tumours to Dietary Serine and glycine Starvation. *Nature* 544 (7650), 372–376. doi:10.1038/nature22056

Markman, B., Javier Ramos, F., Capdevila, J., and Tabernero, J. (2010). EGFR and KRAS in Colorectal Cancer. *Adv. Clin. Chem.* 51, 71–119. doi:10.1016/s0065-2423(10)51004-7

McCarthy, D. J., Chen, Y., and Smyth, G. K. (2012). Differential Expression Analysis of Multifactor RNA-Seq Experiments with Respect to Biological Variation. *Nucleic Acids Res.* 40 (10), 4288–4297. doi:10.1093/nar/gks042

Miller, K. D., Mariotto, A. B., Rowland, J. H., Yabroff, K. R., Alfano, C. M., Jemal, A., et al. (2019). Cancer Treatment and Survivorship Statistics, 2019. *CA Cancer J. Clin.* 69 (1), 363–385. doi:10.3322/caac.2155110.3322/caac.21565

National Health Commission of the People's Republic of China (2020). Chinese Protocol of Diagnosis and Treatment of Colorectal Cancer (2020 Edition). *Zhonghua Wai Ke Za Zhi* 58(8), 561–585. doi:10.3760/cma.j.cn112139-20200518-00390

Ozawa, H., Matsunaga, T., Kamiya, K., Tokumaru, Y., Fujii, M., Tomita, T., et al. (2007). Decreased Expression of Connexin-30 and Aberrant Expression of Connexin-26 in Human Head and Neck Cancer. *Anticancer Res.* 27 (4b), 2189–2195.

Papke, B., and Der, C. J. (2017). Drugging RAS: Know the Enemy. *Science* 355 (6330), 1158–1163. doi:10.1126/science.aam7622

Pietrocola, F., Bravo-San Pedro, J. M., Galluzzi, L., and Kroemer, G. (2017). Autophagy in Natural and Therapy-Driven Anticancer Immunosurveillance. *Autophagy* 13 (12), 2163–2170. doi:10.1080/15548627.2017.1310356

Rudzińska, M., Daglioglu, C., Savvateeva, L. V., Kaci, F. N., Antoine, R., and Zamyatnin Jr, A. A., Jr. (2021). Current Status and Perspectives of Protease Inhibitors and Their Combination with Nanosized Drug Delivery Systems for Targeted Cancer Therapy. *Dddt* 15, 9–20. doi:10.2147/dddt.S285852

Russo, A., Bazan, V., Iacopetta, B., Kerr, D., Soussi, T., and Gebbia, N. (2005). The TP53 Colorectal Cancer International Collaborative Study on the Prognostic and Predictive Significance of P53 Mutation: Influence of Tumor Site, Type of Mutation, and Adjuvant Treatment. *J. Clin. Oncol.* 23 (30), 7518–7528. doi:10.1200/jco.2005.00.471

Schrock, A. B., Ouyang, C., Sandhu, J., Sokol, E., Jin, D., Ross, J. S., et al. (2019). Tumor Mutational Burden Is Predictive of Response to Immune Checkpoint Inhibitors in MSI-High Metastatic Colorectal Cancer. *Ann. Oncol.* 30 (7), 1096–1103. doi:10.1093/annonc/mdz134

Schwitalla, S., Fingerle, A. A., Cammareri, P., Nebelsiek, T., Göktuna, S. I., Ziegler, P. K., et al. (2013). Intestinal Tumorigenesis Initiated by Dedifferentiation and Acquisition of Stem-cell-like Properties. *Cell.* 152 (1-2), 25–38. doi:10.1016/j.cell.2012.12.012

Sentani, K., Oue, N., Sakamoto, N., Anami, K., Naito, Y., Aoyagi, K., et al. (2010). Upregulation of Connexin 30 in Intestinal Phenotype Gastric Cancer and its Reduction during Tumor Progression. *Pathobiology* 77 (5), 241–248. doi:10.1159/000314966

Thein, K. Z., Biter, A. B., and Hong, D. S. (2021). Therapeutics Targeting Mutant KRAS. *Annu. Rev. Med.* 72, 349–364. doi:10.1146/annurev-med-080819-033145

Vogelstein, B., Fearon, E. R., Hamilton, S. R., Kern, S. E., Preisinger, A. C., Leppert, M., et al. (1988). Genetic Alterations during Colorectal-Tumor Development. *N. Engl. J. Med.* 319 (9), 525–532. doi:10.1056/NEJM198809013190901

Wiesweg, M., Kasper, S., Worm, K., Herold, T., Reis, H., Sara, L., et al. (2019). Impact of RAS Mutation Subtype on Clinical Outcome-A Cross-Entity Comparison of Patients with Advanced Non-small Cell Lung Cancer and Colorectal Cancer. *Oncogene* 38 (16), 2953–2966. doi:10.1038/s41388-018-0634-0

Yu, G., Wang, L. G., Han, Y., and He, Q. Y. (2012). clusterProfiler: an R Package for Comparing Biological Themes Among Gene Clusters. *Omics* 16 (5), 284–287. doi:10.1089/omi.2011.0118

Zhu, G., Pei, L., Xia, H., Tang, Q., and Bi, F. (2021). Role of Oncogenic KRAS in the Prognosis, Diagnosis and Treatment of Colorectal Cancer. *Mol. Cancer* 20 (1), 143. doi:10.1186/s12943-021-01441-4

Conflict of Interest: The authors declare that the research was conducted in the absence of any commercial or financial relationships that could be construed as a potential conflict of interest.

Publisher's Note: All claims expressed in this article are solely those of the authors and do not necessarily represent those of their affiliated organizations, or those of the publisher, the editors and the reviewers. Any product that may be evaluated in this article, or claim that may be made by its manufacturer, is not guaranteed or endorsed by the publisher.

frontiers | Frontiers in Cell and Developmental Biology

ORIGINAL RESEARCH
published: 15 June 2022
doi: 10.3389/fcell.2022.913307

N6-Methyladenosine Modification Patterns and Tumor Microenvironment Immune Characteristics Associated With Clinical Prognosis Analysis in Stomach Adenocarcinoma

Zhang Meijing[1†], *Luo Tianhang*[2†] *and Yang Biao*[2*]

[1]Department of Oncology, Changhai Hospital, Second Military Medical University, Shanghai, China, [2]Department of General Surgery, Changhai Hospital, Second Military Medical University, Shanghai, China

OPEN ACCESS

Edited by:
Haitao Wang,
National Cancer Institute (NIH),
United States

Reviewed by:
Lin Zhang,
Clinical Center (NIH), United States
Tiantian Zhang,
Cornell University, United States
Kui Zhang,
The University of Chicago,
United States

***Correspondence:**
Yang Biao
191817524@qq.com

[†]These authors have contributed equally to this work

Specialty section:
This article was submitted to Cancer Cell Biology, a section of the journal Frontiers in Cell and Developmental Biology

Received: 05 April 2022
Accepted: 17 May 2022
Published: 15 June 2022

Citation:
Meijing Z, Tianhang L and Biao Y (2022) N6-Methyladenosine Modification Patterns and Tumor Microenvironment Immune Characteristics Associated With Clinical Prognosis Analysis in Stomach Adenocarcinoma. Front. Cell Dev. Biol. 10:913307. doi: 10.3389/fcell.2022.913307

Background: N6-methyladenosine (m6A) modification is a part of epigenetic research that has gained increasing attention in recent years. m6A modification is widely involved in many biological behaviors of intracellular RNA by regulating mRNA, thus affecting disease progression and tumor occurrence. However, the effects of m6A modification on immune cell infiltration of the tumor microenvironment (TME) are uncertain in stomach adenocarcinoma (STAD).

Methods: The Cancer Genome Map (TCGA) database was used to download transcriptome data, clinicopathological data, and survival data for m6A-regulated genes in 433 STAD tissues that meet the requirements of this study. GSE84437 data were obtained from the Gene Expression Omnibus (GEO) database. The correlation between 23 m6A regulated genes was analyzed using R software. Sample clustering analysis was carried out on the genes of the m6A regulatory factor, and survival analysis and differentiation comparison were made for patients in clustering grouping. Then, the Gene Set Enrichment Analysis (GSEA), the single-sample GSEA (ssGSEA), and other methods were conducted to assess the correlation among m6A modification patterns, TME cell infiltration characteristics, and immune infiltration markers. The m6A modification pattern of individual tumors was quantitatively evaluated using the m6A score scheme of the principal component analysis (PCA).

Results: From the TCGA database, 94/433 (21.71%) samples were somatic cell mutations, and ZC3H13 mutations are the most common. Based on the consensus, matrix k-3 is an optimal clustering stability value to identify three different clusters. Three types of m6A methylation modification patterns were significantly different in immune infiltration. Thus, 1028 differentially expressed genes (DEGs) were identified. The survival analysis of the m6A score found that patients in the high m6A score group had a better prognosis than those in the low m6A score group. Further analysis of the survival curve combining tumor mutation burden (TMB) and m6A scores revealed that patients had a significantly lower prognosis in the low tumor mutant group and the low m6A score group ($p = 0.003$). The results

showed that PD-L1 was significantly higher in the high m6A score group than in the low score group (p < 2.22e-16). The high-frequency microsatellite instability (MSI-H) subtype score was significantly different from the other two groups.

Conclusions: This study systematically evaluated the modification patterns of 23 m6A regulatory factors in STAD. The m6A modification pattern may be a critical factor leading to inhibitory changes and heterogeneity in TME. This elucidated the TME infiltration characteristics in patients with STAD through the evaluation of the m6A modification pattern.

Keywords: stomach adenocarcinoma, N6-methyladenosine, tumor microenvironment, immunotherapy, mutation burden, microsatellites instability

KEY POINTS

- This study systematically evaluated the modification patterns of 23 m6A regulatory factors in STAD.
- This study revealed that m6A modification is significantly associated with TME diversity and complexity.
- The m6A score has the potential in predicting the clinical response of PD-L1 blockade.
- Quantitative evaluation of the m6A modification patterns of individual tumors will strengthen our understanding of TME characteristics and promote effective immunotherapy strategies.

INTRODUCTION

Traditional epigenetics research focuses on DNA methylation, histone modification, non-coding RNA, and chromatin remodeling (Boccaletto et al., 2018). Methylation of N^6 adenosine (m6A) is the primary methylation in eukaryotic mRNA and long non-coding RNA and is regulated by methyltransferases (writers), demethylases (erasers), and binding proteins (readers) (Roundtree et al., 2017; Shen et al., 2022). Substantial m6A methylation is detected in the "RRACH" base sequence through high-throughput sequencing and bioinformatics analysis (Meyer et al., 2012; Jenjaroenpun et al., 2021). It is also rich in areas, such as stop codon and 3′-untranslated region (UTR) (Dominissini et al., 2012). m6A methylation regulates the translation of mRNA, nuclear transport, and degradation, thereby determining the entire life process of mRNA. Other RNAs in the cell, including transport RNA (tRNA), ribosome RNA (rRNA), and long non-coding RNA (lncRNA), also have a large amount of m6A methylation. Moreover, studies have shown that m6A methylation is involved in the complex and delicate regulation of critical functional genes, especially in the development of tumors. Therefore, studying the role of m6A modification is crucial to clarify the tumor mechanism and clinical treatment.

In recent years, immunotherapy usage has revolutionized the regulation of the immune system to exert the anti-tumor effect for the treatment of malignant tumors. However, immunotherapy offers lasting survival benefits in only 20%–30% of patients in clinical practice (Tabernero et al., 2018). Most patients face immunotherapy resistance. Therefore, the major issue of immunotherapy is the lack of accurate prediction of the dominant population and the systematic research and response of drug resistance mechanisms, resulting in excessive or insufficient immunotherapy. Recent studies on the interaction between tumors and tumor microenvironments (TMEs) have provided novel opportunities for immunotherapy. Tumor cells induce immune escape by inhibiting the response and function of infiltrative immune cells by suppressing signaling pathways, such as the programmed cell death protein 1/programmed cell death protein-ligand 1 (PD-1/PD-L1) (Chen and Flies, 2013; Beatty and Gladney, 2015; Xiong et al., 2022). In addition, the metabolic reconstruction of tumor cells consumes excess sugar, and amino acids competitively deprive T cells of the required nutrients, promoting the deactivation and immunosuppression of T cells (Li and Zhang, 2016). On the other hand, the recruitment and amplification of immunosuppressive cells in TME, such as T-regulatory lymphocytes (Tregs), tumor-associated macrophages (TAMs), and myeloid-derived suppressor cell (MDSCs) is also one of the primary mechanisms that induce immunosuppressive TME (Davis et al., 2016; Yang et al., 2021). The immune status of TME is a critical factor affecting tumor progression. TME presents a differentiated degree of immune activation under the action of specific immune cells or molecules. The targeted TME immunotherapy involves the intervention of non-tumor cells and components and can transform the immune response from tumor promotion to tumor suppression (Zou, 2018). Similarly, the combination of anti-tumor and multi-target immunotherapy drugs can avoid adaptive resistance and improve tumor prognosis and survival significantly (Lambrechts et al., 2018; Lee et al., 2020).

Stomach adenocarcinoma (STAD) is one of the most common malignant tumors worldwide. Statistically, the morbidity of malignant tumors ranks fourth, and the mortality rate is third (Chen et al., 2016). STAD is a multi-step, multi-factor disease similar to other malignant tumors. Some studies demonstrated that m6A is closely related to the immune status of TME. The interaction among various mechanisms formed a complex network that promoted the development of tumors (Liu et al., 2022). Reportedly, METTL3 is high in STAD patients and increases with the progression of tumor stages and grades

(Wang et al., 2020; Yang et al., 2020). Strikingly, METTL3 knockout reduces the expression of EMT-related proteins, thereby inhibiting STAD cell proliferation and migration. Some studies have reported that high expression of METTL3 is significantly associated with the clinicopathological characteristics and poor survival in STAD patients and that knocking out METTL3 can inhibit cell proliferation, migration, and invasion. Further RNA-seq and m6A-seq analysis showed that METTL3 promotes STAD development via m6A modification and regulates key proteins on MYC target genes such as *MCM5* and *MCM6*. In addition, it has also been shown that EIF3B promotes the migration and invasion of tumor cells by regulating EMT and STAT3 signaling pathways (Wang et al., 2019). However, the tumor immunosuppressive microenvironment is a complex network regulated by multiple immunosuppressive signals that are constantly changing dynamically; hence, targeting a single immunosuppressive signal alone does not achieve long-term efficacy. Therefore, a multi-targeted immunotherapy strategy is essential to understand the m6A modification combined with TME to screen immunotherapy-sensitive markers. Also, exploring new immunotherapy targets in the future is imperative.

In this study, we analyzed the differences in the expression of m6A using STAD sample transcriptome data and related mutation data from The Cancer Genome Atlas (TCGA) and Gene Expression Omnibus (GEO) databases. Then, we evaluated the correlation between m6A modification patterns and TME cell-infiltrating characteristics. The TME characteristics of the three m6A modification modes and the three immune phenotypes were consistent. We also established a scoring system for m6A modification patterns to quantify the patients individually. The correlation between survival time, clinical response to immunotherapy, tumor mutation burden (TMB), and microsatellite instability (MSI) was assessed based on the quantification of m6A modification patterns. These results confirmed that m6A methylation plays a critical role in the development of STAD through TME, creating opportunities to predict the prognosis of clinical STAD patients and explore new targeted treatments.

METHODS

Data Collection

TCGA and GEO downloaded RNA-seq transcription group and clinical data from 433 STAD patients. This sample selected GSE84437 cohorts with complete clinical information and follow-up data for final inclusion in the study (Yoon et al., 2020). The Fragments Per Kilobase of exon model per Million mapped fragments (FPKM) format data were downloaded using the "fpkm" function in R to convert them to the transcripts per kilobase million (TPM) for the next analysis (Zhao et al., 2020). Then, we performed copy number variation (CNV) data analysis of qualified TCGA-STAD data. The CNV data were downloaded from the UCSC Xena database (http://xena.ucsc.edu/). Data analysis and collation were carried out using R software (version 3.6.1).

m6A RNA Methylation Regulator for Stomach Adenocarcinoma in The Cancer Genome Map

We retrieved the literature related to m6A methylation modification, and a total of 23 acknowledged m6A regulator genes were curated and analyzed to identify distinct m6A methylation modification patterns (Chen et al., 2019; Zaccara et al., 2019; Liu et al., 2022; Mobet et al., 2022). Based on the mRNA expression data available in TCGA, we analyzed 23 m6A RNA methylation regulators (METTL3, METTL14, METTL16, WTAP, VIRMA, ZC3H13, RBM15) RBM15B, FTO, ALKBH5, YTHDC1, YTHDC2, YTHDF1, YTHDF2, YTHDF3, HNRNPC, FMR1, LRPPRC, IGF2BP1, IGF2BP2, IGF2BP3, HNRNPA2B1, and RBMX) data. The expression and the correlation of mRNA of 23 m6A methylation regulators were analyzed. The correlation between PD-1, PD-L1, and m6A RNA methylation regulatory factors was established, and the corresponding heat maps were drawn. ConsensusClustPlus package was used for consistency clustering. The optimal clustering (k-value) was evaluated based on the clustering score of the cumulative distribution function (CDF) curve. The R software ConsensuClusterPlus package was used to draw a heat map and verify the differences using Wilcox rank test through limma packets.

Unsupervised Consensus Clustering of 23 m6A Regulators and Functional Analysis

The m6A differential genes were analyzed using GSEA. $p < 0.05$ and the false discovery rate (FDR) < 0.05 indicated a significantly enriched gene set. GSVA package was used for differential analysis of m6A modification pattern activity (Foroutan et al., 2018). ConsensusClustPlus package was utilized for consistency clustering. We also used the clusterProfiler package for Gene Ontology (GO) and Kyoto Encyclopedia of Genes and Genomes (KEGG) pathway enrichment analyses.

Immune Infiltrating Cell Analysis

TME immune infiltration cells used CIBERSORT (a bioinformatics algorithm) to assess the correlation between m6A expression and the abundance of tumor-infiltrating immune cells (TIIC), including CD4-T cells, CD8-T cells, and macrophages. Immune infiltration cells in TME for STAD were analyzed using ssGSEA (Hanzelmann et al., 2013). The differences between the m6A modification patterns and immune cells were analyzed using differential analysis of immune cells.

Differentially Expressed Genes Among the m6A Phenotypes

We used the R limma package to screen for m6A Differentially Expressed Genes (DEGs) between different m6A phenotypes. The adjusted p-value < 0.05 was set The significance filtering criteria of DEG. GO and KEGG analyses of the differential genes were carried out using the R clusterProfiler and enrichplot packages. The results are shown in bar and bubble charts.

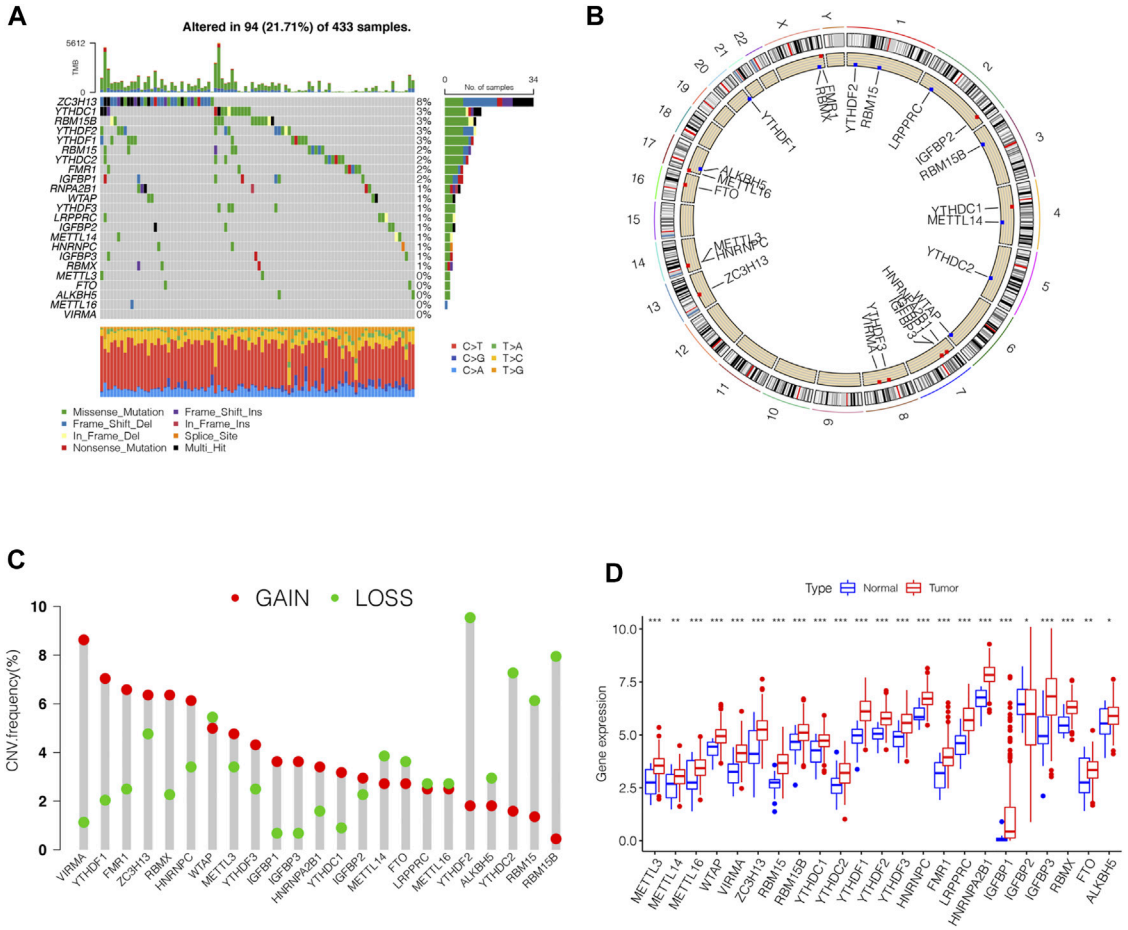

FIGURE 1 | Genetic variation profile of m6A regulators in STAD. **(A)** Mutation frequency of the m6A regulators of stomach adenocarcinoma patients in the TCGA-STAD cohort. **(B)** Location of CNV changes of 23 m6A regulators on the chromosome. **(C)** A histogram plotting the CNV mutation frequency of each gene obtained by statistical analysis of the copy number of m6A. The abscissa was the m6A-related gene, and the ordinate was the mutation frequency. **(D)** The box plot of m6A differential expression analysis in the tumor and normal samples. The asterisks represented the statistical p value ($^{***}p < 0.0001$, $^{**}p < 0.01$, $^{*}p < 0.05$).

Prognostic Signature of m6A-Related Genes

The differences in genes in different m6A clusters in STAD patients were quantified using the principal component analysis (PCA). First, we extracted the overlapping genes from DEGs. Then, consensus clustering algorithms were employed to test the number and stability of gene clusters. Finally, PCA was used to analyze the different genes related to prognosis. Next, we established m6A-related features based on the results of the analysis. In addition, PCA maximized the integrity of the data. This method was used to assess the m6A gene characteristics of STAD patients, termed the m6A score. The m6A score was calculated using the following formula (Sotiriou et al., 2006; Zeng et al., 2019): $\text{m6Ascore} = \sum(\text{PC1}_i + \text{PC2}_i)$, where i represents the expression of m6A-related genes. Patients were divided into high- and low-score groups based on the ranking statistics. Subsequently, we used immunophenoscore (IPS) to detect the characteristics of the tumor immune landscape (Charoentong et al., 2017). IPS was used to detect the efficacy of anti-CTLA-4 and anti-PD-1 treatment regimens and calculated using four types of immune-related genes: MHC molecules (MHC), immunomodulators (CP), and effector cells (EC), and suppressor cells (SC).

Statistical Analysis

Statistical analysis was carried out using R 3.6.1 software. The comparison of the expression levels of core genes between different genotype groups did not show normal distribution, as shown in the median and quartile number of spacings (P25, P75). Wilcoxon testing was used for group comparisons. A single-factor Cox analysis of 23 m6A methylation regulators used the survival package and screening condition $p < 0.05$ to determine the correlation between RNA m6A methylation regulation in STAD tumor tissue and prognosis related to mRNA expression. The log-rank Kaplan–Meier survival curve analyzed the progenitive correlation. Spearman's test was used in the

analysis of the correlation between the core genes and the infiltration degree of different immune cells. $0.1 \leq |r| \leq 1.0$ was defined as relevant. $p < 0.05$ indicated statistically significant differences.

RESULTS

Genetic Variation Profile of m6A Regulators in Stomach Adenocarcinoma

In this study, we identified the role of 23 m6A regulation genes in STAD, including 13 readers, 8 writers, and 2 erasers. After downloading the relevant mutation data from the TCGA database, we identified somatic cell mutations in 94/433 (21.71%) samples; among these, ZC3H13 mutations were the most common (**Figure 1A**). The position of the m6A regulator CNV mutation on the chromosome is observed on the Circos plot (**Figure 1B**). Further analysis of CNV mutations revealed that VIRMA, YTHDF1, and FMR1 showed extensive CNV amplification, while YTHDF2, RBM15B, and YTHDC2 showed widespread CNV deficiency (**Figure 1C**). Next, we investigated whether changes in CNV altered the expression of regulatory m6A in STAD and found that almost all m6A regulators were expressed significantly higher in STAD tissue than in normal tissue, except IGFBP2 (**Figure 1D**). These results indicated significant genetic variation characteristics of m6A regulatory in STAD, suggesting that the complexity of m6A modification and tumor heterogeneity play a fundamental role in STAD development.

Identification of m6A Methylation Modification Patterns in Stomach Adenocarcinoma

GSE84437 dataset with complete survival and clinical information in the GEO database and the TCGA-STAD (n = 443) data were merged for the analysis of the correlation of tumor mutation load. The results showed that TTN and TP53 had the highest TMB. The top 10 genes of the mutant burden are shown in **Supplementary Table S1**. According to the most common mutation of ZC3H13, the m6A regulator genes were divided into ZC3H13 wild-type and ZC3H13 mutation type. The results of the TMB and expression correlation analysis of the m6A regulator genes are shown in **Supplementary Figure S1**. The prognostic correlation analysis of the m6A regulatory genes by Cox analysis method identified a correlation between *RBM15*, *IGFBP3*, *HNRNRPPC*, *HNRNPA2B1*, *IGFBP1*, *IGFBP2*, and *LRPPRC* and prognosis (**Supplementary Table S2**). Next, we conducted a survival analysis of the m6A regulatory genes. Each m6A regulator gene was assigned to high- or a low-expression group according to the optimal cutoff value in the stomach adenocarcinoma tissue. The results showed that the groups with low expression of *FTO*, *IGFBP3*, *IGFBP2*, *IGFBP1*, and *ZC3H13* had better survival rates than those patients in the high-expression group, while those with high expression of *RBMX*, *HNRNPA2B1*, *LRPPRC*, *FMR1*, *HNRNPC*, *YTHDF2*, *YTHDC2*, *RBM15B*, *RBM15*, *WTAP*, and *METTL3* had better survival rates than patients in the low-expression group (**Supplementary Figure S2**). The m6A prognostic network illustrated that the expression of most genes are positively correlated among writers, readers, and erasers, except that *YTHDF3*, *IGFBP2*, *LRPPRC*, and *IGFBP3* were negatively correlated among writers, readers, and erasers (**Figure 2A**). The non-negative matrix factorization (NMF) clustering has a consensus with respect to the expression of m6A regulators. Based on the consensus, matrix k-3 was an optimal clustering stability value; finally, three different clusters were identified (**Supplementary Figure S3**): m6Acluster-A (n = 317), m6Acluster-B (n = 204), and m6Acluster-C (n = 283). **Figure 2B** shows that m6Acluster-C has a better survival advantage, while m6Acluster-A has a poor prognosis (p = 0.005) among the three clusters.

Distinct Immune Landscapes in m6A Modification Patterns

By using GSVA, m6Acluster-A was significantly enriched in environmental information processing and signaling interaction; m6Acluster-B was significantly enriched in the immune system and biosynthesis of other secondary metabolites; m6Acluster-C was significantly enriched in environmental information processing and signal transduction (**Figures 3A–C**). Next, we used ssGSEA, which showed a rich innate immune cell immersion in m6Acluster-A. **Figure 3D** shows significant differences in the penetration characteristics of TME cells in the three clusters. The PCA results showed significant differences between the transcriptomes of the three m6A modification patterns (**Figure 3E**). The typed heat map of m6A revealed that the m6A-related genes were highly expressed in cluster-B and lowly in clusters A and C (**Figure 3F**).

m6A-Related Genes' Functional Annotation

Although we divided STAD patients into three gene clusters based on the consensus clustering algorithm, the correlation between the m6A-related genes was not clarified. Hence, we analyzed the differences between m6A gene clusters (**Figure 4A**) and identified 1028 DEGs (**Supplementary Table S2**). The GO enrichment bar and bubble charts showed that the differential genes occurred in almost all cellular functions. In biological process (BP), the main enrichment was in RNA localization; in cellular component (CC), it was in the nuclear pore; in molecular function (MF), the main enrichment was in the ATPase activity (**Figures 4B,C**). The KEGG enrichment bar and bubble charts exhibited the involvement of the differential genes in the signaling pathway of nucleocytoplasmic transport (**Figures 4D,E**).

Identification of m6A-Related Genes' Phenotypes and m6A Scores

To further analyze the DEGs associated with m6A phenotypes, we used a single-factor Cox method to identify the differential genes associated with STAD prognosis. Similar to the m6A modification pattern, we classified the m6A genomic

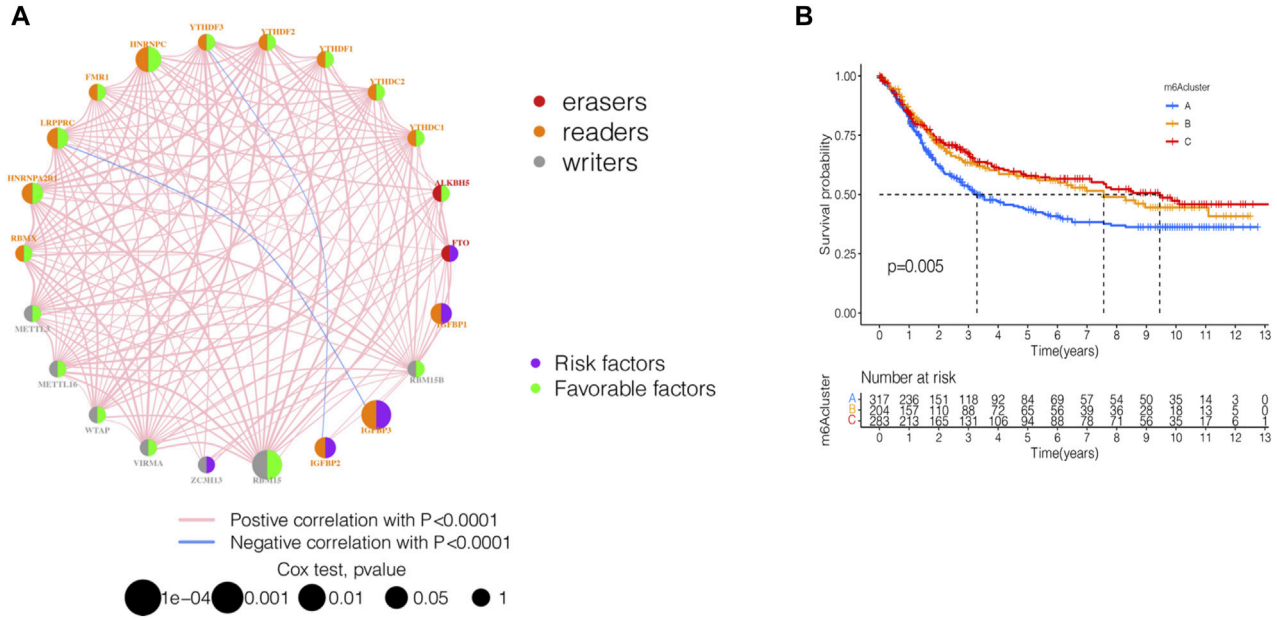

FIGURE 2 | Identification of m6A methylation modification patterns in STAD. **(A)** Interaction of 23 m6A regulators and their prognostic significance in STAD. The circle size represented the effect of each regulator on the prognosis, and the range of values calculated by Cox test was $p < 0.001$, $p < 0.01$, $p < 0.05$, and $p < 1$, respectively. **(B)** Kaplan–Meier curves of m6A modification patterns. Kaplan-Meier curves with Log-rank p-value 0.005 showed a significant survival difference among three m6A modification patterns.

phenotype into three categories: genecluster-A (n = 347), genecluster-B (n = 237), and genecluster-C (n = 220) (**Supplementary Figure S4**). The genecluster heat map containing clinical information showed a high expression of genecluster-C and low expression of genecluster-B (**Figure 5A**). The survival analysis of the three groups revealed that genecluster-B had the worst prognosis (p < 0.001) (**Figure 5B**). The difference analysis of genotype m6A showed significant differences among the three genotypes (**Figure 5C**). Considering the complexity of the quantification of m6A modification, we illustrated the workflow of m6A score construction with the Sankey diagram (**Figure 5D**). Next, we then rated m6A based on m6A correlation characteristics and divided it into the high m6Ascore group and the low m6Ascore group. The results of immunocyte difference analysis using m6A scores showed a significant positive correlation between m6A scores and activated CD4.T.cellna (**Figure 5E**). The results of the m6A score difference analysis showed that the scores were expressed in both the m6A cluster and the genecluster. The m6Acluster-B had the highest m6A score among the m6Aclusters (**Figure 5F**), while the genecluster-C had the highest score among geneclusters (**Figure 5G**).

m6A Scores' Clinical Prognosis Analysis and Somatic Tumor Mutations

The survival analysis of the m6A score found that patients in the high m6A score group had a better prognosis than those in the low score group (**Figure 6A**). The analysis of the m6A score and TMB revealed a difference between patients in the high m6A score group and those in the low m6A score group; patients in the high m6A score group had high TMB ($p < 0.001$, **Figure 6B**). The correlation analysis showed a significant positive correlation between the m6A score and TMB (R = 0.35, p = 6.8e-12, **Figure 6C**). The survival analysis of TMB found that patients with a high number of mutations had a better survival duration than those with low mutations (p < 0.001, **Figure 6D**). Further analysis of the survival curve combining TMB and m6A scores found that patients had a significantly lower prognosis in the low tumor mutant and the low m6A score group (p = 0.003, **Figure 6E**). The STAD samples of the m6A score groups were analyzed based on the significant mutant gene (SMG). It was found that TTN and TP53 had high somatic mutation rates in both m6A score groups and high somatic mutation rates in the high m6A score groups (**Figures 6F,G**).

Clinical Evaluation of m6A Scores

Next, we analyzed the clinical relevance of the m6A score. As shown in **Figure 7A**, STAD patient deaths occurred in the low m6A score group. The rank test results showed that patients in the high m6A score group had prolonged survival (**Figure 7B**). To further analyze the clinical relevance, we divided the patients into the T1-T2 and the T3-T4 groups. The results of survival analyses of both groups showed that patients in the high m6A score group had a better prognosis than those in the low m6A score group (**Figures 7C,D**). To detect the differences in PD-L1 expression in the m6A score and support-related immunotherapy, we tested the expression of PD-L1 in the m6A score and observed that PD-L1 was significantly higher in the

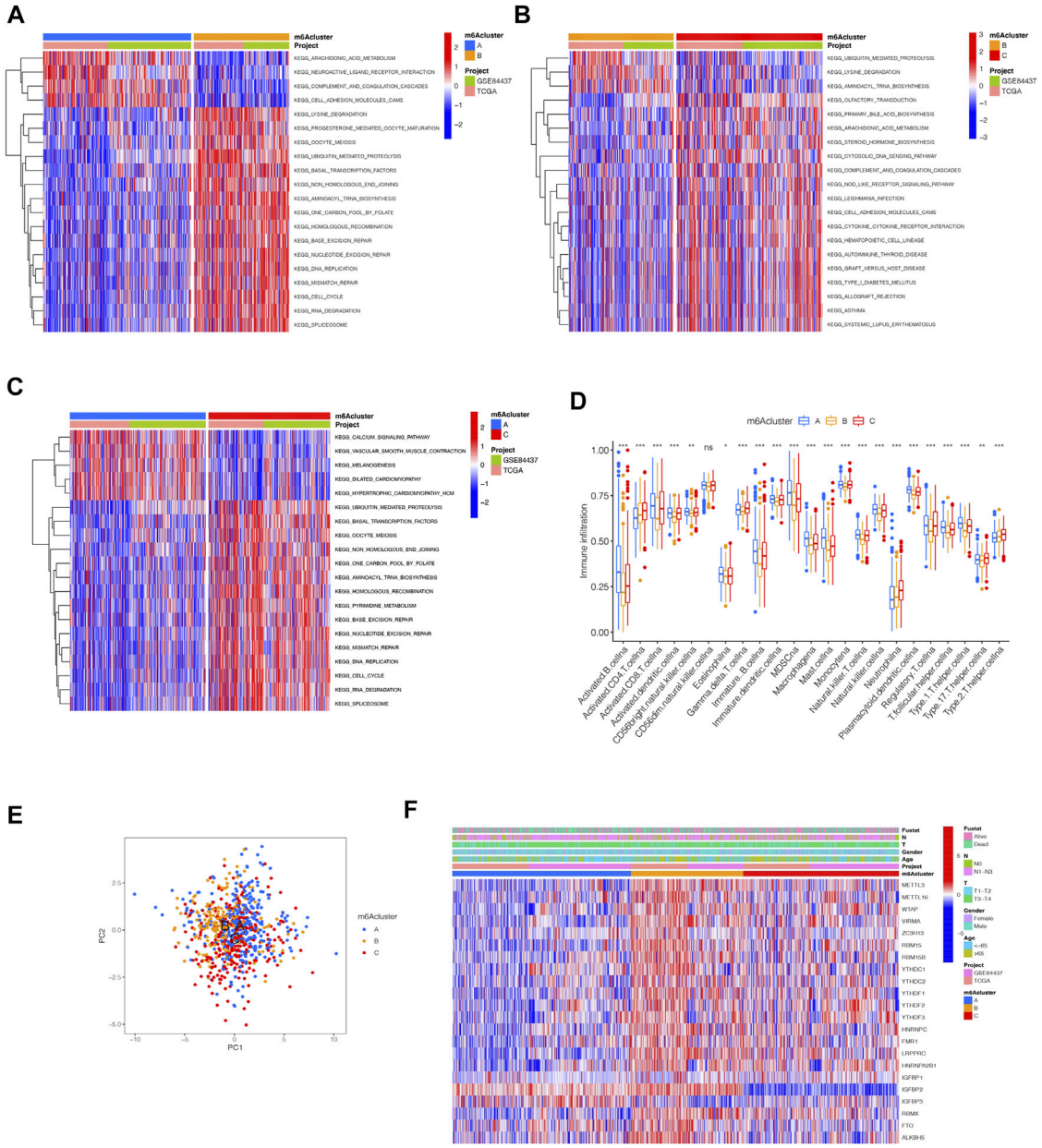

FIGURE 3 | Distinct immune landscapes in m6A modification patterns and the biological characteristics of each pattern. **(A–C)** GSVA analyzed the differences between functional pathways in m6A modification patterns (adjusted *p*-value < 0.05). **(A)**, m6Acluster A vs. m6Acluster B; **(B)**, m6Acluster B vs. m6Acluster C; **(C)**, m6Acluster A vs. m6Acluster C. **(D)** Differential expression analysis of 23 immune cells among three m6A modification patterns. The asterisks represented the statistical *p* value (***$p < 0.0001$, **$p < 0.01$, *$p < 0.05$). **(E)** Scatter plot of PCA for m6A methylation modification pattern. **(F)** Unsupervised clustering of 23 m6A regulators of STAD.

high m6A score group than in the low score group ($p < 2.22e-16$, **Figure 7E**).

Role of the m6A Scores in Immunotherapy

Presently, immunotherapy is becoming a prominent treatment method. Anti-HER-2 antibodies, anti-VEGF antibodies, tyrosine-kinase inhibitor (TKI), and immuno-checkpoint inhibitors (ICIs) have achieved preliminary results in the treatment of STAD. Thus, we tested the expression of IPS and MSI in the m6A score to predict the patient's response to ICI treatment. **Figure 8A** shows that the IPS of the m6A score was not significantly different in CTLA-4/PD-1 immunotherapy in two groups. In the other three groups, the IPS of the low m6A score group increased significantly compared to the high m6A score group (**Figures 8B–D**). To explore the critical clinical significance of chemotherapy response to MSI gastric cancer, we divided MSI into three groups, high-frequency microsatellite instability (MSI-H), low-frequency microsatellite instability (MSI-L), and

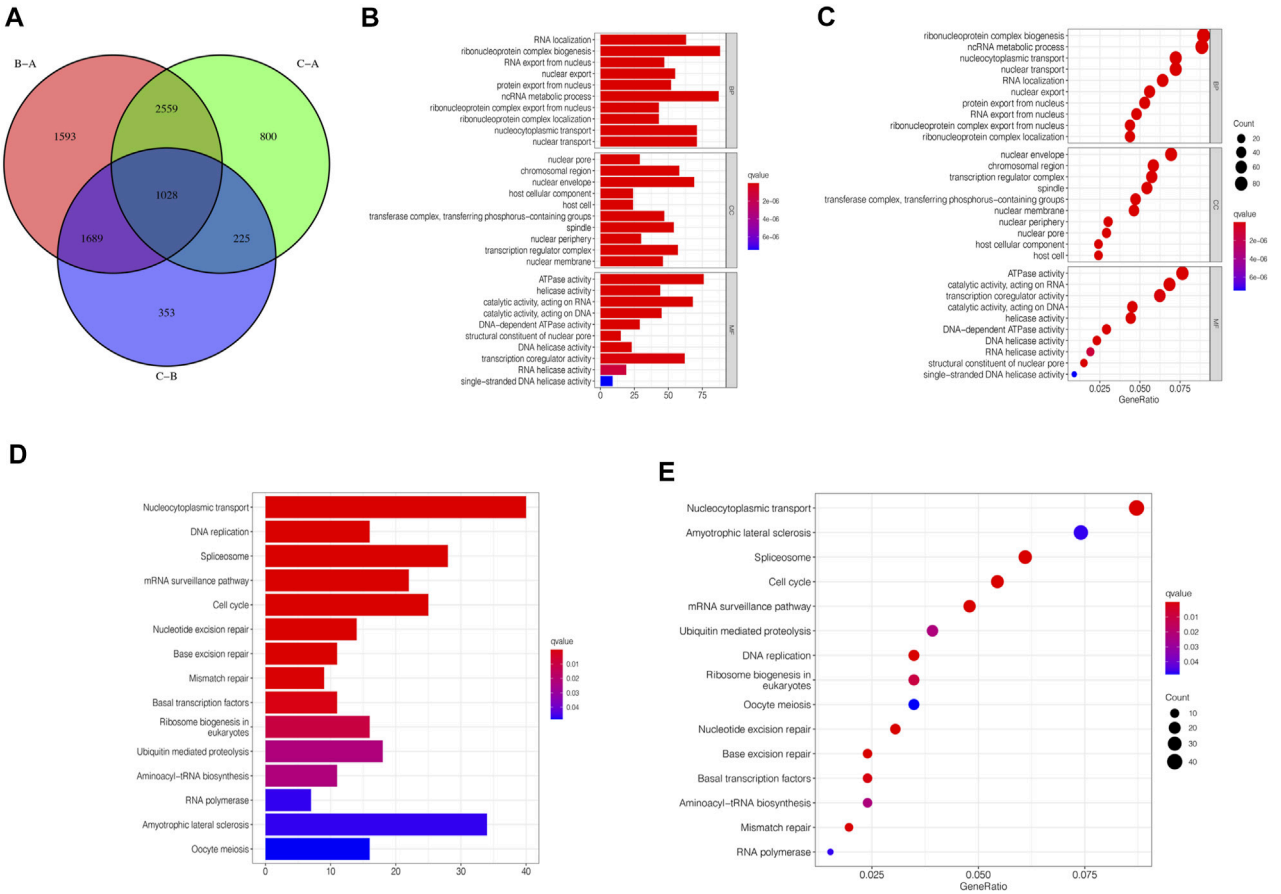

FIGURE 4 | m6A-related genes' functional annotation. **(A)** 1028 m6A-related DEGs between three m6A clusters are shown in the Venn diagram. **(B)** Functional annotation for m6A-related genes using GO enrichment analysis on the bar chart. **(C)** Functional annotation for m6A-related genes using GO enrichment analysis on the bubble chart. **(D)** Functional annotation for m6A-related genes using KEGG enrichment analysis on the bar chart. **(E)** Functional annotation for m6A-related genes using KEGG enrichment analysis on the bubble chart.

microsatellite stability (MSS), according to the MSI diagnostic criteria proposed by the Cancer Institute (NCI). As seen in **Figure 8E**, MSS was high in the high and low m6A score groups. The MSI-H subtype score was significantly different from the other two groups and had a higher score (**Figure 8F**).

DISCUSSION

m6A modification plays an important role in gene regulation and tumor development (Zhao et al., 2017). Overexpression or low expression of m6A-related genes can alter m6A modification in tumors and affect tumor development (Chen et al., 2019; Shulman and Stern-Ginossar, 2020). Thus, understanding the molecular mechanism of m6A modification and identifying the abnormal expression of m6A regulatory factors in clinical biopsy specimens is crucial for the clinical treatment and prognosis of early tumor diagnosis. Although the function of m6A in different cell types and microenvironments is being revealed gradually, the role of multiple m6A regulators in TME cell infiltration and the molecular mechanism of the anti-tumor immune response is yet unclear. Therefore, STAD immunotherapy was explored with respect to the characteristics of TME cell infiltration in different m6A modification patterns.

In the current study, we used 23 m6A methylation-related genes and found three types of m6A methylation modification patterns that differed significantly in immune infiltration. m6Acluster-A had high immune cell number and lymphocyte infiltration, m6Acluster-B was involved in the Wnt, TGF-β, JAK2, and other signaling pathways, and m6Acluster-C was deficient in immune cell infiltration. These three types of m6A methylation modification patterns correspond to immune-inflammatory type (immune inflamed), immuno-exclusion type (immune exclusive), and immune desert type (immune desert), respectively (Chen and Mellman, 2017). A comprehensive analysis of the infiltration characteristics of TME cells in the m6A methylation modification pattern in STAD provided a new strategy for exploring STAD-targeted therapeutic drugs. The immune inflammatory tumors are referred to as tumors with high levels of PD-L1 expression in cancer cells and excess immune cells and tumor-insulated lymphocytes (TILs) in the tumor. In the trials of PD-1/L1

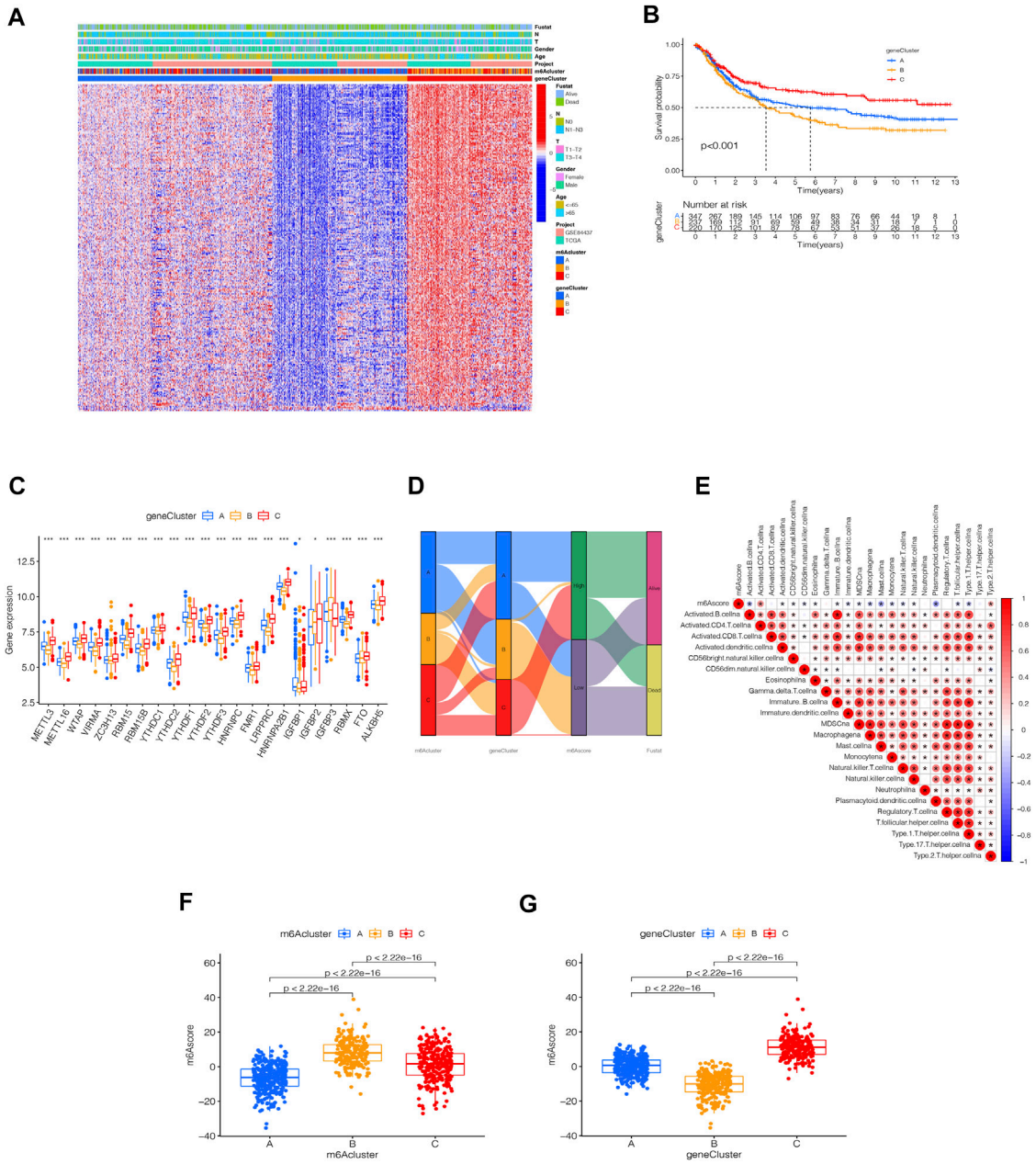

FIGURE 5 | Identification of m6A-related genes' phenotypes and m6A scores. **(A)** Heat map of genetic modification patterns. **(B)** Survival curves of different geneclusters ($p < 0.0001$, Log-rank test). **(C)** Box plot of the differential expression analysis of m6A-related genes among different geneclusters. The asterisks represented the statistical p value ($^{***}p < 0.0001$, $^{**}p < 0.01$, $^{*}p < 0.05$). The one-way ANOVA test was used to test the statistical differences among three gene clusters. **(D)** Sankey diagrams of different genotypes. **(E)** Correlation analysis between the m6A score and immune cells, with red indicating positive correlation and blue indicating a negative correlation. The Kruskal-Wallis test was used to compare the statistical difference between three gene clusters ($p < 0.001$). **(F)** Differential expression analysis of the m6A score in the m6A cluster. **(G)** Difference analysis of m6A score in genecluster ($p < 0.001$, Kruskal-Wallis test)

inhibitor monotherapy of non-small cell lung cancer, such as KEYNOTE-042 and IMpower110, patients with high PD-L1 expression (≥50%) were likely to have prolonged survival (Mok et al., 2019; Herbst et al., 2020). Even in the high expression subgroup, the objective remission rate (ORR) of treatment was only about 40%. Therefore, the inflammatory tumors need to be investigated in-depth to improve the benefits of treatment. For example, previous studies suggested that PD-L1 had a high expression, TILs were fully infiltrated, and immunotherapy was effective. However, subsequent studies hinted that it might be necessary to distinguish between highly expressed PD-L1 in TME and immune or cancer cells. If PD-L1 came from immune cells, there were more TILS in the TME, especially CD8-T cells. On the other hand, TILs were abundant in

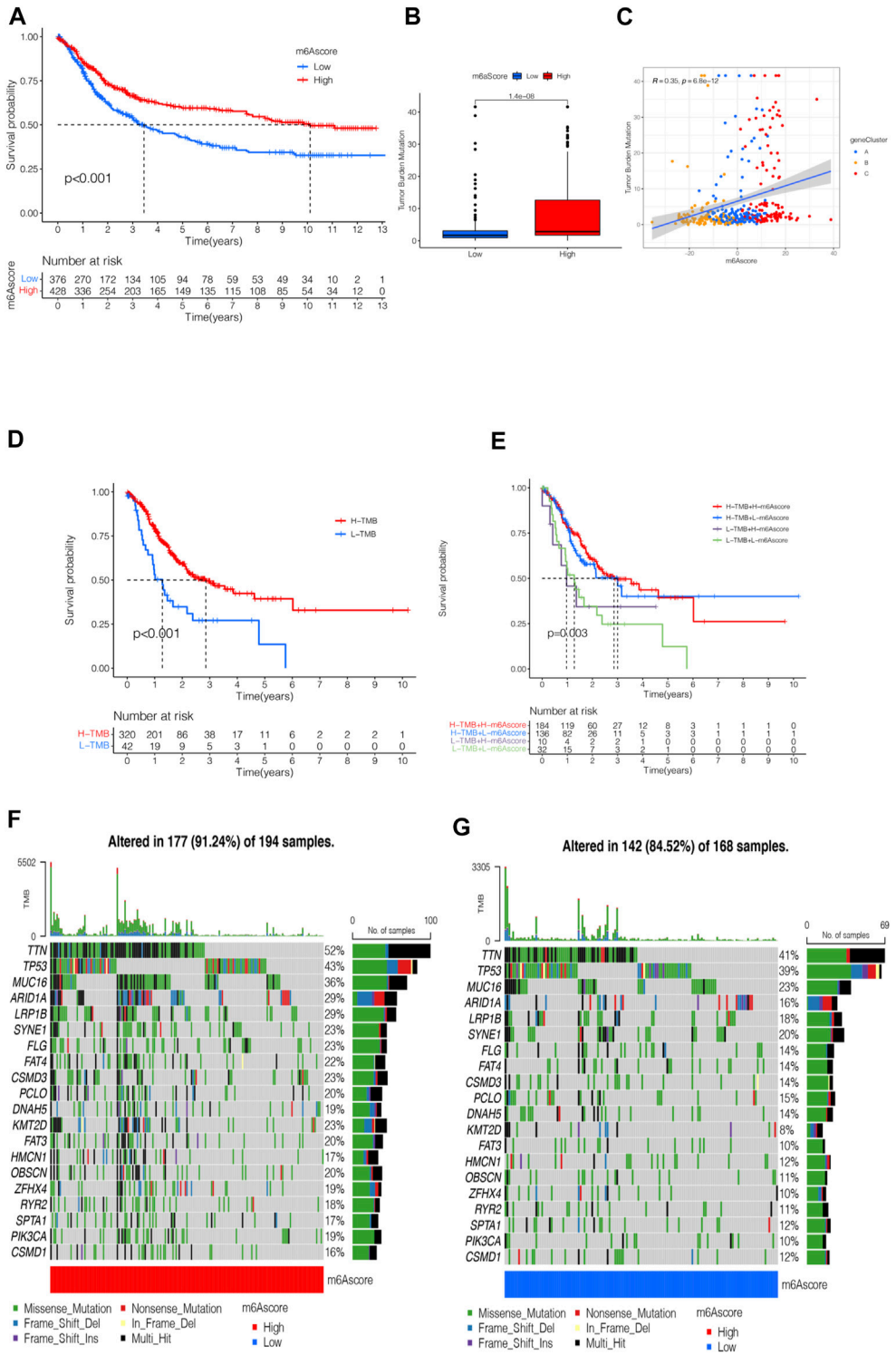

FIGURE 6 | m6A scores' clinical prognosis analysis and somatic tumor mutations. **(A)** Survival analysis of high- and low-m6A score groups using Kaplan-Meier curves ($p < 0.001$, Log-rank test). **(B)** Stratified analysis of the m6A score for STAD patients by tumor mutation burden ($p < 0.001$, Wilcoxon test). **(C)** A scatter plot describing the positive correlation between the m6A score and TMB. **(D)** Survival analysis of TMB ($p < 0.001$, Log-rank test). **(E)** Survival analysis of TMB combined with m6A score ($p = 0.003$, Log-rank test). **(F)** Waterfall chart of the high-m6A score group. **(G)** Waterfall chart of the low-m6A score group.

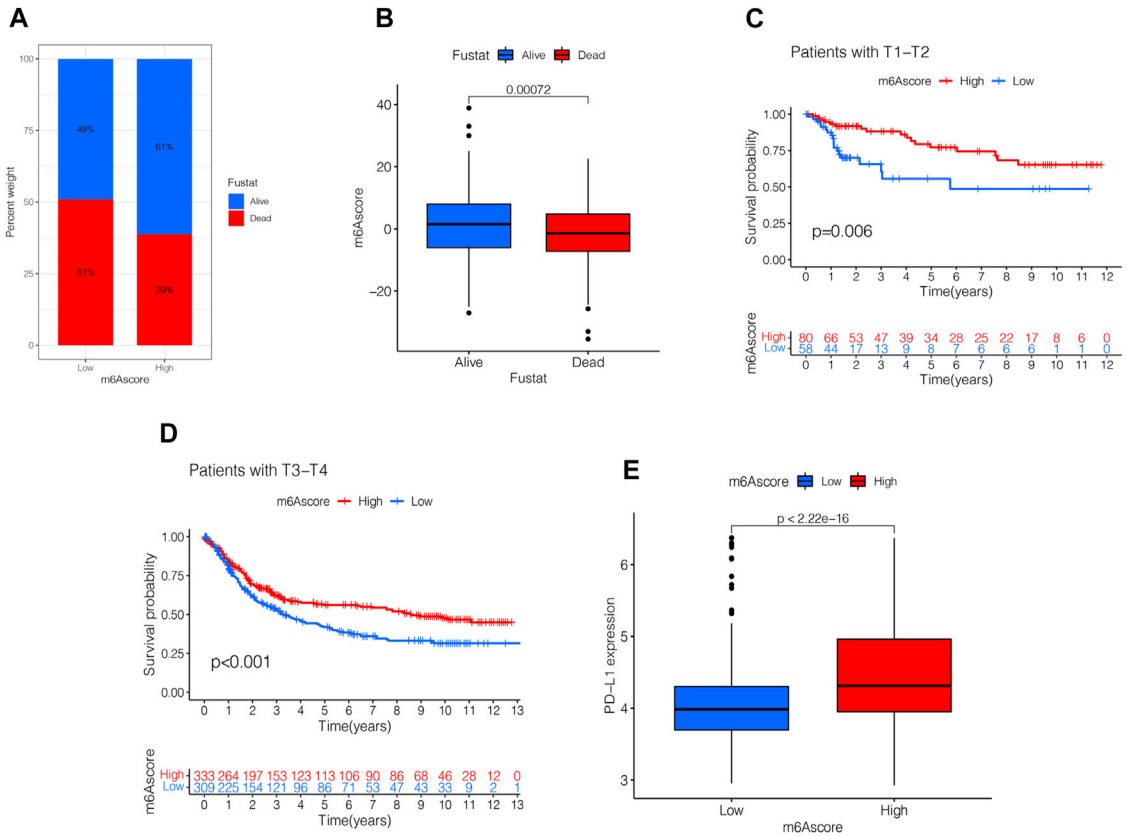

FIGURE 7 | Validation and application of the m6A score in clinical evaluation. **(A)** Proportion of survival and death in high- and low-m6A score groups. **(B)** Comparison of the m6A score between survival and dead patients ($p < 0.001$, Wilcoxon test). **(C)** Stratified analysis of the m6A score for STAD patients by T1-T2 ($p = 0.006$, Log-rank test). **(D)** Stratified analysis of m6A score for STAD patients by T3-T4 ($p < 0.001$, Log-rank test). **(E)** Stratified analysis of m6A score for STAD patients by PD-L1 ($p < 0.0001$, Wilcoxon test).

the tumor, tumor and matrix interface, and matrix. Thus, optimal response conditions were created for immunotherapy, such that patients may have a better response to the treatment of PD-1/L1 inhibitors. Conversely, if PD-L1 came from tumor cells, TILs were mostly immersed in the matrix around the tumor. Therefore, the infiltration characteristics of TME cells in m6A methylation modification patterns provided potential therapeutic targets and novel ideas for the prevention of STAD.

In addition, we identified DEGs based on the m6A methylation modification patterns. Further analysis showed that these DEGs had m6A-related characteristic genes closely related to tumor prognosis and immune pathways. These m6A-related characteristic genes were genotyped according to the cluster analysis. The results of the analysis of the phenotype genes showed that they were closely related to cell-matrix and immune activation, which further validated the role of m6A methylation in TME. Then, we adjusted the mRNA levels according to m6A regulatory genes and classified them into high- and low-expression groups according to the mRNA expression median value. Subsequently, the m6A score model was constructed to evaluate the m6A modification patterns in individual patients with STAD, and the effects of individual heterogeneity were excluded. This provided accurate guidance for immunotherapy in patients with STAD. According to the m6A score difference analysis results, m6Acluster-B with immuno-exclusion type had the highest m6A score, while m6Acluster-A with immune-inflammatory type had the lowest m6A score. The immuno-correlated analysis established a positive correlation between m6A scores and $CD4^+$ T cells. These results showed that the m6A score could determine the TME-infiltrated tumor immunophenotype and guide precision immunotherapy in patients with STAD. Several studies have reported that the higher the TMB in cancer patients, the better the prognosis (Cheng et al., 2015; Li et al., 2016; Kelly, 2017; Wei et al., 2021). Therefore, TMB can be used as a predictive biomarker for patients with STAD during ICI progression, facilitating clinical decision-making. Our analysis found that the m6A score was significantly positively correlated with TMB, which was consistent with previous findings. Subsequent studies found a correlation between the m6A score in mutation burden, PD-L1 expression, and MSI state. Additionally, the predictive advantages of the m6A score in immunotherapy of patients with STAD were determined.

A large number of studies have found that m6A-related genes play a major role in the progression and metastasis of STAD. METTL3 was the main catalytic component of methyl transfer

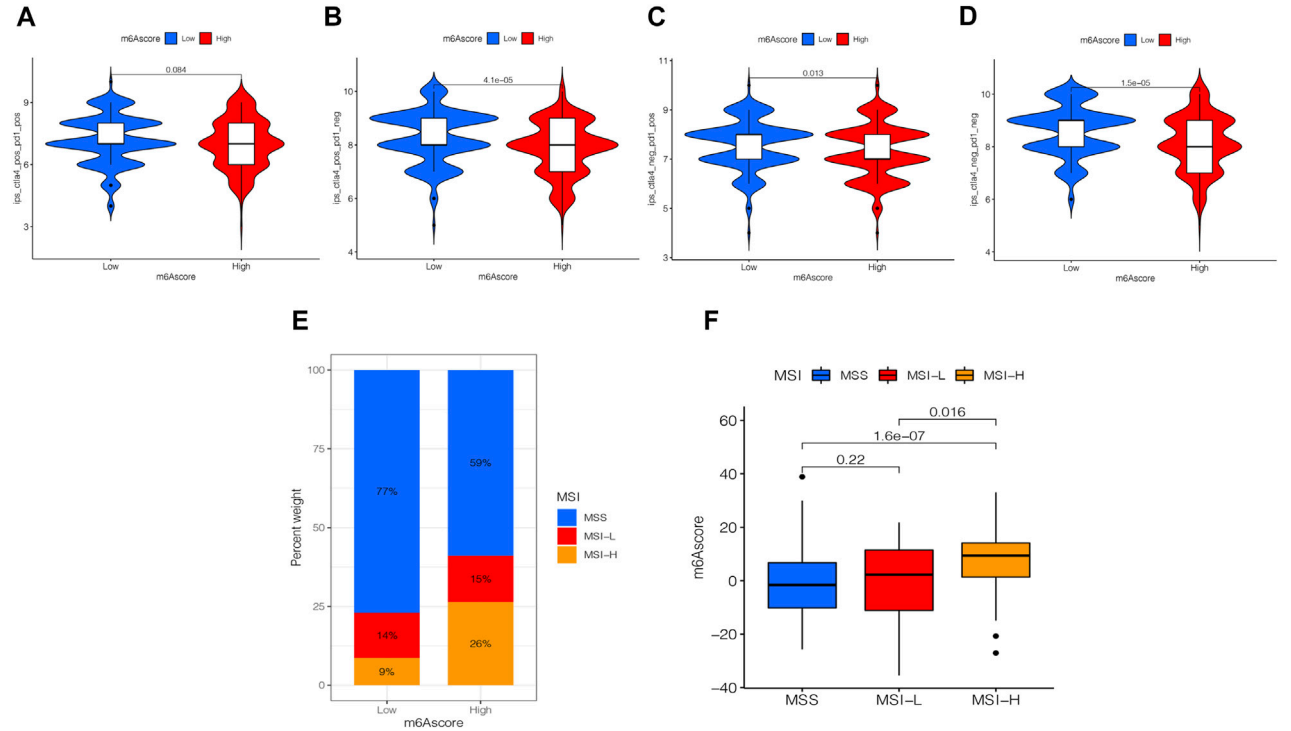

FIGURE 8 | Analysis of the m6A score in anti-PD-L1 and CTLA-4 immunotherapy. **(A)** Differential analysis for the low m6A score group and the high m6A score group in immunophenoscore (IPS) with CTLA4 (+)/PD1 (+) ($p = 0.084$, Wilcoxon test). **(B)** Differential analysis for the low m6A score group and the high m6A score group in IPS with CTLA4 (+)/PD1 (–) ($p < 0.0001$, Wilcoxon test). **(C)** Differential analysis for the low m6A score group and the high m6A score group in IPS with CTLA4 (–)/PD1 (+) ($p = 0.013$, Wilcoxon test). **(D)** Differential analysis for the low m6A score group and the high m6A score group in IPS with CTLA4 (–)/PD1 (–) ($p < 0.0001$, Wilcoxon test). **(E)** The proportion of the m6A score in groups with high or low MSI and stable status. **(F)** Differences in the m6A score among high or low MSI and stable status. The differences between the three groups were compared through the Kruskal-Wallis test. MSS, microsatellite stable; MSI-H, high microsatellite instability; MSI-L, low microsatellite instability.

enzyme complexes, and its abnormal expression can alter the expression of *m6A* mRNA, affecting the proliferation, metastasis, invasion, and apoptosis of STAD. Yue et al. (2019) demonstrated that elevated METTL3 expression was positively correlated with poor prognosis in patients and thus contributed to the epithelial-mesenchymal transition process and metastasis. Jiang et al. (2020) demonstrated that METTL3 knockout increases the expression of suppressor of cytokine signaling (SOCS) protein families in STAD cells and that SOCS2 expression is negatively correlated with STAD cell proliferation. This phenomenon suggested that a decline in METTL3 elevates SOCS2 expression and inhibits STAD cell proliferation. A recent study found that m6A and METTL3 expression levels increased in STAD and that elevated METTL3 expression indicated high malignancy and poor prognosis in patients (Sun et al., 2020). FTO was the first m6A methylation enzyme to be discovered. Some studies found that FTO was associated with STAD development and might be a vital molecular target for monitoring STAD prognosis. Zhang et al. (2019) demonstrated that low m6A signals were associated with poor clinicopathological characteristics of STAD. The mechanism studies revealed that FTO overexpression could reduce m6A methylation levels, activate Wnt/PI3K-AKT pathways, and promote malignant phenotypes of STAD. The YTH family protein is bound to mRNA containing m6A, which regulates the positioning and stability of mRNA. This family of proteins was associated with the development of STAD. Based on the biological information from various human cancer databases, one study found that about 7% of STAD patients had YTHDF1 mutations and that high expression of YTHDF1 was associated with high tumor proliferation rates and poor overall survival (Pi et al., 2021). *In vivo* and *in vitro* experiments confirmed that YTHDF1 promotes the translation of the Wnt pathway key receptor protein frizzled 7 (FZD7) in a m6A-dependent manner and enhanced the expression of FZD7. Subsequently, the Wnt/β-catenin signaling pathway was triggered; which facilitated the occurrence of STAD. These results confirmed our findings and demonstrated that m6A-related genes in TME play a critical role in the metabolism, drug resistance, and metastasis of STAD, suggesting that m6A modification can be used as a target for the prevention and treatment of STAD.

The systematic study on the m6A score revealed its role in gastric cancer patients in clinical practice. First, the m6A score could be used to evaluate m6A methylation patterns in patients with STAD, which elaborated the corresponding TME cell infiltration characteristics. This enhanced our understanding of the immune phenotype of STAD, thereby improving the clinical treatment conversion effect.

In this study, we found that the m6A score was closely related to the clinicopathological characteristics of STAD, including TNM, TMB, and MSI. Therefore, the m6A score can be used as an independent prognostic biomarker for STAD to guide clinical treatment, as well as a supplementary assessment criterion for immunotherapy to predict the clinical effects of immunotherapy. Furthermore, it can also be used as a sensitive index of precision immunotherapy for STAD. Importantly, the present study confirmed the role of m6A regulatory factors or m6A phenotype-related genes in STAD. Targeting these genes can alter the characteristics of TME cell infiltration and improve the effectiveness of targeted immunotherapy, thereby opening a new avenue for epigenetics and tumor research and the underlying regulatory mechanisms.

CONCLUSION

In summary, this study systematically evaluated the modification patterns of 23 m6A regulatory factors in STAD. Thus, it was proved that different modification patterns may be critical factors leading to inhibitory changes and heterogeneity in TME. This will elucidate TME infiltration characteristics in patients with STAD based on the evaluation of m6A modification patterns. This promoted basic research in relevant areas and created opportunities for clinical STAD patients to predict prognosis and explore novel immunotherapies.

DATA AVAILABILITY STATEMENT

The datasets presented in this study can be found in online repositories. The names of the repository/repositories and accession number(s) can be found in the article/ **Supplementary Material**.

AUTHOR CONTRIBUTIONS

YB and LTH designed the work; ZMJ and YB wrote the main manuscript text; ZMJ prepared figures and tables.

ACKNOWLEDGMENTS

The data for this work were obtained from the TCGA and GEO databases. The authors acknowledge contributions from these resources and the staff who expand and improve the databases.

SUPPLEMENTARY MATERIAL

The Supplementary Material for this article can be found online at: https://www.frontiersin.org/articles/10.3389/fcell.2022.913307/full#supplementary-material

REFERENCES

Beatty, G. L., and Gladney, W. L. (2015). Immune Escape Mechanisms as a Guide for Cancer Immunotherapy. *Clin. Cancer Res.* 21 (4), 687–692. doi:10.1158/1078-0432.CCR-14-1860

Boccaletto, P., Machnicka, M. A., Purta, E., Piątkowski, P., Bagiński, B., Wirecki, T. K., et al. (2018). MODOMICS: a Database of RNA Modification Pathways. 2017 Update. *Nucleic Acids Res.* 46 (D1), D303–D307. doi:10.1093/nar/gkx1030

Charoentong, P., Finotello, F., Angelova, M., Mayer, C., Efremova, M., Rieder, D., et al. (2017). Pan-cancer Immunogenomic Analyses Reveal Genotype-Immunophenotype Relationships and Predictors of Response to Checkpoint Blockade. *Cell Rep.* 18 (1), 248–262. doi:10.1016/j.celrep.2016.12.019

Chen, D. S., and Mellman, I. (2017). Elements of Cancer Immunity and the Cancer-Immune Set Point. *Nature* 541 (7637), 321–330. doi:10.1038/nature21349

Chen, L., and Flies, D. B. (2013). Molecular Mechanisms of T Cell Co-stimulation and Co-inhibition. *Nat. Rev. Immunol.* 13 (4), 227–242. doi:10.1038/nri3405

Chen, W., Zheng, R., Baade, P. D., Zhang, S., Zeng, H., Bray, F., et al. (2016). Cancer Statistics in China, 2015. *CA A Cancer J. Clin.* 66 (2), 115–132. doi:10.3322/caac.21338

Chen, X.-Y., Zhang, J., and Zhu, J.-S. (2019). The Role of M(6)A RNA Methylation in Human Cancer. *Mol. Cancer* 18 (1), 103. doi:10.1186/s12943-019-1033-z

Cheng, D. T., Mitchell, T. N., Zehir, A., Shah, R. H., Benayed, R., Syed, A., et al. (2015). Memorial Sloan Kettering-Integrated Mutation Profiling of Actionable Cancer Targets (MSK-IMPACT): A Hybridization Capture-Based Next-Generation Sequencing Clinical Assay for Solid Tumor Molecular Oncology. *J. Mol. Diagnostics* 17 (3), 251–264. doi:10.1016/j.jmoldx.2014.12.006

Davis, R. J., Van Waes, C., and Allen, C. T. (2016). Overcoming Barriers to Effective Immunotherapy: MDSCs, TAMs, and Tregs as Mediators of the Immunosuppressive Microenvironment in Head and Neck Cancer. *Oral Oncol.* 58, 59–70. doi:10.1016/j.oraloncology.2016.05.002

Dominissini, D., Moshitch-Moshkovitz, S., Schwartz, S., Salmon-Divon, M., Ungar, L., Osenberg, S., et al. (2012). Topology of the Human and Mouse m6A RNA Methylomes Revealed by m6A-Seq. *Nature* 485 (7397), 201–206. doi:10.1038/nature11112

Foroutan, M., Bhuva, D. D., Lyu, R., Horan, K., Cursons, J., and Davis, M. J. (2018). Single Sample Scoring of Molecular Phenotypes. *BMC Bioinforma.* 19 (1), 404. doi:10.1186/s12859-018-2435-4

Hänzelmann, S., Castelo, R., and Guinney, J. (2013). GSVA: Gene Set Variation Analysis for Microarray and RNA-Seq Data. *BMC Bioinforma.* 14, 7. doi:10.1186/1471-2105-14-7

Herbst, R. S., Giaccone, G., de Marinis, F., Reinmuth, N., Vergnenegre, A., Barrios, C. H., et al. (2020). Atezolizumab for First-Line Treatment of PD-L1-Selected Patients with NSCLC. *N. Engl. J. Med.* 383 (14), 1328–1339. doi:10.1056/NEJMoa1917346

Jenjaroenpun, P., Wongsurawat, T., Wadley, T. D., Wassenaar, T. M., Liu, J., Dai, Q., et al. (2021). Decoding the Epitranscriptional Landscape from Native RNA Sequences. *Nucleic Acids Res.* 49 (2), e7. doi:10.1093/nar/gkaa620

Jiang, L., Chen, T., Xiong, L., Xu, J. H., Gong, A. Y., Dai, B., et al. (2020). Knockdown of m6A Methyltransferase METTL3 in Gastric Cancer Cells Results in Suppression of Cell Proliferation. *Oncol. Lett.* 20 (3), 2191–2198. doi:10.3892/ol.2020.11794

Kelly, R. J. (2017). Immunotherapy for Esophageal and Gastric Cancer. *Am. Soc. Clin. Oncol. Educ. Book* 37, 292–300. doi:10.14694/EDBK_17523110.1200/edbk_175231

Lambrechts, D., Wauters, E., Boeckx, B., Aibar, S., Nittner, D., Burton, O., et al. (2018). Phenotype Molding of Stromal Cells in the Lung Tumor Microenvironment. *Nat. Med.* 24 (8), 1277–1289. doi:10.1038/s41591-018-0096-5

Lee, H. W., Chung, W., Lee, H.-O., Jeong, D. E., Jo, A., Lim, J. E., et al. (2020). Single-cell RNA Sequencing Reveals the Tumor Microenvironment and Facilitates Strategic Choices to Circumvent Treatment Failure in a Chemorefractory Bladder Cancer Patient. *Genome Med.* 12 (1), 47. doi:10.1186/s13073-020-00741-6

Li, X., Wu, W. K. K., Xing, R., Wong, S. H., Liu, Y., Fang, X., et al. (2016). Distinct Subtypes of Gastric Cancer Defined by Molecular Characterization Include

Novel Mutational Signatures with Prognostic Capability. *Cancer Res.* 76 (7), 1724–1732. doi:10.1158/0008-5472.CAN-15-2443

Li, Z., and Zhang, H. (2016). Reprogramming of Glucose, Fatty Acid and Amino Acid Metabolism for Cancer Progression. *Cell. Mol. Life Sci.* 73 (2), 377–392. doi:10.1007/s00018-015-2070-4

Liu, L., Li, H., Hu, D., Wang, Y., Shao, W., Zhong, J., et al. (2022). Insights into N6-Methyladenosine and Programmed Cell Death in Cancer. *Mol. Cancer* 21 (1), 32. doi:10.1186/s12943-022-01508-w

Meyer, K. D., Saletore, Y., Zumbo, P., Elemento, O., Mason, C. E., and Jaffrey, S. R. (2012). Comprehensive Analysis of mRNA Methylation Reveals Enrichment in 3′ UTRs and Near Stop Codons. *Cell* 149 (7), 1635–1646. doi:10.1016/j.cell.2012.05.003

Mobet, Y., Liu, X., Liu, T., Yu, J., and Yi, P. (2022). Interplay between M(6)A RNA Methylation and Regulation of Metabolism in Cancer. *Front. Cell Dev. Biol.* 10, 813581. doi:10.3389/fcell.2022.813581

Mok, T. S. K., Wu, Y. L., Kudaba, I., Kowalski, D. M., Cho, B. C., Turna, H. Z., et al. (2019). Pembrolizumab versus Chemotherapy for Previously Untreated, PD-L1-Expressing, Locally Advanced or Metastatic Non-small-cell Lung Cancer (KEYNOTE-042): a Randomised, Open-Label, Controlled, Phase 3 Trial. *Lancet* 393 (10183), 1819–1830. doi:10.1016/S0140-6736(18)32409-7

Pi, J., Wang, W., Ji, M., Wang, X., Wei, X., Jin, J., et al. (2021). YTHDF1 Promotes Gastric Carcinogenesis by Controlling Translation of FZD7. *Cancer Res.* 81 (10), 2651–2665. doi:10.1158/0008-5472.CAN-20-0066

Roundtree, I. A., Evans, M. E., Pan, T., and He, C. (2017). Dynamic RNA Modifications in Gene Expression Regulation. *Cell* 169 (7), 1187–1200. doi:10.1016/j.cell.2017.05.045

Shen, C., Wang, K., Deng, X., and Chen, J. (2022). DNA N(6)-methyldeoxyadenosine in Mammals and Human Disease. *Trends Genet.* 38 (5), 454–467. doi:10.1016/j.tig.2021.12.003

Shulman, Z., and Stern-Ginossar, N. (2020). The RNA Modification N(6)-methyladenosine as a Novel Regulator of the Immune System. *Nat. Immunol.* 21 (5), 501–512. doi:10.1038/s41590-020-0650-4

Sotiriou, C., Wirapati, P., Loi, S., Harris, A., Fox, S., Smeds, J., et al. (2006). Gene Expression Profiling in Breast Cancer: Understanding the Molecular Basis of Histologic Grade to Improve Prognosis. *J. Natl. Cancer Inst.* 98 (4), 262–272. doi:10.1093/jnci/djj052

Sun, Y., Li, S., Yu, W., Zhao, Z., Gao, J., Chen, C., et al. (2020). N(6)-methyladenosine-dependent Pri-miR-17-92 Maturation Suppresses PTEN/TMEM127 and Promotes Sensitivity to Everolimus in Gastric Cancer. *Cell Death Dis.* 11 (10), 836. doi:10.1038/s41419-020-03049-w

Tabernero, J., Hoff, P. M., Shen, L., Ohtsu, A., Shah, M. A., Cheng, K., et al. (2018). Pertuzumab Plus Trastuzumab and Chemotherapy for HER2-Positive Metastatic Gastric or Gastro-Oesophageal Junction Cancer (JACOB): Final Analysis of a Double-Blind, Randomised, Placebo-Controlled Phase 3 Study. *Lancet Oncol.* 19 (10), 1372–1384. doi:10.1016/S1470-2045(18)30481-9

Wang, L., Wen, X., Luan, F., Fu, T., Gao, C., Du, H., et al. (2019). EIF3B Is Associated with Poor Outcomes in Gastric Cancer Patients and Promotes Cancer Progression via the PI3K/AKT/mTOR Signaling Pathway. *Cmar* 11, 7877–7891. doi:10.2147/CMAR.S207834

Wang, Q., Chen, C., Ding, Q., Zhao, Y., Wang, Z., Chen, J., et al. (2020). METTL3-mediated M(6)A Modification of HDGF mRNA Promotes Gastric Cancer Progression and Has Prognostic Significance. *Gut* 69 (7), 1193–1205. doi:10.1136/gutjnl-2019-319639

Wei, X.-L., Xu, J.-Y., Wang, D.-S., Chen, D.-L., Ren, C., Li, J.-N., et al. (2021). Baseline Lesion Number as an Efficacy Predictive and Independent Prognostic Factor and its Joint Utility with TMB for PD-1 Inhibitor Treatment in Advanced Gastric Cancer. *Ther. Adv. Med. Oncol.* 13, 175883592198899. doi:10.1177/1758835921988996

Xiong, J., He, J., Zhu, J., Pan, J., Liao, W., Ye, H., et al. (2022). Lactylation-driven METTL3-Mediated RNA M(6)A Modification Promotes Immunosuppression of Tumor-Infiltrating Myeloid Cells. *Mol. Cell* 82 (9), 1660–1677 e10. doi:10.1016/j.molcel.2022.02.033

Yang, D.-D., Chen, Z.-H., Yu, K., Lu, J.-H., Wu, Q.-N., Wang, Y., et al. (2020). METTL3 Promotes the Progression of Gastric Cancer via Targeting the MYC Pathway. *Front. Oncol.* 10, 115. doi:10.3389/fonc.2020.00115

Yang, M., Li, J., Gu, P., and Fan, X. (2021). The Application of Nanoparticles in Cancer Immunotherapy: Targeting Tumor Microenvironment. *Bioact. Mater.* 6 (7), 1973–1987. doi:10.1016/j.bioactmat.2020.12.010

Yoon, S.-J., Park, J., Shin, Y., Choi, Y., Park, S. W., Kang, S.-G., et al. (2020). Deconvolution of Diffuse Gastric Cancer and the Suppression of CD34 on the BALB/c Nude Mice Model. *BMC Cancer* 20 (1), 314. doi:10.1186/s12885-020-06814-4

Yue, B., Song, C., Yang, L., Cui, R., Cheng, X., Zhang, Z., et al. (2019). METTL3-mediated N6-Methyladenosine Modification Is Critical for Epithelial-Mesenchymal Transition and Metastasis of Gastric Cancer. *Mol. Cancer* 18 (1), 142. doi:10.1186/s12943-019-1065-4

Zaccara, S., Ries, R. J., and Jaffrey, S. R. (2019). Reading, Writing and Erasing mRNA Methylation. *Nat. Rev. Mol. Cell Biol.* 20 (10), 608–624. doi:10.1038/s41580-019-0168-5

Zeng, D., Li, M., Zhou, R., Zhang, J., Sun, H., Shi, M., et al. (2019). Tumor Microenvironment Characterization in Gastric Cancer Identifies Prognostic and Immunotherapeutically Relevant Gene Signatures. *Cancer Immunol. Res.* 7 (5), 737–750. doi:10.1158/2326-6066.CIR-18-0436

Zhang, C., Zhang, M., Ge, S., Huang, W., Lin, X., Gao, J., et al. (2019). Reduced m6A Modification Predicts Malignant Phenotypes and Augmented Wnt/PI3K-Akt Signaling in Gastric Cancer. *Cancer Med.* 8 (10), 4766–4781. doi:10.1002/cam4.2360

Zhao, B. S., Roundtree, I. A., and He, C. (2017). Post-transcriptional Gene Regulation by mRNA Modifications. *Nat. Rev. Mol. Cell Biol.* 18 (1), 31–42. doi:10.1038/nrm.2016.132

Zhao, S., Ye, Z., and Stanton, R. (2020). Misuse of RPKM or TPM Normalization when Comparing across Samples and Sequencing Protocols. *RNA* 26 (8), 903–909. doi:10.1261/rna.074922.120

Zou, W. (2018). Mechanistic Insights into Cancer Immunity and Immunotherapy. *Cell Mol. Immunol.* 15 (5), 419–420. doi:10.1038/s41423-018-0011-5

Conflict of Interest: The authors declare that the research was conducted in the absence of any commercial or financial relationships that could be construed as a potential conflict of interest.

Publisher's Note: All claims expressed in this article are solely those of the authors and do not necessarily represent those of their affiliated organizations, or those of the publisher, the editors and the reviewers. Any product that may be evaluated in this article, or claim that may be made by its manufacturer, is not guaranteed or endorsed by the publisher.

frontiers | Frontiers in Oncology

REVIEW
published: 24 June 2022
doi: 10.3389/fonc.2022.925041

Recent Insight on Regulations of FBXW7 and Its Role in Immunotherapy

Liangliang Xing[1†], Leidi Xu[1†], Yong Zhang[1], Yinggang Che[1], Min Wang[1], Yongxiang Shao[2], Dan Qiu[1], Honglian Yu[3], Feng Zhao[1] and Jian Zhang[1*]*

[1] Department of Pulmonary Medicine, Xijing Hospital, Air Force Medical University, Xi'an, China, [2] Department of Anus and Intestine Surgery, The 942th Hospital of Joint Logistics Support Force, Yinchuan, China, [3] Department of Hemato-Oncology, The 942th Hospital of Joint Logistics Support Force, Yinchuan, China

OPEN ACCESS

Edited by:
Xuebing Li,
Tianjin Medical University General Hospital, China

Reviewed by:
Lin Lin,
Tianjin Medical University General Hospital, China
Fengjie Guo,
South China University of Technology, China
Yue Zhen Deng,
Central South University, China

***Correspondence:**
Jian Zhang
13991802890@163.com
Feng Zhao
xjzhaof@fmmu.edu.cn

[†]These authors have contributed equally to this work

Specialty section:
This article was submitted to Pharmacology of Anti-Cancer Drugs, a section of the journal Frontiers in Oncology

Received: *21 April 2022*
Accepted: *24 May 2022*
Published: *24 June 2022*

Citation:
Xing L, Xu L, Zhang Y, Che Y, Wang M, Shao Y, Qiu D, Yu H, Zhao F and Zhang J (2022) Recent Insight on Regulations of FBXW7 and Its Role in Immunotherapy. Front. Oncol. 12:925041. doi: 10.3389/fonc.2022.925041

SCF^{FBXW7} E3 ubiquitin ligase complex is a crucial enzyme of the ubiquitin proteasome system that participates in variant activities of cell process, and its component FBXW7 (F-box and WD repeat domain–containing 7) is responsible for recognizing and binding to substrates. The expression of FBXW7 is controlled by multiple pathways at different levels. FBXW7 facilitates the maturity and function maintenance of immune cells *via* functioning as a mediator of ubiquitination-dependent degradation of substrate proteins. FBXW7 deficiency or mutation results in the growth disturbance and dysfunction of immune cell, leads to the resistance against immunotherapy, and participates in multiple illnesses. It is likely that FBXW7 coordinating with its regulators and substrates could offer potential targets to improve the sensitivity and effects of immunotherapy. Here, we review the mechanisms of the regulation on FBXW7 and its tumor suppression role in immune filed among various diseases (mostly cancers) to explore novel immune targets and treatments.

Keywords: FBXW7, ubiquitination, epigenetic regulation, immunity, immunotherapy

1. INTRODUCTION

Degradation is one of most significant bioprocesses of metabolism in almost all forms of life. For most eukaryotic cells, three pathways were discovered to degrade multiple proteins: (1) lysosomal pathway, (2) caspase pathway, and (3) ubiquitin proteasome pathway. Among them, the ubiquitin-proteasome pathway is the most irreplaceable specific protein degradation pathway, which can participate in various biological processes including cell proliferation, division, differentiation, and apoptosis, by promoting protein degradation (1, 2). The ubiquitin proteasome system (UPS) performs its protein-degrading function by three enzymes: the ubiquitin-activating enzyme (E1), the ubiquitin-conjugating enzyme (E2), and the ubiquitin ligase (E3). Among them, E3 ubiquitin ligase is the most critical component of UPS that can specifically recognize proteins to complete their ubiquitination. Emerging evidence exhibits that E3 shows a tendency weighing more in tumor suppressing than that in activating (3, 4). Skp1–Cullin1–F-box (SCF)^{FBXW7} consisting of Skp1, CUL1, F-box, and RBX1, is a well-learned category of E3 ligase in Really Interesting New Gene (RING) family (5). FBXW7 (F-box and WD repeat domain–containing 7) is usually deemed as a negative regulator of human cancers and is the most crucial F-box protein in E3 ligase so far (6).

Studies have indicated that FBXW7 is also involved in the regulation of immunity (7–11). Theories have explained the correlation between immunity and tumorigenesis, including tumor immunosurveillance and tumor immunoediting theory (12). Tumor immunoediting theory is a refinement of tumor immunosurveillance to explain the immune evsion of mutated cells and the progression of tumors. According to this theory, tumors develop in three stages. The first step is the elimination phase—the healthy body detects and eliminates mutated cells through immune surveillance; the second is the equilibrum phase—the immune system is so vulnerable that is uncapable of clearing out all of the mutated cells and leaves a significant number of the tumor cells remaining inside the body; and the final step is the escape phase—the tumor cells take a dominant position and become resistant to the attack launched by the immune system with the emergence of clinical signs and symptoms. Because immunity shows a close correlation with tumorigenesis, immunotherapy has been explored to fight against multiple cancers (13). Multiple immunotherapies have been developed, such as tumor vaccine, Bacille Calmette-Guerin (BCG), chimeric antigen receptor–engineered T lymphocytes, adoptive cellular therapy, and immune checkpoint inhibitors (ICIs). Among them, ICIs (including anti–PD-1/anti–PD-L1 and anti–CTLA-4) are mostly applied into the clinic, especially anti–PD-1/anti–PD-L1. Three immune patterns were characterized according to the anti-tumor reaction to PD-L1/PD-1 treatment (14). The first is the immune-inflamed phenotype featured by the existence of CD4- and CD8-positive T cells in the tumor parenchyma. The second is the immune-excluded phenotype featured by plentiful immune cells existing in the stroma without the ability of invading tumor parenchyma. The last one is the immune-desert phenotype featured by the absence of T cells in either parenchyma or stroma. A lot of research studies have found that SCF^{FBXW7} acting as a tumor suppressor is involved in tumorigenesis and resistance to immunotherapy by maintaining immune evasion (9, 15, 16).

This review mainly focuses on the FBXW7 functions in different cancers immunotherapy based on its structure and regulations in different levels, its involvement in multiple biological processes, as well its effect on immune cells and cytokines, which eventually draws a blueprint of targeting FBXW7 in immunotherapy.

2. SKP1–CULLIN1–F-BOX PROTEIN COMPLEX

The UPS plays a significant role in multiple bioprocess including cell propagation, division, and differentiation to decide the destiny of cell (7). It consists of three functionally interconnected enzymes: E1, E2, and E3. RING finger–type proteins and Homologous to the E6-AP Carboxyl Terminus (HECT) domain–type proteins are the largest two families of E3 ligase. In the RING family, E3 ligases transfer ubiquitin molecules directly from the E2 ubiquitin complex to the substrate without binding to ubiquitin molecules. The SCF ubiquitin ligase complex is a crucial member mainly composed of four units: Skp1 (composed of 163 residues), CUL1 (composed of 776 residues), F-box (composed of ~430 to >1,000 residues), and RBX1 (also called ROC1, composed of 108 residues) (17–20). CUL1 functions as a skeleton protein to interplay with the remaining three subunits (20). CUL1 interacts with RBX1via C terminus while it interacts with SKP1 *via* its N terminus. Moreover, F-box interacts with Skp1 *via* the F-box motif (21). SCF complex is deemed as one of the critical controllers of the mechanism in cell cycle for they regulate pivotal proteins progressing cell cycle (22). The F-box is the part of SCF complex responsible for recognizing and binding substrates. So far, nearly 70 F-box proteins have been found in humans as well as in other species (23). These proteins are further divided into three categories: Those rich in leucine repeats are called FBXL; the domain containing WD40 is called FBXW; the others are FBXO (with another or without motif except F-box protein) (24). FBXW7 (F-box with 7 tandem WD40 repeats) is the most famous FBXW protein for its significance in cellular processes including cell proliferation, division, and differentiation and is also known as FBW7, hAgo, hCDC4, and Sel10 (7).

3. FBXW7—THE MOST CRITICAL F-BOX PROTEIN IN THE RING FAMILY OF E3 UBIQUITIN LIGASE

3.1. Structure and Locations

FBXW7 is the most widely researched F-box protein for its tumor suppression role up to now. It was first identified in budding yeast in 1973 by Hartwell et al. and then named CDC4 (25). This gene is highly conserved in multiple species. During the research on regulation of SEL-10 to LIN-12, the conserved gene CDC4 was also found in human cells and was named FBXW7 in terms of its structure, attracting increasing attention from then (26–28). FBXW7 gene that consists of 13 coding exons and 4 non-coding exons is located in the 4q31q.3 region of the human chromosome (a region frequently associated with deletion mutations in human tumors), and the gene length of FBXW7 is approximately 210 kb (6, 29). According to the difference between the 5′ untranslated region (5'UTR) and N-terminal coding region, the spliced variants of FBXW7 are divided into three subtypes: FBXW7α, FBXW7β, and FBXW7γ. Same gene as it comes from, the corresponding proteins translated by the three subtypes are located differently in subcellular regions: FBXW7α is located in the cytoplasm; FBXW7β is located in the cytoplasm; FBXW7γ is located in the nucleolus (30a). Different localization of FBXW7 can regulate their respective functions, which may be related to different pathways to bind to substrates. The three subtypes of FBXW7 share the following important conserved sequences: (1) the F-box domain, performing the function of recruiting SCF complexes through Skp1; (2) D domain, promoting the formation of FBXW7 dimer; and (3) WD40 domain, responsible for substrate recognition. Apart from the distinguishment in intracellular localization, three subtypes of FBXW7 also

expressed discrepantly in different tissue types. A study in 2002 found that FBXW7α is widely expressed in human tissues, whereas FBXW7β and FBXW7γ are highly expressed mainly in the heart, brain, and skeletal muscle (29). Four years later, another mice model study came to similar conclusions (31). Currently, research studies lay emphasis mainly on the function of FBXW7α, whereas the other two subtypes of FBXW7-related biological studies are relatively rare.

3.2. Regulation of FBXW7

3.2.1. FBXW7 Regulation at Transcriptional Level

Since we have known the structure and locations of FBXW7, we want to figure out the mechanisms on how it is regulated. Regulation of FBXW7 at transcriptional level represents a tendency to negatively regulating the expression of FBXW7. RAN-binding protein 10 (RANBP10) promotes the stabilization of c-myc *via* binding to the region P4 of FBW7 promotor and inhibiting its transcription, which induces the progression of glioblastoma (32). A complex of PHF1/PRMT5–WDR77/CRL4B represses transcription of FBWX7 by taking up its promotor, which leads to the progression of cancer (33). C/EBPδ functions as an inhibitor binding to the promoter of FBW7α and decreases the abundance of FBXW7α mRNA, contributing to improved activity of HIF-1 *via* stabilizing mTOR (34). Furthermore, a feedback loop consisting of FBXW7, Hes5, and NOTCH intracellular domain (NICD) is involved in the inactivation of FBXW7 mRNA (35). In this loop, Hes5 binds to the N-box in the promotor of FBXW7 to suppress its transcription, which can affect the fate of intestinal and neural stem cells. Moreover, the inactivation of FBXW7 mediated by Hes5 participates in the inhibition of TGF-β pathway as well (36). TRIP13 confers the carcinogenicity of glioblastoma *via* binding to the promoter near FBXW7 gene and further stabilizing c-myc by suppressing expression of FBXW7 (37). Intriguingly, P53 activates the transcription of FBXW7β by binding to a site in exon 1b, acting as a resistance against genotoxic pressure from UV radiation and adriamycin (38).

3.2.2. Epigenetic Regulation of FBXW7

3.2.2.1. Methylation and Demethylation Modification

Several studies have uncovered the correlation of DNA methylation with FBXW7 expression. In the study of Akhoondi et al., they found that the ratio of methylation of the FBXW7β promoter in cancer cell line is 43%, whereas the number in primary breast cancer is 51% (39). Data suggested that FBXW7β of methylated group was downregulated both in cancer cell line and in primary breast cancer compared with the unmethylated group. They also found that although methylation was connected with advanced tumors, the hazard ratio (HR) for patients' death with FBXW7β methylation on the opposite showed a downtrend. Gu et al. discovered that, with the methylation of the CpG sequence in FBXW7β's promoter, a significant decline of the expression of FBXW7β was observed (40a). The methylation in FBXW7β promoter was found to be positively associated with thymoma histological subtype that presents a positive correlation with prognosis of patients (41b). In addition, the methylation level of FBXW7 gene 5′ upstream areas of p53-mutated samples was significantly higher than that of wild-type samples, which may due to the suppression of FBXW7 expression by p53 mutations through the hypermethylation in designated areas (42). More epigenetic silencing of FBXW7 was exhibited in human papillomavirus-IMM (HPV-IMM) than HPV16-KRT, which may work in the stratification of cervical squamous cell carcinoma (CSCC) affected by HPV16 to provide reasonable treatment for patients (43). Furthermore, lysine demethylase 5B (KDM5B), a histone demethylase of FBXW7, was unveiled to suppress FBXW7 expression *via* demethylation of H3K4me3 at promoter region (44). The mechanism of FBXW7 epigenetic modulation has been applied into clinical treatment for patient of lung cancer as decitabine is able to demethylate the epigenetically silenced FBXW7 gene and reactivate it (45)

3.2.2.2. Histone Acetylation

In addition to DNA methylation, histone acetylation is also implicated in regulation of FBXW7. A research to detect the DNA methylation, histone methylation, histone acetylation, and chromatin remodeling uncovered that H3K27 acetylation suppressed by the mutation or knockdown in CREBBP or EP300 in B-lymphoma cells weakened the expression of FBXW7, leading to the activation of NOTCH pathway and thereby caused the tumor-associated macrophage (TAM) polarizing to M2 phenotype and proliferation of tumor cells (46). Histone acetylation could also work synergistically with DNA methylation. Data acquired from The Cancer Genome Atlas (TCGA) revealed that high DNA methylation of the FBXW7 was accompanied with high KDM5c (a histone demethylase) expression, which might ascribe to the recruitment of DNMT3b induced by interaction of KDM5c and H3K4me3 of FBXW7 downstream so that the CpG of FBXW7 could be methylated, followed with inhibited FBXW7 expression (47a).

3.2.2.3. Chromatin Remodeling

Chromatin remodeling is involved in the mediation of FBXW7 as well. An experiment conducted by Masayuki Hagiwara disclosed that the expression of FBXW7 was restrained by the overexpression of MUC1-1C, which activates the components, including MBD3, MTA1, and CHD4, of the nucleosome remodeling and deacetylation (NuRD) complex to facilitate Interferon Gamma Receptor 1 (IFNGR1) expression (48, 49). Another study demonstrated that FBXW7 has an intimated relation with chromatin remodeling through whole-exome sequencing of 57 cancers (50). Although the direct relationship between FBXW7 and chromatin remodeling was not demonstrated, we speculate that FBXW7 expression could be inhibited by means of chromatin remodeling. However, more work remains to be done to explore the deeper mechanisms. In this way, the substrate of FBXW7, IFNGR1, showed a trend of increasing expression and further promoted the tumorigenesis and metastasis of cancer (51).

Collectively, epigenetic modification regulates FBXW7 in three ways: methylation and demethylation modification, Histone acetylation and Chromatin remodeling.

3.2.2.4. RNA Epitranscriptomic Modification of FBXW7

A previous research conducted by our team revealed that N6-methyladenosine (m^6A) is involved in the methylated modification of FBW7 mRNA (52). M^6A refers to the methylation of N6-adenosine in eukaryotic mRNA controlled by writers—methyltransferases, erasers—demethylases, and readers—binding proteins, which is a universal modification of mRNA and affects various pathphysiological processes including tumorgensis (53, 54). METTL3 is one of the methyltransferases which methylates m^6A of FBXW7 mRNA and facilitates its translational efficiency to repress lung adenocarcinoma (52). Interestingly, not only is FBXW7 regulated through m^6A, but it also regulates the m^6A of other mRNAs. FBXW7 targets YTHDF2 protein, the m6A reader of BMF mRNA, rescuing the YTHDF2-mediated inactivation of BMF mRNA and repressing the growth and progression of ovarian cancer (55).

3.2.3. Regulation of FBXW7 Mediated by Non-Coding RNA

3.2.3.1. MicroRNA Regulation of FBXW7

Non-coding RNA also functions in regulation of FBXW7. MicroRNA (miRNA) is a kind of non-coding RNA that can suppress the mRNA and intervene the subsequent protein synthesis *via* binding to the 3′UTR. Plenty of miRNAs have been uncovered to bind to the 3′UTR of FBXW7 and inhibit the protein translation. Overexpression of miR-223 plays roles in different situations by the counteraction of FBXW7. MiR-223 functions in gastric cancer for carcinostasis and drug resistance (56, 57), gives rise to physiologic cardiac hypertrophy (58), and protects CRC cells against apoptosis and promotes its proliferation as well (59). Moreover, a KLF5/mi-R27a/FBXW7 axis was reported to enhance migration and invasion of ccRCC when FBXW7 was reduced by mi-R27a (60). Apart from involvement in cancer, downregulation of FBXW7 by miR-322 demonstrates a possible curing method to protect myocardium from ischemia/reperfusion injury. Collectively, there are still other miRNAs, such as miR129 (61), miR-92a-3p (62), miR182 (63), miR-27a-3p (64, 65), miR-212/132 (66), miR-223-3p (67), miR-103a-3p (68), miR-25 (69), miR–25–3p (70), miR-144 (71), miR-101 (72), miR-188-5p (73), and miR-500a-3p (74), functioning discrepantly to mediate different cell phenotypes but *via* the identical mechanism of targeting FBXW7.

3.2.3.2. Long Non-Coding RNA Regulation of FBXW7

Long non-coding RNAs (lncRNAs) are non-coding RNAs with more than 200 nucleotides in length and without the function of coding proteins (75). LncRNAs take part in various biological activities by interplaying with DNAs, RNAs, and proteins (76, 77), which means lncRNAs regulate FBXW7 at different levels directly or indirectly. A lncRNA-associated-feedback loop was explored by Pengfei Zhang et al. demostrated that lncRNA-MIF (c-myc inhibitory factor) functioning as a competing endogenous RNA (ceRNA) for miR586 weakened the suppression of miR-586 on FBXW7 (78). Therefore, the substrate of FBXW7, c-myc, was repressed subsequently as FBXW7 was upregulated by the lncRNA-MIF–associated feedback loop and the aerobic glycolysis and pro-oncogenicity triggered by c-myc was eliminated. As c-myc was repressed by FBXW7, its induction to lncRNA-MIF was attenuated, which in turn results in the reduction of lncRNA-MIF abundance. Moreover, lncRNAs of similar roles served as miRNA "sponges" include MALAT1 (79), CASC2 (80), TINCR (81), MT1JP (82), FER1L4 (83), MIR22HG (84), TTN-AS1 (85), LINC00173 (86), and PADNA (87). Other mechanisms of lncRNAs regulating the expression of FBXW7 are displayed as well. A research carried out by Lianzhi Wu et al. revealed the pathway that FBXW7 directly recruited by MALAT1 contributed to the degradation of CRY2 (88). LncRNA BDNF-AS was capable of recruiting WDR5 to contribute to CpG island methylation of FBXW7, by which FBXW7 was downregulated and the ubiquitination of its substrate VDAC3 was diminished (89a). Another study verified that lncRNA SEMA3B-AS1 integrates with HMGB1, a transcription factor of FBXW7, and then facilitates the expression of FBXW7, resulting in the enhanced ubiquitination-mediated degradation (90). In addition, lncRNA TUG1 facilitates the expression of FBXW7 at protein level instead of mRNA level to destabilize SIRT1, leading to the abrogation of neuronal mitophagy (91).

3.2.3.3. Circular RNA Regulation of FBXW7

Circular RNA (circRNA) is distinguished by its structure of covalently closed loop without polyadenylated tail or 5′ to 3′ polarity (92). Parallel to lncRNAs, most circRNAs regulate FBXW7 as miRNA "sponges". For instance, hsa_circ_11780 (93), circFBXW4 (94), Hsa_circ_001988 (95), circ_CLASP2 (96), circBRAF (97), circ_0000094 (98), hsa_circ_0001306 (99), hsa_circ_0022742 (100), circPSD3 (101), and circKL (102) were confirmed to sponge different miRNAs to impact the expression of FBXW7, respectively. Intriguingly, although the majority of circRNAs are deemed unable to code proteins as non-coding RNAs, a special circRNA associated with FBXW7 has been confirmed the function of coding protein. Circ-FBXW7 was a product of the circulation of cyclization of exons 3 and 4 in the FBXW7 gene that can code a neo-protein named FBXW7-185aa (103, 104). One study revealed that the FBXW7-185aa coded by circ-FBXW7 regulating FBXW7 protein *via* competitively binding to USP28 in glioma (104). Another study discovered two pathways in triple-negative breast cancer to control the expression of FBXW7: One displayed that circ-FBXW7 sponges miR-197-3p to promote the expression of FBXW7. The other demonstrated a similar pathway to that in glioma—FBXW7-185aa competitively binding to USP28 to protect the function of FBXW 7 (103).

In brief, three kinds of non-coding RNAs, including miRNAs, lncRNAs, and circRNAs, regulate the expression of FBXW7 in their own ways. In addition, some miRNAs work synergistically with lncRNAs or circRNAs to fulfill the function together.

3.2.4 Dimerization of FBXW7

Although the protein translation process has been completed, the abundance of FBXW7 can also been influenced. Dimerization is not only a widely phenomenon for all F-box proteins but also a critical regulatory mechanism for FBW7-mediated ubiquitination to substrates as well (105–108). FBXW7

owns three shared domains among all different isoforms as depicted, and the D domain mainly mediates FBXW7′ dimerization (107). Dimerization of FBXW7 may exert the following effects: (1) impacting the location of different isoforms; (2) raising the possibility for several substrates to be regulated by FBXW7; (3) capable of regulating the autoubiquitination of FBXW7; (4) functioning as a buffer to endure mutations that impair the FBXW7 substrate and hinder the substrate degradation mediated by monomeric FBXW7; (5) and increasing ubiquitination rate and processivity (5, 105, 108). However, take the examples of c-myc and cyclin E (108), widely seen as it is, not all substrates ubiquitination need dimerization of FBXW7. Intriguingly, a latest research revealed that LSD1, often regarded as a demethylase of histone, directly bound to FBXW7 to disturb the formation of dimerization to facilitate autoubiquitination rather than activate the demethylation of FBXW7, which might offer a new target for cancer treatment (109).

3.2.5 Phosphorylation of FBXW7

Phosphorylation of FBXW7 also occurs after FBXW7 translation. Activation of ERK1/2 kinase occurs in many drug-resistant tumor cells (110, 111), and FBXW7 is phosphorylated at Thr^{205} and further degraded by UPS (112). The instability of FBXW7 caused by phosphorylation has been verified in many experiments. Mun et al. investigated that Erk1/2 kinase participated in the inhibition of FBXW7 expression in drug-resistant cells (A549-Taxolr cells and T47D-Doxr cells), which led to an increase in heat-shock factor 1 (HSF1) and promoted transcriptional activation of MDR1 (113). This phosphorylation-dependent regulation of FBXW7 by ERK1/2 was also confirmed by other studies. Shu et al. found that ERK1/2-mediated phosphorylation of FBXW7 was involved in transcriptional regulation of FOS-like 1 (Fra-1) by Neuregulin 1 *via* stabilizing downstream c-myc that could bind to the promoter of Fra-1, thereby promoting metastasis of triple negative breast cancer (114). Another example of FBXW7 phosphorylation by ERK kinase at the T^{205} residue was verified likely to affect the ferroptosis of pancreatic carcinoma cells (115). In addition, FBXW7-myc-PLK1 forms a regulatory loop that controlled neuroblastoma tumor progression, in which FBXW7 was phosphorylated at Thr^{284} and Ser^{58} by PLK1 (116). Similar regulatory loop was also discovered in medulloblastoma (117). Phosphorylation of FBXW7 by related kinases not only contributes to the degradation of FBXW7 but also improves the catalytic activity of FBXW7 to downstream substrates. The process of FBXW7 phosphorylation at Ser^{227} mediated by serum and glucocorticoidregulated kinase 1 (SGK1) or Phosphoinositide 3-kinase (PI3K) enhances the ubiquitination ability of FBXW7 (118, 119). Furthermore, phosphorylation of FBXW7α at Ser^{10}/Ser^{18} mediated by protein kinase (PK) C was found both *in vitro* and in mammals, and phosphorylation of Ser^{10} had been validated to affect nuclear localization of FBXW7α (120). Other results had been obtained both in human and Xenopus eggs in regard to PKC phosphorylation of FBXW7 that FBXW7α phosphorylated by PKC at Ser^{18} residues occurred during mitosis, which stabilized FBXW7 itself but interfered with ubiquitination of downstream cyclin E (121).

3.2.6 Autoubiquitination of FBXW7

Not only can FBXW7 degrade its substrates in the ubiquitination dependent way, but it is also competent for its autoubiquitination. It is a universal phenomenon that F-box is ubiquitinated for its necessity to strike the functional balance of SCF complex *via* the autoubiquitination (122, 123). F-box is more apt to be degraded compared with other components in SCF complex for its instability. The process of F-box ubiquitination takes place within the SCF complex itself without the assistance of other F-box proteins as the ubiquitination is required to be complete (124). Ubiquitin binding to FBXW7 was reported to facilitate ubiquitination and degradation of FBXW7, for which was predominant in the competition against the substrates of the FBXW7 (125). Moreover, FBXW7 autoubiquitination is also promoted through its dimerization (105). Another investigation revealed that CSN6 increased neddylation of Cullin-1 to contribute to FBXW7 autoubiquitination as a K48 linkage (126). In contrast, PML promotes FBXW7 expression *via* inhibiting ubiquitination and degradation of FBXW7 in the K48-linked way to enhance antiviral immunoreaction against influenza virus (127).

3.2.7 Biomechanical Regulation of FBXW7

What we have mentioned above are biological pathways to regulate FBXW7 expression. Interestingly, a biomechanical pathway that controls FBXW7 was unveiled recently (128). The investigation conducted by Haiyan Zhang suggested that mechanical overloading downregulated FBXW7 in chondrocyte of patients with osteoarthritis. The critical step that they found contributing to FBXW7 suppression occurred in the synthesis of mRNA. As a result of FBXW7 downregulation, MKK7–JNK pathway was activated and further facilitated the senility of chondrocyte. It offers us a promising curing target on treatment osteoarthritis and a fire-new viewpoint to explore the undiscovered pathways of the regulation of FBXW7.

3.3. The Pattern of FBXW7 Binding to Its Substrates

3.3.1. CPDs of Substrates

Previous studies found that a large proportion of substrates of FBXW7 was unable to bind FBXW7 E3 ligase until the CDC4 phospho-degrons (CPDs) of substrates were phosphorylated by protein kinase (129–131). Optimal sequences refer to CPDs sequences interacting with FBXW7 that contain essential residues. Specifically, there should be at least one hydrophobic amino acid at the sites −5, −3, −2, and −1; it is usually threonine or serine that takes up site zero; the +1 and +2 sites are generally proline; the +4 site may be one of serine, threonine, glutamate, and aspartic acid (7). Only when the 0 and +4 amino acids are phosphorylated by kinases can the substrate be discerned by the WD40 domain and participate in the UPS pathway for degradation. Intriguingly, not all CPDs of substrates follow this rule. CPDs with unfavorable residues of

some proteins partially different from the optimal sequence are called semi-optimal CPDs. However, a portion of substrates CPDs remains undiscovered (7). In addition, some substrates possess more than one CPD sequence. KLF5 was reported to be degraded by FBXW7 with any of three CPDs phosphorylated by GSK-3β, which result in its repressed bio-activity in cell propagation (129). FBXW7 dimerization is likely to play a role in its interaction with the CPDs of protein as it was surveyed that the dimer structure can interact with the two CPDs of cyclin E to enhance the binding ability of cyclin E and promote its ubiquitination degradation (105, 107).

3.3.2. UPS-Dependent Degradation of Substrates

Multifarious substrates of FBXW7 have been previously reported before (7). E3 ligase recognizes the substrates once the CPDs of substrates are phosphorylated and then transfer ubiquitin molecules to the substrates (generally to a lysine side chain) to facilitate the ubiquitination of substrates (132). More than one poly-ubiquitin chain or multiple mono-ubiquitins are required to initiate the degradation (133). When substrates acquire enough ubiquitin chains, they will be captured and cut into peptides in an Adenosine Triphosphate (ATP)-dependent manner by the 26S proteosome (134). The UPS-dependent degradation of substrates mediated by SCF^{FBXW7} is shown in (**Figure 1**).

3.4. Interaction of Deubiquitinating Enzymes and FBXW7

Generally, as proteins are captured by 26S proteosome, deubiquitinating enzymes (DUBs) directly cut off ubiquitin from ubiquitin-binding proteins in various cell bioprocesses (135). Specifically, here, we introduce unusual pathways for DUBs regulating protein. USP28 (one of DUBs) could counteract the effect of FBXW7α degrading myc in the nucleus by forming a special complex with myc and FBW7α (136a; 137). Similarly, USP28 could stabilize HIF-1α by antagonizing FBXW7 rather than interacting with HIF-1α, which impacts the cancer cell activity and capillary formation (138). Analogous mechanism was observed on the regulation of NICD1 and c-jun in intestinal homeostasis and tumorigenesis (139). Interestingly, another study found that partial reduction of USP28 stabilizes FBXW7 and facilitates degradation of its substrates, whereas the absence of USP28 can facilitate FBXW7 ubiquitination, and overexpression of USP28 preferentially counteracts autocatalytic ubiquitination of FBXW7, leading to the increased stability of both FBXW7 and of its substrates simultaneously (140). USP36 is another DUB antagonizing the degradation of c-myc mediated by FBXW7γ to maintain the stability of c-myc in nucleolus (141–143). Moreover, USP9X interacts with FBXW7 and protects it from autoubiquitination, which results in the suppression on substrates of FBXW7 and maintain intestinal homeostasis *via* controlling c-myc and NOTCH1 (144). In short, DUBs not only interact with proteins to cut off ubiquitins but also interact with FBXW7 to influence its function on substrates.

4. FBXW7 IN IMMUNITY

4.1 FBXW7-Mediated Immune Evasion Promotes Carcinogenicity

Both the regulations and degradation functions of FBXW7 have been reviewed above, and we want to further explore whether it is involved in immunity for immunity has a crucial connection with most diseases including cancers. Immunity has an intimated correlation with the health of mammals from birth to death in controlling the equilibrium state of bodies and causing harmful response under unbalanced immune homeostasis. Chances are that immune evasion happens when immunity is suppressed.

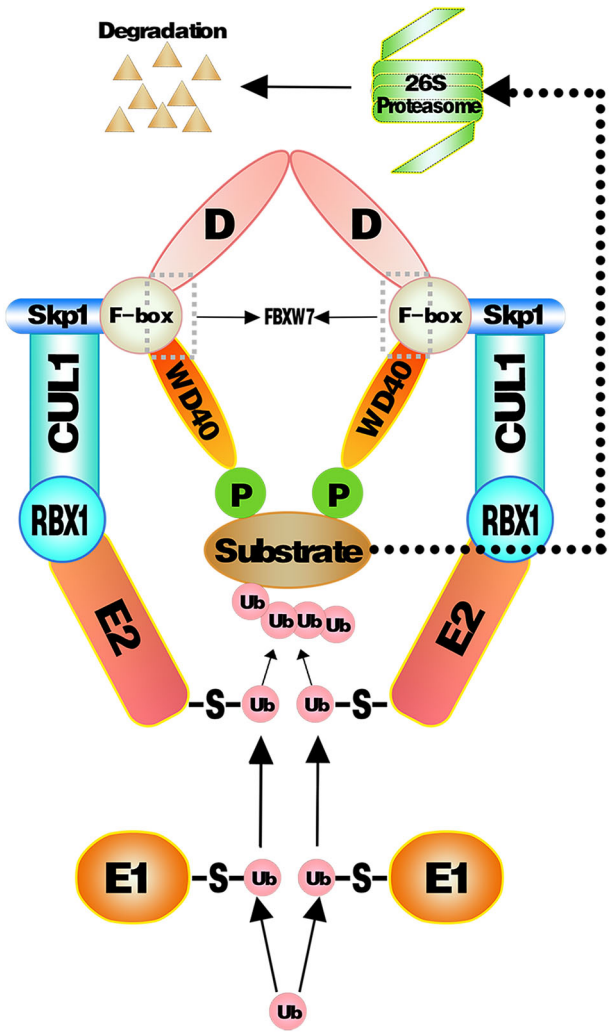

FIGURE 1 | Substrates proteins targeted and ubiquitinated by SCF^{FBXW7} complex. Ubiquitin molecules are activated by E1 and then transferred to E2. E3 recognizes phosphorylated substrates and combined to E2 ubiquitin to transfer ubiquitin from E2 to substrates. As sufficient ubiquitin chains form onto substrates, they will be captured and cut into peptides in an ATP-dependent way by the 26S proteosome.

Studies have demonstrated that FBXW7 is involved in the regulation of immune evasion occurring both in anti-virus and anti-tumor immunoreaction. Porcine epidemic diarrhea virus (PEDV) was found to promote FBXW7 degradation in a UPS-dependent way to attenuate the antiviral reaction (145). Nonstructural protein (nsp2) encoded by PEDV was identified to be the component interplaying with FBXW7 and contributing to degradation of FBXW7 *via* disturbing the stability of retinoic acid-inducible gene I (RIG-I), which results in reduced production of IFN I (145, 146). The involvement of FBXW7 in immune evasion was also reported in cancer cells (15). Eyes absent homolog 2 (EYA2) could be recognized by SCF^{FBXW7} and further accept the final destiny of being degraded. FBXO7, one of the F-box proteins, is capable of binding and stabilizing EYA2 in an SCF-independent way to protect EYA2 against FBXW7-mediated degradation so as to facilitate AXL-mediated immune evasion (15).

As it is known, immune evasion is one of the mechanisms of tumorigenesis. Therefore, FBXW7 might be involved in immunity-related tumorigenesis and immunotherapy resistance.

4.2 FBXW7 Influences the Cancer Progression Through Its Effect on Immune Cells

4.2.1. Macrophages

Macrophages are involved both in innate immune response and adaptive immune response. FBXW7 participates in the polarization of tumor-associated macrophages *via* different pathways (9, 46). The CCAAT/enhancer-binding protein-δ (C/EBPδ, Cebpd), an inflammation related gene regulated by NF-κB and ATF3, functions to amplify innate immune response *via* identifying the status of Toll-like receptor 4 (TLR4)–induced signals (TLR4 could induce the activation of macrophages) (16). FBXW7 was revealed to weaken the inflammatory pathway by targeting C/EBPδ as it was phosphorylated to further negatively regulate TLR4 and its reaction to ligand lipopolysaccharide (LPS) (147). Another research found that MiR-223 downregulated FBXW7 and TLR4 expression in macrophages, which modulated the inflammatory reaction of macrophage to LPS (148). However, when FBXW7 was repressed by estrogen receptor α (Erα) in breast cancer, high expression of C/EBPδ was revealed to attenuate the carcinogenicity of cancer cells through suppressing expression of the SNAI2, which is different from a previous research correlated with the role of C/EBPδ in breast cancer (34, 149). Mice lacking in FBXW7 show improved expression of chemokine C-C Motif Chemokine Ligand 2 (CCL2) in serum, which contributed to the recruitment of macrophages and monocytic myeloid-derived cells and then led to the metastasis of tumor (11). The similar negative relationship between FBXW7 and CCL2 was observed in serum of human later (150). By contrast, the deficiency of FBXW7 in CX3CR1hi macrophages enhanced the abundance of CCL2/CCL7 to induce intestinal inflammation (151). In the study of Zhang et al., FBXW7 inhibited by calcium/calmodulin-dependent protein kinase IV (CaMKIV) promoted the upregulation of mTOR in macrophages, resulting in the LPS-induced autophagy of macrophages subsequently (152). FBXW7 deficiency in myeloid cells promotes the recruitment of monocyte-macrophages in pulmonary tissue, facilitating the collagen deposition induced by bleomycin and finally developing into progressive pulmonary fibrosis (153). Moreover, the suppression of MCL-1 by FBXW7 in M2 macrophages demonstrated an improved apoptosis and repressed EMT phenotype of colon cancer cells (8). Data from timer 2.0 show that the expression of FBXW7 displays a positive correlation with macrophages infiltration level in colon adenocarcinoma (COAD) (**Figure 2**). A metabolism-related pathway of FBXW7 deficiency in myeloid results in the loss of substrate flux *via* pentose phosphate pathway, which causes a decreasing production of equivalents [nicotinamide adenine dinucleotide phosphate (NADPH) and Glutathione (GSH)] and then increases the reactive oxygen species in macrophages to promote the inflammation (154).

4.2.2. NK Cells

EYA2 mentioned above can be degraded by SCF^{FBXW7}-mediated ubiquitination. Downregulation of EYA2 leads to weakened mesenchymal phenotypes, improved immunogenicity of cancer cells, decreased carcinogenicity including tumor growth and metastasis, increased infiltration level of natural killer cells (NK cells), and cytotoxic T cells. As a result, a favorable anti–PD-L1 therapy occurs in mice tumor models (15). The correlation between FBXW7 and NK cells demonstrates a positive interaction for curing tumors. Infiltration level of NK cells basically is positively associated with FBXW7 expression in different cancer (**Figure 3**).

4.2.3. Lymphocytes

FBXW7 is a critical regulator to maintain the quiescence and self-renewal of hematopoietic stem cells (HSCs) *via* regulating four critical genes, including Ccnd1, Evi1, Pbx3, and Meis1, participating in differentiation of HSCs. On regulation of lymphocytes, FBXW7 deficiency of progenitors in bone marrow lose the ability to colonize the thymus, resulting in a significant shortage of T lymphocyte progenitors and an obvious decline of all B lymphocytes, and FBXW7 is considered as a driver gene for CLL ascribe to its mutations and degradation of NOTCH1 (155, 156).

4.2.3.1. B Lymphocytes

B lymphocyte plays an important role in keeping of immunity and immune tolerance (157). FBXW7 is of critical significance to maintain the mature B lymphocytes populations in mice. B-cell receptors (BCRs) stimulation of B cells lead to their apoptosis and stasis of proliferation and growth, owing to FBXW7 deficiency in mice (10). The volume of FBXW7-deficeient B cells is smaller that of normal group after accepting the stimulation of anti-IgM, displaying that FBXW7 matters a lot to BCR-mediated proliferation and survival of B cells (157). On condition that FBXW7 is absent in B cells, Ig class-switching is destroyed, functions of GC (germinal center) including CSR (class switch recombination) and affinity maturation of antibody are badly impaired, and memory antibody response is whittled,

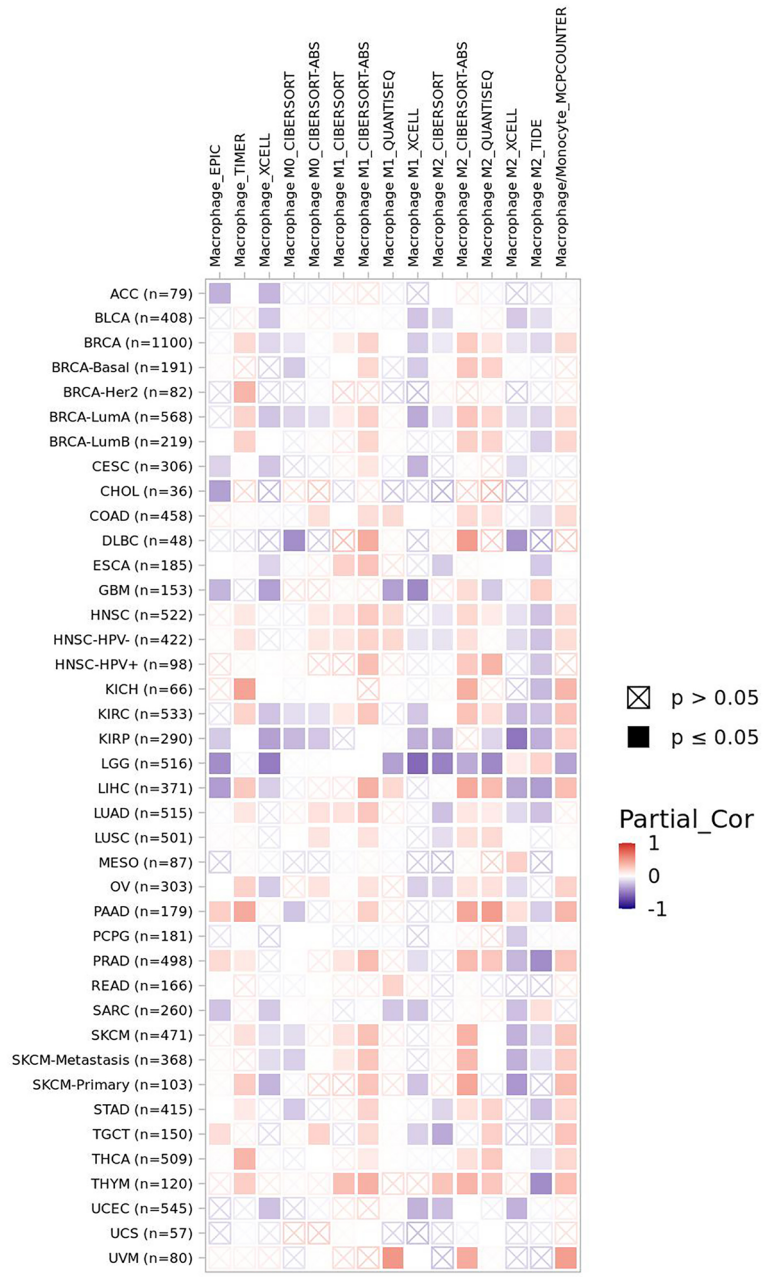

FIGURE 2 | The correlation of FBXW7 expression with macrophages infiltration level in diverse cancer types (data from timer 2.0).

which might be the result of FBXW7 affecting BCL6, a protein of great importance to initiate and maintain the GC reaction (157). As shown in the mice model case of collagen-induced arthritis, a slower disease induction stage, a later disease onset, a lighter disease severity, a lower disease incidence, and a gentler joint destruction occur in FBXW7-deleted mice compared with control group, in accordance with the parallelly decreased anti-CII autoantibodies (157). Collectively, a latent treatment related to FBXW7 to cure GC-connected and autoantibody-induced autoimmune diseases is offered. FBXW7 expression presents a positive correlation of B-cell infiltration level in most cancers (**Figure 4**).

4.2.3.2. T Lymphocytes

FBXW7 deletion in T cells results in enhanced cell proliferation, which expresses both CD4 and CD8 (double-positive, DP); however, the anticipation improvement of single-positive (SP) T cells does not appear as expected, instead DP cells may develop

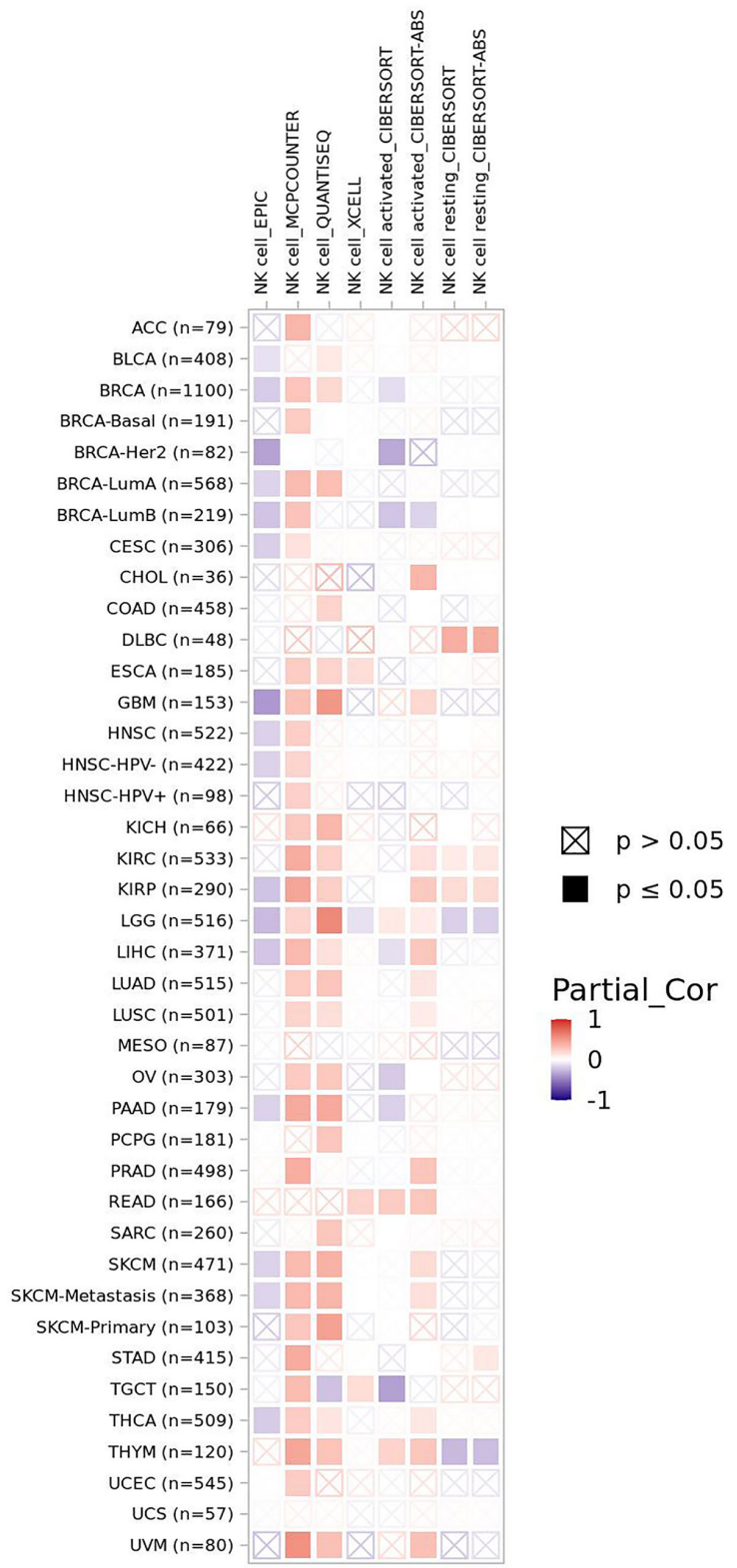

FIGURE 3 | The correlation of FBXW7 expression with NK cells infiltration level in diverse cancer types (data from timer 2.0).

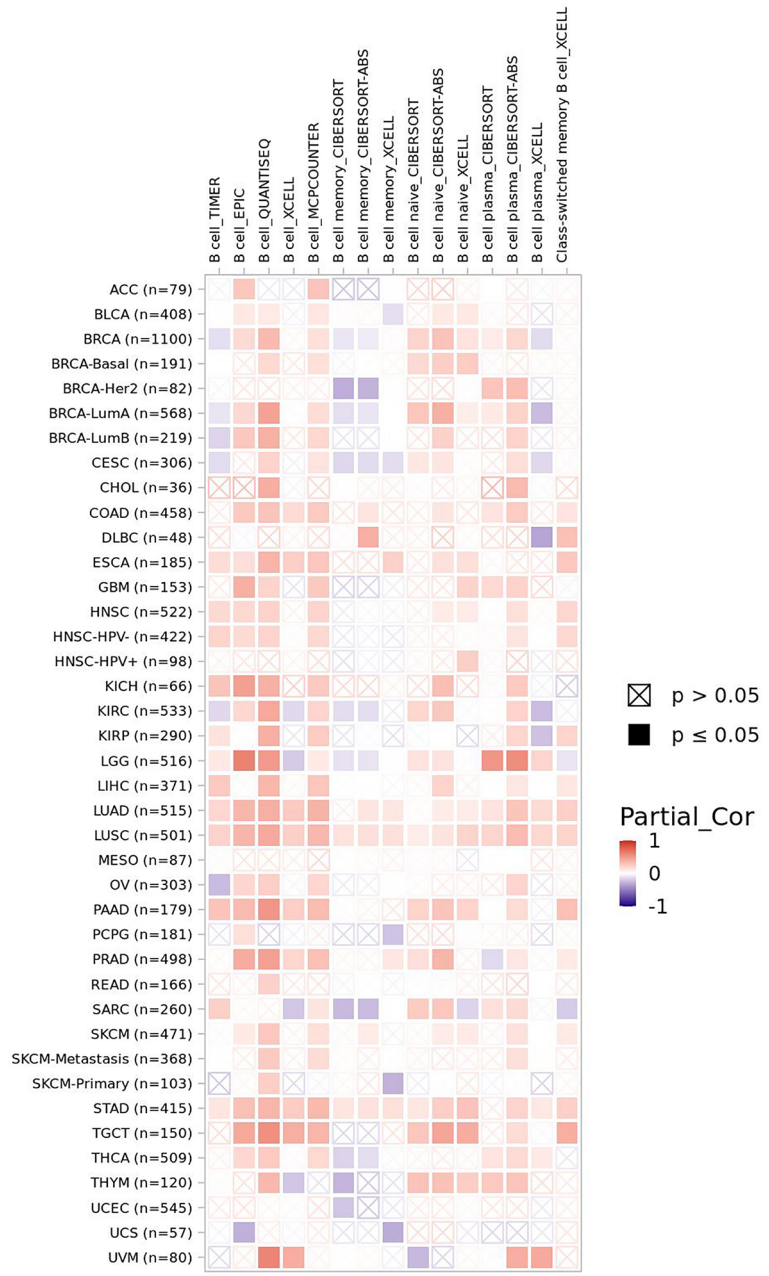

FIGURE 4 | The correlation of FBXW7 expression with B-cell infiltration level in diverse cancer types (data from timer 2.0).

into lymphoma due to uncontrollable cell cycle caused by accumulated c-myc at last (158). It demonstrates that either DP cells are uncapable of performing positive selection or the proliferative and survival ability of SP T cell is injured due to the loss of FBXW7. The former explanation was excluded because positive selection does not take part in cell circle progression, and the latter explanation was remained for it is consistent with the result of experiment. GATA3, a T-cell differentiation regulator, was revealed to be a substrate of FBXW7 taking an effect on the development and differentiation of T cells at the DN (CD4/CD8 double-negative) phase (159). Sox12 is able to promote the degradation of GATA3 mediated by FBXW7 in Th2 cells to inhibit the differentiation of Th2 cells and subsequently weaken allergic inflammation (160). The loss of FBXW7 was also reported to lead to T-ALL (161). NOTCH1/FBXW7 mutation shows a positive correlation with prednisone response against T-ALL (162, 163). The reason patients with FBXW7 mutations demonstrate an incline of prednisone response might lie in the

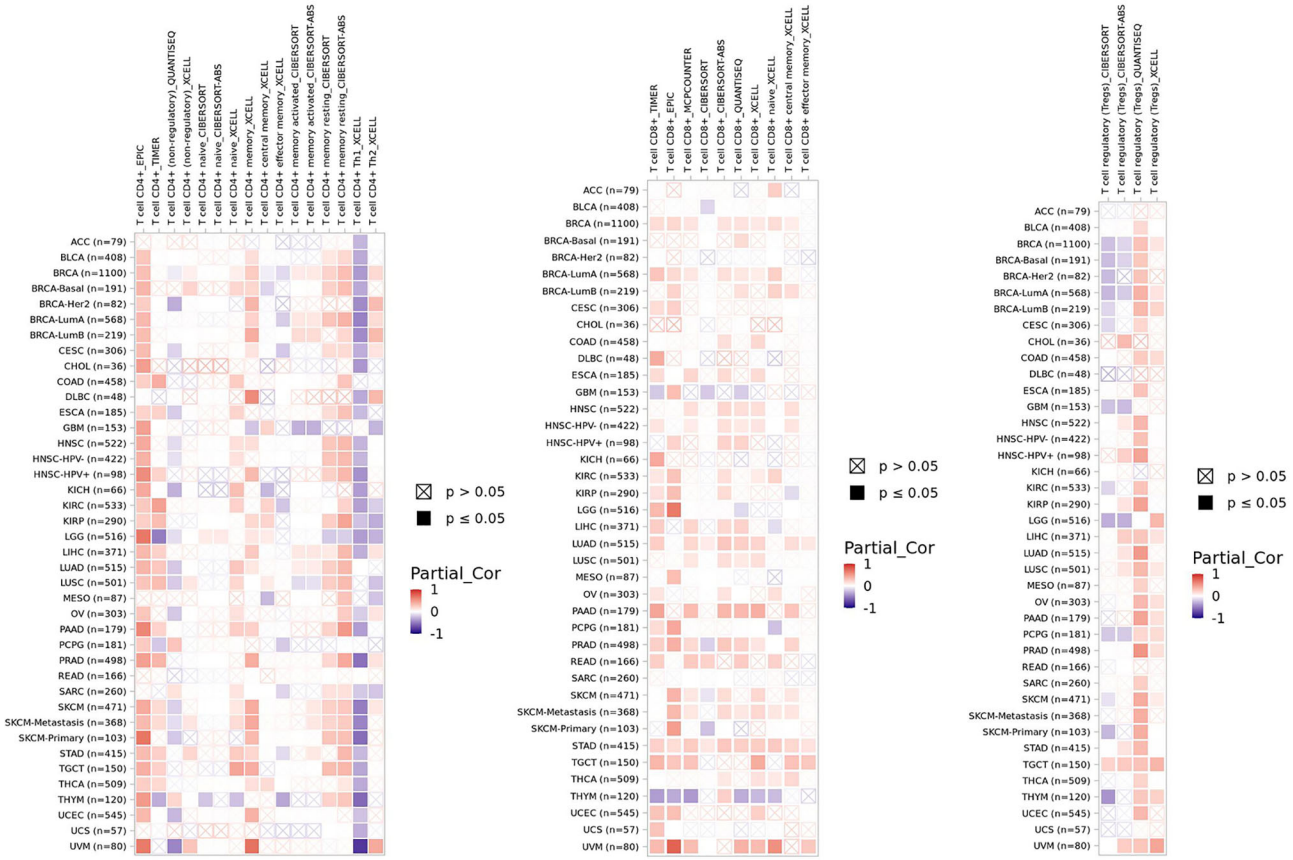

FIGURE 5 | The correlation of FBXW7 expression with $CD4^+$ T cells, $CD8^+$ T cells, and Tregs infiltration level in diverse cancer types (data from timer 2.0).

glucocorticoid receptor α (GRα) serving as one of the targets of FBXW7 (164). All mutations of FBXW7 gene are limited within exons 9 and 10, which are the regions functioning to encode the C-terminal binding site to bind substrates (163). Moreover, enhancer of zeste homolog 2 (EZH2) is reported to activate the expression of T-cell multifunctional cytokines and facilitate its survival owing to inhibiting NUMB and FBXW7 that target NOTCH for degradation (165). Here, we show the correlation of FBXW7 expression with $CD4^+$ T cells, $CD8^+$ T cells, and Tregs infiltration level in multiple cancer types (**Figure 5**).

To summarize, four kinds of immune cells including macrophages, NK cells, B lymphocytes, and T lymphocytes areregulated by FBXW7. Because FBXW7 functions as a regulator of immune cells, we want to figure out how it works in immunotherapy.

4.3. FBXW7 Is Involved in Immunotherapy in Multiple Cancers

4.3.1. Renal Cell Cancer

FBXW7 mutation has been discovered in plentiful human cancers including renal cell cancer (**Figure 6**), and it is one the 10 most frequently mutated genes in metastatic tissues of renal cancer (166). NFAT1 is one of the critical factors of activated T-cell (NFAT) family participating in innate and adaptive immunoreaction (167, 168). NFAT1 improves the expression of PD-L1 by means of boosting TNF abundance in renal cancer to promote the proliferation of renal cancer cells and regulate immunoreaction *via* multiple signaling pathways (169). The expression of PD-L1 regulated by RRM2–ANXA1–AKT axis affects sensitivity to sunitinib and ICIs to cancer cells in renal cell cancer (170). FBXW7 induces the degradation of NFAT1 that is phosphorylated by PI3K/AKT/GSK-3β in a UPS-mediated pathway. Downregulation of the expression of NFAT1 follows with downregulation of PD-L1, which facilitates the tumor cytotoxicity of PD-1 antibodies and infiltration of T lymphocytes (169).

4.3.2 Prostate Cancer

MUC1-C, which could facilitate the expression of IFNGR1 *via* inhibiting FBXW7 expression, drives dedifferentiation of castrate-resistant prostate cancer (CRPC) cell in a chromatin remodeling-dependent way (48). The enhanced stability of IFNGR1 leads to stimulation of the type II interferon-gamma (IFN-γ) inflammatory reaction pathway in prostate carcinomas. In return, the silencing of MUC1-C improves the expression of FBXW7 both at the level of mRNA and proteins. IFN-γ

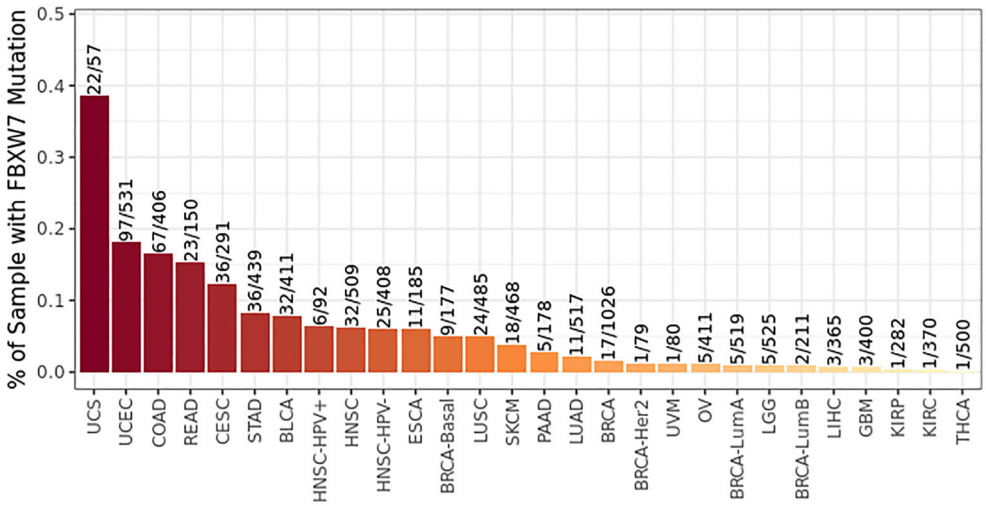

FIGURE 6 | FBXW7 is mutated in multiple cancers (data from timer 2.0).

stimulating the IFNGR1 receptor complex induces the transcription factors including Signal Transducer and Activator of Transcription 1 (STAT1) and Interferon Regulatory Factor 1 (IRF1) to actuate the type II IFN response genes and chronic inflammatory reaction in prostate carcinoma cells (48).

4.3.3 Glioblastoma

As a specific inhibitor for NEDD8-activating enzyme, Pevonedistat (also known as MLN4924) is capable of suppressing the degradation function of FBXW7 E3 ligase and leading to the improved stability of c-myc, a critical transcriptional activation factor of PD-L1 binding to the promoter region of PD-L1 gene (171), to promote the expression of PD-L1 (172). In this way, the killing effect of T cells was weakened *via* PD-L1 improvement. However, the inactivation of the cytotoxic effect of T cells induced by Pevonedistat was rescued by PD-L1 blockade. Then, an interesting phenomenon occurs; the treatment of Glioblastoma acquired a better effect through the integration of pevonedistat and anti–PD-L1 drugs than that of each drug alone. In short, the integration of pevonedistat and anti–PD-L1 drugs offers a novel method to cure glioblastoma.

4.3.4 Breast Cancer

HSF1 phosphorylated by gsk3β and ERK1 at Ser303 and Ser307 is revealed as one of the substrates of FBXW7 (173). Nevertheless, the phosphorylation at another amino acid residue, Thr^{120}, by PIM2 protects it from being degrading by FBXW7 and results in the accumulation of HSF1, which subsequently induces the expression of PD-L1 in breast cancer and enhances growth of breast cancer (174). This may offer a potential target for anti–PD-L1 drugs treatment.

In addition, the investigation by Singh et al. illustrates that E74-like transcription factor 5 (Elf5) facilitates the expression of FBXW7 through binding to the enhancer region of FBXW7 (51). The deficiency of Elf5 downregulates the expression of FBXW7 and confers the accumulation of IFNGR1 as a result of the deleted ubiquitination of IFNGR1 in breast cancer cells. The IFN-γ signaling pathway therewith is promoted *via* the elevation of IFNGR1 abundance, which facilitates the propagation of neutrophils as well as the potential proliferation and metastasis of breast cancer. The abundance of PD-L1 is improved due to elevation of IFNGR1. As anticipated, the carcinogenicity induced by IFNGR1 could be blocked by PD1 and PD-L1 inhibitors.

4.3.5 Colorectal Cancer

Phoaphoinositide 3-kinase γ (PI3Kγ) is an isotype of PI3K that elicits an effect on the regulation of metabolic pathways in inflammation and oncogenicity (175). PI3Kγ expresses lavishly in macrophages but has no expression in cancer cells (176). As discussed above, an axis concerning FBXW7–MCL-1 is associated with the features of macrophages in colorectal cancer, and suppression of PI3Kγ elicits the reversion of cancer progression in a FBXW7–MCL-1–dependent way (8). PI3Kγ alters the function of macrophages between the status of immunological tolerance and immune surveillance by affecting abundance of cytokines (pro-inflammatory factors: IL-1α, IL-1β, CXCL10, IL-8, and IL-12β; anti-inflammatory factors: TGF-β and IL-10) (8). Hence, PI3Kγ of macrophage is likely to fulfill a function for immunotherapy in colon cancer.

4.3.6 Melanoma

FBXW7 mutation functions as a driver to initiate melanoma by activating NOTCH1 (177). In addition, EZH2 improves the abundance of NOTCH *via* suppressing the inhibitors (NUMB and FBXW7) of NOTCH to attenuate the activation of Bcl-2 and to weaken the polyfunctionality and survival of effector T cells (165). Gstalder et al. found that dysfunction of FBXW7 caused by mutation has a correlation with the resistance to pembrolizumab in melanoma patients (178). To uncover the sealed mechanism,

they constructed a FBXW7 deficiency melanoma model in mice and obtained similar consequence as patients. Absence of FBXW7 remolds tumor immune microenvironment into an inclination of weaker response to anti-virus and anti-tumors by means of decreasing IFN-γ–related genes, which are with respect to type I interferon stimulation or viral sensing and the amount of multiple immune cells in tumors. In contrast, the presence of FBXW7 maintaining the stability of Rig-I and melanoma differentiation-associated protein 5 (Mda5) facilitates the dsRNA sensing to further enhance interferon pathway and then boost the sensitivity of anti–PD-1 against tumors. Moreover, the viral sensing pathway could be restored by overexpressing mitochondrial antiviral-signaling protein (Mavs) or interferon regulatory factor 1 (Irf1). Nevertheless, the only fly in the ointment is that the mechanism of FBXW7 affecting Rig-1 and Mda5 still needs further exploration.

4.3.7 Lung Cancer

FBXW7 mutation is associated with unfavorable response to patients with Lung Squamous Cell Carcinoma (LUSC) treated with adjuvant therapy (179), which is conversed to its effects in chemotherapy as a tumor suppression gene. Zhong et al. revealed an evident augment of M2-like TAM and aggressive tumor progression *via* inoculating subcutaneously with Lewis lung cancer cells (LLCs) into mice without myeloid FBXW7 (9). The mechanisms that M2-like TAMs facilitate the propagation and metastasis of LLCs may be as follows. FBXW7 induces degradation of c-myc in a UPS-dependent pathway at the post-translational level. Consequently, the deficiency of FBXW7 results in the accumulation of c-myc, which ulteriorly improves the expression of M2-related genes both at the level of mRNA and proteins. Then, the polarization of M2 macrophages occurs and polarized M2 macrophages facilitate the expression of pro-tumor factors to motivate the progression of LLCs. In this way, chances are that novel targets for tumor immunotherapy are found out. In comparison, a clinical research (180) of non–small cell lung cancer unveiled that patients with mutation of FBXW7 profit more from immunotherapy than those of without mutations, which might be on account of improved infiltration level of M1 macrophages and CD8 T cells as well as the enhanced immunogenicity associated with FBXW7 mutation.

4.3.8 Hematological Malignancies

T-cell receptor (TCR) gene therapy serves as an unconventional immunotherapy that isolates TCR genes from antigen-specific T lymphocytes and then transfer TCR gene into T lymphocytes of patients to amplify abundant antigen-specific lymphocytes (181). Then, antigen-specific lymphocytes are adoptively transferred into patients to exert the function of anti-tumor. As mentioned, FBXW7 is often mutated in hematological malignancies. The mutation of FBXW7 is used to isolate CD8 T cells from healthy donor. CD8 T cells specific for an HLA-A*11:01–presented mutant FBXW7(mFBXW7) peptide were triumphantly isolated, which are capable of recognizing targeting cells edited to express mFBXW7. The recurrent mutation of pR465H in FBXW7 was found to encode an HLA-A*11:01–presented neoepitope, which could be applied into the treatment of hematological malignancies *via* TCR gene therapy.

4.3.9 Coronavirus Disease 2019

Coronavirus disease 2019 (COVID-19), which is caused by severe acute respiratory syndrome coronavirus 2 (SARS-CoV-2), is still a severe ongoing contagious disease causing thousands of millions of deaths worldwide. In human lung cells, RIG-I suppresses the replication of SARS-CoV-2 without the participation of type I/III IFN (182). The 3′UTR of viral RNA is recognized by RIG-I *via* its helicase domains rather than the C-terminal domain. FBW7 is capable of maintaining the stability of RIG-I (178). Therefore, it is possible that FBW7 is capable of interfering with the viral RNA synthesis in the early stage of SARS-CoV-2 invasion *via* stabling RIG-I. Moreover, the expression of PD-1and PD-L1 was reported to increase in patients with severe COVID-19 (183). The abundance of PD-1 demonstrates a closed correlation with the severity of the disease (184). It is rational that ICIs could serve as a promising treatment against COVID-19 in this way. However, patients treating with PD-1/PD-L1 blockade show neither advantages nor disadvantages to their recovery (183).

4.3.10 Others

Furthermore, the mutation of FBXW7 is reported to be associated with immunotherapy resistance in endometrial and pancreatic cancer (185) (details are unknown).

All in all, FBXW7 functions discrepantly in immunotherapy of different cancers. However, it fails to work in COVID-19. More work should be done to investigate the function of FBXW7 in various cancers for so many proteins can be ubiquitinated by SCF^{FBXW7}.

5. CONCLUSION

In general, FBXW7 functions as a suppressor of tumor by means of promoting the degradation of proteins correlated with carcinogenicity, such as c-myc, cyclin E, NOTCH1, and HIF1α (186–191). The mechanism of FBXW7 recognizing proteins and inducing the UPS-dependent degradation has been almost elucidated. Therefore, here, we lay emphasis on its own regulation by various pathways, such as epigenetic regulation, miRNA, circRNA, lncRNA, dimerization, phosphorylation, and autoubiquitination to offer neo-targets for exploring the novel methods of cancer or other diseases treatment *via* regulating the expression of FBXW7. Moreover, previous studies have attached more importance to the effect of FBXW7 on carcinostasis and chemoradiotherapy (64, 117, 192–194) and targeted therapies (195–197), whereas its influence on immunotherapy is ignored to a certain extent. In consequence, we summarize the role of FBXW7 principally in immune cells and in immunotherapy. Here, we demonstrate the relative substrates of FBXW7 functioning in immunity in different cancers (**Figure 7**). In accordance with its role as tumor suppressor, mutation or downregulation of FBXW7 is more likely to contribute to

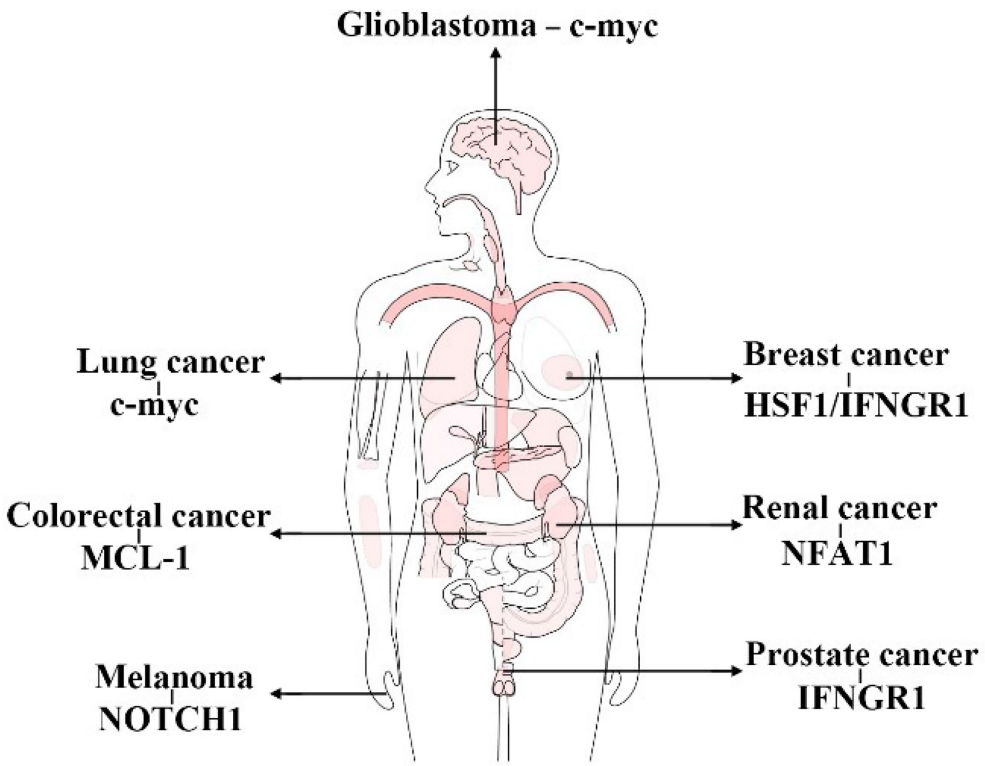

FIGURE 7 | Substrates of FBXW7 functioning in immunity in different cancers. (This figure takes GEPIA as a template).

resistance of immunotherapy rather than the opposite. Nevertheless, increasing efforts still need to be taken in unveiling the mysterious regulations, such as how FBXW7 regulating Rig-1 and Mda5 (178). In summary, FBXW7 could be utilized as a target to improve the sensitivity of immunotherapy or that with the combination of other treatment to benefit patients suffering from cancers.

AUTHOR CONTRIBUTIONS

JZ and FZ designed this review. YZ and Yinggang Che searched the references. LLX and LX wrote the manuscript. MW and DQ revised the manuscript. YS and HY drew the figures. All authors contributed to the article and approved the submitted version.

FUNDING

This work was supported by National Natural Science Foundation of China (81773153).

ACKNOWLEDGMENTS

The authors would like to thank all the researchers of references cited in this review.

REFERENCES

1. Nakajima T, Morita K, Ohi N, Arai T, Nozaki N, Kikuchi A, et al. Degradation of Topoisomerase IIalpha During Adenovirus E1A-Induced Apoptosis is Mediated by the Activation of the Ubiquitin Proteolysis System. *J Biol Chem* (1996) 271(40):24842–9. doi: 10.1074/jbc.271.40.24842
2. Hochstrasser M. Ubiquitin, Proteasomes, and the Regulation of Intracellular Protein Degradation. *Curr Opin Cell Biol* (1995) 7(2):215–23. doi: 10.1016/0955-0674(95)80031-x
3. Díaz VM, de Herreros AG. F-Box Proteins: Keeping the Epithelial-to-Mesenchymal Transition (EMT) in Check. Semin. *Cancer Biol* (2016) 36:71–9. doi: 10.1016/j.semcancer.2015.10.003
4. Zheng N, Zhou Q, Wang Z, Wei W. Recent Advances in SCF Ubiquitin Ligase Complex: Clinical Implications. *Biochim Biophys Acta* (2016) 1866(1):12–22. doi: 10.1016/j.bbcan.2016.05.001
5. Hao B, Oehlmann S, Sowa ME, Harper JW, Pavletich NP. Structure of a Fbw7-Skp1-Cyclin E Complex: Multisite-Phosphorylated Substrate Recognition by SCF Ubiquitin Ligases. *Mol Cell* (2007) 26(1):131–43. doi: 10.1016/j.molcel.2007.02.022
6. Yeh CH, Bellon M, Nicot C. FBXW7: A Critical Tumor Suppressor of Human Cancers. *Mol Cancer* (2018) 17(1):115. doi: 10.1186/s12943-018-0857-2
7. Yumimoto K, Nakayama KI. Recent Insight Into the Role of FBXW7 as a Tumor Suppressor. Semin. *Cancer Biol* (2020) 67(Pt 2):1–15. doi: 10.1016/j.semcancer.2020.02.017

8. Lee YS, Song SJ, Hong HK, Oh BY, Lee WY, Cho YB. The FBW7-MCL-1 Axis is Key in M1 and M2 Macrophage-Related Colon Cancer Cell Progression: Validating the Immunotherapeutic Value of Targeting PI3Kγ. *Exp Mol Med* (2020) 52(5):815–31. doi: 10.1038/s12276-020-0436-7
9. Zhong L, Zhang Y, Li M, Song Y, Liu D, Yang X, et al. E3 Ligase FBXW7 Restricts M2-Like Tumor-Associated Macrophage Polarization by Targeting C-Myc. *Aging (Albany NY)* (2020) 12(23):24394–423. doi: 10.18632/aging.202293
10. Ramezani-Rad P, Leung CR, Apgar JR, Rickert RC. E3 Ubiquitin Ligase Fbw7 Regulates the Survival of Mature B Cells. *J Immunol (Baltimore Md 1950)* (2020) 204(6):1535–42. doi: 10.4049/jimmunol.1901156
11. Yumimoto K, Akiyoshi S, Ueo H, Sagara Y, Onoyama I, Ueo H, et al. F-Box Protein FBXW7 Inhibits Cancer Metastasis in a non-Cell-Autonomous Manner. *J Clin Invest* (2015) 125(2):621–35. doi: 10.1172/JCI78782
12. Dunn GP, Bruce AT, Ikeda H, Old LJ, Schreiber RD. Cancer Immunoediting: From Immunosurveillance to Tumor Escape. *Nat Immunol* (2002) 3(11):991–8. doi: 10.1038/ni1102-991
13. Varadé J, Magadán S, González-Fernández Á. Human Immunology and Immunotherapy: Main Achievements and Challenges. *Cell Mol Immunol* (2021) 18(4):805–28. doi: 10.1038/s41423-020-00530-6
14. Chen DS, Mellman I. Elements of Cancer Immunity and the Cancer–Immune Set Point. *Nature* (2017) 541(7637):321–30. doi: 10.1038/nature21349
15. Shen JZ, Qiu Z, Wu Q, Zhang G, Harris R, Sun D, et al. A FBXO7/EYA2-SCFFBXW7 Axis Promotes AXL-Mediated Maintenance of Mesenchymal and Immune Evasion Phenotypes of Cancer Cells. *Mol Cell* (2022) 82 (6):1123–1139.e8. doi: 10.1016/j.molcel.2022.01.022
16. Litvak V, Ramsey SA, Rust AG, Zak DE, Kennedy KA, Lampano AE, et al. Function of C/EBPdelta in a Regulatory Circuit That Discriminates Between Transient and Persistent TLR4-Induced Signals. *Nat Immunol* (2009) 10 (4):437–43. doi: 10.1038/ni.1721
17. Craig KL, Tyers M. The F-Box: A New Motif for Ubiquitin Dependent Proteolysis in Cell Cycle Regulation and Signal Transduction. *Prog Biophys Mol Biol* (1999) 72(3):299–328. doi: 10.1016/s0079-6107(99)00010-3
18. Krek W. Proteolysis and the G1-S Transition: The SCF Connection. *Curr Opin Genet Dev* (1998) 8(1):36–42. doi: 10.1016/s0959-437x(98)80059-2
19. Skowyra D, Craig KL, Tyers M, Elledge SJ, Harper JW. F-Box Proteins are Receptors That Recruit Phosphorylated Substrates to the SCF Ubiquitin-Ligase Complex. *Cell* (1997) 91(2):209–19. doi: 10.1016/s0092-8674(00)80403-1
20. Zheng N, Schulman BA, Song L, Miller JJ, Jeffrey PD, Wang P, et al. Structure of the Cul1–Rbx1–Skp1–F Boxskp2 SCF Ubiquitin Ligase Complex. *Nature* (2002) 416(6882):703–9. doi: 10.1038/416703a
21. Bai C, Sen P, Hofmann K, Ma L, Goebl M, Harper JW, et al. SKP1 Connects Cell Cycle Regulators to the Ubiquitin Proteolysis Machinery Through a Novel Motif, the F-Box. *Cell* (1996) 86(2):263–74. doi: 10.1016/s0092-8674 (00)80098-7
22. Wang Z, Liu P, Inuzuka H, Wei W. Roles of F-Box Proteins in Cancer. *Nat Rev Cancer* (2014) 14(4):233–47. doi: 10.1038/nrc3700
23. Jin J, Cardozo T, Lovering RC, Elledge SJ, Pagano M, Harper JW. Systematic Analysis and Nomenclature of Mammalian F-Box Proteins. *Genes Dev* (2004) 18(21):2573–80. doi: 10.1101/gad.1255304
24. Kipreos ET, Pagano M. The F-Box Protein Family. *Genome Biol* (2000) 1(5): REVIEWS3002–REVIEWS3002. doi: 10.1186/gb-2000-1-5-reviews3002
25. Hartwell LH, Culotti J, Reid B. Genetic Control of the Cell-Division Cycle in Yeast. I. Detection of Mutants. *Proc Natl Acad Sci U.S.A.* (1970) 66(2):352–9. doi: 10.1073/pnas.66.2.352
26. Gupta-Rossi N, Le Bail O, Gonen H, Brou C, Logeat F, Six E, et al. Functional Interaction Between SEL-10, an F-Box Protein, and the Nuclear Form of Activated Notch1 Receptor*. *J Biol Chem* (2001) 276(37):34371–8. doi: 10.1074/jbc.M101343200
27. Wu G, Lyapina S, Das I, Li J, Gurney M, Pauley A, et al. SEL-10 is an Inhibitor of Notch Signaling That Targets Notch for Ubiquitin-Mediated Protein Degradation. *Mol Cell Biol* (2001) 21(21):7403–15. doi: 10.1128/MCB.21.21.7403-7415.2001
28. öberg C, Li J, Pauley A, Wolf E, Gurney M, Lendahl U. The Notch Intracellular Domain Is Ubiquitinated and Negatively Regulated by the Mammalian Sel-10 Homolog*. *J Biol Chem* (2001) 276(38):35847–53. doi: 10.1074/jbc.M103992200
29. Spruck CH, Strohmaier H, Sangfelt O, Müller HM, Hubalek M, Müller-Holzner E, et al. Hcdc4 Gene Mutations in Endometrial Cancer[1]. *Cancer Res* (2002) 62(16):4535–9.
30. Welcker M, Orian A, Grim JA, Eisenman RN, Clurman BE. A Nucleolar Isoform of the Fbw7 Ubiquitin Ligase Regulates C-Myc and Cell Size. *Curr Biol* (2004) 14(20):1852–7. doi: 10.1016/j.cub.2004.09.083
31. Matsumoto A, Onoyama I, Nakayama KI. Expression of Mouse Fbxw7 Isoforms is Regulated in a Cell Cycle- or P53-Dependent Manner. *Biochem Bioph Res Co* (2006) 350(1):114–9. doi: 10.1016/j.bbrc.2006.09.003
32. Hou J, Liu Y, Huang P, Wang Y, Pei D, Tan R, et al. RANBP10 Promotes Glioblastoma Progression by Regulating the FBXW7/c-Myc Pathway. *Cell Death Dis* (2021) 12(11):967–7. doi: 10.1038/s41419-021-04207-4
33. Liu R, Gao J, Yang Y, Qiu R, Zheng Y, Huang W, et al. PHD Finger Protein 1 (PHF1) is a Novel Reader for Histone H4R3 Symmetric Dimethylation and Coordinates With PRMT5-WDR77/CRL4B Complex to Promote Tumorigenesis. *Nucleic Acids Res* (2018) 46(13):6608–26. doi: 10.1093/nar/gky461
34. Balamurugan K, Wang J, Tsai H, Sharan S, Anver M, Leighty R, et al. The Tumour Suppressor C/Ebpδ Inhibits FBXW7 Expression and Promotes Mammary Tumour Metastasis. *EMBO J* (2010) 29(24):4106–17. doi: 10.1038/emboj.2010.280
35. Sancho R, Blake SM, Tendeng C, Clurman BE, Lewis J, Behrens A. Fbw7 Repression by Hes5 Creates a Feedback Loop That Modulates Notch-Mediated Intestinal and Neural Stem Cell Fate Decisions. *PloS Biol* (2013) 11(6):e1001586–e1001586. doi: 10.1371/journal.pbio.1001586
36. Chen L, Hu B, Han Z, Liu W, Zhu J, Chen X, et al. Repression of FBXW7 by HES5 Contributes to Inactivation of the TGF-β Signaling Pathway and Alleviation of Endometriosis. *FASEB J* (2021) 35(2):e20938. doi: 10.1096/fj.202000438RRR
37. Zhang G, Zhu Q, Fu G, Hou J, Hu X, Cao J, et al. TRIP13 Promotes the Cell Proliferation, Migration and Invasion of Glioblastoma Through the FBXW7/c-MYC Axis. *Br J Cancer* (2019) 121(12):1069–78. doi: 10.1038/s41416-019-0633-0
38. Kimura T, Gotoh M, Nakamura Y, Arakawa H. Hcdc4b, a Regulator of Cyclin E, as a Direct Transcriptional Target of P53. *Cancer Sci* (2003) 94(5):431–6. doi: 10.1111/j.1349-7006.2003.tb01460.x
39. Akhoondi S, Lindström L, Widschwendter M, Corcoran M, Bergh J, Spruck C, et al. Inactivation of FBXW7/hCDC4-β Expression by Promoter Hypermethylation is Associated With Favorable Prognosis in Primary Breast Cancer. *Breast Cancer Res* (2010) 12(6):R105. doi: 10.1186/bcr2788
40. Gu Z, Inomata K, Mitsui H, Horii A. Promoter Hypermethylation is Not the Major Mechanism for Inactivation of the FBXW7 Beta-Form in Human Gliomas. *Genes Genet Syst* (2008) 83(4):347–52. doi: 10.1266/ggs.83.347
41. Gu Z, Mitsui H, Inomata K, Honda M, Endo C, Sakurada A, et al. The Methylation Status of FBXW7 Beta-Form Correlates With Histological Subtype in Human Thymoma. *Biochem Biophys Res Commun* (2008) 377 (2):685–8. doi: 10.1016/j.bbrc.2008.10.047
42. Kitade S, Onoyama I, Kobayashi H, Yagi H, Yoshida S, Kato M, et al. FBXW7 is Involved in the Acquisition of the Malignant Phenotype in Epithelial Ovarian Tumors. *Cancer Sci* (2016) 107(10):1399–405. doi: 10.1111/cas.13026
43. Lu X, Jiang L, Zhang L, Zhu Y, Hu W, Wang J, et al. Immune Signature-Based Subtypes of Cervical Squamous Cell Carcinoma Tightly Associated With Human Papillomavirus Type 16 Expression, Molecular Features, and Clinical Outcome. *Neoplasia* (2019) 21(6):591–601. doi: 10.1016/j.neo.2019.04.003
44. Chen B, Chen H, Lu S, Zhu X, Que Y, Zhang Y, et al. KDM5B Promotes Tumorigenesis of Ewing Sarcoma *via* FBXW7/CCNE1 Axis. *Cell Death Dis* (2022) 13(4):354. doi: 10.1038/s41419-022-04800-1
45. Kim MJ, Chen G, Sica GL, Deng X. Epigenetic Modulation of FBW7/Mcl-1 Pathway for Lung Cancer Therapy. *Cancer Biol Ther* (2021) 22(1):55–65. doi: 10.1080/15384047.2020.1856756
46. Huang YH, Cai K, Xu PP, Wang L, Huang CX, Fang Y, et al. CREBBP/EP300 Mutations Promoted Tumor Progression in Diffuse Large B-Cell Lymphoma Through Altering Tumor-Associated Macrophage Polarization *via* FBXW7-NOTCH-CCL2/CSF1 Axis. *Signal Transd Target Ther* (2021) 6(1):10. doi: 10.1038/s41392-020-00437-8
47. Lin H, Ma N, Zhao L, Yang G, Cao B. KDM5c Promotes Colon Cancer Cell Proliferation Through the FBXW7-C-Jun Regulatory Axis. *Front Oncol* (2020) 10:535449. doi: 10.3389/fonc.2020.535449
48. Hagiwara M, Fushimi A, Bhattacharya A, Yamashita N, Morimoto Y, Oya M, et al. MUC1-C Integrates Type II Interferon and Chromatin Remodeling Pathways in Immunosuppression of Prostate Cancer. *Oncoimmunology* (2022) 11(1):2029298–2029298. doi: 10.1080/2162402X.2022.2029298

49. Hata T, Rajabi H, Takahashi H, Yasumizu Y, Li W, Jin C, et al. MUC1-C Activates the NuRD Complex to Drive Dedifferentiation of Triple-Negative Breast Cancer Cells. *Cancer Res* (2019) 79(22):5711–22. doi: 10.1158/0008-5472.CAN-19-1034
50. Zhao S, Choi M, Overton JD, Bellone S, Roque DM, Cocco E, et al. Landscape of Somatic Single-Nucleotide and Copy-Number Mutations in Uterine Serous Carcinoma. *P Natl Acad Sci USA* (2013) 110(8):2916–21. doi: 10.1073/pnas.1222577110
51. Singh S, Kumar S, Srivastava RK, Nandi A, Thacker G, Murali H, et al. Loss of ELF5-FBXW7 Stabilizes IFNGR1 to Promote the Growth and Metastasis of Triple-Negative Breast Cancer Through Interferon-γ Signalling. *Nat Cell Biol* (2020) 22(5):591–602. doi: 10.1038/s41556-020-0495-y
52. Wu Y, Chang N, Zhang Y, Zhang X, Xu L, Che Y, et al. METTL3-Mediated M (6)A mRNA Modification of FBXW7 Suppresses Lung Adenocarcinoma. *J Exp Clin Cancer Res* (2021) 40(1):90. doi: 10.1186/s13046-021-01880-3
53. Chong W, Shang L, Liu J, Fang Z, Du F, Wu H, et al. M(6)A Regulator-Based Methylation Modification Patterns Characterized by Distinct Tumor Microenvironment Immune Profiles in Colon Cancer. *Theranostics* (2021) 11(5):2201–17. doi: 10.7150/thno.52717
54. Bokar JA, Shambaugh ME, Polayes D, Matera AG, Rottman FM. Purification and cDNA Cloning of the AdoMet-Binding Subunit of the Human mRNA (N6-Adenosine)-Methyltransferase. *RNA* (1997) 3(11):1233–47.
55. Xu F, Li J, Ni M, Cheng J, Zhao H, Wang S, et al. FBW7 Suppresses Ovarian Cancer Development by Targeting the N(6)-Methyladenosine Binding Protein YTHDF2. *Mol Cancer* (2021) 20(1):45. doi: 10.1186/s12943-021-01340-8
56. Gao H, Ma J, Cheng Y, Zheng P. Exosomal Transfer of Macrophage-Derived miR-223 Confers Doxorubicin Resistance in Gastric Cancer. *Onco Targets Ther* (2020) 13:12169–79. doi: 10.2147/OTT.S283542
57. Li J, Guo Y, Liang X, Sun M, Wang G, De W, et al. MicroRNA-223 Functions as an Oncogene in Human Gastric Cancer by Targeting FBXW7/Hcdc4. *J Cancer Res Clin Oncol* (2012) 138(5):763–74. doi: 10.1007/s00432-012-1154-x
58. Yang L, Li Y, Wang X, Mu X, Qin D, Huang W, et al. Overexpression of miR-223 Tips the Balance of Pro- and Anti-Hypertrophic Signaling Cascades Toward Physiologic Cardiac Hypertrophy. *J Biol Chem* (2016) 291(30):15700–13. doi: 10.1074/jbc.M116.715805
59. Liu L, Tao T, Liu S, Yang X, Chen X, Liang J, et al. An RFC4/Notch1 Signaling Feedback Loop Promotes NSCLC Metastasis and Stemness. *Nat Commun* (2021) 12(1):2693–3. doi: 10.1038/s41467-021-22971-x
60. Liu Z, Liu X, Liu S, Cao Q. Cholesterol Promotes the Migration and Invasion of Renal Carcinoma Cells by Regulating the KLF5/miR-27a/FBXW7 Pathway. *Biochem Biophys Res Commun* (2018) 502(1):69–75. doi: 10.1016/j.bbrc.2018.05.122
61. Meng Q, Wu W, Pei T, Xue J, Xiao P, Sun L, et al. miRNA-129/FBW7/NF-κb, a Novel Regulatory Pathway in Inflammatory Bowel Disease. *Mol Ther Nucleic Acids* (2020) 19:731–40. doi: 10.1016/j.omtn.2019.10.048
62. Zeng R, Huang J, Sun Y, Luo J. Cell Proliferation is Induced in Renal Cell Carcinoma Through miR-92a-3p Upregulation by Targeting FBXW7. *Oncol Lett* (2020) 19(4):3258–68. doi: 10.3892/ol.2020.11443
63. Liu S, Liu H, Deng M, Wang H. MiR-182 Promotes Glioma Progression by Targeting FBXW7. *J Neurol Sci* (2020) 411:116689. doi: 10.1016/j.jns.2020.116689
64. Lu B, Feng Z, Fan B, Shi Y. Blocking miR-27a-3p Sensitises Taxol Resistant Osteosarcoma Cells Through Targeting Fbxw7. *Bull Cancer* (2021) 108 (6):596–604. doi: 10.1016/j.bulcan.2021.01.006
65. Ben W, Zhang G, Huang Y, Sun Y. MiR-27a-3p Regulated the Aggressive Phenotypes of Cervical Cancer by Targeting Fbxw7. *Cancer Manag Res* (2020) 12:2925–35. doi: 10.2147/CMAR.S234897
66. Bai C, Ren Q, Liu H, Li X, Guan W, Gao Y. miR-212/132-Enriched Extracellular Vesicles Promote Differentiation of Induced Pluripotent Stem Cells Into Pancreatic Beta Cells. *Front Cell Dev Biol* (2021) 9:673231. doi: 10.3389/fcell.2021.673231
67. Wang Y, Shi S, Wang Y, Zhang X, Liu X, Li J, et al. miR-223-3p Targets FBXW7 to Promote Epithelial-Mesenchymal Transition and Metastasis In Breast Cancer. *Thorac Cancer* (2022) 13(3):474–82. doi: 10.1111/1759-7714.14284
68. Ren L, Yang J, Meng X, Zhang J, Zhang Y. The Promotional Effect of microRNA-103a-3p in Cervical Cancer Cells by Regulating The Ubiquitin Ligase FBXW7 Function. *Hum Cell* (2022) 35(2):472–85. doi: 10.1007/s13577-021-00649-2
69. Feng X, Zou B, Nan T, Zheng X, Zheng L, Lan J, et al. MiR-25 Enhances Autophagy and Promotes Sorafenib Resistance of Hepatocellular Carcinoma *via* Targeting FBXW7. *Int J Med Sci* (2022) 19(2):257–66. doi: 10.7150/ijms.67352
70. Wang J, Li T, Wang B. Exosomal Transfer of Mir−25–3p Promotes the Proliferation and Temozolomide Resistance of Glioblastoma Cells by Targeting FBXW7. *Int J Oncol* (2021) 59(2):64. doi: 10.3892/ijo.2021.5244
71. Tian X, Liu Y, Wang Z, Wu S. miR-144 Delivered by Nasopharyngeal Carcinoma-Derived EVs Stimulates Angiogenesis Through the FBXW7/HIF-1α/VEGF-A Axis. *Mol Ther Nucleic Acids* (2021) 24:1000–11. doi: 10.1016/j.omtn.2021.03.016
72. Li Y, Wang J, Ma Y, Du W, Feng K, Wang S. miR-101-Loaded Exosomes Secreted by Bone Marrow Mesenchymal Stem Cells Requires the FBXW7/HIF1α/FOXP3 Axis, Facilitating Osteogenic Differentiation. *J Cell Physiol* (2021) 236(6):4258–72. doi: 10.1002/jcp.30027
73. Yi X, Lou L, Wang J, Xiong J, Zhou S. Honokiol Antagonizes Doxorubicin Resistance in Human Breast Cancer *via* miR-188-5p/FBXW7/c-Myc Pathway. *Cancer Chemother Pharmacol* (2021) 87(5):647–56. doi: 10.1007/s00280-021-04238-w
74. Lin H, Zhang L, Zhang C, Liu P. Exosomal MiR-500a-3p Promotes Cisplatin Resistance and Stemness *via* Negatively Regulating FBXW7 in Gastric Cancer. *J Cell Mol Med* (2020) 24(16):8930–41. doi: 10.1111/jcmm.15524
75. Schmitz SU, Grote P, Herrmann BG. Mechanisms of Long Noncoding RNA Function in Development and Disease. *Cell Mol Life Sci* (2016) 73(13):2491–509. doi: 10.1007/s00018-016-2174-5
76. Ponting CP, Oliver PL, Reik W. Evolution and Functions of Long Noncoding RNAs. *Cell* (2009) 136(4):629–41. doi: 10.1016/j.cell.2009.02.006
77. Wang KC, Chang HY. Molecular Mechanisms of Long Noncoding RNAs. *Mol Cell* (2011) 43(6):904–14. doi: 10.1016/j.molcel.2011.08.018
78. Zhang P, Cao L, Fan P, Mei Y, Wu M. LncRNA-MIF, a C-Myc-Activated Long non-Coding RNA, Suppresses Glycolysis by Promoting Fbxw7-Mediated C-Myc Degradation. *EMBO Rep* (2016) 17(8):1204–20. doi: 10.15252/embr.201642067
79. Cao S, Wang Y, Li J, Lv M, Niu H, Tian Y. Tumor-Suppressive Function of Long Noncoding RNA MALAT1 in Glioma Cells by Suppressing miR-155 Expression and Activating FBXW7 Function. *Am J Cancer Res* (2016) 6 (11):2561–74.
80. Wang Y, Liu Z, Yao B, Li Q, Wang L, Wang C, et al. Long non-Coding RNA CASC2 Suppresses Epithelial-Mesenchymal Transition of Hepatocellular Carcinoma Cells Through CASC2/miR-367/FBXW7 Axis. *Mol Cancer* (2017) 16(1):123. doi: 10.1186/s12943-017-0702-z
81. Liu X, Ma J, Xu F, Li L. TINCR Suppresses Proliferation and Invasion Through Regulating miR-544a/FBXW7 Axis In Lung Cancer. *Biomed Pharmacother* (2018) 99:9–17. doi: 10.1016/j.biopha.2018.01.049
82. Zhang G, Li S, Lu J, Ge Y, Wang Q, Ma G, et al. LncRNA MT1JP Functions as a ceRNA in Regulating FBXW7 Through Competitively Binding To miR-92a-3p in Gastric Cancer. *Mol Cancer* (2018) 17(1):87. doi: 10.1186/s12943-018-0829-6
83. Huo W, Qi F, Wang K. Long non-Coding RNA FER1L4 Inhibits Prostate Cancer Progression *via* Sponging miR-92a-3p and Upregulation of FBXW7. *Cancer Cell Int* (2020) 20:64. doi: 10.1186/s12935-020-1143-0
84. Chen H, Ali M, Ruben A, Stelmakh D, Pak M. E2F6-Mediated Downregulation of MIR22HG Facilitates the Progression of Laryngocarcinoma by Targeting the miR-5000-3p/FBXW7 Axis. *Mol Cell Biol* (2020) 40(10):e00496–19. doi: 10.1128/MCB.00496-19
85. Miao S, Wang J, Xuan L, Liu X. LncRNA TTN-AS1 Acts as Sponge for miR-15b-5p to Regulate FBXW7 Expression in Ovarian Cancer. *Biofactors* (2020) 46(4):600–7. doi: 10.1002/biof.1622
86. Zhang J, Zhou M, Zhao X, Wang G, Li J. Long Noncoding RNA LINC00173 is Downregulated in Cervical Cancer and Inhibits Cell Proliferation and Invasion by Modulating the miR-182-5p/FBXW7 Axis. *Pathol Res Pract* (2020) 216(8):152994. doi: 10.1016/j.prp.2020.152994
87. Yuning F, Liang C, Tenghuan W, Zhenhua N, Shengkai G. Knockdown of lincRNA PADNA Promotes Bupivacaine-Induced Neurotoxicity by miR-194/FBXW7 Axis. *Mol Med* (2020) 26(1):79. doi: 10.1186/s10020-020-00209-8
88. Wu L, Liu Q, Fan C, Yi X, Cheng B. MALAT1 Recruited the E3 Ubiquitin Ligase FBXW7 to Induce CRY2 Ubiquitin-Mediated Degradation and

Participated in Trophoblast Migration and Invasion. *J Cell Physiol* (2021) 236 (3):2169–77. doi: 10.1002/jcp.30003
89. Huang G, Xiang Z, Wu H, He Q, Dou R, Lin Z, et al. The lncRNA BDNF-AS/WDR5/FBXW7 Axis Mediates Ferroptosis in Gastric Cancer Peritoneal Metastasis by Regulating VDAC3 Ubiquitination. *Int J Biol Sci* (2022) 18 (4):1415–33. doi: 10.7150/ijbs.69454
90. Huang G, Xiang Z, Wu H, He Q, Dou R, Yang C, et al. The lncRNA SEMA3B-AS1/HMGB1/FBXW7 Axis Mediates the Peritoneal Metastasis of Gastric Cancer by Regulating BGN Protein Ubiquitination. *Oxid Med Cell Longev* (2022) 2022:5055684–5055684. doi: 10.1155/2022/5055684
91. Xue L, Chen S, Xue S, Liu P, Liu H. LncRNA TUG1 Compromised Neuronal Mitophagy in Cerebral Ischemia/Reperfusion Injury by Targeting Sirtuin 1. *Cell Biol Toxicol* (2022). doi: 10.1007/s10565-022-09700-w
92. Chen LL, Yang L. Regulation of circRNA Biogenesis. *RNA Biol* (2015) 12 (4):381–8. doi: 10.1080/15476286.2015.1020271
93. Liu Y, Yang C, Cao C, Li Q, Jin X, Shi H. Hsa_circ_RNA_0011780 Represses the Proliferation and Metastasis of Non-Small Cell Lung Cancer by Decreasing FBXW7 *via* Targeting miR-544a. *Onco Targets Ther* (2020) 13:745–55. doi: 10.2147/OTT.S236162
94. Chen X, Li HD, Bu FT, Li XF, Chen Y, Zhu S, et al. Circular RNA Circfbxw4 Suppresses Hepatic Fibrosis *via* Targeting the miR-18b-3p/FBXW7 Axis. *Theranostics* (2020) 10(11):4851–70. doi: 10.7150/thno.42423
95. Sun D, Wang G, Xiao C, Xin Y. Hsa_circ_001988 Attenuates GC Progression *In Vitro* and *In Vivo via* Sponging miR-197-3p. *J Cell Physiol* (2021) 236 (1):612–24. doi: 10.1002/jcp.29888
96. Zhang Q, Long J, Li N, Ma X, Zheng L. Circ_CLASP2 Regulates High Glucose-Induced Dysfunction of Human Endothelial Cells Through Targeting miR-140-5p/FBXW7 Axis. *Front Pharmacol* (2021) 12:594793. doi: 10.3389/fphar.2021.594793
97. Zhang J, Chen Z, Liu X, Yang C, Xie D. Gain of circBRAF Represses Glioma Progression by Regulating miR-1290/FBXW7 Axis. *Neurochem Res* (2021) 46 (5):1203–13. doi: 10.1007/s11064-021-03259-4
98. Hou Y, Sun J, Huang J, Yao F, Chen X, Zhu B, et al. Circular RNA circRNA_0000094 Sponges microRNA-223-3p and Up-Regulate F-Box and WD Repeat Domain Containing 7 to Restrain T Cell Acute Lymphoblastic Leukemia Progression. *Hum Cell* (2021) 34(3):977–89. doi: 10.1007/s13577-021-00504-4
99. Wu Y, Fan T, Zhao Y, Hu R, Yan D, Sun D, et al. Circular RNA Hsa_Circ_0001306 Functions as a Competing Endogenous RNA to Regulate FBXW7 Expression by Sponging miR-527 in Hepatocellular Carcinoma. *J Cancer* (2021) 12(21):6531–42. doi: 10.7150/jca.61381
100. Liu S, Wang L, Wu X, Wu J, Liu D, Yu H. Overexpression of Hsa_Circ_0022742 Suppressed Hyperglycemia-Induced Endothelial Dysfunction by Targeting the miR-503-5p/FBXW7 Axis. *Microvasc Res* (2022) 139:104249. doi: 10.1016/j.mvr.2021.104249
101. Xie X, Li H, Gao C, Lai Y, Liang J, Chen Z, et al. Downregulation of Circular RNA Circpsd3 Promotes Metastasis by Modulating FBXW7 Expression in Clear Cell Renal Cell Carcinoma. *J Oncol* (2022) 2022:5084631. doi: 10.1155/2022/5084631
102. Cao J, Yu U, Li L, Yuan X, Chen S, Xu H, et al. circKL Inhibits the Growth and Metastasis of Kidney Cancer by Sponging Mir−182−5p and Upregulating FBXW7. *Oncol Rep* (2022) 47(4):75. doi: 10.3892/or.2022.8286
103. Ye F, Gao G, Zou Y, Zheng S, Zhang L, Ou X, et al. Circfbxw7 Inhibits Malignant Progression by Sponging miR-197-3p and Encoding a 185-Aa Protein in Triple-Negative Breast Cancer. *Mol Ther Nucleic Acids* (2019) 18:88–98. doi: 10.1016/j.omtn.2019.07.023
104. Yang Y, Gao X, Zhang M, Yan S, Sun C, Xiao F, et al. Novel Role of FBXW7 Circular RNA in Repressing Glioma Tumorigenesis. *J Natl Cancer Institute* (2018) 110(3):304–15. doi: 10.1093/jnci/djx166
105. Welcker M, Larimore EA, Swanger J, Bengoechea-Alonso MT, Grim JE, Ericsson J, et al. Fbw7 Dimerization Determines the Specificity and Robustness of Substrate Degradation. *Genes Dev* (2013) 27(23):2531–6. doi: 10.1101/gad.229195.113
106. Welcker M, Clurman BE. FBW7 Ubiquitin Ligase: A Tumour Suppressor at the Crossroads of Cell Division, Growth and Differentiation. *Nat Rev Cancer* (2008) 8(2):83–93. doi: 10.1038/nrc2290
107. Tang X, Orlicky S, Lin Z, Willems A, Neculai D, Ceccarelli D, et al. Suprafacial Orientation of the SCFCdc4 Dimer Accommodates Multiple Geometries for Substrate Ubiquitination. *Cell* (2007) 129(6):1165–76. doi: 10.1016/j.cell.2007.04.042
108. Welcker M, Clurman BE. Fbw7/hCDC4 Dimerization Regulates its Substrate Interactions. *Cell Div* (2007) 2:7. doi: 10.1186/1747-1028-2-7
109. Lan H, Tan M, Zhang Q, Yang F, Wang S, Li H, et al. LSD1 Destabilizes FBXW7 and Abrogates FBXW7 Functions Independent of its Demethylase Activity. *Proc Natl Acad Sci U.S.A.* (2019) 116(25):12311–20. doi: 10.1073/pnas.1902012116
110. Mirmohammadsadegh A, Mota R, Gustrau A, Hassan M, Nambiar S, Marini A, et al. ERK1/2 is Highly Phosphorylated in Melanoma Metastases and Protects Melanoma Cells From Cisplatin-Mediated Apoptosis. *J Invest Dermatol* (2007) 127(9):2207–15. doi: 10.1038/sj.jid.5700870
111. Jeong EK, Lee SY, Jeon HM, Ju MK, Kim CH, Kang HS. Role of Extracellular Signal-Regulated Kinase (ERK)1/2 in Multicellular Resistance To Docetaxel in MCF-7 Cells. *Int J Oncol* (2010) 37(3):655–61. doi: 10.3892/ijo_00000714
112. Ji S, Qin Y, Shi S, Liu X, Hu H, Zhou H, et al. ERK Kinase Phosphorylates and Destabilizes the Tumor Suppressor FBW7 in Pancreatic Cancer. *Cell Res* (2015) 25(5):561–73. doi: 10.1038/cr.2015.30
113. Mun GI, Choi E, Lee Y, Lee YS. Decreased Expression of FBXW7 by ERK1/2 Activation in Drug-Resistant Cancer Cells Confers Transcriptional Activation of MDR1 by Suppression of Ubiquitin Degradation Of HSF1. *Cell Death Dis* (2020) 11(5):395. doi: 10.1038/s41419-020-2600-3
114. Shu L, Chen A, Li L, Yao L, He Y, Xu J, et al. (2022). NRG1 Regulates Fra-1 Transcription and Metastasis of Triple-Negative Breast Cancer Cells *via* the C-Myc Ubiquitination as Manipulated by ERK1/2-Mediated Fbxw7 Phosphorylation. *Oncogene* (2022) 41(6):907–19. doi: 10.1038/s41388-021-02142-4
115. Ye Z, Zhuo Q, Hu Q, Xu X, Mengqi L, Zhang Z, et al. FBW7-NRA41-SCD1 Axis Synchronously Regulates Apoptosis and Ferroptosis in Pancreatic Cancer Cells. *Redox Biol* (2021) 38:101807–7. doi: 10.1016/j.redox.2020.101807
116. Xiao D, Yue M, Su H, Ren P, Jiang J, Li F, et al. Polo-Like Kinase-1 Regulates Myc Stabilization and Activates a Feedforward Circuit Promoting Tumor Cell Survival. Mol. *Cell* (2016) 64(3):493–506. doi: 10.1016/j.molcel.2016.09.016
117. Wang D, Pierce A, Veo B, Fosmire S, Danis E, Donson A, et al. A Regulatory Loop of FBXW7-MYC-PLK1 Controls Tumorigenesis of MYC-Driven Medulloblastoma. *Cancers (Basel)* (2021) 13(3):387. doi: 10.3390/cancers13030387
118. Schülein C, Eilers M, Popov N. PI3K-Dependent Phosphorylation of Fbw7 Modulates Substrate Degradation and Activity. *FEBS Lett* (2011) 585 (14):2151–7. doi: 10.1016/j.febslet.2011.05.036
119. Mo JS, Ann EJ, Yoon JH, Jung J, Choi YH, Kim HY, et al. Serum- and Glucocorticoid-Inducible Kinase 1 (SGK1) Controls Notch1 Signaling by Downregulation of Protein Stability Through Fbw7 Ubiquitin Ligase. *J Cell Sci* (2011) 124(Pt 1):100–12. doi: 10.1242/jcs.073924
120. Durgan J, Parker PJ. Regulation of the Tumour Suppressor Fbw7α by PKC-Dependent Phosphorylation and Cancer-Associated Mutations. *Biochem J* (2010) 432(1):77–87. doi: 10.1042/BJ20100799
121. Zitouni S, Méchali F, Papin C, Choquet A, Roche D, Baldin V, et al. The Stability of Fbw7α in M-Phase Requires its Phosphorylation by PKC. *PloS One* (2017) 12(8):e0183500–e0183500. doi: 10.1371/journal.pone.0183500
122. Kus BM, Caldon CE, Andorn-Broza R, Edwards AM. Functional Interaction of 13 Yeast SCF Complexes With a Set of Yeast E2 Enzymes *In Vitro*. *Proteins: Structure Function Bioinf* (2004) 54(3):455–67. doi: 10.1002/prot.10620
123. Zhou P, Howley PM. Ubiquitination and Degradation of the Substrate Recognition Subunits of SCF Ubiquitin-Protein Ligases. *Mol Cell* (1998) 2 (5):571–80. doi: 10.1016/s1097-2765(00)80156-2
124. Galan JM, Peter M. Ubiquitin-Dependent Degradation of Multiple F-Box Proteins by an Autocatalytic Mechanism. *P Natl Acad Sci USA* (1999) 96 (16):9124–9. doi: 10.1073/pnas.96.16.9124
125. Pashkova N, Gakhar L, Winistorfer SC, Yu L, Ramaswamy S, Piper RC. WD40 Repeat Propellers Define a Ubiquitin-Binding Domain That Regulates Turnover of F Box Proteins. *Mol Cell* (2010) 40(3):433–43. doi: 10.1016/j.molcel.2010.10.018
126. Chen J, Shin J, Zhao R, Phan L, Wang H, Xue Y, et al. CSN6 Drives Carcinogenesis by Positively Regulating Myc Stability. *Nat Commun* (2014) 5:5384–4. doi: 10.1038/ncomms6384
127. Yan H, Wang H, Zhong M, Wu S, Yang L, Li K, et al. PML Suppresses Influenza Virus Replication by Promoting FBXW7 Expression. *Virol Sin* (2021) 36(5):1154–64. doi: 10.1007/s12250-021-00399-3

128. Zhang H, Shao Y, Yao Z, Liu L, Zhang H, Yin J, et al. Mechanical Overloading Promotes Chondrocyte Senescence and Osteoarthritis Development Through Downregulating FBXW7. *Ann Rheumatol Dis* (2022) 81(5):676–86. doi: 10.1136/annrheumdis-2021-221513
129. Liu N, Li H, Li S, Shen M, Xiao N, Chen Y, et al. The Fbw7/human CDC4 Tumor Suppressor Targets Proproliferative Factor KLF5 for Ubiquitination and Degradation Through Multiple Phosphodegron Motifs. *J Biol Chem* (2010) 285(24):18858–67. doi: 10.1074/jbc.M109.099440
130. Orlicky S, Tang X, Willems A, Tyers M, Sicheri F. Structural Basis for Phosphodependent Substrate Selection and Orientation by the SCFCdc4 Ubiquitin Ligase. *Cell* (2003) 112(2):243–56. doi: 10.1016/S0092-8674(03)00034-5
131. Nash P, Tang X, Orlicky S, Chen Q, Gertler FB, Mendenhall MD, et al. Multisite Phosphorylation of a CDK Inhibitor Sets a Threshold for the Onset of DNA Replication. *Nature* (2001) 414(6863):514–21. doi: 10.1038/35107009
132. Deshaies RJ, Joazeiro CA. RING Domain E3 Ubiquitin Ligases. *Annu Rev Biochem* (2009) 78:399–434. doi: 10.1146/annurev.biochem.78.101807.093809
133. Xu P, Duong DM, Seyfried NT, Cheng D, Xie Y, Robert J, et al. Quantitative Proteomics Reveals the Function of Unconventional Ubiquitin Chains in Proteasomal Degradation. *Cell* (2009) 137(1):133–45. doi: 10.1016/j.cell.2009.01.041
134. Ravid T, Hochstrasser M. Diversity of Degradation Signals in the Ubiquitin-Proteasome System. *Nat Rev Mol Cell Biol* (2008) 9(9):679–90. doi: 10.1038/nrm2468
135. Chung CH, Baek SH. Deubiquitinating Enzymes: Their Diversity and Emerging Roles. *Biochem Biophys Res Commun* (1999) 266(3):633–40. doi: 10.1006/bbrc.1999.1880
136. Popov N, Herold S, Llamazares M, Schülein C, Eilers M. Fbw7 and Usp28 Regulate Myc Protein Stability in Response to DNA Damage. *Cell Cycle* (2007) 6(19):2327–31. doi: 10.4161/cc.6.19.4804
137. Popov N, Wanzel M, Madiredjo M, Zhang D, Beijersbergen R, Bernards R, et al. The Ubiquitin-Specific Protease USP28 is Required for MYC Stability. *Nat Cell Biol* (2007) 9(7):765–74. doi: 10.1038/ncb1601
138. Flügel D, Görlach A, Kietzmann T. GSK-3β Regulates Cell Growth, Migration, and Angiogenesis *via* Fbw7 and USP28-Dependent Degradation of HIF-1α. *Blood* (2012) 119(5):1292–301. doi: 10.1182/blood-2011-08-375014
139. Diefenbacher ME, Popov N, Blake SM, Schülein-Völk C, Nye E, Spencer-Dene B, et al. The Deubiquitinase USP28 Controls Intestinal Homeostasis and Promotes Colorectal Cancer. *J Clin Invest* (2014) 124(8):3407–18. doi: 10.1172/JCI73733
140. Schülein-Völk C, Wolf E, Zhu J, Xu W, Taranets L, Hellmann A, et al. Dual Regulation of Fbw7 Function and Oncogenic Transformation by Usp28. *Cell Rep* (2014) 9(3):1099–109. doi: 10.1016/j.celrep.2014.09.057
141. Zhang J, Ren P, Xu D, Liu X, Liu Z, Zhang C, et al. Human UTP14a Promotes Colorectal Cancer Progression by Forming a Positive Regulation Loop With C-Myc. *Cancer Lett* (2019) 440-441:106–15. doi: 10.1016/j.canlet.2018.10.010
142. Sun XX, Sears RC, Dai MS. Deubiquitinating C-Myc: USP36 Steps Up in the Nucleolus. *Cell Cycle* (2015) 14(24):3786–93. doi: 10.1080/15384101.2015.1093713
143. Sun X, He X, Yin L, Komada M, Sears RC, Dai M. The Nucleolar Ubiquitin-Specific Protease USP36 Deubiquitinates and Stabilizes C-Myc. *P Natl Acad Sci USA* (2015) 112(12):3734–9. doi: 10.1073/pnas.1411713112
144. Khan OM, Carvalho J, Spencer-Dene B, Mitter R, Frith D, Snijders AP, et al. The Deubiquitinase USP9X Regulates FBW7 Stability and Suppresses Colorectal Cancer. *J Clin Invest* (2018) 128(4):1326–37. doi: 10.1172/JCI97325
145. Li M, Wu Y, Chen J, Shi H, Ji Z, Zhang X, et al. Innate Immune Evasion of Porcine Epidemic Diarrhea Virus Through Degradation of the FBXW7 Protein *via* the Ubiquitin-Proteasome Pathway. *J Virol* (2022) 96(5):e0088921. doi: 10.1128/JVI.00889-21
146. Song Y, Lai L, Chong Z, He J, Zhang Y, Xue Y, et al. E3 Ligase FBXW7 is Critical for RIG-I Stabilization During Antiviral Responses. *Nat Commun* (2017) 8:14654–4. doi: 10.1038/ncomms14654
147. Balamurugan K, Sharan S, Klarmann KD, Zhang Y, Coppola V, Summers GH, et al. Fbxw7α Attenuates Inflammatory Signalling by Downregulating C/Ebpδ and its Target Gene Tlr4. Nat. *Commun* (2013) 4:1662. doi: 10.1038/ncomms2677
148. Deiuliis JA, Syed R, Duggineni D, Rutsky J, Rengasamy P, Zhang J, et al. Visceral Adipose MicroRNA 223 Is Upregulated in Human and Murine Obesity and Modulates the Inflammatory Phenotype of Macrophages. *PLoS One* (2016) 11(11):e0165962–e0165962. doi: 10.1371/journal.pone.0165962
149. Mendoza-Villanueva D, Balamurugan K, Ali HR, Kim S, Sharan S, Johnson RC, et al. The C/Ebpδ Protein is Stabilized by Estrogen Receptor α Activity, Inhibits SNAI2 Expression and Associates With Good Prognosis in Breast Cancer. *Oncogene* (2016) 35(48):6166–76. doi: 10.1038/onc.2016.156
150. Masuda T, Noda M, Kogawa T, Kitagawa D, Hayashi N, Jomori T, et al. Phase I Dose-Escalation Trial to Repurpose Propagermanium, an Oral CCL2 Inhibitor, in Patients With Breast Cancer. *Cancer Sci* (2020) 111(3):924–31. doi: 10.1111/cas.14306
151. He J, Song Y, Li G, Xiao P, Liu Y, Xue Y, et al. Fbxw7 Increases CCL2/7 in CX3CR1hi Macrophages to Promote Intestinal Inflammation. *J Clin Invest* (2019) 129(9):3877–93. doi: 10.1172/JCI123374
152. Zhang X, Howell GM, Guo L, Collage RD, Loughran PA, Zuckerbraun BS, et al. CaMKIV-Dependent Preservation of mTOR Expression is Required for Autophagy During Lipopolysaccharide-Induced Inflammation and Acute Kidney Injury. *J Immunol (Baltimore Md 1950)* (2014) 193(5):2405–15. doi: 10.4049/jimmunol.1302798
153. He J, Du Y, Li G, Xiao P, Sun X, Song W, et al. Myeloid Fbxw7 Prevents Pulmonary Fibrosis by Suppressing TGF-β Production. *Front Immunol* (2021) 12:760138. doi: 10.3389/fimmu.2021.760138
154. Wang C, Chao Y, Xu W, Liu Z, Wang H, Huang K. Myeloid FBW7 Deficiency Disrupts Redox Homeostasis and Aggravates Dietary-Induced Insulin Resistance. *Redox Biol* (2020) 37:101688–8. doi: 10.1016/j.redox.2020.101688
155. Close V, Close W, Kugler SJ, Reichenzeller M, Yosifov DY, Bloehdorn J, et al. FBXW7 Mutations Reduce Binding of NOTCH1, Leading to Cleaved NOTCH1 Accumulation and Target Gene Activation in CLL. *Blood* (2019) 133(8):830–9. doi: 10.1182/blood-2018-09-874529
156. Thompson BJ, Jankovic V, Gao J, Buonamici S, Vest A, Lee JM, et al. Control of Hematopoietic Stem Cell Quiescence by the E3 Ubiquitin Ligase Fbw7. *J Exp Med* (2008) 205(6):1395–408. doi: 10.1084/jem.20080277
157. Feng C, Li L, Zhou L, Li D, Liu M, Han S, et al. Critical Roles of the E3 Ubiquitin Ligase FBW7 in B-Cell Response and the Pathogenesis of Experimental Autoimmune Arthritis. *Immunology* (2021) 164(3):617–36. doi: 10.1111/imm.13398
158. Onoyama I, Tsunematsu R, Matsumoto A, Kimura T, de Alborán IM, Nakayama K, et al. Conditional Inactivation of Fbxw7 Impairs Cell-Cycle Exit During T Cell Differentiation and Results in Lymphomatogenesis. *J Exp Med* (2007) 204(12):2875–88. doi: 10.1084/jem.20062299
159. Kitagawa K, Shibata K, Matsumoto A, Matsumoto M, Ohhata T, Nakayama KI, et al. Fbw7 Targets GATA3 Through Cyclin-Dependent Kinase 2-Dependent Proteolysis and Contributes to Regulation of T-Cell Development. *Mol Cell Biol* (2014) 34(14):2732–44. doi: 10.1128/MCB.01549-13
160. Suehiro KI, Suto A, Suga K, Furuya H, Iwata A, Iwamoto T, et al. Sox12 Enhances Fbw7-Mediated Ubiquitination and Degradation of GATA3 in Th2 Cells. *Cell Mol Immunol* (2021) 18(7):1729–38. doi: 10.1038/s41423-020-0384-0
161. Matsuoka S, Oike Y, Onoyama I, Iwama A, Arai F, Takubo K, et al.). Fbxw7 Acts as a Critical Fail-Safe Against Premature Loss of Hematopoietic Stem Cells and Development of T-ALL. *Gene Dev* (2008) 22(8):986–91. doi: 10.1101/gad.1621808
162. Zuurbier L, Homminga I, Calvert V, Winkel MT, Buijs-Gladdines JGCA, Kooi C, et al. NOTCH1 and/or FBXW7 Mutations Predict for Initial Good Prednisone Response But Not for Improved Outcome in Pediatric T-Cell Acute Lymphoblastic Leukemia Patients Treated on DCOG or COALL Protocols. *Leukemia* (2010) 24(12):2014–22. doi: 10.1038/leu.2010.204
163. Kox C, Zimmermann M, Stanulla M, Leible S, Schrappe M, Ludwig W, et al. The Favorable Effect of Activating NOTCH1 Receptor Mutations on Long-Term Outcome in T-ALL Patients Treated on the ALL-BFM 2000 Protocol can be Separated From FBXW7 Loss of Function. *Leukemia* (2010) 24(12):2005–13. doi: 10.1038/leu.2010.203
164. Malyukova A, Brown S, Papa R, O'Brien R, Giles J, Trahair TN, et al. FBXW7 Regulates Glucocorticoid Response in T-Cell Acute Lymphoblastic Leukaemia by Targeting the Glucocorticoid Receptor for Degradation. *Leukemia* (2013) 27(5):1053–62. doi: 10.1038/leu.2012.361

165. Zhao E, Maj T, Kryczek I, Li W, Wu K, Zhao L, et al. Cancer Mediates Effector T Cell Dysfunction by Targeting microRNAs and EZH2 *via* Glycolysis Restriction. *Nat Immunol* (2016) 17(1):95–103. doi: 10.1038/ni.3313
166. van der Mijn JC, Eng KW, Chandra P, Fernandez E, Ramazanoglu S, Sigaras A, et al. The Genomic Landscape of Metastatic Clear Cell Renal Cell Carcinoma After Systemic Therapy. *Mol Oncol* (2022). doi: 10.1002/1878-0261.13204
167. Qin JJ, Nag S, Wang W, Zhou J, Zhang WD, Wang H, et al. NFAT as Cancer Target: Mission Possible? *Biochim Biophys Acta* (2014) 1846(2):297–311. doi: 10.1016/j.bbcan.2014.07.009
168. Xanthoudakis S, Viola JP, Shaw KT, Luo C, Wallace JD, Bozza PT, et al. An Enhanced Immune Response in Mice Lacking the Transcription Factor NFAT1. *Science* (1996) 272(5263):892–5. doi: 10.1126/science.272.5263.892
169. Liu W, Ren D, Xiong W, Jin X, Zhu L. A Novel FBW7/NFAT1 Axis Regulates Cancer Immunity in Sunitinib-Resistant Renal Cancer by Inducing PD-L1 Expression. *J Exp Clin Cancer Res CR* (2022) 41(1):38–8. doi: 10.1186/s13046-022-02253-0
170. Xiong W, Zhang B, Yu H, Zhu L, Yi L, Jin X. RRM2 Regulates Sensitivity to Sunitinib and PD-1 Blockade in Renal Cancer by Stabilizing ANXA1 and Activating the AKT Pathway. *Adv Sci (Weinh)* (2021) 8(18):e2100881. doi: 10.1002/advs.202100881
171. Casey SC, Tong L, Li Y, Do R, Walz S, Fitzgerald KN, et al. MYC Regulates the Antitumor Immune Response Through CD47 and PD-L1. *Science* (2016) 352(6282):227–31. doi: 10.1126/science.aac9935
172. Zhou S, Zhao X, Yang Z, Yang R, Chen C, Zhao K, et al. Neddylation Inhibition Upregulates PD-L1 Expression and Enhances the Efficacy of Immune Checkpoint Blockade in Glioblastoma. *Int J Cancer* (2019) 145 (3):763–74. doi: 10.1002/ijc.32379
173. Kourtis N, Moubarak RS, Aranda-Orgilles B, Lui K, Aydin IT, Trimarchi T, et al. FBXW7 Modulates Cellular Stress Response and Metastatic Potential Through HSF1 Post-Translational Modification. *Nat Cell Biol* (2015) 17 (3):322–32. doi: 10.1038/ncb3121
174. Yang T, Ren C, Lu C, Qiao P, Han X, Wang L, et al. Phosphorylation of HSF1 by PIM2 Induces PD-L1 Expression and Promotes Tumor Growth in Breast Cancer. *Cancer Res* (2019) 79(20):5233–44. doi: 10.1158/0008-5472.CAN-19-0063
175. Vanhaesebroeck B, Stephens L, Hawkins P. PI3K Signalling: The Path to Discovery and Understanding. *Nat Rev Mol Cell Biol* (2012) 13(3):195–203. doi: 10.1038/nrm3290
176. Martin EL, Souza DG, Fagundes CT, Amaral FA, Assenzio B, Puntorieri V, et al. Phosphoinositide-3 Kinase Gamma Activity Contributes to Sepsis and Organ Damage by Altering Neutrophil Recruitment. *Am J Respir Crit Care Med* (2010) 182(6):762–73. doi: 10.1164/rccm.201001-0088OC
177. Aydin IT, Melamed RD, Adams SJ, Castillo-Martin M, Demir A, Bryk D, et al. FBXW7 Mutations in Melanoma and a New Therapeutic Paradigm. *J Natl Cancer Inst* (2014) 106(6):dju107. doi: 10.1093/jnci/dju107
178. Gstalder C, Liu D, Miao D, Lutterbach B, Devine AL, Lin C, et al. Inactivation of Fbxw7 Impairs dsRNA Sensing and Confers Resistance to PD-1 Blockade. *Cancer Discovery* (2020) 10(9):1296–311. doi: 10.1158/2159-8290.CD-19-1416
179. Choi M, Kadara H, Zhang J, Parra ER, Rodriguez-Canales J, Gaffney SG, et al. Mutation Profiles in Early-Stage Lung Squamous Cell Carcinoma With Clinical Follow-Up and Correlation With Markers of Immune Function. *Ann Oncol* (2017) 28(1):83–9. doi: 10.1093/annonc/mdw437
180. Liu XY, Cui YN, Li J, Zhang Z, Guo RH. Effect of FBXW7 Gene Mutation on the Prognosis of Immunotherapy in Patients With non-Small Cell Lung Cancer. *Zhonghua Yi Xue Za Zhi* (2022) 102(13):914–21. doi: 10.3760/cma.j.cn112137-20211021-02332
181. Xue S, Gillmore R, Downs A, Tsallios A, Holler A, Gao L, et al. Exploiting T Cell Receptor Genes for Cancer Immunotherapy. *Clin Exp Immunol* (2005) 139(2):167–72. doi: 10.1111/j.1365-2249.2005.02715.x
182. Yamada T, Sato S, Sotoyama Y, Orba Y, Sawa H, Yamauchi H, et al. RIG-I Triggers a Signaling-Abortive Anti-SARS-CoV-2 Defense in Human Lung Cells. *Nat Immunol* (2021) 22(7):820–8. doi: 10.1038/s41590-021-00942-0
183. Aygun H. Vitamin D can Reduce Severity in COVID-19 Through Regulation of PD-L1. *Naunyn-Schmiedeberg's Arch Pharmacol* (2022) 395(4):487–94. doi: 10.1007/s00210-022-02210-w
184. Diao B, Wang C, Tan Y, Chen X, Liu Y, Ning L, et al. Reduction and Functional Exhaustion of T Cells in Patients With Coronavirus Disease 2019 (COVID-19). *Front Immunol* (2020) 11:827. doi: 10.3389/fimmu.2020.00827
185. Lin PC, Yeh YM, Hsu HP, Chan RH, Lin BW, Chen PC, et al. Comprehensively Exploring the Mutational Landscape and Patterns of Genomic Evolution in Hypermutated Cancers. *Cancers (Basel)* (2021) 13 (17):4317. doi: 10.3390/cancers13174317
186. Cassavaugh JM, Hale SA, Wellman TL, Howe AK, Wong C, Lounsbury KM. Negative Regulation of HIF-1α by an FBW7-Mediated Degradation Pathway During Hypoxia. *J Cell Biochem* (2011) 112(12):3882–90. doi: 10.1002/jcb.23321
187. O'Neil J, Grim J, Strack P, Rao S, Tibbitts D, Winter C, et al. FBW7 Mutations in Leukemic Cells Mediate NOTCH Pathway Activation and Resistance to Gamma-Secretase Inhibitors. *J Exp Med* (2007) 204(8):1813–24. doi: 10.1084/jem.20070876
188. Thompson BJ, Buonamici S, Sulis ML, Palomero T, Vilimas T, Basso G, et al. The SCFFBW7 Ubiquitin Ligase Complex as a Tumor Suppressor in T Cell Leukemia. *J Exp Med* (2007) 204(8):1825–35. doi: 10.1084/jem.20070872
189. Yada M, Hatakeyama S, Kamura T, Nishiyama M, Tsunematsu R, Imaki H, et al. Phosphorylation-Dependent Degradation of C-Myc is Mediated by the F-Box Protein Fbw7. *EMBO J* (2004) 23(10):2116–25. doi: 10.1038/sj.emboj.7600217
190. Welcker M, Orian A, Jin J, Grim JE, Harper JW, Eisenman RN, et al. The Fbw7 Tumor Suppressor Regulates Glycogen Synthase Kinase 3 Phosphorylation-Dependent C-Myc Protein Degradation. *Proc Natl Acad Sci U.S.A.* (2004) 101(24):9085–90. doi: 10.1073/pnas.0402770101
191. Welcker M, Singer J, Loeb KR, Grim J, Bloecher A, Gurien-West M, et al. Multisite Phosphorylation by Cdk2 and GSK3 Controls Cyclin E Degradation. *Mol Cell* (2003) 12(2):381–92. doi: 10.1016/s1097-2765(03)00287-9
192. Liu Z, Ma T, Duan J, Liu X, Liu L. MicroRNA−223−induced Inhibition of the FBXW7 Gene Affects the Proliferation and Apoptosis of Colorectal Cancer Cells *via* the Notch and Akt/mTOR Pathways. *Mol Med Rep* (2021) 23 (2):154. doi: 10.3892/mmr.2020.11793
193. Zhang P, Shao Y, Quan F, Liu L, Yang J. FBP1 Enhances the Radiosensitivity by Suppressing Glycolysis *via* the FBXW7/mTOR Axis In Nasopharyngeal Carcinoma Cells. *Life Sci* (2021) 283:119840. doi: 10.1016/j.lfs.2021.119840
194. Gombodorj N, Yokobori T, Tanaka N, Suzuki S, Kuriyama K, Kumakura Y, et al. Correlation Between High FBXW7 Expression in Pretreatment Biopsy Specimens and Good Response to Chemoradiation Therapy in Patients With Locally Advanced Esophageal Cancer: A Retrospective Study. *J Surg Oncol* (2018) 118(1):101–8. doi: 10.1002/jso.25127
195. Chen Z, Yu D, Owonikoko TK, Ramalingam SS, Sun SY. Induction of SREBP1 Degradation Coupled With Suppression of SREBP1-Mediated Lipogenesis Impacts the Response of EGFR Mutant NSCLC Cells to Osimertinib. *Oncogene* (2021) 40(49):6653–65. doi: 10.1038/s41388-021-02057-0
196. Song X, Shen L, Tong J, Kuang C, Zeng S, Schoen RE, et al. Mcl-1 Inhibition Overcomes Intrinsic and Acquired Regorafenib Resistance in Colorectal Cancer. *Theranostics* (2020) 10(18):8098–110. doi: 10.7150/thno.45363
197. Hidayat M, Mitsuishi Y, Takahashi F, Tajima K, Yae T, Miyahara K, et al. Role of FBXW7 in the Quiescence of Gefitinib-Resistant Lung Cancer Stem Cells in EGFR-Mutant non-Small Cell Lung Cancer. *Bosn J Basic Med Sci* (2019) 19(4):355–67. doi: 10.17305/bjbms.2019.4227

Conflict of Interest: The authors declare that the research was conducted in the absence of any commercial or financial relationships that could be construed as a potential conflict of interest.

frontiers | Frontiers in Pharmacology

ORIGINAL RESEARCH
published: 07 July 2022
doi: 10.3389/fphar.2022.901518

Identifying an Immune-Related Gene ST8SIA1 as a Novel Target in Patients With Clear-Cell Renal Cell Carcinoma

Xu Hu[1], *Yanfei Yang*[2], *Yaohui Wang*[1], *Shangqing Ren*[1,3]* *and Xiang Li*[1]*

[1]Institute of Urology, Department of Urology, West China Hospital, West China Medical School, Sichuan University, Chengdu, China, [2]The Third Xiangya Hospital of Central South Hospital, Changsha, China, [3]Robot Minimally Invasive Center, Sichuan Provincial People's Hospital, Chengdu, China

Clear-cell renal cell carcinoma (ccRCC) is one of the most common urological cancers. The tumor microenvironment plays an important role in tumor development. The present study was conducted to identify novel immune-related biomarkers. The differentially expressed genes were identified using the ESTIMATE algorithm base on GEO and TCGA databases. The Kaplan–Meier survival curve and univariate and multivariate analyses were performed. The association between ST8SIA1 and the immune system was explored. The gene set enrichment analysis (GSEA) and online databases were used for functional annotation. ST8SIA1 was identified as a potential prognostic gene. Elevated ST8SIA1 was observed in the tumor tissues compared with adjacent normal tissues and associated with higher T stage and advanced TNM stage (all $p < 0.05$). The mRNA and protein levels of ST8SIA1 in cancer tissues and cells are also upregulated. The Kaplan–Meier survival curve and univariate and multivariate analyses showed that higher expression of ST8SIA1 was associated with worse OS (all $p < 0.05$). ST8SIA1 expression levels were negatively correlated with tumor purity and positively associated with infiltrated immune cells and expression of immune checkpoint genes. Function analysis also revealed that ST8SIA1 was significantly associated with immune-related pathways. In conclusion, ST8SIA1 was identified as an immune-related gene and a potential target in ccRCC patients. Further relevant studies are required to validate our findings.

Keywords: clear-cell renal cell carcinoma, immune-related, ST8SIA1, prognosis, target

OPEN ACCESS

Edited by:
Ya Meng,
Zhuhai Precision Medical Center, China

Reviewed by:
Ming Zhao,
the First Affiliated Hospital of Chengdu Medical College, China
Wolfgang A. Zimmermann,
LMU Munich University Hospital, Germany

***Correspondence:**
Shangqing Ren
rsq0516@163.com
Xiang Li
hx_uro@sina.com

Specialty section:
This article was submitted to Pharmacology of Anti-Cancer Drugs, a section of the journal Frontiers in Pharmacology

Received: *22 March 2022*
Accepted: *06 June 2022*
Published: *07 July 2022*

Citation:
Hu X, Yang Y, Wang Y, Ren S and Li X (2022) Identifying an Immune-Related Gene ST8SIA1 as a Novel Target in Patients With Clear-Cell Renal Cell Carcinoma. Front. Pharmacol. 13:901518. doi: 10.3389/fphar.2022.901518

INTRODUCTION

Renal cancer is one of the most common urological cancers, with an estimated 431,288 new cases and 179,368 deaths in 2020 worldwide (Sung et al., 2021). Renal cell carcinoma (RCC) accounts for approximately 90% of all kidney malignancies (Ljungberg et al., 2019). RCC includes three main histological types: clear-cell RCC (ccRCC), papillary RCC, and chromophobe RCC; ccRCC is the most common (80–90%) and aggressive type (Ljungberg et al., 2019). For localized disease, surgical resection with curative intent is the standard treatment. However, approximately 20–30% of patients will develop local or distant recurrence after surgery (Williamson et al., 2016; Jamil et al., 2020). Moreover, about 30% of patients had metastatic diseases at initial diagnosis (Siegel et al., 2022). To be noted, the clinical outcome of advanced diseases is very poor and the 5-year relative survival rate for the distant-stage disease is only about 14% (Siegel et al., 2022).

Immunotherapy such as immune checkpoint inhibitors is becoming a promising treatment for advanced RCC (Bedke et al., 2021). Immune checkpoint inhibitors have shown encouraging results, which could improve outcomes of advanced or metastatic RCC (Motzer et al., 2019; Rini et al., 2019; Motzer et al., 2021). However, the response rates of patients who receive immune checkpoint inhibitors are not high. Reportedly, the tumor microenvironment plays an important role in the tumor development and response to immunotherapies (Binnewies et al., 2018). Moreover, ccRCC is also a highly immune cell-infiltrated cancer (Chevrier et al., 2017). Therefore, it is necessary to explore the potential prognostic genes in ccRCC patients that are immune-related.

The cells within the tumor microenvironment are an important component of the tumor tissue and strongly affect the behavior and malignancy of the tumor (Binnewies et al., 2018). Infiltrating immune and stromal cells are necessary components for the function of the tumor microenvironment, which are reported to be associated with tumor growth, recurrence, and metastasis (Hanahan and Coussens, 2012; Becht et al., 2016). An algorithm named Estimation of Stromal and Immune cells in Malignant Tumours using Expression Data (ESTIMATE) was designed to estimate the immune and stromal cells in malignant tumor tissues, which could also calculate the immune and stromal score (Yoshihara et al., 2013). Therefore, the present study aimed to explore the novel immune-related genes as prognostic factors in ccRCC patients based on The Cancer Genome Atlas (TCGA) and Gene Expression Omnibus (GEO) databases by applying the ESTIMATE algorithm.

MATERIALS AND METHODS

Data Collection

The expression profiling data of GSE126964 (n = 66) were downloaded from the GEO database (http://www.ncbi.nlm.nih.gov/geo) to identify differentially expressed genes (DEGs). The RNA-seq and clinical data of ccRCC (TCGA-KIRC data) obtained from the TCGA data portal were downloaded from the University of California Santa Cruz (UCSC) Xena database (https://xenabrowser.net/datapages/). After excluding incomplete data, a total of 527 TCGA-KIRC patients were included in the analysis.

Identification of Differentially Expressed Genes

The GSE126964 and TCGA-KIRC cohorts were divided into low and high score groups separately according to the median value of immune and stromal scores. DEGs were screened by using the package limma (version R 3.6.3). The criteria of DEGs selection are |log2 fold change (FC)|>1 and adjusted $p < 0.05$. DEGs selected from GSE126964 and TCGA-KIRC patients with low scores compared to those with high scores were shown via heatmap (**Supplementary Figure S1**). Furthermore, Venn diagrams (https://bioinfogp.cnb.csic.es/tools/venny/) were conducted to identify common DEGs (**Supplementary Figure S1**). The 12 common DEGs in GSE126964 and TCGA-KIRC were identified, including ST8SIA1. Gangliosides are important in tumorigenesis and the development of cancers (Liu et al., 2018). Biswas et al. also observed that select gangliosides (GM2, GD2, and GD3) were associated with T-cell dysfunction in RCC patients (Biswas et al., 2009). ST8SIA1, also known as GD3 synthase (GD3S), is highly expressed in several tumors and plays an important role in the development and progression of cancer. However, the exact mechanism of GD3S in RCC remains unknown. So, the ST8SIA1 was chosen for further analysis and identified as a potential key immune-related gene in the ccRCC patients.

Survival and Statistical Analysis in the TCGA-KIRC Cohort

The patients were divided into low and high score groups based on the optimal cutoff value of gene expression, which is obtained using package survivalROC (version R 3.6.3). First, the expression level of the prognostic gene between tumor and normal tissues was compared. Furthermore, the pathological characteristics' (pT, pN, pM, and stage) boxplots were also conducted based on TCGA-KIRC data by using the Wilcoxon signed-rank test. Overall survival (OS) was compared between the low and high score groups by applying the Kaplan–Meier survival curve and the log-rank test. Univariate and multivariate analyses were also conducted to identify the prognostic factors of OS. In addition, the nomogram of OS was constructed based on the multivariate analysis. Furthermore, the concordance index (C-index), the calibration curve, and the decision curve analysis (DCA) were generated to evaluate the performance of the nomogram. All statistical analyses were carried out using R software version 3.6.3. Additionally, the comparison of mRNA expression levels of ST8SIA1 between ccRCC and normal tissue was also validated based on the Oncomine database (https://www.oncomine.org/) (Rhodes et al., 2004). The cBioPortal (https://www.cbioportal.org/) database was applied to acquire genomic alteration of ST8SIA1 in KIRC from TCGA (Cerami et al., 2012).

The Association Between Prognostic Gene and Immune Microenvironment

TISIDB (http://cis.hku.hk/TISIDB/index.php) was used to investigate correlations between tumors and the immune system (Ru et al., 2019). To explore the correlation of the expression level of ST8SIA1 with immune cell infiltration level and expression of immune checkpoints genes, TIMER 2.0 (http://timer.cistrome.org/) was used (Li et al., 2020). In addition, the expression correlation of ST8SIA1 with immune checkpoints genes was also evaluated using the GEPIA ((http://gepia.cancer-pku.cn/) database (Tang et al., 2017). There were significant correlations when the p-value <0.05 and |Rho|>0.1.

The Functions of Prognostic Gene in TCGA-KIRC

The gene set enrichment analysis (GSEA) 4.0.2 (https://www.gsea-msigdb.org/gsea/index.jsp) was applied to explore the relationship between the ST8SIA1 and HALLMARK pathways. ST8SIA1 was divided into low and high score categories to annotate phenotype. Based on the default values of parameters, the 1,000 random sample permutations were conducted. LinkedOmics (http://www.linkedomics.org/login.php), a publicly available portal including multi-omics data from TCGA, was used to obtain the genes associated with ST8SIA1 in KIRC and relevant functions, including the KEGG pathway and Gene Ontology (GO) (Vasaikar et al., 2018). CancerSEA (http://biocc.hrbmu.edu.cn/CancerSEA/home.jsp), the database that uncovers functional states of cancer cells at a single-cell resolution, was applied to explore the function of ST8SIA1 at a single-cell resolution (Yuan et al., 2019).

Quantitative Real-Time Polymerase Chain Reaction

The HK-2, 786-O, and ACHN cell lines were obtained from American Type Culture Collection (ATCC). Total RNA from cells was isolated using a RaPure Total RNA Kit (Magen Biotechnology, China) according to the manufacturer's manual. Complementary DNA (cDNA) was synthesized by using oligo (dT) primer and the RevertAid First Strand cDNA Synthesis Kit (Thermo Fisher Scientific, United States). Quantitative real-time PCR was performed using the QuantiNova SYBR Green PCR Kit (Qiagen, Germany) in a PCR system (Bio-Rad, United States). The PCR conditions were as follows: initial denaturation at 95°C for 2 min, followed by 95°C for 5 s and 60°C for 10 s for cycles. The gene primers were as follows: ST8SIA1, forward 5'-TACTCTCTCTTCCCACAGG-3', and reverse 5'-GACAAAGGAGGGAGATTGC-3'. Relative gene expression was calculated using the $2^{-\Delta\Delta Ct}$ method and normalized with GAPDH.

Immunohistochemical Analysis

The 46 ccRCC tumor tissues and 37 adjacent normal kidney tissues were used for immunohistochemistry. Then, xylene and a graded alcohol series were used for deparaffinization and hydration. After the citric acid solution was applied for antigen retrieval, the sections were incubated with normal goat serum for 30 min and primary antibody against ST8SIA1 (1:200; 24918-1-AP; ProteinTech Group, Inc.) at 4 °C overnight. Subsequently, the sections were incubated with secondary antibodies at room temperature for 30 min, and staining was performed using DAB. Then, the sections were counterstained with hematoxylin and observed under a microscope.

The immunohistochemical score was evaluated using the criterion reported previously (Zhu et al., 2020). The staining intensity level ranged from 0 to 3 (no staining, weakly positive, moderately positive, and strongly positive). Based on the fraction of positively stained tumor cells, the score ranged from 0 to 4 (negative, ≤ 25%, 26–50%, 51–75%, and > 75%). The final score was calculated by multiplying these two scores, ranging from 0 to 12 (−; +; ++; +++), and ≤3 was defined as low expression.

Statistical Analysis

All statistical analyses were performed by an online database or R software. Two-sided *p*-values less than 0.05 were considered statistically significant.

RESULTS

The Identification of DEGs in ccRCC Patients

The gene expression profiles were compared between low and high score groups based on the immune/stromal scores in the GSE126964 and TCGA-KIRC cohorts. In the GSE126964 dataset, 201 DEGs (2 upregulated and 199 downregulated genes) and 391 DEGs (24 upregulated and 367 downregulated genes) were obtained based on the differences in stromal and immune scores, respectively. Similarly, in the TCGA-KIRC cohort, the comparisons based on the stromal and immune scores generated 572 DEGs (20 upregulated and 552 downregulated genes) and 669 DEGs (18 upregulated and 651 downregulated genes), respectively. As shown in the Venn diagrams, only 12 DEGs were commonly downregulated both in the GSE126964 and TCGA-KIRC cohorts (**Supplementary Figure S1**). The ST8SIA1 (ST8 alpha-N-acetyl-neuraminide alpha-2,8-sialyltransferase 1) was identified as a potential key immune-related gene in the ccRCC patients.

Association Between ST8SIA1 Expression and Clinicopathological Characteristics

The expression of ST8SIA1 was higher in the KIRC tissue compared with adjacent normal tissue ($p = 0.006$; **Figure 1A**). In the Oncomine database, meta-analysis also revealed ST8SIA1 was highly expressed in the tumor tissue ($p = 0.03$; **Supplementary Figure S2**). In the TCGA-KIRC cohort, higher expression of ST8SIA1 was significantly associated with advanced T stage and TNM stage (all $p < 0.001$; **Figures 1B,C**). Furthermore, high ST8SIA1 expression may be associated with lymph node metastasis and distant metastasis but did not reach a significant difference (**Supplementary Figure S2**). ST8SIA1 expression was also positively correlated with the grade of tumor (Rho = 0.198, $p < 0.001$; **Figure 1D**). The Kaplan–Meier curve revealed that higher ST8SIA1 expression (using optimal cutoff value) was associated with worse OS ($p = 0.002$; **Figure 1E**). The univariate analysis demonstrated that age, T stage, N stage, M stage, TNM stage, and ST8SIA1 expression were associated with OS (**Table 1**). Moreover, the multivariate analysis also revealed that higher ST8SIA1 expression was significantly associated with worse OS ($p = 0.015$; **Table 1**). Based on the multivariate analysis, the nomogram of OS was constructed (**Figure 1F**), with a C-index of 0.747. The calibration plots for predicting OS fitted well between the nomogram-predicted probability and actual observation at 3- and 5-year follow-ups (**Supplementary Figure S2**). Based on the DCA

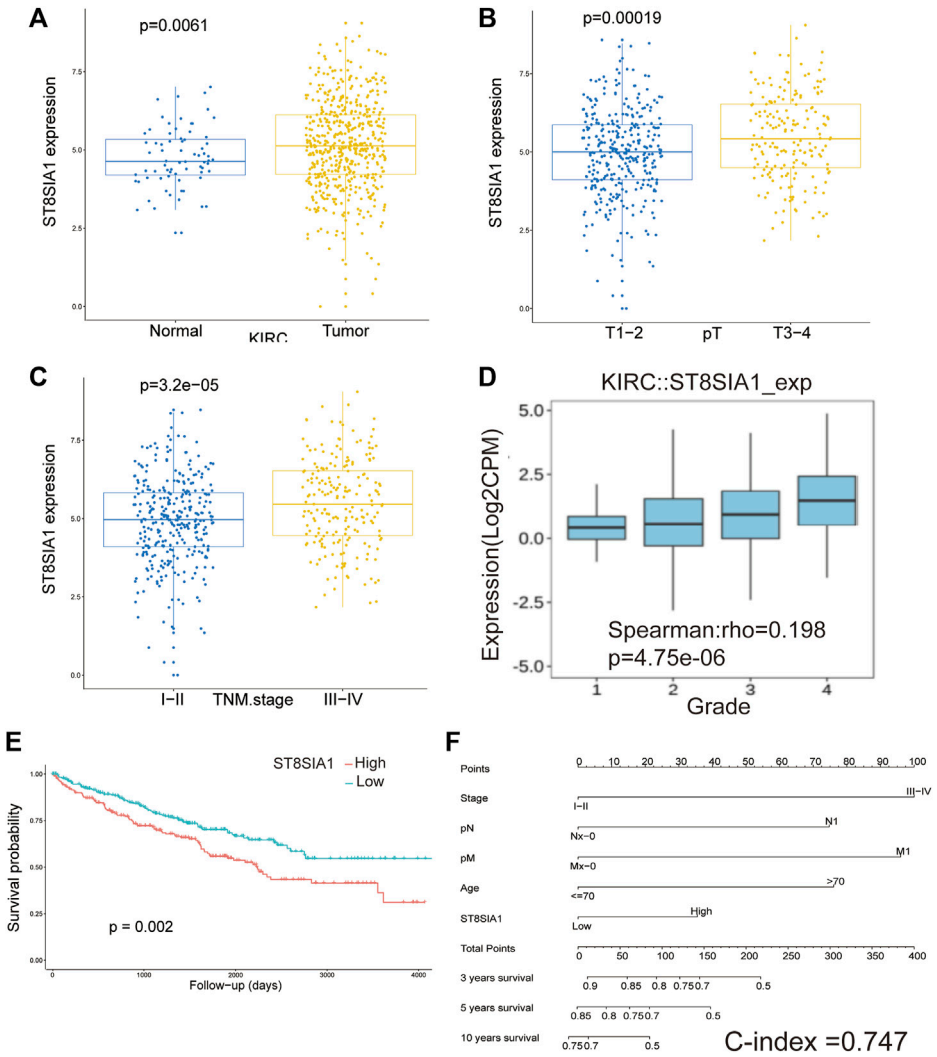

FIGURE 1 | The mRNA expression level of ST8SIA1 in renal cancer and adjacent normal tissues in TCGA-KIRC **(A)**; the mRNA expression level of ST8SIA1 between the different T stage **(B)** and TNM stage **(C)** in TCGA-KIRC; the correlation between ST8SIA1 mRNA expression and tumor grade based on the TISIDB database **(D)**; the Kaplan–Meier curve analysis of OS grouped by ST8SIA1 expression (using optimal cutoff value) **(E)**; nomogram incorporating ST8SIA1 expression predicts probability of OS **(F)**.

TABLE 1 | Univariate and multivariate Cox regression analyses of overall survival for clear-cell renal cell carcinoma patients in TCGA cohort.

Variables	Univariate analysis			Multivariate analysis		
	HR	95% CI	*p*-value	HR	95% CI	*p*-value
Age (>70 vs. ≤ 70)	1.84	1.35–2.52	<0.001[a]	2.37	1.72–3.21	<0.001[a]
Gender (female vs. male)	0.93	0.68–1.26	0.631			
Year of diagnosis (>2006 vs. ≤ 2006)	0.83	0.57–1.2	0.323			
T stage (T3–4 vs. T1–2)	3.12	2.31–4.23	<0.001[a]	1.03	0.56–1.88	0.929
N stage (N1 vs. NX-0)	3.85	2.13–7.14	<0.001[a]	2.13	1.12–4.17	0.021[a]
M stage (M1 vs. MX-0)	4.35	3.23–5.88	<0.001[a]	2.78	1.89–4	<0.001[a]
TNM stage (III–IV vs. I–II)	3.82	2.79–5.24	<0.001[a]	2.30	1.15–4.59	0.019[a]
ST8SIA1 expression (high vs. low)	1.59	1.18–2.13	0.002[a]	1.45	1.08–1.96	0.015[a]

[a]p<*0.05*.

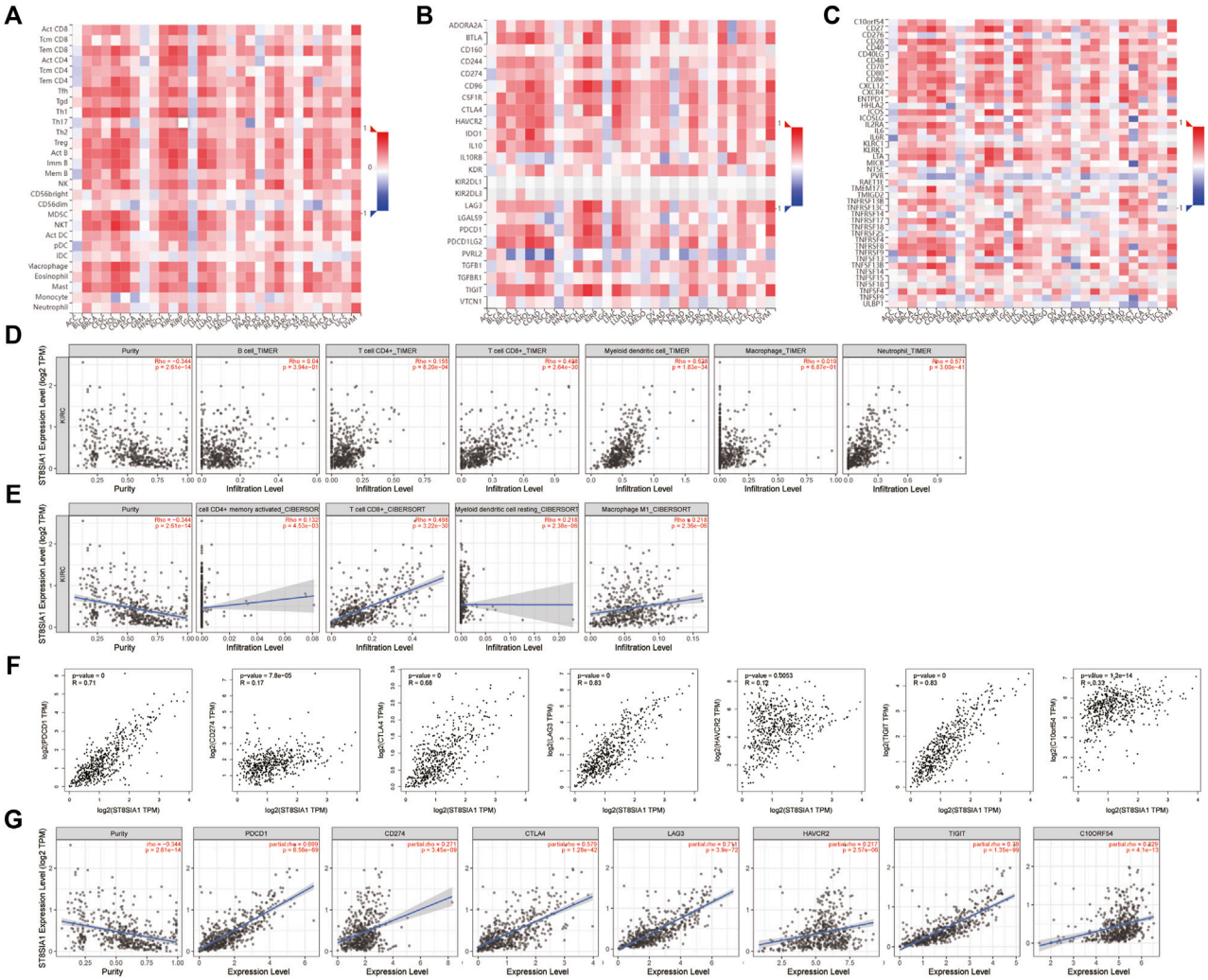

FIGURE 2 | correlation analysis of ST8SIA1 expression and abundance of tumor-infiltrating lymphocytes **(A)**, immunoinhibitory **(B)**, and immunostimulatory **(C)** genes expression across different cancers from TCGA using the TISIDB database, KICH: chromophobe renal cell carcinoma, KIRC: clear renal cell carcinoma, KIRP: renal papillary cell carcinoma; The association of ST8SIA1 expression with immune cell infiltration levels in KIRC using the TIMER **(D)** and CIBERSORT **(E)** algorithms; The association of ST8SIA1 expression with immune checkpoint genes' expression in KIRC using GEPIA **(F)** and TIMER 2.0 **(G)** databases.

curves (**Supplementary Figure S2**), the nomogram showed larger net benefits across a wide range of threshold probability than the AJCC stage model both for 3-year and 5-year OS, indicating better clinical utilities. As for genomic alteration, ST8SIA1 was rarely mutated with a relatively low frequency of 1.1% based on the cBioportal database, indicating ST8SIA1 is highly conserved (**Supplementary Figure S3**).

Association Between ST8SIA1 Expression and Immune Cell Infiltration Level

Based on the TISIDB database, the correlation between the expression level of ST8SIA1 and the immune system was explored. As shown in **Figures 2A–C**, the ST8SIA1 expression level was positively correlated to the abundance of most tumor-infiltrating lymphocytes and immunoinhibitory and immunostimulatory gene expressions across different cancers from TCGA. ST8SIA1 was also found to be associated with immune subtypes in KIRC (**Supplementary Figure S4**), we found that ST8SIA1 expression was the highest in the C2 subtype (IFN-gamma dominant) and the lowest in the C5 subtype (immunologically quiet). Based on the TIMER and CIBERSORT algorithms, a negative relationship between ST8SIA1 expression and tumor purity was observed (Rho = -0.334; $p < 0.001$; **Figures 2D,E**). Conversely, the TIMER algorithm (**Figure 2D**) revealed that ST8SIA1 expression was positively associated with the infiltrating levels of $CD4^+$ T cell (Rho = 0.155, $p < 0.001$), $CD8^+$ T cell (Rho = 0.498, $p < 0.001$), neutrophils (Rho = 0.571, $p < 0.001$), and dendritic cells (Rho = 0.528, $p < 0.001$). The CIBERSORT algorithm (**Figure 2E**) demonstrated that the infiltration levels of M1 macrophage

TABLE 2 | The enrichment analysis of Hallmark pathway associated with ST8SIA1 expression using GSEA.

Name	NES	NOM p-val	FDR q-val
HALLMARK_ALLOGRAFT_REJECTION	2.737	0	0
HALLMARK_INTERFERON_GAMMA_RESPONSE	2.702	0	0
HALLMARK_INTERFERON_ALPHA_RESPONSE	2.642	0	0
HALLMARK_INFLAMMATORY_RESPONSE	2.328	0	0
HALLMARK_IL6_JAK_STAT3_SIGNALING	2.318	0	0
HALLMARK_EPITHELIAL_MESENCHYMAL_TRANSITION	2.155	0	0
HALLMARK_COMPLEMENT	2.142	0	0
HALLMARK_KRAS_SIGNALING_UP	1.983	0	0
HALLMARK_TNFA_SIGNALING_VIA_NFKB	1.956	0	0
HALLMARK_IL2_STAT5_SIGNALING	1.952	0	0

NES: normalized enrichment score; NOM: nominal; FDR: false discovery rate.

(Rho = 0.218, $p < 0.001$), activated $CD4^+$ memory T cell (Rho = 0.132, $p < 0.001$), $CD8^+$ T cell (Rho = 0.498, $p < 0.001$), and resting myeloid dendritic cell (Rho = 0.218, $p < 0.001$) were positively associated with ST8SIA1 expression. Furthermore, the arm-level gain of ST8SIA1 had a significant negative correlation with the infiltration level of $CD8^+$ T cells in KIRC (**Supplementary Figure S4**).

Association Between the Expression Levels of ST8SIA1 and Immune Checkpoint Genes

PDCD1 (PD-1), CD274 (PD-L1), and CTLA4 are well-known important immune checkpoint genes. Several novel immune checkpoints genes have been proposed recently, such as LAG3, HAVCR2 (TIM3), TIGIT, and VSIR (C10orf54) (Morad et al., 2021). Based on the GEPIA database (**Figure 2F**), the expression level of ST8SIA1 was significantly positively associated with the expression of PDCD1 (Rho = 0.71, $p < 0.001$), CD274 (Rho = 0.17, $p < 0.001$), CTLA4 (Rho = 0.68, $p < 0.001$), LAG3 (Rho = 0.83, $p < 0.001$), HAVCR2 (Rho = 0.12, $p = 0.005$), TIGIT (Rho = 0.83, $p < 0.001$), and VSIR (Rho = 0.33, $p < 0.001$). Adjusted by tumor purity (**Figure 2G**), the ST8SIA1 expression level was also significantly positively associated with the expression of PDCD1 (Rho = 0.699, $p < 0.001$), CD274 (Rho = 0.271, $p < 0.001$), CTLA4 (Rho = 0.579, $p < 0.001$), LAG3 (Rho = 0.711, $p < 0.001$), HAVCR2 (Rho = 0.217, $p = 0.005$), TIGIT (Rho = 0.79, $p < 0.001$), and VSIR (Rho = 0.329, $p < 0.001$).

The Function of ST8SIA1 in KIRC

The hallmark pathways were identified between low and high ST8SIA1 expression in the TCGA-KIRC cohort using GESA. Almost all of the top 10 pathways that correlated with elevated ST8SIA1 expression are immune-related (**Table 2**). Based on the LinkedOmics database, genes coexpressed with ST8SIA1 in KIRC were identified. The heatmaps show the top 50 genes, the expression of which exhibited significant positive or negative correlation with ST8SIA1 expression (**Figures 3A,B**). The GO and KEGG analyses of significant coexpressed genes showed that most enriched pathways are immune-related (**Figures 3C–F**). Furthermore, single-cell analysis using CancerSEA was performed to investigate the functions of ST8SIA1. In a single-cell resolution in RCC, ST8SIA1 expression was positively associated with the expression of stemness and differentiation signature genes (**Supplementary Figure S4**).

The mRNA and Protein Level of ST8SIA1 in Tissue and Cell

To verify the expression level of ST8SIA1, we performed the immunohistochemical analysis of 46 ccRCC tumor tissues and 37 adjacent normal kidney tissues (**Figures 4A–D**). We observed that 19 tumor tissues out of 46 have a >3 score, and 5 normal tissues of 37 have a >3 score (19/46 vs. 5/37; $p < 0.05$). A total of 8 tumor tissues out of 46 have a > 6 score, while no normal tissue has a > 6 score. To validate the selective expression of ST8SIA1 in tumor cells, the quantitative real-time PCR in RCC cell lines (786-O and ACHN) and a normal kidney epithelial cell line (HK-2) was performed. The ST8SIA1 mRNA was highly expressed in RCC cell lines, compared with a normal kidney cell line (**Figures 4E,F**).

DISCUSSION

The tumor microenvironment, which consists of tumor cells, and various infiltrating immune and stromal cells, plays a critical role in tumor growth, progression, and drug resistance (Binnewies et al., 2018). ccRCC is a highly vascularized and immune cell–infiltrated cancer, resulting in two revolutionary therapies including antiangiogenic therapy and immunotherapy (Qian et al., 2009; Chevrier et al., 2017). While a heterogeneous tumor microenvironment might be associated with therapy resistance and low response rate, it may affect the prognosis of patients.

With the wide application of bioinformatics, several studies have reported different immune-related genes that are associated with the prognosis of cancer patients. For example, Du et al. also revealed an immune-related prognostic factor (TGFBI) in ccRCC patients (Du et al., 2020). In addition, Liu et al. demonstrated that type 2 papillary RCC is associated with immune infiltration and explored potential new targets (CCL19/CCR7, CXCL12/CXCR4, and CCL20/CCR6) (Liu et al., 2020). In the present study, we screened immune-related DEGs based on the stromal/immune scores using the ESTIMATE algorithm in the GSE126964 and

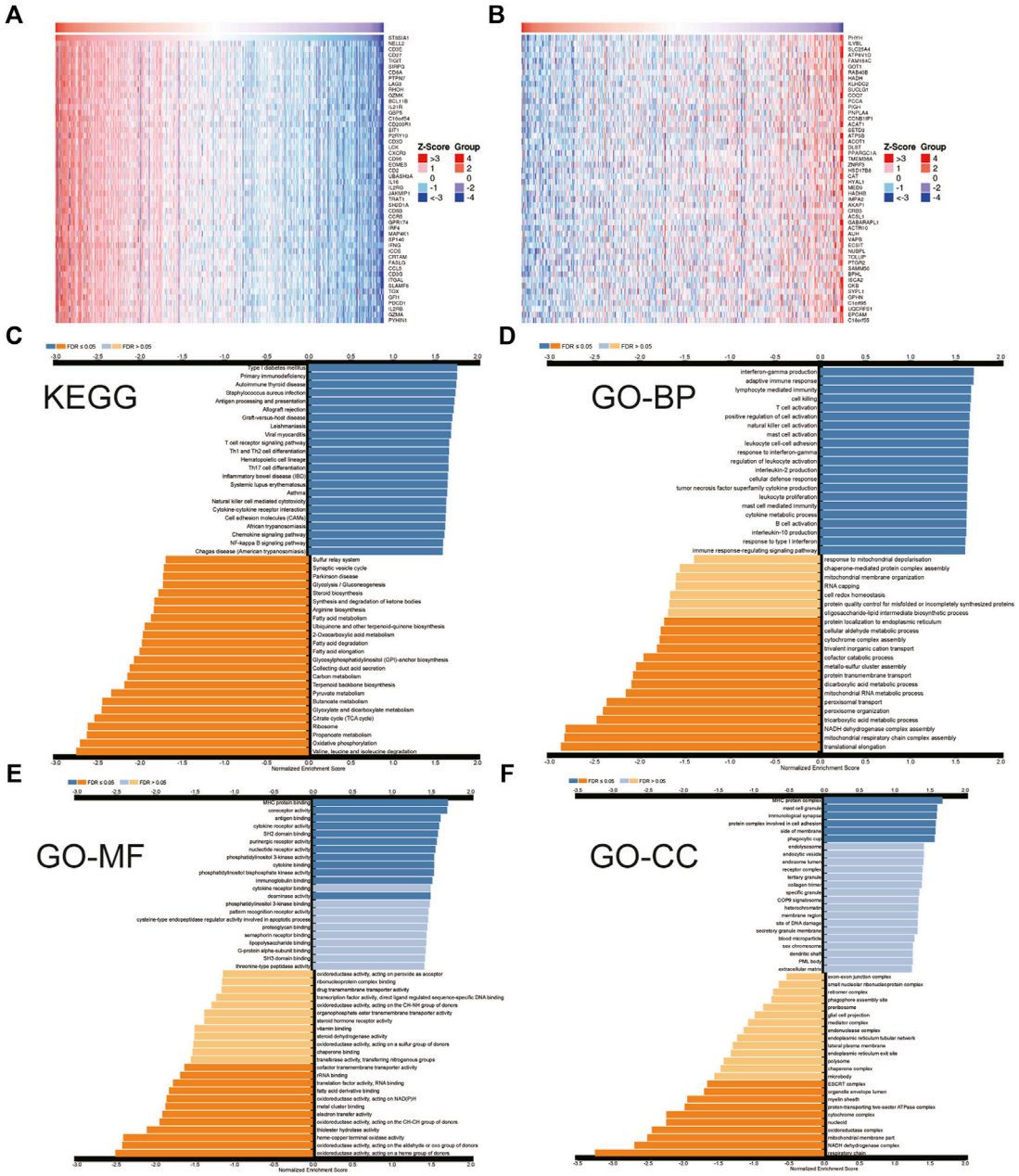

FIGURE 3 | Heatmap of top 50 genes that have positive **(A)** and negative **(B)** correlations with ST8SIA1 expression in TCGA-KIRC using the LinkedOmics database; the KEGG pathway **(C)** and Gene Ontology (GO) biological process (BP), molecular function (MF), cellular component (CC) enrichment **(D–F)** of genes coexpressed with ST8SIA1.

TCGA-KIRC cohorts. ST8SIA1 was identified as the immune-related prognostic gene after reviewing relevant research studies. We found that ST8SIA1 was more expressed in the KIRC tissue than adjacent normal tissue. Higher expression of ST8SIA1 was significantly associated with higher T stage and advanced TNM stage, which indicated that ST8SIA1 was associated with survival. Moreover, univariate and multivariate analyses also revealed that ST8SIA1 was associated with worse OS. Based on TIMER, TISIDB, and GEPIA databases, we observed that ST8SIA1 was significantly associated with infiltration levels of various immune cells. However, different immune cells play different roles in antitumor immunity. Furthermore, the ST8SIA1 expression was positively associated with the expression of several immune checkpoints, indicating a potential suppressive antitumor immunity. GSEA and the LinkedOmics database revealed that ST8SIA1 was significantly enriched in immune-related pathways and functions. All aforementioned findings suggested that ST8SIA1 was highly associated with the immune system and

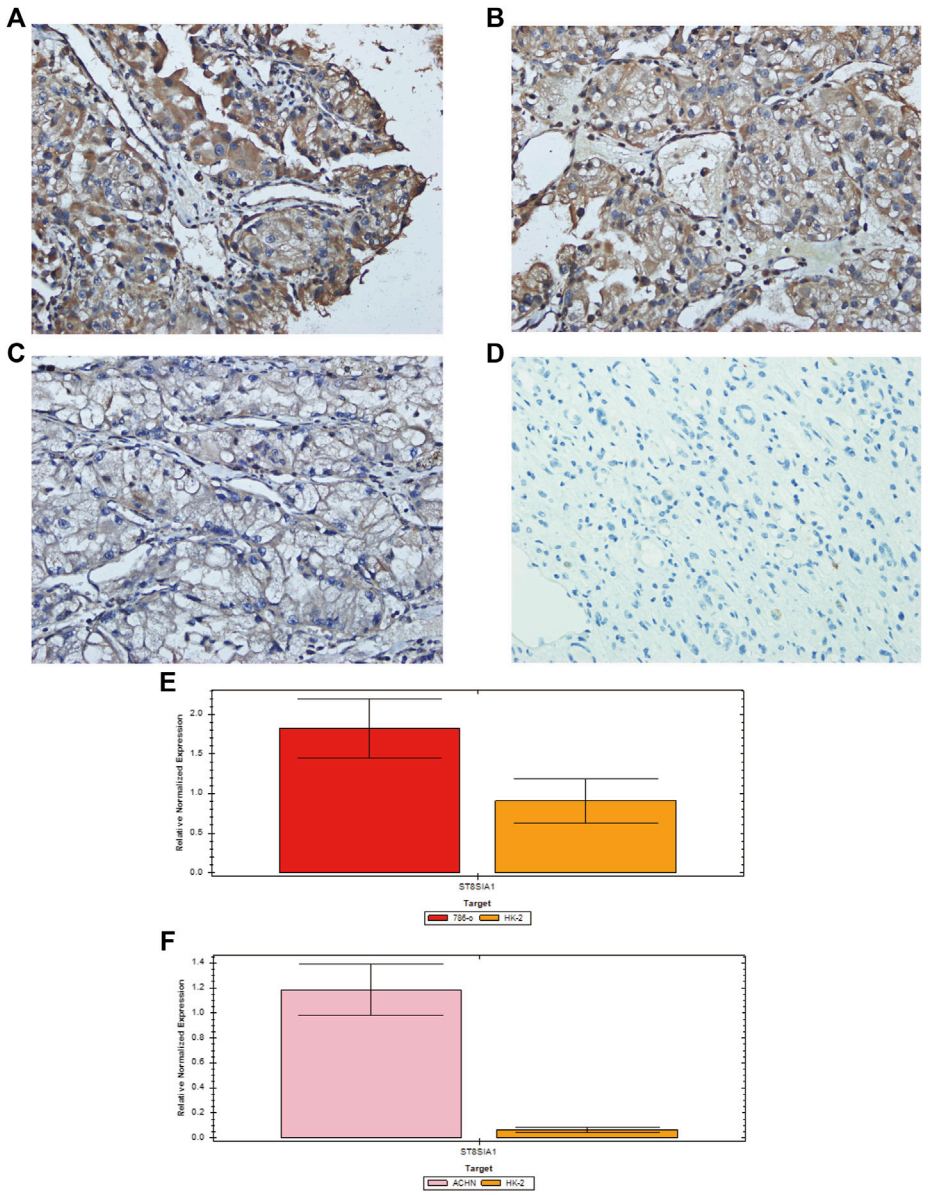

FIGURE 4 | Representative immunohistochemical staining of ST8SIA1 protein in ccRCC tissues [**(A)** +++, **(B)** ++, **(C)** +, magnification: × 400] and normal kidney tissue [**(D)** –, magnification: × 400]; Quantitative real-time PCR of ST8SIA1 in 786-O **(E)** and ACHN **(F)** cells compared with HK-2 cell.

may be a potential target, but these results were obtained through bioinformatics; further studies are required to explore its exact role.

ST8SIA1, also known as GD3 synthase (GD3S), is highly expressed in several tumors, and plays an important role in the development and progression of cancer. In human melanoma SK-MEL-2 cells, GD3S is highly expressed and regulated by transcription factors NF-κB (Kang et al., 2007). Inhibition of GD3S could decrease the cell viability of melanoma cells (Kang et al., 2007). Ramos et al. have found that high expression of GD3S is associated with the phenotype of melanoma brain metastasis, and the overall survival is significantly worse. ST8SIA1 overexpression enhanced cell proliferation and colony formation in melanoma cells (Ramos et al., 2020). In human breast tumors, GD3S could lead to increased stem cell properties and metastatic competence via activation of the c-Met signaling pathway (Sarkar et al., 2015). Glioma is also a highly malignant tumor with a high recurrence rate. GD3S is also highly expressed in glioma. Suppression of GD3S could decrease glioma stem cell–associated properties (Yeh et al., 2016). Ko et al. found that GD3S was highly expressed in lung cancer, and inhibition of GD3S by siRNA could reduce the expression of GD2 and inhibit cell proliferation, migration, and invasion (Ko et al., 2006).

The enzyme GD3S is involved in the synthesis of disialogangliosides with three glycosyl groups (GD3) and is important in tumorigenesis and the development of cancers

(Liu et al., 2018). Certain gangliosides, such as GD3, can promote tumor-associated angiogenesis and strongly regulate cell adhesion and thus initiate tumor metastasis. Moreover, ganglioside antigens on the cell surface, or shed from the cells, act as immunosuppressors (Birklé et al., 2003). In ovarian cancer, GD3 inhibits the NKT cell response as an immune escape mechanism via binding the CD1d antigenic-binding site (Webb et al., 2012). In cutaneous T-cell lymphoma, GD3 inhibits the production of IL-17A as a mechanism of suppressive antitumor immunity (Kume et al., 2021). Biswas et al. observed that selected gangliosides (GM2, GD2, and GD3) are associated with T-cell dysfunction in RCC patients (Biswas et al., 2009). However, the exact mechanism of GD3S in RCC remains unknown. Based on GSEA, we observed that interferon-γ, interferon-α, and IL6-JAK-STAT3 pathways were enriched, which may be connected with the upregulation of immune checkpoint genes and thus may play a role in suppressive antitumor immunity. Further experimental studies are required to explore the exact mechanism.

There are some advantages and limitations in the present study. GEO and TCGA have relatively large sample sizes and comprehensive genomic data, providing a good foundation for analysis. To our knowledge, there is no report that focuses on ST8SIA1 expression in ccRCC patients. Furthermore, we explored the function of ST8SIA1 and its association with immune systems. We also performed immunohistochemical analysis and quantitative real-time PCR to validate the expression level of ST8SIA1. However, though the present study was well-designed and performed carefully, the exact mechanism of ST8SIA1 in ccRCC patients still needs to be explored through relevant experiments.

In conclusion, higher expression of ST8SIA1 was associated with adverse factors as well as worse overall survival. ST8SIA1 was identified as an immune-related gene and potential target in ccRCC patients. Further relevant studies are required to validate our findings.

DATA AVAILABILITY STATEMENT

The datasets presented in this study can be found in online repositories. The names of the repository/repositories and accession number(s) can be found in the article/ **Supplementary Material**.

ETHICS STATEMENT

The studies involving human participants were reviewed and approved by Sichuan University West China Hospital. The patients/participants provided their written informed consent to participate in this study.

AUTHOR CONTRIBUTIONS

XH and YY performed the data analysis. XH, YW, and SR collected the data. XH, SR and XL designed this study and drafted and reviewed the manuscript.

FUNDING

This work was supported by Sichuan Science and Technology Program (2022YFS0133 and 2022NSFSC1526).

SUPPLEMENTARY MATERIAL

The Supplementary Material for this article can be found online at: https://www.frontiersin.org/articles/10.3389/fphar.2022.901518/full#supplementary-material

REFERENCES

Becht, E., de Reyniès, A., Giraldo, N. A., Pilati, C., Buttard, B., Lacroix, L., et al. (2016). Immune and Stromal Classification of Colorectal Cancer Is Associated with Molecular Subtypes and Relevant for Precision Immunotherapy. *Clin. Cancer Res.* 22 (16), 4057–4066. doi:10.1158/1078-0432.Ccr-15-2879

Bedke, J., Albiges, L., Capitanio, U., Giles, R. H., Hora, M., Lam, T. B., et al. (2021). The 2021 Updated European Association of Urology Guidelines on Renal Cell Carcinoma: Immune Checkpoint Inhibitor-Based Combination Therapies for Treatment-Naive Metastatic Clear-cell Renal Cell Carcinoma Are Standard of Care. *Eur. Urol.* 80 (4), 393–397. doi:10.1016/j.eururo.2021.04.042

Binnewies, M., Roberts, E. W., Kersten, K., Chan, V., Fearon, D. F., Merad, M., et al. (2018). Understanding the Tumor Immune Microenvironment (TIME) for Effective Therapy. *Nat. Med.* 24 (5), 541–550. doi:10.1038/s41591-018-0014-x

Birklé, S., Zeng, G., Gao, L., Yu, R. K., and Aubry, J. (2003). Role of Tumor-Associated Gangliosides in Cancer Progression. *Biochimie* 85 (3-4), 455–463. doi:10.1016/s0300-9084(03)00006-3

Biswas, S., Biswas, K., Richmond, A., Ko, J., Ghosh, S., Simmons, M., et al. (2009). Elevated Levels of Select Gangliosides in T Cells from Renal Cell Carcinoma Patients Is Associated with T Cell Dysfunction. *J. Immunol.* 183 (8), 5050–5058. doi:10.4049/jimmunol.0900259

Cerami, E., Gao, J., Dogrusoz, U., Gross, B. E., Sumer, S. O., Aksoy, B. A., et al. (2012). The cBio Cancer Genomics Portal: an Open Platform for Exploring Multidimensional Cancer Genomics Data. *Cancer Discov.* 2 (5), 401–404. doi:10.1158/2159-8290.Cd-12-0095

Chevrier, S., Levine, J. H., Zanotelli, V. R. T., Silina, K., Schulz, D., Bacac, M., et al. (2017). An Immune Atlas of Clear Cell Renal Cell Carcinoma. *Cell* 169 (4), 736. doi:10.1016/j.cell.2017.04.016

Du, G. W., Yan, X., Chen, Z., Zhang, R. J., Tuoheti, K., Bai, X. J., et al. (2020). Identification of Transforming Growth Factor Beta Induced (TGFBI) as an Immune-Related Prognostic Factor in Clear Cell Renal Cell Carcinoma (ccRCC). *Aging (Albany NY)* 12 (9), 8484–8505. doi:10.18632/aging.103153

Hanahan, D., and Coussens, L. M. (2012). Accessories to the Crime: Functions of Cells Recruited to the Tumor Microenvironment. *Cancer Cell* 21 (3), 309–322. doi:10.1016/j.ccr.2012.02.022

Jamil, M. L., Keeley, J., Sood, A., Dalela, D., Arora, S., Peabody, J. O., et al. (2020). Long-term Risk of Recurrence in Surgically Treated Renal Cell Carcinoma: A Post Hoc Analysis of the Eastern Cooperative Oncology Group-American College of Radiology Imaging Network E2805 Trial Cohort. *Eur. Urol.* 77 (2), 277–281. doi:10.1016/j.eururo.2019.10.028

Kang, N. Y., Kim, C. H., Kim, K. S., Ko, J. H., Lee, J. H., Jeong, Y. K., et al. (2007). Expression of the Human CMP-NeuAc:GM3 Alpha2,8-Sialyltransferase (GD3 Synthase) Gene through the NF-kappaB Activation in Human Melanoma SK-MEL-2 Cells. *Biochim. Biophys. Acta* 1769 (11-12), 622–630. doi:10.1016/j.bbaexp.2007.08.001

Ko, K., Furukawa, K., Takahashi, T., Urano, T., Sanai, Y., Nagino, M., et al. (2006). Fundamental Study of Small Interfering RNAs for Ganglioside GD3 Synthase

Gene as a Therapeutic Target of Lung Cancers. *Oncogene* 25 (52), 6924–6935. doi:10.1038/sj.onc.1209683

Kume, M., Kiyohara, E., Matsumura, Y., Koguchi-Yoshioka, H., Tanemura, A., Hanaoka, Y., et al. (2021). Ganglioside GD3 May Suppress the Functional Activities of Benign Skin T Cells in Cutaneous T-Cell Lymphoma. *Front. Immunol.* 12, 651048. doi:10.3389/fimmu.2021.651048

Li, T., Fu, J., Zeng, Z., Cohen, D., Li, J., Chen, Q., et al. (2020). TIMER2.0 for Analysis of Tumor-Infiltrating Immune Cells. *Nucleic Acids Res.* 48 (W1), W509–w514. doi:10.1093/nar/gkaa407

Liu, J., Zheng, X., Pang, X., Li, L., Wang, J., Yang, C., et al. (2018). Ganglioside GD3 Synthase (GD3S), a Novel Cancer Drug Target. *Acta Pharm. Sin. B* 8 (5), 713–720. doi:10.1016/j.apsb.2018.07.009

Liu, T., Zhang, M., and Sun, D. (2020). Immune Cell Infiltration and Identifying Genes of Prognostic Value in the Papillary Renal Cell Carcinoma Microenvironment by Bioinformatics Analysis. *Biomed. Res. Int.* 2020, 5019746. doi:10.1155/2020/5019746

Ljungberg, B., Albiges, L., Abu-Ghanem, Y., Bensalah, K., Dabestani, S., Fernández-Pello, S., et al. (2019). European Association of Urology Guidelines on Renal Cell Carcinoma: The 2019 Update. *Eur. Urol.* 75 (5), 799–810. doi:10.1016/j.eururo.2019.02.011

Morad, G., Helmink, B. A., Sharma, P., and Wargo, J. A. (2021). Hallmarks of Response, Resistance, and Toxicity to Immune Checkpoint Blockade. *Cell* 184 (21), 5309–5337. doi:10.1016/j.cell.2021.09.020

Motzer, R. J., Rini, B. I., McDermott, D. F., Arén Frontera, O., Hammers, H. J., Carducci, M. A., et al. (2019). Nivolumab Plus Ipilimumab versus Sunitinib in First-Line Treatment for Advanced Renal Cell Carcinoma: Extended Follow-Up of Efficacy and Safety Results from a Randomised, Controlled, Phase 3 Trial. *Lancet Oncol.* 20 (10), 1370–1385. doi:10.1016/s1470-2045(19)30413-9

Motzer, R. J., Powles, T., Atkins, M. B., Escudier, B., McDermott, D. F., Alekseev, B. Y., et al. (2022). Final Overall Survival and Molecular Analysis in IMmotion151, a Phase 3 Trial Comparing Atezolizumab Plus Bevacizumab vs Sunitinib in Patients with Previously Untreated Metastatic Renal Cell Carcinoma. *JAMA Oncol.* 8, 275. doi:10.1001/jamaoncol.2021.5981

Qian, C. N., Huang, D., Wondergem, B., and Teh, B. T. (2009). Complexity of Tumor Vasculature in Clear Cell Renal Cell Carcinoma. *Cancer* 115 (10 Suppl. l), 2282–2289. doi:10.1002/cncr.24238

Ramos, R. I., Bustos, M. A., Wu, J., Jones, P., Chang, S. C., Kiyohara, E., et al. (2020). Upregulation of Cell Surface GD3 Ganglioside Phenotype Is Associated with Human Melanoma Brain Metastasis. *Mol. Oncol.* 14 (8), 1760–1778. doi:10.1002/1878-0261.12702

Rhodes, D. R., Yu, J., Shanker, K., Deshpande, N., Varambally, R., Ghosh, D., et al. (2004). ONCOMINE: a Cancer Microarray Database and Integrated Data-Mining Platform. *Neoplasia* 6 (1), 1–6. doi:10.1016/s1476-5586(04)80047-2

Rini, B. I., Plimack, E. R., Stus, V., Gafanov, R., Hawkins, R., Nosov, D., et al. (2019). Pembrolizumab Plus Axitinib versus Sunitinib for Advanced Renal-Cell Carcinoma. *N. Engl. J. Med.* 380 (12), 1116–1127. doi:10.1056/NEJMoa1816714

Ru, B., Wong, C. N., Tong, Y., Zhong, J. Y., Zhong, S. S. W., Wu, W. C., et al. (2019). TISIDB: an Integrated Repository Portal for Tumor-Immune System Interactions. *Bioinformatics* 35 (20), 4200–4202. doi:10.1093/bioinformatics/btz210

Sarkar, T. R., Battula, V. L., Werden, S. J., Vijay, G. V., Ramirez-Peña, E. Q., Taube, J. H., et al. (2015). GD3 Synthase Regulates Epithelial-Mesenchymal Transition and Metastasis in Breast Cancer. *Oncogene* 34 (23), 2958–2967. doi:10.1038/onc.2014.245

Siegel, R. L., Miller, K. D., Fuchs, H. E., and Jemal, A. (2022). Cancer Statistics, 2022. *CA Cancer J. Clin.* 72 (1), 7–33. doi:10.3322/caac.21708

Sung, H., Ferlay, J., Siegel, R. L., Laversanne, M., Soerjomataram, I., Jemal, A., et al. (2021). Global Cancer Statistics 2020: GLOBOCAN Estimates of Incidence and Mortality Worldwide for 36 Cancers in 185 Countries. *CA Cancer J. Clin.* 71 (3), 209–249. doi:10.3322/caac.21660

Tang, Z., Li, C., Kang, B., Gao, G., Li, C., and Zhang, Z. (2017). GEPIA: a Web Server for Cancer and Normal Gene Expression Profiling and Interactive Analyses. *Nucleic Acids Res.* 45 (W1), W98–w102. doi:10.1093/nar/gkx247

Vasaikar, S. V., Straub, P., Wang, J., and Zhang, B. (2018). LinkedOmics: Analyzing Multi-Omics Data within and across 32 Cancer Types. *Nucleic Acids Res.* 46 (D1), D956–d963. doi:10.1093/nar/gkx1090

Webb, T. J., Li, X., Giuntoli2nd, Lopez, R. L. P. H., Lopez, P. H., Heuser, C., Schnaar, R. L., et al. (2012). Molecular Identification of GD3 as a Suppressor of the Innate Immune Response in Ovarian Cancer. *Cancer Res.* 72 (15), 3744–3752. doi:10.1158/0008-5472.Can-11-2695

Williamson, T. J., Pearson, J. R., Ischia, J., Bolton, D. M., and Lawrentschuk, N. (2016). Guideline of Guidelines: Follow-Up after Nephrectomy for Renal Cell Carcinoma. *BJU Int.* 117 (4), 555–562. doi:10.1111/bju.13384

Yeh, S. C., Wang, P. Y., Lou, Y. W., Khoo, K. H., Hsiao, M., Hsu, T. L., et al. (2016). Glycolipid GD3 and GD3 Synthase Are Key Drivers for Glioblastoma Stem Cells and Tumorigenicity. *Proc. Natl. Acad. Sci. U. S. A.* 113 (20), 5592–5597. doi:10.1073/pnas.1604721113

Yoshihara, K., Shahmoradgoli, M., Martínez, E., Vegesna, R., Kim, H., Torres-Garcia, W., et al. (2013). Inferring Tumour Purity and Stromal and Immune Cell Admixture from Expression Data. *Nat. Commun.* 4, 2612. doi:10.1038/ncomms3612

Yuan, H., Yan, M., Zhang, G., Liu, W., Deng, C., Liao, G., et al. (2019). CancerSEA: a Cancer Single-Cell State Atlas. *Nucleic Acids Res.* 47 (D1), D900–d908. doi:10.1093/nar/gky939

Zhu, W. K., Xu, W. H., Wang, J., Huang, Y. Q., Abudurexiti, M., Qu, Y. Y., et al. (2020). Decreased SPTLC1 Expression Predicts Worse Outcomes in ccRCC Patients. *J. Cell Biochem.* 121 (2), 1552–1562. doi:10.1002/jcb.29390

Conflict of Interest: The authors declare that the research was conducted in the absence of any commercial or financial relationships that could be construed as a potential conflict of interest.

Publisher's Note: All claims expressed in this article are solely those of the authors and do not necessarily represent those of their affiliated organizations, or those of the publisher, the editors, and the reviewers. Any product that may be evaluated in this article, or claim that may be made by its manufacturer, is not guaranteed or endorsed by the publisher.

frontiers | Frontiers in Oncology

ORIGINAL RESEARCH
published: 22 July 2022
doi: 10.3389/fonc.2022.912694

Stemness Analysis Uncovers That The Peroxisome Proliferator-Activated Receptor Signaling Pathway Can Mediate Fatty Acid Homeostasis In Sorafenib-Resistant Hepatocellular Carcinoma Cells

Tingze Feng[1†], Tianzhi Wu[1†], Yanxia Zhang[2†], Lang Zhou[1†], Shanshan Liu[1,3], Lin Li[1], Ming Li[1], Erqiang Hu[1], Qianwen Wang[1], Xiaocong Fu[1], Li Zhan[1], Zijing Xie[1], Wenqin Xie[1], Xianying Huang[4], Xuan Shang[2*] and Guangchuang Yu[1,4*]*

[1] Department of Bioinformatics, School of Basic Medical Sciences, Southern Medical University, Guangzhou, China, [2] Department of Medical Genetics, School of Basic Medical Sciences, Southern Medical University, Guangzhou, China, [3] Country Guangdong Provincial Key Laboratory of Viral Hepatitis Research, Hepatology Unit and Department of Infectious Diseases, Nanfang Hospital, Southern Medical University, Guangzhou, China, [4] Division of Vascular and Interventional Radiology, Department of General Surgery, Nanfang Hospital, Southern Medical University, Guangzhou, China

Hepatocellular carcinoma (HCC) stem cells are regarded as an important part of individualized HCC treatment and sorafenib resistance. However, there is lacking systematic assessment of stem-like indices and associations with a response of sorafenib in HCC. Our study thus aimed to evaluate the status of tumor dedifferentiation for HCC and further identify the regulatory mechanisms under the condition of resistance to sorafenib. Datasets of HCC, including messenger RNAs (mRNAs) expression, somatic mutation, and clinical information were collected. The mRNA expression-based stemness index (mRNAsi), which can represent degrees of dedifferentiation of HCC samples, was calculated to predict drug response of sorafenib therapy and prognosis. Next, unsupervised cluster analysis was conducted to distinguish mRNAsi-based subgroups, and gene/geneset functional enrichment analysis was employed to identify key sorafenib resistance-related pathways. In addition, we analyzed and confirmed the regulation of key genes discovered in this study by combining other omics data. Finally, Luciferase reporter assays were performed to validate their regulation. Our study demonstrated that the stemness index obtained from transcriptomic is a promising biomarker to predict the response of sorafenib therapy and the prognosis in HCC. We revealed the peroxisome proliferator-activated receptor signaling pathway (the PPAR signaling pathway), related to fatty acid biosynthesis, that was a potential sorafenib resistance pathway that had not been reported before. By analyzing the core regulatory genes of the PPAR signaling pathway, we identified four candidate target genes, *retinoid X receptor beta* (*RXRB*), *nuclear receptor subfamily 1 group H member 3* (*NR1H3*), *cytochrome P450 family 8*

OPEN ACCESS

Edited by:
Haitao Wang,
National Cancer Institute (NIH),
United States

Reviewed by:
Venkata Ramireddy Narala,
Yogi Vemana University, India
Fan Feng,
The 302th Hospital of PLA, China
Yuejun Wang,
University of California, San Francisco,
United States
Dake Zhang,
Beihang University, China

***Correspondence:**
Xianying Huang
147932441@qq.com
Xuan Shang
shangrabbit@163.com
Guangchuang Yu
gcyu1@smu.edu.cn

†These authors have contributed equally to this work

Specialty section:
This article was submitted to Pharmacology of Anti-Cancer Drugs, a section of the journal Frontiers in Oncology

Received: *04 April 2022*
Accepted: *22 June 2022*
Published: *22 July 2022*

Citation:
Feng T, Wu T, Zhang Y, Zhou L, Liu S, Li L, Li M, Hu E, Wang Q, Fu X, Zhan L, Xie Z, Xie W, Huang X, Shang X and Yu G (2022) Stemness Analysis Uncovers That The Peroxisome Proliferator-Activated Receptor Signaling Pathway Can Mediate Fatty Acid Homeostasis In Sorafenib-Resistant Hepatocellular Carcinoma Cells. Front. Oncol. 12:912694. doi: 10.3389/fonc.2022.912694

subfamily B member 1 (*CYP8B1*) and *stearoyl-CoA desaturase* (*SCD*), as a signature to distinguish the response of sorafenib. We proposed and validated that the *RXRB* and *NR1H3* could directly regulate *NR1H3* and *SCD*, respectively. Our results suggest that the combined use of *SCD* inhibitors and sorafenib may be a promising therapeutic approach.

Keywords: hepatocellular carcinoma, sorafenib resistance, PPAR signaling pathway, stemness index, prognosis

INTRODUCTION

Primary liver cancer (PLC) is the fourth most common cause of cancer-related deaths worldwide and the sixth-most common cancer in the world, according to data provided by the World Health Organization (WHO) (1–3). HCC is the most common form of liver cancer and accounts for approximately 80% of all cases of PLC (4). Numerous patients were first diagnosed with advanced-stage HCC (5). Sorafenib, which is administered only as a first-line chemotherapeutic agent in advanced HCC patients, is the most prevalent oral small-molecule multi-kinase inhibitor and has been in use for over a decade (5, 6). Sorafenib can inhibit tumor cell proliferation and angiogenesis, thereby inducing cancer cell apoptosis, which not only blocks the Ras/MEK/ERK-mediated cell signaling pathway but also blocks tumor angiogenesis, by inhibiting kinases such as vascular endothelial growth factor receptor (VEGFR) and platelet-derived growth factor receptor (PDGFR) (1, 6). However, some HCC patients exhibited congenital resistance to sorafenib or acquired resistance after treatment (6, 7). Only a few patients with HCC exhibited extended survival after receiving sorafenib treatment (8). Therefore, we need to develop a method for predicting the response of HCC patients to sorafenib, to facilitate the precise treatment of advanced HCC patients. Importantly, we need to identify the primary and additional mechanisms of acquired sorafenib resistance.

Stemness was defined as the ability of cells to self-renewal and interact with their environment to maintain a balance between quiescence, proliferation, and regeneration (9, 10). Normal adult stem cells exhibit stemness when involved in tissue homeostasis, whereas cancer stem cells (CSCs) display stemness when involved in malignant growth (10, 11). Moreover, it had been proven that non-CSCs can dedifferentiate into CSCs by the stimuli of the tumor microenvironment (11, 12). Cancer progression necessitates the gradual loss of a differentiated phenotype and restoration of progenitor and stem cell-like features (11, 13, 14). Both patient prognosis and drug response are likely to be related to the state of tumor cells (15). Evidence has shown that an assessment of tumor stemness can reflect tumor status, and liver cancer stem cells can mediate tumor growth and sorafenib resistance development (7, 16). Undifferentiated HCC is more likely to result in tumor metastasis, disease recurrence, poor prognosis, and drug resistance (7, 17). However, there is a lack of systematic studies examining the relationship between sorafenib resistance and the HCC stemness index. In recent years, despite several efforts to identify potential biomarkers in HCC patients' prognosis, only a few have focused on drug response (18). Numerous HCC risk signatures were identified by gene expression for predicting HCC patient prognosis. Whereas these signatures were typically validated using only a single dataset or were not externally validated (19), resulting in unreliable clinical outcome prediction. There is still an urgent need for reliable and robust markers that can be used for predicting the prognosis of different HCC cohorts and the effect of drug therapy, which are also of great value for the precise treatment of patients. Several studies have shown that the stemness index is effective for the prediction of prognosis and drug resistance in multiple malignancies (20–23). Here, we aimed to explore the regulatory mechanism under sorafenib-resistant conditions using the stemness index.

In this study, the cancer stemness was assessed by extracting sets of transcriptomic features (mRNAsi), using the one-class logistic regression (OCLR) machine-learning algorithm, which was proposed in a recent study (22). We systematically analyzed HCC stem-like indices using a total of 7 independent HCC cohorts and the OCLR algorithm. We identified mRNAsi-related subgroups that can distinguish between different responses to sorafenib treatment and evaluated the prognostic significance of mRNAsi in several datasets. To our knowledge, this was the first attempt to use the tumor stemness index to explore the potential mechanisms of sorafenib drug resistance development. Moreover, we identified that four genes, which were found to be involved in the PPAR signaling pathway, might play a role in sorafenib resistance development. The signature for predicting sorafenib treatment effectiveness has been extracted. We additionally discussed the regulation of SCD and its upstream genes in the PPAR signaling pathway by combining other omics data such as somatic mutations of key genes, transcription factor binding site for key genes, and methylation level of the SCD promoter. And luciferase reporter assays were performed to validate regulations of key genes.

MATERIALS AND METHODS

Patient Cohorts and Clinical Data

Publicly available data regarding HCC cohorts were systematically screened and checked, and matched with individual clinical annotations. In total, we obtained seven HCC cohorts, involving a total of 991 samples; of these, five cohorts were used for the survival study (TCGA-HCC, ICGC-JP, GSE14520 (24), GSE76427 (25), GSE116174), and the other two were used for a sorafenib drug response study (GSE109211 (26) cohort and GSE143477 (27) cohort). The expression profiles of the TCGA cohort were obtained through a data portal (https://xenabrowser.net/) (28), along with both somatic mutation data

and clinical data of tumor samples. Besides, the GSE14520, GSE76427, GSE116174, GSE109211, and GSE143477 cohorts were obtained from the Gene Expression Omnibus (http://www.ncbi.nlm.nih.gov/geo/). Sixty-seven samples treated with sorafenib were contained in the GSE109211. The sorafenib samples of GSE109211 were divided into "responder" (n=21) and "non-responder" (n=46) groups in terms of recurrence-free survival (RFS). Compared with the responder group in GSE109211, sorafenib non-responders were defined as patients in whom sorafenib had no effect (sorafenib resistance). GSE143477 contains three sorafenib-resistant samples and three sorafenib-sensitive samples. The expression profiles and clinical information regarding the ICGC-JP cohort were downloaded from the ICGC Data Portal (https://dcc.icgc.org/). Three methods were adopted to collect clinical information: 1) Information was downloaded from the database if the authors had uploaded it; 2) Information was extracted from the original literature; and 3) It was obtained from the corresponding authors if necessary. All the information regarding these cohorts has been summarized in **Table 1**.

Calculation of mRNAsi for HCC

We collected samples from seven HCC cohorts, and derived their mRNA expression data and corresponding clinical information (survival or response to sorafenib), to characterize the mRNA stemness features of HCC patients, as demonstrated in the flowchart (**Figure 1**). We used an OCLR model based on the Progenitor Cell Biology Consortium (PCBC) embryonic stem cell data (29), to characterize the stemness signature. We collected 229 stem cell samples with 13013 protein-coding genes for use in the training dataset and assessed the stemness weight of each gene using the R package, *gelnet* (version 1.2.1) (30). The stemness weight of each gene has been shown in **Table S1**. These values were then applied to characterize the stemness features for each patient in a total of 6 HCC cohorts and obtain information regarding their mRNAsi. The mRNAsi, which range from 0 to 1, could serve as an indicator for assessing the degree of dedifferentiation of tumor samples.

We selected tumor samples from the TCGA-HCC cohort for inclusion in the survival training set and calculated the mRNAsi for the training set. We further classified the HCC patients in the TCGA-HCC cohort into the high-mRNAsi and low-mRNAsi groups, based on a median mRNAsi value of 0.55.

To verify the hypothesis that the lower the tumor differentiation, the higher the malignancy, and the worse the patient prognosis, we calculated the mRNAsi for five HCC cohorts. Tumor samples in the TCGA-HCC cohort were selected for inclusion in the training set and classified into the high-mRNAsi and low-mRNAsi groups, based on a median mRNAsi value of 0.55. Kaplan-Meier analysis (K-M analysis) was performed for the two groups. We validated the mRNAsi cutoff for prognosis prediction for the ICGC cohort and three GEO cohorts. In each cohort, tumor samples were divided into the high and low groups based on the mRNAsi cutoff value of 0.55. The validation of the prognostic significance of mRNAsi was also performed based on K-M analysis. R packages such as *survival* and *survminer* (31–33) were used for performing K-M analysis and log-rank tests in all cohorts.

Identification of the Relationship Between mRNAsi Subgroups and Sorafenib Response

After testing the hypothesis that mRNAsi can predict prognosis in HCC patients, we further hypothesized that mRNAsi may be associated with drug treatment sensitivity based on the activity of multiple inhibitors that were shown to be highly correlated with cancer stemness index mRNAsi (22). First, we identified differentially expressed genes (DEGs) between the high and low mRNAsi subgroups in the GSE109211 cohort. Sixty-seven samples were divided into two segments based on the median mRNAsi in the sorafenib cohort (median = 0.2513743). Additionally, 845 DEGs were analyzed among two segments using R package *limma* (34)(| log2foldchange| > 1.5, adjusted p-value < 0.01).

Then, hierarchical clustering was performed based on DEGs using the R package *ConsensusClusterPlus* (35), which used an algorithm to determine the cluster count and membership during unsupervised analysis. The process has repeated a total of 1000 times, to ensure the stability of the classification process; these samples were clustered into two groups based on the estimated number of clusters. The relationship between mRNAsi subgroups and the response to sorafenib was assessed and visualized using the R package *ggstatplot* (36).

Identification of Hub Pathways and Genes Involved in Sorafenib Resistance

After analyzing the relationship between mRNAsi subgroups and drug resistance, we further explored and evaluated the functional mechanisms that the DEGs between two subgroups might participate in, to identify molecular changes at the pathway level. WikiPathway enrichment analysis and visualization were performed *via clusterProfiler* (37) and *enrichplot* packages. For

TABLE 1 | Information regarding the HCC cohorts used in this study.

Cohort Names	Sample Size	Direction of Analysis	PMID	Link
TCGA-HCC	330	Prognosis	NA	https://xenabrowser.net/
ICGC-JP	229	Prognosis	NA	https://dcc.icgc.org/releases/release_28/Projects/LIRI-JP
GSE14520		Prognosis	21159642	
GSE76427		Prognosis	29117471	
GSE116174	359	Prognosis	NA	https://www.ncbi.nlm.nih.gov/geo/query/
GSE109211	67	Sorafenib response	30108162	
GSE143477	6	Sorafenib response	32554246	

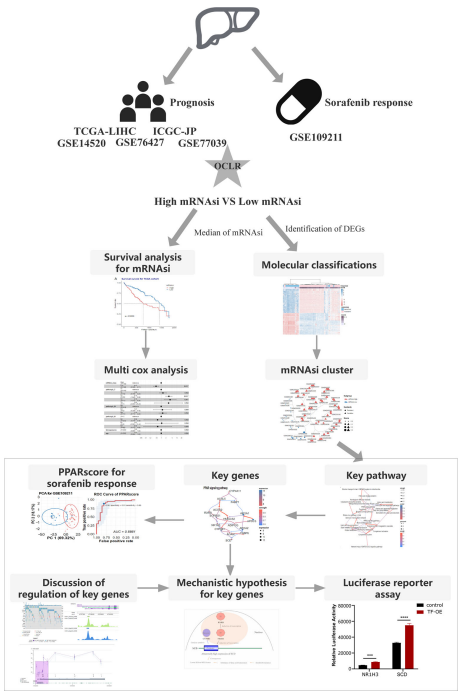

FIGURE 1 | The flowchart demonstrates the analytical process of calculating HCC stemness and its association with the response to sorafenib treatment and HCC patient prognosis.

focused critical pathways, the key regulatory genes involved also need to be analyzed. *CBNplot* (38), which exhibited a Bayesian network inference approach, was employed to explore molecular regulatory relationships. We set the parameter *R* (the number of bootstraps) to 10000 to ensure that the gene or pathway regulatory network can be stably inferred.

Generation and Validation of a PPAR-Related Signature for Sorafenib Resistance

We additionally examined whether the four hub genes identified by *CBNplot* could be used to distinguish the response to sorafenib. Principal component analysis (PCA) and visualization were performed *via FactomineR* (39), *ggplot2*, and *ggstatplot* (36). To assess the possibility of resistance to sorafenib, we used the first 2 principal components (number of dimensions: 2) to construct a PPAR-relevant gene signature. The signature scores contained the coordinates of samples in the first 2 principal components (PCs), which indicate the correlation between a sample and two principal components. The use of this method can enable the score to focus on the set with the largest block of correlated (or non-correlated) genes in the set. We then defined the PPAR-related signature score using a method similar to that used in Zhang's study (40–42). *PPARscore* was defined as the risk score of sorafenib and was evaluated by adding the values for *Dimi1* and *Dimi2*. *Dimi1* was defined as the coordinate on PC1 of sample *i*. *Dimi2* was defined as the coordinate on PC2 of sample *i*. The formula used is as follows:

$$PPARscore = Dimi1 + Dimi2$$

Sixty-seven samples were divided into two segments according to the best threshold of *PPARscore*, which was the point closest to the upper left corner in the Receiver-operating characteristic (ROC) curve. Patients with PCA scores greater than the *PPARscore* cutoff (cutoff = -0.56) had a higher likelihood of developing sorafenib resistance. The *PPARscore* and its cutoff were validated in another sorafenib cohort, i.e., GSE143477.

Analysis of Somatic Mutations for Hub Genes

We checked the mutation data of hub genes in the TCGA-HCC cohort, to examine whether the hub genes were affected by genomic alterations. We downloaded somatic variants in the mutation annotation format (MAF) and visualized the files. We compared the frequencies of somatic mutations in the top 10 mutational genes and key genes in the PPAR signaling pathway. The maftools R package was adopted for analysis (43).

Visualization of Transcription Factor Binding Site for Key Genes

Cistrome Data Browser, a resource of human cis-regulatory data derived from Chromatin immunoprecipitation followed by sequencing (ChIP-seq). ChIP-seq profiling assays provide the genome-wide locations of transcription factor (TF) binding sites.

We queried the potential binding transcript factors for specific genes in the Cistrome Data Browser (44, 45). Two *RXRB* ChIP-seq samples were used to analyze the binding of *RXRB* to the *NR1H3* promoter (ENCODE Project Consortium et al.) (46). In addition, four *NR1H3* ChIP-seq samples were used to analyze the binding of *NR1H3* to the *SCD* promoter (Savic D. et al.) (47).

Luciferase Reporter Assay

To examine the effect of *RXRB* on *NR1H3* and *NR1H3* on *SCD* transcriptional activity, we constructed pGL4.18 vectors composed of *NR1H3* or *SCD* promoters. Empty pcDNA3.1 plasmid, pcDNA3.1-*RXRB*, or pcDNA3.1-*NR1H3* plasmid was co-transfected with pGL4.18-promoter vectors and phRL-TK plasmids using Lipofectamine 2000 in MHCC-97h cells. MHCC-97h cells were then harvested and luciferase activity was analyzed by using Dual-Luciferase® Reporter Assay System kit (Promega). In order to compare the transfection efficiency, the firefly luciferase values were revised by the corresponding Renilla luciferase values.

Visualization of Promoter DNA Methylation

We examined whether the expression levels of key genes related to the response to sorafenib were affected by methylation. We determined and visualized the methylation status of the SCD promoter using MEXPRESS (48), which is a web tool for generating fast queries and visualizing methylation data for the TCGA-HCC cohort.

Statistical Analysis

Univariate survival analysis was performed *via* K-M survival analysis and the log-rank test. Correlation coefficients were assessed *via* Spearman analysis. Analyses of differentially expressed genes were performed based on the *limma* package, and K-M analysis was performed using the *survival* package and *survminer* package. Gene functional enrichment analysis was conducted *via clusterProfiler*. The mRNAsi-related subgroups were visualized using *ggtree*, *via* the generation of gene clustering trees (49). ROC curve was performed, and the area under the ROC curve was used to assess the predictive performance of *PPARscore* using the R package *pROC*. Different expressions between two groups (sorafenib-sensitive or sorafenib-resistant) were assessed using the Wilcoxon Rank Sum Test and P values adjusted by the hommel method. All statistical analyses were performed using R (Version 4.0.2), and the statistical significance was defined based on whether $P < 0.05$ or $P < 0.01$.

RESULTS

mRNAsi Is Significantly Correlated With the Response to Sorafenib

The mRNAsi value was calculated as Spearman's correlation between the weight vectors of the stemness signature using a *gelnet* trained OCLR model, based on the stem cell data (29, 30) and mRNA expression data for each of the HCC samples. Its value ranges between 0 to 1; a higher mRNAsi represents a lower level of differentiation in a sample, signaling drug resistance (16, 17). We explored mRNAsi subgroups to distinguish the response to sorafenib therapy. First, the mRNAsi scores of samples in the sorafenib cohort GSE109211 were calculated, and the samples were classified into the high and low subgroups using the median value of mRNAsi (0.2513743). Then, differential expression analysis was performed. Finally, 845 DEGs were identified using the screening criteria ($|logFC| > 1.5$, adj.P-value < 0.01) (**Figure 2A**). We could utilize those DEGs to cluster for identifying mRNAsi subgroups.

To investigate the relationship between DEGs, mRNAsi, and the response to sorafenib, we implemented a consensus clustering analysis for 67 patients from the GSE109211 cohort based on the expression pattern of 845 DEGs. The results revealed that there were two distinct patient clusters based on changes in the Cumulative Distribution Function (CDF) area and consensus matrix (**Figure S1**). As shown in **Figure 2B** and **Figure 2C**, the responses to sorafenib were notably different among the two subgroups. We termed two clustered subgroups as the mRNAsi-high subgroup and the mRNAsi-low subgroup. Only 8% of patients in the mRNAsi-high subgroup were sensitive to sorafenib, while 89% of patients in the mRNAsi-low subgroup exhibited a response to the therapy. The difference in the responses to sorafenib in the two mRNAsi-related subgroups was statistically significant (Test of proportion for mRNAsi-high subgroup p-value = 7.76e-9; Test of proportion for mRNAsi-low subgroup p-value = 5.79e-4). These results demonstrated that our mRNAsi-related subgroups could distinguish the drug response to sorafenib therapy in HCC patients.

The PPAR Signaling Pathway Is the Key Pathway for Sorafenib Resistance

To determine DEGs-enriched pathways, 845 DEGs, identified by samples' mRNAsi (greater than median value or not), were first used to perform over-representation analysis (ORA). As shown in **Figure 3A**, the identified enriched pathways did not include the commonly reported sorafenib-associated pathway (Ras-MEK-ERK pathway) but were related to lipid metabolism. To exclude the analysis bias, more differentially expressed genes were included between the high-mRNAsi and low-mRNAsi subgroups in differential expression analysis. Then, we selected 1853 DEGs ($|logFC| > 1.5$, adj.P-value < 0.01) in total, to repeat pathway analysis, and similar analysis results were collected. Indeed, DEGs between the high-mRNAsi and low-mRNAsi subgroups were mainly enriched in lipid metabolism-associated biological processes, such as the PPAR signaling pathway (https://www.wikipathways.org/index.php/Pathway : WP3942) and fatty acid omega-oxidation (**Figure 3B**). It was worth noting that fatty acid biosynthesis and one of the PPAR subtypes PPARG had been reported to be associated with the efficacy of sorafenib (50, 51).

Hence, to determine the causal relationships between our enriched pathways and the response to sorafenib treatment, we first inferred regulatory relationships between the enriched pathways *via* Bayesian network (BN) inference. BN inference revealed the interactions between the current enriched pathways

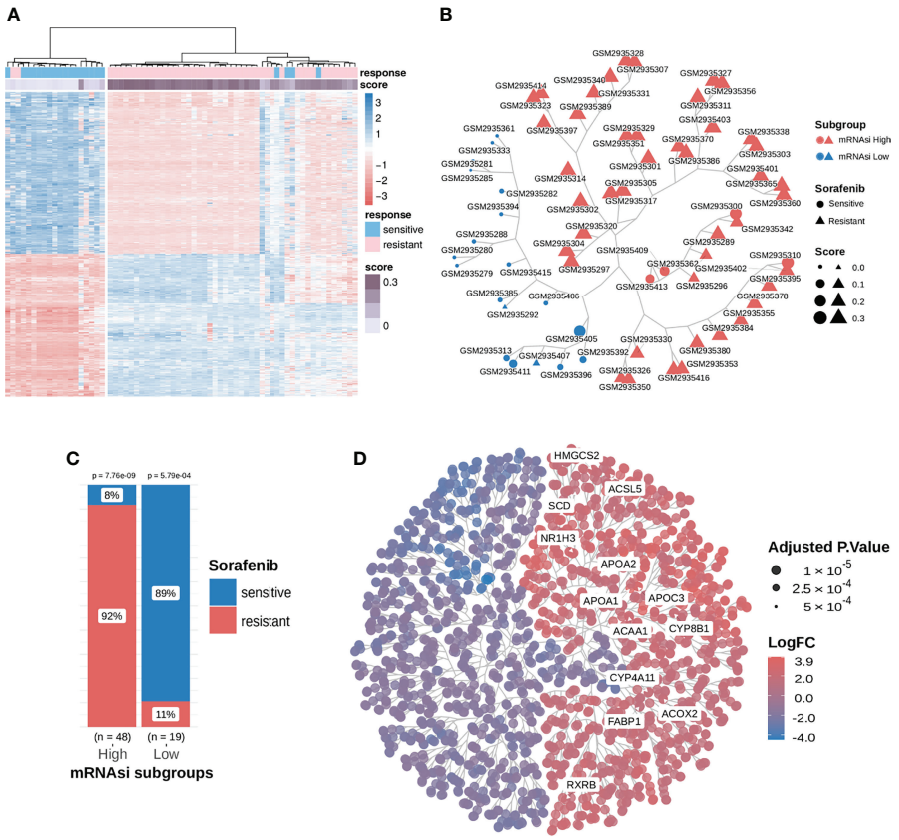

FIGURE 2 | Consensus clustering facilitated the identification of distinct mRNAsi-related clusters associated with different responses to sorafenib treatment; samples in the mRNAsi-high cluster were resistant to sorafenib and exhibited higher stemness proportions. **(A)** We extracted and compared 845 DEGs using subgroup classification in the sorafenib cohort GSE109211. **(B)** Tree-based visualization of the two mRNAsi subgroups. **(C)** The proportion of different responses to sorafenib (responder or non-responder) in the two mRNAsi subgroups with statistical significance. **(D)** Tree cluster of 1853 differentially expressed genes. Genes in the PPAR signaling pathway have been highlighted. See also **Figure S1**.

and other pathways. It provided a more comprehensive insight into the regulatory impact. As shown in **Figure 3C**, the most notable finding was that the PPAR signaling pathway could trigger fatty acid biosynthesis. The PPARA signaling pathway had been identified as activated in CSCs (52), and PPARA and PPARG can enhance stemness and tumorigenicity by PPAR-fatty acid oxidation program (53). We further identified the PPAR signaling pathway regulating fatty acids biosynthesis in low differentiated samples (high-mRNAsi subgroup) (**Figures 3C, E**). The results of our analysis suggested that the PPAR signaling pathway was the "bridge" between fatty acid imbalance and maintenance of cancer cell stemness.

As shown in **Figures 2D**, **3E**, notably, several genes were highly expressed in the PPAR signaling pathway. In addition, we conducted a GSEA analysis between the two mRNAsi-related subgroups using logFC. And we found that the PPAR signaling pathway and its upstream pathway nuclear receptors meta-pathway were significantly enriched in the high mRNAsi group. This result further demonstrated that the PPAR signaling pathway was a sorafenib resistance-related pathway (**Figure 3F**). This considerably different expression (NES=1.615) in two mRNAsi subgroups suggested that the PPAR signaling pathway was a sorafenib response-related pathway that deserved our attention. We hypothesized that genes involved in lipid metabolism might be related to the response to sorafenib in HCC patients and that these genes were overlooked in previous reports.

SCD Is One of the Hub Genes in the PPAR Signaling Pathway That Plays a Role in Sorafenib Resistance Development

In the PPAR signaling pathway, *SCD* was reported to code for an enzyme crucial for the conversion of saturated C16/C18 fatty acids into monounsaturated fatty acids and regulation of the saturated fatty acid:monounsaturated fatty acid (SFA : MUFA) ratio. Furthermore, we inferred that the *SCD* expressed in the PPAR signaling pathway might play a vital role in sorafenib resistance. Upon visualizing the expression of the entire pathway, we found that most genes, including *SCD*, were highly expressed, compared to those in the mRNAsi-low subgroup (**Figures 2D**, **3E**).

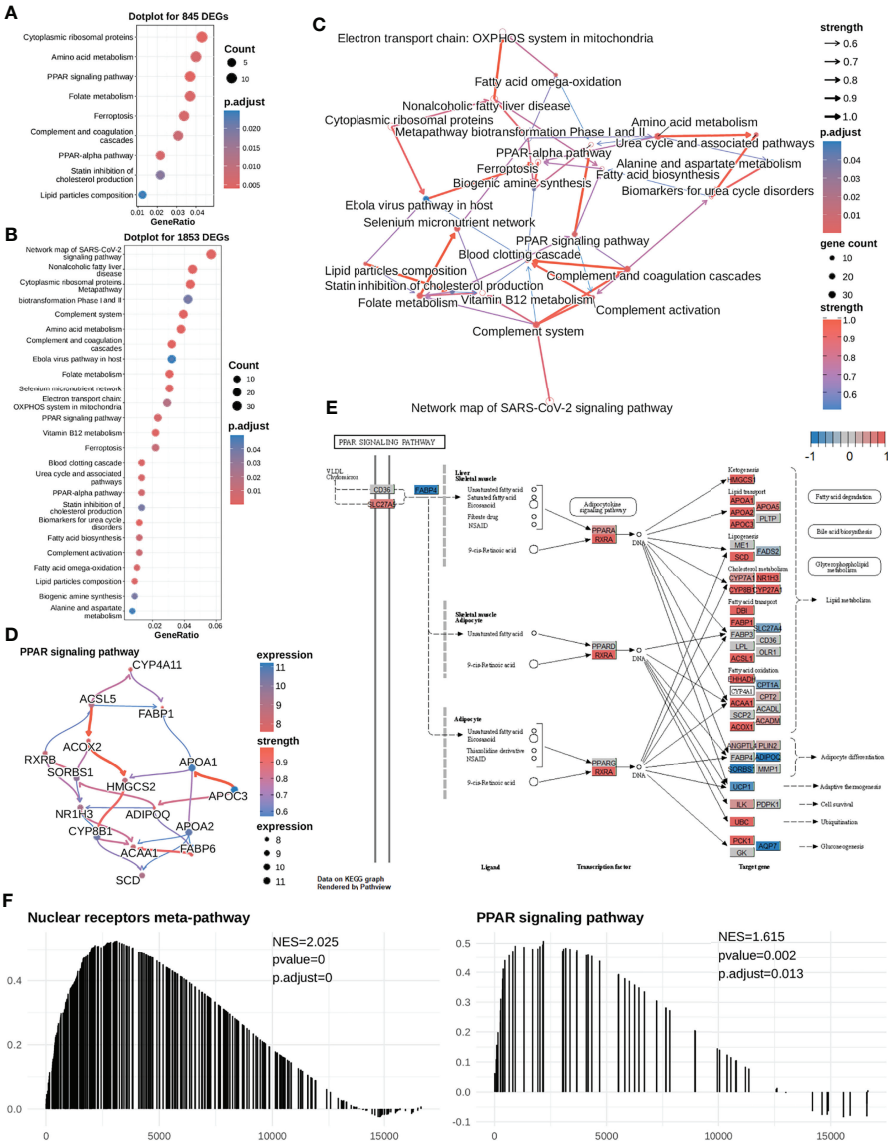

FIGURE 3 | The high mRNAsi subgroup (sorafenib resistant) exhibits higher expression levels of most genes in the PPAR signaling pathway in HCC cells. **(A)** We first selected 845 DEGs for performing functional analysis and found that these DEGs were significantly enriched in the PPAR signaling pathway, cytoplasmic ribosomal proteins, folate metabolism, etc. **(B)** Next, we selected 1853 DEGS for performing enrichment analysis and found that the DEGs were significantly enriched in lipid metabolism-related pathways. **(C)** Enriched pathway regulatory network for 26 pathways. **(D)** The gene regulatory network for the PPAR signaling pathway. **(E)** Visualization of expression of the PPAR signaling pathway (most genes were highly expressed in the mRNAsi-high subgroup). The expression of the gene in both mRNAsi subgroups ranges from -1 to 1. A value closer to 1 means that the gene is highly expressed in the high-mRNAsi subgroup (red color); conversely, it is highly expressed in the low-mRNAsi subgroup (blue color). Most of the genes in the PPAR signaling pathway are highly expressed in the high-mRNAsi subgroup. **(F)** Meanwhile, GSEA was performed to compare the high-mRNAsi and low-mRNAsi subgroups, to identify upstream pathways of PPAR signaling that were up-regulated in the mRNAsi-high subgroup, NES =2.049. PPAR signaling pathways were up-regulated in the mRNAsi-high subgroup, NES = 1.642.

After noting the apparent differences in *SCD* expression, we inferred the gene regulatory network in the PPAR signaling pathway and searched for *SCD* genes with regulatory functions. As shown in **Figure 3D**, upon combining literature reports (50) and regulatory networks inferred from the enriched result, we could focus on a regulatory route from *RXRB* to *NR1H3* to *CYP8B1*, and finally to *SCD*. It was well known that i) the *RXRB* TF could induce the transcription of *NR1H3* (54), ii) the *NR1H3* TF could induce the transcription of *SCD* (55), and iii) the *CYP8B1* enzyme could catalyze the synthesis of lipid and cholesterol (56). Our result indicated that the high level of expression of *SCD* and its upstream genes in the PPAR signaling pathway diminished the therapeutic efficacy of sorafenib.

We further checked the correlation between related genes and their expression levels in different responses to sorafenib. Three genes (*NR1H3*, *CYP8B1*, *SCD*) were induced transcription by subtypes of PPARs (https://www.wikipathways.org/index.php/Pathway:WP3942) (57). We found that *PPARA* was slightly different expressed in two responses to sorafenib, which meant *PPARA* was responsible for the change in the expression level of its downstream target genes (**Figure 4A**, **Figure S2**). The expression levels of all the four key genes were higher in sorafenib non-responders than in sorafenib responders (**Figure 4A**). To assess the accuracy of inferred stem-related sorafenib resistance indices, we conducted correlation analysis and observed high levels of relevance between mRNAsi and the expression levels of *RXRB*, *NR1H3*, *CYP8B1*, and *SCD* (**Figure 4B**).

The PPAR-Related Signature Can Be Used to Predict the Response to Sorafenib

To assess the predictive accuracy of the four-gene signature (*RXRB*, *NR1H3*, *CYP8B1*, and *SCD*), we used PCA to assess the ability of the signature to predict the effectiveness of sorafenib therapy, using the expression levels of the four genes. As shown in **Figure 4C**, the expression of these genes was also significantly correlated with the response to sorafenib. Hence, we calculated the four-gene signature, named *PPARscore*, for sorafenib samples using the coordinates of samples on the first 2 principal components. The Receiver-operating characteristic (ROC) analysis showed that *PPARscore* achieved an Area Under Curve (AUC) of 0.88, which *PPARscore* equaled -0.56 with the highest sensitivity and specificity (**Figure 4E**). We classified samples into two groups based on the best threshold of *PPARscore*. If the *PPARscore* was greater than -0.56, it means that the likelihood of sorafenib resistance development is higher. The PPAR-related signature was significantly correlated with sorafenib resistance (**Figure 4D**, **Table S3**). Finally, we validated *PPARscore* in another sorafenib cohort, i.e., GSE143477 (**Figure 4C**, **Table S4**). The scores of three sorafenib-resistant samples were greater than -0.56 and those of three sorafenib-sensitive samples were less than -0.56 (**Table S4**). We also

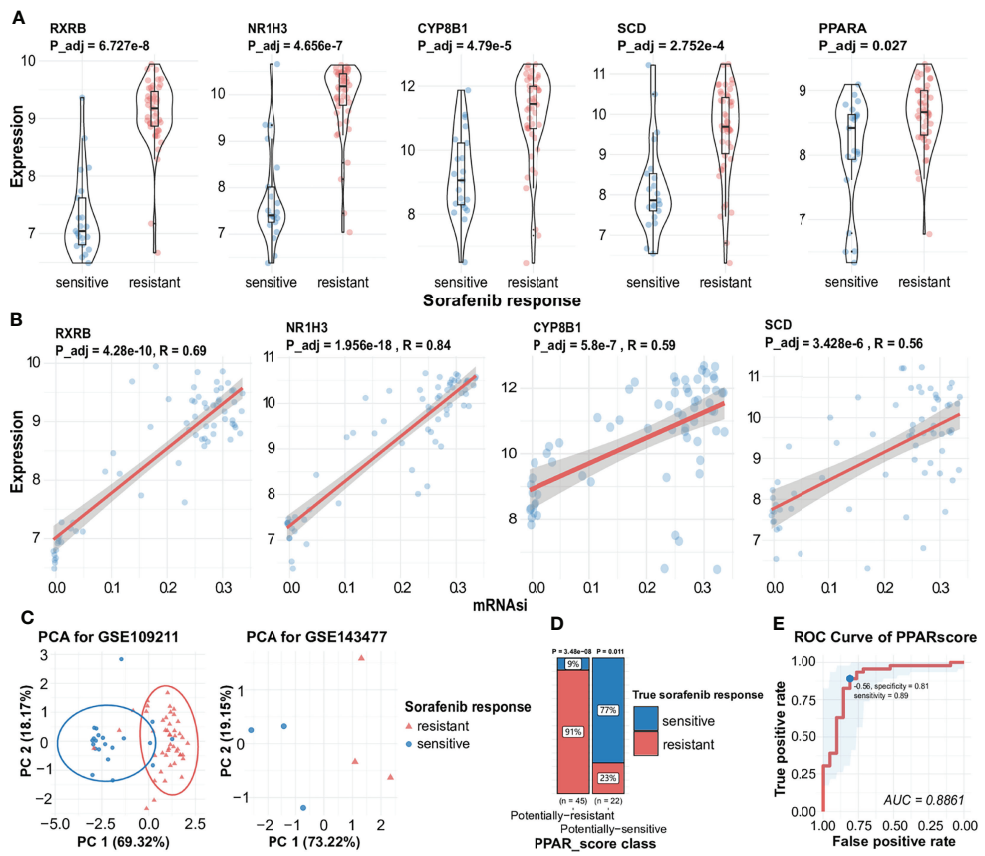

FIGURE 4 | Expression of key genes during the generation of different responses to sorafenib, the correlation between key genes and mRNAsi, and visualization of PPAR-related signature. **(A)** Expression of *RXRB*, *NR1H3*, *CYP8B1 SCD*, and *PPARA* during different responses to sorafenib treatment with statistical significance. **(B)** Correlation analysis facilitated the identification of a significant positive association between mRNAsi and several sorafenib resistance genes (*RXRB*, *NR1H3*, *CYP8B1*, *SCD*). **(C)** AUC results are indicative of the expression of four genes in the sorafenib cohort GSE109211 (the left) and PCA results indicate the expression of four genes in the validated sorafenib cohort GSE143477 (the right). See also **Figure S2**. **(D)** The proportion of different responses to sorafenib (responder or non-responder) in two groups of samples for four-gene scores. **(E)** ROC of *PPARscore*, the AUC value of *PPARscore* was 0.8861. The point with the highest specificity and sensitivity in the curve was -0.56.

examined whether the expression of the four genes showed a similar trend in the GSE143477 cohort. The expression levels of *RXRB*, *NR1H3*, and *SCD* were higher in samples exhibiting sorafenib resistance (**Figure S2**). These results suggested that the expression levels of *RXRB*, *NR1H3*, *CYP8B1*, and *SCD* in the PPAR signaling pathway were strongly associated with the response to sorafenib.

Differences in the Expression of Key Genes are Not Related to the Somatic Mutation Frequency

We explored the potential regulatory mechanisms of the core genes described above. Variations in genetic expression may be attributable to the occurrence of key somatic mutations in genes within the transcriptome across patients with different phenotypes and specific types of cancer (58). We assessed the expression of key genes related to the response to sorafenib, to examine the possibility that the response to sorafenib is affected by mutations, by comparing the frequencies of somatic mutations for the top 10 mutational genes and key genes in the PPAR pathway (**Figure 5A**). We then identified key genes in the PPAR pathway that exhibited low mutation rates in the TCGA HCC dataset. This result proved that somatic mutation frequencies in key genes were not responsible for the changes in the expression of key genes. Therefore, we ruled out the possibility that mutation frequency affected the function and expression of these genes. The result mirrored the Bayesian inference that these gene-phenotype-related alterations occur mainly at the transcriptional level.

Transcription Factors in the PPAR Signaling Pathway Induce the Expression of NR1H3 and SCD

We also assessed the potential mechanism of occurrence of alterations in gene expression, because TFs can activate gene expression by binding to the targeted gene promoter (59). We combined regulatory networks inferred from enriched results and literature reports (50, 60), and focused on a regulatory route from *RXRB* to *NR1H3* to *CYP8B1* and finally to *SCD*. Although it was well known that *RXRB* and *NR1H3* could separately bind to *NR1H3* and *SCD* (54, 55), we demonstrated that *RXRB* and *NR1H3* could act as TFs and bind to the promoter regions of *NR1H3* and *SCD*, respectively. First, *RXRB* could bind to the promoter region of *NR1H3* in HepG2 hepatocellular carcinoma cells. Each track corresponds to a HepG2 sample. (**Figure 5C**). Second, *NR1H3* could bind to *SCD* in HT29 colorectal adenocarcinoma cells (no similar study was performed with hepatocellular carcinoma cells) (**Figure 5D**). An analysis of these results showed that there is abundant evidence to support the regulatory relationship between these genes.

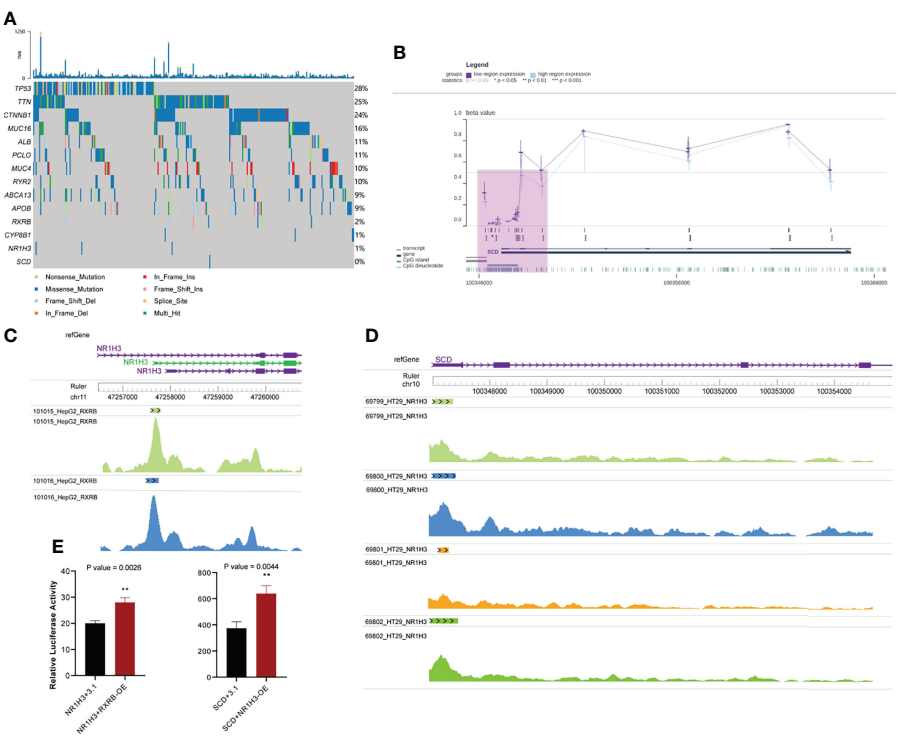

FIGURE 5 | Other omics analysis of key genes. **(A)** Somatic mutations in the top 10 mutated genes and key genes in the PPAR signaling pathway. **(B)** Visualization of methylation of the *SCD* promoter region in HCC. The purple shaded area represents the *SCD* promoter region **(C)** Chips of *RXRB* bind to the promoter region of *NR1H3*. **(D)** Chips of *NR1H3* bind to the promoter region of *SCD*. **(E)** Relative dual luciferase activities of *NR1H3* and *SCD* promoters were determined at 48 h in MHCC-97h cells (Left: *NR1H3*; Right: *SCD*. pcDNA3.1-RXRB and pcDNA3.1-NR1H3 plasmid were empty pcDNA3.1 plasmids as the control). Data results were shown as mean ± SEM (n ≥ 3). P-values were calculated by two-tailed t-tests. **P<0.01; OE, overexpression; SEM, standard error of the mean.

Moreover, we validated whether *RXRB* and *NR1H3* could directly regulate *NR1H3* and *SCD* by luciferase reporter assay. In MHCC-97h cells, enforced *RXRB* or *NR1H3* expression significantly increased the *NR1H3* or *SCD* promoter activity. *NR1H3* or *SCD* showed transcriptional activity in response to *RXRB* or *NR1H3*. The above data demonstrated that *RXRB* or *NR1H3* can respectively bind to the *NR1H3* or *SCD* promoter and induce its transcription (**Figure 5E**).

Similar Methylation Levels in *SCD* Promoter Regions Between Patients

Epigenetic modifications can modulate the binding of TFs to DNA; for example, DNA hypermethylation represses the binding of TFs to gene promoters (61). We checked the methylation level of the *SCD* promoter in the TCGA-HCC cohort using the MEXPRESS web server. Regardless of the level of *SCD* expression in HCC, the level of methylation in the *SCD* promoter was low (**Figure 5B**). This result suggested that the methylation of *SCD* promoter has hardly any effects on the binding of transcription factors to it. There were significant differences in the expression of *SCD* in sorafenib-resistant and sensitive groups, and *SCD* expression is probably regulated by *NR1H3*, while *NR1H3* is regulated by *RXRB*.

Mechanistic Hypothesis Involving Four PPAR-Related Genes

Based on our BN inference results (**Figure 3D**) and literature reports, we proposed the hypothesis that four gene cascades result in sorafenib resistance. As shown in **Figure 6**, the *RXRB* TF induced the transcription of *NR1H3* and the transcription of *SCD* was induced by the TF *NR1H3* and the enzyme *CYP8B1*. The high level of expression of *SCD* results in a lower SFA : MUFA ratio, and further causes an imbalance in fatty acid homeostasis and sorafenib resistance development.

mRNAsi Is a Valuable Prognostic Predictor for HCC Patients

We also calculated the mRNAsi for HCC samples obtained from five cohorts. A higher mRNAsi represents a lower level of differentiation of a sample (20). Survival analysis was performed only using samples obtained from patients for whom the survival duration was less than 5 years. Upon selecting the median mRNAsi value of 0.55 as the cut-off value in the TCGA HCC cohort, a 5-year survival analysis was performed. K-M analysis revealed that patients with a low mRNAsi had a better OS than those with a high mRNAsi (P = 0.00039; **Figure 7A**). Then, the prognostic value of mRNAsi was validated using the ICGC-JP cohort and three GEO cohorts with the same cutoff (**Figure 7B**; P < 0.0001; **Figure 7C**; P = 0.015). To examine whether the mRNAsi was independent of other clinical and pathological factors, we performed a multivariable cox proportional hazard analysis, by including individual clinical variables and mRNAsi subgroups in these datasets. As shown in **Figure 7D**, in the TCGA-HCC cohort, the mRNAsi class and the TNM Staging System (TNM) were significantly associated with the OS during multivariate analysis. The mRNAsi class was significantly associated with the OS in ICGC-JP cohorts (**Figure 7E**). But the adjusted P value of mRNAsi class is no longer significant in three GEO cohorts (**Figure 7F**). These results suggest that mRNAsi may is a robust predictive factor of HCC patient survival.

DISCUSSION

HCC is the most common primary liver cancer in adults and is the leading cause of cancer-related mortality worldwide (62, 63). Sorafenib is the only first-line chemotherapeutic treatment administered to advanced HCC patients (5, 6). Sorafenib therapy has proven to be effective in the treatment of patients with advanced HCC. Given that the overall rate of response to sorafenib therapy is still low (1, 7), it is crucial to identify patients who can benefit the most from sorafenib therapy. Here, the predictive value of the stemness index for response to sorafenib treatment was first confirmed. Despite evaluating different markers in sorafenib-resistant HCC for several years, we did not discover a promising index that could predict the response to sorafenib therapy. This highlights the need to identify a biomarker for sorafenib treatment in HCC. By applying mRNAsi to sorafenib therapy cohorts, novel mRNAsi-based

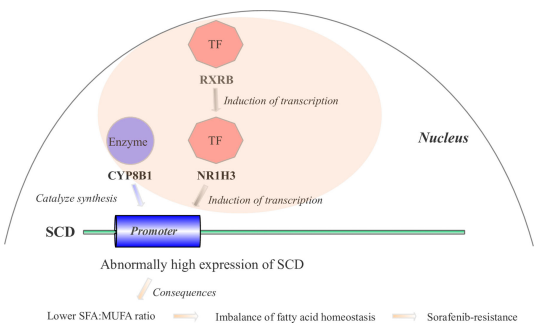

FIGURE 6 | The mechanistic hypothesis for four hub genes in the PPAR signaling pathway. Abnormally high expression levels of four hub genes result in sorafenib resistance through a cascade reaction in the PPAR pathway.

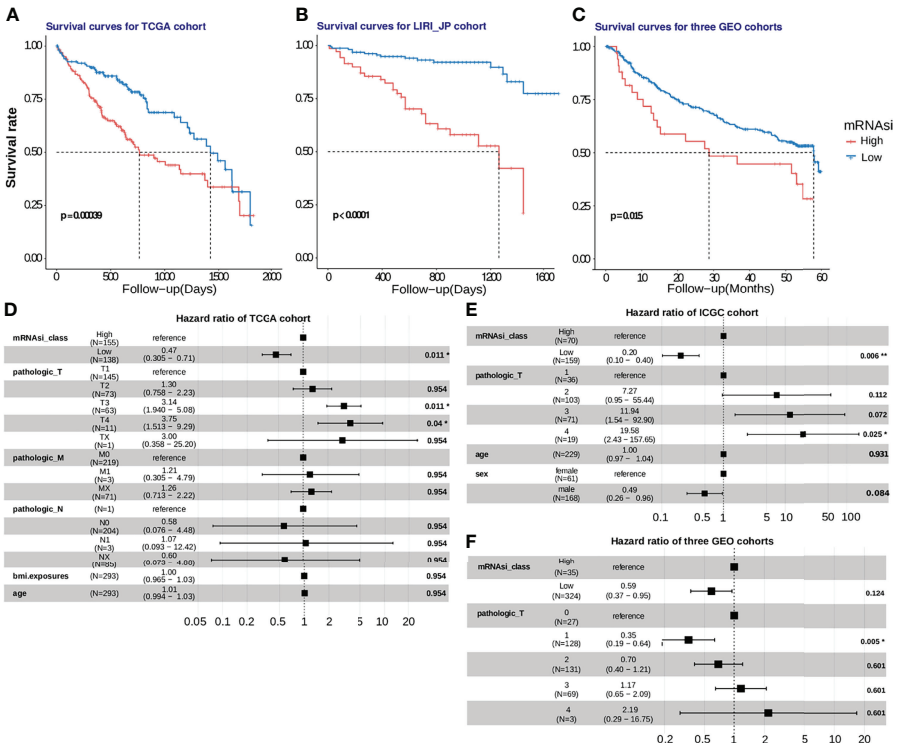

FIGURE 7 | Development and validation of the mRNAsi cutoff value in five HCC cohorts. **(A)** In the TCGA-HCC cohort, patients with high stemlike indices (mRNAsi > 0.55) suffered from worse survival outcomes, compared to those in the low-mRNAsi group with log-rank test P =0.00039. **(B, C)** The mRNAsi cutoff value was further verified using the ICGC-JP cohort and 3 GEO cohorts, and the mRNAsi-based cutoff was a significant hazard factor for HCC patients with log-rank test p<0.0001 and p = 0.016. **(D, E, F)**. The hazard ratios of mRNAsi were shown using a forest plot in the training and validation cohorts.

subgroups that could enable us to understand the response to sorafenib were clustered. Two mRNAsi-based subgroups were strongly correlated with the sensitivity to sorafenib therapy. Hence, we performed a functional enrichment analysis of DEGs, to determine whether common sorafenib-related pathways were differentially expressed in these two subgroups. We also assessed the effect of several selected DEGs on the results of enrichment analysis (845 DEGs, followed by 1853 DEGs, along with 845 genes included in the unsupervised cluster have been shown in **Table S2**). Hence, in order to further clarify the relationship between enriched pathways, we performed Bayesian network inference using *CBNplot*, which helped us to identify the previously overlooked regulatory relationship between pathways. It was inferred that the PPAR signaling pathway regulated fatty acid biosynthesis. This suggested that the change in lipid metabolism might be related to the response to sorafenib in HCC patients, but had been overlooked in previous reports.

It is known that fatty acids (FAs) can be broadly classified as saturated FAs and unsaturated FAs. Different ratios of unsaturated to saturated fatty acids (UFA: SFA ratio) can affect tumor cell survival, as high levels of saturated fatty acids result in lethal lipotoxicity (50). However, unsaturated fatty acids cannot induce reactions to metabolic stress and thus repress lipotoxicity (55). The PPAR signaling pathway can mediate not only saturated fatty acid synthesis, but also monounsaturated fatty acid synthesis (64). Stearoyl-coenzyme A desaturase 1 (*SCD*) can convert saturated fatty acids into monounsaturated fatty acids in the PPAR signaling pathway (65). The role of *SCD* in facilitating hepatocarcinoma cell proliferation and efficacy of sorafenib treatment has been confirmed (50, 66). We identified that the PPAR pathway regulating fatty acid biosynthesis also affects the efficacy of treatment with sorafenib. Recent studies have verified that PPAR can enhance stemness and tumorigenicity in individuals consuming a high-fat diet (53, 67). This explained why the PPAR signaling pathway is strongly associated with mRNAsi stemness indices and sorafenib resistance. It has been demonstrated that the inhibition of PPARG, one subtype of the peroxisome proliferator-activated receptor, could reverse the metabolic reprogramming of compensatory glutamine and further sensitize HCC cells to sorafenib (51). This implies that the PPAR signaling pathway plays an important role not only in glutamine metabolism but also in fatty acid homeostasis. In addition, we demonstrated that the different levels of expression of PPAR-related genes were correlated with sorafenib resistance, and were not attributable to somatic gene mutations. The rate of occurrence of somatic mutations in resistance-related genes was almost zero. It has also been demonstrated that TFs such as *RXRB* and *NR1H3* can bind to the promoter regions of their target genes (*NR1H3*, *SCD*). We also verified that the methylation level of the SCD promoter hardly affected its binding with NR1H3. Finally, we proposed the

hypothesis that key genes cascades result in sorafenib resistance, based on literature reports and gene regulatory networks. The PPAR signaling pathway is activated in samples with obvious stemness feature (higher stemness indices). Four genes, *RXRB*, *NR1H3*, *CYP8B1* and *SCD*, were involved in PPAR signaling pathway (57) act as sorafenib-resistant related genes. It is known to *RXRB* induce the transcription of *NR1H3 (*54). And the transcription of *SCD* was induced by the TF *NR1H3 (*55). The *CYP8B1*, as a catalyze enzyme, induced lipogenesis, whose overexpression increased *SCD* expression (68, 69). *NR1H3* as TF and *CYP8B1* as catalyzing enzyme induce *SCD* expression. Finally, increased expression of *SCD* results in greater content of MUFA and lower SFA : MUFA ratio, causing an imbalance in fatty acid homeostasis (50, 55). The imbalance in fatty acid homeostasis subsequently increased and maintain the stemness of cancer cells and further resulted in sorafenib resistance development (50, 70).

The prognosis of individual patients varies greatly due to high levels of heterogeneity (62). Hence, we need to urgently develop novel diagnostic or prognostic biomarkers that can predict multiple HCC cohorts. Accumulating evidence demonstrates that mRNAsi can predict the prognosis of other cancers (71, 72). Based on this, we employed a trained one-class regression model, and scored the mRNAsi for each of the HCC patients, by determining the Spearman correlation between the weight vectors of the stemness signature, mRNA expression data, and the mRNAsi threshold, to predict a better or worse prognosis, and set it at 0.55. Survival analysis was performed using data of patients with HCC from the TCGA cohort and validated with data from the ICGC-JP cohort and three GEO cohorts. K-M analysis demonstrated the effective stratification of low- and high-risk patients according to different results for overall survival, suggesting that the stemness index could be used as a robust prognostic marker. Multivariate cox regression analysis suggested that the prognostic capacity of the stemness likeness was independent of other clinical data. In general, the lower mRNAsi score represented a better survival prognosis, and an mRNAsi value of 0.55 can be used as a cutoff for predicting the prognosis of HCC patients, which was validated in both the TCGA cohort and the four independent datasets.

However, several limitations were associated with our work, and need to be optimized in the future. The validation of other omics was different from that of the HCC cohort used to identify mRNAsi-related subgroups.

In this study, we performed a systematic analysis of the mRNAsi subgroups that were strongly correlated with the response to sorafenib. Simultaneously, HCC stem-like indices that were based on multiple independent cohorts were used to validate the robust prognostic ability of mRNAsi. To our knowledge, this is the first attempt to explore the potential mechanisms of the development of sorafenib drug resistance by assessing the tumor stemness likeness. Through an analysis of differentially expressed pathways between two mRNAsi-related subgroups in sorafenib cohorts, we identified the PPAR signaling pathway to be associated with sorafenib therapy. The key genes *RXRB*, *NR1H3*, *CYP8B1*, and *SCD* were identified in the PPAR signaling pathway, and their regulatory relationships were also examined. They can be used as candidate targets for researching drug resistance mechanisms. In particular, *SCD* has been experimentally validated to be responsible for sorafenib resistance (50, 66). We also derived the four-gene signature that would enable us to predict the effectiveness of sorafenib therapy and formulated a mechanistic hypothesis for the four PPAR-related genes. Based on the results of our study, we thought that, in addition to commonly reported pathways, PPAR-related activities associated with fatty acid metabolism might also affect the response to sorafenib treatment. Furthermore, based on a combination of experimental evidence derived from previously conducted research (50, 66), we suggested that the combined use of SCD inhibitors and sorafenib may be a promising therapeutic approach that could be used in the future.

DATA AVAILABILITY STATEMENT

The original contributions presented in the study are included in the article/**Supplementary Material**. Further inquiries can be directed to the corresponding authors.

AUTHOR CONTRIBUTIONS

TF, TW, YZ, and LZ (4th Author) were the major contributors who made substantial contributions to the conception, data collection, and manuscript writing of this project. SL, ML, EH, QW, XF, and LZ (11th Author) provided crucial technical support to this study. LL, ZX, and WX provide support in data visualization for this study. XH, XS, and GY supervised this study, provided support in all aspects throughout the progression of this study, and approved the final version of the manuscript.

ACKNOWLEDGMENTS

We thank TopEdit (www.topeditsci.com) for its linguistic assistance during the preparation of this manuscript.

SUPPLEMENTARY MATERIAL

The Supplementary Material for this article can be found online at: https://www.frontiersin.org/articles/10.3389/fonc.2022.912694/full#supplementary-material

REFERENCES

1. Feng M, Pan Y, Kong R, Shu S. Therapy of Primary Liver Cancer. *Innovation* (2020) 1:100032. doi: 10.1016/j.xinn.2020.100032

2. Jiang Y-Q, Cao S-E, Cao S, Chen J-N, Wang G-Y, Shi W-Q, et al. Preoperative Identification of Microvascular Invasion in Hepatocellular Carcinoma by XGBoost and Deep Learning. *J Cancer Res Clin Oncol* (2021) 147:821–33. doi: 10.1007/s00432-020-03366-9

3. Gryziak M, Woźniak K, Kraj L, Stec R. Milestones in the Treatment of Hepatocellular Carcinoma: A Systematic Review. *Crit Rev Oncol/Hematol* (2021) 157:103179. doi: 10.1016/j.critrevonc.2020.103179
4. Llovet JM, Kelley RK, Villanueva A, Singal AG, Pikarsky E, Roayaie S, et al. Hepatocellular Carcinoma. *Nat Rev Dis Primers* (2021) 7:6. doi: 10.1038/s41572-020-00240-3
5. Colagrande S, Inghilesi AL, Aburas S, Taliani GG, Nardi C, Marra F. Challenges of Advanced Hepatocellular Carcinoma. *WJG* (2016) 22:7645. doi: 10.3748/wjg.v22.i34.7645
6. Niu L, Liu L, Yang S, Ren J, Lai PBS, Chen GG. New Insights Into Sorafenib Resistance in Hepatocellular Carcinoma: Responsible Mechanisms and Promising Strategies. *Biochim Biophys Acta (BBA) - Rev Cancer* (2017) 1868:564–70. doi: 10.1016/j.bbcan.2017.10.002
7. Xia S, Pan Y, Liang Y, Xu J, Cai X. The Microenvironmental and Metabolic Aspects of Sorafenib Resistance in Hepatocellular Carcinoma. *EBioMedicine* (2020) 51:102610. doi: 10.1016/j.ebiom.2019.102610
8. Cabral LKD, Tiribelli C, Sukowati CHC. Sorafenib Resistance in Hepatocellular Carcinoma: The Relevance of Genetic Heterogeneity. *Cancers* (2020) 12:1576. doi: 10.3390/cancers12061576
9. Prasad S, Ramachandran S, Gupta N, Kaushik I, Srivastava SK. Cancer Cells Stemness: A Doorstep to Targeted Therapy. *Biochim Biophys Acta (BBA) - Mol Basis Dis* (2020) 1866:165424. doi: 10.1016/j.bbadis.2019.02.019
10. Aponte PM, Caicedo A. Stemness in Cancer: Stem Cells, Cancer Stem Cells, and Their Microenvironment. *Stem Cells Int* (2017) 2017:1–17. doi: 10.1155/2017/5619472
11. Friedmann-Morvinski D, Verma IM. Dedifferentiation and Reprogramming: Origins of Cancer Stem Cells. *EMBO Rep* (2014) 15:244–53. doi: 10.1002/embr.201338254
12. Chaffer CL, Brueckmann I, Scheel C, Kaestli AJ, Wiggins PA, Rodrigues LO, et al. Normal and Neoplastic Nonstem Cells can Spontaneously Convert to a Stem-Like State. *Proc Natl Acad Sci USA* (2011) 108:7950–5. doi: 10.1073/pnas.1102454108
13. Ge Y, Gomez NC, Adam RC, Nikolova M, Yang H, Verma A, et al. Stem Cell Lineage Infidelity Drives Wound Repair and Cancer. *Cell* (2017) 169:636–50.e14. doi: 10.1016/j.cell.2017.03.042
14. Visvader JE, Lindeman GJ. Cancer Stem Cells: Current Status and Evolving Complexities. *Cell Stem Cell* (2012) 10:717–28. doi: 10.1016/j.stem.2012.05.007
15. Hanahan D. Hallmarks of Cancer: New Dimensions. *Cancer Discovery* (2022) 12:31–46. doi: 10.1158/2159-8290.CD-21-1059
16. Gan G, Shi Z, Liu D, Zhang S, Zhu H, Wang Y, et al. 3-Hydroxyanthranic Acid Increases the Sensitivity of Hepatocellular Carcinoma to Sorafenib by Decreasing Tumor Cell Stemness. *Cell Death Discovery* (2021) 7:173. doi: 10.1038/s41420-021-00561-6
17. Shibue T, Weinberg RA. EMT, CSCs, and Drug Resistance: The Mechanistic Link and Clinical Implications. *Nat Rev Clin Oncol* (2017) 14:611–29. doi: 10.1038/nrclinonc.2017.44
18. Zucman-Rossi J, Villanueva A, Nault J-C, Llovet JM. Genetic Landscape and Biomarkers of Hepatocellular Carcinoma. *Gastroenterology* (2015) 149:1226–39.e4. doi: 10.1053/j.gastro.2015.05.061
19. Zou Z-M, Chang D-H, Liu H, Xiao Y-D. Current Updates in Machine Learning in the Prediction of Therapeutic Outcome of Hepatocellular Carcinoma: What Should We Know? *Insights Imaging* (2021) 12:31. doi: 10.1186/s13244-021-00977-9
20. Huang K, Wu Y, Xie Y, Huang L, Liu H. Analyzing Mrnasi-Related Genes Identifies Novel Prognostic Markers and Potential Drug Combination for Patients With Basal Breast Cancer. *Dis Markers* (2021) 2021:1–15. doi: 10.1155/2021/4731349
21. Zhang Y, Tseng JT-C, Lien I-C, Li F, Wu W, Li H. Mrnasi Index: Machine Learning in Mining Lung Adenocarcinoma Stem Cell Biomarkers. *Genes* (2020) 11:257. doi: 10.3390/genes11030257
22. Malta TM, Sokolov A, Gentles AJ, Burzykowski T, Poisson L, Weinstein JN, et al. Machine Learning Identifies Stemness Features Associated With Oncogenic Dedifferentiation. *Cell* (2018) 173:338–54.e15. doi: 10.1016/j.cell.2018.03.034
23. Pan S, Zhan Y, Chen X, Wu B, Liu B. Identification of Biomarkers for Controlling Cancer Stem Cell Characteristics in Bladder Cancer by Network Analysis of Transcriptome Data Stemness Indices. *Front Oncol* (2019) 9:613. doi: 10.3389/fonc.2019.00613
24. Roessler S, Jia H-L, Budhu A, Forgues M, Ye Q-H, Lee J-S, et al. A Unique Metastasis Gene Signature Enables Prediction of Tumor Relapse in Early-Stage Hepatocellular Carcinoma Patients. *Cancer Res* (2010) 70:10202–12. doi: 10.1158/0008-5472.CAN-10-2607
25. Grinchuk OV, Yenamandra SP, Iyer R, Singh M, Lee HK, Lim KH, et al. Tumor-Adjacent Tissue Co-Expression Profile Analysis Reveals Pro-Oncogenic Ribosomal Gene Signature for Prognosis of Resectable Hepatocellular Carcinoma. *Mol Oncol* (2018) 12:89–113. doi: 10.1002/1878-0261.12153
26. Pinyol R, Montal R, Bassaganyas L, Sia D, Takayama T, Chau G-Y, et al. Molecular Predictors of Prevention of Recurrence in HCC With Sorafenib as Adjuvant Treatment and Prognostic Factors in the Phase 3 STORM Trial. *Gut* (2019) 68:1065–75. doi: 10.1136/gutjnl-2018-316408
27. Wang M, Wang Z, Zhi X, Ding W, Xiong J, Tao T, et al. SOX9 Enhances Sorafenib Resistance Through Upregulating ABCG2 Expression in Hepatocellular Carcinoma. *Biomed Pharmacother* (2020) 129:110315. doi: 10.1016/j.biopha.2020.110315
28. Goldman MJ, Craft B, Hastie M, Repečka K, McDade F, Kamath A, et al. Visualizing and Interpreting Cancer Genomics Data *via* the Xena Platform. *Nat Biotechnol* (2020) 38:675–8. doi: 10.1038/s41587-020-0546-8
29. Salomonis N, Dexheimer PJ, Omberg L, Schroll R, Bush S, Huo J, et al. Integrated Genomic Analysis of Diverse Induced Pluripotent Stem Cells From the Progenitor Cell Biology Consortium. *Stem Cell Rep* (2016) 7:110–25. doi: 10.1016/j.stemcr.2016.05.006
30. Sokolov A, Carlin DE, Paull EO, Baertsch R, Stuart JM. Pathway-Based Genomics Prediction Using Generalized Elastic Net. *PLoS Comput Biol* (2016) 12:e1004790. doi: 10.1371/journal.pcbi.1004790
31. Therneau TM, Grambsch PM. *Modeling Survival Data: Extending the Cox Model*. New York, NY: Springer New York (2000). doi: 10.1007/978-1-4757-3294-8
32. Therneau T. *A Package for Survival Analysis in R* . Available at: https://CRAN.R-project.org/package=survival.
33. Alboukadel. *Survminer: Drawing Survival Curves Using "Ggplot2."* (2020). Available at: https://CRAN.R-project.org/package=survminer.
34. Ritchie ME, Phipson B, Wu D, Hu Y, Law CW, Shi W, et al. Limma Powers Differential Expression Analyses for RNA-Sequencing and Microarray Studies. *Nucleic Acids Res* (2015) 43:e47–7. doi: 10.1093/nar/gkv007
35. Wilkerson MD, Hayes DN. ConsensusClusterPlus: A Class Discovery Tool With Confidence Assessments and Item Tracking. *Bioinformatics* (2010) 26:1572–3. doi: 10.1093/bioinformatics/btq170
36. Patil I. Visualizations With Statistical Details: The "Ggstatsplot" Approach. *JOSS* (2021) 6:3167. doi: 10.21105/joss.03167
37. Wu T, Hu E, Xu S, Chen M, Guo P, Dai Z, et al. Clusterprofiler 4.0: A Universal Enrichment Tool for Interpreting Omics Data. *Innovation* (2021) 100141. doi: 10.1016/j.xinn.2021.100141
38. Sato N, Tamada Y, Yu G, Okuno Y. *CBNplot* : Bayesian Network Plots for Enrichment Analysis. *Bioinformatics* (2022) btac175. doi: 10.1093/bioinformatics/btac175
39. Lê S, Josse J, Husson F. FactoMineR : An *R* Package for Multivariate Analysis. *J Stat Soft* (2008) 25:1–18. doi: 10.18637/jss.v025.i01
40. Zeng D, Li M, Zhou R, Zhang J, Sun H, Shi M, et al. Tumor Microenvironment Characterization in Gastric Cancer Identifies Prognostic and Immunotherapeutically Relevant Gene Signatures. *Cancer Immunol Res* (2019) 7:737–50. doi: 10.1158/2326-6066.CIR-18-0436
41. Sotiriou C, Wirapati P, Loi S, Harris A, Fox S, Smeds J, et al. Gene Expression Profiling in Breast Cancer: Understanding the Molecular Basis of Histologic Grade To Improve Prognosis. *JNCI: J Natl Cancer Institute* (2006) 98:262–72. doi: 10.1093/jnci/djj052
42. Zhang B, Wu Q, Li B, Wang D, Wang L, Zhou YL. M6a Regulator-Mediated Methylation Modification Patterns and Tumor Microenvironment Infiltration Characterization in Gastric Cancer. *Mol Cancer* (2020) 19:53. doi: 10.1186/s12943-020-01170-0
43. Mayakonda A, Lin D-C, Assenov Y, Plass C, Koeffler HP. Maftools: Efficient and Comprehensive Analysis of Somatic Variants in Cancer. *Genome Res* (2018) 28:1747–56. doi: 10.1101/gr.239244.118

44. Zheng R, Wan C, Mei S, Qin Q, Wu Q, Sun H, et al. Cistrome Data Browser: Expanded Datasets and New Tools for Gene Regulatory Analysis. *Nucleic Acids Res* (2019) 47:D729–35. doi: 10.1093/nar/gky1094
45. Mei S, Qin Q, Wu Q, Sun H, Zheng R, Zang C, et al. Cistrome Data Browser: A Data Portal for ChIP-Seq and Chromatin Accessibility Data in Human and Mouse. *Nucleic Acids Res* (2017) 45:D658–62. doi: 10.1093/nar/gkw983
46. ENCODE Project Consortium. An Integrated Encyclopedia of DNA Elements in the Human Genome. *Nature* (2012) 489:57–74. doi: 10.1038/nature11247
47. Savic D, Ramaker RC, Roberts BS, Dean EC, Burwell TC, Meadows SK, et al. Distinct Gene Regulatory Programs Define the Inhibitory Effects of Liver X Receptors and PPARG on Cancer Cell Proliferation. *Genome Med* (2016) 8:74. doi: 10.1186/s13073-016-0328-6
48. Koch A, Jeschke J, Van Criekinge W, van Engeland M, De Meyer T. MEXPRESS Update 2019. *Nucleic Acids Res* (2019) 47:W561–5. doi: 10.1093/nar/gkz445
49. Yu G, Smith DK, Zhu H, Guan Y, Lam TT. Ggtree : An R Package for Visualization and Annotation of Phylogenetic Trees With Their Covariates and Other Associated Data. *Methods Ecol Evol* (2017) 8:28–36. doi: 10.1111/2041-210X.12628
50. Rudalska R, Harbig J, Snaebjornsson MT, Klotz S, Zwirner S, Taranets L, et al. Lxrα Activation and Raf Inhibition Trigger Lethal Lipotoxicity in Liver Cancer. *Nat Cancer* (2021) 2:201–17. doi: 10.1038/s43018-020-00168-3
51. Kim M-J, Choi Y-K, Park SY, Jang SY, Lee JY, Ham HJ, et al. Pparδ Reprograms Glutamine Metabolism in Sorafenib-Resistant HCC. *Mol Cancer Res* (2017) 15:1230–42. doi: 10.1158/1541-7786.MCR-17-0061
52. Kuramoto K, Yamamoto M, Suzuki S, Togashi K, Sanomachi T, Kitanaka C, et al. Inhibition of the Lipid Droplet-Peroxisome Proliferator-Activated Receptor α Axis Suppresses Cancer Stem Cell Properties. *Genes (Basel)* (2021) 12:99. doi: 10.3390/genes12010099
53. Mana MD, Hussey AM, Tzouanas CN, Imada S, Barrera Millan Y, Bahceci D, et al. High-Fat Diet-Activated Fatty Acid Oxidation Mediates Intestinal Stemness and Tumorigenicity. *Cell Rep* (2021) 35:109212. doi: 10.1016/j.celrep.2021.109212
54. Svensson S, Ostberg T, Jacobsson M, Norström C, Stefansson K, Hallén D, et al. Crystal Structure of the Heterodimeric Complex of LXRalpha and RXRbeta Ligand-Binding Domains in a Fully Agonistic Conformation. *EMBO J* (2003) 22:4625–33. doi: 10.1093/emboj/cdg456
55. Igal RA. Stearoyl CoA Desaturase-1: New Insights Into a Central Regulator of Cancer Metabolism. *Biochim Biophys Acta (BBA) - Mol Cell Biol Lipids* (2016) 1861:1865–80. doi: 10.1016/j.bbalip.2016.09.009
56. Yang Y, Eggertsen G, Gåfvels M, Andersson U, Einarsson C, Björkhem I, et al. Mechanisms of Cholesterol and Sterol Regulatory Element Binding Protein Regulation of the Sterol 12α-Hydroxylase Gene (CYP8B1). *Biochem Biophys Res Commun* (2004) 320:1204–10. doi: 10.1016/j.bbrc.2004.06.069
57. Fujii H. [PPARs-Mediated Intracellular Signal Transduction]. *Nihon Rinsho* (2005) 63:565–71.
58. Gerstung M, Pellagatti A, Malcovati L, Giagounidis A, Porta MGD, Jädersten M, et al. Combining Gene Mutation With Gene Expression Data Improves Outcome Prediction in Myelodysplastic Syndromes. *Nat Commun* (2015) 6:5901. doi: 10.1038/ncomms6901
59. Chen H, Zhang P, Radomska HS, Hetherington CJ, Zhang D-E, Tenen DG. Octamer Binding Factors and Their Coactivator Can Activate the Murine PU.1 (Spi-1) Promoter. *J Biol Chem* (1996) 271:15743–52. doi: 10.1074/jbc.271.26.15743
60. Ma X-L, Sun Y-F, Wang B-L, Shen M-N, Zhou Y, Chen J-W, et al. Sphere-Forming Culture Enriches Liver Cancer Stem Cells and Reveals Stearoyl-CoA Desaturase 1 as a Potential Therapeutic Target. *BMC Cancer* (2019) 19:760. doi: 10.1186/s12885-019-5963-z
61. Moore LD, Le T, Fan G. DNA Methylation and Its Basic Function. *Neuropsychopharmacol* (2013) 38:23–38. doi: 10.1038/npp.2012.112
62. Forner A, Reig M, Bruix J. Hepatocellular Carcinoma. *Lancet* (2018) 391:1301–14. doi: 10.1016/S0140-6736(18)30010-2
63. Bray F, Ferlay J, Soerjomataram I, Siegel RL, Torre LA, Jemal A. Global Cancer Statistics 2018: GLOBOCAN Estimates of Incidence and Mortality Worldwide for 36 Cancers in 185 Countries. *CA: A Cancer J Clin* (2018) 68:394–424. doi: 10.3322/caac.21492
64. Antonosante A, d'Angelo M, Castelli V, Catanesi M, Iannotta D, Giordano A, et al. The Involvement of PPARs in the Peculiar Energetic Metabolism of Tumor Cells. *IJMS* (2018) 19:1907. doi: 10.3390/ijms19071907
65. Piccinin E, Cariello M, Moschetta A. Lipid Metabolism in Colon Cancer: Role of Liver X Receptor (LXR) and Stearoyl-CoA Desaturase 1 (Scd1). *Mol Aspects Med* (2021) 78:100933. doi: 10.1016/j.mam.2020.100933
66. Ma MKF, Lau EYT, Leung DHW, Lo J, Ho NPY, Cheng LKW, et al. Stearoyl-CoA Desaturase Regulates Sorafenib Resistance *via* Modulation of ER Stress-Induced Differentiation. *J Hepatol* (2017) 67:979–90. doi: 10.1016/j.jhep.2017.06.015
67. Tysoe O. PPAR Mediates Intestinal Stem Cell Tumorigenesis. *Nat Rev Endocrinol* (2021) 17:514–4. doi: 10.1038/s41574-021-00530-0
68. Pathak P, Chiang JYL. Sterol 12α-Hydroxylase Aggravates Dyslipidemia by Activating the Ceramide/mTORC1/SREBP-1C Pathway via FGF21 and FGF15. *Gene Expr* (2019) 19:161–173. doi: 10.3727/105221619X15529371970455
69. Patankar JV, Wong CK, Morampudi V, Gibson WT, Vallance B, Ioannou GN, et al. Genetic ablation of Cyp8b1 preserves host metabolic function by repressing steatohepatitis and altering gut microbiota composition. *Am J of Physiol-Endocrinol and Metab* (2018) 314:E418–32. doi: 10.1152/ajpendo.00172.2017
70. Mukherjee A, Kenny HA, Lengyel E. Unsaturated Fatty Acids Maintain Cancer Cell Stemness. *Cell Stem Cell* (2017) 20:291–92. doi: 10.1016/j.stem.2017.02.008
71. Petralia F, Tignor N, Reva B, Koptyra M, Chowdhury S, Rykunov D, et al. Integrated Proteogenomic Characterization across Major Histological Types of Pediatric Brain Cancer. *Cell* (2020) 183:1962–85.e31. doi: 10.1016/j.cell.2020.10.044
72. Luo M, Shang L, Brooks MD, Jiagge E, Zhu Y. Targeting Breast Cancer Stem Cell State Equilibrium through Modulation of Redox Signaling. *Cell Metabolism* (2018) 28:69–86.e6. doi: 10.1016/j.cmet.2018.06.006

Conflict of Interest: The authors declare that the research was conducted in the absence of any commercial or financial relationships that could be construed as a potential conflict of interest.

frontiers | Frontiers in Pharmacology

TYPE Original Research
PUBLISHED 09 August 2022
DOI 10.3389/fphar.2022.958070

OPEN ACCESS

EDITED BY
Haitao Wang,
Center for *Cancer* Research, National *Cancer* Institute (NIH), United States

REVIEWED BY
Jiankang Fang,
University of Pennsylvania, United States
Lin Zhang,
Clinical Center (NIH), United States
Kui Zhang,
The University of Chicago, United States

*CORRESPONDENCE
Hong Qiu,
qiuhong@hust.edu.cn

SPECIALTY SECTION
This article was submitted to Pharmacology of Anti-Cancer Drugs, a section of the journal Frontiers in Pharmacology

RECEIVED 31 May 2022
ACCEPTED 11 July 2022
PUBLISHED 09 August 2022

CITATION
Zhang X, Li Y, Hu P, Xu L and Qiu H (2022), Identification of molecular patterns and prognostic models of epithelial–mesenchymal transition- and immune-combined index in the gastric cancer.
Front. Pharmacol. 13:958070.
doi: 10.3389/fphar.2022.958070

Identification of molecular patterns and prognostic models of epithelial–mesenchymal transition- and immune-combined index in the gastric cancer

Xiuyuan Zhang, Yiming Li, Pengbo Hu, Liang Xu and Hong Qiu*

Department of Oncology, Tongji Hospital, Tongji Medical College, Huazhong University of Science and Technology, Wuhan, China

Background: Epithelial–mesenchymal transition (EMT) and the immune microenvironment play important roles in the progression of gastric cancer (GC), but the joint role of both in GC is not clear.

Methods: We identified EMT- and immune-related genes (EIRGs), and the molecular subtypes of EIRGs were identified by unsupervised cluster analysis. Then, we constructed an accurate EIRG_score model by using differential genes of molecular subtypes. The correlation of EIRG_score with prognosis, immune infiltration, gene mutation, chemotherapeutic drug sensitivity, and immunotherapy response was comprehensively analyzed. In addition, we investigated the biological function of EIRG_score via *in vitro* experiments.

Results: A total of 808 GC patients were classified into two molecular subtypes, which were enriched in EMT and immune-related biological pathways and significantly correlated with prognosis and immune infiltration. The constructed EIRG_score had an important role in predicting prognosis and immunotherapeutic response. The higher EIRG_score was associated with worse prognosis, higher abundance of immunosuppressive cell infiltration, lower immune checkpoint genes expression, lower tumor mutation burden, microsatellite instability-high, lower chemotherapeutic drug sensitivity, and poorer immunotherapeutic response.

Conclusion: EIRG_score may be used as a biomarker to assess prognosis and guide precise treatment.

KEYWORDS

epithelial–mesenchymal transition, gastric cancer, tumor microenvironment, immunotherapy, biomarker

Introduction

Gastric cancer (GC) is one of the most common digestive tumors, ranking fifth in incidence and mortality rates worldwide (Sung et al., 2021). The 5-year survival rate of GC is only approximately 20% (Etemadi et al., 2020). The current treatment for GC is mainly radical surgery, and the survival rate of early GC is up to 90% after surgical resection, but the treatment for middle and advanced GC is not optimistic, and conventional chemotherapy does not achieve the desired effect (Thrumurthy et al., 2015; Li et al., 2021). At present, immunotherapy has achieved a series of promising results in the treatment of GC (Coutzac et al., 2019). However, immunotherapy needs to identify specific populations to be more effective; therefore, we urgently need new biomarkers that have a role in identification.

The tumor microenvironment (TME) is a heterogeneous structure composed of tumor cells and immune cells, stromal cells, and so on. Cells in the TME interact in a paracrine manner with other cell types, which enables tumor cells to escape host immune surveillance (Sadeghi Rad et al., 2021). The GC microenvironment is mainly composed of stromal and immune cells with immune escape characteristics, such as cancer-associated fibroblasts (CAFs), tumor-associated macrophages (TAMs), and T regulatory cells (Tregs) (Seeneevassen et al., 2021); therefore, it is considered to be an immunosuppressive tumor.

Epithelial–mesenchymal transition (EMT) is a process by which epithelial cells acquire mesenchymal characteristics that promote tumor invasion metastasis and drug resistance (Pastushenko and Blanpain, 2019). Previous studies have identified that EMT can affect TME. Epithelial tumors are infiltrated with large numbers of cytotoxic $CD8^+$ T cells, but tumors with mesenchymal function contain Tregs cells and TAMs and can polarize into M2 subtypes (Dongre et al., 2017). EMT can also decrease the level of MHC class I on the cell surface and escape the killing function of T cells (Garcia-Lora et al., 2003) and can also induce cancer cells to express PD-L1, causing immune escape (Noman et al., 2017). In addition, TME components such as CAFs and TAMs can secrete growth factors and cytokines such as transforming growth factor-β (TGF-β) and interleukin-6 (IL-6), which can promote EMT (Dongre and Weinberg, 2019). Thus, EMT and TME interactions affect tumor progression.

In this study, we focused on the interaction between EMT and immunity. First, we obtained EMT- and immune-related genes (EIRGs) and classified GC patients into two molecular subtypes according to EIRGs. Then, patients were classified into two genetic subtypes based on differentially expressed genes (DEGs) identified by molecular subtypes. We further established the EIRG_score to predict overall survival (OS) and explored the immune status of GC to predict the response to immunotherapy.

Materials and methods

Data collection

We downloaded transcriptome data and clinical information of GC patients through the Cancer Genome Atlas (TCGA) database and the Gene Expression Omnibus (GEO) database. RNA sequencing data in the form of fragments per kilobase million (FPKM) and somatic mutation data in the form of MAF were downloaded via TCGA-STAD (n = 407), and the FPKM form was converted to transcripts per kilobase million form. We collected GSE84437 (n = 433) from the GEO database and combined and normalized the two datasets using the "ComBat" function of the "affy" and "sva" packages of R.

Clustering analysis of EIRGs

In total, 1184 EMT-associated genes and 1959 immune-related genes were obtained from previous studies and the ImmPort database (https://www.immport.org/) (Gao et al., 2021). We intersected the EMT- and immune-related genes using a Venn diagram and subsequently performed differential expression analysis (FC > 1, $p < 0.05$) using the "limma" package to obtain 82 DEGs as EIRGs. The EIRGs were subjected to unsupervised clustering analysis by the "ConsensusClusterPlus" package. Principal component analysis (PCA) was then performed using the "stat" package to investigate the variability of different molecular subtypes. Detailed data are available in Supplementary Table S2.

Gene set variation analysis

We downloaded the "h.all.v7.4. symbols" geneset from the GSEA-MSigDB database (http://www.gsea-msigdb.org/) and performed Gene set variation analysis (GSVA) to explore the biological role of different clusters using the "GSVA" package. The cutoff was logFC > 0.1 and adj.P.Val < 0.05, and GO and KEGG analyses were performed using the "clusterProfiler" package (Yu et al., 2012), with $p < 0.05$ as a filtering condition.

Immune cell infiltration analysis

To investigate different molecular subtypes of TME, we performed immune cell infiltration analysis using ssGSEA and the "CIBERSORT" algorithm (Newman et al., 2015) to assess the relative abundance of M2 macrophages, T, myeloid-derived suppressor cells (MDSCs) and other immune cells. To ensure the accuracy of the results, we only included results with $p < 0.05$.

Gene enrichment analysis

GO and KEGG enrichment analysis can be used as a way to explore gene function. In this study, we divided the expression of KIF2C into high- and low-risk groups according to the median and then performed enrichment analysis using the "clusterprofiler" (Yu et al., 2012) in R.

Differentially expressed gene analysis of molecular subtypes of EIRGs.

We obtained 5,503 DEGs by using the "limma" package for differential analysis of different molecular subtypes with a screening criterion of $p < 0.001$. We obtained 1,669 genes associated with prognosis by univariate Cox regression of DEGs with $p < 0.05$ as the screening criterion. Gene clustering analysis was then performed using the "ConsensusClusterPlus" package to obtain GeneCluster.

Construction and validation of the EIRG_score model

We constructed a prognostic model consisting of 18 genes using Lasso regression and multivariate Cox regression of prognosis-related DEGs with the "glmnet" package of R. EIRG_score was calculated using the following equation: Risk score = (exp gen1 × coef gen1) + (exp gen2 × coef gen2) +... + (exp gen18 × coef gen18), where exp is the value of gene expression and coef is the estimated regression coefficient. Patients were classified into high- and low-risk groups by using the median of the risk score. Survival analysis was performed using the "survival" package and the "survminer" package. ROC curves at 1, 3, and 5 years were plotted using the "timeROC" package.

Constructing and evaluating nomogram

The nomogram can be used for multiple indicators to predict disease progression (Iasonos et al., 2008), and we constructed the nomogram by integrating clinicopathological data and EIRG_score through the "rms" package to predict 1-, 3-, and 5-year survival rates. Calibration curves were used to assess the agreement of the nomogram with the actual situation.

Assessing the relationship between EIRG_score and immunotherapy response

Tumor immune dysfunction and exclusion (TIDE) algorithm predicts the response of a single sample or subtype to immune checkpoint inhibitors (ICIs) (Jiang et al., 2018), and immunophenoscores (IPS) can predict immunotherapy response. TIDE scores can be obtained from http://tide.dfci.harvard.edu/, and immunotherapy cohort IPS data can be obtained from the TCIA database (http://tcia.at/). The correlation of EIRG_score with TIDE and IPS was plotted by the "ggpubr" package.

In vitro experimental validation

All cell lines in this study were obtained from the Laboratory of Oncology, Tongji Hospital, Huazhong University of Science and Technology. GES-1, BGC-823, and SGC-7901 were cultured using RPMI-1640 complete medium. qRT-PCR was used to verify the mRNA expression levels of the cell lines, siRNA transfection was used to knock down AKR1B1, and Cell Counting Kit 8 (CCK8) and transwell assay were used to study proliferation and migration. The above-detailed procedures are shown in Supplementary Table S1. All experiments were performed with three biological replicates.

Immunohistochemistry

To verify the protein level expression of AKR1B1, we collected 5 GC tissues and five normal tissues from our hospital for immunohistochemical analysis. Tumor sections were first baked, subsequently desliced in xylene, and hydrated in graded ethanol; after retrieval in heat-sensitive citrate antigen, tissue sections were incubated overnight at 4°C ℃ with the primary antibody to AKR1B1 (YT0194, Immunoway, USA) and for 60 min at 25°C with horseradish peroxidase–conjugated antibody. Staining was performed by incubation with diaminobenzidine. At last, these treated tissue sections were observed under a microscope.

Statistical analysis

All statistical analyses were performed using R software (version 4.1.0). The Wilcoxon test was used for comparison between the two groups. Survival curves for each subgroup were plotted using the Kaplan–Meier plotter. Correlation coefficients were calculated using Spearman's analysis. $p < 0.05$ was considered to be statistically significant.

Results

Identification of molecular subtypes of EIRGs in GC

After obtaining 1184 EMT- and 1959 immune-related genes, we obtained 199 intersecting genes associated with both

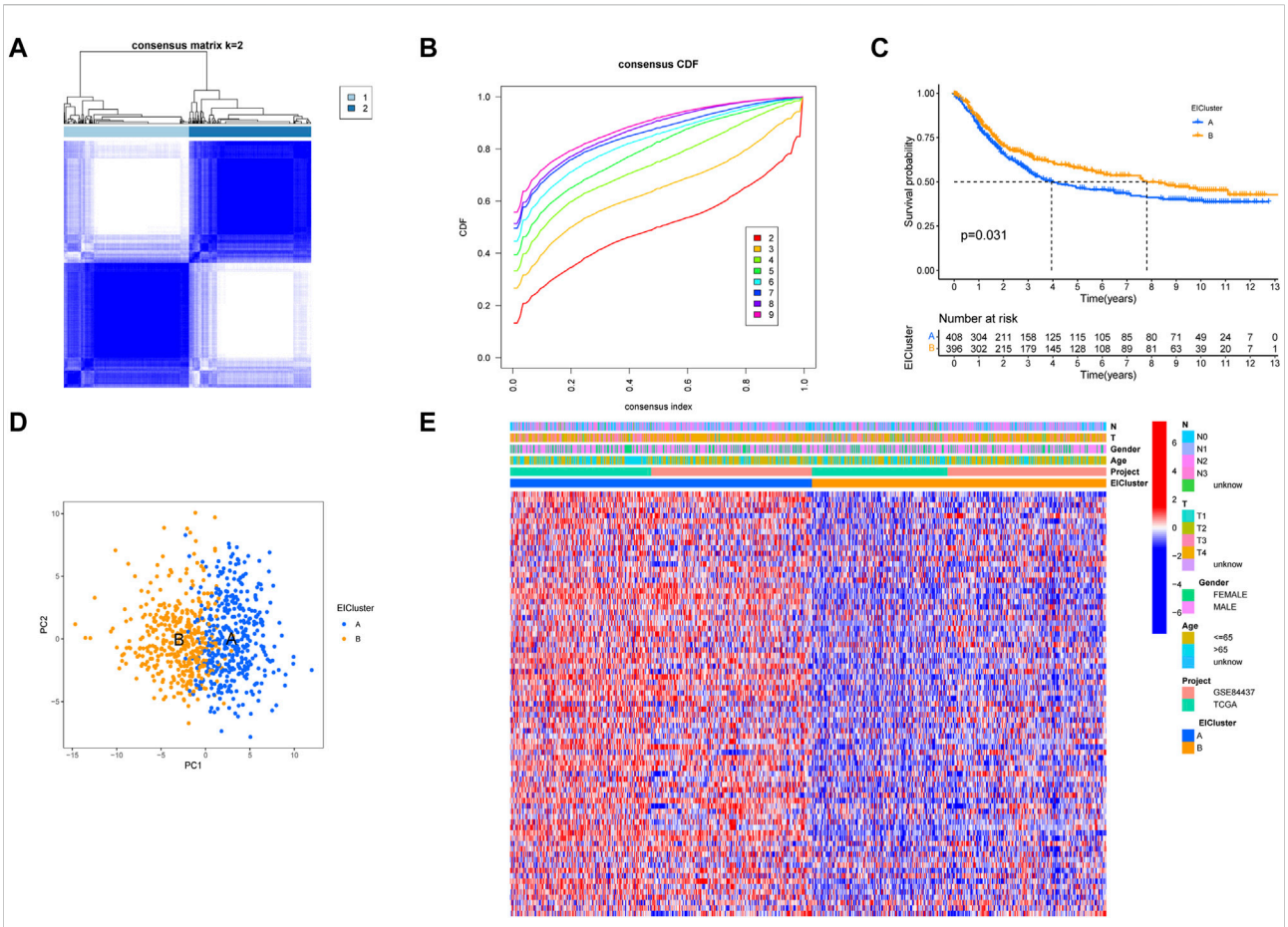

FIGURE 1
Construction of molecular subtypes of epithelial–mesenchymal transition- and immune-related genes (EIRGs) **(A)** consensus matrix heatmap defining two clusters (k = 2) and their correlation area. **(B)** cumulative distribution function graph. **(C)** survival curves of molecular subtypes. *p*-values are calculated using the log-rank test. **(D)** principal component analysis (PCA) between the two subtypes. **(E)** Clinicopathological characteristics and differences in expression levels of the two different subtypes.

immunity and EMT using a Venn diagram and subsequently performed differential expression analysis on the 199 intersecting genes to obtain 82 EIRGs (Supplementary Figure S1). To deeply investigate the expression characteristics of EIRGs in GC, we performed an unsupervised cluster analysis on GC patients (n = 808) based on EIRGs. When k = 2, the boundaries of the consistency matrix were clear (Figure 1A), and combined with the results of the cumulative distribution function (CDF) (Figure 1B), we took k = 2 as the optimal number of clusters and divided the cohort into two subtypes (EIcluster), namely, group A (n = 409) and group B (n = 399). By KM survival analysis (Figure 1C), we found that group A had a longer OS than group B ($p < 0.05$). To verify the stratification effect, we performed PCA analysis, and the results indicated a significant difference between the two subtypes and a good stratification effect (Figure 1D). Figure 1E shows the expression of EIRGs in the subtypes and the relationship with clinicopathological features.

GSVA analysis of different molecular subtypes of EIRGs and immune infiltration analysis

Through a GSVA analysis study, we found that subtype A was mainly enriched in EMT, interferon-gamma response, IL6 JAK STAT3 signaling, TNFA signaling via NFKB, and other biological activities (Figure 2A). To investigate the role of molecular subtypes in the immune microenvironment of GC, we evaluated the TME score of molecular subtypes by an estimate algorithm. A higher TME score means more abundant immune cells or stromal cells in TME, and the results showed that subtype A had a higher TME score than subtype B (Figure 2B). We then performed immune cell infiltration analysis of the subtypes by ssGSEA, and the results showed that subtype A had more abundant immune cell infiltration than subtype B, including MDSCs, Tregs, and macrophages (Figure 2C).

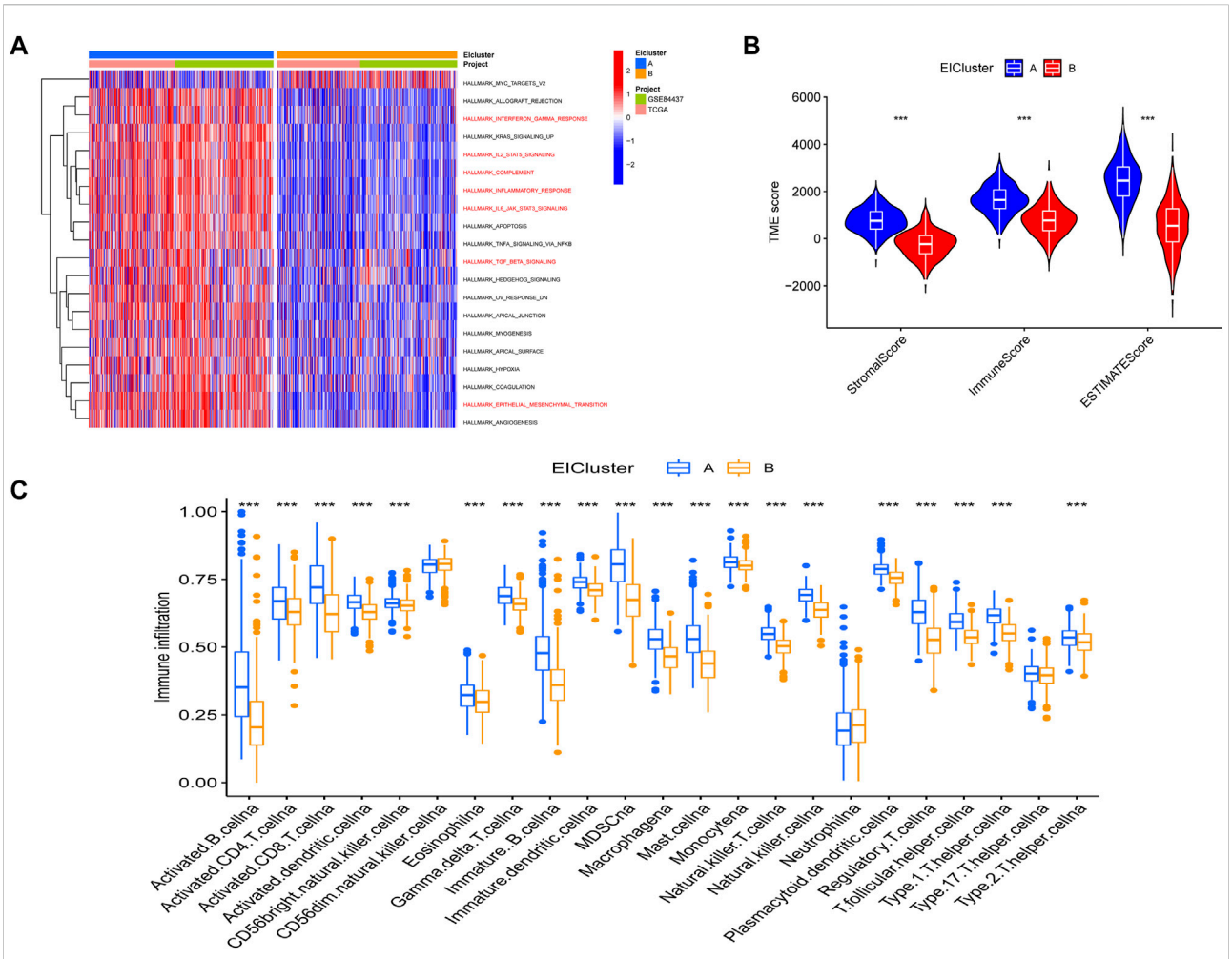

FIGURE 2
(A) Gene set variation analysis (GSVA) between two different subtypes, where red and blue represent activating and inhibiting pathways, respectively **(B)** correlation of molecular subtypes with tumor microenvironment score. **(C)** immune cell infiltration analysis of molecular subtypes. *$p < 0.05$, **$p < 0.01$, ***$p < 0.001$. p-values are calculated using the Wilcoxon test.

Clustering analysis of genes related to molecular subtypes of EIRGs

We obtained 5,503 differential genes by using the limma package and enriched the DEGs via GO and KEGG analyses. GO analysis indicated that EIRGs are involved in the regulation of immune functions (Figure 3A), and KEGG analysis indicated that EIRGs are implicated in tumor- and immune-related pathways; as seen, EIRG has a vital function in tumor progression and immune regulation (Figure 3B). We subjected the DEGs to unsupervised cluster analysis, and the boundaries of the consistency matrix were clear when k = 2 (Figure 4A). Combined with the CDF results, we divided the cohort into two gene subtypes (GeneCluster) (Figure 4B). KM survival curves showed that group A had worse OS than group B ($p < 0.001$) (Figure 4C), and PCA results also showed significant differences between the two subtypes (Figure 4D). We then performed GSVA and immune infiltration analysis on the subtypes and found that group A was enriched in EMT and KRAS signaling, whereas group B was enriched in MTORC1 signaling, oxidative phosphorylation, and other biological activities (Figure 5A); the two subtypes were significantly correlated with immune infiltration, and the proportion of immune cells was greater in subtype A than in subtype B (Figure 5B).

Construction and validation of the prognostic EIRG_score

The EIRG_score was constructed by molecular subtyping of prognostic DEGs, and 30 genes were identified using Lasso

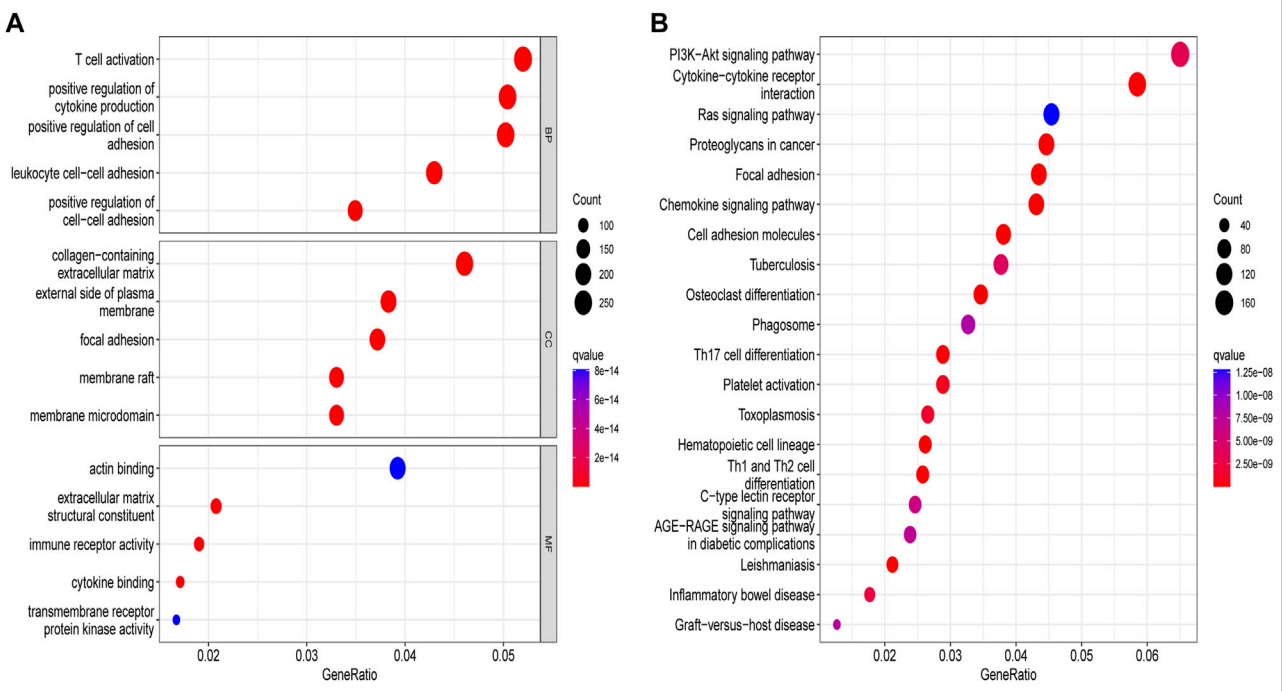

FIGURE 3
Enrichment analysis of molecular subtypes of DEGs. **(A)** gene ontology analysis **(B)** Kyoto encyclopedia of genes and genomes analysis.

regression analysis (Supplementary Figure S2) We then performed a multivariate Cox regression analysis on the 30 prognosis-related genes and finally obtained 18 hub genes for the construction of the EIRG_score model. The formula for the EIRG_score is as follows: The EIRG_score = (0.1921 × AKR1B1 exp.) + (−0.5852 × TRIM69exp.) + (0.1580 × FSTL3 exp.) + (0.3813 × PRDM6 exp.) + (0.6983 × SLC39A4 exp.) + (0.2299 × SENP7 exp.) + (0.2981 × DDIT4 exp.) + (0.5647 × MAN2A1 exp.) + (0.4436 × GLP2R exp.) + (0.2084 × EDN1 exp.) + (−0.3576 × EAF2 exp.) + (−0.3131 × FDX1 exp.) + (0.3803 × CNGA3 exp.) + (−0.4340 × ADAT3 exp.) + (−0.6221 × SH3BP2 exp.) + (0.8502 × S100Z exp.) + (−0.3144 × TBX3 exp.) + (−0.2143 × FRMD3 exp.). We divided the patients into training cohort (n = 402) and test cohort (n = 402) by using the "caret" package. We divided the patients into high- and low-risk groups using the median of EIRG_score in the training cohort. Detailed clinical data are available in Supplementary Table S3. The distribution of EIRG_score with EIRG molecular subtypes and GeneCluster is shown in Figure 6.

The survival curve indicated that in all groups, the high-risk group had a worse prognosis than the low-risk group ($p < 0.001$) (Figures 7A–C). In addition, the predicted 1-, 3-, and 5-year survival AUC values for EIRG_score were 0.719, 0.806, and 0.820 in the training cohort and 0.673, 0.730, and 0.733 in the all cohort, respectively (Figures 7D–F). The risk curve of EIRG_score shows that the score is negatively correlated with prognosis.

We downloaded the GSE62254 database (n = 300) as an external validation and calculated the score using the formula of EIRG_score from the training cohort. The patients were divided into two groups of high and low risks according to the median, and the survival analysis showed that the prognosis of the high-risk group was worse than that of the low-risk group (Supplementary Figure S3A). Using ROC curve analysis, the AUC values of EIRG_score for predicting 1-, 3-, and 5-year survival were 0.627, 0.687, and 0.651, respectively (Supplementary Figure S3B). The results indicated that EIRG_score had a positive effect in predicting the survival of GC patients.

Construction and validation of a nomogram

To more conveniently predict the prognosis of GC patients, we constructed a nomogram based on EIRG_score and clinicopathological characteristics (age, T-stage, N-stage, etc.) to predict the 1-, 3-, and 5-year OS rate of GC patients (Figure 8A). The calibration curves showed that the actual observed results were well consistent with the predicted results (Figure 8B). The ROC curve showed that the AUC values of the 1-, 3-, and 5-year OS of the nomogram were 0.711,0.762, and 0.774, respectively

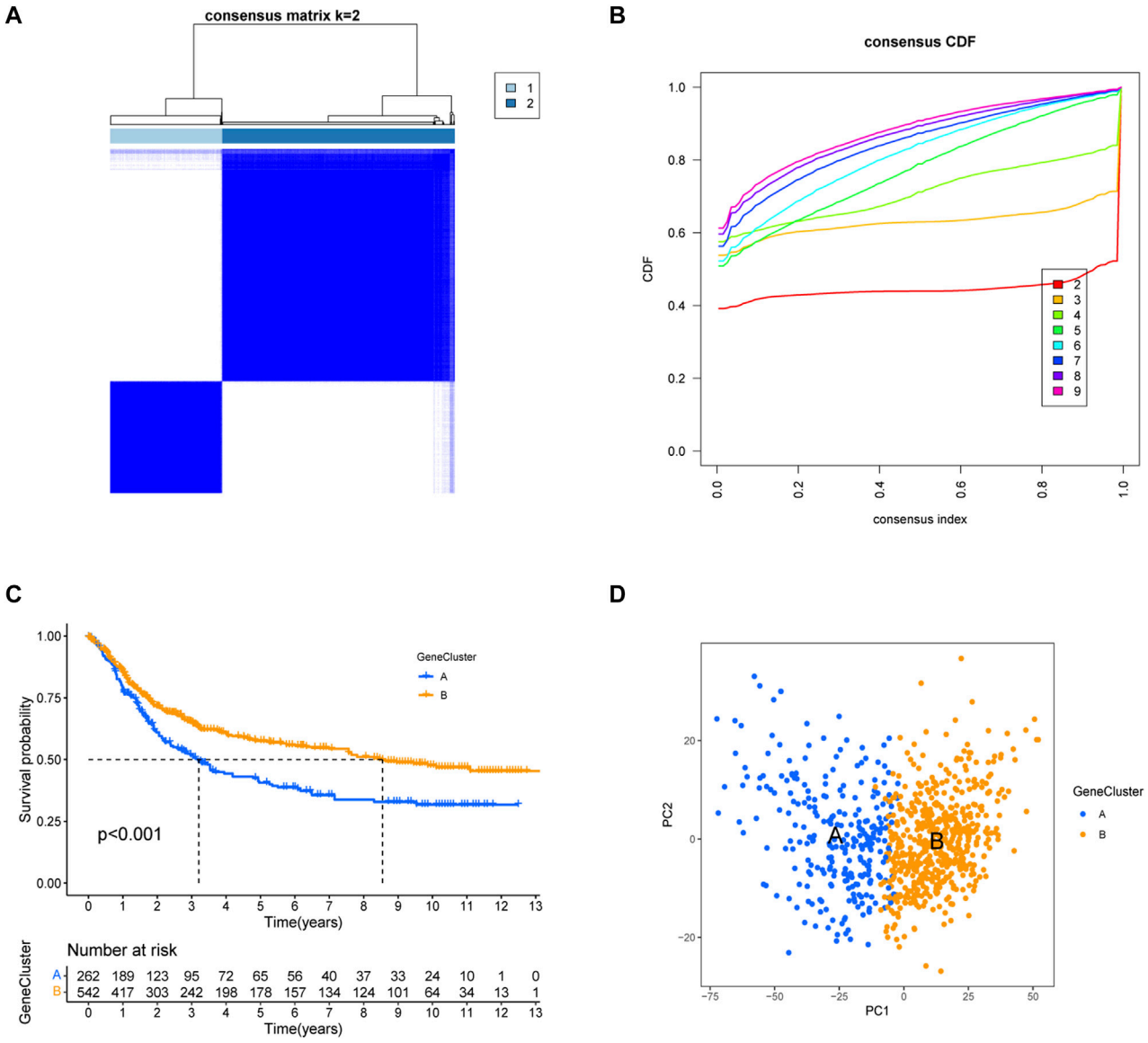

FIGURE 4
Construction of gene subtypes of EIRGs. **(A)** consensus matrix heatmap defining two clusters (k = 2) and their correlation area. **(B)** distribution function graph. **(C)** Survival curves of molecular subtypes. **(D)** PCA between the two subtypes.

(Figure 8C), which indicated that the predictive efficacy of the nomogram was satisfactory.

Immune infiltration analysis of EIRG_score

We analyzed the relationship between EIRG_score and 22 immune cell infiltrations by the cibersort algorithm. The results showed that the high EIRG_score group had a higher abundance in Tregs, M2 macrophages, mast cells resting, and lower in M1 macrophages (Figure 9A). Then, we performed correlation analysis and EIRG_score was positively correlated with Tregs and M2 macrophages, which promote immunosuppression, and negatively correlated with M1 macrophages, which inhibit tumor progression (Figure 9B). It can be seen that the EIRG_score correlates with the immunosuppressive microenvironment.

Correlation of EIRG_score with mutations

Tumor mutational burden (TMB) is considered to be a biomarker to predict a good response to immunotherapy.

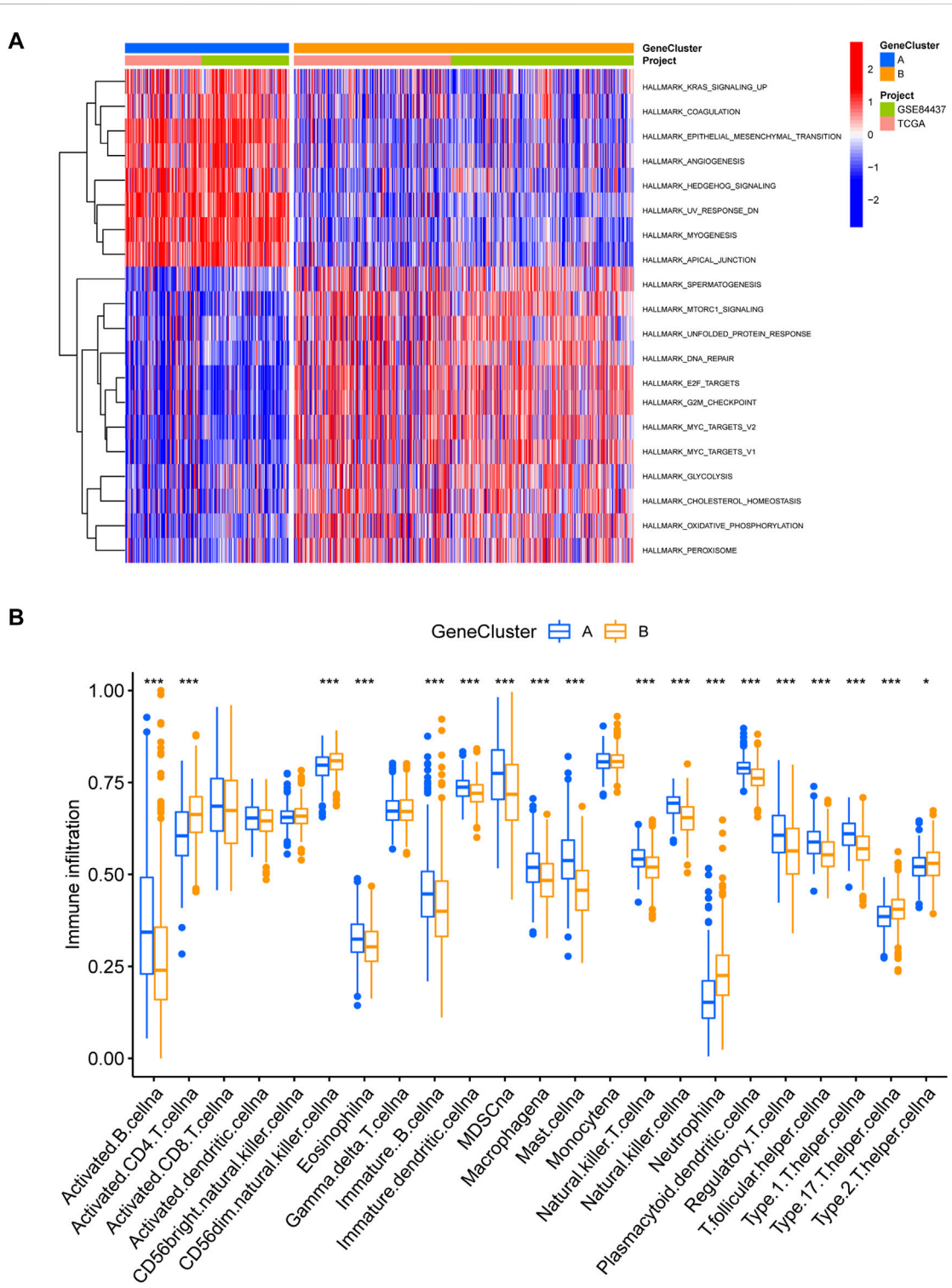

FIGURE 5
Immune infiltration analysis of gene subtypes **(A)** GSVA analysis of gene subtypes, where red and blue represent activation and suppression pathways, respectively. **(B)** immune cell infiltration analysis of gene subtypes. *$p < 0.05$, **$p < 0.01$, ***$p < 0.001$. The p-values are calculated using the Wilcoxon test.

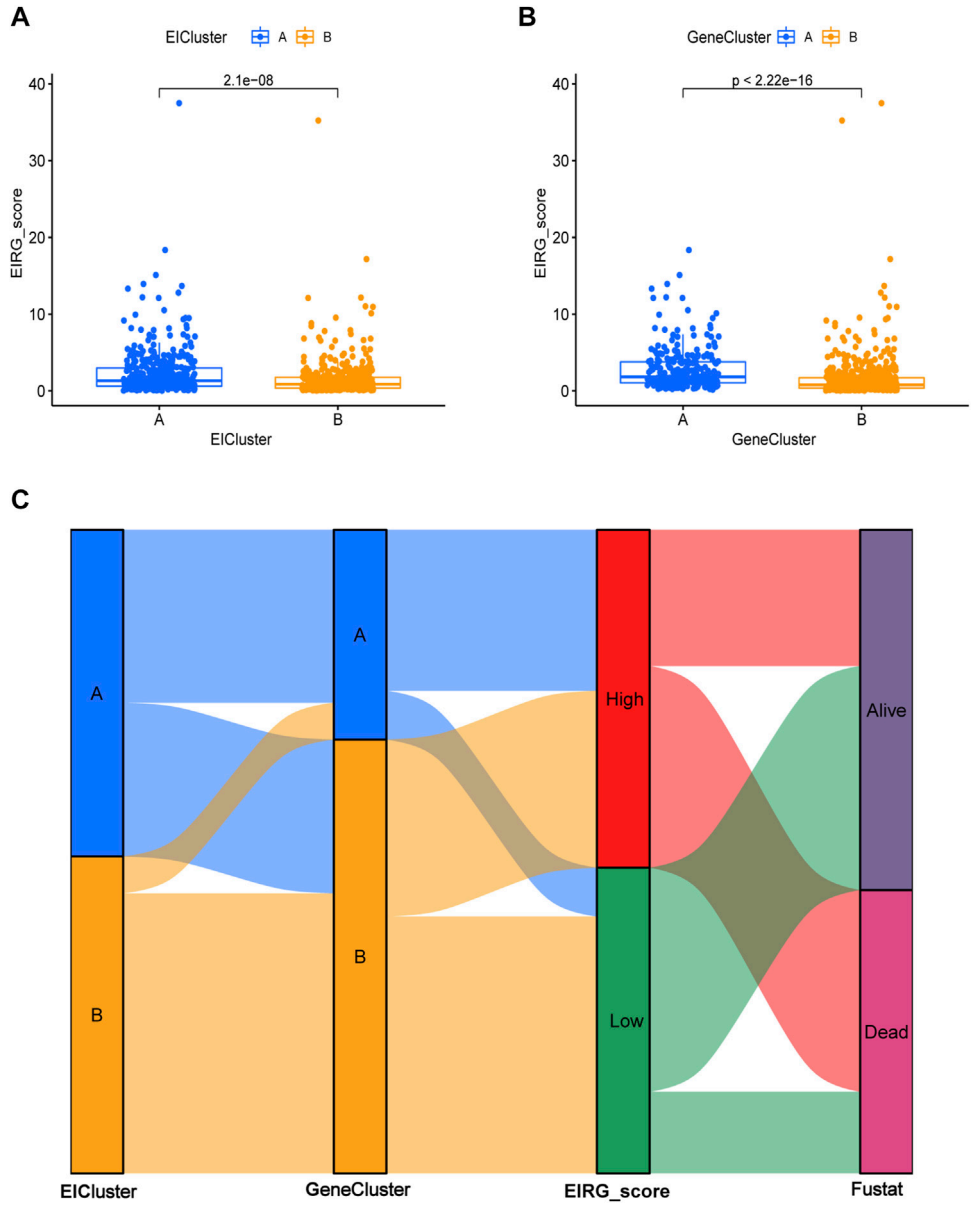

FIGURE 6
Distribution of EIRG_score. **(A)** differences in EIRG_score between different molecular subtypes. **(B)** differences in EIRG_score between different gene subtypes. **(C)** alluvial diagram of the distribution of different EIRG_score and survival outcome subtypes.

Therefore, we studied the correlation between EIRG_score and TMB, and we found that TMB was lower in the high score group than in the low score group (Figure 10A). As shown in Figure 10B, the low EIRG_score + high TMB group had the best prognosis ($p < 0.001$), suggesting that EIRG_score may be negatively correlated with immunotherapy response. Furthermore, we performed somatic mutation analysis for the high and low score groups by the "maftools" package, and we found that the mutation frequency in the high EIRG_score group (83.07%) was lower than that in the low EIRG_score group (93.64%), and the top three mutated genes in both groups were TTN, TP53, and MUC16(Figures 10C–D).

EIRG_score predicts immunotherapy response

First, we analyzed the correlation between EIRG_score and immune checkpoint genes (CD274, CTLA4, LAG3, and PDCD1) and found that ICP genes expression was higher in the low

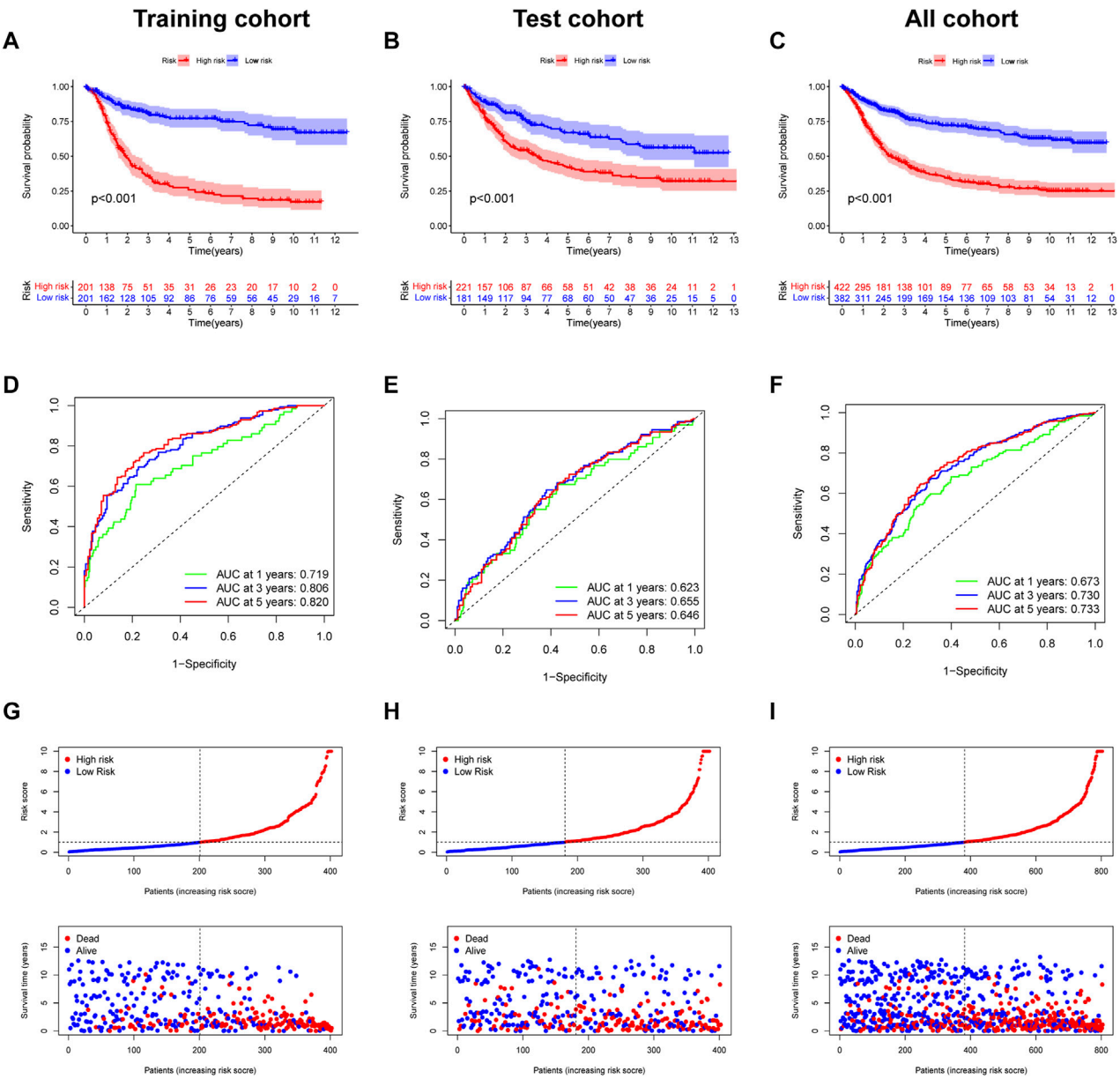

FIGURE 7
Prognostic assessment of EIRG_score. **(A)** Kaplan–Meier (KM) survival analysis of training cohort, **(B)** test cohort, **(C)** all cohorts. **(C)** receiver operating characteristic (ROC) curve analysis of training cohort, **(D)** test cohort, and **(E)** all cohorts. **(F)** Risk score distribution and survival scatter plot of **(G)** training cohort, **(H)** test cohort, and **(I)** all cohorts.

EIRG_score group (Figure 11A). The results of the TIDE algorithm showed that the high EIRG_score group had a higher TIDE score, suggesting that the high EIRG_score may not respond well to ICB (Figure 11B). In addition, we included immunotherapy groups in the TCIA database for in-depth analysis, and the results showed that the low EIRG_score group had better treatment outcomes than the high EIRG_score group in the single anti-CALT4 treatment group, the single anti-PD1 treatment group, and the simultaneous anti-CALT4 and PD1 treatment group (Figures 11C–E). Moreover, the proportion of microsatellite instability-high (MSI-H) was lower in patients in the high EIRG_score group (11%) than in the low EIRG_score group (26%) (Figure 11F).

At last, we investigated the correlation between EIRG_score and chemotherapeutic drug sensitivity by using the "pRRophetic" package. It was found that the IC50 of chemotherapeutic drugs such as cyclopamine, gemcitabine, paclitaxel, and lenalidomide were higher in the high EIRG_score group than in the low EIRG_score group

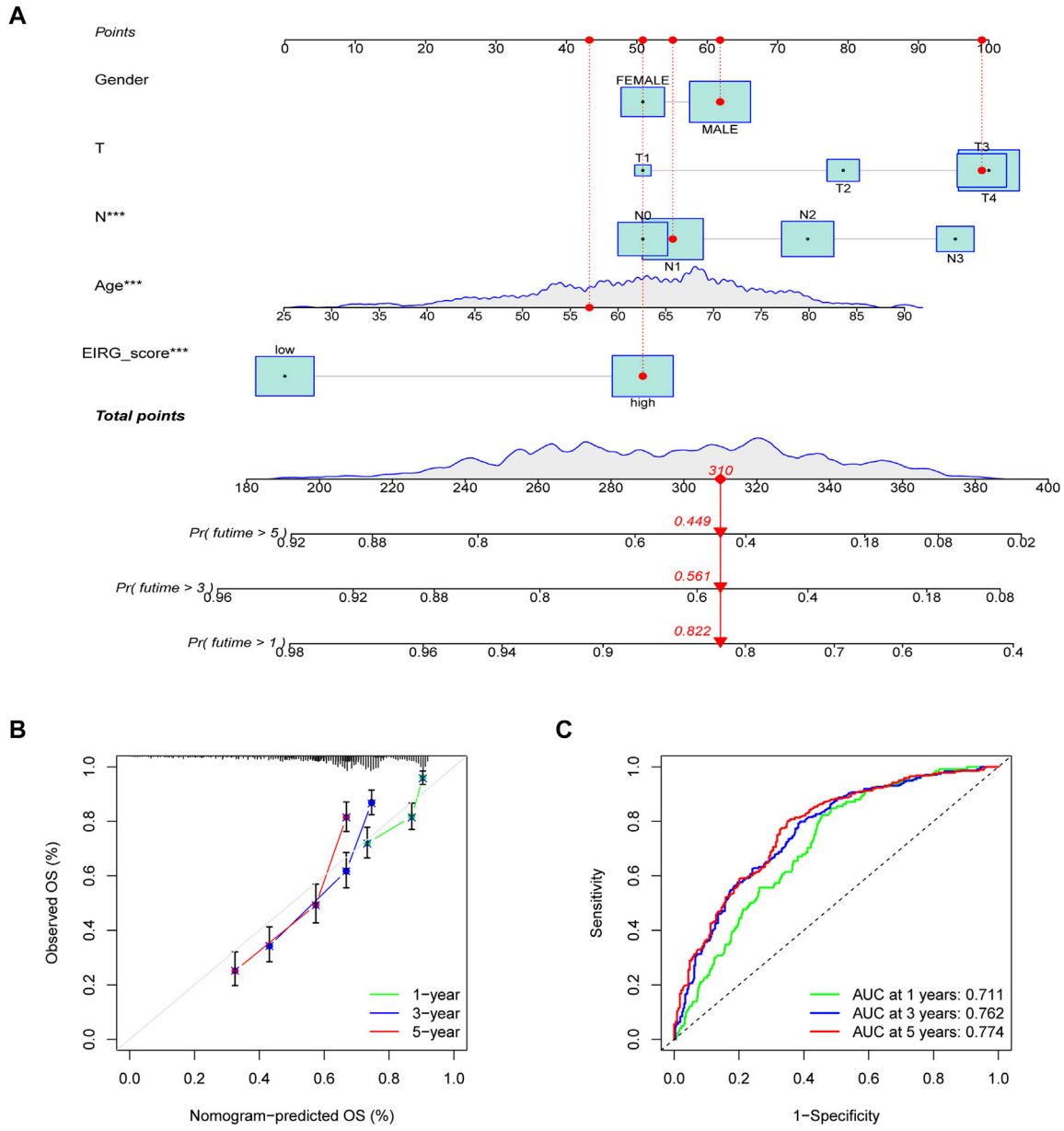

FIGURE 8
Construction and validation of nomogram. **(A)** nomogram for predicting 1-, 3-, and 5-year OS in patients with colorectal cancer in the training group. **(B)** calibration curves with a nomogram. **(C)** ROC curve analysis of the nomogram.

(Supplementary Figure S4), indicating that the high EIRG_score group may be resistant to these drugs.

AKR1B1 affects GC cell proliferation and migration

We explored the biological function of EIRG_score by *in vitro* experiments, and we selected AKR1B1, which has barely been studied in GC, for our study. The UALCAN database (Chandrashekar et al., 2017) and IHC results revealed that AKR1B1 was highly expressed in GC tissues and associated with poor prognosis (Supplementary Figure S5). qRT-PCR results showed that AKR1B1 was highly expressed in GC cell lines, which was consistent with the database results (Figure 12A). Then, we performed AKR1B1 knockdown by transfection of siRNA (Figure 12B), and we discovered through CCK-8 and transwell assays that knockdown of

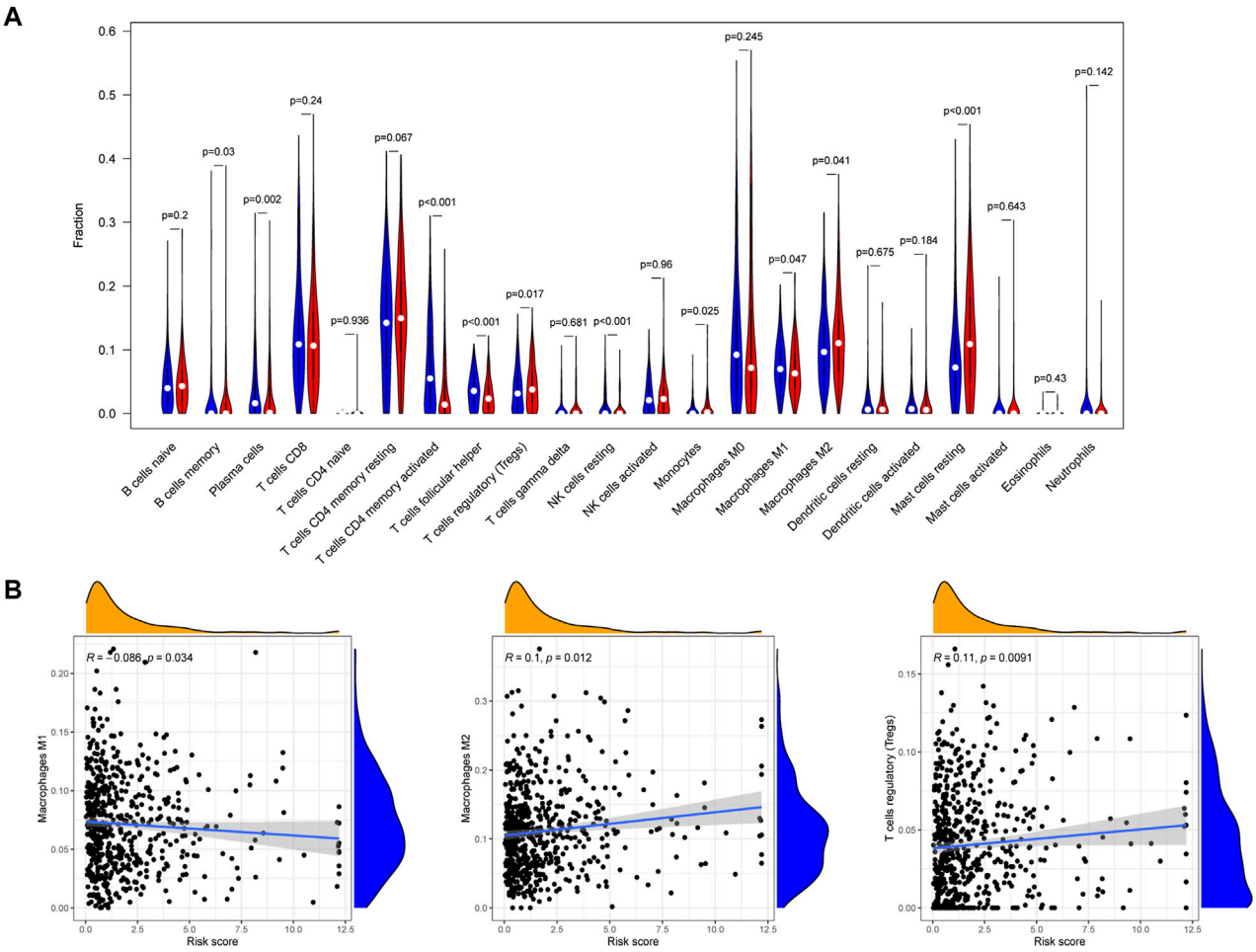

FIGURE 9
Immune infiltration analysis of EIRG_score. **(A)** abundance of 22 types of infiltrating immune cells in EIRG_score. Red represents the high EIRG_score group and blue represents the low EIRG_score group. **(B)** correlation analysis of EIRG_score with M1 macrophages, M2 macrophages, and Tregs. Correlation analysis using the Spearman correlation test.

AKR1B1 significantly inhibited GC cell proliferation and migration (Figures 12C,D). It indicates that AKR1B1 plays a procancer role in GC.

Discussion

Multiple factors are influencing GC development and progression, for example, EMT can promote GC invasion, metastasis, and resistance to chemotherapy. Moreover, the microenvironment of GC can affect tumor progression. Focusing on a single factor alone may not be sufficient to provide a comprehensive understanding of GC. We included the combination of EMT and the immune microenvironment in our study for the first time to explore the combined effects on GC prognosis and immunotherapy.

We collected 1184 EMT- and 1959 immune-related genes from databases and previous studies and identified DEGs through the TCGA database, obtaining 82 overlapping intersection genes as EIRGs. We classified GC patients into two molecular subtypes by EIRGs, and the prognosis of subtype A was worse compared with subtype B. Moreover, there were significant differences between the two subtypes in TME, with subtype A having a higher TME score than subtype B. EIRGs molecular subtypes are enriched in biological pathways such as EMT, IL6-JAK-STAT3 signaling, IL2-STAT5 signaling, and TGF-β signaling, and previous studies have shown that CAFs in GC cells enhance EMT by secreting IL-6 to activate the JAK2/STAT3 pathway in GC cells (Wu et al., 2017). MDSCs and Tregs are more abundant in subtype A than in subtype B. Tregs can suppress $CD8^+$ T cell activation and also secrete IL-10 and TGF-β to inhibit tumor-

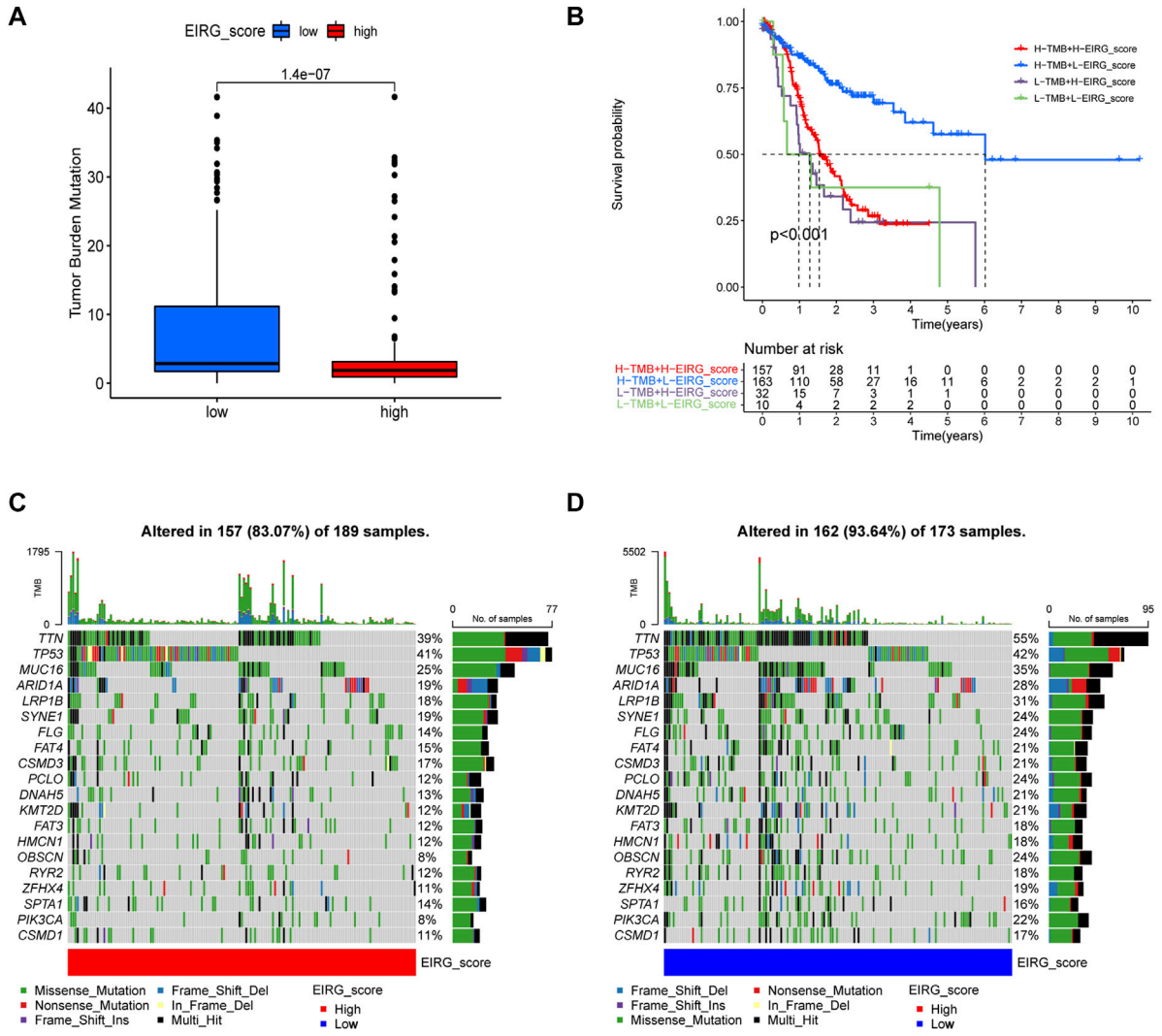

FIGURE 10
Mutation analysis of EIRG_score. **(A)** tumor mutational burden (TMB) of different EIRG_score groups. **(B)** KM survival analysis of EIRG_score and TMB. *p*-values are calculated using the log-rank test. Correlation of mutations between **(C)** high- and **(D)** low-risk group. Each column represents an individual patient. The numbers on the right indicate the mutation frequency of each regulator. The bars on the right show the proportion of each mutation type.

specific T cell infiltration and function, thereby causing immunosuppression (Ahrends and Borst, 2018). MDSCs are immature immunosuppressive myeloid cells that can inhibit $CD8^+$ T cell function through the expression of PD-L1 and CTLA-4 and can induce EMT (Oya et al., 2020), suggesting that subtype A has an immunosuppressive profile (cold tumors) and subtype B has an immune-activating profile (hot tumors).

We performed a differential analysis of the molecular subtypes of EIRG, resulting in two gene subtypes. Genotyping was significantly correlated with the prognosis and immune infiltration of GC. To better assess the prognosis and immunotherapeutic response of GC, we constructed an EIRG_score based on the differential genes of EIRGs molecular subtypes and explored its predictive ability. Compared with the low EIRG_score group, the high EIRG_score group had a worse prognosis, with subtype A, characterized by cold tumors, associated with a higher EIRG_score, and subtype B, characterized by hot tumors, associated with a lower EIRG_score.

Then, we performed an immune infiltration analysis of EIRG_score and found that Tregs in the high EIRG_score group had an increased abundance of M2 macrophage infiltration, whereas in the low EIRG_score group, M1 macrophage infiltration abundance was increased. The correlation results showed that EIRG_score was positively

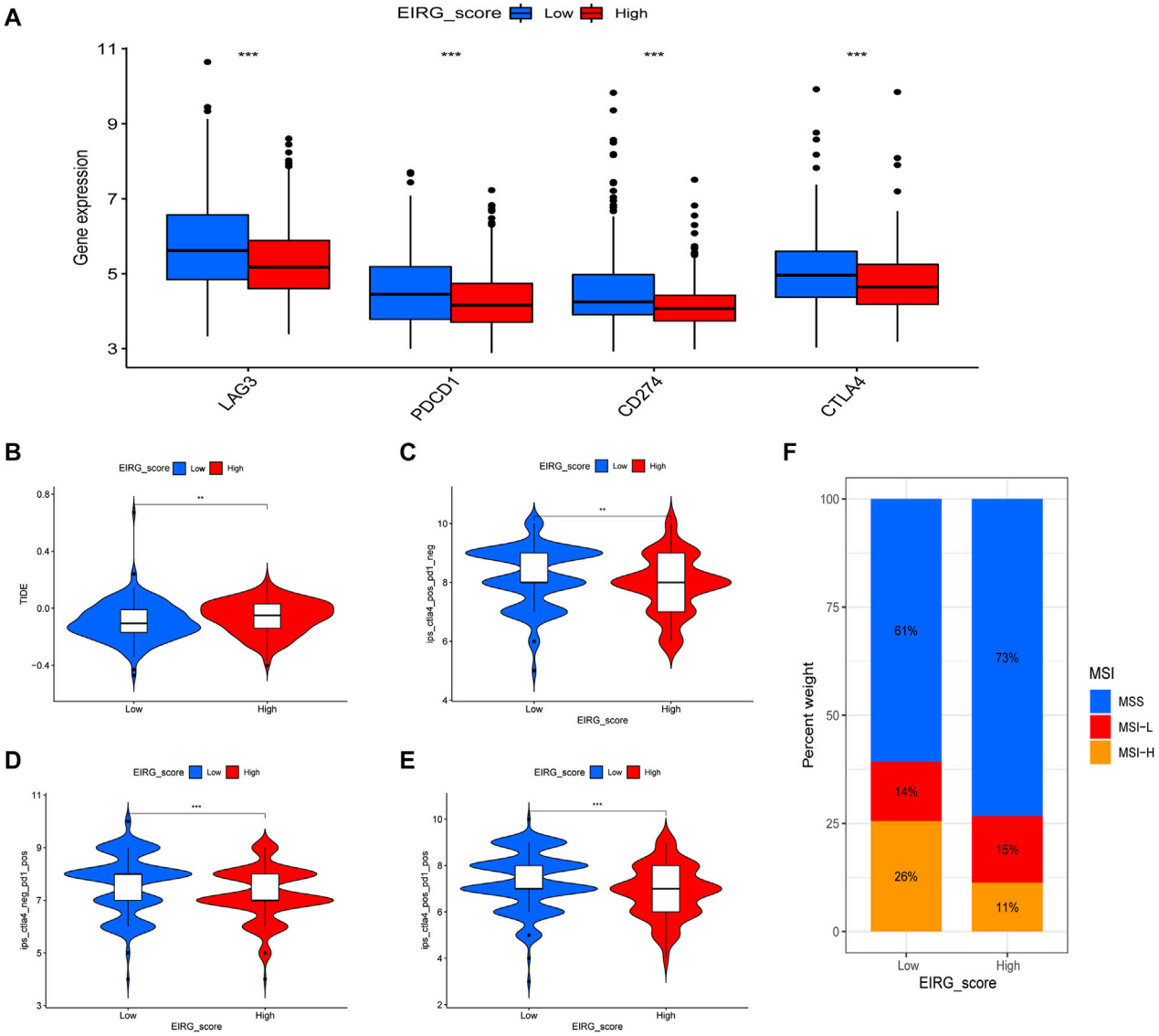

FIGURE 11
EIRG_score predicts immunotherapy response. **(A)** expression of immune checkpoint genes in high and low EIRG_score groups. **(B)** correlation of EIRG_score with tumor immune dysfunction and exclusion score. **(C–E)** correlation between EIRG_score and IPS. **(F)** correlation of EIRG_score with MSI. *$p < 0.05$, **$p < 0.01$, ***$p < 0.001$.

correlated with Tregs and M2 macrophages and negatively correlated with M1 macrophages. Macrophages are mainly divided into M1 and M2 types. M1 macrophages can kill tumors through both antibody-dependent cell–mediated cytotoxicity and direct-mediated cytotoxicity and therefore have tumor suppressive effects (Pan et al., 2020). By contrast, M2 macrophages can promote tumor proliferation, invasion, and angiogenesis and are associated with EMT, which can promote tumor metastasis and cause poor patient prognosis (Rihawi et al., 2021). This may explain the worse prognosis in the high EIRG_score group.

A significant part of immunotherapy is ICIs. However, the majority of patients receiving ICIs do not benefit from them (Sha et al., 2020). Therefore, we wanted to explore whether EIRG_score could be used as a biomarker to predict the efficacy of immunotherapy.

Because of PDL1 expression, TMB and MSI-H are considered to be biomarkers that can predict the efficacy of immunotherapy (Rizzo et al., 2021). Therefore, we explored the correlation between EIRG_score and ICP genes, TMB and MSI-H. We found that the low EIRG_score group had higher ICP gene expression levels, higher TMB, and higher MSI-H

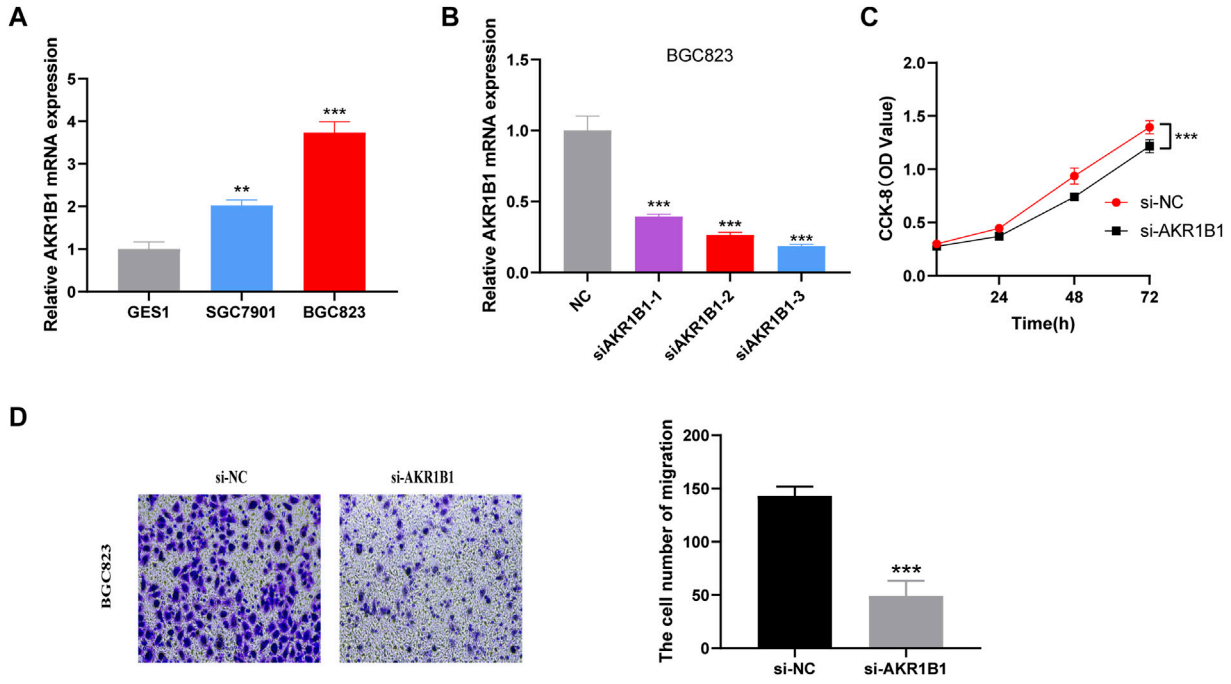

FIGURE 12
Validation of the biological function of AKR1B1 **(A)** quantitative polymerase chain reaction (qPCR) displayed upregulation of AKR1B1 in gastric cancer (GC) cells compared to normal cell line (GES1). Results represent mean ± SD; $n = 3$. ***$p < 0.001$; two-tailed *t*-test. **(B)** validation of knockdown efficiency by qPCR. Results represent mean ± SD. $n = 3$. ***$p < 0.001$; two-tailed *t*-test. **(C)** AKR1B1 siRNA displayed reduced proliferation of BGC823 cell. Results represent mean ± SD; $n = 3$; ***$p < 0.001$; two-tailed *t*-test. **(D)** AKR1B1 knockdown inhibited migration of BGC823 cells. Results represent mean ± SD; $n = 3$. **$p < 0.01$; ***$p < 0.001$; two-tailed *t*-test.

proportion than the high EIRG_score group. Moreover, we combined TMB and EIRG_score for prognostic analysis and found that TMB-high + low EIRG_score had the best prognosis. In addition, we calculated the TIDE score of GC using the TIDE algorithm, and the TIDE scores were higher in the high EIRG_score group, indicating that the high EIRG_score had a poorer response to immunotherapy; in IPS assessment, the IPS scores were higher in the low EIRG_score group in any treatment group, suggesting that the low EIRG_score responded better to immunotherapy. The above results suggest that EIRG_score can be used as a biomarker to identify and screen patients for immunotherapy, and the lower the EIRG_score value, the better the response of GC patients to immunotherapy.

At last, we examined the correlation between EIRG_score and chemotherapeutic drug sensitivity and showed that EIRG_score was positively correlated with the IC50 of several drugs, including paclitaxel. Paclitaxel is a first-line chemotherapy drug that exerts its anticancer effects by inhibiting cell cycle progression, and it was found that paclitaxel can inhibit Tregs, which can reverse immunosuppression (Zhu and Chen, 2019), suggesting that the low EIRG_score group may benefit from it. Previous studies have found that AKR1B1 plays a major role in tumor progression, and the mechanisms of action of AKR1B1 include participation in EMT and immune regulation. In addition, AKR1B1 has regulatory effects on the synthesis of reactive oxygen species and prostaglandins (Khayami et al., 2020). Moreover, AKR1B1 expression was higher in GC patients with poorer OS prognosis, suggesting that AKR1B1 is associated with poorer prognosis in GC (Xiong, 2021). In the present study, we found that AKR1B1 could promote GC cell proliferation and migration, which is consistent with the results of previous studies.

There are still some limitations in our study; on the one hand, it is only a retrospective study of data from public databases, and more prospective and multicenter clinical studies are needed to further confirm our results. On the other hand, more *in vivo* and *in vitro* experiments are needed to investigate the molecular mechanisms underlying the effects of EIRGs.

Conclusion

For the first time, we included EMT- and immune-related genes jointly in our study, comprehensively analyzed the role of

EIRGs in GC, and constructed the EIRG_score model, which can be used as a biomarker for predicting mutation, prognosis, and response to immunotherapy, providing a new thought for precise treatment of GC.

Data availability statement

The datasets presented in this study can be found in online repositories. The names of the repository/repositories and accession number(s) can be found in the article/ Supplementary Material.

Author contributions

XZ contributed to data acquisition and article drafting; YL, PH, and LX provided technical support; HQ contributed to study design and supervision. All authors read and approved the final article.

Conflict of interest

The authors declare that the research was conducted in the absence of any commercial or financial relationships that could be construed as a potential conflict of interest.

Publisher's note

All claims expressed in this article are solely those of the authors and do not necessarily represent those of their affiliated organizations, or those of the publisher, the editors and the reviewers. Any product that may be evaluated in this article, or claim that may be made by its manufacturer, is not guaranteed or endorsed by the publisher.

Supplementary material

The Supplementary Material for this article can be found online at: https://www.frontiersin.org/articles/10.3389/fphar.2022.958070/full#supplementary-material

References

Ahrends, T., and Borst, J. (2018). The opposing roles of CD4 $^{+}$ T cells in anti-tumour immunity. *Immunology* 154 (4), 582–592. doi:10.1111/imm.12941

Chandrashekar, D. S., Bashel, B., Balasubramanya, S. A. H., Creighton, C. J., Ponce-Rodriguez, I., Chakravarthi, B. V. S. K., et al. (2017). Ualcan: A portal for facilitating tumor subgroup gene expression and survival analyses. *Neoplasia* 19 (8), 649–658. doi:10.1016/j.neo.2017.05.002

Coutzac, C., Pernot, S., Chaput, N., and Zaanan, A. (2019). Immunotherapy in advanced gastric cancer, is it the future? *Crit. Rev. Oncol. Hematol.* 133, 25–32. doi:10.1016/j.critrevonc.2018.10.007

Dongre, A., Rashidian, M., Reinhardt, F., Bagnato, A., Keckesova, Z., Ploegh, H. L., et al. (2017). Epithelial-to-Mesenchymal transition contributes to immunosuppression in breast carcinomas. *Cancer Res.* 77 (15), 3982–3989. doi:10.1158/0008-5472.CAN-16-3292

Dongre, A., and Weinberg, R. A. (2019). New insights into the mechanisms of epithelial–mesenchymal transition and implications for cancer. *Nat. Rev. Mol. Cell Biol.* 20 (2), 69–84. doi:10.1038/s41580-018-0080-4

Etemadi, A., Safiri, S., Sepanlou, S. G., Ikuta, K., Bisignano, C., Shakeri, R., et al. (2020). The global, regional, and national burden of stomach cancer in 195 countries, 1990–2017: A systematic analysis for the global burden of disease study 2017. *Lancet. Gastroenterol. Hepatol.* 5 (1), 42–54. doi:10.1016/S2468-1253(19)30328-0

Gao, Y., Liu, J., Cai, B., Chen, Q., Wang, G., Lu, Z., et al. (2021). Development of epithelial-mesenchymal transition-related lncRNA signature for predicting survival and immune microenvironment in pancreatic cancerwithexperiment validation. *Bioengineered* 12 (2), 10553–10567. doi:10.1080/21655979.2021.2000197

Garcia-Lora, A., Algarra, I., and Garrido, F. (2003). MHC class I antigens, immune surveillance, and tumor immune escape. *J. Cell. Physiol.* 195 (3), 346–355. doi:10.1002/jcp.10290

Iasonos, A., Schrag, D., Raj, G. V., and Panageas, K. S. (2008). How to build and interpret a nomogram for cancer prognosis. *J. Clin. Oncol.* 26 (8), 1364–1370. doi:10.1200/JCO.2007.12.9791

Jiang, P., Gu, S., Pan, D., Fu, J., Sahu, A., Hu, X., et al. (2018). Signatures of T cell dysfunction and exclusion predict cancer immunotherapy response. *Nat. Med.* 24 (10), 1550–1558. doi:10.1038/s41591-018-0136-1

Khayami, R., Hashemi, S. R., and Kerachian, M. A. (2020). Role of aldo-keto reductase family 1 member B1 (AKR1B1) in the cancer process and its therapeutic potential. *J. Cell. Mol. Med.* 24 (16), 8890–8902. doi:10.1111/jcmm.15581

Li, K., Zhang, A., Li, X., Zhang, H., and Zhao, L. (2021). Advances in clinical immunotherapy for gastric cancer. *Biochim. Biophys. Acta. Rev. Cancer* 1876 (2), 188615. doi:10.1016/j.bbcan.2021.188615

Newman, A. M., Liu, C. L., Green, M. R., Gentles, A. J., Feng, W., Xu, Y., et al. (2015). Robust enumeration of cell subsets from tissue expression profiles. *Nat. Methods* 12 (5), 453–457. doi:10.1038/nmeth.3337

Noman, M. Z., Janji, B., Abdou, A., Hasmim, M., Terry, S., Tan, T. Z., et al. (2017). The immune checkpoint ligand PD-L1 is upregulated in EMT-activated human breast cancer cells by a mechanism involving ZEB-1 and miR-200. *OncoImmunology* 6 (1), e1263412. doi:10.1080/2162402X.2016.1263412

Oya, Y., Hayakawa, Y., and Koike, K. (2020). Tumor microenvironment in gastric cancers. *Cancer Sci.* 111 (8), 2696–2707. doi:10.1111/cas.14521

Pan, Y., Yu, Y., Wang, X., and Zhang, T. (2020). Tumor-associated macrophages in tumor immunity. *Front. Immunol.* 11, 583084. doi:10.3389/fimmu.2020.583084

Pastushenko, I., and Blanpain, C. (2019). EMT transition States during tumor progression and metastasis. *Trends Cell Biol.* 29 (3), 212–226. doi:10.1016/j.tcb.2018.12.001

Rihawi, K., Ricci, A. D., Rizzo, A., Brocchi, S., Marasco, G., Pastore, L. V., et al. (2021). Tumor-associated macrophages and inflammatory microenvironment in gastric cancer: Novel translational implications. *Int. J. Mol. Sci.* 22 (8), 3805. doi:10.3390/ijms22083805

Rizzo, A., Ricci, A. D., and Brandi, G. (2021). PD-L1, TMB, MSI, and other predictors of response to immune checkpoint inhibitors in biliary tract cancer. *Cancers* 13 (3), 558. doi:10.3390/cancers13030558

Sadeghi Rad, H., Monkman, J., Warkiani, M. E., Ladwa, R., O'Byrne, K., Rezaei, N., et al. (2021). Understanding the tumor microenvironment for effective immunotherapy. *Med. Res. Rev.* 41 (3), 1474–1498. doi:10.1002/med.21765

Seeneevassen, L., Bessède, E., Mégraud, F., Lehours, P., Dubus, P., Varon, C., et al. (2021). Gastric cancer: Advances in carcinogenesis research and new therapeutic strategies. *Int. J. Mol. Sci.* 22 (7), 3418. doi:10.3390/ijms22073418

Sha, D., Jin, Z., Budczies, J., Kluck, K., Stenzinger, A., Sinicrope, F. A., et al. (2020).

Tumor mutational burden as a predictive biomarker in solid tumors. *Cancer Discov.* 10 (2), 1808–1825. doi:10.1158/2159-8290.CD-20-0522

Sung, H., Ferlay, J., Siegel, R. L., Laversanne, M., Soerjomataram, I., Jemal, A., et al. (2021). Global cancer statistics 2020: GLOBOCAN estimates of incidence and mortality worldwide for 36 cancers in 185 countries. *Ca. Cancer J. Clin.* 71 (3), 209–249. doi:10.3322/caac.21660

Thrumurthy, S. G., Chaudry, M. A., Chau, I., and Allum, W. (2015). Does surgery have a role in managing incurable gastric cancer? *Nat. Rev. Clin. Oncol.* 12 (11), 676–682. doi:10.1038/nrclinonc.2015.132

Wu, X., Tao, P., Zhou, Q., Li, J., Yu, Z., Wang, X., et al. (2017). IL-6 secreted by cancer-associated fibroblasts promotes epithelial-mesenchymal transition and metastasis of gastric cancer via JAK2/STAT3 signaling pathway. *Oncotarget* 8 (13), 20741–20750. doi:10.18632/oncotarget.15119

Xiong, Z., Lin, Y., Yu, Y., Zhou, X., Fan, J., Rog, C. J., et al. (2021). Exploration of lipid metabolism in gastric cancer: A novel prognostic genes expression profile. *Front. Oncol.* 11, 712746. doi:10.3389/fonc.2021.712746

Yu, G., Wang, L.-G., Han, Y., and He, Q.-Y. (2012). clusterProfiler: an R Package for comparing biological themes among gene clusters. *OMICS* 16 (5), 284–287. doi:10.1089/omi.2011.0118

Zhu, L., and Chen, L. (2019). Progress in research on paclitaxel and tumor immunotherapy. *Cell. Mol. Biol. Lett.* 24, 40. doi:10.1186/s11658-019-0164-y

frontiers | Frontiers in Pharmacology

TYPE Review
PUBLISHED 22 August 2022
DOI 10.3389/fphar.2022.991052

OPEN ACCESS

EDITED BY
Haitao Wang,
Center for Cancer Research (NIH), United States

REVIEWED BY
Siqi Chen,
Washington University in St. Louis, United States
Guoqiang Liu,
University of Notre Dame, United States
Jiankang Fang,
University of Pennsylvania, United States
Lin Zhang,
Clinical Center (NIH), United States
Ming Zhao,
First Affiliated Hospital of Chengdu Medical College, China
Lingling Hu,
Cornell University, United States

*CORRESPONDENCE
Huabao Xiong,
xionghbl@yahoo.com
Shulong Jiang,
jnsljiang@163.com

SPECIALTY SECTION
This article was submitted to Pharmacology of Anti-Cancer Drugs, a section of the journal Frontiers in Pharmacology

RECEIVED 11 July 2022
ACCEPTED 25 July 2022
PUBLISHED 22 August 2022

CITATION
Tian X, Yan T, Liu F, Liu Q, Zhao J, Xiong H and Jiang S (2022), Link of sorafenib resistance with the tumor microenvironment in hepatocellular carcinoma: Mechanistic insights. *Front. Pharmacol.* 13:991052. doi: 10.3389/fphar.2022.991052

Link of sorafenib resistance with the tumor microenvironment in hepatocellular carcinoma: Mechanistic insights

Xinchen Tian[1], Tinghao Yan[1], Fen Liu[2], Qingbin Liu[2], Jing Zhao[2], Huabao Xiong[3]* and Shulong Jiang[1,2]*

[1]Cheeloo College of Medicine, Shandong University, Jinan, China, [2]Clinical Medical Laboratory Center, Jining First People's Hospital, Jining Medical University, Jining, China, [3]Institute of Immunology and Molecular Medicine, Basic Medical School, Jining Medical University, Jining, China

Sorafenib, a multi-kinase inhibitor with antiangiogenic, antiproliferative, and proapoptotic properties, is the first-line treatment for patients with late-stage hepatocellular carcinoma (HCC). However, the therapeutic effect remains limited due to sorafenib resistance. Only about 30% of HCC patients respond well to the treatment, and the resistance almost inevitably happens within 6 months. Thus, it is critical to elucidate the underlying mechanisms and identify effective approaches to improve the therapeutic outcome. According to recent studies, tumor microenvironment (TME) and immune escape play critical roles in tumor occurrence, metastasis and anti-cancer drug resistance. The relevant mechanisms were focusing on hypoxia, tumor-associated immune-suppressive cells, and immunosuppressive molecules. In this review, we focus on sorafenib resistance and its relationship with liver cancer immune microenvironment, highlighting the importance of breaking sorafenib resistance in HCC.

KEYWORDS

tumor microenvironment, hepatocellular carcinoma, sorafenib resistance, tumor-associated immune-suppressive cells, immunosuppressive factors, hypoxia

1 Introduction

According to the latest global cancer statistics, primary liver cancer (PLC) is the sixth most common diagnosed cancer and the third leading cause of cancer death worldwide, with report of 830,000 deaths in 2020 (Sung et al., 2021). Hepatocellular carcinoma (HCC) is the most common histologic type of PLC, accounting for approximately 80–90% (Yang W et al., 2019; Zhu W et al., 2020). Established risk factors for HCC include hepatitis B and C virus infections, alcohol consumption, smoking, obesity, and aflatoxin contamination (Ma et al., 2019). Currently, multidisciplinary treatment strategies are used for HCC, including surgical resection, liver transplantation, transcatheter arterial chemoembolization (TACE), chemotherapy, radiotherapy and molecular targeted therapy (Gao Y et al., 2019). However, HCC is a highly invasive and metastatic tumor with insidious early clinical manifestations. Therefore, most HCC patients lose

the opporet tunity for surgery or acquire poor surgical outcomes (Dang et al., 2017). Systemic therapy becomes only treatment option for these patients. Meanwhile, sorafenib has been recognized as a standard first-line treatment for advanced HCC (Pinyol et al., 2019).

Sorafenib, an oral multi-kinase inhibitor, was permitted by the U.S. Food and Drug Administration (FDA) for the treatment of renal cell carcinoma, HCC, and thyroid cancer in 2009 (Yang and Stockwell, 2016). Sorafenib exerts anti-proliferation and anti-angiogenesis effects by inhibiting various kinases, such as inhibiting the tyrosine kinase activity of the cell surface: vascular endothelial growth factor receptor (VEGFR) family, platelet-derived growth factor receptor (PDGFR) family, hepatocyte factor receptor (c-Kit) and FMS-like tyrosine kinase (FLT-3) and suppressing the intracellular Raf family kinase (Yang and Stockwell, 2016). According to the phase III sorafenib Asia-Pacific (AP) trial and the sorafenib HCC Assessment Randomized Protocol (SHARP) trial, sorafenib was effective in prolonging 3 months of median overall survival in patients with late-stage HCC (Llovet et al., 2008; Cheng et al., 2009). However, the therapeutic effect of sorafenib is mainly limited by drug resistance. Only about 30% of HCC patients acquired benefits from sorafenib and the resistance always arose within 6 months in HCC patients (Ford et al., 2009). Hence, it is critical to identify underlying mechanisms and effective strategies to improve its therapeutic outcome.

Tumorigenesis is a complex process requiring synergistic changes in both tumor cells and tumor microenvironment (TME) (Franco et al., 2015). TME has been shown to be critical for tumor progression (Yao et al., 2020) and the development of drug resistance (Borden, 2014). TME was usually classified into cellular and non-cellular components, both of which have been reported to significantly influence drug resistance. In this review, we discuss the relationship between different immune-associated components of TME and sorafenib resistance and provide potential targets that could improve the resistance.

2 Sorafenib resistance

It has widely been accepted that sorafenib resistance is classified as primary (intrinsic) and secondary (acquired) resistance. Primary resistance denotes that due to the genetic heterogeneity of tumor cells, liver cancer cells already have the resistance factor(s) before sorafenib treatment, which leads to the insensitivity of sorafenib at the early stage of treatment (Xu et al., 2019). Acquired resistance refers to the phenomenon that tumor cells become less sensitive to sorafenib after a period of treatment, resulting in treatment failure (Niu et al., 2017; Yu et al., 2020). Because primary and secondary resistances greatly limit the therapeutic effect of sorafenib, it is important and necessary to gain an in-depth understanding of them. Published resistance mechanisms are presented in Figure 1.

2.1 Primary resistance

The molecular mechanisms behind the primary resistance of sorafenib are poorly understood. Based on previous reports, the primary resistance are mainly associated with following molecules and cellular change: 1) EGFR (epidermal growth factor receptor) belongs to the ErbB/EGFR family of receptor tyrosine kinases (RTKs) (Yang Y. M. et al., 2020). The binding of EGFRs to their ligands triggers a series of downstream signaling pathways to promote cell proliferation, survival, and invasion (Tan et al., 2020). Ezzoukhry et al. found that activating EGFR contributed to the primary resistance of sorafenib in HCC by activating the RAF-MEK-ERK cascade. Either inhibiting the kinase activity of EGFR or down-regulating its expression significantly increased the effects of sorafenib on the resistance cells (Ezzoukhry et al., 2012). 2) Sestrin 2 is a probable biomarker and therapeutic target for tumor treatment that plays a vital role in the incidence and development of malignance. Some studies identified sestrin 2 as a tumor suppressor gene, while others described it as an oncogene (Qu et al., 2021). A previous study found that the expression of SESN2 was positively associated with the IC50 of sorafenib in HCC cell lines and Sestrin 2 could induce sorafenib primary resistance by activation of the AKT and AMPK pathways (Dai et al., 2018). 3) Yap, a transcriptional coactivator, is a primary nuclear effector of the Hippo signaling pathway (Sadek and Olson, 2020). Activation of the Hippo/Yap pathway occurs early in the development of liver cancer. Dysregulation of this pathway was detected in approximately 65% of HCCs and associated with a much worse prognosis (Lee et al., 2018). Accumulating studies suggest that Yap play a critical role in sorafenib resistance. For example, Wu et al. found that YAP, activating by SET domain containing 1A (SETD1A), could lead to sorafenib primary resistance in HCC (Wu et al., 2020). 4) FcRn (neonatal Fc receptor) is a member of a family of receptors for the Fc portion of IgG and is involved in the recycling and endocytosis of IgG (Dalloneau et al., 2016). FcRn regulates albumin homeostasis in the liver, where albumin is synthesized (Kuo et al., 2010). Guan et al. found that activation of FcRn triggered the primary resistance of sorafenib in HCC by activating the HIF pathway (Guan et al., 2021). 5) AFP (Alpha fetoprotein) is the most commonly used biomarker for HCC (Zhang et al., 2018). It has been shown that high level of AFP is associated with poor prognosis across stages of HCC (Kelley et al., 2020). Negri et al. confirmed that the adverse prognostic implications of elevated baseline serum AFP and suggested that AFP contributed to the development of sorafenib primary resistance (Negri et al., 2021). 6) CSCs

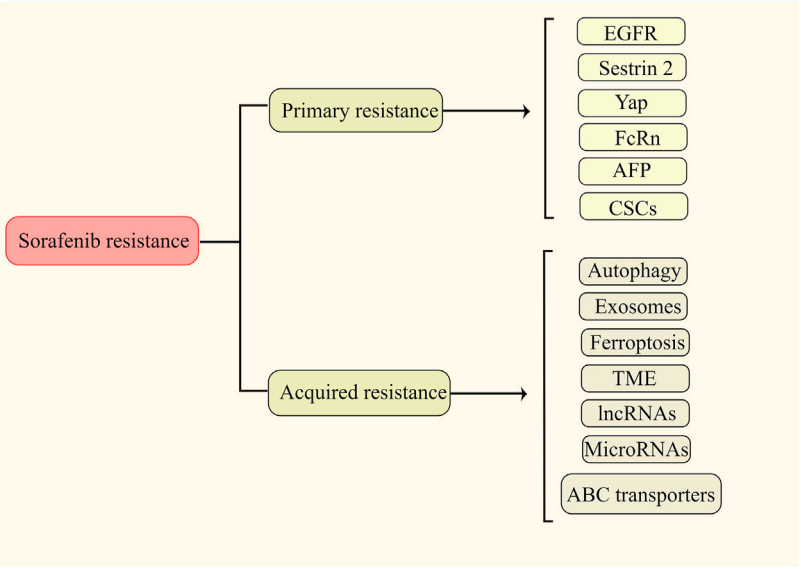

FIGURE 1
Major determinants of the primary and acquired resistance (edited by Figdraw software).

(cancer stem cells) are a subpopulation of cells that have stem cell characteristics and are in an embryonic stem cell state (Wang G et al., 2020). A growing body of research has revealed the critical role of CSCs in intratumoral heterogeneity and primary resistance (Reya et al., 2001). IL-6/STAT3 signaling was shown to be a major pathway to regulate CSCs leading to sorafenib resistance in HCC (Li D et al., 2020). CD133 promotes CSC-like properties by stimulating EGFR-AKT signaling and further reduces the sensitivity to sorafenib in HCC (Jang et al., 2017).

2.2 Acquired resistance

Compared with primary resistance, mechanisms for acquired resistance have been widely discussed. Understanding the mechanisms of acquired resistance often has vital therapeutic implications. 1) ABC transporters. Overexpression of ATP binding box (ABC) transporters is a major cause of multidrug resistance (MDR) (Wu and Fu, 2018) For example, Heme oxygenase 1 (HMOX1) reduces the sensitivity of HCC cells to sorafenib via regulation of the expression of ABC transporters (Zhu et al., 2022). In addition, SOX9 contributes to the resistance of HCC to sorafenib by activation of the Akt/ABCG2 pathway (Wang M et al., 2020). 2) Autophagy. Deregulated autophagy is associated with cancer initiation and progression. A large amount of evidence shows that autophagy is involved in developing sorafenib resistance in HCC through various mechanisms, and inhibition of autophagy restores sorafenib sensitivity. For example, CD24 contributes to sorafenib resistance via activating autophagy in HCC. In addition, through FOXO3-mediated autophagy, RNAm 6) A methylation leads to sorafenib resistance in HCC (Lu et al., 2018; Lin H et al., 2020; Li et al., 2021). 3) Exosomes. Exosomes, as material transport carriers, play a vital role in the exchange of biological information and the regulation of the cellular microenvironment (Jiang et al., 2019). Qu et al. showed that HCC cell-derived exosomes induced sorafenib resistance both *in vivo* and *in vitro* via the HGF/c-Met/Akt pathway in HCC (Qu et al., 2016). 4) Ferroptosis. Ferroptosis is an iron-dependent type of non-apoptotic cell death (Youssef et al., 2018). Sorafenib can induce ferroptosis in HCC (Nie et al., 2018). Therefore, inhibition of ferroptosis may induce sorafenib resistance. For example, YAP/TAZ and ATF4 trigger sorafenib resistance by preventing ferroptosis in HCC (Gao et al., 2021b). In addition, Metallothionein-1G leads to sorafenib resistance by inhibition of ferroptosis (Sun et al., 2016). 5) EMT. A number of investigations have shown that EMT is associated with poor survival in patients with HCC because it facilitates tumor development and progression through driving metastasis (Fukusumi et al., 2018). Moreover, EMT is a significant contributor to sorafenib resistance in HCC. For example, Van Malenstein et al. found that continuing exposure to sorafenib of HCC cells triggered the resistance with EMT (van Malenstein et al., 2013). In addition, EMT induced from overexpression of Snails facilitates sorafenib resistance in HCC (Dong et al., 2017). 6) lncRNAs. Long non-coding RNAs (lncRNAs) are a class of non-coding RNAs that participate in an extensive range of biological processes,

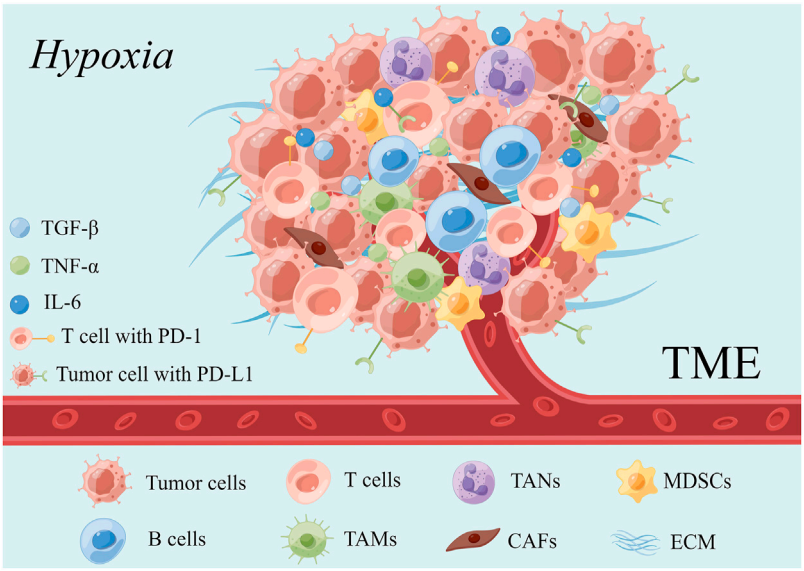

FIGURE 2
Constituents of the TME (edited by Figdraw software).

including cellular proliferation, differentiation and development, exerting a significant influence on normal physiology and disease development (Rodriguez-Mateo et al., 2017). Accumulating studies have shown that some lncRNAs are dysregulated and significantly associated with initiation, metastasis, recurrence, prognosis and drug resistance in HCC (Wei L et al., 2019). Recent studies have confirmed that some lncRNAs participate in sorafenib resistance in HCC. For example, overexpression of LncRNA SNHG1 leads to sorafenib resistance by activation of the Akt pathway (Li et al., 2019). Further, LncRNA NIFK-AS1 was shown to promote sorafenib resistance by m6A methylation in HCC (Chen et al., 2021). Another lncRNA, SNHG3, induces sorafenib resistance by regulating the miR-128/CD151 pathway in HCC (Zhang et al., 2019). 7) MicroRNAs. MicroRNAs (miRNAs) are endogenous small non-coding RNAs consisting of 19–23 nucleotides that regulate eukaryotic gene expression (Asano et al., 2019). Recently, the aberrant regulation of microRNA has been reported to associate with hepatocarcinogenesis and HCC progression (Feng L et al., 2020; Zha and Li, 2020). It was also identified that a variety of miRNAs were involved in sorafenib resistance. For instance, miR-181a contributes to sorafenib resistance by downregulating RASSF1 expression (Azumi et al., 2016). In addition, over-expressed miR-221 leads to sorafenib resistance by inhibiting caspase-3-mediated apoptosis in HCC (Fornari et al., 2017). 8) TME. Development and progression of HCC are a complex process and rely on interactions between the HCC cell and TME. It is generally accepted that TME is linked to aggressive tumor behavior, drug resistance and poor prognosis for cancer patients. Emerging evidence has revealed that various parts of the TME play pivotal roles in sorafenib resistance in HCC (Tang W et al., 2020; Ju et al., 2021). However, these are not the only mechanisms of primary and secondary resistance of sorafenib; the other causes were also being investigated.

3 Tumor microenvironment

TME is a unique internal environment for tumor cells to survive and proliferate. It is a complex network composed of tumor cells, various immune cells, extracellular matrix (ECM) and a variety of cytokines and chemokines (Mao et al., 2021). The composition of the TME is shown in Figure 2. Studies have highlighted that TME tends to be a hypoxic and acidic environment, which can affect the tumor phenotype and promotes the metastasis and proliferation of tumor cells (Abou Khouzam et al., 2022).

In general, TME is infiltrated with many tumor-related immune cells, including anti-tumor immune cells, such as $CD8^+$ cytotoxic T lymphocytes (CTL) and natural killer cells (NK), and immunosuppressive cells. However, these immune cells are presented at a weakened or non-functional state (Binnewies et al., 2018). A large number of CTLs are limited to the border of tumor mass or segmented by fibrotic nests and are exhibited to hamper the killing activity of tumor cells (Binnewies et al., 2018). Meanwhile, regulatory T cells (Treg), myeloid-derived suppressor cells (MDSCs), and tumor-associated macrophages (TAMs) are activated and proliferate

in large numbers in TME to inhibit the function of anti-tumor effector cells and promote the immune escape and metastasis of tumor cells (Khalaf et al., 2021).

Emerging investigations have demonstrated that ECM, a complex network composed of protein crosslinks, provides physical support for cell growth within TME. Hyaluronic acid and collagen are the major compositions of ECM, which increase solid stress and interstitial fluid pressure, compress the tumor vascular system, and participate in tumor growth, angiogenesis, immunosuppression, and chemoradiotherapy resistance (Zhang et al., 2022). Interestingly, ECM deposition was shown to generate "fibrotic nests" that enclose CTLs to a poor immunological state, forming a barrier that prevents CTLs infiltration into the tumor core (Binnewies et al., 2018).

In TME, cancer-associated fibroblasts (CAFs), the most abundant cells, are able to interact with adjacent tumor cells mediating by paracrine signals (cytokines, exosomes, and metabolites) or the ECM. Moreover, CAFs secret matrixmetallo proteinases (MMPs) to reshape the ECM. Moreover, by releasing chemokines, growth factors, and angiogenic factors, they also contribute to the abnormalities and functional defects of vascular structure, thereby accelerating tumor invasion and metastasis and promoting the occurrence of drug resistance (Mao et al., 2021). A recent study found that the exosomes released by gemcitabine-exposed CAFs could more effectively accelerate of tumor cell growth (Richards et al., 2017), suggesting the potential role of CAFs in drug resistance.

In addition, the interactions between cytokines released from the local TME and their receptors make the tumor form an immunosuppressive network, which promotes tumor progression. Several studies have demonstrated that interleukin-6 (IL-6), transforming growth factor-β (TGF-β), TNF-α, CCL2, CCL17, CCL22, and other immune-regulatory cytokines have significant changes in TME and are closely related to tumor grade, invasiveness and sorafenib resistance.

Until now, it has been well established that TME is a complex and dynamic network driving tumor growth and progression. Although regulated by the combined actions of many factors, TME maintains relative stability. Of note, TME-mediated drug resistance is usually the result of the continuous interactions between tumor cells and components of the TME. In this way, targeting various parts of the tumor microenvironment could be one of the effective strategies to overcome the drug resistance.

4 Relationships between sorafenib resistance and tumor microenvironment

4.1 Hypoxia

As a common pathophysiological phenomenon, hypoxia is present in most solid tumors, including HCC (Curtis et al., 2019) (Chiu et al., 2017). The median partial pressure of O2 (pO2) is barely 6 mmHg in human liver tumors. However, in normal human liver tissue, the pO_2 is 30 mm Hg (Bao and Wong, 2021). Tumors have developed a variety of mechanisms to cope with hypoxic stress. Among the various regulatory pathways, hypoxia-inducible factors (HIFs) are the most important transcription factors that regulate a couple of dozen genes in response to a decrease in intracellular oxygen concentration (Wang and Liu, 2020). HIFs are heterodimers composed of a HIF-α subunit (HIF-1α, HIF-2α, or HIF-3α) and a HIF-1β subunit (Bulle and Lim, 2020). As a negative regulator of HIF-mediated gene expression, HIF-3α is not closely related to HIF-1α and HIF-2α (Zou et al., 2011). Therefore, we will primarily discuss HIF-1α and HIF-2α. The HIF-α subunits are tightly regulated by cellular oxygen concentration, whereas the HIFβ-subunit is persistently expressed (Lee et al., 2020). Under normoxic condition, HIF-1α and HIF-2α are catalyzed to be degraded by von Hippel-Lindau tumor suppressor protein (VHL) and cannot activate the transcription of their target genes (Shi et al., 2009). However, HIF-1α and HIF-2α are stabilized under hypoxic conditions leading to transcriptionally inducing the target genes involved in energy metabolism, angiogenesis, proliferation, apoptosis and drug resistance (Shih et al., 2017; Vanhove et al., 2019).

Increasing evidence indicates that hypoxia plays a prominent role in the drug resistance, including sorafenib resistance in various cancers and different therapies resistance in HCC (Alsaab et al., 2018; Wu et al., 2019). Compared with sorafenib-sensitive patients, sorafenib-resistant tumors typically show higher intratumoral hypoxia (Liang et al., 2013). It is worth noting that long-term sorafenib treatment also exacerbates the hypoxic microenvironment of HCC by suppressing tumor angiogenesis (Mo et al., 2021). Sorafenib-induced hypoxia stabilizes HIF-1α and HIF-2α and strengthens the transcription of their downstream target genes (Song et al., 2019). This process acts as an adaptive cytoprotective response to induce sorafenib resistance in liver cancer cells. In addition, sorafenib also triggers the HIF-1α-to-Hif-2α pathway switch, further promoting this adaptive cytoprotective response (Ma et al., 2014). The entire process can enhance the effect via positive feedback loop and form a vicious cycle, accelerating the resistance to sorafenib. Accordingly, inhibition of hypoxia is a promising strategy for overcoming sorafenib resistance. In this section, we mainly discuss the relationship between hypoxia and sorafenib resistance in HCC. The mechanism details are described in Figure 3.

4.1.1 HIF-1α

HIF-1a is frequently upregulated in patients with HCC, and its overexpression is largely related to poor prognosis of HCC patients (Kai et al., 2016). An increasing body of evidence suggests that metabolic alterations in the glycolytic pathway play an essential role in drug resistance (Mondal et al., 2019). Glycolysis-mediated drug resistance is frequently associated with

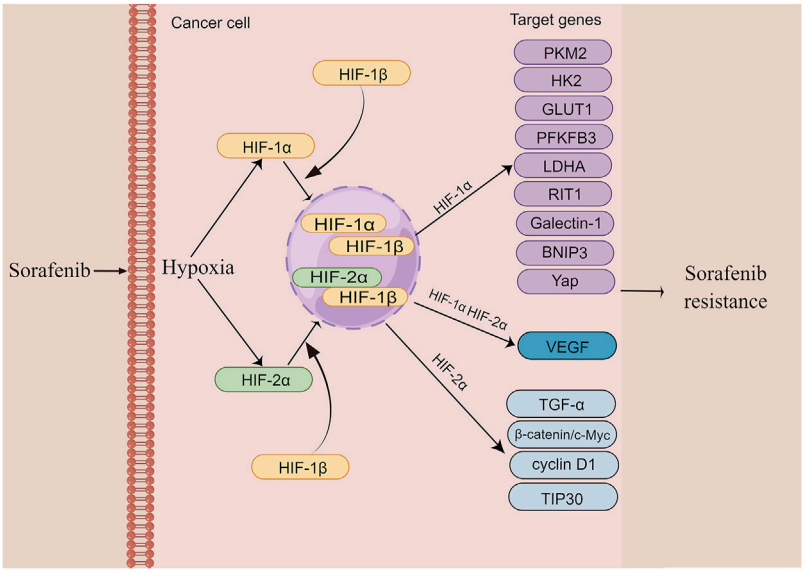

FIGURE 3
The mechanism of hypoxia induces sorafenib resistance in HCC (edited by Figdraw software). Sustained sorafenib treatment induces dysregulation of HIF-1a and HIF-2a expression and promotes transcription of their downstream genes, thereby causing resistance to sorafenib in HCC.

the upregulation of glycolysis-related vital enzymes, including pyruvate kinase type M2 (PKM2), Hexokinase II (HK2), glucose transporter 1 (GLUT1), and PFKFB3 (Xia et al., 2020). Indeed, HIF-1a occupies a significant position in regulating these glycolysis enzymes. For example, the activity of PKM2, which is highly upregulated and initiates sorafenib resistance in HCC, is mediated by HIF-1a (Chen J et al., 2018) In contrast, Simvastatin, a medicine to lower lipid level, can overcome sorafenib resistance by inhibiting HIF-1α/PPAR-γ/PKM2-mediated glycolysis (Feng J et al., 2020). Another drug flavonoid proanthocyanidin B2 was shown to enhance the efficiency of sorafenib by targeting PKM2 (Feng et al., 2019). HK2, which catalyzes glucose to glucose 6-phosphate (G6P) in the glycolytic pathway, is negatively related to poor prognosis in patients with HCC and is also mediated by HIF-1a (Agnihotri and Zadeh, 2016; DeWaal et al., 2018). Compared with the responders, sorafenib-resistant patients showed an elevated level of HK2 (Gao et al., 2021b). Whereas HK2 knockdown synergistically inhibited tumor growth with sorafenib, suggesting that HK2 inhibition significantly improves the efficacy of sorafenib (DeWaal et al., 2018). In addition, HIF-1α was shown to reduce the expression of miR-199a that directly targets PKM2 and HK2 in liver cancer (Guo et al., 2015). As a HIF target gene, GLUT1 expression is associated with resistance to multiple drugs in various cancers (Chigaev, 2015; Sawayama et al., 2019; Guo et al., 2020). It has been demonstrated that genistein inhibited HK2 and GLUT1 to suppress aerobic glycolysis and improve sorafenib sensitivity by downregulation of HIF-1α (Li et al., 2017). PFKFB3 is a member of the 6-phosphofructo-2-kinase/fructose-2,6-bisphosphatases (PFKFB) family and is closely related to many aspects of cancer including cell proliferation, vessel aggressiveness, drug resistance and TME (Shi et al., 2017). The expression of PFKFB3 is markedly induced under hypoxia condition (Niskanen et al., 2018; Sun et al., 2019). Meanwhile, PFKFB3 was found to be elevated after sorafenib treatment and the increased PFKFB3 markedly hampered sorafenib sensitivity in HCC cells. Interestingly, the inhibition of HIF-1α overcomes sorafenib resistance by modulating PFKFB3 in HCC (Long et al., 2019). Ras-like-without-CAAX-1 (RIT1), a member of the Ras family of GTPases, has emerged as an important cause of Noonan syndrome and cancer (Castel et al., 2019). It has been revealed that hypoxia significantly upregulates RIT1 expression in HCC cells via HIF-1α and the over-expressed RIT1 attributes to sorafenib resistance in HCC (Song et al., 2019). A study found that RIT1 was able to promote cell proliferation by activation of AKT. As a result, the combination of sorafenib and AKT inhibitor enhances sorafenib sensitivity in HCC (Sun et al., 2022). Bcl-2 interacting protein 3 (BNIP3), a member of the BH3-only Bcl-2 family, is a hypoxia-regulated protein. HIF-1α increases BNIP3 expression by binding to a hypoxia response element (HRE) within the promoter region of BNIP3 (Burton et al., 2006). The methylation BNIP3 promoter was observed in sorafenib resistant HCC cells under hypoxia (Mendez-Blanco et al., 2019). Galectin-1, belonging to the galectin protein family, is suggested to be a predictive marker of poor prognosis and a potential

therapeutic target for malignant tumors (Wu et al., 2012). As a downstream target of the AKT/mTOR/HIF-1α signaling pathway, Galectin-1 is a possible biomarker for predicting resistance of sorafenib in HCC *in vitro* and *in vivo* (Yeh et al., 2015). Furthermore, Galectin-1 was shown to induce sorafenib resistance in liver cancer by activation of the FAK/PI3K/AKT signaling (Zhang P.F et al., 2016). YAP is activated and translocated into the nucleus under hypoxia (Li et al., 2018). It has been reported that the Hippo/YAP/TAZ pathway is involved in drug resistance, cancer cell stemness and EMT (Gao et al., 2021b). Of note, YAP/TAZ drives sorafenib resistance in HCC by preventing ferroptosis (Gao et al., 2021b). YAP promotes sorafenib resistance in HCC by inducing survival as well (Sun et al., 2021). Furthermore, cirrhotic stiffness induces sorafenib resistance in HCC via YAP (Gao J et al., 2019). Additionally, it has been shown that YAP–IGF1R signaling plays a vital role in sorafenib resistance and targeting YAP–IGF-1R is an effective measure for treating sorafenib-resistant HCC (Ngo et al., 2021). Due to the crucial role of HIF-1a in regulating sorafenib resistance, previous studies have demonstrated that a dozen of drugs improve sorafenib resistance in HCC by indirect targeting HIF-1a. For instance, melatonin reduces HIF-1α protein synthesis by inhibiting the mTORC1/p70S6K/RP-S6 pathway, thereby improving sorafenib sensitivity (Prieto-Dominguez et al., 2017). *Rhizoma Paridis* saponins extracted from the herb *Paris polyphylla* decreases mRNA and protein levels of HIF- 1a and the combination with sorafenib reduces the resistance (Yao et al., 2018). In summary, a deeper understanding of HIF-1a in sorafenib resistance provides a potential therapeutic target for overcoming the resistance. In addition, glycolysis-related pathways seem to be the central element, and further investigation is warranted for metabolomics in sorafenib resistance.

4.1.2 HIF-2a

HIF-1α and HIF-2α have been suggested to exist the reciprocal compensatory mechanism, by which the expression of HIF-2α can be upregulated when HIF-1α is inhibited (Menrad et al., 2010). This switch is conducive to generate dynamic cytokines for tumors' aggressive growth under hypoxia (Koh et al., 2011). Similar to HIF-1α, the expression of HIF-2α is also induced by sorafenib, leading to the insensitivity to sorafenib in HCC cells (Zhao et al., 2014). As such, the re-sensitization of the resistant HCC cells to sorafenib can be improved by regulating HIF-2α and its downstream genes. For example, Ma et al. showed that sorafenib-induced upregulation of HIF-2α and increased expression of vascular endothelial growth factor (VEGF) and cyclin D1 contribute to the resistance of hypoxic HCC cells to sorafenib. Both HIF-1α and HIF-2α, as well as their downstream genes, including VEGF, lactate dehydrogenase A (LDHA) and cyclin D1, are significantly reduced by 2ME2, an antitumor and antiangiogenic agent (Ma et al., 2014). In addition, sodium orthovanadate also overcomes sorafenib resistance in HCC cells by reduction of HIF-1α/HIF-2α protein expression and their nuclear translocation, resulting in downregulation of their downstream genes, including VEGF, LDHA and GLUT1 (Jiang et al., 2018). Interestingly, sorafenib treatment-upregulated HIF-2α by sorafenib feedback enhances sorafenib resistance by activating the TGF-α/EGFR pathway (Zhao et al., 2014). HIF-2α activity mediated by the COX2/PGE2 axis was found to be associated with the activation of TGF-α/EGFR, which in turn promotes HCC development and reduces the sensitivity to sorafenib. The β-catenin/c-Myc pathway is an essential signaling pathway in tumors (Bai et al., 2020). Liu et al. found that activation of β-catenin/c-Myc signaling enhances glycolysis and glutaminolysis, and promotes hepatocarcinogenesis, metastasis, and drug resistance (Liu et al., 2019). Notably, downregulation of HIF-2α improves the antitumor activity of sorafenib in HCC via the β-catenin/C-Myc-dependent pathway (Liu et al., 2015). A 30-kDa Tat-interacting protein (TIP30), a tumor suppressor gene and a downstream target of HIF-2α, was shown to inhibit EMT. TIP30 downregulated by the overexpression of HIF-2α has been identified to result in EMT (Zhu et al., 2015). Surprisingly, metformin was found to enhance the anti-tumor activity of sorafenib by regulation the expression of HIF-2α and TIP30 (You et al., 2016).

4.2 Tumor-associated immune-suppressive cells

The extensive infiltration of tumor-associated immune-suppressive cells in TME is considered a principal factor affecting cancer progression and hindering treatment (Gorgun et al., 2013). When tumor-associated immunosuppressive cells are recruited into TME, they promote the malignant phenotypes of HCC (Riscal et al., 2019). In addition, these immunosuppressive cells establish a complex of interaction network that maintains the immunosuppressive microenvironment and promotes the immune escape of tumor cells (LaGory and Giaccia, 2016). A growing body of literature has recently shown that the infiltration of tumor-associated immunosuppressive cells is a vital link in sorafenib resistance. Therefore, clarification of the relationship between tumor-associated immunosuppressive cells and sorafenib resistance is crucial. The mechanisms of tumor-associated immunosuppressive cells contributing to sorafenib resistance are presented in Figure 4.

4.2.1 Tumor-associated macrophages

TAMs, whose functions are determined by their polarization state, are one of the most abundant types of immune cells in TME (Le et al., 2018). Polarized macrophages have been identified into two broad types: M1 (classically activated macrophages) and M2 (alternatively activated macrophages). TAMs frequently convert

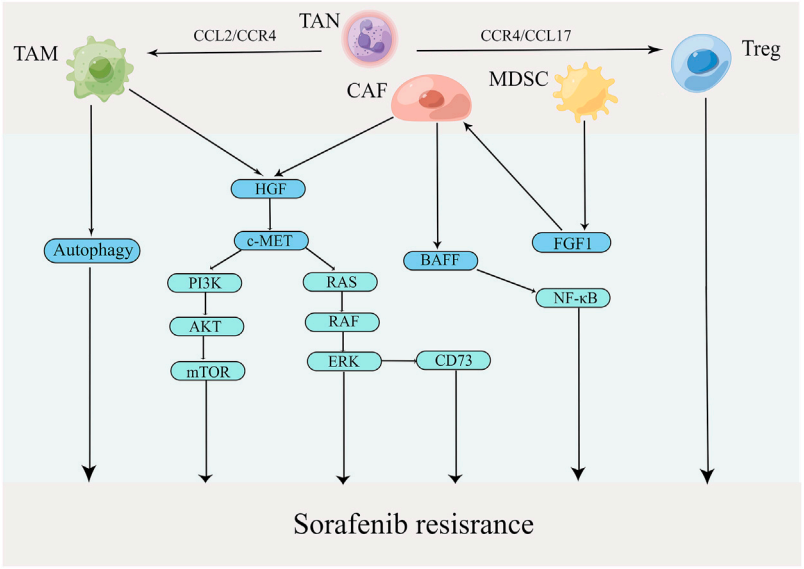

FIGURE 4
Mechanisms by which tumor-associated immune-suppressive cells promote sorafenib resistance in TME (edited by Figdraw software).

M1 to M2 during tumor progression, supporting tumor growth and metastasis by various functions (Zhu Z et al., 2020). Mantovani et al. found that abundant TAMs are associated with poor prognosis in various cancers, especially liver cancer (Mantovani et al., 2006). Furthermore, TAMs are closely related to sorafenib resistance as well. For example, Wei et al. demonstrated that TAMs promoted proliferation, migration and invasion of sorafenib-resistant liver cancer cells (Wei et al., 2017). A recent study showed that TAMs mediated liver cancer resistance to sorafenib by activating the MAPK, PI3K/AKT and HGF/c-Met signaling pathways (Dong et al., 2019). Additionally, a growing number of studies have shown that autophagy that was induced by M2 macrophages is a significant causing factor of sorafenib resistance in HCC (Prieto-Dominguez et al., 2016; Wu et al., 2016; Lin Z et al., 2020). For example, Wei et al. found that M2 macrophages boost autophagy when sorafenib acts on tumor cells; however, this autophagy renders tumor cells resistance to sorafenib (Wei F et al., 2019). Compared with traditional treatments, targeting macrophages has become a new strategy in cancer immunotherapy (Cassetta and Kitamura, 2018; Gunassekaran et al., 2021). The photoimmunotherapy utilizing a TAM-targeted probe IRD-αCD206 was found to suppress the growth and metastasis of sorafenib-resistant tumor (Zhang C et al., 2016). In addition to eliminating TAM cells, repolarizing TAM from M2 to M1 phenotype is another promising intervention approach in cancer (Snuderl et al., 2013). For example, IFN-α, as an immunomodulator, was shown to increase the therapeutic efficacy of sorafenib via a shift in TAM polarization (Zhang et al., 2021). In addition, the compound Kushen, the dried roots of Sophora flavescens Aiton, injection was found to induce polarization TAMs to M1 and thus reverse sorafenib resistance (Yang Y. et al., 2020). Notably, CCL2, a member of the C-C chemokine family, promotes the recruitment of TAMs by activating CCR2, leading to cancer progression (Yang Z et al., 2019). CCR2 antagonist, 747, was able to block TAM recruitment and enhance the efficiency of sorafenib by modulating the CCL2/CCR2 axis, providing a novel therapeutic approach for HCC (Yao et al., 2017). These results indicate the importance of TAMs in sorafenib resistance in HCC.

4.2.2 Cancer-associated fibroblasts

A large number of CAFs in the tumor tissue create a favorable environment for tumor development (Pein et al., 2020). CAFs not only boost tumor growth and metastasis but also mediate immunosuppression and drug resistance by directly interacting with cancer cells or by secreting a wide variety of factors and nutrients (Multhaupt et al., 2016). Mechanistically, CAFs lead to the resistance by impairing drug delivery and biochemical signaling (Meads et al., 2009). In addition, ECM remodeling by CAFs inhibits anti-cancer drug uptake through increasing intratumoral interstitial fluid pressure and vascular collapse (Paraiso and Smalley, 2013). Liu et al. showed that the co-culture of liver tumor organoids with CAFs could decrease the efficiency of sorafenib, 5-FU and regorafenib (Liu et al., 2021). It has also been demonstrated that CAFs induce sorafenib resistance by activation of the BAFF/NF-κB axis in liver cancer cells (Gao L et al., 2021). Another report demonstrated

that HGF secreted by CAFs regulates the expression of CD73 to promote the sorafenib resistance of HCC by modulating the Met-ERK1/2 pathway (Peng et al., 2020). Therefore, CAF is of crucial role in sorafenib resistance and could be a potential immunotherapeutic target for overriding the resistance.

4.2.3 Tumor-associated neutrophils

Emerging evidence indicates that neutrophils, which have been identified to regulate innate and adaptive immune responses, also play essential roles in sorafenib resistance (Gupta and Kaplan, 2016). It has been reported that neutrophils display plasticity. Similar to TAMs, TANs can either be polarized into an anti-tumorigenic "N1" phenotype by IFNs or into a protumorigenic "N2" phenotype when TGF-β is present (Strauss et al., 2021). In clinical trials, enriched N2 TANs in HCC tumor tissues are not only a poor prognostic marker but also a key indicator of the poor efficacy of sorafenib in patients with HCC (Li et al., 2011; Bruix et al., 2017). Clinical data have also shown that sorafenib is more effective in treating patients with less N2 TANs infiltration (Zhou et al., 2016). Hence, the overrepresentated N2 TANs is closely related to sorafenib resistance in liver cancer. Further study has highlighted that N2 TANs recruit macrophages and Treg to promote resistance to sorafenib and the progression of liver cancer (Zhou et al., 2016). Future investigations are required to develop strategy aiming to suppress the recruitment of immunosuppressive cells including N2 TANs for conquering sorafenib resistance.

4.2.4 Myeloid-derived suppressor cells

MDSCs are a heterogeneous cell population comprising of progenitors and precursors of myeloid cells with potent immunosuppressive effect (Mulder et al., 2019). There are three major types of MDSCs: polymorphonuclear MDSCs (PMN-MDSCs), monocytic MDSCs (M-MDSCs) and early-stage MDSCs (eMDSCs). Phenotypically and morphologically, PMN-MDSCs resemble neutrophils, while M-MDSCs are similar to monocytes. eMDSCs are primarily myeloid progenitors and precursors, and represent less than 5% of MDSCs (Veglia et al., 2018; Veglia et al., 2021). Although the phenotypic characteristics of PNM-MDSCs and M-MDSCs differ, both possess potent immunosuppressive properties. MDSCs promote the development of liver cancer through a variety of mechanisms, including inhibition of $CD8^+$ T-cell response, induction of Treg expansion and impairment of NK cell function (Hoechst et al., 2009; Kalathil et al., 2013; de Oliveira et al., 2016). In addition, MDSCs are associated with early recurrence and poor prognosis in HCC patients who have undergone curative resection, radiotherapy and hepatic arterial infusion chemotherapy (Deng et al., 2022). Deng et al. found that MDSCs facilitated CAF activation, resulting in tumor growth, angiogenesis and sorafenib resistance by inducing FGF1 expression (Deng et al., 2022).

4.2.5 Regulatory T cells

Treg cells are defined as a FoxP3+ $CD25^+$ $CD4^+$ T lymphocyte subset (Konopacki et al., 2019). They protect hosts from developing autoimmune diseases and allergies, whereas in malignancies, they promote tumor progression by suppressing effective antitumor immunity. FoxP3+ Treg is a potential therapeutic target to enhance the effect of antitumor immunity (Whiteside, 2018). Gao et al. found that intratumoral CCR4+ Tregs were the leading type of Tregs and closely associated with sorafenib resistance in hepatitis B-related HCC. Moreover, interfering with a CCR4 antagonist or a N-terminus recombinant protein of CCR4 (N-CCR4-Fc) exerts a prominent effect on conquering sorafenib resistance and sensitizes liver cancer to PD-1 checkpoint inhibitor (Gao et al., 2022). It is of considerable interest to identify new approaches that target Tregs for overcoming sorafenib resistance in HCC.

4.3 Immunosuppressive factors

Numerous studies have revealed that some immunosuppressive factors, that were secreted by tumor cells or stromal cells, infiltrate into the tumor site through specific recognition. These immunosuppressive molecules, together with other components of the TME, form a stable immunosuppressive microenvironment to mediate the immune escape of tumor cells and sorafenib resistance. The mechanisms of these factors in sorafenib resistance are shown in Table 1.

4.3.1 PD-L1

Programmed cell death 1-ligand 1 (PD-L1), also known as B7-H1 or CD274, is one of the most critical immune inhibitory molecules in the TME and plays a vital role in tumor cell immune escape (Theodoraki et al., 2018). It has been widely reported that PD-L1 regulates drug resistance and other malignant phenotypes in many types of cancer (Nowicki et al., 2018; Shen et al., 2019; Chen et al., 2020). PD-L1 was found to be overexpressed in sorafenib-resistant HCC cell lines and tumor tissues (Zhang et al., 2020). Liu et al. showed that overexpression of DNA methyltransferase1 (DNMT1) is positively associated with elevated level of PD-L1 in sorafenib-resistant HCC cells, and PD-L1 is able to regulate DNMT1 via the STAT3 signaling pathway. Furthermore, the inhibition of either PD-L1 or DNMT1 sensitizes HCC cells to sorafenib (Liu et al., 2017). In addition, c-Met and PD-L1 were shown to be co-overexpressed in sorafenib-resistant cell lines, and c-Met promoted the expression of PD-L1 through the MAPK/NF-κBp65 cascade. The overexpressed PD-L1 in turn facilitates sorafenib resistance (Xu et al., 2022). By activating Sterol regulatory element-binding protein 1 (SREBP-1) via the PI3K/AKT signaling, PD-L1 promoted EMT in sorafenib-resistant HCC cell lines (Xu et al., 2020). Accordingly, inhibiting

TABLE 1 Immunosuppressive factors and sorafenib resistance in HCC.

Immunosuppressive factor	Cell involved	Pathway	Effects on the tumor	References
PD-L1	HepG2 and Huh7 sorafenib-resistance cells	PD-L1/STAT3/DNMT1	Promote sorafenib resistance	Liu et al., (2017)
	Huh7 sorafenib-resistance cells	c-MET/PD-L1/RAS/RAF/MEK/ERK1/2	Promote sorafenib resistance	Xu et al., (2022)
	HepG2 and Huh7 sorafenib-resistance cells	PI3K/AKT/SREBP-1	Promote sorafenib resistance	Xu et al., (2020)
TGF-β	Hep3B and PLC/PRF/5 cells	TGF-β/EMT/PD-L1	Promote sorafenib resistance	Shrestha et al., (2021b)
	Hep-3B, Huh7, SK-Hep-1, SNU-182, SNU-398 and SNU-449 cells	TGF-β/P38	Inhibit sorafenib resistance	Kang et al., (2017)
	HepG2, Huh7 and PLC/PRF/5 cells	TGF-β/ERK/ETS1/PXR	Promote sorafenib resistance	Bhagyaraj et al., (2019)
	PLC/PRF/5, Hep3B and Huh7 cells	TGF-β/RTK	Promote sorafenib resistance	Ungerleider et al., (2017)
IL-6	PLC/PRF/5 sorafenib-resistance cells	LCSCs/IL-6/STAT3	Promote sorafenib resistance	Li Y et al., (2020)
	Hep3B, HepG2, Huh7 and HepG2.2.15 Hep3B and HepG2.2.15 sorafenib-resistance cells	IL-6/STAT3/DNMT3b/OCT4	Promote sorafenib resistance	Lai S.C et al., (2019)
	HEK-293T, Huh7 and Hep3B cells Huh7 and Hep3B sorafenib-resistance cells	PSMD10/IL-6/STAT3/DANCR	Promote sorafenib resistance	Liu et al., (2020)
CCL2	HepG2, PLC/PRF/5, MHCC97H, HCCLM3, Hepa1-6 and H22cells	CCL2/CCR4/TAM	Promote sorafenib resistance	Zhou et al., (2016)
CCL17	HepG2, PLC/PRF/5, MHCC97H, HCCLM3, Hepa1-6 and H22cells	CCL17/CCR4/Treg	Promote sorafenib resistance	Zhou et al., (2016)
CXCR3	Huh7 sorafenib-resistant cells	CXCR3/MAPK pathway/adipocytokine signaling	Promote sorafenib resistance	Ren et al., (2020)
SDF-1α	HCA-1 cells	SDF-1α/CXCR4	Promote sorafenib resistance	Chen et al., (2014)

PD-L1 is an excellent approach to overcome sorafenib resistance. A previous study revealed that microRNA-1 overcame sorafenib resistance and suppressed the malignant progression of liver cancer cells through inhibition of PD-L1 (Li D et al., 2020). Similar to EMT inhibition, silencing PD-L1 was also shown to sensitize cells to sorafenib (Shrestha et al., 2021b). Strikingly, it has been reported that combination with EMT inhibition, blockade of PD-L1 expression exhibits potent effects on sorafenib resistance by targeting the liver cancer stem cell subpopulation (Shrestha et al., 2021a). Clinical studies have also provided evidence that avelumab, an anti-PD-L1 antibody, shows moderate efficacy and is well tolerated in advanced HCC patients previously treated with sorafenib (Lee et al., 2021). Based on these findings, the combination of PD-L1 inhibitor with sorafenib could be an effective therapeutic strategy for advanced HCC.

4.3.2 TGF-β

It is well known that transforming growth factor-β (TGF-β) exerts dual effects on tumor cells, both positive and negative functions (Massague, 2008). In the early stage of cancer development, TGF-β acts as a tumor suppressor to inhibit cell proliferation and stimulate apoptosis. However, in the late stage of cancer development, TGF-β becomes a tumor-promoting factor to induce EMT, invasion and metastasis. In addition, TGF-β is a key regulator of T cell response. It also regulates the responses mediated by the innate and adaptive immune cells, including dendritic cells, B cells, NK cells, innate lymphocytes, and granulocytes (Tu et al., 2019). In bioinformatic studies, Lin et al. found that mRNA levels of TGF-β were elevated in sorafenib-acquired resistant HCC tissues (Lin H et al., 2020). Numerous studies have shown that overexpressed TGF-β is

associated with HCC progression and sorafenib resistance (Lin et al., 2015; Sharma et al., 2017). Bhagyaraj et al. found that TGF-β increased pregnane X receptor (PXR) expression via the ERK-ETS1 axis and contributed to sorafenib resistance (Bhagyaraj et al., 2019). In addition, TGF-β induces the expression of receptor tyrosine kinases (RTKs) that contribute to sorafenib resistance in HCC (Ungerleider et al., 2017). Therefore, TGF-β plays a crucial role in the process of sorafenib resistance. As EMT is a critical process of drug resistance and as TGF-β is a major signal transduction pathway in EMT (Hahne and Valeri, 2018; Kouno et al., 2019), the sorafenib resistance induced by TGF-β could be closely related to EMT. In addition, Shrestha et al. revealed that TGF-β1-induced EMT increased PD-L1 expression in HCC cells, leading to the resistance of sorafenib. In line with these findings, the combination of targeting PD-L1 and TGF-β1 signals was shown to have a synergic effect on conquering sorafenib resistance (Shrestha et al., 2021b). Another study showed that knockdown of TGF-β could reinforce the phosphorylation of p38 and enhance the sensitivity of HCC cells to sorafenib (Kang et al., 2017). TGF-β has also been shown to induce sorafenib resistance through the ERK/AKT signaling pathway, and valproic acid increases sorafenib sensitivity by suppressing TGF-β-induced ERK/AKT signaling (Matsuda et al., 2014). In addition, miR-101 improves the anti-tumor effect of sorafenib in HCC cells by targeting dual-specificity phosphatase 1 (DUSP1) and inhibiting TGF-β activation (Wei et al., 2015). Consequently, the desensitization of TGF-β is a potential strategy for overcoming sorafenib resistance.

4.3.3 TNF-α

TNF-α, an important pro-inflammatory cytokine, is produced by activated macrophages/monocytes (Yu et al., 2020). Numerous clinical and experimental studies have revealed that patients with liver damage produce large amounts of TNF-α, which are closely related to the incidence and progression of hepatitis, liver cirrhosis and liver cancer (Huang et al., 2017). Liu et al. showed that overexpression of TNF-α was related to poor prognosis in HCC patients (Liu et al., 2013). The elevated level of TNF-α is also associated with the weakened effect of sorafenib treatment (Tan et al., 2019). TNF-α was found to accelerate sorafenib resistance by inducing EMT in HCC cells. Moreover, ulinastatin, an urinary trypsin inhibitor, improves the antitumor effect of sorafenib by inhibition of TNF-α expression and secretion (Tan et al., 2019). A recent study has shown that TNF-α derived from the inflammatory microenvironment of the fibrotic liver promotes sorafenib resistance via STAT3 activation and that STAT3 antagonists reverse HCC resistance to sorafenib (Jiang et al., 2021). Additionally, sorafenib was demonstrated to promote CCL22 expression via the TNF-α/RIP1/NF-κB signaling, and the sorafenib resistance was reversed by inhibition of CCL22 signaling, suggesting CCL22 as a possible therapeutic target for hampering sorafenib resistance (Gao et al., 2020; Marshall et al., 2020).

4.3.4 IL-6

IL-6, a significant driver of hepatocellular carcinogenesis, is involved in tumor progression, metastasis and chemoresistance in HCC (Bharti et al., 2016). A growing body of evidence suggests that HCC cancer stem cells (CSCs) are responsible for the tumor recurrence and sorafenib resistance (Lai Y et al., 2019). Liver cancer stem cells (LCSCs) were shown to accelerate sorafenib resistance via the IL-6/STAT3 signaling pathway, and targeting IL-6 relieves this resistance (Li Y et al., 2020). The IL-6/STAT3 signaling pathway also mediates sorafenib resistance by increasing expression of DNA methyltransferase 3b (DNMT3b) and octamer-binding transcription factor 4 (OCT4). Combination of targeting DNMT3b with nanaomycin A and sorafenib treatment manifested a synergistic inhibitory effect on sorafenib-resistant HCC cells (Lai S.C et al., 2019). In addition, a long-noncoding RNA (lncRNA) DANCR was shown to promote sorafenib resistance by activating the IL-6/STAT3 pathway. Similarly, the activation of the IL-6/STAT3 pathway feedback enhances DANCR expression (Liu et al., 2020). A previous report also demonstrated that celecoxib, an anti-inflammatory medicine, overcame sorafenib resistance by inhibition of the IL-6/STAT3 signaling cascade (Liu et al., 2011). In summary, these findings indicate that the IL-6/STAT3 pathway plays a vital role in promoting sorafenib resistance and could be critical therapeutic targets for defeating the resistance.

4.3.5 Chemokines

Chemokines are a class of cytokines that have similar structures and chemotactic functions. Based on the sequence of cysteine residues at the N-terminus, chemokines are divided into four subtypes: CC-chemokines, CXC-chemokines, C-chemokines and CX3C-chemokines (Affo et al., 2014; Chen W et al., 2018). Chemokines and their receptors, which have been identified to play a critical role in the development and metastasis of cancers, have altered expression in a variety of tumors (Gao et al., 2018; Vela et al., 2019). Recently, an increasing number of studies have reported that CC chemokines and CC receptors (CCRs) are involved in sorafenib resistance. For example, Zhou et al. found that CCL2/CCR2 and CCL17/CCR4 secreted from TANs are responsible for sorafenib resistance by recruiting macrophages and Tregs (Zhou et al., 2016). A CCR2 antagonist, 747, enhances the anti-cancer efficacy of sorafenib by blocking TAMs (Yao et al., 2017). Similar to CCR2, CCR4 is a therapeutic target for sorafenib resistance as well. It has been shown that CCR4 antagonism enhances anti-cancer efficiency of sorafenib and overcomes sorafenib resistance via targeting CCR4+TIL-Tregs (Gao et al., 2022). Sorafenib also increases CCL22 expression by activation of TNF-α/RIP1/NF-κB signaling. In contrast, inhibition of CCL22 surmounts sorafenib

TABLE 2 Therapeutic approaches target TME to overcome sorafenib resistance in HCC.

Drugs	Targets	Cell lines/animal models/patients	References
miR-374b	PKM2-mediated glycolysis pathway	Hep3B-sorafenib resistance cells and HCCLM3-sorafenib resistance cells Hep3B-sorafenib resistant SCID mice subcutaneous HCC model	Zhang et al., (2019)
Simvastatin	HIF-1α/PPAR-γ/PKM2-mediated glycolysis	LM3-sorafenib resistance cells, LM3-sorafenib resistant nude mice subcutaneous HCC model	Feng J et al., (2020)
Proanthocyanidin B2	PKM2/HSP90/HIF-1α	LO2, HCC-LM3, SMMC-7721, Bel-7402, Huh-7 and HepG2 cells LM3 BALB/C nude mice subcutaneous HCC model	Feng et al., (2019)
Dauricine	PKM2, HK2	HepG2, Huh-7, Hep3B, Hepa1-6, H22andHL-7702 cells Huh-7 cells athymic nude mice subcutaneous HCC model	Li et al., (2018)
Genistein	GLUT1,HK2	HCC-LM3, SMMC-7721, Hep3B, Bel-7402, Huh-7 and LO2 cells HCC-LM3 cells BALB/C nu/nu mice subcutaneous HCC model	Li et al., (2017)
Aspirin	PFKFB3	HCC-LM3, SMMC-7721, Hep3B, Bel-7402, Huh7, QSG-7701 and LO2 cells	Li et al., (2017)
MK2206-2HCI	RIT1/PI3K/P38MAPK/AKT	CRL-8024 cells CRL-8024 (EV/RIT1 overexpression)cells BALB/C nude mice subcutaneous HCC model Huh7 (EV/RIT1 knockdown) cells BALB/C nude mice subcutaneous HCC model	Sun et al., (2022)
Verteporfin	YAP-IGF-1R signaling	HepG2215 and Hep3B cells/HepG2215-sorafenib resistance and Hep3B-sorafenib resistance cells HepG2215-sorafenib resistant NOD-SCID mice subcutaneous HCC models	Ngo et al., (2021)
Melatonin	mTORC1/p70S6K/HIF-1α	Hep3B cells	Prieto-Dominguez et al., (2017)
Rhizoma Paridis saponins	mRNA of HIF-1α	H22 cells Kunming mice subcutaneous HCC model	Yao et al., (2018)
2ME2	HIF-1α,HIF-2α	Huh-7 and HepG2 cells Huh-7 cells BALB/c nude mice subcutaneous HCC model	Ma et al., (2014)
Sodium orthovanadate	HIF-1α,HIF-2α	HepG2, Hep3B and SK-Hep-1 cells/HepG2-sorafenib resistance and Huh7-sorafenib resistance cells Huh7-sorafenib resistant BALB/c-nu/nu mice subcutaneous HCC model	Jiang et al., (2018)
Celecoxib and Meloxicam	COX-2/PGE2/COX-2	Huh-7, Hep3B, HepG2 and SMMC-7721 cells Huh-7 and Hep3B cells nude mice subcutaneous HCC model	Dong et al., (2019)
Metformin	HIF-2α	MHCC97H cells/MHCC97H cells orthotopic xenograft model	You et al., (2016)
MK2206-2HCI	RIT1/PI3K/P38MAPK/AKT	CRL-8024 cells CRL-8024 (EV/RIT1 overexpression)cells BALB/C nude mice subcutaneous HCC model Huh7 (EV/RIT1 knockdown) cells BALB/C nude mice subcutaneous HCC model	Sun et al., (2022)
Verteporfin	YAP-IGF-1R signaling	HepG2215 and Hep3B cells/HepG2215-sorafenib resistance and Hep3B-sorafenib resistance cells HepG2215-sorafenib resistant NOD-SCID mice subcutaneous HCC models	Ngo et al., (2021)
Melatonin	mTORC1/p70S6K/HIF-1α	Hep3B cells	Prieto-Dominguez et al., (2017)
Rhizoma Paridis saponins	mRNA of HIF-1α	H22 cells Kunming mice subcutaneous HCC model	Yao et al., (2018)
IRD-αCD206	TAMs	4T1cells, 4T1 cells female BALB/c mice subcutaneous breast cancer model	Zhang C et al., (2016)
IFN-α	Shifting the M2-like polarization of TAM	Hepa1-6 HCC and Huh7 HCC cells Hepa1-6 cells C57BL/6 mice subcutaneous HCC model	Zhang et al., (2021)
Compound kushen injection	Polarization TAMs to M1	Hepa1-6 tumor cells orthotopic HCC model Hepa1-6 and LPC-H12 cells nude mice subcutaneous HCC models	Yang et al., (2020a)
NRF-2/MicroRNA-1	NRF-2/miR-1/PD-L1	Hep3B and HepG2 cells/Hep3B sorafenib resistance cells and HepG2 sorafenib resistance cells Hep3B sorafenib resistant and HepG2 sorafenib resistant BALB/C nude mice subcutaneous HCC model	Li D et al., (2020)
Avelumab	PD-L1	Advanced HCC patients	Lee et al., (2021)
SB431542	TGF-β1-Mediated EMT	Hep3B and PLC/PRF/5 cells	Shrestha et al., (2021b)
Valproic acid	TGF-β/ERK/AKT	HepG2 and PLC/PRF/5 cells	Matsuda et al., (2014)
MiR-101	DUSP1/TGF-β	HepG2 and Huh7 cells	Wei et al., (2015)
Ulinastatin	TNF-α/NF-κB/EMT	HepG2, SK-HEP-1, and Huh-7 Hep3B and PLC/PRF/5 HCC cells SK-HEP-1 cells BALB/c athymic nude mice subcutaneous HCC model	Tan et al., (2019)
S3I-201	STAT3	Hepa1-6, Huh7 and Hep3B cells Orthotopic HCC mouse model with chronic liver injury	Jiang et al., (2021)

(Continued on following page)

TABLE 2 (*Continued*) Therapeutic approaches target TME to overcome sorafenib resistance in HCC.

Drugs	Targets	Cell lines/animal models/patients	References
Nanaomycin A	IL-6/STAT3/DNMT3b/OCT4/DNMT1	Hep3B, HepG2 and Huh7 cells/Hep3B and HepG2.2.15 sorafenib resistance cells	Lai S.C et al., (2019)
Celecoxib	JAK2/IL-6/STAT3	Hep3B, HepG2, Huh-7, SNU-387 and SNU-449 cells	Liu et al., (2011)
747	CCL2/CCR2	Hepa1-6, THP-1, HepG2, LPC-H12, 7702, BEL-7404, SMMC-7721 and PVTT-1 cells Hepa1-6 and LPC-H12 cells BALB/c athymic nude mice subcutaneous HCC models	Yao et al., (2017)
C-021	CCR4	Orthotopic HCC mode	Gao et al., (2022)
C-021	TNF-α-RIP1-NF-κB/CCL22	Hepa1–6 cells, MHCC97 L MHCC97H, HepG2 and HepG2.2.15 cells Hepa1–6 cells BALB/c nude mice subcutaneous HCC models	Gao et al., (2020)
Metapristone	SDF-1/CXCR4 axis	HepG2, Huh7, and SMMC-7721 cells SMCC-7721 cells BALB/c nude mice subcutaneous HCC models	Zheng et al., (2019)
BPRCX807	CXCL12/CXCR4	HCA-1 and JHH-7 cells/orthotopic HCA-1 model JHH-7 cells nude mice subcutaneous HCC models DEN/CCl4-induced liver fibrosis associated HCC model	Song et al., (2021)

resistance (Gao et al., 2020). Furthermore, sorafenib-resistant cells exhibited higher levels of CXC chemokines and CXC-chemokine receptors (CXCRs) (Wu et al., 2017). For example, Ren et al. showed that CXCR3 played a critical role in resistance to sorafenib therapy by modifying the AMPK pathway, adipocytokine signaling and lipid peroxidation (Ren et al., 2020). In addition, sorafenib treatment was found to increase hypoxia and SDF1α/CXCR4 expression in HCC cells and animal tumor models, whereas inhibition of the SDF1α/CXCR4 pathway overcame the sorafenib resistance in HCC (Chen et al., 2014; Chen et al., 2015). Moreover, co-delivery of sorafenib and mifepristone using CXCR4-targeted PLGA-PEG nanoparticles vanishs sorafenib resistance in CXCR4-expressing HCC (Zheng et al., 2019). Recently, a newly discovered CXCR4 antagonist, BPRCX807, enhances the clinical efficacy of sorafenib (Song et al., 2021). Further studies are warranted to determine whether other chemokines are involved in sorafenib resistance.

5 Conclusions and perspectives

Although sorafenib resistance is an important clinical challenge for liver cancer treatment, the underlying mechanisms of sorafenib resistance are complex and still need to be explored. It has been reported that EMT, epigenetic regulation, cancer stem cells, transport processes, autophagy and the crosstalk between the PI3K/AKT and JAK-STAT pathways are involved in sorafenib resistance (Tovar et al., 2017; Tang J et al., 2020). Emerging evidence suggests that the TME plays an essential role in sorafenib resistance. It is worth noting that the therapeutic effect of sorafenib is significantly improved when combined with the drugs targeting hypoxic TME, tumor-associated immune suppressor cells or immunosuppressive factors (Table 2). However, the combination therapy is far from satisfactory since there are several reasons that may affect the poor clinical efficacy: 1) TME is a complex network participated by many elements. However, current studies tend to focus on a single cell type or factor and ignore the mutual regulation of the entire TME, especially the immunosuppressive microenvironment. Thus, the conclusions drawn from these studies are often incomplete or even contradictory. 2) The constructed drug-resistant cell lines and *in vivo* drug-resistant models often differ from the actual drug resistance observed in patients, which is also the most prominent problem in our study. Therefore, sorafenib resistance model should be improved or reestablished.

Since sorafenib is still the primary treatment for advanced HCC, it is of great importance to continue investigating the potential mechanisms of sorafenib resistance in HCC treatment. We believe that the combination therapy using sorafenib and TME-targeting drugs will be an effective strategy to overcome sorafenib resistance and improve outcome in patients with HCC.

Author contributions

Conceptualization, SJ and HX; writing original draft preparation, XT; writing review and editing, QL, FL, JZ, and TY; visualization: XT and TY; supervision: SJ and HX; funding acquisition: SJ. All authors have read and agreed to the published version of the manuscript.

Funding

This work was supported by the National Natural Science Foundation of China (grant no. 81873249 and 82074360), National Natural Science Foundation of Shandong Province

(grant no. ZR2019MH058) and the Young Taishan Scholars Program of Shandong Province (grant no. tsqn201909200).

Conflict of interest

The authors declare that the research was conducted in the absence of any commercial or financial relationships that could be construed as a potential conflict of interest.

Publisher's note

References

Abou Khouzam, R., Zaarour, R. F., Brodaczewska, K., Azakir, B., Venkatesh, G. H., Thiery, J., et al. (2022). The effect of hypoxia and hypoxia-associated pathways in the regulation of antitumor response: Friends or foes? *Front. Immunol.* 13, 828875. doi:10.3389/fimmu.2022.828875

Affo, S., Morales-Ibanez, O., Rodrigo-Torres, D., Altamirano, J., Blaya, D., Dapito, D. H., et al. (2014). CCL20 mediates lipopolysaccharide induced liver injury and is a potential driver of inflammation and fibrosis in alcoholic hepatitis. *Gut* 63 (11), 1782–1792. doi:10.1136/gutjnl-2013-306098

Agnihotri, S., and Zadeh, G. (2016). Metabolic reprogramming in glioblastoma: the influence of cancer metabolism on epigenetics and unanswered questions. *Neuro. Oncol.* 18 (2), 160–172. doi:10.1093/neuonc/nov125

Alsaab, H. O., Sau, S., Alzhrani, R. M., Cheriyan, V. T., Polin, L. A., Vaishampayan, U., et al. (2018). Tumor hypoxia directed multimodal nanotherapy for overcoming drug resistance in renal cell carcinoma and reprogramming macrophages. *Biomaterials* 183, 280–294. doi:10.1016/j.biomaterials.2018.08.053

Asano, N., Matsuzaki, J., Ichikawa, M., Kawauchi, J., Takizawa, S., Aoki, Y., et al. (2019). A serum microRNA classifier for the diagnosis of sarcomas of various histological subtypes. *Nat. Commun.* 10 (1), 1299. doi:10.1038/s41467-019-09143-8

Azumi, J., Tsubota, T., Sakabe, T., and Shiota, G. (2016). miR-181a induces sorafenib resistance of hepatocellular carcinoma cells through downregulation of RASSF1 expression. *Cancer Sci.* 107 (9), 1256–1262. doi:10.1111/cas.13006

Bai, N., Xia, F., Wang, W., Lei, Y., Bo, J., and Li, X. (2020). CDK12 promotes papillary thyroid cancer progression through regulating the c-myc/β-catenin pathway. *J. Cancer* 11 (15), 4308–4315. doi:10.7150/jca.42849

Bao, M. H., and Wong, C. C. (2021). Hypoxia, metabolic reprogramming, and drug resistance in liver cancer. *Cells* 10 (7), 1715. doi:10.3390/cells10071715

Bhagyaraj, E., Ahuja, N., Kumar, S., Tiwari, D., Gupta, S., Nanduri, R., et al. (2019). TGF-beta induced chemoresistance in liver cancer is modulated by xenobiotic nuclear receptor PXR. *Cell Cycle* 18 (24), 3589–3602. doi:10.1080/15384101.2019.1693120

Bharti, R., Dey, G., and Mandal, M. (2016). Cancer development, chemoresistance, epithelial to mesenchymal transition and stem cells: A snapshot of IL-6 mediated involvement. *Cancer Lett.* 375 (1), 51–61. doi:10.1016/j.canlet.2016.02.048

Binnewies, M., Roberts, E. W., Kersten, K., Chan, V., Fearon, D. F., Merad, M., et al. (2018). Understanding the tumor immune microenvironment (TIME) for effective therapy. *Nat. Med.* 24 (5), 541–550. doi:10.1038/s41591-018-0014-x

Borden, K. L. (2014). When will resistance be futile? *Cancer Res.* 74 (24), 7175–7180. doi:10.1158/0008-5472.CAN-14-2607

Bruix, J., Cheng, A. L., Meinhardt, G., Nakajima, K., De Sanctis, Y., and Llovet, J. (2017). Prognostic factors and predictors of sorafenib benefit in patients with hepatocellular carcinoma: Analysis of two phase III studies. *J. Hepatol.* 67 (5), 999–1008. doi:10.1016/j.jhep.2017.06.026

Bulle, A., and Lim, K. H. (2020). Beyond just a tight fortress: contribution of stroma to epithelial-mesenchymal transition in pancreatic cancer. *Signal Transduct. Target. Ther.* 5 (1), 249. doi:10.1038/s41392-020-00341-1

Burton, T. R., Henson, E. S., Baijal, P., Eisenstat, D. D., and Gibson, S. B. (2006). The pro-cell death Bcl-2 family member, BNIP3, is localized to the nucleus of human glial cells: Implications for glioblastoma multiforme tumor cell survival under hypoxia. *Int. J. Cancer* 118 (7), 1660–1669. doi:10.1002/ijc.21547

Cassetta, L., and Kitamura, T. (2018). Macrophage targeting: opening new possibilities for cancer immunotherapy. *Immunology* 155 (3), 285–293. doi:10.1111/imm.12976

Castel, P., Cheng, A., Cuevas-Navarro, A., Everman, D. B., Papageorge, A. G., Simanshu, D. K., et al. (2019). RIT1 oncoproteins escape LZTR1-mediated proteolysis. *Science* 363 (6432), 1226–1230. doi:10.1126/science.aav1444

Chen, J., Yu, Y., Chen, X., He, Y., Hu, Q., Li, H., et al. (2018). MiR-139-5p is associated with poor prognosis and regulates glycolysis by repressing PKM2 in gallbladder carcinoma. *Cell Prolif.* 51 (6), e12510. doi:10.1111/cpr.12510

Chen, M., Zhao, Z., Meng, Q., Liang, P., Su, Z., Wu, Y., et al. (2020). TRIM14 promotes noncanonical NF-κB activation by modulating p100/p52 stability via selective autophagy. *Adv. Sci.* 7 (1), 1901261. doi:10.1002/advs.201901261

Chen, W., Zhang, J., Fan, H. N., and Zhu, J. S. (2018). Function and therapeutic advances of chemokine and its receptor in nonalcoholic fatty liver disease. *Ther. Adv. Gastroenterol.* 11, 1756284818815184. doi:10.1177/1756284818815184

Chen, Y., Huang, Y., Reiberger, T., Duyverman, A. M., Huang, P., Samuel, R., et al. (2014). Differential effects of sorafenib on liver versus tumor fibrosis mediated by stromal-derived factor 1 alpha/C-X-C receptor type 4 axis and myeloid differentiation antigen-positive myeloid cell infiltration in mice. *Hepatology* 59 (4), 1435–1447. doi:10.1002/hep.26790

Chen, Y., Ramjiawan, R. R., Reiberger, T., Ng, M. R., Hato, T., Huang, Y., et al. (2015). CXCR4 inhibition in tumor microenvironment facilitates anti-programmed death receptor-1 immunotherapy in sorafenib-treated hepatocellular carcinoma in mice. *Hepatology* 61 (5), 1591–1602. doi:10.1002/hep.27665

Chen, Y. T., Xiang, D., Zhao, X. Y., and Chu, X. Y. (2021). Upregulation of lncRNA NIFK-AS1 in hepatocellular carcinoma by m(6)A methylation promotes disease progression and sorafenib resistance. *Hum. Cell* 34 (6), 1800–1811. doi:10.1007/s13577-021-00587-z

Cheng, A. L., Kang, Y. K., Chen, Z., Tsao, C. J., Qin, S., Kim, J. S., et al. (2009). Efficacy and safety of sorafenib in patients in the asia-pacific region with advanced hepatocellular carcinoma: a phase III randomised, double-blind, placebo-controlled trial. *Lancet. Oncol.* 10 (1), 25–34. doi:10.1016/S1470-2045(08)70285-7

Chigaev, A. (2015). Does aberrant membrane transport contribute to poor outcome in adult acute myeloid leukemia? *Front. Pharmacol.* 6, 134. doi:10.3389/fphar.2015.00134

Chiu, D. K., Tse, A. P., Xu, I. M., Di Cui, J., Lai, R. K., Li, L. L., et al. (2017). Hypoxia inducible factor HIF-1 promotes myeloid-derived suppressor cells accumulation through ENTPD2/CD39L1 in hepatocellular carcinoma. *Nat. Commun.* 8 (1), 517. doi:10.1038/s41467-017-00530-7

Curtis, M., Kenny, H. A., Ashcroft, B., Mukherjee, A., Johnson, A., Zhang, Y., et al. (2019). Fibroblasts mobilize tumor cell glycogen to promote proliferation and metastasis. *Cell Metab.* 29 (1), 141–155. doi:10.1016/j.cmet.2018.08.007

Dai, J., Huang, Q., Niu, K., Wang, B., Li, Y., Dai, C., et al. (2018). Sestrin 2 confers primary resistance to sorafenib by simultaneously activating AKT and AMPK in hepatocellular carcinoma. *Cancer Med.* 7 (11), 5691–5703. doi:10.1002/cam4.1826

Dalloneau, E., Baroukh, N., Mavridis, K., Maillet, A., Gueugnon, F., Courty, Y., et al. (2016). Downregulation of the neonatal Fc receptor expression in non-small cell lung cancer tissue is associated with a poor prognosis. *Oncotarget* 7 (34), 54415–54429. doi:10.18632/oncotarget.10074

Dang, H., Takai, A., Forgues, M., Pomyen, Y., Mou, H., Xue, W., et al. (2017). Oncogenic activation of the RNA binding protein NELFE and MYC signaling in hepatocellular carcinoma. *Cancer Cell* 32 (1), 101–114. doi:10.1016/j.ccell.2017.06.002

de Oliveira, S., Rosowski, E. E., and Huttenlocher, A. (2016). Neutrophil migration in infection and wound repair: going forward in reverse. *Nat. Rev. Immunol.* 16 (6), 378–391. doi:10.1038/nri.2016.49

Deng, X., Li, X., Guo, X., Lu, Y., Xie, Y., Huang, X., et al. (2022). Myeloid-derived suppressor cells promote tumor growth and sorafenib resistance by inducing FGF1 upregulation and fibrosis. *Neoplasia* 28, 100788. doi:10.1016/j.neo.2022.100788

DeWaal, D., Nogueira, V., Terry, A. R., Patra, K. C., Jeon, S. M., Guzman, G., et al. (2018). Hexokinase-2 depletion inhibits glycolysis and induces oxidative phosphorylation in hepatocellular carcinoma and sensitizes to metformin. *Nat. Commun.* 9 (1), 446. doi:10.1038/s41467-017-02733-4

Dong, J., Zhai, B., Sun, W., Hu, F., Cheng, H., and Xu, J. (2017). Activation of phosphatidylinositol 3-kinase/AKT/snail signaling pathway contributes to epithelial-mesenchymal transition-induced multi-drug resistance to sorafenib in hepatocellular carcinoma cells. *PLoS One* 12 (9), e0185088. doi:10.1371/journal.pone.0185088

Dong, N., Shi, X., Wang, S., Gao, Y., Kuang, Z., Xie, Q., et al. (2019). M2 macrophages mediate sorafenib resistance by secreting HGF in a feed-forward manner in hepatocellular carcinoma. *Br. J. Cancer* 121 (1), 22–33. doi:10.1038/s41416-019-0482-x

Ezzoukhry, Z., Louandre, C., Trecherel, E., Godin, C., Chauffert, B., Dupont, S., et al. (2012). EGFR activation is a potential determinant of primary resistance of hepatocellular carcinoma cells to sorafenib. *Int. J. Cancer* 131 (12), 2961–2969. doi:10.1002/ijc.27604

Feng, J., Dai, W., Mao, Y., Wu, L., Li, J., Chen, K., et al. (2020). Simvastatin re-sensitizes hepatocellular carcinoma cells to sorafenib by inhibiting HIF-1α/PPAR-γ/PKM2-mediated glycolysis. *J. Exp. Clin. Cancer Res.* 39 (1), 24. doi:10.1186/s13046-020-1528-x

Feng, J., Wu, L., Ji, J., Chen, K., Yu, Q., Zhang, J., et al. (2019). PKM2 is the target of proanthocyanidin B2 during the inhibition of hepatocellular carcinoma. *J. Exp. Clin. Cancer Res.* 38 (1), 204. doi:10.1186/s13046-019-1194-z

Feng, L., Zhang, Y., Yang, Q., Guo, L., and Yang, F. (2020). MicroRNA-885 regulates the growth and epithelial mesenchymal transition of human liver cancer cells by suppressing tropomodulin 1 expression. *Arch. Biochem. Biophys.* 693, 108588. doi:10.1016/j.abb.2020.108588

Ford, R., Schwartz, L., Dancey, J., Dodd, L. E., Eisenhauer, E. A., Gwyther, S., et al. (2009). Lessons learned from independent central review. *Eur. J. Cancer* 45 (2), 268–274. doi:10.1016/j.ejca.2008.10.031

Fornari, F., Pollutri, D., Patrizi, C., La Bella, T., Marinelli, S., Casadei Gardini, A., et al. (2017). In hepatocellular carcinoma miR-221 modulates sorafenib resistance through inhibition of caspase-3-mediated apoptosis. *Clin. Cancer Res.* 23 (14), 3953–3965. doi:10.1158/1078-0432.CCR-16-1464

Franco, A. T., Corken, A., and Ware, J. (2015). Platelets at the interface of thrombosis, inflammation, and cancer. *Blood* 126 (5), 582–588. doi:10.1182/blood-2014-08-531582

Fukusumi, T., Guo, T. W., Sakai, A., Ando, M., Ren, S., Haft, S., et al. (2018). The NOTCH4-HEY1 pathway induces epithelial-mesenchymal transition in head and neck squamous cell carcinoma. *Clin. Cancer Res.* 24 (3), 619–633. doi:10.1158/1078-0432.CCR-17-1366

Gao, J., Rong, Y., Huang, Y., Shi, P., Wang, X., Meng, X., et al. (2019). Cirrhotic stiffness affects the migration of hepatocellular carcinoma cells and induces sorafenib resistance through YAP. *J. Cell. Physiol.* 234 (3), 2639–2648. doi:10.1002/jcp.27078

Gao, L., Morine, Y., Yamada, S., Saito, Y., Ikemoto, T., Tokuda, K., et al. (2021). The BAFF/NFκB axis is crucial to interactions between sorafenib-resistant HCC cells and cancer-associated fibroblasts. *Cancer Sci.* 112 (9), 3545–3554. doi:10.1111/cas.15041

Gao, R., Kalathur, R. K. R., Coto-Llerena, M., Ercan, C., Buechel, D., Shuang, S., et al. (2021b). YAP/TAZ and ATF4 drive resistance to Sorafenib in hepatocellular carcinoma by preventing ferroptosis. *EMBO Mol. Med.* 13 (12), e14351. doi:10.15252/emmm.202114351

Gao, Y., Fan, X., Li, N., Du, C., Yang, B., Qin, W., et al. (2020). CCL22 signaling contributes to sorafenib resistance in Hepatitis B virus-associated hepatocellular carcinoma. *Pharmacol. Res.* 157, 104800. doi:10.1016/j.phrs.2020.104800

Gao, Y. J., Liu, L., Li, S., Yuan, G. F., Li, L., Zhu, H. Y., et al. (2018). Down-regulation of CXCL11 inhibits colorectal cancer cell growth and epithelial-mesenchymal transition. *Onco. Targets. Ther.* 11, 7333–7343. doi:10.2147/OTT.S167872

Gao, Y., You, M., Fu, J., Tian, M., Zhong, X., Du, C., et al. (2022). Intratumoral stem-like CCR4+ regulatory T cells orchestrate the immunosuppressive microenvironment in HCC associated with Hepatitis B. *J. Hepatol.* 76 (1), 148–159. doi:10.1016/j.jhep.2021.08.029

Gao, Y., Zheng, Q. C., Xu, S., Yuan, Y., Cheng, X., Jiang, S., et al. (2019). Theranostic nanodots with aggregation-induced emission characteristic for targeted and image-guided photodynamic therapy of hepatocellular carcinoma. *Theranostics* 9 (5), 1264–1279. doi:10.7150/thno.29101

Gorgun, G. T., Whitehill, G., Anderson, J. L., Hideshima, T., Maguire, C., Laubach, J., et al. (2013). Tumor-promoting immune-suppressive myeloid-derived suppressor cells in the multiple myeloma microenvironment in humans. *Blood* 121 (15), 2975–2987. doi:10.1182/blood-2012-08-448548

Guan, X., Wu, Y., Zhang, S., Liu, Z., Fan, Q., Fang, S., et al. (2021). Activation of FcRn mediates a primary resistance response to sorafenib in hepatocellular carcinoma by single-cell RNA sequencing. *Front. Pharmacol.* 12, 709343. doi:10.3389/fphar.2021.709343

Gunassekaran, G. R., Poongkavithai Vadevoo, S. M., Baek, M. C., and Lee, B. (2021). M1 macrophage exosomes engineered to foster M1 polarization and target the IL-4 receptor inhibit tumor growth by reprogramming tumor-associated macrophages into M1-like macrophages. *Biomaterials* 278, 121137. doi:10.1016/j.biomaterials.2021.121137

Guo, Q. R., Wang, H., Yan, Y. D., Liu, Y., Su, C. Y., Chen, H. B., et al. (2020). The role of exosomal microRNA in cancer drug resistance. *Front. Oncol.* 10, 472. doi:10.3389/fonc.2020.00472

Guo, W., Qiu, Z., Wang, Z., Wang, Q., Tan, N., Chen, T., et al. (2015). MiR-199a-5p is negatively associated with malignancies and regulates glycolysis and lactate production by targeting hexokinase 2 in liver cancer. *Hepatology* 62 (4), 1132–1144. doi:10.1002/hep.27929

Gupta, S., and Kaplan, M. J. (2016). The role of neutrophils and NETosis in autoimmune and renal diseases. *Nat. Rev. Nephrol.* 12 (7), 402–413. doi:10.1038/nrneph.2016.71

Hahne, J. C., and Valeri, N. (2018). Non-coding RNAs and resistance to anticancer drugs in gastrointestinal tumors. *Front. Oncol.* 8, 226. doi:10.3389/fonc.2018.00226

Hoechst, B., Voigtlaender, T., Ormandy, L., Gamrekelashvili, J., Zhao, F., Wedemeyer, H., et al. (2009). Myeloid derived suppressor cells inhibit natural killer cells in patients with hepatocellular carcinoma via the NKp30 receptor. *Hepatology* 50 (3), 799–807. doi:10.1002/hep.23054

Huang, S., Li, C., Wang, W., Li, H., Sun, Z., Song, C., et al. (2017). A54 peptide-mediated functionalized gold nanocages for targeted delivery of DOX as a combinational photothermal-chemotherapy for liver cancer. *Int. J. Nanomedicine* 12, 5163–5176. doi:10.2147/IJN.S131089

Jang, J. W., Song, Y., Kim, S. H., Kim, J. S., Kim, K. M., Choi, E. K., et al. (2017). CD133 confers cancer stem-like cell properties by stabilizing EGFR-AKT signaling in hepatocellular carcinoma. *Cancer Lett.* 389, 1–10. doi:10.1016/j.canlet.2016.12.023

Jiang, W., Li, G., Li, W., Wang, P., Xiu, P., Jiang, X., et al. (2018). Sodium orthovanadate overcomes sorafenib resistance of hepatocellular carcinoma cells by inhibiting Na(+)/K(+)-ATPase activity and hypoxia-inducible pathways. *Sci. Rep.* 8 (1), 9706. doi:10.1038/s41598-018-28010-y

Jiang, Y., Chen, P., Hu, K., Dai, G., Li, J., Zheng, D., et al. (2021). Inflammatory microenvironment of fibrotic liver promotes hepatocellular carcinoma growth, metastasis and sorafenib resistance through STAT3 activation. *J. Cell. Mol. Med.* 25 (3), 1568–1582. doi:10.1111/jcmm.16256

Jiang, Y., Han, Q. J., and Zhang, J. (2019). Hepatocellular carcinoma: Mechanisms of progression and immunotherapy. *World J. Gastroenterol.* 25 (25), 3151–3167. doi:10.3748/wjg.v25.i25.3151

Ju, M., Jiang, L., Wei, Q., Yu, L., Chen, L., Wang, Y., et al. (2021). A immune-related signature associated with TME can serve as a potential biomarker for survival and sorafenib resistance in liver cancer. *Onco. Targets. Ther.* 14, 5065–5083. doi:10.2147/OTT.S326784

Kai, A. K., Chan, L. K., Lo, R. C., Lee, J. M., Wong, C. C., Wong, J. C., et al. (2016). Down-regulation of TIMP2 by HIF-1α/miR-210/HIF-3α regulatory feedback circuit enhances cancer metastasis in hepatocellular carcinoma. *Hepatology* 64 (2), 473–487. doi:10.1002/hep.28577

Kalathil, S., Lugade, A. A., Miller, A., Iyer, R., and Thanavala, Y. (2013). Higher frequencies of GARP(+)CTLA-4(+)Foxp3(+) T regulatory cells and myeloid-derived suppressor cells in hepatocellular carcinoma patients are associated with impaired T-cell functionality. *Cancer Res.* 73 (8), 2435–2444. doi:10.1158/0008-5472.CAN-12-3381

Kang, D., Han, Z., Oh, G. H., Joo, Y., Choi, H. J., and Song, J. J. (2017). Down-regulation of TGF-beta expression sensitizes the resistance of hepatocellular carcinoma cells to sorafenib. *Yonsei Med. J.* 58 (5), 899–909. doi:10.3349/ymj.2017.58.5.899

Kelley, R. K., Meyer, T., Rimassa, L., Merle, P., Park, J. W., Yau, T., et al. (2020). Serum alpha-fetoprotein levels and clinical outcomes in the phase III CELESTIAL study of cabozantinib versus placebo in patients with advanced hepatocellular carcinoma. *Clin. Cancer Res.* 26 (18), 4795–4804. doi:10.1158/1078-0432.CCR-19-3884

Khalaf, K., Hana, D., Chou, J. T., Singh, C., Mackiewicz, A., and Kaczmarek, M. (2021). Aspects of the tumor microenvironment involved in immune resistance and drug resistance. *Front. Immunol.* 12, 656364. doi:10.3389/fimmu.2021.656364

Koh, M. Y., Lemos, R., Jr., Liu, X., and Powis, G. (2011). The hypoxia-associated factor switches cells from HIF-1α- to HIF-2α-dependent signaling promoting stem cell characteristics, aggressive tumor growth and invasion. *Cancer Res.* 71 (11), 4015–4027. doi:10.1158/0008-5472.CAN-10-4142

Konopacki, C., Pritykin, Y., Rubtsov, Y., Leslie, C. S., and Rudensky, A. Y. (2019). Transcription factor Foxp1 regulates Foxp3 chromatin binding and coordinates regulatory T cell function. *Nat. Immunol.* 20 (2), 232–242. doi:10.1038/s41590-018-0291-z

Kouno, T., Moody, J., Kwon, A. T., Shibayama, Y., Kato, S., Huang, Y., et al. (2019). C1 CAGE detects transcription start sites and enhancer activity at single-cell resolution. *Nat. Commun.* 10 (1), 360. doi:10.1038/s41467-018-08126-5

Kuo, T. T., Baker, K., Yoshida, M., Qiao, S. W., Aveson, V. G., Lencer, W. I., et al. (2010). Neonatal Fc receptor: from immunity to therapeutics. *J. Clin. Immunol.* 30 (6), 777–789. doi:10.1007/s10875-010-9468-4

LaGory, E. L., and Giaccia, A. J. (2016). The ever-expanding role of HIF in tumour and stromal biology. *Nat. Cell Biol.* 18 (4), 356–365. doi:10.1038/ncb3330

Lai, S. C., Su, Y. T., Chi, C. C., Kuo, Y. C., Lee, K. F., Wu, Y. C., et al. (2019). DNMT3b/OCT4 expression confers sorafenib resistance and poor prognosis of hepatocellular carcinoma through IL-6/STAT3 regulation. *J. Exp. Clin. Cancer Res.* 38 (1), 474. doi:10.1186/s13046-019-1442-2

Lai, Y., Feng, B., Abudoureyimu, M., Zhi, Y., Zhou, H., Wang, T., et al. (2019). Non-coding RNAs: Emerging regulators of sorafenib resistance in hepatocellular carcinoma. *Front. Oncol.* 9, 1156. doi:10.3389/fonc.2019.01156

Le, Y., Gao, H., Bleday, R., and Zhu, Z. (2018). The homeobox protein VentX reverts immune suppression in the tumor microenvironment. *Nat. Commun.* 9 (1), 2175. doi:10.1038/s41467-018-04567-0

Lee, D. W., Cho, E. J., Lee, J. H., Yu, S. J., Kim, Y. J., Yoon, J. H., et al. (2021). Phase II study of avelumab in patients with advanced hepatocellular carcinoma previously treated with sorafenib. *Clin. Cancer Res.* 27 (3), 713–718. doi:10.1158/1078-0432.CCR-20-3094

Lee, P., Chandel, N. S., and Simon, M. C. (2020). Cellular adaptation to hypoxia through hypoxia inducible factors and beyond. *Nat. Rev. Mol. Cell Biol.* 21 (5), 268–283. doi:10.1038/s41580-020-0227-y

Lee, Y. A., Noon, L. A., Akat, K. M., Ybanez, M. D., Lee, T. F., Berres, M. L., et al. (2018). Autophagy is a gatekeeper of hepatic differentiation and carcinogenesis by controlling the degradation of Yap. *Nat. Commun.* 9 (1), 4962. doi:10.1038/s41467-018-07338-z

Li, B., Wei, S., Yang, L., Peng, X., Ma, Y., Wu, B., et al. (2021). CISD2 promotes resistance to sorafenib-induced ferroptosis by regulating autophagy in hepatocellular carcinoma. *Front. Oncol.* 11, 657723. doi:10.3389/fonc.2021.657723

Li, D., Sun, F. F., Wang, D., Wang, T., Peng, J. J., Feng, J. Q., et al. (2020). Programmed death ligand-1 (PD-L1) regulated by NRF-2/MicroRNA-1 regulatory Axis enhances drug resistance and promotes tumorigenic properties in sorafenib-resistant hepatoma cells. *Oncol. Res.* 28 (5), 467–481. doi:10.3727/096504020X15925659763817

Li, H., Li, X., Jing, X., Li, M., Ren, Y., Chen, J., et al. (2018). Hypoxia promotes maintenance of the chondrogenic phenotype in rat growth plate chondrocytes through the HIF-1α/YAP signaling pathway. *Int. J. Mol. Med.* 42 (6), 3181–3192. doi:10.3892/ijmm.2018.3921

Li, S., Li, J., Dai, W., Zhang, Q., Feng, J., Wu, L., et al. (2017). Genistein suppresses aerobic glycolysis and induces hepatocellular carcinoma cell death. *Br. J. Cancer* 117 (10), 1518–1528. doi:10.1038/bjc.2017.323

Li, W., Dong, X., He, C., Tan, G., Li, Z., Zhai, B., et al. (2019). LncRNA SNHG1 contributes to sorafenib resistance by activating the Akt pathway and is positively regulated by miR-21 in hepatocellular carcinoma cells. *J. Exp. Clin. Cancer Res.* 38 (1), 183. doi:10.1186/s13046-019-1177-0

Li, Y., Chen, G., Han, Z., Cheng, H., Qiao, L., and Li, Y. (2020). IL-6/STAT3 signaling contributes to sorafenib resistance in hepatocellular carcinoma through targeting cancer stem cells. *Onco. Targets. Ther.* 13, 9721–9730. doi:10.2147/OTT.S262089

Li, Y. W., Qiu, S. J., Fan, J., Zhou, J., Gao, Q., Xiao, Y. S., et al. (2011). Intratumoral neutrophils: a poor prognostic factor for hepatocellular carcinoma following resection. *J. Hepatol.* 54 (3), 497–505. doi:10.1016/j.jhep.2010.07.044

Liang, Y., Zheng, T., Song, R., Wang, J., Yin, D., Wang, L., et al. (2013). Hypoxia-mediated sorafenib resistance can be overcome by EF24 through Von Hippel-Lindau tumor suppressor-dependent HIF-1α inhibition in hepatocellular carcinoma. *Hepatology* 57 (5), 1847–1857. doi:10.1002/hep.26224

Lin, H., Zhang, R., Wu, W., and Lei, L. (2020). Comprehensive network analysis of the molecular mechanisms associated with sorafenib resistance in hepatocellular carcinoma. *Cancer Genet.* 245, 27–34. doi:10.1016/j.cancergen.2020.04.076

Lin, T. H., Shao, Y. Y., Chan, S. Y., Huang, C. Y., Hsu, C. H., and Cheng, A. L. (2015). High serum transforming growth factor-β1 levels predict outcome in hepatocellular carcinoma patients treated with sorafenib. *Clin. Cancer Res.* 21 (16), 3678–3684. doi:10.1158/1078-0432.CCR-14-1954

Lin, Z., Niu, Y., Wan, A., Chen, D., Liang, H., Chen, X., et al. (2020). RNA m(6) A methylation regulates sorafenib resistance in liver cancer through FOXO3-mediated autophagy. *EMBO J.* 39 (12), e103181. doi:10.15252/embj.2019103181

Liu, F., Dong, X., Lv, H., Xiu, P., Li, T., Wang, F., et al. (2015). Targeting hypoxia-inducible factor-2α enhances sorafenib antitumor activity via β-catenin/C-Myc-dependent pathways in hepatocellular carcinoma. *Oncol. Lett.* 10 (2), 778–784. doi:10.3892/ol.2015.3315

Liu, J., Li, P., Wang, L., Li, M., Ge, Z., Noordam, L., et al. (2021). Cancer-associated fibroblasts provide a stromal niche for liver cancer organoids that confers trophic effects and therapy resistance. *Cell. Mol. Gastroenterol. Hepatol.* 11 (2), 407–431. doi:10.1016/j.jcmgh.2020.09.003

Liu, J., Liu, Y., Meng, L., Liu, K., and Ji, B. (2017). Targeting the PD-L1/DNMT1 axis in acquired resistance to sorafenib in human hepatocellular carcinoma. *Oncol. Rep.* 38 (2), 899–907. doi:10.3892/or.2017.5722

Liu, R., Li, Y., Tian, L., Shi, H., Wang, J., Liang, Y., et al. (2019). Gankyrin drives metabolic reprogramming to promote tumorigenesis, metastasis and drug resistance through activating beta-catenin/c-Myc signaling in human hepatocellular carcinoma. *Cancer Lett.* 443, 34–46. doi:10.1016/j.canlet.2018.11.030

Liu, X. L., Li, F. Q., Liu, L. X., Li, B., and Zhou, Z. P. (2013). TNF-alpha, HGF and macrophage in peritumoural liver tissue relate to major risk factors of HCC Recurrence. *Hepatogastroenterology.* 60 (125), 1121–1126. doi:10.5754/hge12982

Liu, Y., Chen, L., Yuan, H., Guo, S., and Wu, G. (2020). LncRNA DANCR promotes sorafenib resistance via activation of IL-6/STAT3 signaling in hepatocellular carcinoma cells. *Onco. Targets. Ther.* 13, 1145–1157. doi:10.2147/OTT.S229957

Liu, Y., Liu, A., Li, H., Li, C., and Lin, J. (2011). Celecoxib inhibits interleukin-6/interleukin-6 receptor-induced JAK2/STAT3 phosphorylation in human hepatocellular carcinoma cells. *Cancer Prev. Res.* 4 (8), 1296–1305. doi:10.1158/1940-6207.CAPR-10-0317

Llovet, J. M., Ricci, S., Mazzaferro, V., Hilgard, P., Gane, E., Blanc, J. F., et al. (2008). Sorafenib in advanced hepatocellular carcinoma. *N. Engl. J. Med.* 359 (4), 378–390. doi:10.1056/NEJMoa0708857

Long, Q., Zou, X., Song, Y., Duan, Z., and Liu, L. (2019). PFKFB3/HIF-1α feedback loop modulates sorafenib resistance in hepatocellular carcinoma cells. *Biochem. Biophys. Res. Commun.* 513 (3), 642–650. doi:10.1016/j.bbrc.2019.03.109

Lu, S., Yao, Y., Xu, G., Zhou, C., Zhang, Y., Sun, J., et al. (2018). CD24 regulates sorafenib resistance via activating autophagy in hepatocellular carcinoma. *Cell Death Dis.* 9 (6), 646. doi:10.1038/s41419-018-0681-z

Ma, L., Li, G., Zhu, H., Dong, X., Zhao, D., Jiang, X., et al. (2014). 2-Methoxyestradiol synergizes with sorafenib to suppress hepatocellular carcinoma by simultaneously dysregulating hypoxia-inducible factor-1 and -2. *Cancer Lett.* 355 (1), 96–105. doi:10.1016/j.canlet.2014.09.011

Ma, Y., Yang, W., Simon, T. G., Smith-Warner, S. A., Fung, T. T., Sui, J., et al. (2019). Dietary patterns and risk of hepatocellular carcinoma among U.S. Men and women. *Hepatology* 70 (2), 577–586. doi:10.1002/hep.30362

Mantovani, A., Schioppa, T., Porta, C., Allavena, P., and Sica, A. (2006). Role of tumor-associated macrophages in tumor progression and invasion. *Cancer Metastasis Rev.* 25 (3), 315–322. doi:10.1007/s10555-006-9001-7

Mao, X., Xu, J., Wang, W., Liang, C., Hua, J., Liu, J., et al. (2021). Crosstalk between cancer-associated fibroblasts and immune cells in the tumor microenvironment: new findings and future perspectives. *Mol. Cancer* 20 (1), 131. doi:10.1186/s12943-021-01428-1

Marshall, L. A., Marubayashi, S., Jorapur, A., Jacobson, S., Zibinsky, M., Robles, O., et al. (2020). Tumors establish resistance to immunotherapy by regulating Treg recruitment via CCR4. *J. Immunother. Cancer* 8 (2), e000764. doi:10.1136/jitc-2020-000764

Massague, J. (2008). TGFbeta in cancer. *Cell* 134 (2), 215–230. doi:10.1016/j.cell.2008.07.001

Matsuda, Y., Wakai, T., Kubota, M., Osawa, M., Hirose, Y., Sakata, J., et al. (2014). Valproic acid overcomes transforming growth factor-beta-mediated sorafenib resistance in hepatocellular carcinoma. *Int. J. Clin. Exp. Pathol.* 7 (4), 1299–1313.

Meads, M. B., Gatenby, R. A., and Dalton, W. S. (2009). Environment-mediated drug resistance: a major contributor to minimal residual disease. *Nat. Rev. Cancer* 9 (9), 665–674. doi:10.1038/nrc2714

Mendez-Blanco, C., Fondevila, F., Fernandez-Palanca, P., Garcia-Palomo, A., Pelt, J. V., Verslype, C., et al. (2019). Stabilization of hypoxia-inducible factors and BNIP3 promoter methylation contribute to acquired sorafenib resistance in human hepatocarcinoma cells. *Cancers (Basel)* 11 (12), E1984. doi:10.3390/cancers11121984

Menrad, H., Werno, C., Schmid, T., Copanaki, E., Deller, T., Dehne, N., et al. (2010). Roles of hypoxia-inducible factor-1alpha (HIF-1alpha) versus HIF-2alpha in the survival of hepatocellular tumor spheroids. *Hepatology* 51 (6), 2183–2192. doi:10.1002/hep.23597

Mo, Z., Liu, D., Rong, D., and Zhang, S. (2021). Hypoxic characteristic in the immunosuppressive microenvironment of hepatocellular carcinoma. *Front. Immunol.* 12, 611058. doi:10.3389/fimmu.2021.611058

Mondal, S., Roy, D., Sarkar Bhattacharya, S., Jin, L., Jung, D., Zhang, S., et al. (2019). Therapeutic targeting of PFKFB3 with a novel glycolytic inhibitor PFK158 promotes lipophagy and chemosensitivity in gynecologic cancers. *Int. J. Cancer* 144 (1), 178–189. doi:10.1002/ijc.31868

Mulder, W. J. M., Ochando, J., Joosten, L. A. B., Fayad, Z. A., and Netea, M. G. (2019). Therapeutic targeting of trained immunity. *Nat. Rev. Drug Discov.* 18 (7), 553–566. doi:10.1038/s41573-019-0025-4

Multhaupt, H. A., Leitinger, B., Gullberg, D., and Couchman, J. R. (2016). Extracellular matrix component signaling in cancer. *Adv. Drug Deliv. Rev.* 97, 28–40. doi:10.1016/j.addr.2015.10.013

Negri, F., Gnetti, L., Pedrazzi, G., Silini, E. M., and Porta, C. (2021). Sorafenib and hepatocellular carcinoma: is alpha-fetoprotein a biomarker predictive of tumor biology and primary resistance? *Future Oncol.* 17 (27), 3579–3584. doi:10.2217/fon-2021-0083

Ngo, M. T., Peng, S. W., Kuo, Y. C., Lin, C. Y., Wu, M. H., Chuang, C. H., et al. (2021). A yes-associated protein (YAP) and insulin-like growth factor 1 receptor (IGF-1R) signaling loop is involved in sorafenib resistance in hepatocellular carcinoma. *Cancers (Basel)* 13 (15), 3812. doi:10.3390/cancers13153812

Nie, J., Lin, B., Zhou, M., Wu, L., and Zheng, T. (2018). Role of ferroptosis in hepatocellular carcinoma. *J. Cancer Res. Clin. Oncol.* 144 (12), 2329–2337. doi:10.1007/s00432-018-2740-3

Niskanen, H., Tuszynska, I., Zaborowski, R., Heinaniemi, M., Yla-Herttuala, S., Wilczynski, B., et al. (2018). Endothelial cell differentiation is encompassed by changes in long range interactions between inactive chromatin regions. *Nucleic Acids Res.* 46 (4), 1724–1740. doi:10.1093/nar/gkx1214

Niu, L., Liu, L., Yang, S., Ren, J., Lai, P. B. S., and Chen, G. G. (2017). New insights into sorafenib resistance in hepatocellular carcinoma: Responsible mechanisms and promising strategies. *Biochim. Biophys. Acta. Rev. Cancer* 1868 (2), 564–570. doi:10.1016/j.bbcan.2017.10.002

Nowicki, T. S., Hu-Lieskovan, S., and Ribas, A. (2018). Mechanisms of resistance to PD-1 and PD-L1 blockade. *Cancer J.* 24 (1), 47–53. doi:10.1097/PPO.0000000000000303

Paraiso, K. H., and Smalley, K. S. (2013). Fibroblast-mediated drug resistance in cancer. *Biochem. Pharmacol.* 85 (8), 1033–1041. doi:10.1016/j.bcp.2013.01.018

Pein, M., Insua-Rodriguez, J., Hongu, T., Riedel, A., Meier, J., Wiedmann, L., et al. (2020). Metastasis-initiating cells induce and exploit a fibroblast niche to fuel malignant colonization of the lungs. *Nat. Commun.* 11 (1), 1494. doi:10.1038/s41467-020-15188-x

Peng, H., Xue, R., Ju, Z., Qiu, J., Wang, J., Yan, W., et al. (2020). Cancer-associated fibroblasts enhance the chemoresistance of CD73(+) hepatocellular carcinoma cancer cells via HGF-Met-ERK1/2 pathway. *Ann. Transl. Med.* 8 (14), 856. doi:10.21037/atm-20-1038

Pinyol, R., Montal, R., Bassaganyas, L., Sia, D., Takayama, T., Chau, G. Y., et al. (2019). Molecular predictors of prevention of recurrence in HCC with sorafenib as adjuvant treatment and prognostic factors in the phase 3 STORM trial. *Gut* 68 (6), 1065–1075. doi:10.1136/gutjnl-2018-316408

Prieto-Dominguez, N., Mendez-Blanco, C., Carbajo-Pescador, S., Fondevila, F., Garcia-Palomo, A., Gonzalez-Gallego, J., et al. (2017). Melatonin enhances sorafenib actions in human hepatocarcinoma cells by inhibiting mTORC1/p70S6K/HIF-1α and hypoxia-mediated mitophagy. *Oncotarget* 8 (53), 91402–91414. doi:10.18632/oncotarget.20592

Prieto-Dominguez, N., Ordonez, R., Fernandez, A., Garcia-Palomo, A., Muntane, J., Gonzalez-Gallego, J., et al. (2016). Modulation of autophagy by sorafenib: Effects on treatment response. *Front. Pharmacol.* 7, 151. doi:10.3389/fphar.2016.00151

Qu, J., Luo, M., Zhang, J., Han, F., Hou, N., Pan, R., et al. (2021). A paradoxical role for sestrin 2 protein in tumor suppression and tumorigenesis. *Cancer Cell Int.* 21 (1), 606. doi:10.1186/s12935-021-02317-9

Qu, Z., Wu, J., Wu, J., Luo, D., Jiang, C., and Ding, Y. (2016). Exosomes derived from HCC cells induce sorafenib resistance in hepatocellular carcinoma both *in vivo* and *in vitro*. *J. Exp. Clin. Cancer Res.* 35 (1), 159. doi:10.1186/s13046-016-0430-z

Ren, Y., Gu, Y. K., Li, Z., Xu, G. Z., Zhang, Y. M., Dong, M. X., et al. (2020). CXCR3 confers sorafenib resistance of HCC cells through regulating metabolic alteration and AMPK pathway. *Am. J. Transl. Res.* 12 (3), 825–836.

Reya, T., Morrison, S. J., Clarke, M. F., and Weissman, I. L. (2001). Stem cells, cancer, and cancer stem cells. *Nature* 414 (6859), 105–111. doi:10.1038/35102167

Richards, K. E., Zeleniak, A. E., Fishel, M. L., Wu, J., Littlepage, L. E., and Hill, R. (2017). Cancer-associated fibroblast exosomes regulate survival and proliferation of pancreatic cancer cells. *Oncogene* 36 (13), 1770–1778. doi:10.1038/onc.2016.353

Riscal, R., Skuli, N., and Simon, M. C. (2019). Even cancer cells watch their cholesterol. *Mol. Cell* 76 (2), 220–231. doi:10.1016/j.molcel.2019.09.008

Rodriguez-Mateo, C., Torres, B., Gutierrez, G., and Pintor-Toro, J. A. (2017). Downregulation of Lnc-Spry1 mediates TGF-beta-induced epithelial-mesenchymal transition by transcriptional and posttranscriptional regulatory mechanisms. *Cell Death Differ.* 24 (5), 785–797. doi:10.1038/cdd.2017.9

Sadek, H., and Olson, E. N. (2020). Toward the goal of human heart regeneration. *Cell Stem Cell* 26 (1), 7–16. doi:10.1016/j.stem.2019.12.004

Sawayama, H., Ogata, Y., Ishimoto, T., Mima, K., Hiyoshi, Y., Iwatsuki, M., et al. (2019). Glucose transporter 1 regulates the proliferation and cisplatin sensitivity of esophageal cancer. *Cancer Sci.* 110 (5), 1705–1714. doi:10.1111/cas.13995

Sharma, P., Hu-Lieskovan, S., Wargo, J. A., and Ribas, A. (2017). Primary, adaptive, and acquired resistance to cancer immunotherapy. *Cell* 168 (4), 707–723. doi:10.1016/j.cell.2017.01.017

Shen, M., Xu, Z., Xu, W., Jiang, K., Zhang, F., Ding, Q., et al. (2019). Inhibition of ATM reverses EMT and decreases metastatic potential of cisplatin-resistant lung cancer cells through JAK/STAT3/PD-L1 pathway. *J. Exp. Clin. Cancer Res.* 38 (1), 149. doi:10.1186/s13046-019-1161-8

Shi, L., Pan, H., Liu, Z., Xie, J., and Han, W. (2017). Roles of PFKFB3 in cancer. *Signal Transduct. Target. Ther.* 2, 17044. doi:10.1038/sigtrans.2017.44

Shi, S., Yoon, D. Y., Hodge-Bell, K. C., Bebenek, I. G., Whitekus, M. J., Zhang, R., et al. (2009). The aryl hydrocarbon receptor nuclear translocator (Arnt) is required for tumor initiation by benzo[a]pyrene. *Carcinogenesis* 30 (11), 1957–1961. doi:10.1093/carcin/bgp201

Shih, J. W., Chiang, W. F., Wu, A. T. H., Wu, M. H., Wang, L. Y., Yu, Y. L., et al. (2017). Long noncoding RNA LncHIFCAR/MIR31HG is a HIF-1α co-activator driving oral cancer progression. *Nat. Commun.* 8, 15874. doi:10.1038/ncomms15874

Shrestha, R., Bridle, K. R., Cao, L., Crawford, D. H. G., and Jayachandran, A. (2021a). Dual targeting of sorafenib-resistant HCC-derived cancer stem cells. *Curr. Oncol.* 28 (3), 2150–2172. doi:10.3390/curroncol28030200

Shrestha, R., Prithviraj, P., Bridle, K. R., Crawford, D. H. G., and Jayachandran, A. (2021b). Combined inhibition of TGF-β1-induced EMT and PD-L1 silencing Re-sensitizes hepatocellular carcinoma to sorafenib treatment. *J. Clin. Med.* 10 (9), 1889. doi:10.3390/jcm10091889

Snuderl, M., Batista, A., Kirkpatrick, N. D., Ruiz de Almodovar, C., Riedemann, L., Walsh, E. C., et al. (2013). Targeting placental growth factor/neuropilin 1 pathway inhibits growth and spread of medulloblastoma. *Cell* 152 (5), 1065–1076. doi:10.1016/j.cell.2013.01.036

Song, J. S., Chang, C. C., Wu, C. H., Dinh, T. K., Jan, J. J., Huang, K. W., et al. (2021). A highly selective and potent CXCR4 antagonist for hepatocellular carcinoma treatment. *Proc. Natl. Acad. Sci. U. S. A.* 118 (13), e2015433118. doi:10.1073/pnas.2015433118

Song, Z., Liu, T., Chen, J., Ge, C., Zhao, F., Zhu, M., et al. (2019). HIF-1α-induced RIT1 promotes liver cancer growth and metastasis and its deficiency increases sensitivity to sorafenib. *Cancer Lett.* 460, 96–107. doi:10.1016/j.canlet.2019.06.016

Strauss, L., Guarneri, V., Gennari, A., and Sica, A. (2021). Implications of metabolism-driven myeloid dysfunctions in cancer therapy. *Cell. Mol. Immunol.* 18 (4), 829–841. doi:10.1038/s41423-020-00556-w

Sun, L., Xi, S., Zhou, Z., Zhang, F., Hu, P., Cui, Y., et al. (2022). Elevated expression of RIT1 hyperactivates RAS/MAPK signal and sensitizes hepatocellular carcinoma to combined treatment with sorafenib and AKT inhibitor. *Oncogene* 41 (5), 732–744. doi:10.1038/s41388-021-02130-8

Sun, R., Meng, X., Pu, Y., Sun, F., Man, Z., Zhang, J., et al. (2019). Overexpression of HIF-1a could partially protect K562 cells from 1, 4-benzoquinone induced toxicity by inhibiting ROS, apoptosis and enhancing glycolysis. *Toxicol. Vitro* 55, 18–23. doi:10.1016/j.tiv.2018.11.005

Sun, T., Mao, W., Peng, H., Wang, Q., and Jiao, L. (2021). YAP promotes sorafenib resistance in hepatocellular carcinoma by upregulating survivin. *Cell. Oncol.* 44 (3), 689–699. doi:10.1007/s13402-021-00595-z

Sun, X., Niu, X., Chen, R., He, W., Chen, D., Kang, R., et al. (2016). Metallothionein-1G facilitates sorafenib resistance through inhibition of ferroptosis. *Hepatology* 64 (2), 488–500. doi:10.1002/hep.28574

Sung, H., Ferlay, J., Siegel, R. L., Laversanne, M., Soerjomataram, I., Jemal, A., et al. (2021). Global cancer statistics 2020: GLOBOCAN estimates of incidence and mortality worldwide for 36 cancers in 185 countries. *Ca. Cancer J. Clin.* 71 (3), 209–249. doi:10.3322/caac.21660

Tan, W., Luo, X., Li, W., Zhong, J., Cao, J., Zhu, S., et al. (2019). TNF-alpha is a potential therapeutic target to overcome sorafenib resistance in hepatocellular carcinoma. *EBioMedicine* 40, 446–456. doi:10.1016/j.ebiom.2018.12.047

Tan, Z., Gao, L., Wang, Y., Yin, H., Xi, Y., Wu, X., et al. (2020). PRSS contributes to cetuximab resistance in colorectal cancer. *Sci. Adv.* 6 (1), eaax5576. doi:10.1126/sciadv.aax5576

Tang, J., Sui, C. J., Wang, D. F., Lu, X. Y., Luo, G. J., Zhao, Q., et al. (2020). Targeted sequencing reveals the mutational landscape responsible for sorafenib therapy in advanced hepatocellular carcinoma. *Theranostics* 10 (12), 5384–5397. doi:10.7150/thno.41616

Tang, W., Chen, Z., Zhang, W., Cheng, Y., Zhang, B., Wu, F., et al. (2020). The mechanisms of sorafenib resistance in hepatocellular carcinoma: theoretical basis and therapeutic aspects. *Signal Transduct. Target. Ther.* 5 (1), 87. doi:10.1038/s41392-020-0187-x

Theodoraki, M. N., Yerneni, S. S., Hoffmann, T. K., Gooding, W. E., and Whiteside, T. L. (2018). Clinical significance of PD-L1(+) exosomes in plasma of head and neck cancer patients. *Clin. Cancer Res.* 24 (4), 896–905. doi:10.1158/1078-0432.CCR-17-2664

Tovar, V., Cornella, H., Moeini, A., Vidal, S., Hoshida, Y., Sia, D., et al. (2017). Tumour initiating cells and IGF/FGF signalling contribute to sorafenib resistance in hepatocellular carcinoma. *Gut* 66 (3), 530–540. doi:10.1136/gutjnl-2015-309501

Tu, S., Huang, W., Huang, C., Luo, Z., and Yan, X. (2019). Contextual regulation of TGF-beta signaling in liver cancer. *Cells* 8 (10), E1235. doi:10.3390/cells8101235

Ungerleider, N., Han, C., Zhang, J., Yao, L., and Wu, T. (2017). TGFβ signaling confers sorafenib resistance via induction of multiple RTKs in hepatocellular carcinoma cells. *Mol. Carcinog.* 56 (4), 1302–1311. doi:10.1002/mc.22592

van Malenstein, H., Dekervel, J., Verslype, C., Van Cutsem, E., Windmolders, P., Nevens, F., et al. (2013). Long-term exposure to sorafenib of liver cancer cells induces resistance with epithelial-to-mesenchymal transition, increased invasion and risk of rebound growth. *Cancer Lett.* 329 (1), 74–83. doi:10.1016/j.canlet.2012.10.021

Vanhove, K., Graulus, G. J., Mesotten, L., Thomeer, M., Derveaux, E., Noben, J. P., et al. (2019). The metabolic landscape of lung cancer: New insights in a disturbed glucose metabolism. *Front. Oncol.* 9, 1215. doi:10.3389/fonc.2019.01215

Veglia, F., Perego, M., and Gabrilovich, D. (2018). Myeloid-derived suppressor cells coming of age. *Nat. Immunol.* 19 (2), 108–119. doi:10.1038/s41590-017-0022-x

Veglia, F., Sanseviero, E., and Gabrilovich, D. I. (2021). Myeloid-derived suppressor cells in the era of increasing myeloid cell diversity. *Nat. Rev. Immunol.* 21 (8), 485–498. doi:10.1038/s41577-020-00490-y

Vela, M., Bueno, D., Gonzalez-Navarro, P., Brito, A., Fernandez, L., Escudero, A., et al. (2019). Anti-CXCR4 antibody combined with activated and expanded natural killer cells for sarcoma immunotherapy. *Front. Immunol.* 10, 1814. doi:10.3389/fimmu.2019.01814

Wang, G., Xu, J., Zhao, J., Yin, W., Liu, D., Chen, W., et al. (2020). Arf1-mediated lipid metabolism sustains cancer cells and its ablation induces anti-tumor immune responses in mice. *Nat. Commun.* 11 (1), 220. doi:10.1038/s41467-019-14046-9

Wang, M., Wang, Z., Zhi, X., Ding, W., Xiong, J., Tao, T., et al. (2020). SOX9 enhances sorafenib resistance through upregulating ABCG2 expression in hepatocellular carcinoma. *Biomed. Pharmacother.* 129, 110315. doi:10.1016/j.biopha.2020.110315

Wang, Y., and Liu, A. (2020). Carbon-fluorine bond cleavage mediated by metalloenzymes. *Chem. Soc. Rev.* 49 (14), 4906–4925. doi:10.1039/c9cs00740g

Wei, F., Zong, S., Zhou, J., Fan, M., Wang, Y., Cheng, X., et al. (2019). Tumor-associated macrophages attenuate apoptosis-inducing effect of sorafenib in hepatoma cells by increasing autophagy. *Nan Fang. Yi Ke Da Xue Xue Bao* 39 (3), 264–270. doi:10.12122/j.issn.1673-4254.2019.03.02

Wei, L., Wang, X., Lv, L., Liu, J., Xing, H., Song, Y., et al. (2019). The emerging role of microRNAs and long noncoding RNAs in drug resistance of hepatocellular carcinoma. *Mol. Cancer* 18 (1), 147. doi:10.1186/s12943-019-1086-z

Wei, X., Pu, J., Guo, Z., Li, T., Zhu, D., and Wu, Z. (2017). Tumor-associated macrophages promote the proliferation and migration as well as invasion of sorafenib-resistant hepatocellular carcinoma cells. *Xi Bao Yu Fen Zi Mian Yi Xue Za Zhi* 33 (5), 617–622.

Wei, X., Tang, C., Lu, X., Liu, R., Zhou, M., He, D., et al. (2015). MiR-101 targets DUSP1 to regulate the TGF-beta secretion in sorafenib inhibits macrophage-induced growth of hepatocarcinoma. *Oncotarget* 6 (21), 18389–18405. doi:10.18632/oncotarget.4089

Whiteside, T. L. (2018). FOXP3+ Treg as a therapeutic target for promoting anti-tumor immunity. *Expert Opin. Ther. Targets* 22 (4), 353–363. doi:10.1080/14728222.2018.1451514

Wu, F. Q., Fang, T., Yu, L. X., Lv, G. S., Lv, H. W., Liang, D., et al. (2016). ADRB2 signaling promotes HCC progression and sorafenib resistance by inhibiting autophagic degradation of HIF1α. *J. Hepatol.* 65 (2), 314–324. doi:10.1016/j.jhep.2016.04.019

Wu, H., Chen, P., Liao, R., Li, Y. W., Yi, Y., Wang, J. X., et al. (2012). Overexpression of galectin-1 is associated with poor prognosis in human hepatocellular carcinoma following resection. *J. Gastroenterol. Hepatol.* 27 (8), 1312–1319. doi:10.1111/j.1440-1746.2012.07130.x

Wu, J., Chai, H., Li, F., Ren, Q., and Gu, Y. (2020). SETD1A augments sorafenib primary resistance via activating YAP in hepatocellular carcinoma. *Life Sci.* 260, 118406. doi:10.1016/j.lfs.2020.118406

Wu, Q., Zhou, W., Yin, S., Zhou, Y., Chen, T., Qian, J., et al. (2019). Blocking triggering receptor expressed on myeloid cells-1-positive tumor-associated macrophages induced by hypoxia reverses immunosuppression and anti-programmed cell death ligand 1 resistance in liver cancer. *Hepatology* 70 (1), 198–214. doi:10.1002/hep.30593

Wu, S., and Fu, L. (2018). Tyrosine kinase inhibitors enhanced the efficacy of conventional chemotherapeutic agent in multidrug resistant cancer cells. *Mol. Cancer* 17 (1), 25. doi:10.1186/s12943-018-0775-3

Wu, S., Saxena, S., Varney, M. L., and Singh, R. K. (2017). CXCR1/2 chemokine network regulates melanoma resistance to chemotherapies mediated by NF-κB. *Curr. Mol. Med.* 17 (6), 436–449. doi:10.2174/1566524018666171219100158

Xia, S., Pan, Y., Liang, Y., Xu, J., and Cai, X. (2020). The microenvironmental and metabolic aspects of sorafenib resistance in hepatocellular carcinoma. *EBioMedicine* 51, 102610. doi:10.1016/j.ebiom.2019.102610

Xu, G. L., Ni, C. F., Liang, H. S., Xu, Y. H., Wang, W. S., Shen, J., et al. (2020). Upregulation of PD-L1 expression promotes epithelial-to-mesenchymal transition in sorafenib-resistant hepatocellular carcinoma cells. *Gastroenterol. Rep.* 8 (5), 390–398. doi:10.1093/gastro/goaa049

Xu, L. X., He, M. H., Dai, Z. H., Yu, J., Wang, J. G., Li, X. C., et al. (2019). Genomic and transcriptional heterogeneity of multifocal hepatocellular carcinoma. *Ann. Oncol.* 30 (6), 990–997. doi:10.1093/annonc/mdz103

Xu, R., Liu, X., Li, A., Song, L., Liang, J., Gao, J., et al. (2022). c-Met up-regulates the expression of PD-L1 through MAPK/NF-κBp65 pathway. *J. Mol. Med.* 100 (4), 585–598. doi:10.1007/s00109-022-02179-2

Yang, W., Ma, Y., Liu, Y., Smith-Warner, S. A., Simon, T. G., Chong, D. Q., et al. (2019). Association of intake of whole grains and dietary fiber with risk of hepatocellular carcinoma in US adults. *JAMA Oncol.* 5 (6), 879–886. doi:10.1001/jamaoncol.2018.7159

Yang, W. S., and Stockwell, B. R. (2016). Ferroptosis: Death by lipid peroxidation. *Trends Cell Biol.* 26 (3), 165–176. doi:10.1016/j.tcb.2015.10.014

Yang, Y., Sun, M., Yao, W., Wang, F., Li, X., Wang, W., et al. (2020a). Compound kushen injection relieves tumor-associated macrophage-mediated immunosuppression through TNFR1 and sensitizes hepatocellular carcinoma to sorafenib. *J. Immunother. Cancer* 8 (1), e000317. doi:10.1136/jitc-2019-000317

Yang, Y. M., Hong, P., Xu, W. W., He, Q. Y., and Li, B. (2020b). Advances in targeted therapy for esophageal cancer. *Signal Transduct. Target. Ther.* 5 (1), 229. doi:10.1038/s41392-020-00323-3

Yang, Z., Li, H., Wang, W., Zhang, J., Jia, S., Wang, J., et al. (2019). CCL2/CCR2 Axis promotes the progression of salivary adenoid cystic carcinoma via recruiting and reprogramming the tumor-associated macrophages. *Front. Oncol.* 9, 231. doi:10.3389/fonc.2019.00231

Yao, J., Man, S., Dong, H., Yang, L., Ma, L., and Gao, W. (2018). Combinatorial treatment of Rhizoma Paridis saponins and sorafenib overcomes the intolerance of sorafenib. *J. Steroid Biochem. Mol. Biol.* 183, 159–166. doi:10.1016/j.jsbmb.2018.06.010

Yao, M., Ventura, P. B., Jiang, Y., Rodriguez, F. J., Wang, L., Perry, J. S. A., et al. (2020). Astrocytic trans-differentiation completes a multicellular paracrine feedback loop required for medulloblastoma tumor growth. *Cell* 180 (3), 502–520. doi:10.1016/j.cell.2019.12.024

Yao, W., Ba, Q., Li, X., Li, H., Zhang, S., Yuan, Y., et al. (2017). A natural CCR2 antagonist relieves tumor-associated macrophage-mediated immunosuppression to produce a therapeutic effect for liver cancer. *EBioMedicine* 22, 58–67. doi:10.1016/j.ebiom.2017.07.014

Yeh, C. C., Hsu, C. H., Shao, Y. Y., Ho, W. C., Tsai, M. H., Feng, W. C., et al. (2015). Integrated stable isotope labeling by amino acids in cell culture (SILAC) and isobaric tags for relative and absolute quantitation (iTRAQ) quantitative proteomic analysis identifies galectin-1 as a potential biomarker for predicting sorafenib resistance in liver cancer. *Mol. Cell. Proteomics* 14 (6), 1527–1545. doi:10.1074/mcp.M114.046417

You, A., Cao, M., Guo, Z., Zuo, B., Gao, J., Zhou, H., et al. (2016). Metformin sensitizes sorafenib to inhibit postoperative recurrence and metastasis of

hepatocellular carcinoma in orthotopic mouse models. *J. Hematol. Oncol.* 9, 20. doi:10.1186/s13045-016-0253-6

Youssef, L. A., Rebbaa, A., Pampou, S., Weisberg, S. P., Stockwell, B. R., Hod, E. A., et al. (2018). Increased erythrophagocytosis induces ferroptosis in red pulp macrophages in a mouse model of transfusion. *Blood* 131 (23), 2581–2593. doi:10.1182/blood-2017-12-822619

Yu, W., Yang, W., Zhao, M. Y., and Meng, X. L. (2020). Functional metabolomics analysis elucidating the metabolic biomarker and key pathway change associated with the chronic glomerulonephritis and revealing action mechanism of rhein. *Front. Pharmacol.* 11, 554783. doi:10.3389/fphar.2020.554783

Zha, Z., and Li, J. (2020). MicroRNA125a5p regulates liver cancer cell growth, migration and invasion and EMT by targeting HAX1. *Int. J. Mol. Med.* 46 (5), 1849–1861. doi:10.3892/ijmm.2020.4729

Zhang, C., Gao, L., Cai, Y., Liu, H., Gao, D., Lai, J., et al. (2016). Inhibition of tumor growth and metastasis by photoimmunotherapy targeting tumor-associated macrophage in a sorafenib-resistant tumor model. *Biomaterials* 84, 1–12. doi:10.1016/j.biomaterials.2016.01.027

Zhang, J., Zhao, X., Ma, X., Yuan, Z., and Hu, M. (2020). KCNQ1OT1 contributes to sorafenib resistance and programmed deathligand1mediated immune escape via sponging miR506 in hepatocellular carcinoma cells. *Int. J. Mol. Med.* 46 (5), 1794–1804. doi:10.3892/ijmm.2020.4710

Zhang, P. F., Li, K. S., Shen, Y. H., Gao, P. T., Dong, Z. R., Cai, J. B., et al. (2016). Galectin-1 induces hepatocellular carcinoma EMT and sorafenib resistance by activating FAK/PI3K/AKT signaling. *Cell Death Dis.* 7, e2201. doi:10.1038/cddis.2015.324

Zhang, P. F., Wang, F., Wu, J., Wu, Y., Huang, W., Liu, D., et al. (2019). LncRNA SNHG3 induces EMT and sorafenib resistance by modulating the miR-128/CD151 pathway in hepatocellular carcinoma. *J. Cell. Physiol.* 234 (3), 2788–2794. doi:10.1002/jcp.27095

Zhang, T., Jia, Y., Yu, Y., Zhang, B., Xu, F., and Guo, H. (2022). Targeting the tumor biophysical microenvironment to reduce resistance to immunotherapy. *Adv. Drug Deliv. Rev.* 186, 114319. doi:10.1016/j.addr.2022.114319

Zhang, X., Zhou, H., Jing, W., Luo, P., Qiu, S., Liu, X., et al. (2018). The circular RNA hsa_circ_0001445 regulates the proliferation and migration of hepatocellular carcinoma and may serve as a diagnostic biomarker. *Dis. Markers* 2018, 3073467. doi:10.1155/2018/3073467

Zhang, Z., Zhu, Y., Xu, D., Li, T. E., Li, J. H., Xiao, Z. T., et al. (2021). IFN-alpha facilitates the effect of sorafenib via shifting the M2-like polarization of TAM in hepatocellular carcinoma. *Am. J. Transl. Res.* 13 (1), 301–313.

Zhao, D., Zhai, B., He, C., Tan, G., Jiang, X., Pan, S., et al. (2014). Upregulation of HIF-2α induced by sorafenib contributes to the resistance by activating the TGF-α/EGFR pathway in hepatocellular carcinoma cells. *Cell. Signal.* 26 (5), 1030–1039. doi:10.1016/j.cellsig.2014.01.026

Zheng, N., Liu, W., Li, B., Nie, H., Liu, J., Cheng, Y., et al. (2019). Co-delivery of sorafenib and metapristone encapsulated by CXCR4-targeted PLGA-PEG nanoparticles overcomes hepatocellular carcinoma resistance to sorafenib. *J. Exp. Clin. Cancer Res.* 38 (1), 232. doi:10.1186/s13046-019-1216-x

Zhou, S. L., Zhou, Z. J., Hu, Z. Q., Huang, X. W., Wang, Z., Chen, E. B., et al. (2016). Tumor-associated neutrophils recruit macrophages and T-regulatory cells to promote progression of hepatocellular carcinoma and resistance to sorafenib. *Gastroenterology* 150 (7), 1646–1658. doi:10.1053/j.gastro.2016.02.040

Zhu, M., Yin, F., Fan, X., Jing, W., Chen, R., Liu, L., et al. (2015). Decreased TIP30 promotes Snail-mediated epithelial-mesenchymal transition and tumor-initiating properties in hepatocellular carcinoma. *Oncogene* 34 (11), 1420–1431. doi:10.1038/onc.2014.73

Zhu, W., Doubleday, P. F., Catlin, D. S., Weerawarna, P. M., Butrin, A., Shen, S., et al. (2020). A remarkable difference that one fluorine atom confers on the mechanisms of inactivation of human ornithine aminotransferase by two cyclohexene analogues of gamma-aminobutyric acid. *J. Am. Chem. Soc.* 142 (10), 4892–4903. doi:10.1021/jacs.0c00193

Zhu, X., Zhang, Y., Wu, Y., Diao, W., Deng, G., Li, Q., et al. (2022). HMOX1 attenuates the sensitivity of hepatocellular carcinoma cells to sorafenib via modulating the expression of ABC transporters. *Int. J. Genomics* 2022, 9451557. doi:10.1155/2022/9451557

Zhu, Z., Zhu, X., Yang, S., Guo, Z., Li, K., Ren, C., et al. (2020). Yin-yang effect of tumour cells in breast cancer: from mechanism of crosstalk between tumour-associated macrophages and cancer-associated adipocytes. *Am. J. Cancer Res.* 10 (2), 383–392.

Zou, D., Han, W., You, S., Ye, D., Wang, L., Wang, S., et al. (2011). *In vitro* study of enhanced osteogenesis induced by HIF-1α-transduced bone marrow stem cells. *Cell Prolif.* 44 (3), 234–243. doi:10.1111/j.1365-2184.2011.00747.x

frontiers | Frontiers in Pharmacology

TYPE Original Research
PUBLISHED 22 August 2022
DOI 10.3389/fphar.2022.952482

OPEN ACCESS

EDITED BY
Xuebing Li,
Tianjin Medical University General Hospital, China

REVIEWED BY
Shijun Yu,
Tongji University, China
Alessandro Granito,
University of Bologna Department of Medical and Surgical Sciences, Italy
Hui Jia,
Shenyang Medical College, China

*CORRESPONDENCE
Xi-Zhong Shen,
shen.xizhong@zs-hospital.sh.cn
Tao-Tao Liu,
liu.taotao@zs-hospital.sh.cn

†These authors have contributed equally to this work and share first authorship

SPECIALTY SECTION
This article was submitted to Pharmacology of Anti-Cancer Drugs, a section of the journal Frontiers in Pharmacology

RECEIVED 25 May 2022
ACCEPTED 21 July 2022
PUBLISHED 22 August 2022

CITATION
Liu Z-Y, Zhang D-Y, Lin X-H, Sun J-L, Abuduwaili W, Zhang G-C, Xu R-C, Wang F, Yu X-N, Shi X, Deng B, Dong L, Weng S-Q, Zhu J-M, Shen X-Z and Liu T-T (2022), Nalidixic acid potentiates the antitumor activity in sorafenib-resistant hepatocellular carcinoma via the tumor immune microenvironment analysis. *Front. Pharmacol.* 13:952482. doi: 10.3389/fphar.2022.952482

Nalidixic acid potentiates the antitumor activity in sorafenib-resistant hepatocellular carcinoma *via* the tumor immune microenvironment analysis

Zhi-Yong Liu[1,2†], Dan-Ying Zhang[1,2†], Xia-Hui Lin[1,2†], Jia-Lei Sun[1,2], Weinire Abuduwaili[1,2], Guang-Cong Zhang[1,2], Ru-Chen Xu[1,2], Fu Wang[1,2], Xiang-Nan Yu[1,2], Xuan Shi[1,2], Bin Deng[3], Ling Dong[1,2], Shu-Qiang Weng[1,2], Ji-Min Zhu[1,2], Xi-Zhong Shen[1,2,4]* and Tao-Tao Liu[1,2]*

[1]Department of Gastroenterology and Hepatology, Zhongshan Hospital of Fudan University, Shanghai, China, [2]Shanghai Institute of Liver Disease, Shanghai, China, [3]Department of Gastroenterology, The Affiliated Hospital of Yangzhou University, Yangzhou, China, [4]Key Laboratory of Medical Molecular Virology, Shanghai Medical College of Fudan University, Shanghai, China

Sorafenib resistance is often developed and impedes the benefits of clinical therapy in hepatocellular carcinoma (HCC) patients. However, the relationship between sorafenib resistance and tumor immune environment and adjuvant drugs for sorafenib-resistant HCC are not systemically identified. This study first analyzed the expression profiles of sorafenib-resistant HCC cells to explore immune cell infiltration levels and differentially expressed immune-related genes (DEIRGs). The prognostic value of DEIRGs was analyzed using Cox regression and Kaplan–Meier analysis based on The Cancer Genome Atlas. The primary immune cells infiltrated in sorafenib-resistant HCC mice were explored using flow cytometry (FCM). Finally, small-molecule drugs for sorafenib-resistant HCC treatment were screened and validated by experiments. The CIBERSORT algorithm and mice model showed that macrophages and neutrophils are highly infiltrated, while $CD8^+$ T cells are downregulated in sorafenib-resistant HCC. Totally, 34 DEIRGs were obtained from sorafenib-resistant and control groups, which were highly enriched in immune-associated biological processes and pathways. NR6A1, CXCL5, C3, and TGFB1 were further identified as prognostic markers for HCC patients. Finally, nalidixic acid was identified as a promising antagonist for sorafenib-resistant HCC treatment. Collectively, our study reveals the tumor immune microenvironment changes and explores a promising adjuvant drug to overcome sorafenib resistance in HCC.

KEYWORDS

immune gene signature, sorafenib resistance, tumor immune microenvironment, adjuvant drugs, bioinformatics analysis

Introduction

Hepatocellular carcinoma (HCC), the most common type of primary liver cancer, represents the sixth most common cancer and the fourth leading cause of cancer-related death worldwide (Bray et al., 2018; Siegel et al., 2021). Surgical resection and liver transplantation are still the mainstays in HCC treatment; however, the access depends on tumor size, tumor number, extrahepatic metastasis, and clinical status of patients (Roayaie et al., 2015; Kokudo et al., 2019). Sorafenib has been approved as first-line molecular-targeted therapy for advanced HCC patients (Llovet et al., 2008; Cheng et al., 2009; Kokudo et al., 2019), which attenuates cell proliferation by blocking the Raf-MEK-ERK pathway and arrests cell cycle by decreasing cyclin D1. Despite these impressive advances, overall survival remains dismal in sorafenib-treated HCC patients, with median overall survival increased from 4.2 to 6.5 months (Llovet et al., 2008; Keating, 2017). Moreover, many advanced HCC patients developed resistance to sorafenib and exhibited poor prognosis (Lin et al., 2020; Xia et al., 2020). Previous research suggested multiple mechanisms were involved in the development of sorafenib resistance, such as RNA N6-methyladenosine (Lin et al., 2020), cancer stem cell (Leung et al., 2021), hypoxia microenvironment (Wu et al., 2020), and ferroptosis (Sun et al., 2016). While the mechanism of sorafenib resistance in HCC patients remains poorly understood, investigating the underlying mechanisms is still of great significance in developing novel therapeutic strategies and exploring promising adjuvant drugs for HCC patients.

Tumor immune microenvironment (TIME), as a contributory part to regulating the progression of tumors, includes mainly tumor-infiltrating lymphocytes and other assorted immune cells, such as T cells, macrophages, natural killer cells, and dendritic cells (Lei et al., 2020). The immune system functions to constantly observe and eliminate pre-cancerous cells to prevent the progression to tumor. However, suppression of the immune system contributes to tumor escape and progression (Marzagalli et al., 2019). Recently researchers have also found that immunocytes play critical roles in tumor development and chemotherapy response by cross-talking with tumor cells, including tumor-associated neutrophils (Zhou et al., 2016), natural killer cells (Sprinzl et al., 2013), T cells (Zhou et al., 2016), regulatory T cells (Granito et al., 2021), and tumor-associated macrophages (Zhang et al., 2010; Zhou et al., 2016). Although the biological mechanisms of sorafenib resistance have been explored extensively, the relationship between sorafenib resistance and the TIME in HCC remains to be elusive.

Given limited investigation determining the sorafenib-resistant TIME during HCC development and progression, this study aimed to evaluate the relationship between sorafenib resistance and the TIME and explore a promising drug to overcome sorafenib resistance in HCC patients. Our results suggest that NR6A1, CXCL5, C3, and TGFB1 are critical DEIRGs in sorafenib-resistant cells, which are markedly associated with the survival time of HCC patients and infiltration levels of immune cells. NAL may serve as an adjuvant drug for sorafenib-resistant HCC treatment.

Materials and methods

Data acquisition

The transcriptional data of three parental HCC and five sorafenib-resistant HCC xenografts in the GEO dataset (GSE121153) were obtained for immune cell infiltration analysis. Gene expression data of sorafenib-resistant and control HCC cells were downloaded from the GEO dataset (GSE94550) for gene expression differential analysis. Immune-related genes (IRGs) were obtained from the Immunology Database and Analysis Portal (ImmPort; http://www.immport.org/) (Bhattacharya et al., 2018). Transcriptome sequencing profiles and clinical characteristics of LIHC (liver hepatocellular carcinoma) for differentially expressed gene (DEG) examination and survival analysis were obtained from the TCGA GDC data portal (https://portal.gdc.cancer.gov/), including 371 LIHC and 86 non-LIHC tissue samples.

Immune cell infiltration analysis by CIBERSORT

CIBERSORT is an analytical tool to estimate the composition of member cell types in a mixed cell population by gene expression profiles (https://cibersort.stanford.edu/) (Newman et al., 2015). The "CIBERSORT R" package with LM22, a leukocyte gene signature matrix including 22 human immune cell types, was applied to analyze immune cell infiltration among parental and sorafenib-resistant HCC xenografts in the GSE121153 dataset.

Gene set enrichment analysis in sorafenib-resistant hepatocellular carcinoma cells

Gene set enrichment analysis (GSEA) analysis was performed using GSEA software (V4.1.0) with Gene Ontology (GO) and Kyoto Encyclopedia of Genes and Genomes (KEGG) pathway gene sets between sorafenib-resistant and control HCC cells (GSE94550) to explore different biological functions (Subramanian et al., 2005).

Differential expression analysis between sorafenib-resistant and control hepatocellular carcinoma cells

The "limma R" package was performed to analyze the microarray data between sorafenib-resistant and control HCC cells. The threshold of adjusted $p < 0.05$ and absolute fold change (log2) > 1 was established to screen DEGs. DEIRGs were obtained from overlapped DEGs based on the ImmPort database. The volcano plots and heat maps were presented by R.

Functional enrichment analyses for differentially expressed immune-related genes

To explore the functions among DEIRGs, Gene Ontology (GO) functional annotations and KEGG pathway enrichment analysis were conducted using the Database for Annotation, Visualization, and Integrated Discovery (DAVID: https://david.ncifcrf.gov/) (Huang da et al., 2009). The immune-related GO terms of the GO Circle plot were performed by the "GOplot R" package (Walter et al., 2015). Furthermore, the KEGG pathway was plotted using the "ggplot2 R" package.

Association and mutation analysis of differentially expressed immune-related genes

Pearson's analysis of DEIRGs was carried out based on TCGA expression data using the "corrplot R" package. DEIRG mutation analysis in LIHC patients was performed using the "maftools R" package.

Identification of prognosis-related differentially expressed immune-related genes

Univariate Cox regression analysis was conducted to discover potential prognostic biomarkers. The results were plotted by the "forestplot R" package. Those with $p < 0.05$ were selected as prognosis-related DEIRGs. The relationship between potential prognostic DEIRGs and critical targets of the sorafenib-related pathway was explored by Pearson's analysis. Kaplan–Meier analysis was performed to verify the prognostic value of DEIRGs. In addition, the nomogram of prognosis-related DEIRGs, clinical characteristics, pathologic stage, and survival probability of TCGA-LIHC patients were plotted by the "rms" package of R software based on the Cox proportional hazard regression model.

UALCAN analysis

UALCAN (http://ualcan.path.uab.edu) is a comprehensive online platform to explore cancer data and validate the genes of interest (Chandrashekar et al., 2017). UALCAN was used to analyze the relative expression of prognosis-related DEIRGs between normal samples and HCC patients of different clinicopathological stages in TCGA.

Immune cell infiltration and prognosis-related differentially expressed immune-related gene expression

Tumor Immune Estimation Resource (TIMER) was used to analyze the association between tumor-infiltrating immune cells and prognosis-related DEIRGs. TIMER is a public database containing 32 types of cancers and 10,897 TCGA samples and provides a web tool for analysis and visualization of the six kinds of immunocyte infiltration in tumor samples (Li et al., 2017).

Single-cell expression of prognosis-related differentially expressed immune-related genes in liver

The expression of prognosis-related DEIRGs in different liver cell types was explored in The Single-Cell-Type Atlas (https://www.proteinatlas.org/) (Uhlén et al., 2015). The Single-Cell-Type Atlas includes single-cell RNA sequencing (scRNA-seq) data of 13 human tissues. The scRNA-seq comprises 192 different cell type clusters in 12 main cell type groups. The expression of selected genes expressed in each cell type will be plotted using interactive Uniform Manifold Approximation and Projection for Dimension Reduction (UMAP).

Identification of small bioactive molecules

DEIRGs between sorafenib-resistant and control groups were analyzed to identify potential small molecules using the Connectivity Map (CMap) database. The CMap, a web-based tool, can be applied to predict the biochemical interactions of small molecules with disease-related gene signature, thus helping researchers find novel uses for existing drugs and understanding the molecular mechanisms of diseases (Lamb et al., 2006).

Cell culture and sorafenib-resistant cell line establishment

The mouse HCC cell line Hepa1-6 and human HCC cell line Huh7 were purchased from the cell bank of the Chinese Academy of Science (Shanghai, China). The cells were cultured in Dulbecco's modified Eagle's medium (DMEM) (KeyGEN, Nanjing, China) with 10% fetal bovine serum (FBS) (Sigma, Saint Louis, United States) and 100 U/ml of penicillin and 50 μg/ml strepomycin (Gibco, California, United States) in a 37°C humidified incubator containing 5% CO_2. Sorafenib-resistant cell lines were established as previously described (Jiang et al., 2018; Lu et al., 2018; Xu et al., 2020). Hepa1-6 and Huh7 cells were cultured in DMEM containing 1 μM sorafenib for 2 weeks. The sorafenib concentration of the culture medium is increased slowly by 0.5 μM per week for 4–5 months until the cells can survive in 10 μM sorafenib concentration. The sorafenib-resistant cell lines Hepa1-6 and Huh7 were obtained, termed Hepa1-6-SR and Huh7-SR, and continuously cultured in DMEM with sorafenib.

RNA extraction, reverse transcription, and qRT-PCR

Total RNA was extracted by TRIzol reagent (Takara, Japan). Reverse transcription was performed using 1 μg RNA by the Hifair® II 1st Strand cDNA Synthesis Kit (Yeasen, Shanghai, China). The qRT-PCR assay was conducted by Hieff® qPCR SYBR Green Master Mix (Yeasen, Shanghai, China) according to the manufacturer's instruction. β-actin was used as an internal control, and the relative expression levels of target genes were analyzed using the $2^{-\Delta\Delta CT}$ method. The PCR primers used in this study are listed in Supplementary Table S1.

Cell viability assay

Cell viability was assessed using the cell counting kit 8 (CCK-8) (Beyotime, Shanghai, China) according to the manufacturer's protocol. 1×10^4 HCC cells per well were cultured in 96-well plates and treated with different concentrations of sorafenib with or without nalidixic acid (NAL). After incubation at 37°C for indicated times, 10 μL of CCK-8 medium in each well was added to the cells and incubated for additional 60 min. The absorbance was determined at 450 nm using a spectrophotometer (Thermo Fisher, California, United States).

Half-maximal inhibitory concentration (IC_{50}) assay

Sorafenib-resistant cells were cultured in 96-well plates in 1×10^4 cells per well with fresh medium containing nalidixic acid (0, 1, 5, 10, 20, and 50 μg/ml). After 48 h incubation at 37°C, CCK-8 was used to evaluate cell viability by using a spectrophotometer (Thermo Fisher, California, United States) at 450 nm. The IC_{50} values were calculated by comparing the absorbance and inhibition rate.

Tumor xenograft mouse model

All the mice were purchased from Shanghai Laboratory Animal Company (Shanghai, China) and fed in specific pathogen-free (SPF) conditions. The animal study was approved by the Animal Care and Use Committee at Zhongshan Hospital of Fudan University.

To establish a liver orthotopic xenograft mouse model, 5×10^6 Hepa1-6 and Hepa1-6-SR cells were subcutaneously injected into the back flanks of two C57BL/6 mice. After 2 weeks, resecting the subcutaneous tumors and dissecting into 3-mm^3 tissue masses in volume were carried out. Then, the tumor masses were planted into other mouse livers under anesthesia. The mice were euthanized after 4 weeks, and tumors were harvested and weighed.

To establish the subcutaneous xenograft mouse model, 5×10^6 Hepa1-6 and Hepa1-6-SR cells were subcutaneously injected into the back flanks of C57BL/6 mice. After 2 weeks, the tumor-bearing mice were treated with sorafenib (30 μg/g/mouse; daily, oral gavage) and sorafenib combined nalidixic acid (50 μg/g/mouse; daily, oral gavage) for additional 2 weeks. The tumor length and width were recorded every 3 days. Tumor volumes were calculated as length × $width^2$ × 0.5.

Immunohistochemistry

Mouse tumor tissues were fixed in 4% paraformaldehyde and embedded in paraffin. After deparaffinization and rehydration, the tissue sections were subjected to immunohistochemistry (IHC) analysis. The images were captured using a light microscope (Olympus, Tokyo, Japan). The primary antibody Ki-67 (1:500, Abclonal, Wuhan, China) was used in this study.

Multiplex immunofluorescence staining

Multiplex immunofluorescence (mIF) staining was performed using Opal 7-Color fIHC Kit (PerkinElmer, Waltham, United States) according to protocols which have been described previously (Parra et al., 2017; Parra et al., 2018). The

embedded tumor tissues that underwent deparaffinization and rehydration were heated at 95°C for 20 min using Tris–EDTA buffer or citrate buffer to retrieve antigen. Next, the slides were incubated with primary antibodies overnight at 4°C. Then, the slides were washed three times with 2-methyl-2H-isothiazol-3-one and incubated with horseradish peroxidase (HRP)-conjugated secondary antibody for 10 min at room temperature. Next, the slides were incubated at room temperature for 10 min with one of the following Alexa Fluor tyramides included in the Opal 7 kit to detect antibody staining. After BOND Wash Solution washing, the slides were counterstained with DAPI for 5 min to visualize nuclei and then mounted with glycerine. The slides were scanned using the Pannoramic MIDI System (3DHISTECH, Budapest, Hungary). The following primary antibodies are used in this study: CD8 (1:50, Servicebio, Wuhan, China), Ly-6G (1:200, Servicebio, Wuhan, China), and F4/80 (1:200, Servicebio, Wuhan, China).

Flow cytometry

Tumor tissues were resected from mice and minced into small pieces and then were lysed by 1 mg/ml collagenase IV (Sigma, United States) and DNase I (Invitrogen, United States) for 1 h at 37°C. Afterward, the tissue medium was filtrated using a 70-μm filter screen to obtain single-cell suspensions. The cell suspensions were stained with antibodies for 30 min and washed three times by PBS and then were subjected to FCM analysis. The following reagents and antibodies were used in FCM analysis.

Panel A: LIVE/DEAD™ Fixable Stain (Invitrogen, California, United States), anti-mouse CD45-BV605 (Biolegend, California, United States), anti-mouse CD3-PE-cy7 (Biolegend, California, United States), anti-mouse CD4-Efluor450 (BD, New Jersey, United States), anti-mouse CD8-Percp-cy5.5 (Biolegend, California, United States), anti-mouse CD19-BV650 (Biolegend, California, United States), and anti-mouse NK1.1-PE (Biolegend, California, United States).

Panel B: LIVE/DEAD™ Fixable Stain (Invitrogen, California, United States), anti-mouse CD45-BV605 (Biolegend, California, United States), anti-mouse CD11b-Percp-cy5.5 (Biolegend, California, United States), anti-mouse F4/80-PE (Biolegend, California, United States), and anti-mouse Ly6G-APC (Biolegend, California, United States).

Statistical analysis

R software (v4.0.3), GraphPad Prism (v9.0), and SPSS (v21.0) were used for statistical analysis. All experiments were performed at least three times. Data were presented as mean ± SD. Unpaired Student's t tests were used to analyze the difference between two groups. For different group comparison, one-way analysis of variance (ANOVA) was performed. $p < 0.05$ was considered statistically significant.

Results

The immune microenvironment analysis and differentially expressed immune-related gene identification in sorafenib-resistant hepatocellular carcinoma

While clinical practice using sorafenib monotherapy, or in combination with other agents, has been disappointing, it is worthwhile to understand why sorafenib is resistant to therapy using the tumor microenvironment.

At first, the immune microenvironment in five sorafenib-resistant and three parental HCC xenografts was analyzed. The infiltration levels of 22 immunocyte types between sorafenib-resistant and control HCC cells were explored using the CIBERSORT R package. Immunocyte infiltration percentages of each subtype are presented (Figure 1A), and the heatmap was also constructed to determine infiltration levels of the significant 14 immunocyte types (Figure 1B). The infiltration patterns of immunocytes between sorafenib-resistant and parental HCC xenografts were further explored. The results found that six tumor-infiltrating immunocytes ($CD8^+$ T cells, M0 macrophages, M2 macrophages, neutrophils, resting NK cells, and activated dendritic cells) were associated with sorafenib resistance (Figure 1C). The infiltration of $CD8^+$ T cells, M0 macrophages, and activated dendritic cells was downregulated in sorafenib-resistant HCC, while M2 macrophages, neutrophils, and resting NK cells were upregulated. We then performed the GSEA of the expression data based on hallmark gene sets to identify signaling pathways in sorafenib-resistant HCC cells using the GSE94550 dataset. The results revealed that several immune-related signaling pathways, including positive regulation of T cell activation and lymphocyte differentiation, interleukin-12 production, TGF-α signaling *via* NF-κB, and NK cell-mediated cytotoxicity, were enriched (Figure 1D). Meanwhile, sorafenib-mediated pathways are also enriched, including RAB protein signal transduction, apoptosis, and positive regulation of response to endoplasmic reticulum stress (Supplementary Figure S1A).

Next, the DEGs between sorafenib-resistant and control cells were also screened. A total of 292 genes were identified as DEGs, comprising 175 upregulated and 117 downregulated genes (Supplementary Figures S1B,C), and overlapped with 2,498 immune-related genes from the ImmPort database. The included 23 upregulated and 11 downregulated genes were further identified as DEIRGs (Table 1). The volcano plots and heat maps were presented (Figures 2A,B), which provides a compendium of gene expression between sorafenib-resistant and control HCC groups. Together, these data indicate

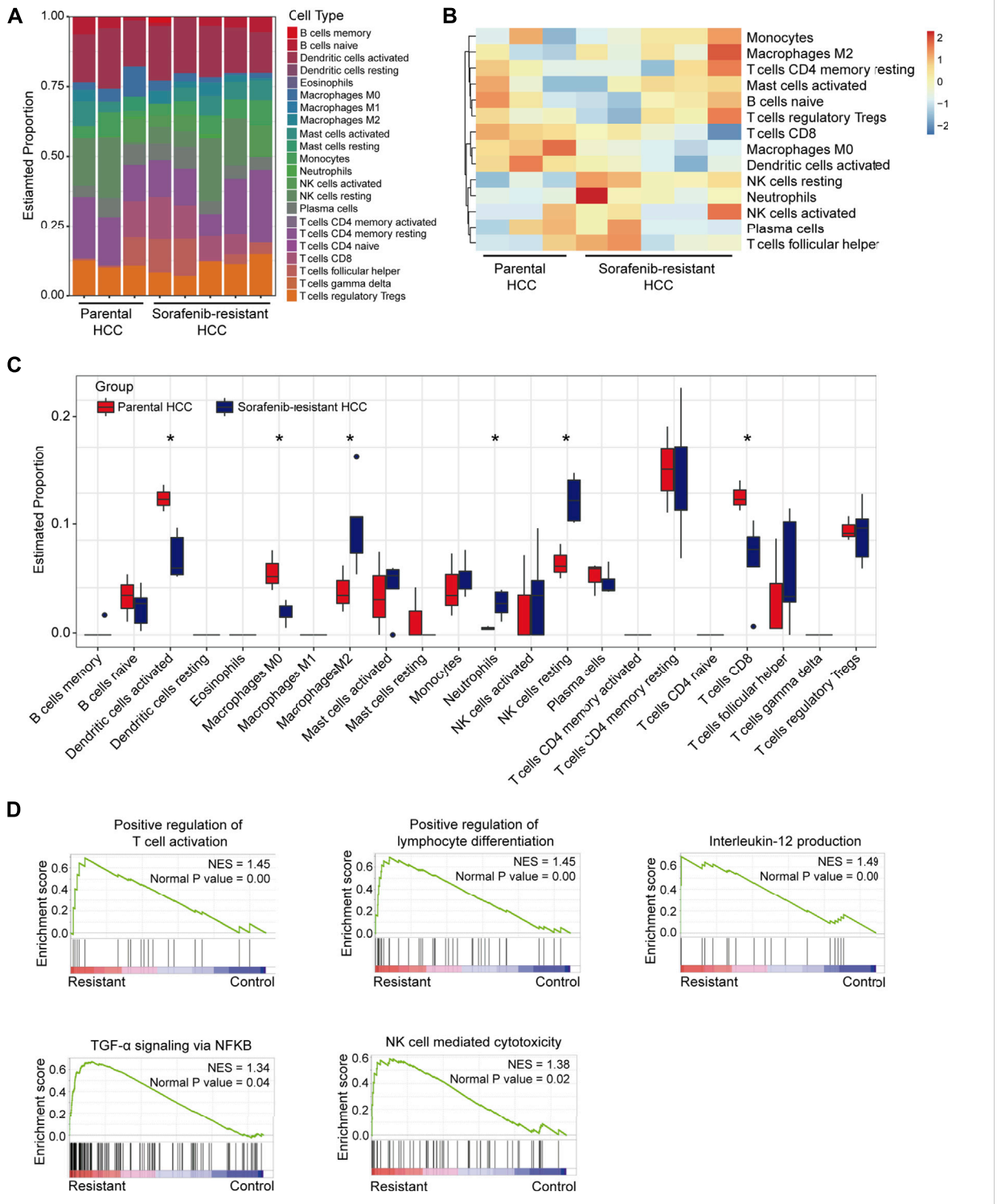

FIGURE 1
Immunocyte infiltration levels and immune-associated signaling pathways in sorafenib-resistant HCC. **(A)** Infiltration levels of 22 types of immune cells in five sorafenib-resistant and three parental HCC xenografts. **(B)** Infiltration heatmap of major 14 types of immune cells. **(C)** Infiltration differences of 22 types of immune cells between sorafenib-resistant and parental HCC xenografts. **(D)** Enrichment plots showing the immune-associated signaling pathways in sorafenib-resistant HCC cells.

TABLE 1 DEIRGs in sorafenib-resistant HCC cells.

ID	ConMean	ResistMean	LogFC	Adjust *p* value
OLR1	7.458849	16.09118	8.63	7.65E-08
CXCL5	8.301718	15.0951	6.79	2.54E-05
SLPI	5.02033	11.18248	6.16	0.00213
TMSB4XP8	11.10576	16.79371	5.69	0.000411
C3	9.039247	13.62951	4.59	0.0239
TNC	4.868948	9.292524	4.42	0.000547
TMSB4X	11.9336	15.99538	4.06	0.000705
STC1	4.098038	8.150799	4.05	0.0142
DEFB1	5.217232	9.037453	3.82	6.15E-05
PLTP	6.982715	10.57509	3.59	5.70E-05
KLRC3	5.133362	8.454206	3.32	0.000379
SEMA3C	5.409964	8.658344	3.25	1.15E-06
SAA2	5.071765	8.300421	3.23	0.0189
TGFB2	9.72438	12.94728	3.22	0.000235
KLRC2	5.564573	8.726469	3.16	8.88E-05
IFNGR1	8.916841	11.81208	2.9	3.45E-05
PDGFD	4.628085	7.490103	2.86	2.21E-06
SAA1	5.578131	8.279558	2.7	0.0346
F2RL1	6.660483	9.310876	2.65	3.67E-05
TGFB1	8.822688	11.33489	2.51	0.00229
TNFRSF10A	6.300875	8.657604	2.36	2.92E-06
GBP2	6.467234	8.828952	2.36	0.0175
ULBP3	4.888659	7.105909	2.22	0.026
DKK1	12.0003	9.934429	−2.07	0.00101
JAG1	14.50584	12.40063	−2.11	0.0148
MBL2	7.87852	5.745177	−2.13	0.000283
SLC40A1	12.60138	10.32488	−2.28	8.62E-05
APOH	13.59051	10.98391	−2.61	0.00799
LGR5	8.182768	5.3616	−2.82	2.16E-05
IL17RB	8.654049	5.802345	−2.85	4.33E-05
NR6A1	10.7923	7.689057	−3.1	2.17E-07
CTSE	10.63313	5.794716	−4.84	0.00499
NTS	9.470508	4.617572	−4.85	0.00079
ANGPTL3	14.94593	9.171327	−5.77	2.64E-06

dysregulated immune-related profiles in sorafenib-resistant HCC cells.

Functional enrichment analyses and mutation signatures of differentially expressed immune-related genes

To explore biological functions of DEIRGs in sorafenib-resistant HCC patients, we conducted functional enrichment analysis using the "GOplot R" package. Based on the GO analysis results, top 10 biological process terms, nine cellular component terms, and 11 molecular function terms are presented (Figure 2C; Supplementary Table S2–S4). Several immune-related GO terms were identified, including "immune response," "inflammatory response," "innate immune response," "type III transforming growth factor beta receptor binding," "type II transforming growth factor beta receptor binding," "acute-phase response," and "transforming growth factor beta receptor binding". The correlations between 12 immune-related GO terms and corresponding DEIRGs are shown (Figure 2D). The dot plot displayed the 10 KEGG pathways with the enrichment levels of DEIRGs (Figure 2E; Supplementary Table S5).

To further explore the underlying signatures of DEIRGs, we constructed a heatmap to show the expression profiles of DEIRGs

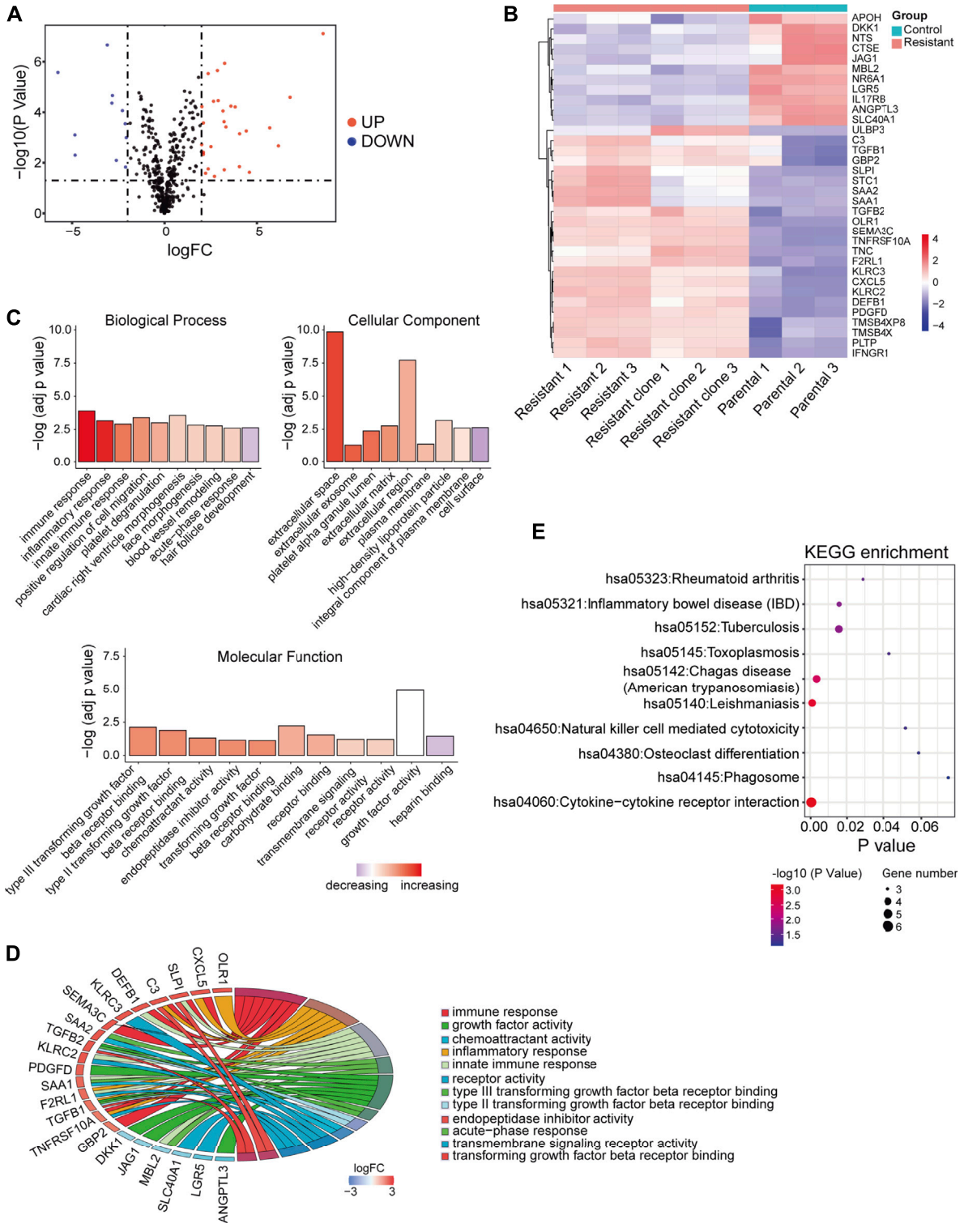

FIGURE 2
DEIRGs between sorafenib-resistant and control cells and functional enrichment analysis. **(A)** Volcano plot of DEIRGs between sorafenib-resistant and control cells. **(B)** Hierarchical clustering heat maps of DEIRGs. **(C)** Bar plot of enriched GO terms in biological process, cell component, and molecular function. **(D)** GOChord plot indicating the relationship between immune-related GO terms and DEIRGs. The color represents upregulation (red) or downregulation (blue). **(E)** Dot plot showing the enriched KEGG pathways in DEIRGs.

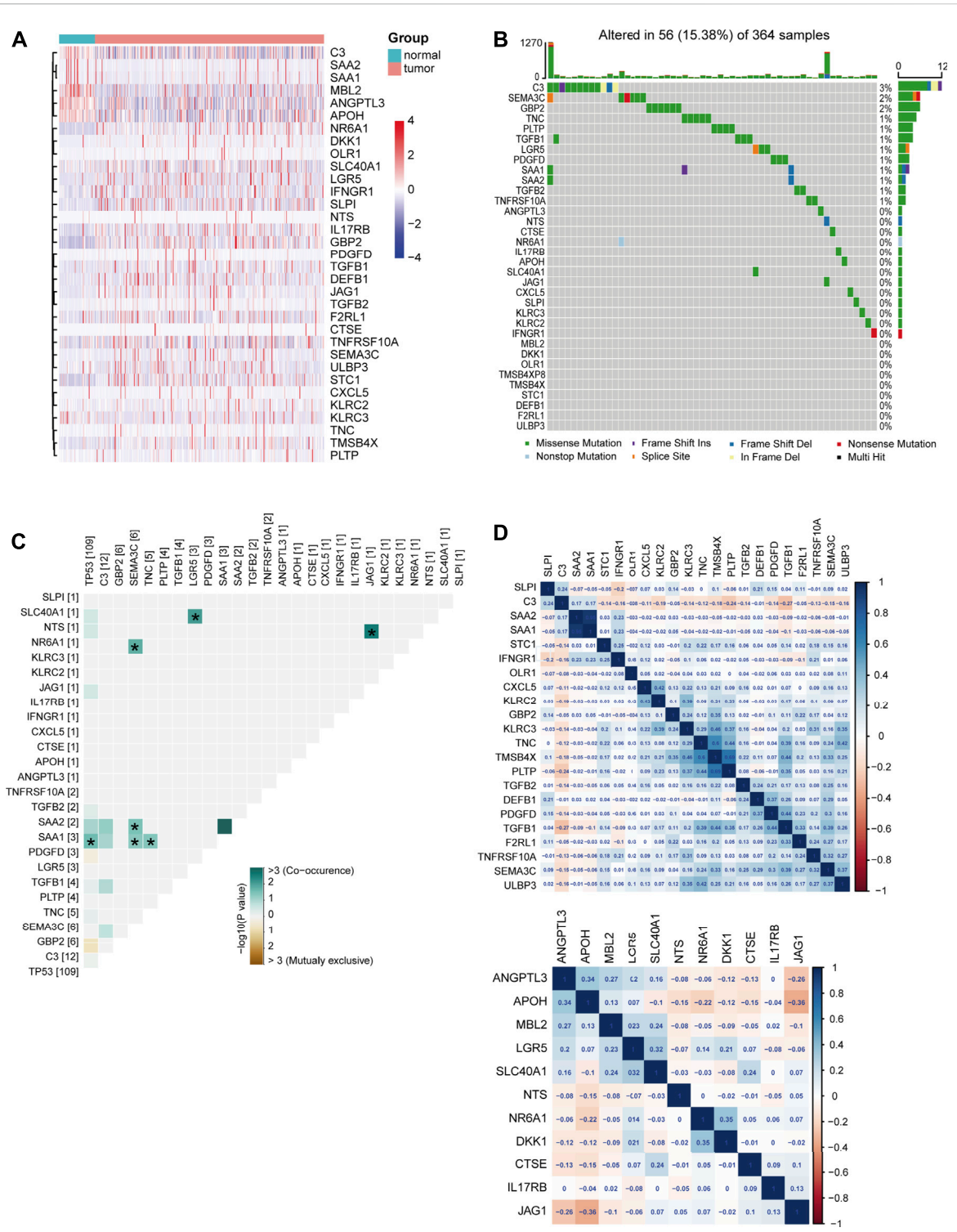

FIGURE 3
Signature of DEIRGs in TCGA-LIHC. **(A)** Expression heatmap of DEIRGs between normal and LIHC patients in TCGA. **(B)** Mutation status of DEIRGs. **(C)** Correlation between mutation status of DEIRGs and *TP53*. **(D)** Expression correlation between DEIRGs. Upper, upregulated DEIRGs; below, downregulated DEIRGs.

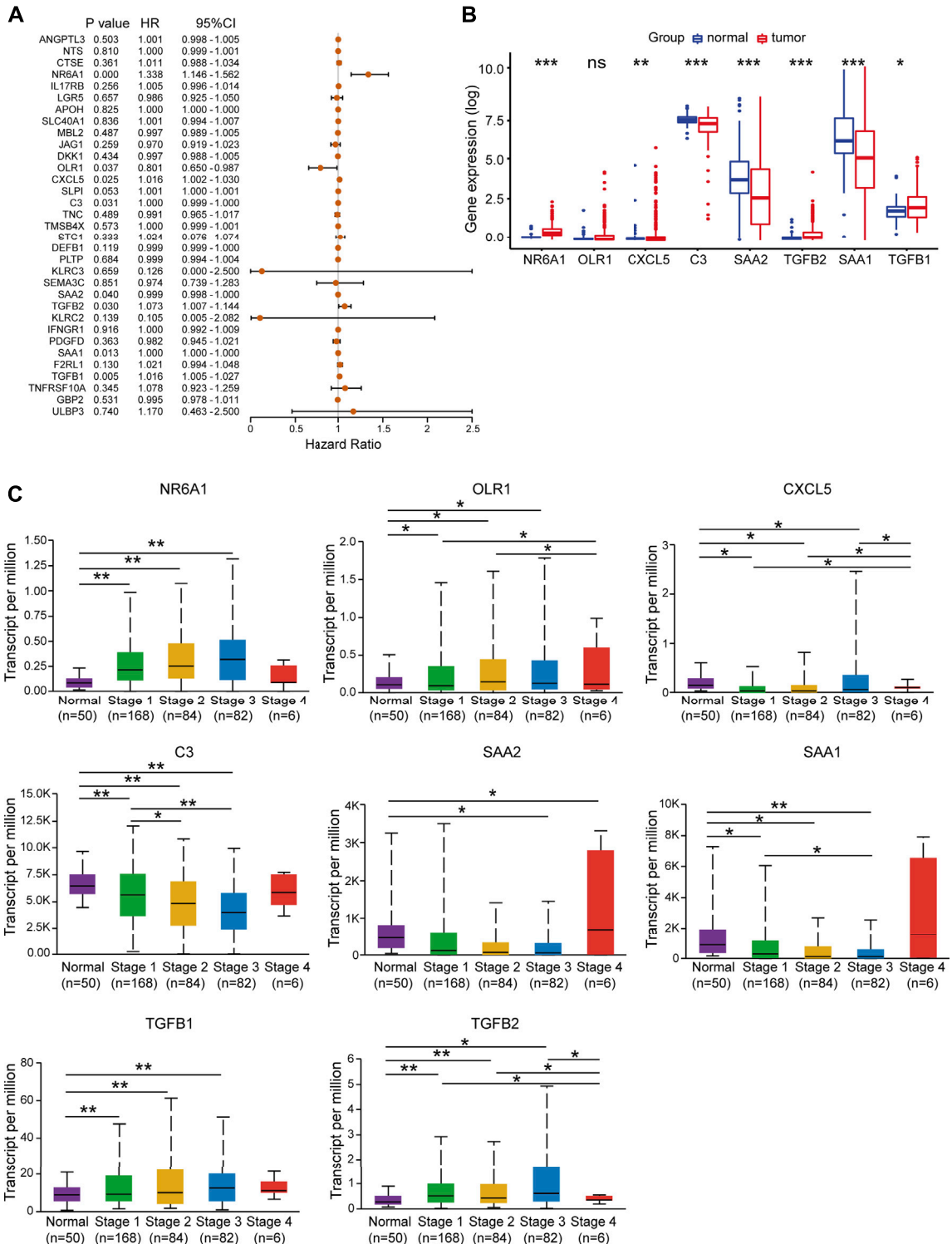

FIGURE 4
Identification of prognosis risk factors of sorafenib resistance. **(A)** Forest plot showing the prognostic values of DEIRGs in univariate Cox proportional hazards regression analysis. **(B)** Expression levels of eight prognosis risk factors between normal and LIHC patients in TCGA. **(C)** Expression levels of eight prognosis risk factors in LIHC patients in different stages.

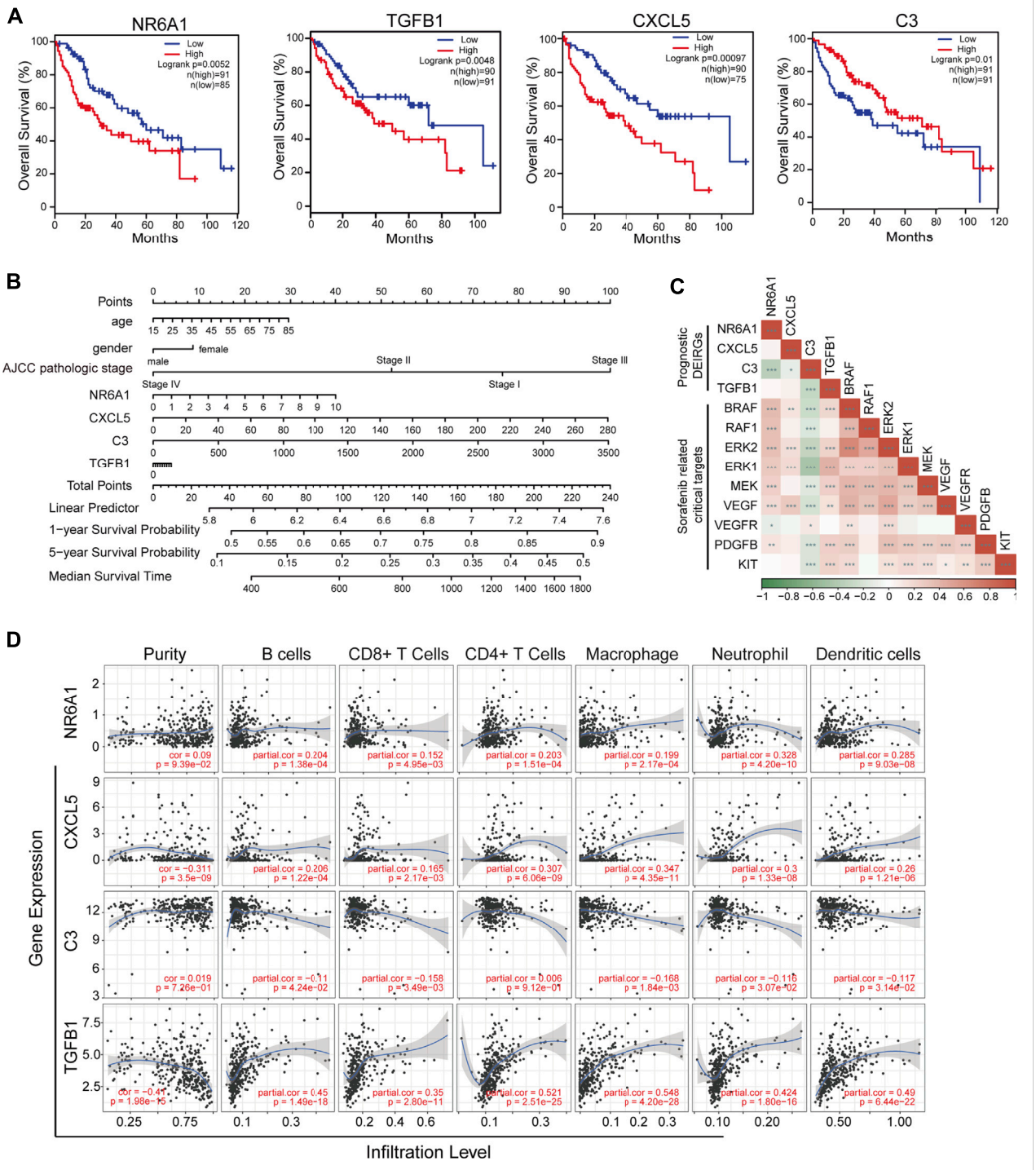

FIGURE 5
Identification of prognostic-related DEIRGs and immune cell infiltration. **(A)** Kaplan–Meier curve analysis overall survival of NR6A1, TGFB1, CXC5, and C3 in LIHC patients. **(B)** Nomogram model showing four independent prognostic DEIRGs and clinical risk factors in LIHC patients. **(C)** Heatmap of expression correlation between the four prognosis risk factors and nine sorafenib-related downstream targets. **(D)** Correlation between immune cell infiltration and prognostic DEIRGs in LIHC patients.

based on the RNA-seq data of LIHC from TCGA (Figure 3A). The mutation signature of DEIRGs was analyzed using the "maftools R" package. The result showed that 25 DEIRGs displayed mutation and C3 has the highest mutation rate (3%;

Figure 3B). *TP53* is the most frequently mutated gene in HCC patients (Yin et al., 2020), and early studies suggested that *TP53* mutation was associated with the response to sorafenib for HCC patients (Gramantieri et al., 2020; Tang et al., 2020). In this study, the correlations between *TP53* and DEIRGs mutations were explored. The results implied that SAA1 is significantly associated with *TP53* mutation (Figure 3C). The correlations of upregulated DEIRGs (upper panel) and downregulated DEIRGs (down panel) were also analyzed (Figure 3D).

The prognostic features of differentially expressed immune-related genes in TCGA-LIHC samples

Next, univariate Cox regression analysis was performed to identify prognosis-related DEIRGs in LIHC ($p < 0.05$). Eight prognosis risk DEIRGs were identified, including six high-risk DEIRGs (NR6A1, CXCL5, C3, TGFB1, TGFB2, and SAA1) and two low-risk DEIRGs (OLR1 and SAA2; Figure 4A). The expression levels of eight prognosis risk DEIRGs in normal and HCC tissues were analyzed. The results found that NR6A1, CXCL5, TGFB1, and TGFB2 were upregulated, while C3, SAA1, and SAA2 were downregulated. Meanwhile, no significant difference was found for OLR1 (Figure 4B), after which the tissue expression of eight prognosis-related DEIRGs between normal and different TNM-stage HCC was evaluated using the UALCAN database (Figure 4C).

To validate the prognostic value of eight selected DEIRGs, we performed Kaplan–Meier analysis for overall survival in TCGA-LIHC patients. According to the survival analysis, four prognostic DEIRGs were identified ($p < 0.05$). The results showed highly expressed NR6A1, CXCL5, and TGFB1, along with lower expressed C3 correlated with poor survival (Figure 5A, Supplementary Figure S2A). A nomogram of integrated scores was developed for predicting 1- and 5-year survival and median survival time. Predictors of the nomogram included four independent prognostic DEIRGs (NR6A1, CXCL5, TGFB1, and C3) and clinical risk factors (including age, gender, and AJCC pathologic stage; Figure 5B). The nomogram model revealed that NR6A1, CXCL5, and C3 were primary risk factors to predict the survival of HCC patients. As a multi-tyrosine kinase inhibitor, sorafenib blocks the RAF-MEK-ERK pathway to inhibit tumor cell proliferation and interacts with vascular endothelial growth factor receptors to attenuate tumor angiogenesis. Therefore, the correlations between four prognostic DEIRGs (including NR6A1, CXCL5, TGFB1, and C3) and sorafenib-mediated nine critical downstream targets (BRAF, RAF1, ERK1, ERK2, MEK, VEGF, VEGFR, PDGFB, and KIT) were individually analyzed in TCGA-LIHC patients. The results revealed that the expression of NR6A1, CXCL5, and TGFB1 was positively correlated with the sorafenib-related key targets, while C3 was negatively related with the sorafenib-related key targets (Figure 5C).

Immune infiltration and single-cell expression of four prognosis-related differentially expressed immune-related genes

The tumor immune estimation resource (TIMER) platform was applied to explore the correlation between infiltration levels of immune cells and the expression of four prognosis-related genes (including NR6A1, CXCL5, TGFB1, and C3). The results demonstrated that CXCL5 and TGFB1 were significantly associated with purity ($p < 0.05$, correlation = −0.311 and −0.41, respectively). Increased expression of NR6A1, CXCL5, and TGFB1 was positively correlated with elevated immune infiltration level ($p < 0.05$); while high C3 expression was negatively associated with the infiltration of B cells, $CD8^+$ T cells, macrophages, neotrophils, and dendritic cells ($p < 0.05$; Figure 5D). Different cell type expression of four selected DEIRGs in the liver was investigated using The Single Cell Type Atlas. The UMAP plots and bar charts showed that NR6A1 and CXCL5 were mainly expressed in cholangiocytes, C3 in hepatocytes, and TGFB1 in T cells, Kupffer cells, Ito cells, and endothelial cells (Supplementary Figures S2B,C), indicating the potential roles of various immunocytes in sorafenib resistance.

Immune cell infiltration analysis in the sorafenib-resistant mouse model

To validate database results, we established a sorafenib-resistant human HCC cell line (Huh7-SR) and mouse HCC cell line (Hepa1-6-SR). The drug resistance of the two cell lines was confirmed using the CCK-8 assay (Figure 6A). NR6A1 was downregulated in sorafenib-resistant cells, while C3, TGFB1, and CXCL5 were upregulated (Figure 6B), which were consistent with former sequencing analysis (Regan-Fendt et al., 2020). To investigate the TIME *in vivo*, we constructed live orthotopic xenograft mice using Hepa1-6 or Hepa1-6-SR cells (Figure 6C). No significant differences were observed for tumor volume and liver/body weight ratio between the two groups (Figure 6D). The immune cell infiltration in tumor tissues was analyzed by FCM (Supplementary Figures S3A,B). The results identified low infiltration levels of $CD8^+$ T cells and high levels of macrophages and neutrophils in sorafenib-resistant mouse HCC tissues. However, no significant infiltration differences were exhibited for $CD4^+$ T cells, B cells, and natural killer (NK) cells (Figure 6E). The mIF of HCC tissues was further performed. The results showed that CD8 was attenuated in sorafenib-resistant tissues, but Ly-6G (neutrophils marker) and F4/80 (macrophages marker) were highly expressed

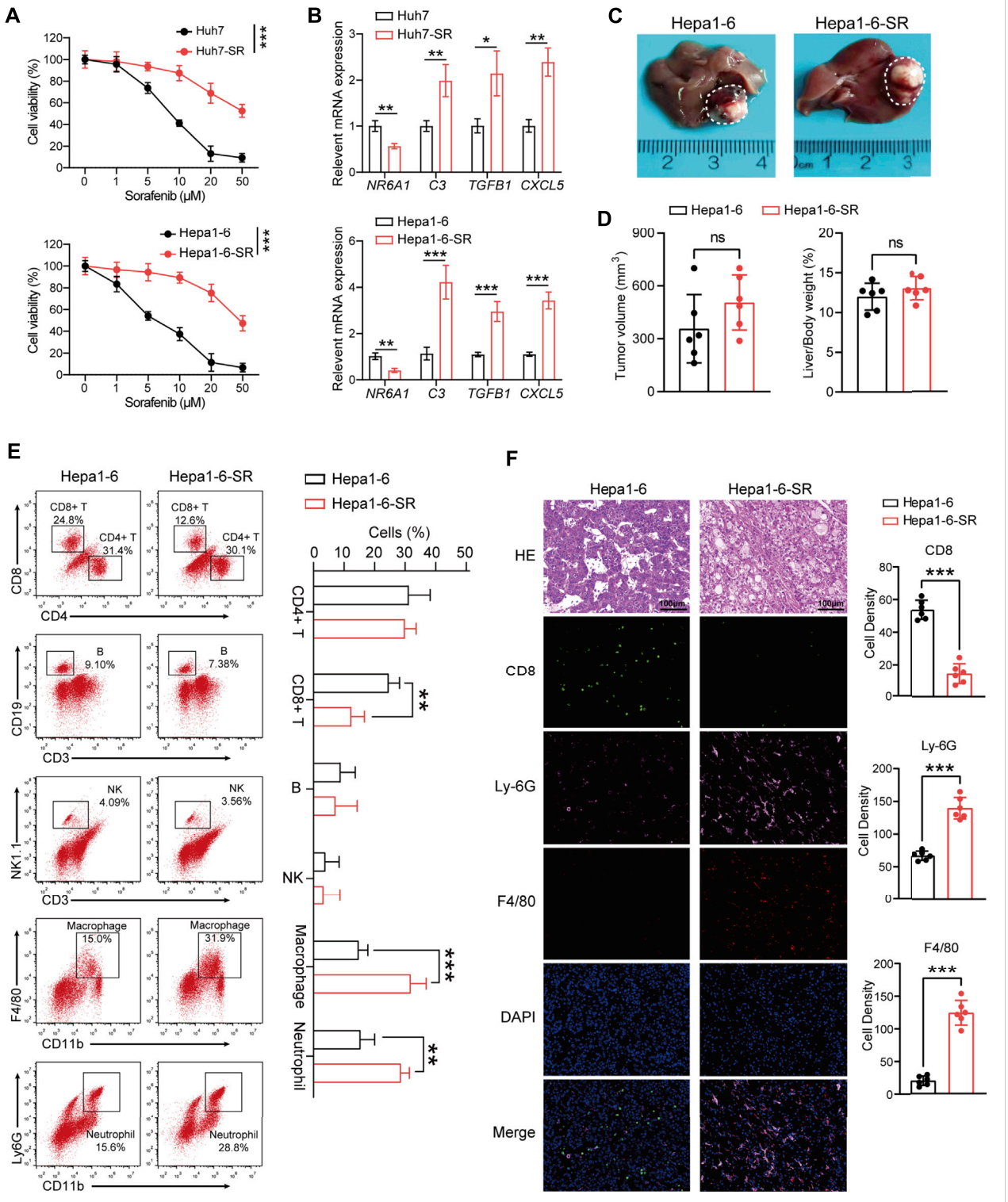

FIGURE 6
Tumor immune microenvironment analysis in the sorafenib-resistant HCC mouse model. **(A)** Two sorafenib-resistant HCC cell lines (Huh7-SR and Hepa1-6-SR) were established and confirmed by CCK-8 assay. **(B)** Expression values of four prognostic DEIRGs in sorafenib-resistant HCC cells. **(C)** Representative images of the liver from a orthotopic xenograft sorafenib-resistant and control HCC mouse model. **(D)** Tumor volume comparison between the control and sorafenib-resistant HCC mouse model. **(E)** Representative immunocyte infiltration analysis using FCM in the mouse model. **(F)** Multiplex immunofluorescence staining CD8, Ly-6G, and F4/80 in control and sorafenib-resistant HCC tissues.

TABLE 2 Results of CMap analysis.

Small molecule	Mean score	n[a]	Enrichment	*p* value	Specificity	Percent non-null[b]
Nalidixic acid	−0.813	5	−0.934	0	0	100
MG-262	−0.676	3	−0.917	0.00096	0.0709	100
Lasalocid	0.598	4	0.839	0.00103	0.0245	100
Butyl hydroxybenzoate	−0.428	5	−0.774	0.00106	0.0068	80
Etynodiol	0.574	4	0.834	0.00115	0	100
Aceclofenac	−0.5	4	−0.835	0.00131	0	100
Colforsin	0.447	5	0.766	0.0016	0.0101	60
Hydrastinine	−0.402	5	−0.74	0.00234	0.0049	60
Sisomicin	0.415	4	0.812	0.00237	0	75
Chlortetracycline	−0.447	5	−0.74	0.00242	0	80
Digoxigenin	0.455	5	0.741	0.00268	0.0614	80
Benzthiazide	−0.435	4	−0.8	0.00316	0.0102	75
11-deoxy-16, 16-dimethyl prostaglandin E2	0.462	4	0.774	0.00495	0.0245	75
Praziquantel	−0.456	4	−0.767	0.00585	0	75
Piracetam	−0.475	4	−0.744	0.00851	0.0122	75

[a]n: The matching result number of each small molecule applied in different concentration and cell lines.
[b]Percent non-null: The percentage of matching score which is not 0.

(Figure 6F). These results help us obtain a clear understanding concerning the TIME changes in sorafenib-resistant HCC tissues.

Nalidixic acid is an antagonist for sorafenib-resistant hepatocellular carcinoma

The CMap provides a convenient strategy for revealing the connections among small molecules, genetic signatures, and diseases (Lamb et al., 2006). Next, the CMap was utilized to screen potential small molecules for sorafenib-resistant HCC according to the expression of DEIRGs. Fifteen small-molecule drugs were identified according to the screening criteria (absolute mean value > 0.4 and $p < 0.01$). Nalidixic acid (NAL) identified as a prominent drug, which negatively correlated with the expression of DEIRGs in sorafenib-resistant HCC cells (Table 2). Therefore, the treatment effect of NAL was evaluated in sorafenib-resistant HCC cells. The results showed that Hepa1-6-SR cells had lower IC_{50} than Hepa1-6 cells (Figure 7A), indicating more sensitivity for NAL treatment. When treated with NAL, the expression of NR6A1 was upregulated, while those of CXCL5, C3, and TGFB1 were downregulated in Huh7-SR and Hepa1-6-SR cells (Figure 7B). Next, the cell proliferation rate was explored using the CCK-8 assay. The results suggested that the combination of NAL and sorafenib effectively inhibited proliferation of Huh7-SR and Hepa1-6-SR cells (Figure 7C). The treatment effect of NAL was further explored using subcutaneous xenograft mice *in vivo*. The group treated with NAL and sorafenib had smaller volume and lower growth rate than other groups (Figures 7D,E). Moreover, the Ki67 staining exhibited that tissue sections from the synergical NAL and sorafenib group showed a lower proportion of proliferation cells than in other groups (Figure 7F). These evidences suggest that NAL can reverse sorafenib resistance and inhibit sorafenib-resistant HCC cell progression *in vitro* and *in vivo*.

Discussion

Sorafenib can block the proliferation and angiogenesis of tumor cells and has been recommended as the first-line regimen for advanced unresectable HCC patients (Heimbach et al., 2018). Researchers also found that the antitumor effects of sorafenib in other tumors, such as prostate cancer, myeloid leukemia, renal cell carcinoma, and desmoid tumor (Escudier et al., 2007; Kharaziha et al., 2012; Gounder et al., 2018; Burchert et al., 2020). Unfortunately, clinical trials indicated that overall survival time was slightly prolonged for HCC patients treated with sorafenib compared with patients receiving placebo (Llovet et al., 2008; Cheng et al., 2009). The main reason for the decrease is HCC heterogeneity and sorafenib resistance (Zhu et al., 2017). Thus, it is urgent to explore resistant mechanisms and evaluate novel synergistic drugs for sorafenib-resistant HCC patients.

Previous studies showed that overexpressed EGFR and its downstream targets, especially Ras, Raf, MEK, and ERK, might predict inadequate sorafenib response (Ezzoukhry et al., 2012). Additionally, a high circulating level of miR-30e-3p suggested the development of sorafenib resistance (Gramantieri et al., 2020). By CRISPR/Cas9 library screening, researchers found that activation of phosphoglycerate dehydrogenase was positively correlated

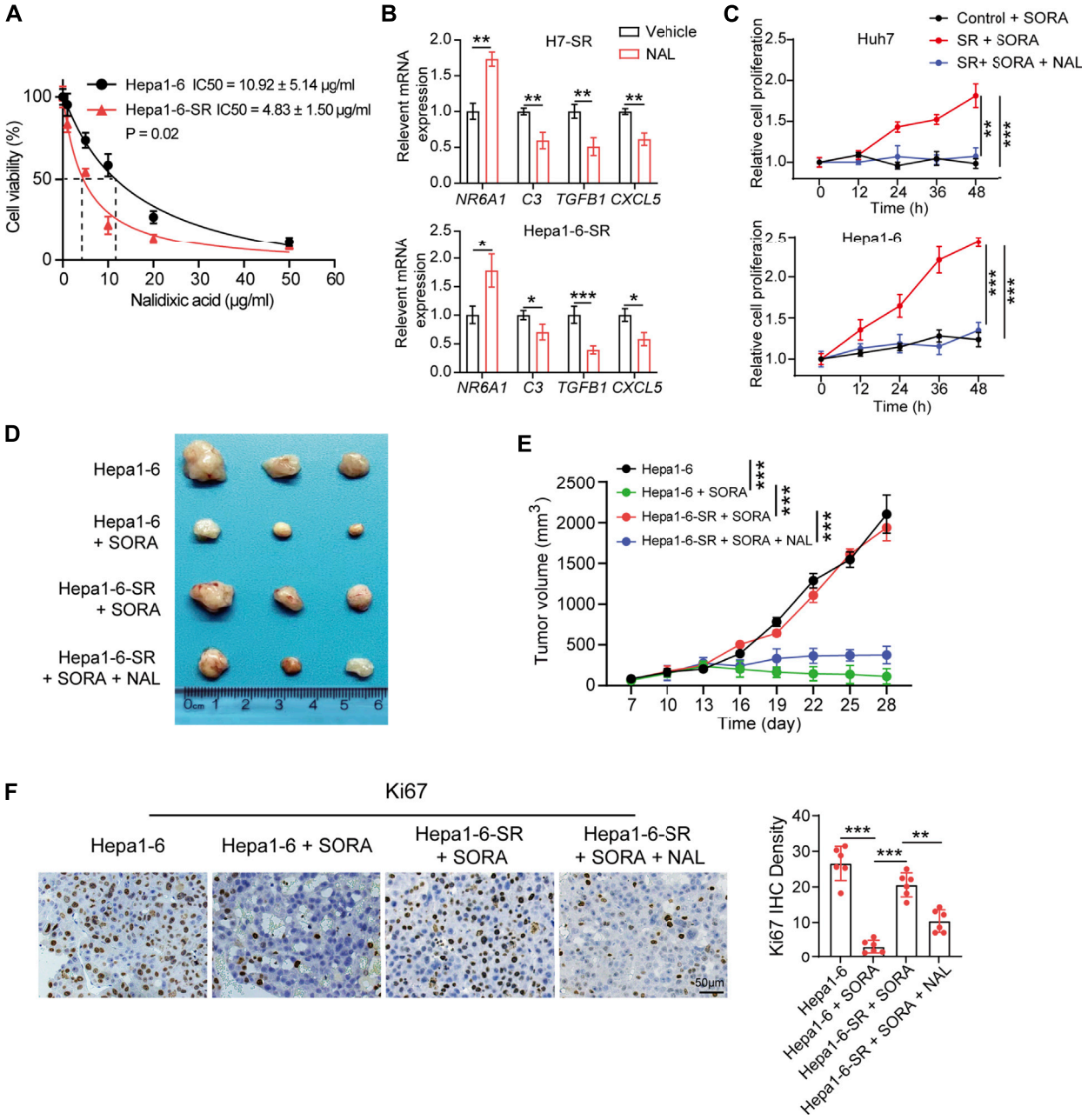

FIGURE 7
Nalidixic acid overcomes sorafenib resistance and inhibits HCC development. **(A)** Cell viability showing the IC_{50} concentrations of nalidixic acid treatment in Hepa1-6-SR and parental Hepa1-6 cells. **(B)** Expression changes of four prognostic DEIRGs (NR6A1, CXCL5, C3, and TGFB1) in sorafenib-resistant HCC cells treated with nalidixic acid. **(C)** CCK-8 assay assessed cell viability in Huh7-SR and Hepa1-6-SR cells treated with sorafenib or sorafenib plus nalidixic acid. **(D)** Representative photos of tumors presented after 4 weeks of different treatments. **(E)** Tumor growth curves of different treatments in the sorafenib-resistant HCC mouse model. **(F)** IHC staining of Ki67 in different treatment groups.

with sorafenib resistance (Wei et al., 2019). Furthermore, CD24 was reported to be upregulated in sorafenib-resistant HCC cell lines, and its depletion led to a significant increase for sorafenib efficacy (Lu et al., 2018). Also, researchers found that part of adverse events occurred during the application of sorafenib, which indicated a better prognosis for HCC patients (Granito et al., 2016). In addition, the tumor microenvironment also plays a critical role in sorafenib response. Hypoxia in solid

tumors is often related with chemotherapy failure, including sorafenib (Méndez-Blanco et al., 2018). Previous studies have also shown that overexpressed hypoxia inducible factor-1α in hypoxic cells regulated various hypoxia-related gene expression to induce sorafenib resistance (Liu et al., 2012). Moreover, Zhou *et al.* proposed that highly expressed CCL2 and CCL17 in tumor-associated neutrophils promoted the infiltration of macrophages and regulatory T cells, thus compromising sorafenib efficacy in HCC (Zhou et al., 2016).

In this study, we assessed immune cell infiltration levels between sorafenib-resistant and parental HCC xenograft using CIBERSORT. The results showed that infiltration levels of M2 macrophages, neutrophils, and resting NK cells were increased, while $CD8^+$ T cells, M0 macrophages, and activated dendritic cells were less infiltrated in sorafenib-resistant HCC. We further confirmed that high levels of macrophages and neutrophils and low levels of $CD8^+$ T cells in the sorafenib-resistant mouse HCC model were observed. Moreover, GSEA results showed that several immune pathways are highly enriched in sorafenib-resistant cells. These results proved that sorafenib resistance was highly associated with dysfunction of immune cells and signaling pathways.

According to recent studies, immune checkpoints and cytokines are closely related to sorafenib resistance (Liu and Qin, 2019). Chen *et al.* found that combinational anti–PD-1 antibody and sorafenib provide a promising option for small subsets of HCC patients (Chen et al., 2016). Furthermore, upregulated CCL22 could forcefully promote sorafenib resistance in HBV-associated HCC (Gao et al., 2020). Here, we analyzed the expression profiles between sorafenib-resistant and control HCC cells and identified 33 DEIRGs. TCGA-LIHC database analysis showed that the selected 33 DEIRGs have a lower mutation rate in HCC patients, in which only SAA1 mutation significantly co-occurred with *TP53* mutation. Further univariate Cox regression and Kaplan–Meier analysis identified that the expression levels of NR6A1, CXCL5, C3, and TGFB1 were significantly associated with overall survival time of HCC patients. TIMER database results showed NR6A1, CXCL5, C3, and TGFB1 were positively associated with immunocyte infiltration.

NR6A1, a nuclear hormone receptor family member, regulated lipogenesis through mTORC1 in HepG2 cells (Wang et al., 2019). However, the relationship between NR6A1 and immunocyte infiltration was less known. CXCL5 is one of the critical proinflammatory chemokines in the TME (Zhang et al., 2020). It can mediate immune cell infiltration and promote angiogenesis, tumor growth, and metastasis by binding to its receptor, C-X-C motif chemokine receptor 2 (CXCR2) (Zhou et al., 2012; Romero-Moreno et al., 2019). In HCC, Zhou et al. found that stem-like cells secreted high levels of CXCL5 to recruit neutrophil infiltration, and increased CXCL5 expression is associated with poor survival (Zhou et al., 2019). It has been reported that TGFB1 was involved in regulating autophagy in tumors (Nüchel et al., 2018; Liang et al., 2020). In addition, researchers found that sorafenib can alleviate hepatic fibrogenesis by inhibiting TGFB1 expression in the 3D co-culture model of fatty hepatocyte and hepatic stellate cells (Romualdo et al., 2021). C3 is an essential component of innate immune system and participates in detecting and clearing potential pathogens in hosts (Delanghe et al., 2014). Highly expressed C3 was found in tumor metastatic models (Boire et al., 2017) and associated with tumor growth (Aykut et al., 2019).

Few systemic therapies have been shown to improve survival time in advanced HCC patients who fail to respond to sorafenib. A clinical trial showed that regorafenib can significantly improve overall survival time than placebo for HCC patients with limited therapy response to sorafenib (Bruix et al., 2017). Regorafenib can act on multiple targets involved in angiogenesis, cell proliferation, and modulate antitumor immunity in HCC (Granito et al., 2021). In this study, we explored the potential molecular drugs that might be effective for sorafenib-resistant HCC patients using the CMap. Among the identified 15 drugs, a highly negative correlation between NAL and the expression of DEIRGs was found. The *in vitro* and *in vivo* studies showed NAL effectively inhibited sorafenib-resistant HCC cells. These findings suggested that NAL was a promising antagonist for sorafenib-resistant HCC treatment. It should be noted that there are still limitations. First, our research data were originally explored by bioinformatics analysis using public resources, and large sample sizes and further experiments are needed to validate our findings. Second, the DEIRGs of sorafenib resistance are valuable to examine the significance of key risk factors, thus predicting therapy response in real-world HCC patients receiving sorafenib. Third, NAL was commonly used as an antibiotic and anti-inflammatory agent (Luo et al., 2022). However, the exact antitumor mechanism and immune microenvironment changes mediated by NAL in sorafenib-resistant HCC patients need further investigation.

In summary, our study explored the TIME in sorafenib-resistant HCC and found low levels of $CD8^+$ T cell infiltration along with high levels of macrophages and neutrophils. NR6A1, CXCL5, C3, and TGFB1 were critical DEIRGs in sorafenib-resistant cells, which were markedly associated with the survival time of HCC patients and infiltration levels of immune cells. Finally, the therapeutic effect of NAL was explored, which might serve as an adjuvant drug for

sorafenib-resistant HCC treatment. These results may help researchers learn the detailed mechanism of drug resistance and facilitate identifying therapeutic targets for HCC patients.

Data availability statement

The datasets presented in this study can be found in online repositories. The names of the repository/repositories and accession number(s) can be found in the article/ Supplementary Material.

Ethics statement

The animal study was reviewed and approved by the Animal Care and Use Committee, Zhongshan Hospital of Fudan University.

Author contributions

Z-YL, D-YZ, X-HL, and T-TL generated the hypothesis and designed the study. Z-YL, D-YZ, X-HL, J-LS, WA, G-CZ, R-CX, FW, X-NY, XS, BD, and X-ZS collected the data. Z-YL, D-YZ, X-HL, J-LS, WA, G-CZ, LD, S-QW, and J-MZ analyzed and interpreted the data. Z-YL, D-YZ, X-HL, X-ZS, and T-TL wrote the manuscript. The authors read and approved the final manuscript.

Funding

This study was partly supported by the National Natural Science Foundation of China (Nos. 81472673, 81672720, and 82173122), and the funding from Shanghai Municipal Population and Family Planning Commission (No. 20174Y0151).

Conflict of interest

The authors declare that the research was conducted in the absence of any commercial or financial relationships that could be construed as a potential conflict of interest.

Publisher's note

All claims expressed in this article are solely those of the authors and do not necessarily represent those of their affiliated organizations, or those of the publisher, the editors, and the reviewers. Any product that may be evaluated in this article, or claim that may be made by its manufacturer, is not guaranteed or endorsed by the publisher.

Supplementary material

The Supplementary Material for this article can be found online at: https://www.frontiersin.org/articles/10.3389/fphar.2022.952482/full#supplementary-material

References

Aykut, B., Pushalkar, S., Chen, R., Li, Q., Abengozar, R., Kim, J. I., et al. (2019). The fungal mycobiome promotes pancreatic oncogenesis via activation of MBL. *Nature* 574, 264–267. doi:10.1038/s41586-019-1608-2

Bhattacharya, S., Dunn, P., Thomas, C. G., Smith, B., Schaefer, H., Chen, J., et al. (2018). ImmPort, toward repurposing of open access immunological assay data for translational and clinical research. *Sci. Data* 5, 180015. doi:10.1038/sdata.2018.15

Boire, A., Zou, Y., Shieh, J., Macalinao, D. G., Pentsova, E., and Massagué, J. (2017). Complement component 3 adapts the cerebrospinal fluid for leptomeningeal metastasis. *Cell* 168, 1101–1113. doi:10.1016/j.cell.2017.02.025

Bray, F., Ferlay, J., Soerjomataram, I., Siegel, R. L., Torre, L. A., and Jemal, A. (2018). Global cancer statistics 2018: GLOBOCAN estimates of incidence and mortality worldwide for 36 cancers in 185 countries. *Ca. Cancer J. Clin.* 68, 394–424. doi:10.3322/caac.21492

Bruix, J., Qin, S., Merle, P., Granito, A., Huang, Y. H., Bodoky, G., et al. (2017). Regorafenib for patients with hepatocellular carcinoma who progressed on sorafenib treatment (RESORCE): A randomised, double-blind, placebo-controlled, phase 3 trial. *Lancet* 389, 56–66. doi:10.1016/s0140-6736(16)32453-9

Burchert, A., Bug, G., Fritz, L. V., Finke, J., Stelljes, M., Röllig, C., et al. (2020). Sorafenib maintenance after allogeneic hematopoietic stem cell transplantation for acute myeloid leukemia with FLT3-internal tandem duplication mutation (SORMAIN). *J. Clin. Oncol.* 38, 2993–3002. doi:10.1200/jco.19.03345

Chandrashekar, D. S., Bashel, B., Balasubramanya, S. A. H., Creighton, C. J., Ponce-Rodriguez, I., Chakravarthi, B., et al. (2017). Ualcan: A portal for facilitating tumor subgroup gene expression and survival analyses. *Neoplasia* 19, 649–658. doi:10.1016/j.neo.2017.05.002

Chen, J., Ji, T., Zhao, J., Li, G., Zhang, J., Jin, R., et al. (2016). Sorafenib-resistant hepatocellular carcinoma stratified by phosphorylated ERK activates PD-1 immune checkpoint. *Oncotarget* 7, 41274–41284. doi:10.18632/oncotarget.8978

Cheng, A. L., Kang, Y. K., Chen, Z., Tsao, C. J., Qin, S., Kim, J. S., et al. (2009). Efficacy and safety of sorafenib in patients in the asia-pacific region with advanced hepatocellular carcinoma: A phase III randomised, double-blind, placebo-controlled trial. *Lancet. Oncol.* 10, 25–34. doi:10.1016/s1470-2045(08)70285-7

Delanghe, J. R., Speeckaert, R., and Speeckaert, M. M. (2014). Complement C3 and its polymorphism: Biological and clinical consequences. *Pathology* 46, 1–10. doi:10.1097/pat.0000000000000042

Escudier, B., Eisen, T., Stadler, W. M., Szczylik, C., Oudard, S., Siebels, M., et al. (2007). Sorafenib in advanced clear-cell renal-cell carcinoma. *N. Engl. J. Med.* 356, 125–134. doi:10.1056/NEJMoa060655

Ezzoukhry, Z., Louandre, C., Trécherel, E., Godin, C., Chauffert, B., Dupont, S., et al. (2012). EGFR activation is a potential determinant of primary resistance of hepatocellular carcinoma cells to sorafenib. *Int. J. Cancer* 131, 2961–2969. doi:10.1002/ijc.27604

Gao, Y., Fan, X., Li, N., Du, C., Yang, B., Qin, W., et al. (2020). CCL22 signaling contributes to sorafenib resistance in hepatitis B virus-

associated hepatocellular carcinoma. *Pharmacol. Res.* 157, 104800. doi:10.1016/j.phrs.2020.104800

Gounder, M. M., Mahoney, M. R., Van Tine, B. A., Ravi, V., Attia, S., Deshpande, H. A., et al. (2018). Sorafenib for advanced and refractory desmoid tumors. *N. Engl. J. Med.* 379, 2417–2428. doi:10.1056/NEJMoa1805052

Gramantieri, L., Pollutri, D., Gagliardi, M., Giovannini, C., Quarta, S., Ferracin, M., et al. (2020). MiR-30e-3p influences tumor phenotype through MDM2/TP53 Axis and predicts sorafenib resistance in hepatocellular carcinoma. *Cancer Res.* 80, 1720–1734. doi:10.1158/0008-5472.can-19-0472

Granito, A., Marinelli, S., Negrini, G., Menetti, S., Benevento, F., and Bolondi, L. (2016). Prognostic significance of adverse events in patients with hepatocellular carcinoma treated with sorafenib. *Ther. Adv. Gastroenterol.* 9, 240–249. doi:10.1177/1756283x15618129

Granito, A., Muratori, L., Lalanne, C., Quarneti, C., Ferri, S., Guidi, M., et al. (2021). Hepatocellular carcinoma in viral and autoimmune liver diseases: Role of CD4+ CD25+ Foxp3+ regulatory T cells in the immune microenvironment. *World J. Gastroenterol.* 27, 2994–3009. doi:10.3748/wjg.v27.i22.2994

Heimbach, J. K., Kulik, L. M., Finn, R. S., Sirlin, C. B., Abecassis, M. M., Roberts, L. R., et al. (2018). AASLD guidelines for the treatment of hepatocellular carcinoma. *Hepatology* 67, 358–380. doi:10.1002/hep.29086

Huang da, W., Sherman, B. T., and Lempicki, R. A. (2009). Systematic and integrative analysis of large gene lists using DAVID bioinformatics resources. *Nat. Protoc.* 4, 44–57. doi:10.1038/nprot.2008.211

Jiang, W., Li, G., Li, W., Wang, P., Xiu, P., Jiang, X., et al. (2018). Sodium orthovanadate overcomes sorafenib resistance of hepatocellular carcinoma cells by inhibiting Na(+)/K(+)-ATPase activity and hypoxia-inducible pathways. *Sci. Rep.* 8, 9706. doi:10.1038/s41598-018-28010-y

Keating, G. M. (2017). Sorafenib: A review in hepatocellular carcinoma. *Target. Oncol.* 12, 243–253. doi:10.1007/s11523-017-0484-7

Kharaziha, P., Rodriguez, P., Li, Q., Rundqvist, H., Björklund, A. C., Augsten, M., et al. (2012). Targeting of distinct signaling cascades and cancer-associated fibroblasts define the efficacy of Sorafenib against prostate cancer cells. *Cell Death Dis.* 3, e262. doi:10.1038/cddis.2012.1

Kokudo, N., Takemura, N., Hasegawa, K., Takayama, T., Kubo, S., Shimada, M., et al. (2019). Clinical practice guidelines for hepatocellular carcinoma: The Japan Society of Hepatology 2017 (4th JSH-HCC guidelines) 2019 update. *Hepatol. Res.* 49, 1109–1113. doi:10.1111/hepr.13411

Lamb, J., Crawford, E. D., Peck, D., Modell, J. W., Blat, I. C., Wrobel, M. J., et al. (2006). The connectivity map: Using gene-expression signatures to connect small molecules, genes, and disease. *Science* 313, 1929–1935. doi:10.1126/science.1132939

Lei, X., Lei, Y., Li, J. K., Du, W. X., Li, R. G., Yang, J., et al. (2020). Immune cells within the tumor microenvironment: Biological functions and roles in cancer immunotherapy. *Cancer Lett.* 470, 126–133. doi:10.1016/j.canlet.2019.11.009

Leung, H. W., Leung, C. O. N., Lau, E. Y., Chung, K. P. S., Mok, E. H., Lei, M. M. L., et al. (2021). EPHB2 activates β-catenin to enhance cancer stem cell properties and drive sorafenib resistance in hepatocellular carcinoma. *Cancer Res.* 81, 3229–3240. doi:10.1158/0008-5472.can-21-0184

Li, T., Fan, J., Wang, B., Traugh, N., Chen, Q., Liu, J. S., et al. (2017). Timer: A web server for comprehensive analysis of tumor-infiltrating immune cells. *Cancer Res.* 77, e108–e110. doi:10.1158/0008-5472.can-17-0307

Liang, C., Xu, J., Meng, Q., Zhang, B., Liu, J., Hua, J., et al. (2020). TGFB1-induced autophagy affects the pattern of pancreatic cancer progression in distinct ways depending on SMAD4 status. *Autophagy* 16, 486–500. doi:10.1080/15548627.2019.1628540

Lin, Z., Niu, Y., Wan, A., Chen, D., Liang, H., Chen, X., et al. (2020). RNA m(6) A methylation regulates sorafenib resistance in liver cancer through FOXO3-mediated autophagy. *Embo J.* 39, e103181. doi:10.15252/embj.2019103181

Liu, L. P., Ho, R. L., Chen, G. G., and Lai, P. B. (2012). Sorafenib inhibits hypoxia-inducible factor-1α synthesis: Implications for antiangiogenic activity in hepatocellular carcinoma. *Clin. Cancer Res.* 18, 5662–5671. doi:10.1158/1078-0432.ccr-12-0552

Liu, X., and Qin, S. (2019). Immune checkpoint inhibitors in hepatocellular carcinoma: Opportunities and challenges. *Oncologist* 24, S3–s10. doi:10.1634/theoncologist.2019-IO-S1-s01

Llovet, J. M., Ricci, S., Mazzaferro, V., Hilgard, P., Gane, E., Blanc, J. F., et al. (2008). Sorafenib in advanced hepatocellular carcinoma. *N. Engl. J. Med.* 359, 378–390. doi:10.1056/NEJMoa0708857

Lu, S., Yao, Y., Xu, G., Zhou, C., Zhang, Y., Sun, J., et al. (2018). CD24 regulates sorafenib resistance via activating autophagy in hepatocellular carcinoma. *Cell Death Dis.* 9, 646. doi:10.1038/s41419-018-0681-z

Luo, T., Xu, J., Cheng, W., Zhou, L., Marsac, R., Wu, F., et al. (2022). Interactions of anti-inflammatory and antibiotic drugs at mineral surfaces can control environmental fate and transport. *Environ. Sci. Technol.* 56, 2378–2385. doi:10.1021/acs.est.1c06449

Marzagalli, M., Ebelt, N. D., and Manuel, E. R. (2019). Unraveling the crosstalk between melanoma and immune cells in the tumor microenvironment. *Semin. Cancer Biol.* 59, 236–250. doi:10.1016/j.semcancer.2019.08.002

Méndez-Blanco, C., Fondevila, F., García-Palomo, A., González-Gallego, J., and Mauriz, J. L. (2018). Sorafenib resistance in hepatocarcinoma: Role of hypoxia-inducible factors. *Exp. Mol. Med.* 50, 1–9. doi:10.1038/s12276-018-0159-1

Newman, A. M., Liu, C. L., Green, M. R., Gentles, A. J., Feng, W., Xu, Y., et al. (2015). Robust enumeration of cell subsets from tissue expression profiles. *Nat. Methods* 12, 453–457. doi:10.1038/nmeth.3337

Nüchel, J., Ghatak, S., Zuk, A. V., Illerhaus, A., Mörgelin, M., Schönborn, K., et al. (2018). TGFB1 is secreted through an unconventional pathway dependent on the autophagic machinery and cytoskeletal regulators. *Autophagy* 14, 465–486. doi:10.1080/15548627.2017.1422850

Parra, E. R., Uraoka, N., Jiang, M., Cook, P., Gibbons, D., Forget, M. A., et al. (2017). Validation of multiplex immunofluorescence panels using multispectral microscopy for immune-profiling of formalin-fixed and paraffin-embedded human tumor tissues. *Sci. Rep.* 7, 13380. doi:10.1038/s41598-017-13942-8

Parra, E. R., Villalobos, P., Behrens, C., Jiang, M., Pataer, A., Swisher, S. G., et al. (2018). Effect of neoadjuvant chemotherapy on the immune microenvironment in non-small cell lung carcinomas as determined by multiplex immunofluorescence and image analysis approaches. *J. Immunother. Cancer* 6, 48. doi:10.1186/s40425-018-0368-0

Regan-Fendt, K., Li, D., Reyes, R., Yu, L., Wani, N. A., Hu, P., et al. (2020). Transcriptomics-based drug repurposing approach identifies novel drugs against sorafenib-resistant hepatocellular carcinoma. *Cancers (Basel)* 12, E2730. doi:10.3390/cancers12102730

Roayaie, S., Jibara, G., Tabrizian, P., Park, J. W., Yang, J., Yan, L., et al. (2015). The role of hepatic resection in the treatment of hepatocellular cancer. *Hepatology* 62, 440–451. doi:10.1002/hep.27745

Romero-Moreno, R., Curtis, K. J., Coughlin, T. R., Miranda-Vergara, M. C., Dutta, S., Natarajan, A., et al. (2019). The CXCL5/CXCR2 axis is sufficient to promote breast cancer colonization during bone metastasis. *Nat. Commun.* 10, 4404. doi:10.1038/s41467-019-12108-6

Romualdo, G. R., Da Silva, T. C., de Albuquerque Landi, M. F., Morais, J., Barbisan, L. F., Vinken, M., et al. (2021). Sorafenib reduces steatosis-induced fibrogenesis in a human 3D co-culture model of non-alcoholic fatty liver disease. *Environ. Toxicol.* 36, 168–176. doi:10.1002/tox.23021

Siegel, R. L., Miller, K. D., Fuchs, H. E., and Jemal, A. (2021). Cancer statistics, 2021. *Ca. Cancer J. Clin.* 71, 7–33. doi:10.3322/caac.21654

Sprinzl, M. F., Reisinger, F., Puschnik, A., Ringelhan, M., Ackermann, K., Hartmann, D., et al. (2013). Sorafenib perpetuates cellular anticancer effector functions by modulating the crosstalk between macrophages and natural killer cells. *Hepatology* 57, 2358–2368. doi:10.1002/hep.26328

Subramanian, A., Tamayo, P., Mootha, V. K., Mukherjee, S., Ebert, B. L., Gillette, M. A., et al. (2005). Gene set enrichment analysis: A knowledge-based approach for interpreting genome-wide expression profiles. *Proc. Natl. Acad. Sci. U. S. A.* 102, 15545–15550. doi:10.1073/pnas.0506580102

Sun, X., Niu, X., Chen, R., He, W., Chen, D., Kang, R., et al. (2016). Metallothionein-1G facilitates sorafenib resistance through inhibition of ferroptosis. *Hepatology* 64, 488–500. doi:10.1002/hep.28574

Tang, J., Sui, C. J., Wang, D. F., Lu, X. Y., Luo, G. J., Zhao, Q., et al. (2020). Targeted sequencing reveals the mutational landscape responsible for sorafenib therapy in advanced hepatocellular carcinoma. *Theranostics* 10, 5384–5397. doi:10.7150/thno.41616

Uhlén, M., Fagerberg, L., Hallström, B. M., Lindskog, C., Oksvold, P., Mardinoglu, A., et al. (2015). Proteomics. Tissue-based map of the human proteome. *Science* 347,

1260419. doi:10.1126/science.1260419

Walter, W., Sánchez-Cabo, F., and Ricote, M. (2015). GOplot: an R package for visually combining expression data with functional analysis. *Bioinformatics* 31, 2912–2914. doi:10.1093/bioinformatics/btv300

Wang, Y., Wan, X., Hao, Y., Zhao, Y., Du, L., Huang, Y., et al. (2019). NR6A1 regulates lipid metabolism through mammalian target of rapamycin complex 1 in HepG2 cells. *Cell Commun. Signal.* 17, 77. doi:10.1186/s12964-019-0389-4

Wei, L., Lee, D., Law, C. T., Zhang, M. S., Shen, J., Chin, D. W., et al. (2019). Genome-wide CRISPR/Cas9 library screening identified PHGDH as a critical driver for Sorafenib resistance in HCC. *Nat. Commun.* 10, 4681. doi:10.1038/s41467-019-12606-7

Wu, H., Wang, T., Liu, Y., Li, X., Xu, S., Wu, C., et al. (2020). Mitophagy promotes sorafenib resistance through hypoxia-inducible ATAD3A dependent Axis. *J. Exp. Clin. Cancer Res.* 39, 274. doi:10.1186/s13046-020-01768-8

Xia, S., Pan, Y., Liang, Y., Xu, J., and Cai, X. (2020). The microenvironmental and metabolic aspects of sorafenib resistance in hepatocellular carcinoma. *EBioMedicine* 51, 102610. doi:10.1016/j.ebiom.2019.102610

Xu, J., Wan, Z., Tang, M., Lin, Z., Jiang, S., Ji, L., et al. (2020). N(6)-methyladenosine-modified CircRNA-SORE sustains sorafenib resistance in hepatocellular carcinoma by regulating β-catenin signaling. *Mol. Cancer* 19, 163. doi:10.1186/s12943-020-01281-8

Yin, L., Zhou, L., and Xu, R. (2020). Identification of tumor mutation burden and immune infiltrates in hepatocellular carcinoma based on multi-omics analysis. *Front. Mol. Biosci.* 7, 599142. doi:10.3389/fmolb.2020.599142

Zhang, W., Wang, H., Sun, M., Deng, X., Wu, X., Ma, Y., et al. (2020). CXCL5/CXCR2 axis in tumor microenvironment as potential diagnostic biomarker and therapeutic target. *Cancer Commun. (Lond).* 40, 69–80. doi:10.1002/cac2.12010

Zhang, W., Zhu, X. D., Sun, H. C., Xiong, Y. Q., Zhuang, P. Y., Xu, H. X., et al. (2010). Depletion of tumor-associated macrophages enhances the effect of sorafenib in metastatic liver cancer models by antimetastatic and antiangiogenic effects. *Clin. Cancer Res.* 16, 3420–3430. doi:10.1158/1078-0432.ccr-09-2904

Zhou, S. L., Dai, Z., Zhou, Z. J., Wang, X. Y., Yang, G. H., Wang, Z., et al. (2012). Overexpression of CXCL5 mediates neutrophil infiltration and indicates poor prognosis for hepatocellular carcinoma. *Hepatology* 56, 2242–2254. doi:10.1002/hep.25907

Zhou, S. L., Yin, D., Hu, Z. Q., Luo, C. B., Zhou, Z. J., Xin, H. Y., et al. (2019). A positive feedback loop between cancer stem-like cells and tumor-associated neutrophils controls hepatocellular carcinoma progression. *Hepatology* 70, 1214–1230. doi:10.1002/hep.30630

Zhou, S. L., Zhou, Z. J., Hu, Z. Q., Huang, X. W., Wang, Z., Chen, E. B., et al. (2016). Tumor-associated neutrophils recruit macrophages and T-regulatory cells to promote progression of hepatocellular carcinoma and resistance to sorafenib. *Gastroenterology* 150, 1646–1658. e1617. doi:10.1053/j.gastro.2016.02.040

Zhu, Y. J., Zheng, B., Wang, H. Y., and Chen, L. (2017). New knowledge of the mechanisms of sorafenib resistance in liver cancer. *Acta Pharmacol. Sin.* 38, 614–622. doi:10.1038/aps.2017.5

frontiers | Frontiers in Pharmacology

TYPE Review
PUBLISHED 01 September 2022
DOI 10.3389/fphar.2022.990445

OPEN ACCESS

EDITED BY
Heng Sun,
University of Macau, China

REVIEWED BY
Josh Haipeng Lei,
University of Macau, China
Xiaodong Shu,
University of Macau, China

*CORRESPONDENCE
Shan Yu,
yushan@hrbmu.edu.cn
Hong Qiao,
qhong0823@163.com

SPECIALTY SECTION
This article was submitted to Pharmacology of Anti-Cancer Drugs, a section of the journal Frontiers in Pharmacology

RECEIVED 10 July 2022
ACCEPTED 10 August 2022
PUBLISHED 01 September 2022

CITATION
Wu Y, Yu S and Qiao H (2022), Understanding the functional inflammatory factors involved in therapeutic response to immune checkpoint inhibitors for pan-cancer. *Front. Pharmacol.* 13:990445. doi: 10.3389/fphar.2022.990445

Understanding the functional inflammatory factors involved in therapeutic response to immune checkpoint inhibitors for pan-cancer

Yanmeizhi Wu[1], Shan Yu[2]* and Hong Qiao[1]*

[1]Department of Endocrinology, The Second Affiliated Hospital of Harbin Medical University, Harbin, China, [2]Department of Pathology, The Second Affiliated Hospital of Harbin Medical University, Harbin, China

Immune checkpoint inhibitors (ICIs) fight tumor progression by activating immune conditions. The inflammatory factors are playing a functional role in programmed death-1 (PD-1) or other immune checkpoints. They are involved in regulating the expression of programmed death ligand-1 (PD-L1), the only predictor recognized by the guidelines in response to ICIs. In addition, abundant components of the tumor microenvironment (TME) all interact with various immune factors contributing to the response to ICIs, including infiltration of various immune cells, extracellular matrix, and fibroblasts. Notably, the occurrence of immune-related adverse events (irAEs) in patients receiving ICIs is increasingly observed in sundry organs. IrAEs are often regarded as an inflammatory factor-mediated positive feedback loop associated with better response to ICIs. It deserves attention because inflammatory factors were observed to be different when targeting different immune checkpoints or in the presence of different irAEs. In the present review, we address the research progresses on regulating inflammatory factors for an intentional controlling anti-cancer response with immune checkpoint inhibitors.

KEYWORDS

immune checkpoint inhibitors, inflammatory factors, programmed death-1, immune-related adverse events, tumor microenvironment

1 Introduction

Immunotherapy modulates the body's immune system to fight immune evasion and immune silencing of tumors. Immune checkpoint inhibitors (ICIs) have the effect of stimulating activation and proliferation on T cells, so it is more beneficial to destroy tumor cells. Currently available immune checkpoint inhibitors are mainly programmed death-1 (PD-1) and its ligand (PD-L1), targeting cytotoxic T lymphocyte antigen-4 (CTLA-4). Further ICIs are being discovered and studied (Parry et al., 2005; Rosenberg et al., 2016), such as Lymphocyte Activation Gene-3 and T cell immunoglobulin mucin-3. Responses to ICIs have only been observed in certain solid tumors, such as gastrointestinal

malignancies and unresectable or metastatic melanoma. And it is often accompanied by the possibility of resistance to ICIs (Haslam and Prasad, 2019; Puccini et al., 2020). The major reasons that account for diverse responses to ICIs are the contributions of multiple components of the tumor microenvironment (TME), including immune cells, fibroblasts, and the extracellular matrix (ECM). Thus, the interaction of inflammatory factors with components in the TME modulates responses to ICIs from different perspectives.

The number of patients being treated with ICIs is increasing, and thus cases of immune-related adverse events (irAEs) are also reported in a wide range of organs (June and Bluestone, 2017; Poto et al., 2022). Although the presence of irAEs is generally believed to be associated with better responses to ICIs, unpredictable and uncontrollable irAEs are a major obstacle preventing a complete course of ICIs therapy. The types of inflammatory factors involved in different irAEs are different, and the inflammatory factors associated with different therapeutic targets are not the same (Teulings et al., 2015; Berner et al., 2019). In addition, the discordance of inflammatory factors in TME and irAEs has also led to a new hypothesis that inflammatory factors mediate different signaling pathways involved in tumor response to ICIs and triggering of tissue-specific irAEs.

We aim to highlight the role of inflammatory factors in the TME on the response to ICIs, and also to address the involvement of inflammatory factors in the occurrence of irAEs.

2 Inflammatory factors on response to immune checkpoint inhibitors in the tumor microenvironment

Research on immune checkpoints has shown that most of them act as “brakes” in immune function, i.e., ICIs reactivate T cells to more effectively clear cancer cells (Ljunggren et al., 2018). At present, ICIs widely used in clinical applications mainly include anti-PD-1/PD-L1 and anti-CTLA-4. Additional immune checkpoint molecules are under study (Bagchi et al., 2021). The combination of PD-L1 and PD-1 will accelerate the apoptosis of immune cells, especially those with PD-1 positive. CTLA-4 also inhibits T cell activity and is up-regulated upon T cell activation (Valk et al., 2008). However, PD-L1 was a predictor for the response to ICIs rather than CTLA-4. One classification of TME is based on tumor-infiltrating lymphocytes (TILs) and PD-L1 expression, which are the main predictors of response to ICIs (Powles et al., 2014). Among them, one type with PD-L1 positive and abundant TIL infiltration had the best response to ICIs treatment (Teng et al., 2015). Furthermore, cancer ECM influences the response to immunotherapy through secreted regulators and suppressors (Umair et al., 2018; Bagaev et al., 2021). The ECM status provides important complementary information on the capture capacity of T cells (Mariathasan et al., 2018) and is considered a major common denominator of anti-ICIs (Jensen et al., 2021). Among them, cancer-associated fibroblasts (CAFs) are involved in constituting ECM fibrosis to hinder T cell infiltration and T cell activity, which produces a marked effect on immunotherapy resistance (Wang et al., 2018a; Mariathasan et al., 2018). The following summarizes the effects of inflammatory factors on the response of ICIs in TME from three aspects: PD-L1 abundance, TIL density, and ECM status (Figure 1).

2.1 Inflammatory factors regulating programmed death ligand-1 abundance

The abundance of PD-L1 in TME could predict therapeutic response to ICIs in multiple cancers, such as melanoma (Caroline et al., 2015) and cancer in lung (Borghaei et al., 2015) and bladder (Rosenberg et al., 2016). Inflammatory-related signaling was confirmed to regulate the expression of PD-L1 (Ji et al., 2015) but was detected not only on T cells (Fehrenbacher et al., 2016). PD-L1 is commonly detected by adaptive and innate immune cells, as well as epithelial cells, especially under inflammatory conditions (Sharpe et al., 2007). Many classical inflammatory factors have a hand in the regulation of PD-L1, which are discussed below respectively.

2.1.1 Interferons

Interferons (IFNs) are secreted in large quantities by various activated immune cells, mainly by T cells and natural killer cells (NK cells). Importantly, PD-L1 of target cells can be triggered by IFN-γ (Garcia-Diaz et al., 2017). T cells secreted IFN-γ through the JAK1/JAK2-STAT1/STAT3 pathway (Karachaliou et al., 2018; Na et al., 2018; Thiem et al., 2019; Fujita, 2021). The JAK1/JAK2-STAT1 pathway has also been observed to stimulate IFN-γ secretion in NK cells (Bellucci et al., 2015). Further, IFN-γ receptor can also stimulate JAK-STAT, and STAT1 signaling is preferred (Platanias, 2005). In contrast, IFN-γ induces protein kinase D isoform 2 (PKD2), an important isoform that inhibits PD-L1 and promotes a strong antitumor immune response (Chen et al., 2012). Silencing of Male Germ Cell Associated Kinase (MAK), CRK Like Proto-Oncogene (CRKL) and PI3K signaling pathways also impair PD-L1 depending on IFN-γ (Garcia-Diaz et al., 2017). In melanoma, nuclear factor-κB(NF-κB) signal is required for IFN-γ to upregulate PD-L1 (Gowrishankar et al., 2015). Furthermore, IFN-γ receptor 1 inhibition can reduce PD-L1 expression in acute myeloid leukemia mice through the MEK-ERK and myeloid differentiation factor88 (MYD88)-tumor necrosis factor receptor-associated factor6 (TRAF6) pathways (Abiko et al., 2015). Since IFN-γ of TME is generally considered to be beneficial for immunotherapy, tumor cells may undergo survival-stressed proliferation when the IFN-γ signaling pathway is defective (Abril-Rodriguez and Ribas, 2017). This

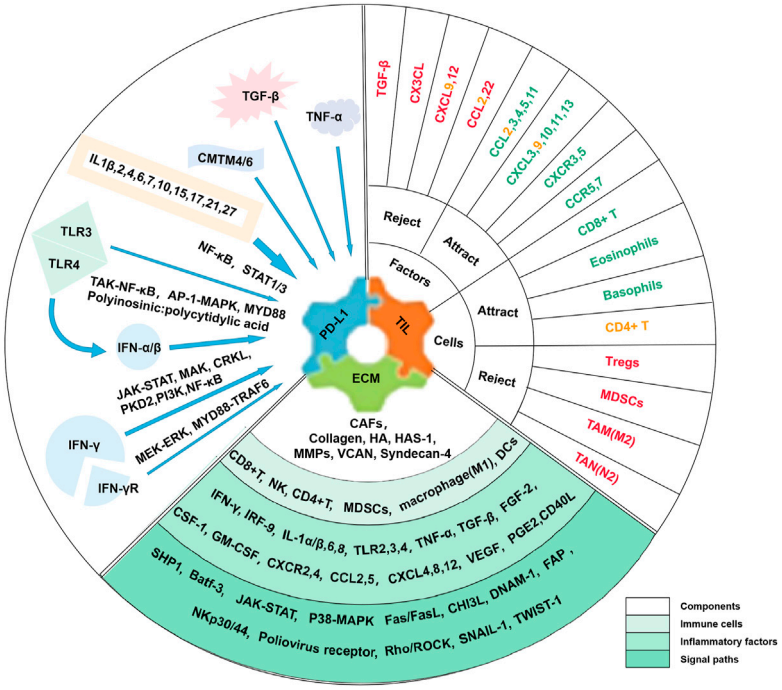

FIGURE 1
Influence of Inflammatory Factors on Responses to ICIs in TME. In the TME, inflammatory factors affecting tumor response to ICIs were mainly associated with three factors, including PD-L1 abundance, TIL density, and ECM status. Many inflammatory factors affect PD-L1 expression, such as IFN-γ. Inflammatory factors and immune cells are both involved in influencing TIL infiltration with different roles. Among them, green factors or cells attract T cells to homing or promote TIL infiltration, while red ones reject T cell homing or inhibit TIL infiltration. Factors or cells that are yellow have been reported to have a dual effect. Factors affecting ECM status include biological and physical factors, and the components, immune cells and inflammatory factors, and signal paths involved are listed.

is one of the currently recognized causes of adaptive resistance during immunotherapy (Yi et al., 2018). Thus, an intact IFN-γ signaling pathway is a determinant for robust antitumor effects that persist throughout the course of ICIs treatment. It is worth noting that the close relationship between IFN-γ levels and PD-L1 was not necessarily observed in all cell types. For example, when sarcoma mice were treated with an IFN-γ blocking antibody, PD-L1 was largely abolished on tumor cells but not on tumor-associated macrophages (Noguchi et al., 2017). Therefore, more studies on the interaction of IFN-γ and PD-L1 need to be carried out.

IFN-α/β, also induces PD-L1 in cancer cells, endothelial cells and leukocytes (Schreiner et al., 2004; Eppihimer et al., 2015; Garcia-Diaz et al., 2017). IFN-α sensitizes the STAT1 signal, further increasing PD-L1 (Meng et al., 2020). However, there are limited reports on the correlation of IFN-α/β with response to ICIs, which may be due to the small effect of IFN-α/β on PD-L1 directly.

2.1.2 Toll-like receptors

Toll-like receptors (TLRs) family, secreted by both myeloid cells and lymphocytes (Loke and Allison, 2003; Gang et al., 2013), connect innate immunity and adaptive immunity. On the one hand, PD-L1 expression is regulated by TLR4 through MyD88-dependent or MyD88-independent pathways (Lu et al., 2008). Besides, TLR4 activates the downstream NF-kB signaling pathway through transforming growth factor kinase 1 (TAK1) and activates the MAPK pathway through the transcription factor AP-1 (Qian et al., 2008). On the other hand, IFN-α production is activated by TLR4 ligands in plasmacytoid dendritic cells (PDCs) (Zhang et al., 2020). TLR3 can also cause increased PD-L1 expression in DCs (Pulko et al., 2009), endothelial cells (Cole et al., 2011) and neuroblastoma cells (Boes and Meyer-Wentrup, 2015) under conditions stimulated by polyinosinic:polycytidylic acid. However, the relevant mechanism is still unclear.

2.1.3 Interleukin (ILs)

Interleukin (ILs) are a class of lymphokine that interacts between immune cells. On the one hand, a number of ILs upregulate PD-L1 on immune cells, including IL-10 (Cole et al., 2011) and IL-17 (Zhao et al., 2011) in monocytes, IL-4 (Ou et al., 2012) and IL-6 (Kim et al., 2008) in dendritic cells. IL-1β upregulates PD-L1 *via* the NF-κB (Kondo et al., 2010), and IL-27 *via* STAT1 and

STAT3 signaling pathways (Karakhanova et al., 2011). In addition, IL-2, 7, 15 and 21 also increased PD-L1 *in vitro* (Kinter et al., 2008). On the other hand, IL in tumor cells can also cause high PD-L1, like IL-4, IL-17 in prostate and colon cancer cells (Wang et al., 2017), IL-27 in ovarian cancer cells (Carbotti et al., 2015), IL-10 in myelodysplastic syndrome blasts (Kondo et al., 2010), renal cell carcinoma (Quandt et al., 2014). IL-12-mediated regulation of PD-L1 may be more complex because IL-12 raises PD-L1 *via* NF-κB in macrophages while lowering PD-L1 when IFN-γ lacking (Xiong et al., 2014).

2.1.4 Other factors

Transforming growth factor (TGF)-β production by CD8+ T cells was required for cells to consistently express PD-L1 (Baas et al., 2016). Meanwhile, TGF-β induced DCs to express PD-L1 *in vitro* in lung cancer (Ni et al., 2012) and hepatocellular carcinoma (Song et al., 2014), respectively. Tumor necrosis factor (TNF)-α in endothelial cells was observed to be relevant to high PD-L1 (Mazanet and Hughes, 2002). More reports are in autoimmune diseases such as Paget's disease (Iga et al., 2019) and rheumatoid arthritis (Wasén et al., 2018). The regulation of PD-L1 expression by these promising inflammatory factors in the TME and further clarification of their roles in response to ICI therapy are warranted. In addition, CKLF (Chemokine-like factor)-like MARVEL transmembrane domain containing (CMTM)4/6 present on the cell surface binds to PD-L1 on protein level rather than transcription (Mezzadra et al., 2017).

2.2 Inflammatory factors regulating tumor-infiltrating lymphocyte density

Along with PD-L1 positivity, tumors respond well to ICIs when TILs are abundant and show drug resistance otherwise (Na et al., 2018). Thus, TIL density acts as a predictor of response to treatment with ICIs, too. It has been found that abundant TILs are associated with both adaptive upregulation of PD-L1 and the clinical benefit of immunotherapy (Xing et al., 2018). Pre-existing TILs are liberated by PD-L1/PD-L1 inhibitors and then promote tumor regression (Yagi et al., 2017; Tomioka et al., 2018). However, TILs on response to anti-CTLA-4 therapy is controversial. Baseline TIL status before treatment has been reported to predict a good therapeutic effect in melanoma (Chen et al., 2016), but no prognostic benefit has also been observed (Huang et al., 2011). Although anti-CTLA-4 is not prominent in immunotherapy as a monotherapy, it is being clinically tested in a variety of cancers as an effective means of enhancing anti-tumor response when applied with other therapies, such as chemotherapy and radiotherapy. This section focuses on those inflammatory factors and immune cells in the TME that attract or reject homing T cells and thus positively or negatively correlate with ICI responses.

2.2.1 Tumor-infiltrating lymphocyte cells associated with immune checkpoint inhibitor responsiveness

TCRs (T cell receptors) are massively amplified in metastatic pancreatic cancer following anti-CTLA-4 (Hopkins et al., 2018). Within the TME, the enrichment of T cells with the same TCR is a hallmark of effective treatment with ICI therapy (Ro et al., 2017; Arakawa et al., 2019). CD8+ T cells are regarded as the key to "stem cell-like" antitumor immunity due to their unique expression of the transcription factor TCF1 (Siddiqui et al., 2019). After ipilimumab, those patients with CD45RA- had better responses, both for CD4+ T and CD8+ T cells (Subrahmanyam et al., 2018). In a study of nivolumab in non-small cell lung cancer, 18% of patients (23/126) exhibited complete or partial responses after treatment. Responders had more CD62LlowCD4+ T cells in the predose circulation than non-responders (Kagamu et al., 2020). Similar results in metastatic melanoma had shown that 9 of the 32 patients responded to ICIs. More memory CD4+ T cells were in the cancer tissues of the 9 responders, which were not only related to the expression of CD62L, but also to CCR7 and CD28 (Sade-Feldman et al., 2019). Therefore, the frequency of pre-treatment TIL populations and their dynamic changes may serve as important predictive biomarkers for distinguishing between ICI responders and non-ICI responders.

2.2.2 Inflammation factors related to T cell homing

Chemotactic cytokines are a class of small cytokines that induce the orientation of responding cells into the site of infection during the immune response. Some chemokines are themselves pro-inflammatory factors, such as IL-8 (Maekawa et al., 2022), while others are regulated by inflammatory factors (Figure 2). Chemokine CC receptor (CCR) 7 binds to its selectin ligand, and chemotactic mature T cells migrate to specific targets. The phenomenon of immune desertification in the TME is a consequence of CCR7 deficiency (Berghuis et al., 2011). The expression of chemokine CC ligand (CCL) 5 is guided by IFN-α and gathers T cells in prostate cancer (Harlin et al., 2009). When triggering WNT/b-catenin, CCL4 downregulation results in failure of effector T cell recruitment and activation (Stefani et al., 2015). Both TLR4 and IL-6 levels were positively correlated with chemokine CXC receptor (CXCR) 3 expression, which may regulate the infiltration of CD+8 T cells (Muthuswamy et al., 2016). In tumor-infiltrating PDCs, CXCR4 is regulated to activate the TNF-α through NF-κB (Han et al., 2021). Inhibition of IFN-γ-induced SDF-1/MIP-1α pathway also reduces CXCR4 and CCR5 (Creery et al., 2004). The chemokine CXC ligand (CXCL) 9 and CXCL10 also contributed to the infiltration of TILs (Liu et al., 2015; Peng et al., 2015). STAT3 signaling can downregulate the CXCR3/CXCL10 axis in CD8+ T cells (Yue et al., 2015), thereby reducing

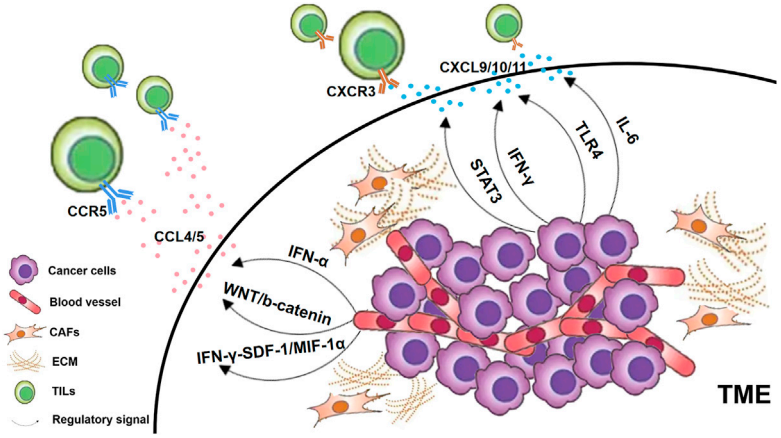

FIGURE 2
Chemokines regulated by inflammatory factors. In general, cancer cells in the TME, CAFs and ECM can all secrete chemokine ligands. Those T lymphocytes that express chemokine receptors on their cell surfaces are attracted to specific chemokine ligands and thus home to the TME as TILs. CXCR3-CXCL9/10/11 is a key chemokine reported to be associated with TILs infiltration, which is regulated by various signaling pathways as shown in the figure. In addition, CCR5-CCL4/5 has also been found to be associated with the infiltration of TILs through multiple pathways.

their ability to penetrate the TME. CXCL9 and CXCL10 can be activated *via* IFN-α to promote TILs increasing in the cancer of the prostate gland (Harlin et al., 2009). CXCL11 was correlated with TLR4 levels positively (Muthuswamy et al., 2016). Regardless of tumor subtype, T cells from breast cancer patients treated with anti-PD-1 were clonally expanded, mediated CD8+ T cell homing *via* CXCL13, and attracted CD4+ T cells by CXCR5 (Bassez et al., 2021). In addition, CCR5, CCL2, CCL3, CCL11 and CX3CL1 were also positively associated with T cell infiltration (Peng et al., 2015; Manou et al., 2020; Bassez et al., 2021).

However, chemokines do not always work as expected (Bassez et al., 2021). A study of patients with metastatic urothelial carcinoma who received PD-L1 blocker found that TILs could not reach the tumor center and were trapped in the surrounding matrix (Mariathasan et al., 2018). Tumor-derived chemokines are one of the main reasons for misdirecting activated T cells to the stromal cells surrounding the tumor. For example, stromal cells surrounding pancreatic tumors produce CXCL12, which attracts effector T cells and prevents them from entering the tumor core (van der Woude et al., 2017). The CXCL9/CXCR3 axis may also have a dual role in promoting T cell migration and tumor cell metastasis (Billottet et al., 2013). High expression of CCL2, CCL22, and CXCL12 normally attracts immunosuppressive cells (Harlin et al., 2009). For non-small cell lung cancer, CCL2 blockade reduces immunosuppression and enhances cancer immunotherapy (Fridlender et al., 2010).

The TGF-β has been concerned due to its negative impact on T cells. Blocking the TGF-β signaling pathway contributes to the transition of the TME to an immune-inflammation-rich state, which has significant advantages in tumor control when combined with ICI (Mariathasan et al., 2018; Ravi et al., 2018). Moreover, stimulation of PD-1/PD-L1 by TGF-β receptor (TGF-βRII) results in a reduction in the host's rejection of the graft, suggesting that similar processing may also be involved in the TME (Baas et al., 2016).

2.2.3 Regulatory immune cells

Several regulatory immune cells influence TIL infiltration (Gabrilovich, 2017; Mantovani et al., 2017) (Table 1), mainly including regulatory T (Treg) cells, myeloid-derived suppressor cells (MDSCs) and monocytes.

Tregs can either restrict the amount of effector T cells by depleting IL-2 (Setoguchi et al., 2005) or inhibit the function of effector T cells by producing TGF-β and IL-10 (Takahashi et al., 1998; Camisaschi et al., 2010). In turn, TGF-β and IL-10 expand Treg cells (Chen et al., 1994). In addition, Treg cells produce perforin and granzymes to kill effector T cells (Mantovani et al., 2017). Activated Treg cells express LAG-3 (Huang et al., 2004) and CTLA-4, which promote indoleamine 2,3-dioxygenase (IDO) secretion (Mellor and Munn, 2004), thereby causing T cell dysfunction (Uyttenhove et al., 2003). Small numbers of Tregs are associated with increased ICIs response and patient survival (Read et al., 2006; Friedline et al., 2009). In bladder cancer patients, however, CTLA-4 blockade resulted in an increased proportion of Tregs (Liakou et al., 2008). This suggests that the baseline status of immune cells and ICIs-related changes are of different predictive significance and that effector T cells/Treg ratio may be a more effective method for predicting response to treatment with ICIs (Sharma et al., 2021). Significantly, the effect of anti-CTLA-4 depends on antibody-dependent cytotoxic activity (ADCC) to deplete CTLA-4-expressing Treg cells in the TME, and its deletion

TABLE 1 Regulation of TIL infiltration by Regulatory immune cells.

		Inflammatory factors	Outcomes	References
APC	Treg	Depletion of IL-2	Inhibiting the proliferation of effector T cell	Setoguchi et al. (2005)
		Expression of LAG-3	Inhibiting the activation of T cell	Huang et al. (2004)
		TGF-β, IL-10	Killing effector T cells	Takahashi et al. (1998), Camisaschi et al. (2010)
		IDO		Mellor and Munn (2004)
		Perforin, granzyme		Mantovani et al. (2017)
	MDSCs	STAT3	Promoting the expression of PD-L1	Ko et al. (2009)
		NADPH	Inhibiting the migration of T cell	Nagaraj et al. (2007)
		COX-2/PGE-2	Inhibiting T cell reactivity	Obermajer et al. (2011)
		Arginase, iNOs		Orillion et al. (2017), ChristmasEntinostat et al. (2018)
		CXCR2, CSF-1R/CSF-1		Mok et al. (2014), Kumar et al. (2017a)
		5-aza-2′-deoxycytidine		Daurkin et al. (2010)
	TAMs	LILRB2-SHP1/2-ERK/P38	Differentiate to TAM-1	Gordon et al. (2017)
		CD47	Promoting TAM activity	Li et al. (2019)
	TANs	CCL5, CXCL9, CXCL10	Eosinophils promote TAM-1 differentiation and T cell migration	Eruslanov et al. (2014)
		CCL3, CCL4	Basophils promote T cell infiltration	Singhal et al. (2016)
	Monocytes	—	Contributes to anti-PD-1/CTLA-4 responses	Carretero et al. (2015); Sektioglu et al. (2016)
	DCs	EZH2	Contributes to anti-PD-1 responses	Bolton et al. (2015)

will abolish the anti-tumor effect of anti-CTLA-4 (Bulliard et al., 2013; Selby et al., 2013). PD-1 inhibitors on Treg cells remain unclear.

Correlations between MDSCs abundance and response to ICIs have been revealed in numerous clinical trials (Meyer et al., 2014; Weber et al., 2016). MDSCs suppress the immune system by expressing PD-L1 (Noman et al., 2014), secreting IL-10 and TGFβ (Hart et al., 2011; Trikha and Carson3rd, 2014), and recruiting Tregs with CD40 (Pan et al., 2010). MDSCs impede response to ICIs not only with ipilimumab (Liakou et al., 2008) but also with anti-PD-L1 therapy (McDermott et al., 2018). MDSCs can reduce T cell reactivity (Messmer et al., 2015). In renal cell cancer, the inhibition of STAT3 aggregates MDSC, further leading to T cell suppression (Ko et al., 2009). MDSCs abolish the directional migration of CD8+ T cells when upregulated by NADPH oxidase (Nagaraj et al., 2007; Lu et al., 2011). Decreased recruitment and differentiation of MDSCs through obstruction of COX-2/PGE2 resulted in improved CTL frequency and immune responses (Obermajer et al., 2011). In addition, the immunosuppressive function of MDSCs was suppressed by downregulating arginase and iNOS, resulting in a shift in tumor dynamics towards more responsive ICIs (Orillion et al., 2017; ChristmasEntinostat et al., 2018). Targeting CXCR2 reduces the number of MDSCs in pancreatic cancer (Steele et al., 2016). Treatment against the receptors of MDSCs or their ligands CSF-1R/CSF-1 combined with immunotherapy can improve antitumor T cell activity and tumor regression (Mok et al., 2014). The combined use of CSF-1R inhibition and CXCR2 antagonism can also reduce the number of MDSCs and improve anti-PD-1 efficacy (Kumar et al., 2017a). Targeted drugs that inhibit the recruitment of tumor-infiltrating CXCR2+ MDSCs can enhance the response of ICIs (Sun et al., 2019). In addition, inhibition of MDSCs by the DNA demethylating agent 5-aza-2′-deoxycytidine also promotes antitumor immune responses (Daurkin et al., 2010).

Increased frequency of circulating monocytes at baseline predicts better ICI response (Martens et al., 2016; Krieg et al., 2018). Macrophages, granulocytes and DCs are of importance. The phagocytic capacity of tumor-associated macrophages (TAMs) is regulated by the PD-1/PD-L1 (Gordon et al., 2017). Differentiation of PD-1+ TAMs impairs effector T cell function (Li et al., 2019). Type 1 polarization (TAM-1) of TAMs is prevented by blocking leukocyte immunoglobulin-like receptor B2 (LILRB2), which improves anti-PD-L1 responses (Chen et al., 2018). CD47 blockade increases the efficiency of anti-PD-L1 in melanoma to by modulating the activity of TAMs (Sockolosky et al., 2016). Tumor-associated neutrophils (TANs) can be divided into type 1 (TAN-1) and type 2 (TAN-2), the former stimulating infiltration of effector T cells (Eruslanov et al., 2014) and the latter an immunosuppressive phenotype (Singhal et al., 2016). Increased eosinophils contribute to the polarization of macrophages in favor of TAM-1, which is further mediated by CCL5, CXCL9 and CXCL10 (Carretero et al., 2015). Conversely, basophils attract CD8+ T cells in the TME by producing CCL3 and CCL4 (Sektioglu et al., 2016). Differentiation of peripheral DCs also modulates the response to anti-PD-1 (Bolton et al., 2015).

2.3 Inflammatory factors participating in extracellular matrix

Cancer ECM is formed through secreted regulators and repressors (Ho et al., 2020). CAFs participate in the process of tumor fibrosis and contribute to the ECM (Jensen et al., 2021). Fibrosis of the ECM through TGF-β signal (Nissen et al., 2019), is considered to be one of the key factors affecting the response to immunotherapy (Bagaev et al., 2021). A combined anti-CTLA-4 and anti-PD1 approach was linked to ECM components to enhance retention within the ECM, suggesting that ECM modulation may be an effective approach to enhance the efficacy of ICIs therapy (Ishihara et al., 2017).

2.3.1 Extracellular matrix formation affects immune cells and inflammatory factors

The formation of ECM determines the migration and localization of immune cells to a certain extent (Hynes, 2009; Hallmann et al., 2015). Based on TME extracellular components, tumors are classified as immune-inflammatory tumors, immune-rejective tumors, and immune-desert tumors (Hegde and Chen, 2020). Immunorejecting tumors respond worse to ICIs than immunoinflammatory tumors, as T cells are blocked away from the tumor (Tumeh et al., 2014; Chen and Mellman, 2017). First, the dense ECM acts as a physical barrier to hinder the infiltration of TILs. Abundant collagen blocks homing T cells despite being activated (Evanko et al., 2012). Elevated collagen level causes patients to resist anti-PD-1/PD-L1 (Peng et al., 2020). Hyaluronic acid (HA) also prevents the move of effector cells (Jacobetz et al., 2013). Chemokine-dependent T cells were observed to infiltrate restricted due to the dense HA surrounding lung cancer tissue (Salmon et al., 2012). Second, immune cells are regulated by the composition of the ECM (Cooper et al., 2016). Collagen inhibits T cell activity by signaling through SHP-1 (Peng et al., 2020). HA promotes inflammation in the TME and increases Treg activity through TLR signaling (Nikitovic et al., 2015). Matrix metalloproteinases (MMPs) promote tolerance polarization in DCs by binding to TLR2 (Godefroy et al., 2014). Vascular endothelial growth factor (VEGF), which is abundantly present, also has inhibitory effects on DCs (Burbage and Amigorena, 2020). Chondroitin sulfate proteoglycan (VCAN) is directly associated with the reduction of TIL (Gorter et al., 2010), as it prevents T cell adhesion and migration (Peng et al., 2020). Meanwhile, it can also indirectly inhibit CTL infiltration by recruiting MDSCs (Wight et al., 2014) and regulating Batf3 DCs (Hope et al., 2017). Third, some ECM components influence inflammatory factor levels. For example, MMP-9 increases TNF-α, IL-1β, IL-6 levels (Liao et al., 2021). Low doses of collagen synergize with CXCL12 to induce the release of CD40L *via* p38-MAPK activation (Nakashima et al., 2020). Collagen peptides can significantly inhibit the secretion of IL-1β, TNF-α and PGE2 (Wang et al., 2018b). Thus, type III collagen propeptide is a predictor of metastatic melanoma response to ICIs (Hurkmans et al., 2020), and type IV collagen fragments can also identify melanoma patients who benefit from anti-CTLA-4 (Jensen et al., 2020).

2.3.2 Immune cells and inflammatory factors affect extracellular matrix remodeling

Remodeling of the ECM is thought to be a key factor in immune cell trafficking and activation of the immune cycle (Huse, 2017). In bladder cancer patients, PD-L1 expression is discordant at metastatic sites and the primary tumor, suggesting the dynamic nature of the ECM (Mukherji et al., 2016). TGF-β has been reported to increase the synthesis and deposition of type I collagen and downregulate MMP-2 (Türlü et al., 2021). Activation of the RhoA/ROCK signaling pathway and transcription of SNAIL1 and TWIST1 genes are both triggered by TGF-β (Gaggioli et al., 2007; García-Palmero et al., 2016; Chung et al., 2021). At the same time, TGF-βR is also necessary for the deposition of collagen and fibronectin (Shuang and Chakrabarty, 2010; Robert et al., 2018). TNF-α and fibroblast growth factor (FGF)-2 are also important adjuvants in the process of promoting collagen synthesis (Katsumata et al., 2019; Muchová et al., 2021). In contrast, IL-1α/β promotes IL-6 and IL-8 and inhibits ECM, by regulating the expression of Versioncan (Chang et al., 2017; Osei et al., 2020). Interferon regulatory factor 9 regulates VCAN transcription independently of JAK-STAT signaling (Brunn et al., 2021). Immune cells are also involved in engineering ECM components (Bhattacharjee et al., 2019). For example, macrophages produce Hyaluronic Acid Synthase 1 *via* TLR2 and Syndecan-4 *via* TLR2, TLR3 and TLR4 (Chang et al., 2017). Also, the M1 macrophages to produce MMP-10 contribute to vascular remodeling through STAT1 signaling (Chi et al., 2022). TGF-β secreted by CD4+ T cells is also involved in vascular reorganization (Li et al., 2020).

2.3.3 Cancer-associated fibroblasts

Activated CAFs often build a matrix-dense barrier in the ECM to protect tumor cells and trap T cells, which affects the efficacy of ICIs (Godefroy et al., 2014). In metastatic urothelial carcinoma patients treated with PD-L1 monoclonal antibody, activated TGF-β signaling pathway in CAFs may hinder T cells from infiltrating tumors (Mariathasan et al., 2018). In co-culture with triple-negative breast cancer, TNF-α and IL-1β induced CXCL8/CCL5 secretion to suppress CD8+ T cells (Liubomirski et al., 2019). The resistance of breast cancer bone metastases to ICB is thought to be the release and resorption of TGF-β after osteoclast induction of osteogenesis, reducing the number of Th1 (Jiao et al., 2019). In addition, p-STAT-3, which is associated with metastatic brain tumors, reduces CD8+ T cell activity and increases the abundance of CD74+ macrophages, potentially playing a role in ICIs (Priego et al., 2018). CAFs have been reported to increase the expression of Fas and PD-1 to control the binding with PD-L2 for the former and Fas ligand for the latter

(Lakins et al., 2018). Loss of Chitinase-3-like 1 in CAFs also increases the TILs (Cohen et al., 2017). Meanwhile, CAF inhibits NK protein (NKp) 44, 30, DNAX accessory molecule-1 (DNAM-1), and poliovirus receptors (Calon et al., 2014; TomokoInoueKatsuyukiTaguchi et al., 2016), which are the activating receptors of NK cells. High levels of IL-6 secreted by CAFs summon MDSCs and amplify PD-L1 in hepatocellular cancer (Liu et al., 2017). CSF-1 in the TME contributes to the reduction of chemotactic factors in CAFs. CSF-1 receptor and CXCR2 are key items for MDSCs gathering (Kumar et al., 2017b). CTLA-4 antibodies were more effective when combined with the GM-CSF vaccine (van Elsas et al., 1999). CAFs can also secrete other negative factors, such as CXCL12, CCL2, and VEGF (Grum-Schwensen et al., 2005; Chen et al., 2017). CXCL12/CXCL12R helps sensitize to anti-PD-L1 therapy, resulting in T cell aggregation and cancer regression (Feig et al., 2013). In gastric and colon cancers, fibroblast activation protein (FAP) in CAFs leads to more CCL2 and less IFN-γ, eventually damaging the outcome of ICIs therapy (Chen et al., 2017), while FAP Inhibition reverses this resistance (Wen et al., 2017). DNA vaccines against FAP induce activation of CD8+ and CD4+ T cells to enhance responses to ICIs (Xia et al., 2016). A pan-cancer analysis showed that TGF-β signaling in CAFs activated "ECM-up" signaling, independent of CAFs or TGF-β activation, a predictor associated with anti-PD-1 resistance, even better than T Cellular inflammatory signaling and mutational burden (Chakravarthy et al., 2018).

Given the complexity and dynamics of the tumor microenvironment, a single biomarker may not be sufficient, and a combination of multiple markers is supposed to be paneled (Binnewies et al., 2018; Kitano et al., 2018). Initial tumor biopsy assessment of PD-L1 abundance, TIL infiltration, and ECM status, combined with longitudinal assessment of changes in each factor during treatment, may have a unique potential to predict tumor phenotypes that respond to ICIs.

3 Inflammatory factors on immune-related adverse effects to immune checkpoint inhibitors in the circulation

Treatment with ICIs induces systemic and local inflammatory responses (Tsukamoto et al., 2018), starting from the interaction between inflammatory factors and their recruitment to immune cells. Inflammatory factors mediate each other. For example, the combination of anti-PD-L1 and anti-IL-6 antibodies increases IFN-γ and Th1 in melanoma mice (Tsukamoto et al., 2018), turning off IL-6/STAT3 pathway, which further activates IFN-γ/STAT1 for causing local inflammation (Xiang et al., 2020). In addition, inflammatory factors contribute to the accumulation of immune cells. TNF-α contributes to Th17 differentiation in colon cancer treated with anti-CTLA-4 (Beck et al., 2006), possibly due to IL-23/Th17 axis activation (Liu et al., 2021). In addition, eosinophils in the skin (Voskens et al., 2013) and macrophages in acute diabetes (Hu et al., 2020) are also the result of the application of ICIs by IFN-α or γ.

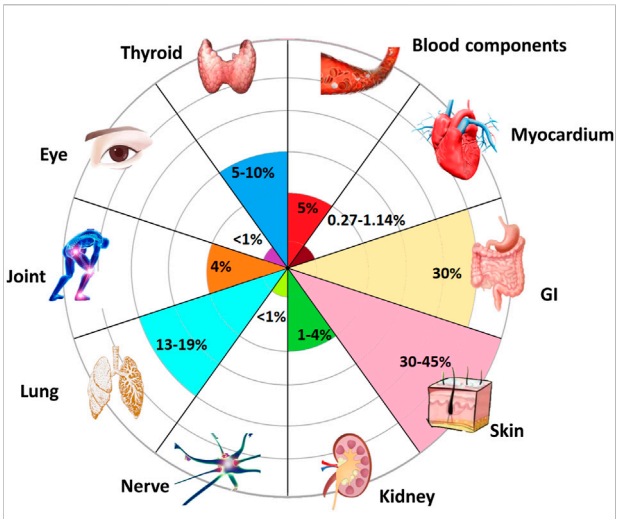

FIGURE 3
Organs susceptible to inflammatory toxicity induced by ICIs. Almost all organs may develop irAEs after receiving ICIs (Poto et al., 2022). Among them, the most common side effects occurred in skin, with an incidence rate of 40%. Gastrointestinal (GI) system with the occurrence of 30%. Followed by lungs and thyroid. The incidence of joints, blood components, and kidneys are all around 5%, while ocular, myocardial, and nerve involvement have been reported rare with a rate less than 1%.

Further, the expansion of the inflammatory factor cascade leads to immune damage to normal tissues, which is the main cause of side effects. IrAEs can occur in various organs (Figure 3) and are associated with good responses to ICIs (Saleh et al., 2019). However, an overresponse can hinder the course of ICIs treatment (Saleh et al., 2019), and the presence of severe irAEs leads to discontinuation of ICIs therapy temporarily or permanently according to guidelines. Induction of increased immune-promoting cells, such as a marked expansion of Th17 cells, is an independent risk factor for severe colitis in patients receiving ipilimumab (Tarhini et al., 2015). In contrast, immunosuppressive cells, such as Treg cells, tend to be depleted after treatment with ICIs (Simpson et al., 2013). The influx of myeloid cells also stimulates organ damage (Nam et al., 2019). In addition, different irAEs may have their specific cytokine profiles (Table 2). Circulating baseline IL-17 levels may help predict patients who are likely to develop severe diarrhea and colitis after treatment with ICIs (Young et al., 2018). However, IL-22 was not elevated (Luoma et al., 2020). The inflammatory response in rheumatoid arthritis is often accompanied by abundant TNF-α and IL-6 (Mcinnes et al.,

TABLE 2 Differences of irAEs in Inflammatory Factors.

	irAEs	Inflammatory factors	References	Anti-TNF	References	Anti-IL6	References
Digestive system	Diarrhea, colitis	IL-17	Young et al. (2018)	Efficient	Perez-Ruiz et al. (2019)	Aggravate	Korzenik et al. (2019)
Endocrine System	Thyroiditis	IL-1β, 2, GM-CSF	Kurimoto et al. (2020)	—		—	
Circulatory system	Myocarditis	—		Aggravate	Kwon et al. (2003)	—	
Motor system	Arthritis	TNF-α, IL-6	Mcinnes et al. (2016)	Efficient	Cappelli et al. (2018)	Efficient	Sang et al. (2017)
Respiratory system	Pneumonia	—		Aggravate	Akiyama et al. (2016)	Efficient	Stroud et al. (2019)
Nervous system	Demyelination, encephalitis	—		—		Efficient	Stroud et al. (2019)
Skin	Psoriasis, alopecia areata	IL-2,6,17,23,CXCL9,10,11, IFN-γ, TNF-α	Dulos et al. (2012), Mcinnes et al. (2016), Murata et al. (2017), Goldinger et al. (2016), Vivar et al. (2017)	—		—	

2016). PD-1 blockade results in increases in IFN-γ, TNF-α, IL-2, 6, 17, and 23 (Dulos et al., 2012; Mcinnes et al., 2016). These changes may trigger psoriasis when treated with PD-1 inhibitors (Murata et al., 2017). However, IL-8 was not associated with dermatitis (Tanaka et al., 2017). In addition, upregulation of CXCL9, CXCL10, and CXCL11 has also been observed to correlate with PD-1 drug-related skin toxicity (Goldinger et al., 2016; Vivar et al., 2017). Prior to treatment, higher concentrations of IL-1β, 2, and GM-CSF were exposed in thyroid irAE (Kurimoto et al., 2020). Anti-TNF monoclonal antibodies prevent colitis (Perez-Ruiz et al., 2019), but at the same time may exacerbate cardiotoxicity associated with ICIs (Kwon et al., 2003) and may exacerbate interstitial lung disease (Akiyama et al., 2016). Pneumonitis, serum sickness, encephalitis, and systemic inflammatory response syndrome were all improved when anti-IL-6 antibodies were used to treat severe IRAE (Stroud et al., 2019). However, it increases the risk of inflammatory bowel disease (Korzenik et al., 2019). Arthritis induced by ICIs can also be ameliorated by inhibition of IL-6 and TNF-α (Sang et al., 2017; Cappelli et al., 2018). Other cytokines, such as IL-12p70, 1α, 1RA and 13, IFN-α2, CSF, CX3CL1, and FGF-2, were also differentially expressed in the plasma of severe irAEs patients before and during ICIs treatment (Tarhini et al., 2015), but they The association with specific classes of IRAEs and their associated mechanisms are unclear.

4 Conclusion and future perspectives

Less than half of the cases respond to ICIs (Young et al., 2018), and there is a lack of effective predictors. A personalized panel composed of various inflammatory factors is a proposed predictive tool, the main factors including IFN, TLR, IL, TNF-α and TGF-β. They were selected for affecting PD-L1 expression and immune cell infiltration. They not only activate signaling pathways or regulate chemokines but also participate in ECM remodeling or balance pro- and anti-inflammatory effects.

IrAEs occurred more frequently when ICIs treatment was shifted from monotherapy to combination therapy (Johnson et al., 2020). Balancing anti-inflammatory and pro-inflammatory is expected to resolve the dilemma between anticancer and anti-irAEs of ICIs therapy, so some combination drugs have been tried other than glucocorticoids. The first is inflammatory pathway inhibitors. PI3K blockade fights cancer and reduces side effects by silencing inflammatory pathways (Eschweiler et al., 2022). The second is inflammatory factor inhibitors, which have a bidirectional effect. Anti- and pro-inflammatory are regulated by TNF through binding to different receptors (TNFR1 and TNFR2) (Chen et al., 2021), and by IL-6 through activation of different signals (JAK-STAT3 or PI3K-Akt) (Nguyen et al., 2014). The third is small molecule inhibitors of immune checkpoints and nanoparticles (Zhang et al., 2019). Small-molecule inhibitors can reduce affinity to reduce IRAEs, while nanoparticles facilitate targeting to improve anticancer efficacy.

The influence of inflammatory factors is not only applicable to ICIs treatment, but also to other immunotherapies. Immune-related side effects are triggered consistently across various immunotherapies, all resulting from cytokine cascades (Weber et al., 2015). For example, in adaptive immune cell therapy, IL-6, IL-1 are the

main triggers of cytokine release syndrome. Likewise, up-regulated IFN and IL-2 caused gastrointestinal reactions and thyroid damage during cytokine therapy. Due to the universality of the effects and side effects of inflammatory factors in various immunotherapies, the understanding of inflammatory factors in ICIs may be extended to immunotherapy in pan-cancer and benefit more patients.

Author contributions

YW did the literature research and wrote the article. SY and HQ revised the manuscripts. All authors read and approved the final manuscript.

Conflict of interest

The authors declare that the research was conducted in the absence of any commercial or financial relationships that could be construed as a potential conflict of interest.

Publisher's note

References

Abiko, K., Matsumura, N., Hamanishi, J., HorikawaN. MuRakami, R., Yamaguchi, K., et al. (2015). IFN-γ from lymphocytes induces PD-L1 expression and promotes progression of ovarian cancer. *Br. J. Cancer* 112 (9), 1501–1509. doi:10.1038/bjc.2015.101

Abril-Rodriguez, G., and Ribas, A. (2017). SnapShot: Immune checkpoint inhibitors. *Cancer Cell* 31 (6), 848. doi:10.1016/j.ccell.2017.05.010

Akiyama, M., Kaneko, Y., Yamaoka, K., Kondo, H., and Takeuchi, T. (2016). Association of disease activity with acute exacerbation of interstitial lung disease during tocilizumab treatment in patients with rheumatoid arthritis: A retrospective, case-control study. *Rheumatol. Int.* 36, 881–889. doi:10.1007/s00296-016-3478-3

Arakawa, A., Vollmer, S., Tietze, J., Galinski, A., Heppt, M. V., Burdek, M., et al. (2019). Clonality of CD4+ blood T cells predicts longer survival with CTLA4 or PD-1 checkpoint inhibition in advanced melanoma. *Front. Immunol.* 10, 1336. doi:10.3389/fimmu.2019.01336

Baas, M., Besançon, A., Goncalves, T., Valette, F., Yagita, H., Sawitzki, B., et al. (2016). TGFβ-dependent expression of PD-1 and PD-L1 controls CD8+ T cell anergy in transplant tolerance[J]. *Elife* 5, e08133. doi:10.7554/eLife.08133

Bagaev, A., Kotlov, N., Nomie, K., Svekolkin, V., Gafurov, A., Isaeva, O., et al. (2021). Conserved pan-cancer microenvironment subtypes predict response to immunotherapy. *Cancer Cell* 39 (6), 845–865.e7. e7. doi:10.1016/j.ccell.2021.04.014

Bagchi, S., Yuan, R., and Engleman, E. G. (2021). Immune checkpoint inhibitors for the treatment of cancer: Clinical impact and mechanisms of response and resistance. *Annu. Rev. Pathol.* 16 (1), 223–249. doi:10.1146/annurev-pathol-042020-042741

Bassez, A., Vos, H., Van Dyck, L., Floris, G., Arijs, I., Desmedt, C., et al. (2021). A single-cell map of intratumoral changes during anti-PD1 treatment of patients with breast cancer. *Nat. Med.* 27 (5), 820–832. doi:10.1038/s41591-021-01323-8

Beck, K. E., Blansfield, J. A., Tran, K. Q., Feldman, A. L., Hughes, M. S., Royal, R. E., et al. (2006). Enterocolitis in patients with cancer after antibody blockade of cytotoxic T-lymphocyte-associated antigen 4. *J. Clin. Oncol.* 24 (15), 2283–2289. doi:10.1200/JCO.2005.04.5716

Bellucci, R., Martin, A., Bommarito, D., Wang, K., Hansen, S. H., Freeman, G. J., et al. (2015). Interferon-γ-induced activation of JAK1 and JAK2 suppresses tumor cell susceptibility to NK cells through upregulation of PD-L1 expression. *Oncoimmunology* 4 (6), e1008824. doi:10.1080/2162402X.2015.1008824

Berghuis, D., Santos, S. J., Baelde, H. J., Taminiau, A. H., Egeler, R. M., Schilham, M. W., et al. (2011). Pro-inflammatory chemokine-chemokine receptor interactions within the Ewing sarcoma microenvironment determine CD8(+) T-lymphocyte infiltration and affect tumour progression. *J. Pathol.* 223, 347–357. doi:10.1002/path.2819

Berner, F., Bomze, D., Diem, S., Ali, O. H., Fassler, M., Ring, S., et al. (2019). Association of checkpoint inhibitor-induced toxic effects with shared cancer and tissue antigens in non-small cell lung cancer. *JAMA Oncol.* 5 (7), 1043–1047. doi:10.1001/jamaoncol.2019.0402

Bhattacharjee, O., Ayyangar, U., Kurbet, A. S., Ashok, D., and Raghavan, S. (2019). Unraveling the ECM-immune cell crosstalk in skin diseases. *Front. Cell Dev. Biol.* 7, 68. doi:10.3389/fcell.2019.00068

Billottet, C., Quemener, C., and Bikfalvi, A. (2013). CXCR3, a double-edged sword in tumor progression and angiogenesis. *Biochim. Biophys. Acta* 1836 (2), 287–295. doi:10.1016/j.bbcan.2013.08.002

Binnewies, M., Roberts, E. W., Kersten, K., Chan, V., Fearon, D. F., Merad, M., et al. (2018). Understanding the tumor immune microenvironment (TIME) for effective therapy. *Nat. Med.* 24 (5), 541–550. doi:10.1038/s41591-018-0014-x

Boes, M., and Meyer-Wentrup, F. (2015). TLR3 triggering regulates PD-L1 (CD274) expression in human neuroblastoma cells. *Cancer Lett.* 361 (1), 49–56. doi:10.1016/j.canlet.2015.02.027

Bolton, H. A., Zhu, E., Terry, A. M., Guy, T. V., Koh, W. P., Tan, S. Y., et al. (2015). Selective Treg reconstitution during lymphopenia normalizes DC costimulation and prevents graft-versus-host disease. *J. Clin. Invest* 125, 3627–3641. doi:10.1172/JCI76031

Borghaei, H., Paz-Ares, L., Horn, L., Spigel, D. R., Steins, M., Ready, N. E., et al. (2015). Nivolumab versus docetaxel in advanced nonsquamous non-small-cell lung cancer. *N. Engl. J. Med. Overseas. Ed.* 373, 1627–1639. doi:10.1056/nejmoa1507643

Brunn, D., Turkowski, K., Günther, S., Weigert, A., Muley, T., Kriegsmann, M., et al. (2021). Interferon regulatory factor 9 promotes lung cancer progression via regulation of versican. *Cancers (Basel)* 13 (2), 208. doi:10.3390/cancers13020208

Bulliard, Y., Jolicoeur, R., Windman, M., Rue, S. M., Ettenberg, S., Knee, D. A., et al. (2013). Activating Fc γ receptors contribute to the antitumor activities of immunoregulatory receptor-targeting antibodies. *J. Exp. Med.* 210, 1685–1693. doi:10.1084/jem.20130573

Burbage, M., and Amigorena, S. (2020). A dendritic cell multitasks to tackle cancer. *Nature* 584 (7822), 533–534. doi:10.1038/d41586-020-02339-9

Calon, A., Tauriello, D., and Batlle, E. (2014). TGF-beta in CAF-mediated tumor growth and metastasis. *Semin. Cancer Biol.* 25, 15–22. doi:10.1016/j.semcancer.2013.12.008

Camisaschi, C., Casati, C., Rini, F., Perego, M., De Filippo, A., Triebel, F., et al. (2010). LAG-3 expression defines a subset of CD4(+)CD25(high)Foxp3(+) regulatory T cells that are expanded at tumor sites. *J. Immunol.* 184, 6545–6551. doi:10.4049/jimmunol.0903879

Cappelli, L. C., Brahmer, J. R., Forde, P. M., Le, D. T., Lipson, E. J., Naidoo, J., et al. (2018). Clinical presentation of immune checkpoint inhibitor-induced inflammatory arthritis differs by immunotherapy regimen[J]. *Seminars Arthritis Rheumatism* 48 (3), 553–557. doi:10.1016/j.semarthrit.2018.02.011

Carbotti, G., Barisione, G., Airoldi, I., Mezzanzanica, D., Bagnoli, M., Ferrero, S., et al. (2015). IL-27 induces the expression of Ido and PD-L1 in human cancer cells. *Oncotarget* 6 (41), 43267–43280. doi:10.18632/oncotarget.6530

Caroline, R., Long, G. V., Brady, B., Dutriaux, C., Maio, M., Mortier, L., et al. (2015). Nivolumab in previously untreated melanoma without BRAF mutation[J]. *N. Engl. J. Med.* 372 (4), 320–330.

Carretero, R., Sektioglu, I. M., Garbi, N., Salgado, O. C., Beckhove, P., and Hammerling, G. J. (2015). Eosinophils orchestrate cancer rejection by normalizing tumor vessels and enhancing infiltration of CD8(+) T cells. *Nat. Immunol.* 16 (6), 609–617. doi:10.1038/ni.3159

Chakravarthy, A., Khan, L., Bensler, N. P., Bose, P., and De Carvalho, D. D. (2018). TGF-β-associated extracellular matrix genes link cancer-associated fibroblasts to immune evasion and immunotherapy failure. *Nat. Commun.* 9 (1), 4692. doi:10.1038/s41467-018-06654-8

Chang, M. Y., Kang, I., Gale, M., Manicone, A. M., Kinsella, M. G., Braun, K. R., et al. (2017). Versican is produced by Trif- and type I interferon-dependent signaling in macrophages and contributes to fine control of innate immunity in lungs. *Am. J. Physiol. Lung Cell. Mol. Physiol.* 313 (6), L1069–L1086. doi:10.1152/ajplung.00353.2017

Chen, A. Y., Wolchok, J. D., and Bass, A. R. (2021). TNF in the era of immune checkpoint inhibitors: Friend or foe?[J]. *Nat. Rev. Rheumatol.* 17 (4), 213–223. doi:10.1038/s41584-021-00584-4

Chen, D. S., and Mellman, I. (2017). Elements of cancer immunity and the cancer-immune set point. *Nature* 541 (7637), 321–330. doi:10.1038/nature21349

Chen, H. M., Touw, W., Wang, Y. S., Kang, K., Mai, S., Zhang, J., et al. (2018). Blocking immunoinhibitory receptor LILRB2 reprograms tumor-associated myeloid cells and promotes antitumor immunity. *J. Clin. Invest.* 128 (12), 5647–5662. doi:10.1172/JCI97570

Chen, J., Feng, Y., Lu, L., Wang, H., Dai, L., Li, Y., et al. (2012). Interferon-γ-induced PD-L1 surface expression on human oral squamous carcinoma via PKD2 signal pathway. *Immunobiology* 217 (4), 385–393. doi:10.1016/j.imbio.2011.10.016

Chen, L., Qiu, X., Wang, X., and He, J. (2017). FAP positive fibroblasts induce immune checkpoint blockade resistance in colorectal cancer via promoting immunosuppression. *Biochem. Biophys. Res. Commun.* 487 (1), 8–14. doi:10.1016/j.bbrc.2017.03.039

Chen, P. L., Roh, W., Reuben, A., Cooper, Z. A., Spencer, C. N., Prieto, P. A., et al. (2016). Analysis of immune signatures in longitudinal tumor samples yields insight into biomarkers of response and mechanisms of resistance to immune checkpoint blockade. *Cancer Discov.* 6 (8), 827–837. doi:10.1158/2159-8290.CD-15-1545

Chen, Y., Kuchroo, V., Inobe, J., Hafler, D. A., and Weiner, H. L. (1994). Regulatory T cell clones induced by oral tolerance: Suppression of autoimmune encephalomyelitis. *Science* 265 (5176), 1237–1240. doi:10.1126/science.7520605

Chi, P. L., Cheng, C. C., Hung, C. C., Wang, M. T., Liu, H. Y., Ke, M. W., et al. (2022). MMP-10 from M1 macrophages promotes pulmonary vascular remodeling and pulmonary arterial hypertension. *Int. J. Biol. Sci.* 18 (1), 331–348. doi:10.7150/ijbs.66472

ChristmasEntinostat, B. J., Rafie, C. I., Hopkins, A. C., Scott, B. A., Ma, H. S., Cruz, K. A., et al. (2018). Entinostat converts immune-resistant breast and pancreatic cancers into checkpoint-responsive tumors by reprogramming tumor-infiltrating MDSCs. *Cancer Immunol. Res.* 6, 1561–1577. doi:10.1158/2326-6066.CIR-18-0070

Chung, J. Y. F., Chan, M. K. K., Li, J. S. F., Chan, A. S. W., Tang, P. C. T., Leung, K. T., et al. (2021). TGF-B signaling: From tissue fibrosis to tumor microenvironment. *Int. J. Mol. Sci.* 22 (14), 7575. doi:10.3390/ijms22147575

Cohen, N., Shani, O., Raz, Y., Sharon, Y., Hoffman, D., Abramovitz, L., et al. (2017). Fibroblasts drive an immunosuppressive and growth-promoting microenvironment in breast cancer via secretion of Chitinase 3-like 1. *Oncogene* 36, 4457–4468. doi:10.1038/onc.2017.65

Cole, J. E., Navin, T. J., Cross, A. J., Goddard, M. E., Alexopoulou, L., Mitra, A. T., et al. (2011). Unexpected protective role for Toll-like receptor 3 in the arterial wall. *Proc. Natl. Acad. Sci. U. S. A.* 108 (6), 2372–2377. doi:10.1073/pnas.1018515108

Cooper, Z. A., Reuben, A., Spencer, C. N., Prieto, P. A., Austin-Breneman, J. L., Jiang, H., et al. (2016). Distinct clinical patterns and immune infiltrates are observed at time of progression on targeted therapy versus immune checkpoint blockade for melanoma. *Oncoimmunology* 5 (3), e1136044. doi:10.1080/2162402X.2015.1136044

Creery, D., Weiss, W., Lim, W. T., AZiZ, Z., Angel, J. B., and KumAr, A. (2004). Down-regulation of CXCR-4 and CCR-5 expression by interferon-gamma is associated with inhibition of chemotaxis and human immunodeficiency virus (HIV) replication but not HIV entry into human monocytes. *Clin. Exp. Immunol.* 137 (1), 156–165. doi:10.1111/j.1365-2249.2004.02495.x

Daurkin, I., Eruslanov, E., Vieweg, J., and Kusmartsev, S. (2010). Generation of antigen-presenting cells from tumor-infiltrated CD11b myeloid cells with DNA demethylating agent 5-aza-2'-deoxycytidine. *Cancer Immunol. Immunother.* 59, 697–706. doi:10.1007/s00262-009-0786-4

Dulos, J., Carven, G. J., Boxtel, S. V., Evers, S., Driessen-Engels, L. J. A., Hobo, W., et al. (2012). PD-1 blockade augments Th1 and Th17 and suppresses Th2 responses in peripheral blood from patients with prostate and advanced melanoma cancer. *J. Immunother.* 35 (2), 169–178. doi:10.1097/CJI.0b013e318247a4e7

Eppihimer, M. J., Gunn, J., Freeman, G. J., Greenfield, E. A., Chernova, T., Erickson, J., et al. (2015). Expression and regulation of the PD-L1 immunoinhibitory molecule on microvascular endothelial cells. *Microcirculation* 9 (2), 133–145. doi:10.1038/sj/mn/7800123

Eruslanov, E. B., Bhojnagarwala, P. S., Quatromoni, J. G., Stephen, T. L., Ranganathan, A., Deshpande, C., et al. (2014). Tumor-associated neutrophils stimulate T cell responses in early-stage human lung cancer. *J. Clin. Invest.* 124 (12), 5466–5480. doi:10.1172/JCI77053

Eschweiler, S., Ramírez-Suástegui, C., Li, Y., King, E., Chudley, L., Thomas, J., et al. (2022). Intermittent PI3Kδ inhibition sustains anti-tumour immunity and curbs irAEs. *Nature* 605 (7911), 741–746. doi:10.1038/s41586-022-04685-2

Evanko, S. P., Potter-Perigo, S., Bollyky, P. L., Nepom, G. T., and Wight, T. N. (2012). Hyaluronan and versican in the control of human T-lymphocyte adhesion and migration. *Matrix Biol.* 31 (2), 90–100. doi:10.1016/j.matbio.2011.10.004

Fehrenbacher, L., Spira, A., Ballinger, M., Kowanetz, M., Vansteenkiste, J., Mazieres, J., et al. (2016). Atezolizumab versus docetaxel for patients with previously treated non-small-cell lung cancer (POPLAR): A multicentre, open-label, phase 2 randomised controlled trial. *Lancet* 387 (10030), 1837–1846. doi:10.1016/S0140-6736(16)00587-0

Feig, C., Jones, J. O., Kraman, M., Wells, R. J. B., Deonarine, A., Chan, D. S., et al. (2013). Targeting CXCL12 from FAP-expressing carcinoma-associated fibroblasts synergizes with anti-PD-L1 immunotherapy in pancreatic cancer. *Proc. Natl. Acad. Sci. U. S. A.* 110 (50), 20212–20217. doi:10.1073/pnas.1320318110

Fridlender, Z. G., Buchlis, G., Kapoor, V., Cheng, G., Sun, J., Singhal, S., et al. (2010). CCL2 blockade augments cancer immunotherapy. *Cancer Res.* 70 (1), 109–118. doi:10.1158/0008-5472.CAN-09-2326

Friedline, R. H., Brown, D. S., Nguyen, H., Kornfeld, H., Lee, J., Zhang, Y., et al. (2009). CD4+ regulatory T cells require CTLA-4 for the maintenance of systemic tolerance. *J. Exp. Med.* 206 (2), 421–434. doi:10.1084/jem.20081811

Fujita, M. (2021). EGCG inhibits tumor growth in melanoma by targeting JAK-STAT signaling and its downstream PD-L1/PD-L2-PD1 Axis in tumors and enhancing cytotoxic T-cell responses[J]. *Pharmaceuticals* 14 (11), 1081.

Gabrilovich, D. I. (2017). Myeloid-derived suppressor cells. *Cancer Immunol. Res.* 5 (1), 3–8. doi:10.1158/2326-6066.CIR-16-0297

Gaggioli, C., Hooper, S., Hidalgo-Carcedo, C., Grosse, R., Marshall, J. F., Harrington, K., et al. (2007). Fibroblast-led collective invasion of carcinoma cells with differing roles for RhoGTPases in leading and following cells. *Nat. Cell Biol.* 9 (12), 1392–1400. doi:10.1038/ncb1658

Gang, H., Qianjun, W., Yongliang, Z., Qiangguo, G., Yun, B., et al. (2013). NF-κB plays a key role in inducing CD274 expression in human monocytes after lipopolysaccharide treatment[J]. *Plos One* 8 (4), e61602.

Garcia-Diaz, A., Shin, D. S., Moreno, B. H., Saco, J., Escuin-Ordinas, H., Rodriguez, G. A., et al. (2017). Interferon receptor signaling pathways regulating PD-L1 and PD-L2 expression. *Cell Rep.* 19 (6), 1189–1201. doi:10.1016/j.celrep.2017.04.031

García-Palmero, I., Torres, S., Bartolomé, R. A., Pelaez-GArciA, A., Larriba, M. J., Lopez-LucendoM., et al. (2016). Twist1-induced activation of human fibroblasts promotes matrix stiffness by upregulating palladin and collagen α1(VI). *Oncogene* 35 (40), 5224–5236. doi:10.1038/onc.2016.57

Godefroy, E., Gallois, A., Idoyaga, J., Merad, M., Tung, N., Monu, N., et al. (2014). Activation of toll-like receptor-2 by endogenous matrix metalloproteinase-2 modulates dendritic-cell-mediated inflammatory responses. *Cell Rep.* 9 (5), 1856–1870. doi:10.1016/j.celrep.2014.10.067

Goldinger, S. M., Stieger, P., Meier, B., Micaletto, S., Contassot, E., French, L. E., et al. (2016). Cytotoxic cutaneous adverse drug reactions during anti-PD-1 therapy. *Clin. Cancer Res.* 22 (16), 4023–4029. doi:10.1158/1078-0432.CCR-15-2872

Gordon, S. R., Maute, R. L., Dulken, B. W., Hutter, G., George, B. M., McCracken, M. N., et al. (2017). PD-1 expression by tumour-associated macrophages inhibits phagocytosis and tumour immunity. *Nature* 545 (7655), 495–499. doi:10.1038/nature22396

Gorter, A., Zijlmans, H. J., van Gent, H., Trimbos, J. B., Fleuren, G. J., and Jordanova, E. S. (2010). Versican expression is associated with tumor-infiltrating CD8-positive T cells and infiltration depth in cervical cancer. *Mod. Pathol.* 23 (12), 1605–1615. doi:10.1038/modpathol.2010.154

Gowrishankar, K., Gunatilake, D., Gallagher, S. J., Tiffen, J., Rizos, H., and Hersey, P. (2015). Inducible but not constitutive expression of PD-L1 in human melanoma cells is dependent on activation of NF-κB[J]. *Plos One* 10 (4), e0123410. doi:10.1371/journal.pone.0123410

Grum-Schwensen, B., Klingelhofer, J., Berg, C. H., El-Naaman, C., Grigorian, M., Lukanidin, E., et al. (2005). Suppression of tumor development and metastasis formation in mice lacking the S100A4(mts1) gene. *Cancer Res.* 65 (9), 3772–3780. doi:10.1158/0008-5472.CAN-04-4510

Hallmann, R., Zhang, X., Di Russo, J., Li, L., Song, J., Hannocks, M. J., et al. (2015). The regulation of immune cell trafficking by the extracellular matrix. *Curr. Opin. Cell Biol.* 36, 54–61. doi:10.1016/j.ceb.2015.06.006

Han, N., Li, X., Wang, Y., Wang, L., Zhang, C., Zhang, Z., et al. (2021). Increased tumor-infiltrating plasmacytoid dendritic cells promote cancer cell proliferation and invasion via TNF-α/NF-κB/CXCR-4 pathway in oral squamous cell carcinoma. *J. Cancer* 12 (10), 3045–3056. doi:10.7150/jca.55580

Harlin, H., Meng, Y., Peterson, A. C., Zha, Y., Tretiakova, M., Slingluff, C., et al. (2009). Chemokine expression in melanoma metastases associated with CD8+ T-cell recruitment. *Cancer Res.* 69 (7), 3077–3085. doi:10.1158/0008-5472.CAN-08-2281

Hart, K. M., Byrne, K. T., Molloy, M. J., Usherwood, E. M., and Berwin, B. (2011). IL-10 immunomodulation of myeloid cells regulates a murine model of ovarian cancer. *Front. Immunol.* 2, 29. doi:10.3389/fimmu.2011.00029

Haslam, A., and Prasad, V. (2019). Estimation of the percentage of US patients with cancer who are eligible for and respond to checkpoint inhibitor immunotherapy drugs. *JAMA Netw. Open* 2 (5), e192535. doi:10.1001/jamanetworkopen.2019.2535

Hegde, P. S., and Chen, D. S. (2020). Top 10 challenges in cancer immunotherapy. *Immunity* 52, 17–35. doi:10.1016/j.immuni.2019.12.011

Ho, Y. J., Li, J. P., Fan, C. H., Liu, H. L., and Yeh, C. K. (2020). Ultrasound in tumor immunotherapy: Current status and future developments. *J. Control. Release* 323, 12–23. doi:10.1016/j.jconrel.2020.04.023

Hope, C., Emmerich, P. B., Papadas, A., Pagenkopf, A., Matkowskyj, K. A., Van De Hey, D. R., et al. (2017). Versican-derived matrikines regulate batf3-dendritic cell differentiation and promote T cell infiltration in colorectal cancer. *J. Immunol.* 199 (5), 1933–1941. doi:10.4049/jimmunol.1700529

Hopkins, A. C., Yarchoan, M., Durham, J. N., Yusko, E. C., Rytlewski, J. A., Robins, H. S., et al. (2018). T cell receptor repertoire features associated with survival in immunotherapy-treated pancreatic ductal adenocarcinoma. *JCI Insight* 3 (13), 122092. doi:10.1172/jci.insight.122092

Hu, H., Zakharov, P. N., Peterson, O. J., and Unanue, E. R. (2020). Cytocidal macrophages in symbiosis with CD4 and CD8 T cells cause acute diabetes following checkpoint blockade of PD-1 in NOD mice. *Proc. Natl. Acad. Sci. U. S. A.* 117 (49), 31319–31330. doi:10.1073/pnas.2019743117

Huang, C. T., Workman, C. J., Flies, D., Pan, X., Marson, A. L., Zhou, G., et al. (2004). Role of LAG-3 in regulatory T cells. *Immunity* 21 (4), 503–513. doi:10.1016/j.immuni.2004.08.010

Huang, R. R., Jalil, J., Economou, J. S., Chmielowski, B., Koya, R. C., Mok, S., et al. (2011). CTLA4 blockade induces frequent tumor infiltration by activated lymphocytes regardless of clinical responses in humans. *Clin. Cancer Res.* 17 (12), 4101–4109. doi:10.1158/1078-0432.CCR-11-0407

Hurkmans, D. P., Jensen, C., Koolen, S. L. W., Aerts, J., Karsdal, M. A., Mathijssen, R. H. J., et al. (2020). Blood-based extracellular matrix biomarkers are correlated with clinical outcome after PD-1 inhibition in patients with metastatic melanoma. *J. Immunother. Cancer* 8 (2), e001193. doi:10.1136/jitc-2020-001193

Huse, M. (2017). Mechanical forces in the immune system. *Nat. Rev. Immunol.* 17, 679–690. doi:10.1038/nri.2017.74

Hynes, R. O. (2009). The extracellular matrix: Not just pretty fibrils. *Science* 326 (5957), 1216–1219. doi:10.1126/science.1176009

Iga, N., Otsuka, A., Yamamoto, Y., Nakashima, C., Honda, T., Kitoh, A., et al. (2019). Accumulation of exhausted CD8+ T cells in extramammary Paget's disease. *PLoS ONE* 14 (1), e0211135. doi:10.1371/journal.pone.0211135

Ishihara, J., Fukunaga, K., Ishihara, A., Larsson, H. M., Potin, L., Hosseinchi, P., et al. (2017). Matrix-binding checkpoint immunotherapies enhance antitumor efficacy and reduce adverse events. *Sci. Transl. Med.* 9 (415), eaan0401. doi:10.1126/scitranslmed.aan0401

Jacobetz, M. A., Chan, D. S., Neesse, A., Bapiro, T. E., Cook, N., Frese, K. K., et al. (2013). Hyaluronan impairs vascular function and drug delivery in a mouse model of pancreatic cancer. *Gut* 62 (1), 112–120. doi:10.1136/gutjnl-2012-302529

Jensen, C., Nissen, N. I., Arenstorff, C., Karsdal, M. A., and Willumsen, N. (2021). Serological assessment of collagen fragments and tumor fibrosis may guide immune checkpoint inhibitor therapy. *J. Exp. Clin. Cancer Res.* 40 (1), 326. doi:10.1186/s13046-021-02133-z

Jensen, C., Sinkeviciute, D., Madsen, D. H., Onnerfjord, P., Hansen, M., Schmidt, H., et al. (2020). Granzyme B degraded type IV collagen products in serum identify melanoma patients responding to immune checkpoint blockade. *Cancers (Basel)* 12 (10), 2786. doi:10.3390/cancers12102786

Ji, M., Liu, Y., Li, Q., Li, X. D., Zhao, W. Q., Zhang, H., et al. (2015). PD-1/PD-L1 pathway in non-small-cell lung cancer and its relation with EGFR mutation. *J. Transl. Med.* 13 (1), 5. doi:10.1186/s12967-014-0373-0

Jiao, S., Subudhi, S. K., Aparicio, A., Ge, Z., Guan, B., Miura, Y., et al. (2019). Differences in tumor microenvironment dictate T helper lineage polarization and response to immune checkpoint therapy. *Cell* 179 (5), 1177–1190. e13. doi:10.1016/j.cell.2019.10.029

Johnson, D. B., Reynolds, K. L., Sullivan, R. J., Balko, J. M., Patrinely, J. R., Cappelli, L. C., et al. (2020). Immune checkpoint inhibitor toxicities: Systems-based approaches to improve patient care and research[J]. *Lancet Oncol.* 21 (8), e398–e404. doi:10.1016/S1470-2045(20)30107-8

June, C. H., and Bluestone, J. A. (2017). Is autoimmunity the achilles' heel of cancer immunotherapy? [j]. *Nat. Med.* 23 (8), 540–547. doi:10.1038/nm.4321

Kagamu, H., Kitano, S., Ou, Y., Yoshimura, K., Horimoto, K., Kitazawa, M., et al. (2020). CD4+ T-cell immunity in the peripheral blood correlates with response to anti-PD-1 therapy. *Cancer Immunol. Res.* 8 (3), 334–344. doi:10.1158/2326-6066.CIR-19-0574

Karachaliou, N., Gonzalez-Cao, M., Crespo, G., Drozdowskyj, A., Aldeguer, E., Gimenez-Capitan, A., et al. (2018). Interferon gamma, an important marker of response to immune checkpoint blockade in non-small cell lung cancer and melanoma patients. *Ther. Adv. Med. Oncol.* 10, 1758834017749748. doi:10.1177/1758834017749748

Karakhanova, S., Bedke, T., Enk, A. H., and Mahnke, K. (2011). IL-27 renders DC immunosuppressive by induction of B7-H1. *J. Leukoc. Biol.* 89 (6), 837–845. doi:10.1189/jlb.1209788

Katsumata, K., Ishihara, J., Mansurov, A., Ishihara, A., Raczy, M. M., Yuba, E., et al. (2019). Targeting inflammatory sites through collagen affinity enhances the therapeutic efficacy of anti-inflammatory antibodies. *Sci. Adv.* 5 (11), eaay1971. doi:10.1126/sciadv.aay1971

Kim, S. H., Oh, J., Choi, J. Y., Jang, J. Y., Kang, M. W., and Lee, C. E. (2008). Identification of human thioredoxin as a novel IFN-gamma-induced factor: Mechanism of induction and its role in cytokine production. *BMC Immunol.* 9, 64. doi:10.1186/1471-2172-9-64

Kinter, A. L., Godbout, E. J., Mcnally, J. P., Sereti, I., Roby, G. A., O'Shea, M. A., et al. (2008). The common gamma-chain cytokines IL-2, IL-7, IL-15, and IL-21 induce the expression of programmed death-1 and its ligands. *J. Immunol.* 181 (10), 6738–6746. doi:10.4049/jimmunol.181.10.6738

Kitano, S., Nakayama, T., and Yamashita, M. (2018). Biomarkers for immune checkpoint inhibitors in melanoma. *Front. Oncol.* 8 (7), 270. doi:10.3389/fonc.2018.00270

Ko, J. S., Zea, A. H., Rini, B. I., Ireland, J. L., Elson, P., Cohen, P., et al. (2009). Sunitinib mediates reversal of myeloid-derived suppressor cell accumulation in renal cell carcinoma patients. *Clin. Cancer Res.* 15, 2148–2157. doi:10.1158/1078-0432.CCR-08-1332

Kondo, A., Yamashita, T., Tamura, H., Zhao, W., Tsuji, T., Shimizu, M., et al. (2010). Interferon-gamma and tumor necrosis factor-alpha induce an immunoinhibitory molecule, B7-H1, via nuclear factor-kappaB activation in blasts in myelodysplastic syndromes. *Blood* 116 (7), 1124–1131. doi:10.1182/blood-2009-12-255125

Korzenik, J., Larsen, M. D., Nielsen, J., Kjeldsen, J., and Norgard, B. M. (2019). Increased risk of developing Crohn's disease or ulcerative colitis in 17 018 patients while under treatment with anti-TNFα agents, particularly etanercept, for autoimmune diseases other than inflammatory bowel disease. *Aliment. Pharmacol. Ther.* 50, 289–294. doi:10.1111/apt.15370

Krieg, C., Nowicka, M., Guglietta, S., Schindler, S., Hartmann, F. J., Weber, L. M., et al. (2018). High-dimensional single-cell analysis predicts response to anti-PD-1 immunotherapy. *Nat. Med.* 24 (2), 144–153. doi:10.1038/nm.4466

Kumar, V., Donthireddy, L., Marvel, D., Condamine, T., Wang, F., Lavilla-Alonso, S., et al. (2017). Cancer-associated fibroblasts neutralize the anti-tumor effect of CSF1 receptor blockade by inducing PMN-MDSC infiltration of tumors[J]. *Cancer Cell* 32 (5), 654–668. e5. doi:10.1016/j.ccell.2017.10.005

Kumar, V., Donthireddy, L., Marvel, D., Condamine, T., Wang, F., Lavilla-Alonso, S., et al. (2017). Cancer-associated fibroblasts neutralize the anti-tumor effect of CSF1 receptor blockade by inducing PMN-MDSC infiltration of tumors. *Cancer Cell* 32, 654–668. doi:10.1016/j.ccell.2017.10.005

Kurimoto, C., Inaba, H., Ariyasu, H., Iwakura, H., Ueda, Y., Uraki, S., et al. (2020). Predictive and sensitive biomarkers for thyroid dysfunctions during treatment with immune-checkpoint inhibitors. *Cancer Sci.* 111, 1468–1477. doi:10.1111/cas.14363

Kwon, H. J., Cote, T. R., Cuffe, M. S., Kramer, J. M., and Braun, M. M. (2003). Case reports of heart failure after therapy with a tumor necrosis factor antagonist. *Ann. Intern. Med.* 138 (10), 807–811. doi:10.7326/0003-4819-138-10-200305200-00008

Lakins, M. A., Ghorani, E., Munir, H., Martins, C. P., and Shields, J. D. (2018). Cancer-associated fibroblasts induce antigen-specific deletion of CD8 + T Cells to protect tumour cells. *Nat. Commun.* 9 (1), 948. doi:10.1038/s41467-018-03347-0

Li, B., Song, T. N., Wang, F. R., Yin, C., Li, Z., Lin, J. P., et al. (2019). Tumor-derived exosomal HMGB1 promotes esophageal squamous cell carcinoma progression through inducing PD1+ TAM expansion. *Oncogenesis* 8 (3), 17. doi:10.1038/s41389-019-0126-2

Li, S., Liu, M., Do, M. H., Chou, C., Stamatiades, E. G., Nixon, B. G., et al. (2020). Cancer immunotherapy via targeted TGF-β signalling blockade in TH cells. *Nature* 587 (7832), 121–125. doi:10.1038/s41586-020-2850-3

Liakou, C. I., Kamat, A., Tang, D. N., Chen, H., Sun, J., Troncoso, P., et al. (2008). CTLA-4 blockade increases IFNgamma-producing CD4+ICOShi cells to shift the ratio of effector to regulatory T cells in cancer patients. *Proc. Natl. Acad. Sci. U. S. A.* 105 (39), 14987–14992. doi:10.1073/pnas.0806075105

Liao, Y., Zhu, E., and Zhou, W. (2021). Ox-LDL aggravates the oxidative stress and inflammatory responses of THP-1 macrophages by reducing the inhibition effect of miR-491-5p on MMP-9. *Front. Cardiovasc. Med.* 8, 697236. doi:10.3389/fcvm.2021.697236

Liu, H., Shen, J., and Lu, K. (2017). IL-6 and PD-L1 blockade combination inhibits hepatocellular carcinoma cancer development in mouse model. *Biochem. Biophys. Res. Commun.* 486 (2), 239–244. doi:10.1016/j.bbrc.2017.02.128

Liu, J., Feng, L., Yu, P., Wang, L., Chen, X., Wang, D., et al. (2015). Local production of the chemokines CCL5 and CXCL10 attracts CD8+ T lymphocytes into esophageal squamous cell carcinoma. *Oncotarget* 6 (28), 24978–24989. doi:10.18632/oncotarget.4617

Liu, J. M., Jin, Q. X., Fujimoto, M., Li, F. F., Jin, L. B., Yu, R., et al. (2021). Dihydroartemisinin alleviates imiquimod-induced psoriasis-like skin lesion in mice involving modulation of IL-23/Th17 Axis. *Front. Pharmacol.* 12, 704481. doi:10.3389/fphar.2021.704481

Liubomirski, Y., Lerrer, S., Meshel, T., Morein, D., Rubinstein-Achiasaf, L., Sprinzak, D., et al. (2019). Notch-mediated tumor-stroma-inflammation networks promote invasive properties and CXCL8 expression in triple-negative breast cancer. *Front. Immunol.* 10, 804. doi:10.3389/fimmu.2019.00804

Ljunggren, H. G., Jonsson, R., and Höglund, P. (2018). Seminal immunologic discoveries with direct clinical implications: The 2018 Nobel Prize in Physiology or Medicine honours discoveries in cancer immunotherapy. *Scand. J. Immunol.* 88 (6), e12731. doi:10.1111/sji.12731

Loke, P., and Allison, J. P. (2003). PD-L1 and PD-L2 are differentially regulated by Th1 and Th2 cells. *Proc. Natl. Acad. Sci. U. S. A.* 100 (9), 5336–5341. doi:10.1073/pnas.0931259100

Lu, T., Ramakrishnan, R., Altiok, S., Youn, J. I., Cheng, P., Celis, E., et al. (2011). Tumor-infiltrating myeloid cells induce tumor cell resistance to cytotoxic T cells in mice. *J. Clin. Invest.* 121, 4015–4029. doi:10.1172/JCI45862

Lu, Y. C., Yeh, W. C., and Ohashi, P. S. (2008). LPS/TLR4 signal transduction pathway. *Cytokine* 42 (2), 145–151. doi:10.1016/j.cyto.2008.01.006

Luoma, A. M., Suo, S., Williams, H. L., Sharova, T., Sullivan, K., Manos, M., et al. (2020). Molecular pathways of colon inflammation induced by cancer immunotherapy. *Cell* 182 (3), 655–671. e622. doi:10.1016/j.cell.2020.06.001

Maekawa, N., Konnai, S., Asano, Y., Sajiki, Y., Deguchi, T., Okagawa, T., et al. (2022). Exploration of serum biomarkers in dogs with malignant melanoma receiving anti-PD-L1 therapy and potential of COX-2 inhibition for combination therapy. *Sci. Rep.* 12 (1), 9265. doi:10.1038/s41598-022-13484-8

Manou, D., Bouris, P., Kletsas, D., Gotte, M., Greve, B., Moustakas, A., et al. (2020). Serglycin activates pro-tumorigenic signaling and controls glioblastoma cell stemness, differentiation and invasive potential. *Matrix Biol. Plus* 6-7, 100033. doi:10.1016/j.mbplus.2020.100033

Mantovani, A., Marchesi, F., Malesci, A., Laghi, L., and Allavena, P. (2017). Tumour-associated macrophages as treatment targets in oncology. *Nat. Rev. Clin. Oncol.* 14, 399–416. doi:10.1038/nrclinonc.2016.217

Mariathasan, S., Turley, S. J., Nickles, D., Castiglioni, A., Yuen, K., Wang, Y., et al. (2018). TGFβ attenuates tumour response to PD-L1 blockade by contributing to exclusion of T cells. *Nature* 554 (7693), 544–548. doi:10.1038/nature25501

Martens, A., Wistuba-Hamprecht, K., Yuan, J., Postow, M. A., Wong, P., Capone, M., et al. (2016). Increases in absolute lymphocytes and circulating CD4+ and CD8+ T cells are associated with positive clinical outcome of melanoma patients treated with ipilimumab. *Clin. Cancer Res.* 22 (19), 4848–4858. doi:10.1158/1078-0432.CCR-16-0249

Mazanet, M. M., and Hughes, C. (2002). B7-H1 is expressed by human endothelial cells and suppresses T cell cytokine synthesis. *J. Immunol.* 169 (7), 3581–3588. doi:10.4049/jimmunol.169.7.3581

McDermott, D. F., Huseni, M. A., Atkins, M. B., Motzer, R. J., Rini, B. I., Escudier, B., et al. (2018). Clinical activity and molecular correlates of response to atezolizumab alone or in combination with bevacizumab versus sunitinib in renal cell carcinoma. *Nat. Med.* 24 (6), 749–757. doi:10.1038/s41591-018-0053-3

Mcinnes, I. B., Buckley, C. D., and Isaacs, J. D. (2016). Cytokines in rheumatoid arthritis - shaping the immunological landscape. *Nat. Rev. Rheumatol.* 12, 63–68. doi:10.1038/nrrheum.2015.171

Mellor, A. L., and Munn, D. H. (2004). Ido expression by dendritic cells: Tolerance and tryptophan catabolism. *Nat. Rev. Immunol.* 4, 762–774. doi:10.1038/nri1457

Meng, S., Liu, L. L., Hou, J., Xu, Y., Qin, L., Liu, W., et al. (2020). PD-L1 upregulation by IFN-α/γ-mediated Stat1 suppresses anti-HBV T cell response[J]. *PLoS One* 15 (7), e0228302.

Messmer, M. N., Netherby, C. S., Banik, D., and Abrams, S. I. (2015). Tumor-induced myeloid dysfunction and its implications for cancer immunotherapy. *Cancer Immunol. Immunother.* 64, 1–13. doi:10.1007/s00262-014-1639-3

Meyer, C., Cagnon, L., Costa-Nunes, C. M., Baumgaertner, P., Montandon, N., Leyvraz, L., et al. (2014). Frequencies of circulating MDSC correlate with clinical outcome of melanoma patients treated with ipilimumab. *Cancer Immunol. Immunother.* 63, 247–257. doi:10.1007/s00262-013-1508-5

Mezzadra, R., Chong, S., Jae, L. T., Gomez-Eerland, R., de Vries, E., Wu, W., et al. (2017). Identification of CMTM6 and CMTM4 as PD-L1 protein regulators. *Nature* 549 (7670), 106–110. doi:10.1038/nature23669

Mok, S., Koya, R. C., Tsui, C., Xu, J., Robert, L., Wu, L., et al. (2014). Inhibition of CSF-1 receptor improves the antitumor efficacy of adoptive cell transfer immunotherapy. *Cancer Res.* 74, 153–161. doi:10.1158/0008-5472.CAN-13-1816

Muchová, J., Hearnden, V., Michlovská, L., Vistejnova, L., Zavadakova, A., Smerkova, K., et al. (2021). Mutual influence of selenium nanoparticles and FGF2-stab® on biocompatible properties of collagen/chitosan 3D scaffolds: *In vitro* and ex ovo evaluation. *J. Nanobiotechnology* 19 (1), 103. doi:10.1186/s12951-021-00849-w

Mukherji, D., Jabbour, M. N., Saroufim, M., Temraz, S., Nasr, R., Charafeddine, M., et al. (2016). Programmed death-ligand 1 expression in muscle-invasive bladder cancer cystectomy specimens and lymph node metastasis: A reliable treatment selection biomarker? *Clin. Genitourin. Cancer* 14 (2), 183–187. doi:10.1016/j.clgc.2015.12.002

Murata, S., Kaneko, S., Harada, Y., Aoi, N., and Morita, E. (2017). Case of de novo psoriasis possibly triggered by nivolumab. *J. Dermatol.* 44, 99–100. doi:10.1111/1346-8138.13450

Muthuswamy, R., Corman, J. M., Dahl, K., Chatta, G. S., and Kalinski, P. (2016). Functional reprogramming of human prostate cancer to promote local attraction of effector CD8(+) T cells. *Prostate* 76 (12), 1095–1105. doi:10.1002/pros.23194

Na, L., Formisano, L., Gonzalez-Ericsson, P. I., Sanchez, V., Dean, P. T., Opalenik, S. R., et al. (2018). Melanoma response to anti-PD-L1 immunotherapy requires JAK1 signaling, but not JAK2[J]. *OncoImmunology* 7 (3), e1438106.

Nagaraj, S., Gupta, K., Pisarev, V., Kinarsky, L., Sherman, S., Kang, L., et al. (2007). Altered recognition of antigen is a mechanism of CD8+ T cell tolerance in cancer. *Nat. Med.* 13, 828–835. doi:10.1038/nm1609

Nakashima, D., Onuma, T., Tanabe, K., Kito, Y., Uematsu, K., Mizutani, D., et al. (2020). Synergistic effect of collagen and CXCL12 in the low doses on human platelet activation. *PLoS One* 15 (10), e0241139. doi:10.1371/journal.pone.0241139

Nam, S., Lee, A., Lim, J., and Lim, J. S. (2019). Analysis of the expression and regulation of PD-1 protein on the surface of myeloid-derived suppressor cells (MDSCs). *Biomol. Ther.* 27 (1), 63–70. doi:10.4062/biomolther.2018.201

Nguyen, D. P., Li, J., and Tewari, A. K. (2014). Inflammation and prostate cancer: The role of interleukin 6 (IL-6). *BJU Int.* 113 (6), 986–992. doi:10.1111/bju.12452

Ni, X. Y., Sui, H. X., Liu, Y., Ke, S. Z., Wang, Y. N., and Gao, F. G. (2012). TGF-beta of lung cancer microenvironment upregulates B7H1 and GITRL expression in dendritic cells and is associated with regulatory T cell generation[D]. *Oncol. Rep.* 28, 615–621. doi:10.3892/or.2012.1822

Nikitovic, D., Tzardi, M., Berdiaki, A., Tsatsakis, A., and Tzanakakis, G. N. (2015). Cancer microenvironment and inflammation: Role of hyaluronan. *Front. Immunol.* 6, 169. doi:10.3389/fimmu.2015.00169

Nissen, N. I., Karsdal, M., and Willumsen, N. (2019). Collagens and Cancer associated fibroblasts in the reactive stroma and its relation to Cancer biology. *J. Exp. Clin. Cancer Res.* 38 (1), 115. doi:10.1186/s13046-019-1110-6

Noguchi, T., Ward, J. P., Gubin, M. M., Arthur, C. D., Lee, S. H., Hundal, J., et al. (2017). Temporally distinct PD-L1 expression by tumor and host cells contributes to immune escape. *Cancer Immunol. Res.* 5 (2), 106–117. doi:10.1158/2326-6066.CIR-16-0391

Noman, M. Z., Desantis, G., Janji, B., Hasmim, M., Karray, S., Dessen, P., et al. (2014). PD-L1 is a novel direct target of HIF-1α, and its blockade under hypoxia enhanced MDSC-mediated T cell activation. *J. Exp. Med.* 211, 781–790. doi:10.1084/jem.20131916

Obermajer, N., Muthuswamy, R., Lesnock, J., Edwards, R. P., and Kalinski, P. (2011). Positive feedback between PGE2 and COX2 redirects the differentiation of human dendritic cells toward stable myeloid-derived suppressor cells. *Blood* 118, 5498–5505. doi:10.1182/blood-2011-07-365825

Orillion, A., Hashimoto, A., Damayanti, N., Shen, L., Adelaiye-Ogala, R., Arisa, S., et al. (2017). Entinostat neutralizes myeloid-derived suppressor cells and enhances the antitumor effect of PD-1 inhibition in murine models of lung and renal cell carcinoma. *Clin. Cancer Res.* 23, 5187–5201. doi:10.1158/1078-0432.CCR-17-0741

Osei, E. T., Mostaço-Guidolin, L., Hsieh, A., Warner, S. M., Al-Fouadi, M., Wang, M., et al. (2020). Epithelial-interleukin-1 inhibits collagen formation by airway fibroblasts: Implications for asthma. *Sci. Rep.* 10 (1), 8721. doi:10.1038/s41598-020-65567-z

Ou, J. N., Wiedeman, A. E., and Stevens, A. M. (2012). TNF-α and TGF-β counter-regulate PD-L1 expression on monocytes in systemic lupus erythematosus. *Sci. Rep.* 2, 295. doi:10.1038/srep00295

Pan, P. Y., Ma, G., Weber, K. J., Ozao-Choy, J., Wang, G., Yin, B., et al. (2010). Immune stimulatory receptor CD40 is required for T-cell suppression and T regulatory cell activation mediated by myeloid-derived suppressor cells in cancer. *Cancer Res.* 70, 99–108. doi:10.1158/0008-5472.CAN-09-1882

Parry, R. V., Chemnitz, J. M., Frauwirth, K. A., Lanfranco, A. R., Braunstein, I., Kobayashi, S. V., et al. (2005). CTLA-4 and PD-1 receptors inhibit T-cell activation by distinct mechanisms. *Mol. Cell. Biol.* 25 (21), 9543–9553. doi:10.1128/MCB.25.21.9543-9553.2005

Peng, D., Kryczek, I., Nagarsheth, N., Zhao, L., Wei, S., Wang, W., et al. (2015). Epigenetic silencing of TH1-type chemokines shapes tumour immunity and immunotherapy[J]. *Nature* 527 (7577), 249–253. doi:10.1038/nature15520

Peng, D. H., Rodriguez, B. L., Diao, L., Chen, L., Wang, J., Byers, L. A., et al. (2020). Collagen promotes anti-PD-1/PD-L1 resistance in cancer through LAIR1-dependent CD8+ T cell exhaustion. *Nat. Commun.* 11 (1), 4520. doi:10.1038/s41467-020-18298-8

Perez-Ruiz, E., Minute, L., Otano, I., Alvarez, M., Ochoa, M. C., Belsue, V., et al. (2019). Prophylactic TNF blockade uncouples efficacy and toxicity in dual CTLA-4 and PD-1 immunotherapy[J]. *Nature* 569 (7756), 1–7. doi:10.1038/s41586-019-1162-y

Platanias, L. C. (2005). Mechanisms of type-I- and type-II-interferon-mediated signalling. *Nat. Rev. Immunol.* 5 (5), 375–386. doi:10.1038/nri1604

Poto, R., Troiani, T., Criscuolo, G., Marone, G., Ciardiello, F., Tocchetti, C. G., et al. (2022). Holistic approach to immune checkpoint inhibitor-related adverse events. *Front. Immunol.* 30 (13), 804597. doi:10.3389/fimmu.2022.804597

Powles, T., Eder, J. P., Fine, G. D., Braiteh, F. S., Loriot, Y., Cruz, C., et al. (2014). MPDL3280A (anti-PD-L1) treatment leads to clinical activity in metastatic bladder cancer. *Nature* 194 (7528), 558–562. doi:10.1038/nature13904

Priego, N., Zhu, L., Monteiro, C., Mulders, M., Wasilewski, D., Bindeman, W., et al. (2018). STAT3 labels a subpopulation of reactive astrocytes required for brain metastasis[J]. *Nat. Med.* 24, 1024–1035. doi:10.1038/s41591-018-0044-4

Puccini, A., Battaglin, F., Iaia, M. L., Lenz, H. J., and Salem, M. E. (2020). Overcoming resistance to anti-PD1 and anti-PD-L1 treatment in gastrointestinal malignancies. *J. Immunother. Cancer* 8 (1), e000404. doi:10.1136/jitc-2019-000404

Pulko, V., Liu, X., Krco, C. J., Harris, K. J., Frigola, X., Kwon, E. D., et al. (2009). TLR3-stimulated dendritic cells up-regulate B7-H1 expression and influence the magnitude of CD8 T cell responses to tumor vaccination. *J. Immunol.* 183 (6), 3634–3641. doi:10.4049/jimmunol.0900974

Qian, Y., Deng, J., Geng, L., Xie, H., Jiang, G., Zhou, L., et al. (2008). TLR4 signaling induces B7-H1 expression through MAPK pathways in bladder cancer cells. *Cancer Invest.* 26 (8), 816–821. doi:10.1080/07357900801941852

Quandt, D., Jasinski-Bergner, S., Müller, U., Schulze, B., and Seliger, B. (2014). Synergistic effects of IL-4 and TNFα on the induction of B7-H1 in renal cell carcinoma cells inhibiting allogeneic T cell proliferation. *J. Transl. Med.* 12, 151. doi:10.1186/1479-5876-12-151

Ravi, R., Noonan, K. A., Pham, V., Bedi, R., Zhavoronkov, A., Ozerov, I. V., et al. (2018). Bifunctional immune checkpoint-targeted antibody-ligand traps that simultaneously disable TGFβ enhance the efficacy of cancer immunotherapy. *Nat. Commun.* 9 (1), 741. doi:10.1038/s41467-017-02696-6

Read, S., Greenwald, R., Izcue, A., Robinson, N., Mandelbrot, D., Francisco, L., et al. (2006). Blockade of CTLA-4 on CD4+CD25+ regulatory T cells abrogates their function *in vivo*. *J. Immunol.* 177 (7), 4376–4383. doi:10.4049/jimmunol.177.7.4376

Ro, W., Che, P. L., Reube, A., Spencer, C. N., Prieto, P. A., Miller, J. P., et al. (2017). Integrated molecular analysis of tumor biopsies on sequential CTLA-4 and PD-1 blockade reveals markers of response and resistance[J]. *Sci. Transl. Med.* 9 (379), eaah3560. doi:10.1126/scitranslmed.aah3560

Robert, F., Douglas, N., Christine, B., Popratiloff, A., and Uittenbogaart, C. H. (2018). TGF-B sustains tumor progression through biochemical and mechanical signal transduction[J]. *Cancers* 10 (6), 199. doi:10.3390/cancers10060199

Rosenberg, J. E., Hoffman-Censits, J., Powles, T., van der Heijden, M. S., Balar, A. V., Necchi, A., et al. (2016). Atezolizumab in patients with locally advanced and metastatic urothelial carcinoma who have progressed following treatment with platinum-based chemotherapy: A single-arm, multicentre, phase 2 trial. *Lancet* 387, 1909–1920. doi:10.1016/S0140-6736(16)00561-4

Sade-Feldman, M., Yizhak, K., Bjorgaard, S. L., Ray, J. P., de Boer, C. G., Jenkins, R. W., et al. (2019). Defining T cell states associated with response to checkpoint immunotherapy in melanoma. *Cell* 175 (4), 998–1013. doi:10.1016/j.cell.2018.10.038

Saleh, K., Khalife-Saleh, N., and Kourie, H. R. (2019). Do immune-related adverse events correlate with response to immune checkpoint inhibitors?[J]. *Immunotherapy* 11, 257–259. doi:10.2217/imt-2018-0201

Salmon, H., Franciszkiewicz, K., Damotte, D., Dieu-Nosjean, M. C., Validire, P., Trautmann, A., et al. (2012). Matrix architecture defines the preferential localization and migration of T cells into the stroma of human lung tumors. *J. Clin. Invest.* 122 (3), 899–910. doi:10.1172/JCI45817

Sang, T., Tayar, J., Trinh, V. A., Suarez-Almazor, M., Garcia, S., Hwu, P., et al. (2017). Successful treatment of arthritis induced by checkpoint inhibitors with tocilizumab: A case series. *Ann. Rheum. Dis.* 76, 2061–2064. doi:10.1136/annrheumdis-2017-211560

Schreiner, B., Mitsdoerffer, M., Kieseier, B. C., Chen, L., Hartung, H. P., Weller, M., et al. (2004). Interferon-beta enhances monocyte and dendritic cell expression of B7-H1 (PD-L1), a strong inhibitor of autologous T-cell activation: Relevance for the immune modulatory effect in multiple sclerosis. *J. Neuroimmunol.* 155 (1-2), 172–182. doi:10.1016/j.jneuroim.2004.06.013

Sektioglu, I. M., Carretero, R., Bulbuc, N., Bald, T., Tuting, T., Rudensky, A. Y., et al. (2016). Basophils promote tumor rejection via chemotaxis and infiltration of CD8+ T cells. *Cancer Res.* 77, 291–302. doi:10.1158/0008-5472.CAN-16-0993

Selby, M. J., Engelhardt, J. J., Quigley, M., Henning, K. A., Chen, T., Srinivasan, M., et al. (2013). Anti-CTLA-4 antibodies of IgG2a isotype enhance antitumor activity through reduction of intratumoral regulatory T cells. *Cancer Immunol. Res.* 1, 32–42. doi:10.1158/2326-6066.CIR-13-0013

Setoguchi, R., Hori, S., Takahashi, T., and Sakaguchi, S. (2005). Homeostatic maintenance of natural Foxp3(+) CD25(+) CD4(+) regulatory T cells by interleukin (IL)-2 and induction of autoimmune disease by IL-2 neutralization. *J. Exp. Med.* 201 (5), 723–735. doi:10.1084/jem.20041982

Sharma, N., Atolagbe, O. T., Ge, Z., and Allison, J. P. (2021). LILRB4 suppresses immunity in solid tumors and is a potential target for immunotherapy[J]. *J. Exp. Med.* 218 (7), e20201811. doi:10.1084/jem.20201811

Sharpe, A. H., Wherry, E. J., Ahmed, R., and Freeman, G. J. (2007). The function of programmed cell death 1 and its ligands in regulating autoimmunity and infection. *Nat. Immunol.* 8 (3), 239–245. doi:10.1038/ni1443

Shuang, H., and Chakrabarty, S. (2010). Regulation of fibronectin and laminin receptor expression, fibronectin and laminin secretion in human colon cancer cells by transforming growth factor-beta 1. *Int. J. Cancer* 57 (5), 742–746. doi:10.1002/ijc.2910570522

Siddiqui, I., Schaeuble, K., Chennupati, V., Fuertes Marraco, S. A., Calderon-Copete, S., Pais Ferreira, D., et al. (2019). Intratumoral Tcf1+PD-1+cd8+ T cells with stem-like properties promote tumor control in response to vaccination and checkpoint blockade immunotherapy. *Immunity* 50 (1), 195–211. doi:10.1016/j.immuni.2018.12.021

Simpson, T. R., Li, F., Montalvo-Ortiz, W., Sepulveda, M. A., Bergerhoff, K., Arce, F., et al. (2013). Fc-dependent depletion of tumor-infiltrating regulatory T cells co-defines the efficacy of anti-CTLA-4 therapy against melanoma. *J. Exp. Med.* 210, 1695–1710. doi:10.1084/jem.20130579

Singhal, S., Bhojnagarwala, P. S., O'Brien, S., Moon, E. K., Garfall, A. L., Rao, A. S., et al. (2016). Origin and role of a subset of tumor-associated neutrophils with antigen-presenting cell features in early-stage human lung cancer[J]. *Cancer Cell* 30, 120–135. doi:10.1016/j.ccell.2016.06.001

Sockolosky, J. T., Dougan, M., Ingram, J. R., Ho, C. C. M., Kauke, M. J., Almo, S. C., et al. (2016). Durable antitumor responses to CD47 blockade require adaptive immune stimulation. *Proc. Natl. Acad. Sci. U. S. A.* 113 (19), E2646–E2654. doi:10.1073/pnas.1604268113

Song, S., Yuan, P., Wu, H., Chen, J., Fu, J., Li, P., et al. (2014). Dendritic cells with an increased PD-L1 by TGF-β induce T cell anergy for the cytotoxicity of hepatocellular carcinoma cells. *Int. Immunopharmacol.* 20 (1), 117–123. doi:10.1016/j.intimp.2014.02.027

Steele, C. W., Karim, S. A., Leach, J. D. G., Bailey, P., Upstill-Goddard, R., Rishi, L., et al. (2016). CXCR2 inhibition profoundly suppresses metastases and augments immunotherapy in pancreatic ductal adenocarcinoma. *Cancer Cell* 29, 832–845. doi:10.1016/j.ccell.2016.04.014

Stefani, S., Riyue, B., and Gajewski, T. F. (2015). Melanoma-intrinsic β-catenin signalling prevents anti-tumour immunity[J]. *Nature* 523 (7559), 231–235.

Stroud, C. R., Hegde, A., Cherry, C., Naqash, A. R., Sharma, N., Addepalli, S., et al. (2019). Tocilizumab for the management of immune mediated adverse events secondary to PD-1 blockade. *J. Oncol. Pharm. Pract.* 25 (3), 551–557. doi:10.1177/1078155217745144

Subrahmanyam, P. B., Dong, Z., Gusenleitner, D., Giobbie-Hurder, A., Severgnini, M., Zhou, J., et al. (2018). Distinct predictive biomarker candidates for response to anti-CTLA-4 and anti-PD-1 immunotherapy in melanoma patients. *J. Immunother. Cancer* 6 (1), 18. doi:10.1186/s40425-018-0328-8

Sun, L., Clavijo, P. E., Robbins, Y., Patel, P., Friedman, J., Greene, S., et al. (2019). Inhibiting myeloid-derived suppressor cell trafficking enhances T cell immunotherapy. *JCI Insight* 4 (7), e126853. doi:10.1172/jci.insight.126853

Takahashi, T., Kuniyasu, Y., Toda, M., SakaguchiN.ItohM.IwataM., et al. (1998). Immunologic self-tolerance maintained by CD25+CD4+ naturally anergic and suppressive T cells: Induction of autoimmune disease by breaking their anergic/suppressive state. *Int. Immunol.* 10 (12), 1969–1980. doi:10.1093/intimm/10.12.1969

Tanaka, R., Okiyama, N., Okune, M., Ishitsuka, Y., Watanabe, R., Furuta, J., et al. (2017). Serum level of interleukin-6 is increased in nivolumab-associated psoriasiform dermatitis and tumor necrosis factor-alpha is a biomarker of nivolumab recativity[J]. *J. Dermatological Sci.* 86, 71–73. doi:10.1016/j.jdermsci.2016.12.019

Tarhini, A. A., Zahoor, H., Lin, Y., Malhotra, U., Sander, C., Butterfield, L. H., et al. (2015). Baseline circulating IL-17 predicts toxicity while TGF-β1 and IL-10 are prognostic of relapse in ipilimumab neoadjuvant therapy of melanoma. *J. Immunother. Cancer* 3 (1), 39. doi:10.1186/s40425-015-0081-1

Teng, M., Ngiow, S. F., Ribas, A., and Smyth, M. J. (2015). Classifying cancers based on T-cell infiltration and PD-L1. *Cancer Res.* 75 (11), 2139–2145. doi:10.1158/0008-5472.CAN-15-0255

Teulings, H. E., Limpens, J., Jansen, S. N., Zwinderman, A. H., Reitsma, J. B., Spuls, P. I., et al. (2015). Vitiligo-like depigmentation in patients with stage III-IV melanoma receiving immunotherapy and its association with survival: A systematic review and meta-analysis. *J. Clin. Oncol.* 33 (7), 773–781. doi:10.1200/JCO.2014.57.4756

Thiem, A., Hesbacher, S., Kneitz, H., di Primio, T., Heppt, M. V., Hermanns, H. M., et al. (2019). IFN-gamma-induced PD-L1 expression in melanoma depends on p53 expression. *J. Exp. Clin. Cancer Res.* 38 (1), 397. doi:10.1186/s13046-019-1403-9

Tomioka, N., Azuma, M., Ikarashi, M., Yamamoto, M., Sato, M., Watanabe, K. I., et al. (2018). The therapeutic candidate for immune checkpoint inhibitors elucidated by the status of tumor-infiltrating lymphocytes (TILs) and programmed death ligand 1 (PD-L1) expression in triple negative breast cancer (TNBC). *Breast Cancer* 25, 34–42. doi:10.1007/s12282-017-0781-0

Tomoko, I., Katsuyuki, A., Kawana, K., Taguchi, A., Nagamatsu, T., Fujimoto, A., et al. (2016). Cancer-associated fibroblast suppresses killing activity of natural killer cells through downregulation of poliovirus receptor (PVR/CD155), a ligand of activating NK receptor. *Int. J. Oncol.* 49, 1297–1304. doi:10.3892/ijo.2016.3631

Trikha, P., and Carson3rd, W. E. (2014). Signaling pathways involved in MDSC regulation. *Biochim. Biophys. Acta* 1846, 55–65. doi:10.1016/j.bbcan.2014.04.003

Tsukamoto, H., Fujieda, K., Miyashita, A., Fukushima, S., Ikeda, T., and Kubo, Y. (2018). Combined blockade of IL6 and PD-1/PD-L1 signaling abrogates mutual regulation of their immunosuppressive effects in the tumor microenvironment[J]. *Cancer Res.* 78, 5011–5022. doi:10.1158/0008-5472.CAN-18-0118

Tumeh, P. C., Harview, C. L., Yearley, J. H., Shintaku, I. P., Taylor, E. J. M., Robert, L., et al. (2014). PD-1 blockade induces responses by inhibiting adaptive immune resistance. *Nature* 515 (7528), 568–571. doi:10.1038/nature13954

Türlü, C., Willumsen, N., Marando, D., Schjerling, P., Biskup, E., Hannibal, J., et al. (2021). A human cellular model for colorectal anastomotic repair: The effect of localization and transforming growth factor-β1 treatment on collagen deposition and biomarkers. *Int. J. Mol. Sci.* 22 (4), 1616. doi:10.3390/ijms22041616

Umair, M. M., Athanasios, P., Adam, P., Evan, F., Zachary, M., Sibgha, G., et al. (2018). Tumor matrix remodeling and novel immunotherapies: The promise of matrix-derived immune biomarkers[J]. *J. Immunother. Cancer* 6 (1), 65.

Uyttenhove, C., Pilotte, L., Theate, I., Stroobant, V., Colau, D., Parmentier, N., et al. (2003). Evidence for a tumoral immune resistance mechanism based on tryptophan degradation by indoleamine 2, 3-dioxygenase. *Nat. Med.* 9, 1269–1274. doi:10.1038/nm934

Valk, E., Rudd, C. E., and Schneider, H. (2008). CTLA-4 trafficking and surface expression. *Trends Immunol.* 29 (6), 272–279. doi:10.1016/j.it.2008.02.011

van der Woude, L. L., Gorris, M. A. J., Halilovic, A., Figdor, C. G., and de Vries, I. J. M. (2017). Migrating into the tumor: A roadmap for T cells[J]. *Trends Cancer* 3 (11), 797. doi:10.1016/j.trecan.2017.09.006

van Elsas, A., Hurwitz, A. A., and Allison, J. P. (1999). Combination immunotherapy of B16 melanoma using anti-cytotoxic T lymphocyte-associated antigen 4 (CTLA-4) and granulocyte/macrophage colony-stimulating factor (GM-CSF)-producing vaccines induces rejection of subcutaneous and metastatic tumors accompanied by autoimmune depigmentation. *J. Exp. Med.* 190 (3), 355–366. doi:10.1084/jem.190.3.355

Vivar, K. L., Deschaine, M., Messina, J., Divine, J. M., Rabionet, A., Patel, N., et al. (2017). Epidermal programmed cell death-ligand 1 expression in TEN associated with nivolumab therapy. *J. Cutan. Pathol.* 44, 381–384. doi:10.1111/cup.12876

Voskens, C. J., Goldinger, S. M., Loquai, C., Robert, C., Kaehler, K. C., Berking, C., et al. (2013). The price of tumor control: An analysis of rare side effects of anti-CTLA-4 therapy in metastatic melanoma from the ipilimumab network. *PLoS One* 8, e53745. doi:10.1371/journal.pone.0053745

Wang, J., Luo, D., Liang, M., Zhang, T., Yin, X., Zhang, Y., et al. (2018). Spectrum-effect relationships between high-performance liquid chromatography (HPLC) fingerprints and the antioxidant and anti-inflammatory activities of collagen peptides. *Molecules* 23 (12), 3257. doi:10.3390/molecules23123257

Wang, L., Abdel, S., Szabo, P. M., Chasalow, S. D., Castillo-Martin, M., Domingo-Domenech, J., et al. (2018). EMT- and stroma-related gene expression and resistance to PD-1 blockade in urothelial cancer. *Nat. Commun.* 9 (1), 3503. doi:10.1038/s41467-018-05992-x

Wang, X., Yang, L., Huang, F., Zhang, Q., Liu, S., Ma, L., et al. (2017). Inflammatory cytokines IL-17 and TNF-α up-regulate PD-L1 expression in human prostate and colon cancer cells. *Immunol. Lett.* 184, 7–14. doi:10.1016/j.imlet.2017.02.006

Wasén, C., Erlandsson, M., Bossios, A., Ekerljung, L., Malmhall, C., Toyra Silfversward, S., et al. (2018). Smoking is associated with low levels of soluble PD-L1 in rheumatoid arthritis. *Front. Immunol.* 9, 1677. doi:10.3389/fimmu.2018.01677

Weber, J., Gibney, G., Kudchadkar, R., Yu, B., Cheng, P., Martinez, A. J., et al. (2016). Phase I/II study of metastatic melanoma patients treated with nivolumab who had progressed after ipilimumab. *Cancer Immunol. Res.* 4, 345–353. doi:10.1158/2326-6066.CIR-15-0193

Weber, J. S., Yang, J. C., Atkins, M. B., and Disis, M. L. (2015). Toxicities of immunotherapy for the practitioner. *J. Clin. Oncol.* 33 (18), 2092–2099. doi:10.1200/JCO.2014.60.0379

Wen, X., He, X., Jiao, F., Wang, C., Sun, Y., Ren, X., et al. (2017). Fibroblast activation protein-α-positive fibroblasts promote gastric cancer progression and resistance to immune checkpoint blockade. *Oncol. Res.* 25 (4), 629–640. doi:10.3727/096504016X14768383625385

Wight, T. N., Kinsella, M. G., Evanko, S. P., Potter-Perigo, S., and Merrilees, M. J. (2014). Versican and the regulation of cell phenotype in disease. *Biochim. Biophys. Acta* 1840 (8), 2441–2451. doi:10.1016/j.bbagen.2013.12.028

Xia, Q., Zhang, F. F., Geng, F., Liu, C. L., Xu, P., Lu, Z. Z., et al. (2016). Anti-tumor effects of DNA vaccine targeting human fibroblast activation protein alpha by producing specific immune responses and altering tumor microenvironment in the 4T1 murine breast cancer model[J]. *Cancer Immunol. Immunother.* 65 (5), 613–624. doi:10.1007/s00262-016-1827-4

Xiang, X., Feng, D., Hwang, S., Ren, T., Wang, X., Trojnar, E., et al. (2020). Interleukin-22 ameliorates acute-on-chronic liver failure by reprogramming impaired regeneration pathways in mice. *J. Hepatol.* 72 (4), 736–745. doi:10.1016/j.jhep.2019.11.013

Xing, X., Guo, J., Wen, X., Li, B., Dong, B., Feng, Q., et al. (2018). Analysis of PD1, PDL1, PDL2 expression and T cells infiltration in 1014 gastric cancer patients. *Oncoimmunology* 7, e1356144. doi:10.1080/2162402X.2017.1356144

Xiong, H. Y., Ma, T. T., Wu, B. T., Lin, Y., and Tu, Z. G. (2014). IL-12 regulates B7-H1 expression in ovarian cancer-associated macrophages by effects on NF-κB signalling. *Asian pac. J. Cancer Prev.* 15 (14), 5767–5772. doi:10.7314/apjcp.2014.15.14.5767

Yagi, T., Baba, Y., Ishimoto, T., Iwatsuki, M., Miyamoto, Y., Yoshida, N., et al. (2017). PD-L1 expression, tumor-infiltrating lymphocytes, and clinical outcome in patients with surgically resected esophageal cancer[J]. *Ann. Surg.* 269 (3), 1. doi:10.1097/SLA.0000000000002616

Yi, G., Yang, J., Cai, Y., Fu, S., Zhang, N., Fu, X., et al. (2018). IFN-γ-mediated inhibition of lung cancer correlates with PD-L1 expression and is regulated by PI3K-akt signaling: IFN-γ-mediated signaling and function in lung adenocarcinoma[J]. *Int. J. Cancer* 143 (4), 931–943. doi:10.1002/ijc.31357

Young, A., Quandt, Z., and Bluestone, J. A. (2018). The balancing act between cancer immunity and autoimmunity in response to immunotherapy. *Cancer Immunol. Res.* 6 (12), 1445–1452. doi:10.1158/2326-6066.CIR-18-0487

Yue, C., Shen, S., Deng, J., Priceman, S. J., Li, W., Huang, A., et al. (2015). STAT3 in CD8+ T cells inhibits their tumor accumulation by downregulating CXCR3/CXCL10 Axis. *Cancer Immunol. Res.* 3 (8), 864–870. doi:10.1158/2326-6066.CIR-15-0014

Zhang, R., Zhu, Z., Lv, H., Li, F., Sun, S., Li, J., et al. (2019). Immune checkpoint blockade mediated by a small-molecule nanoinhibitor targeting the PD-1/PD-L1 pathway synergizes with photodynamic therapy to elicit antitumor immunity and antimetastatic effects on breast cancer. *Small* 15 (49), e1903881. doi:10.1002/smll.201903881

Zhang, W., Lim, S. M., Hwang, J., Ramalingam, S., Kim, M., and Jin, J. O. (2020). Monophosphoryl lipid A-induced activation of plasmacytoid dendritic cells enhances the anti-cancer effects of anti-PD-L1 antibodies[J]. *Cancer Immunol. Immunother.* 70, 1–12. doi:10.1007/s00262-020-02715-4

Zhao, Q., Xiao, X., Wu, Y., Wei, Y., Zhu, L. Y., Zhou, J., et al. (2011). Interleukin-17-educated monocytes suppress cytotoxic T-cell function through B7-H1 in hepatocellular carcinoma patients. *Eur. J. Immunol.* 41 (8), 2314–2322. doi:10.1002/eji.201041282

frontiers | Frontiers in Pharmacology

TYPE Original Research
PUBLISHED 21 October 2022
DOI 10.3389/fphar.2022.1013672

OPEN ACCESS

EDITED BY
Xuebing Li,
Tianjin Medical University General Hospital, China

REVIEWED BY
Yangyang Feng,
University of Macau, China
Yuqing Wang,
University of Macau, China

*CORRESPONDENCE
Yanguo Liu,
liuyanguo@sdu.edu.cn
Xiuwen Wang,
xiuwenwang12@sdu.edu.cn

SPECIALTY SECTION
This article was submitted to Pharmacology of Anti-Cancer Drugs, a section of the journal Frontiers in Pharmacology

RECEIVED 07 August 2022
ACCEPTED 12 October 2022
PUBLISHED 21 October 2022

CITATION
Yang R, Zhang W, Shang X, Chen H, Mu X, Zhang Y, Zheng Q, Wang X and Liu Y (2022), Neutrophil-related genes predict prognosis and response to immune checkpoint inhibitors in bladder cancer.
Front. Pharmacol. 13:1013672.
doi: 10.3389/fphar.2022.1013672

Neutrophil-related genes predict prognosis and response to immune checkpoint inhibitors in bladder cancer

Rui Yang[1], Wengang Zhang[1], Xiaoling Shang[1], Hang Chen[2], Xin Mu[3], Yuqing Zhang[1], Qi Zheng[1], Xiuwen Wang[1]* and Yanguo Liu[1]*

[1]Department of Medical Oncology, Qilu Hospital, Cheeloo College of Medicine, Shandong University, 107 Wenhuaxi Road, Jinan, Shandong, China, [2]School of Basic Medical Sciences, Shandong First Medical University, Jinan, China, [3]Department of Medical Imaging Center, Third People's Hospital of Jinan, Jinan, China

Neutrophils play a key role in the occurrence and development of cancer. However, the relationship between neutrophils and cancer prognosis remains unclear due to their great plasticity and diversity. To explore the effects of neutrophils on the clinical outcome of bladder cancer, we acquired and analyzed gene expression data and clinical information of bladder cancer patients from IMvigor210 cohort and The Cancer Genome Atlas dataset (TCGA) database. We established a neutrophil-based prognostic model incorporating five neutrophil-related genes (EMR3, VNN1, FCGRT, HIST1H2BC, and MX1) and the predictive value of the model was validated in both an internal and an external validation cohort. Multivariate Cox regression analysis further proved that the model remained an independent prognostic factor for overall survival and a nomogram was constructed for clinical practice. Additionally, FCGRT was identified as the key neutrophil-related gene linked to an adverse prognosis of bladder cancer. Up-regulation of FCGRT indicated activated cancer metabolism, immunosuppressive tumor environment, and dysregulated functional status of immune cells. FCGRT overexpression was also correlated with decreased expression of PD-L1 and low levels of tumor mutation burden (TMB). FCGRT predicted a poor response to immunotherapy and had a close correlation with chemotherapy sensitivity. Taken together, a novel prognostic model was developed based on the expression level of neutrophil-related genes. FCGRT served as a promising candidate biomarker for anti-cancer drug response, which may contribute to individualized prognostic prediction and may contribute to clinical decision-making.

Abbreviations: NMIBC, non-muscular invasive bladder cancer; MIBC, muscular invasive bladder cancer; ICIs, immune checkpoint inhibitors; TCGA, The Cancer Genome Atlas dataset; LASSO, Least Absolute Shrinkage and Selection Operator; ROC, the receiver operating characteristic; DEGs, differentially expressed genes; GO, Gene Ontology; KEGG, Kyoto Gene Genome Encyclopedia; GSVA, gene set variation analysis; ssGSEA, single sample gene set enrichment analysis; OS, overall survival; AUC, area under the curve; ECOG, Eastern Cooperative Oncology Group; TME, tumor microenvironment. NGS, next-generation sequencing.

KEYWORDS
neutrophil, FCGRT, bladder cancer, immunotherapy, tumor microenvironment

1 Introduction

Bladder cancer is one of the most common cancers globally, with an estimated 573278 new cases and 212,536 cancer deaths worldwide reported in 2020 (Sung et al., 2021). Based on clinical staging, bladder cancer can be divided into non-muscular invasive bladder cancer (NMIBC), muscular invasive bladder cancer (MIBC), and metastatic bladder cancer, each with different molecular drivers and specific treatment strategies (Sung et al., 2021). For decades, few advances have been made in bladder cancer therapeutics until the advent and application of immune checkpoint inhibitors (ICIs), which expand limited treatment options and show great promise, especially in patients with locally advanced or metastatic bladder cancer who develop intolerance or resistance to conventional first-line therapy (Wu et al., 2021). However, the improved outcomes brought about by ICIs are limited to selected patients and the prognosis remains poor. The 5-year overall survival rate for NMIBC is nearly 90%, compared with 60%–70% in MIBC and only 5%–30% in metastatic bladder cancer (Patel et al., 2020). Thus, effective immunotherapy indicators and prognostic biomarkers must be explored to identify bladder cancer patients who will benefit from ICI therapies and to facilitate risk stratification.

Neutrophils are key mediators of chronic inflammation and innate inflammatory response, as well as important regulators of cancer development (Hedrick and Malanchi, 2022). Instead of terminally differentiated cell populations, tumor-associated neutrophils are susceptible to environmental factors and exhibit great plasticity and diversity, which facilitate tumor growth or interfere with it (Jaillon et al., 2020). Accumulating evidence has suggested that neutrophils affect cancer prognosis and response to different modalities of anticancer treatment, ranging from chemotherapy to immunotherapy. Tumor-associated neutrophil infiltration, peripheral blood neutrophil-to-lymphocyte ratio, and neutrophil-based transcriptional signatures have generally been reported to correlate with poor clinical outcome and low drug sensitivity in many malignant diseases (Templeton et al., 2014; Gentles et al., 2015; Shaul and Fridlender, 2019). However, the prognostic role of neutrophils in bladder cancer remains unknown, nor is the predictive value of neutrophils in specific therapeutic regimens.

To investigate the effects of neutrophils on the prognosis of bladder cancer, we analyzed the gene expression profiles and clinical information of patients in the IMvigor210 cohort. A prognostic model based on neutrophil-related genes was established and validated. The relationships between neutrophil-related genes and the tumor microenvironment phenotype and drug sensitivity were further examined to identify potential immunotherapy response indicators and novel therapeutic targets.

2 Materials and methods

2.1 Data source and processing

IMvigor210 is an open-label, multicenter, single-arm Phase II clinical study evaluating the efficacy and safety of atezolizumab in patients with locally advanced or metastatic urothelial carcinoma who are not eligible for cisplatin-based chemotherapy. We downloaded clinical information and transcriptome data of 298 metastatic bladder cancer patients from http://research-pub.gene.com/IMvigor210CoreBiologies for our analysis. Overall, 298 patients were randomly divided into two data sets in a 7:3 ratio by the R package "Caret": training set (n = 179) and internal validation set (n = 119). Data of 395 bladder cancer patients from The Cancer Genome Atlas dataset (TCGA) was downloaded as an external validation set.

2.2 Source of neutrophil-related gene

Neutrophil-related genes were retrieved from published studies, which can be classified into four gene sets: genes involved in neutrophil function, specificity, polarization, and infiltration, respectively. For genes involved in neutrophil function, 52 genes were extracted from the observation by Rincón et al. (Rincón et al., 2018). They were vital for the function of cell surface receptors, reactive oxygen species, guanine nucleotide exchange factors, and adhesion receptors in neutrophils. For genes involved in neutrophil specificity, 30 genes specifically expressed in neutrophils were obtained from research defining the immune landscape of human colon cancer (Bindea et al., 2013). For genes involved in neutrophil polarization, a continuum of neutrophil states (human N1–5) was identified in human lung cancer by single-cell transcriptomics and 30 genes enriched between the five neutrophil subsets were identified as neutrophil phenotype genes (Zilionis et al., 2019). Finally, 60 genes associated with neutrophil infiltration were obtained from the LM22, a leukocyte gene signature matrix applied in the CIBERSORT algorithm, which was widely used for the estimation of immune cell abundance from tissue expression profiles (Newman et al., 2015). After removing the duplicated genes in the four gene sets, a total of 172 genes were identified and they were defined as neutrophil-related genes for subsequent analyses.

2.3 Construction and validation of the risk model

Univariate COX regression was conducted in bladder cancer patients using the R packages "survival" and "SurvMiner" to select prognostic neutrophil-related genes, which could be used as candidates for construction of a prognostic model. The forest map of prognostic neutrophil-related genes was constructed using the R package "forestPlot." The prognostic genes were then identified by Least Absolute Shrinkage and Selection Operator (LASSO) regression analysis *via* the R packages "glmnet" and a 5-gene risk model was established. The function "predict" in the R package "glmnet" was used to calculate the risk score of individual patients. Patients were divided into high- and low-risk groups according to the median risk scoreThe prognostic value of the 5-gene risk model was verified using the Kaplan-Meier curve and log-rank method *via* the R packages "survival" and "survminer", and the sensitivity and specificity of the model were evaluated by the receiver operating characteristic (ROC) curve analysis *via* the R package "survivalROC".

2.4 Nomogram construction

To determine the probability of survival predicted by the risk model and to facilitate its clinical use, a nomogram was drawn using the R package "rms."

2.5 Survival analysis

Kaplan–Meier plots were drawn to elucidate the effect of each prognostic gene on overall survival (OS) of bladder cancer patients. The Log-rank test was used to evaluate their relationships.

2.6 Analysis of differentially expressed genes

The R package "limma" was used to select differentially expressed genes (DEGs). DEGs meeting the following criteria were considered significant: adjusted p-values <0.05 and | log2 fold change (FC)|≥0.5.

2.7 Pathway enrichment analysis

Gene Ontology (GO) and Kyoto Gene Genome Encyclopedia (KEGG) pathway analyses were performed *via* R package 'clusterprofiler', with a cutoff value of FDR <0.05. To study the differences in biological processes between the high and low expression groups of FCGRT, we applied gene set variation analysis (GSVA) with the R package "GSVA."

2.8 Immune cell infiltration

To assess the composition of immune cells in the tumor microenvironment, we used the ESTIMATE algorithm to evaluate the immune score, tumor purity, and stromal score of tumor samples. The relative abundance of 24 tumor-infiltrating immune cells was obtained by single sample gene set enrichment analysis (ssGSEA) through the R package "GSVA." We then obtained gene sets of exhausted CD8+T cells, naive NKT cells, and nonactivated NK cells from the Molecular Signatures Database (MSigDB) and calculated their enrichment using the GSEA algorithm.

3 Results

3.1 Establishment of the neutrophil-based prognostic model

To determine the correlation between neutrophil-related genes and overall survival (OS) of bladder cancer patients, a univariate Cox regression analysis was performed in the training cohort of the IMvigor210 dataset. Consequently, eight neutrophil-related genes were found to be associated with prognosis, including six genes detrimental to OS (CD93, EMR3, HAL, LILRA2, VNN1, FCGRT) and two genes favorable to OS (MX1, HIST1H2BC) (Figure 1A). These prognostic genes were then subjected to LASSO regression analysis to construct a neutrophil-based prognostic model. After calculating the active coefficients, the prognostic model achieved the best fit when λ points for -4 and 5 key prognostic genes (EMR3, VNN1, FCGRT, HIST1H2BC, and MX1) were incorporated (Figures 1B–D). The individual-level risk score determined by the prognostic model was used for risk stratification and prognosis prediction.

3.2 Validation of the neutrophil-based prognostic model

The risk score for each patient in the training cohort was calculated using the neutrophil-based prognostic model and the median risk score of 0.69 was identified as the cutoff point. According to the cut-off point, bladder cancer patients in the training cohort were divided into high-risk and low-risk groups. Survival analysis showed that patients in the high-risk group had significantly shorter OS than patients in the low-risk group (p = 0.034, HR = 1.309, 95%CI: 1.019–1.682) (Figure 2A). Then a ROC curve was drawn to assess the predictive performance of the prognostic model. As shown in Figure 2B, the area under the curve (AUC) was 0.704. The analysis of the internal validation

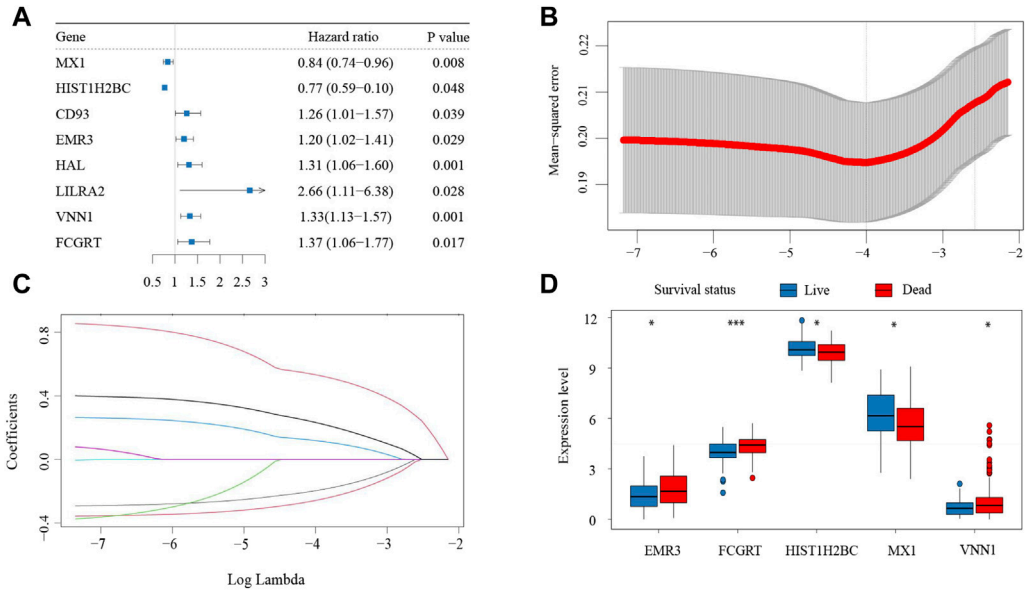

FIGURE 1
Establishment of the neutrophil-based prognostic model **(A)** Forest plot of eight neutrophil-related genes associated with survival. **(B)** Cross-validation for parameter selection **(C)** LASSO coefficient profile plot against the log lambda sequence. **(D)** Expression of the five prognostic genes in patients with different clinical outcomes. LASSO, least absolute shrinkage and selection operator.

cohort from the IMvigor210 dataset corroborated these findings. Patients with a high-risk score had poorer clinical outcomes (p = 0.012, HR = 1.578, 95%CI: 1.101–2.262) and the AUC was 0.604 (Figures 2C,D). Furthermore, data from the TCGA dataset were downloaded as an external validation cohort. Consistent with the previous conclusions, the results showed that a high-risk score was closely related to an inferior OS (p = 0.013, HR = 1.425, 95%CI: 1.076–1.889) (Figures 2E,F).

3.3 Construction of predictive nomogram

To further demonstrate the prognostic value of the neutrophil-based prognostic model, a multivariate Cox regression analysis was performed. The risk score was confirmed to be an independent prognostic factor for OS (HR: 11.43, 95% CI: 3.00–43.57, p < 0.001) (Figure 3A). Furthermore, the Eastern Cooperative Oncology Group (ECOG) score and immune phenotypes were also independent indicators of prognosis. Subsequently, for the convenience in clinical application, we established a nomogram to predict 1- and 3-year OS in bladder cancer patients. According to the results of the multivariate analysis, the risk score, the ECOG score and immune phenotypes were included in the nomogram. The total point scores for all parameters were matched with the survival time scales (Figure 3B).

3.4 Correlation of neutrophil-related genes with prognosis in bladder cancer

With the aim of exploring the function of five neutrophil-related genes incorporated into the prognostic model, a survival analysis was performed. The Kaplan–Meier curves revealed that all five genes played a role in the prognosis of bladder cancer, while FCGRT had the strongest predictive power for survival (p = 0.035, HR = 1.245, 95%CI: 1.015–1.526) (Figure 4A; Supplementary Figure S1). To gain insight into the involvement of FCGRT in bladder cancer development, patients in the IMvigor210 cohort were divided into two groups based on the mean expression of FCGRT. The principal component analysis showed that the gene expression profiles were significantly different between the FCGRT high and FCGRT low groups (Figure 4B). The "limma" package was then used in the R environment to identify DEGs between the two groups. A total of 159 DEGs were selected with a cutoff p-value of 0.05 and |fold-change| >1.5 (Figure 4C).

3.5 Relationship between FCGRT expression and cancer metabolism and immunity

Functional enrichment analysis was performed using the GO and KEGG databases to elucidate the biological functions

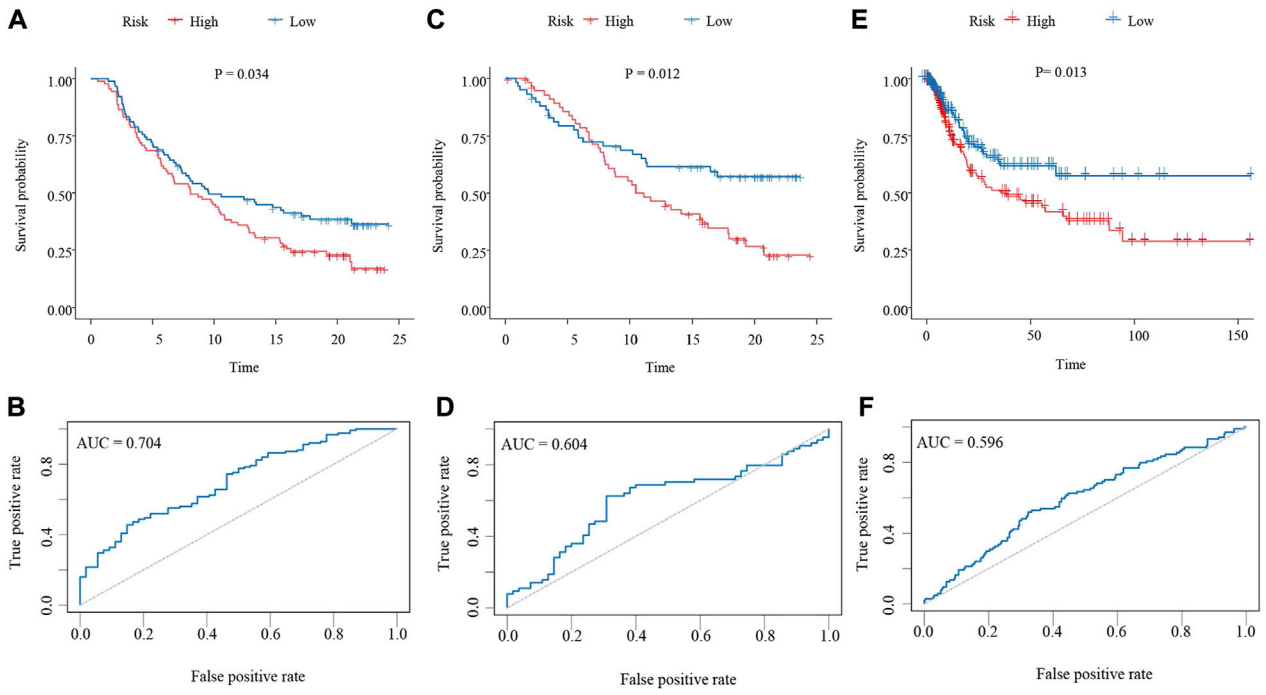

FIGURE 2
Validation of the neutrophil-based prognostic model **(A,C,E)** Kaplan–Meier survival curves of bladder cancer patients from the high-risk group and the low-risk group. **(A)**, training dataset (p = 0.034, HR = 1.309, 95%CI: 1.019–1.682). **(C)**, internal validation dataset (p = 0.012, HR = 1.578, 95%CI: 1.101–2.262). **(E)**, external validation dataset (p = 0.013, HR = 1.425, 95%CI: 1.076–1.889). **(B,D,F)** ROC curves evaluating the sensitivity and specificity of the neutrophil-based prognostic model. **(B)**, training dataset. **(D)**, internal validation dataset. **(F)**, external validation dataset. ROC, receiver operating characteristic.

of DEGs. GO enrichment analysis revealed that upregulated DEGs were mainly enriched in neutrophil chemotaxis and neutrophil migration, while downregulated genes were enriched in cytoskeleton organization and skin development (Figures 5A,B). KEGG enrichment analysis demonstrated that both upregulated and downregulated DEGs were involved in metabolism related pathways, such as protein digestion and absorption, tyrosine metabolism, and linolenic acid metabolism (Figure 5C). The GSEA analysis shared similar conclusions with the KEGG analysis. High expression of FCGRT was closely correlated with gene signatures that feature metabolic processe, including drug metabolism and nutrient metabolism (Figures 5D,E). Furthermore, the GSEA analysis showed that genes upregulated in the FCGRT high group were predominantly enriched in the immune process, such as antigen processing and presentation, the cytokine and chemokine signaling pathway, and B cell receptor signaling pathway (Figure 5F). The results allowed to reasonably infer that FCGRT was closely associated with antitumor immunity and remodeling of the tumor microenvironment. In addition, three mismatch repair pathways were suppressed in the FCGRT high group, suggesting a correlation between FCGRT and the DNA damage and repair process, which requires further exploration (Figure 5G).

3.6 FCGRT-shaped immunosuppressive context

To explore the influence of FCGRT on the immune context of bladder cancer, ESTIMATE analysis was performed to evaluate the level of immune infiltration in tumor tissue. The results showed that the FCGRT high group had higher stromal and immune scores compared to the FCGRT low group (Figure 6A). ssGSEA analysis was then applied to calculate the proportion of each type of immune cells within tumor microenvironment (TME). The proportion of all tumor-infiltrating lymphocytes was significantly elevated in the FCGRT high group, except for activated $CD4^+$ T cells and type 2 T helper cells (Figure 6B). However, the ratio of $CD8^+$ T cells to Treg cells was decreased, indicating an immunosuppressive environment (Figure 6C). Then unsupervised group analysis revealed that the immune profiles of FCGRT high group and FCGRT low group were significantly

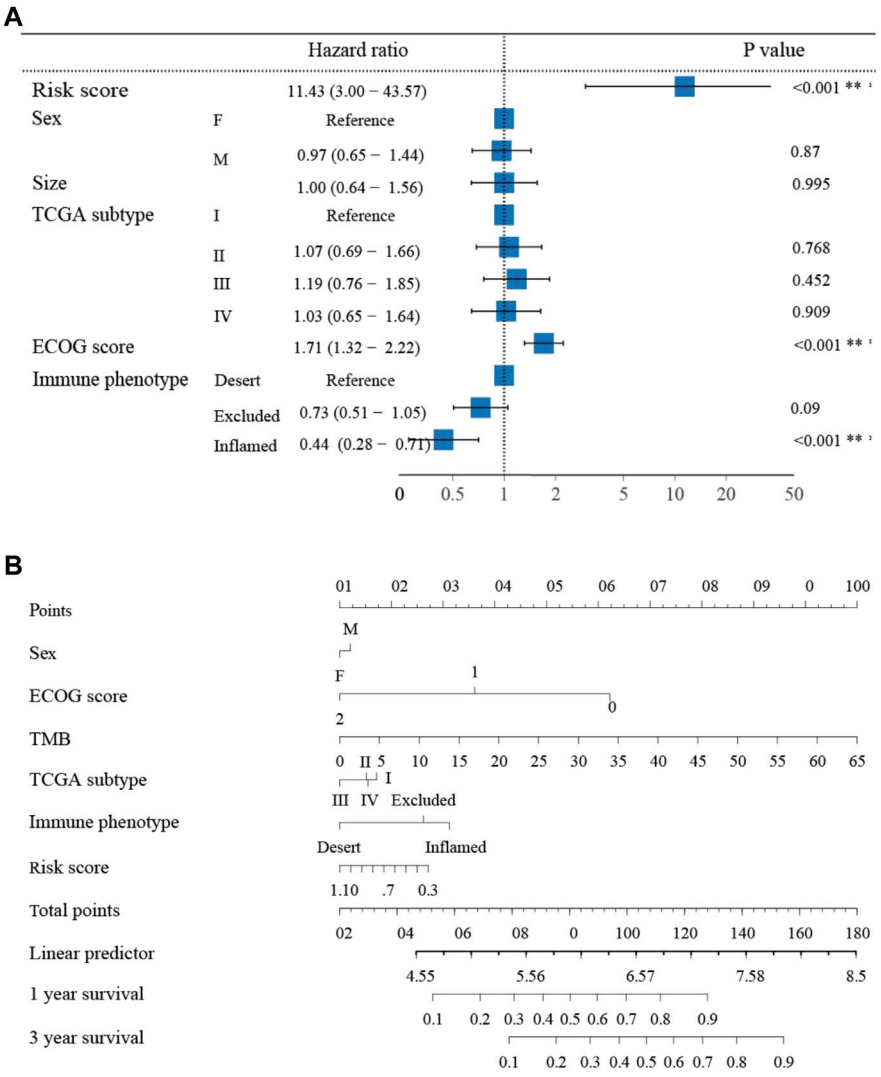

FIGURE 3
The nomogram to predict 1- and 3-year overall survival of bladder cancer patients **(A)** Multivariate Cox regression analysis revealing clinical characteristics related to prognosis. **(B)** The nomogram predicting overall survival of bladder cancer patients.

different (Figure 7A). Further correlation analysis indicated close ties between FCGRT expression and immune cell infiltration, among which NK cells, macrophages and MDSCs exhibited the strongest association with FCGRT level (Figure 7B).

We also investigated the relationship between FCGRT expression and the functional status of immune cells. GSEA analysis showed that the exhausted $CD8^+$ T cell gene set and the unstimulated NK cell gene set were significantly enriched in FCGRT high group (Figures 7C,D), implying that FCGRT could potentially orchestrate the dysfunction of $CD8^+$ T cell and NK cell. Furthermore, the NKT cell, another important antitumor immune cell, was found to display a naïve phenotype in FCGRT high group (Figure 7E). Taken together, our results show that FCGRT influenced the tumor immune microenvironment through various mechanisms and shaped an immunosuppressive context in general.

3.7 Predictive value of FCGRT in responsiveness to anti-tumor drugs

Given the immunophenotype discrepancy between the FCGRT high and FCGRT low group, it was hypothesized that FCGRT hold promise in predicting the immunotherapy response. We explored the correlation between FCGRT expression and recognized immunotherapy markers, including

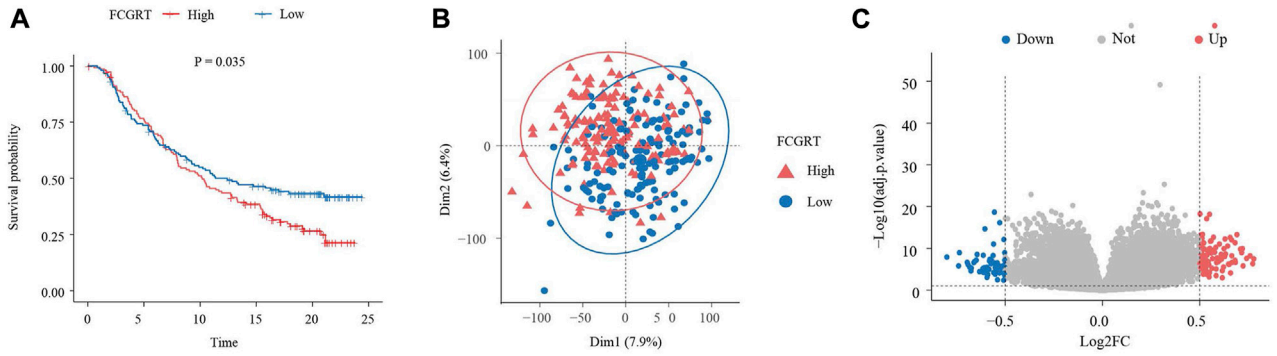

FIGURE 4
Identification of DEGs in FCGRT high and FCGRT low group **(A)** Kaplan–Meier survival curve of overall survival based on FCGRT expression (p = 0.035, HR = 1.245, 95%CI: 1.015–1.526) **(B)** Comparison of gene expression profiles of the FCGRT high and FCGRT low group. **(C)** The Volcano plot of DEGs. DEGs, differentially expressed genes.

PD-L1 and the TMB. As shown in Figures 8A,B, patients with high FCGRT showed reduced PD-L1 expression and decreased TMB level (p = 0.003, p = 0.002). The overall response rate of FCGRT high group was only 16%, which was much lower than 30% of the FCGRT low group (p = 0.006) (Figure 8C). Furthermore, patients who responded to ICIs exhibited decreased FCGRT level (p = 0.007) (Figure 8D). These results suggested that FCGRT could serve as a potential biomarker of poor immunotherapy efficacy in bladder cancer. We also analyzed the correlation between FCGRT expression and sensitivity to chemotherapy and targeted therapy. The results showed that the estimated IC50 values of cisplatin, docetaxel, doxorubicin, erlotinib and lapatinib were significantly higher in the FCGRT high group, while the estimated IC50 values of gemcitabine, methotrexate, and gefitinib did not show statistical differences between the two groups (Figures 9A–H).

4 Discussion

Bladder cancer is the most common malignancy of the urinary system (Bellmunt et al., 2022). Despite advances in targeted therapy and immune regimen, the prognosis of bladder cancer remains unfavorable. Therefore, effective prognostic and therapeutic markers are needed to optimize disease management. The current risk stratification of bladder cancer is based on clinicopathological features, such as clinical stages and tumor grades, none of which exhibits high specificity and sensitivity (Soria et al., 2019). Furthermore, these conventional prediction tools have focused primarily on the intrinsic characteristics of cancer, ignoring the contribution of TME to cancer genesis and development (Kluth et al., 2015). Tumor-associated neutrophils are critical components of TME and its involvement in cancer development has become more and more prominent in recent years. Neutrophils play an important role in the initiation, development and progression of bladder cancer (Thompson et al., 2015). They can directly or indirectly regulate bladder cancer development by boosting inflammation, promoting angiogenesis, and mediating immunosuppression. Neutrophils also play a role in predicting treatment responses and prognosis of bladder cancer. Neutrophils and neutrophil extracellular traps (NETs) have been reported to influence the efficacy of BCG immunotherapy and mediate resistance to radiation therapy (Liu et al., 2019; Shinde-Jadhav et al., 2021). High circulating neutrophil counts and elevated neutrophil-to-lymphocyte ratio (NLR) are associated with adverse clinical outcomes for patients with bladder cancer (Tang Du et al., 2017). Additionally, tumor-infiltrating neutrophils exhibit pro-carcinogenic effects and predict poor prognosis (Liu et al., 2018). To further elucidate the relationship between neutrophils and the prognosis of bladder cancer, we analyzed the transcriptomic data from the IMvigor210 cohort and constructed a prognostic model based on the expression profile of neutrophil-related genes. Moreover, FCGRT was found to participate in cancer metabolic reprogramming and mediate an immunosuppressive tumor microenvironment. Furthermore, we validated the significance of FCGRT in predicting responses to anti-cancer drugs in bladder cancer.

Advances in next-generation sequencing (NGS) technology allow access to genomic profiles of cancer. The application of NGS has identified multiple mutations and gene expression signatures that aid in precise cancer classification and prognosis prediction. Previous studies have shown that immune cell related genes were closely correlated with clinical outcomes of bladder cancer, such as myeloid cells and antitumor T cells (Eckstein et al., 2020; Wang et al., 2021). In the current study, we first investigated the role of neutrophil-related genes in the prognosis of bladder cancer. It was found that eight neutrophil-related genes, namely CD93, EMR3, HAL, LILRA2, VNN1, FCGRT, MX1, and HIST1H2BC, had a strong correlation

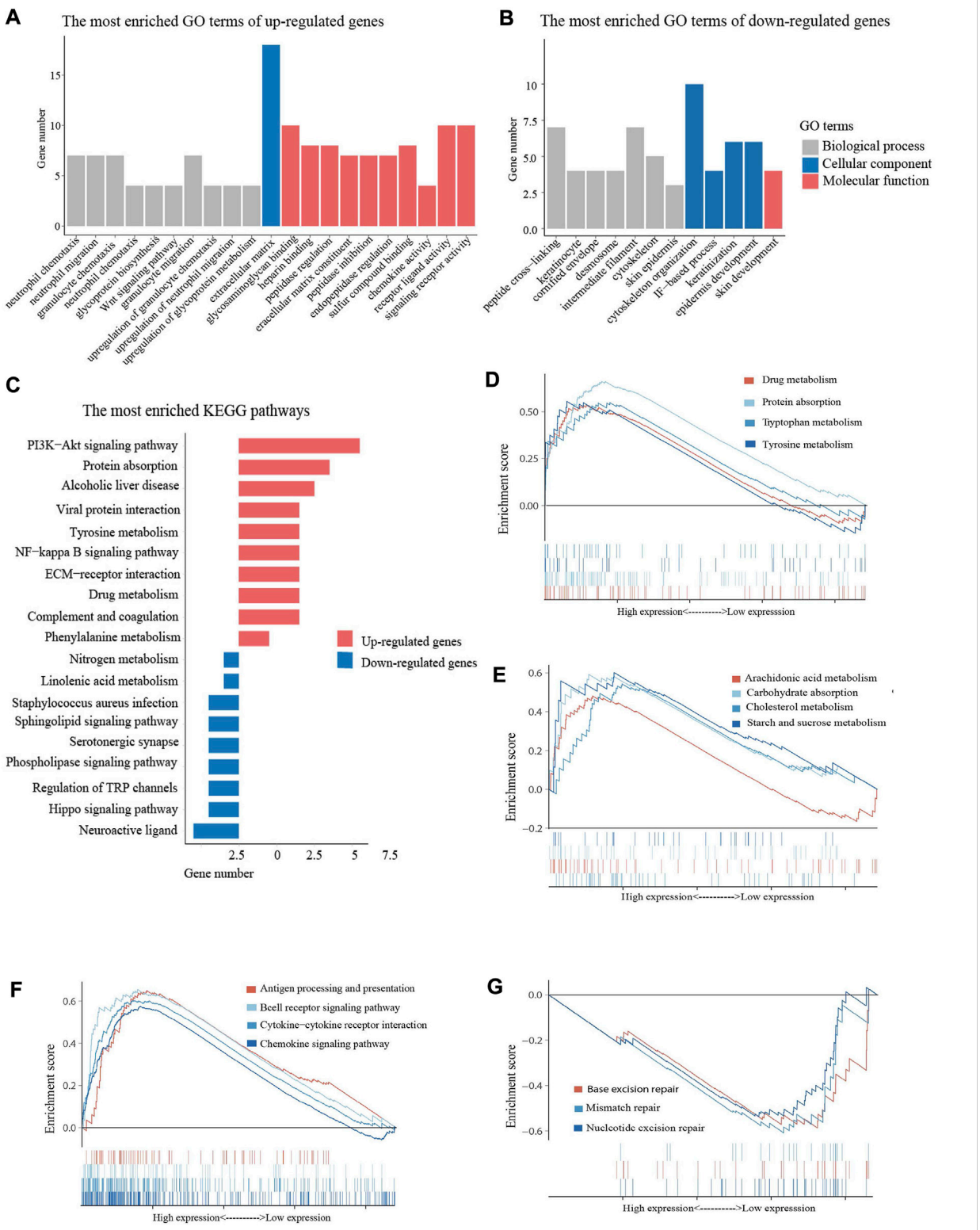

FIGURE 5
Enrichment analysis of DEGs **(A)** The most enriched GO terms of up-regulated DEGs. **(B)** The most enriched GO terms of down-regulated DEGs **(C)** The bar graph of the most enriched KEGG pathways. **(D,E)** Metabolism related pathways in GSEA enrichment analysis **(F)** Immunity related pathways in GSEA enrichment analysis. **(F)** DDR related pathways in GSEA enrichment analysis. DEGs, differentially expressed genes. GO, Gene Ontology. KEGG, Kyoto Encyclopedia of Genes and Genomes. GSEA, gene set enrichment analysis. DDR, DNA damage and repair.

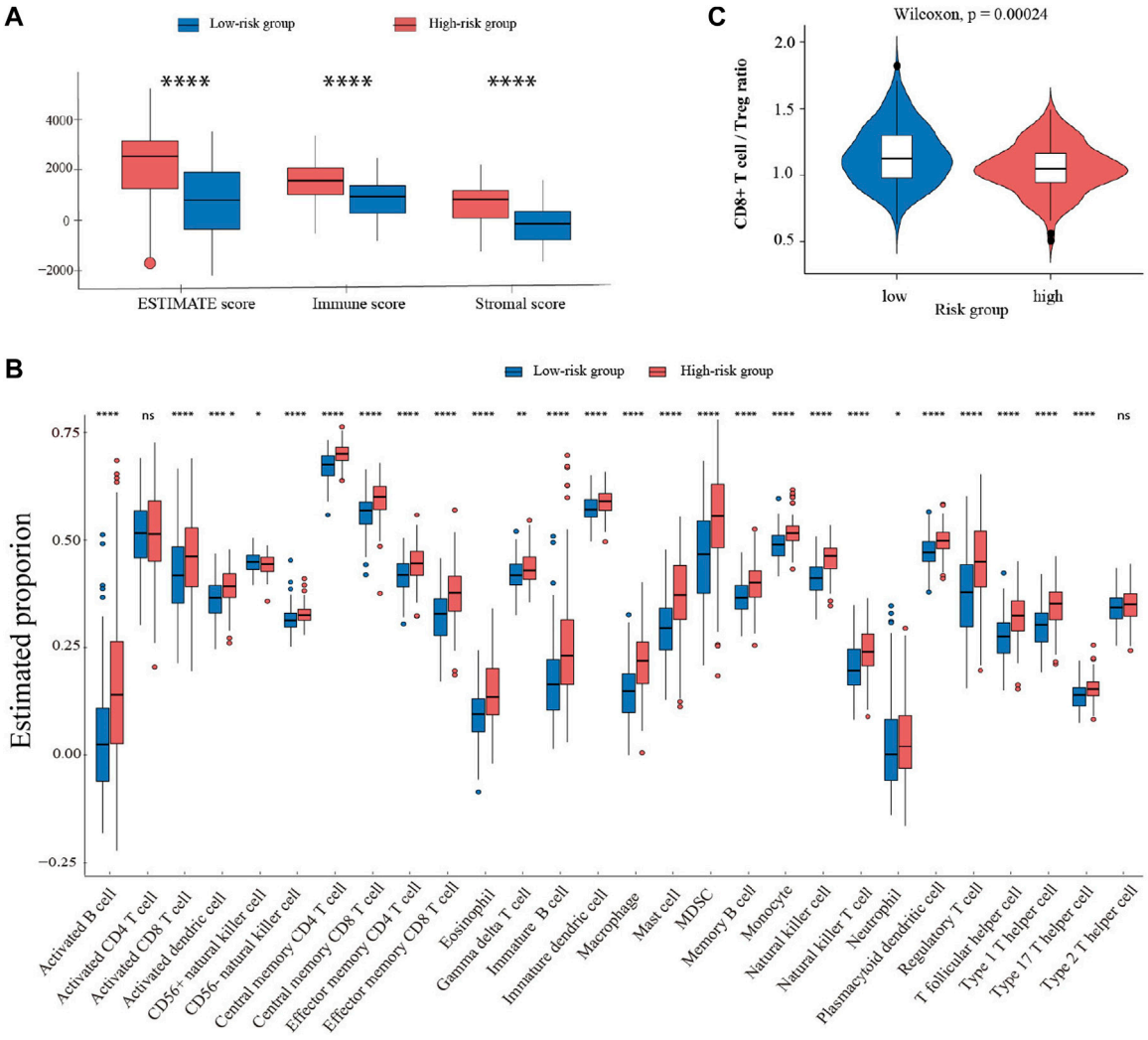

FIGURE 6
Comparison of immune profiles in two groups with different FCGRT expression **(A)** Boxplot of the ESTIMATE score. **(B)** The abundance of each immune cell type in the two groups. **(C)** The ratio of CD8+T/Treg cells in the FCGRT high group.

with the prognosis of bladder cancer. Among them, CD93 and HIST1H2BC were specifically expressed in neutrophils and constituted the distinctive transcriptional profile of neutrophils, facilitating the identification of neutrophils within the tumor microenvironment (Bindea et al., 2013). VNNI, EMR3, LILRA2, and HAL all played significant roles in neutrophil infiltration (Newman et al., 2015). They were widely employed to quantify the number of infiltrating neutrophils in various tissues or malignancies. FCGRT was critical to neutrophil function (Patel and Bussel, 2020). The FCGRT gene-encoded neonatal Fc receptor for IgG (FcRn) participated in IgG-mediated antigen phagocytosis by neutrophils, hence enhancing immune defenses against pathogenic pathogens. MX1 was closely related to the phenotypic heterogeneity of neutrophils (Zilionis et al., 2019). According to single-cell transcriptomics, human neutrophils could be divided into five subsets (N1-N5), and MX1 was prominently enriched in the N2 neutrophil subtype and served as a marker gene for this specific neutrophil population.

Incorporated five genes (MX1, HIST1H2BC, EMR3, VNN1, and FCGRT), an effective prognostic model was constructed. MX1 is an interferon-induced GTPase localized in the cytoplasm. MX1 had been studied mainly for its antiviral properties until recent studies reported its biological functions in tumorigenesis (Calmon et al., 2009). *In vitro* experiments revealed that MX1 was able to inhibit cancer cell migration and reduce metastasis of prostate and melanoma cancer (Mushinski et al.,

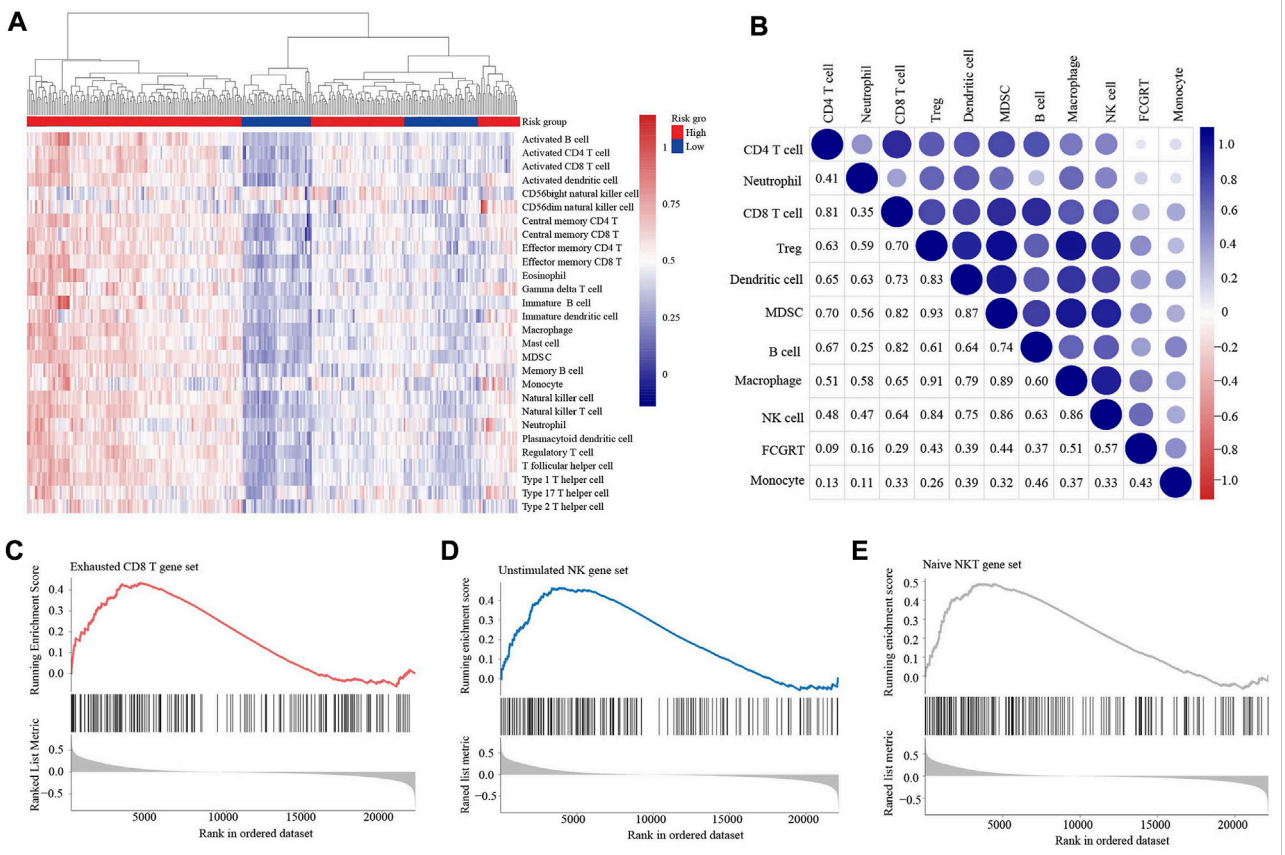

FIGURE 7
FCGRT-shaped immunosuppressive context **(A)** Heatmap of the infiltration profile of 28 immune cells in the two groups. **(B)** Correlation between FCGRT expression and immune cell infiltration. The *p*-value of the correlation is indicated in box. **(C–E)** The enriched gene sets in the FCGRT high group.

2009). HIST1H2BC is a member of the histone H2B family. Emerging evidence has shown that histone modification plays a key role in tumorigenicity, and mutations in histone H2B have been identified as important cancer drivers (Bajbouj et al., 2021; Markouli et al., 2021). However, few reports have described its correlation with cancer prognosis, which deserves further investigation. EMR3, an adherent G protein-coupled receptor, is highly expressed in neutrophils, monocytes, and macrophages (Matmati et al., 2007). EMR3 has been reported to mediate the aggressive phenotype of glioblastoma (Kane et al., 2010). The knockdown of EMR-3 reduced cell invasion capacity by more than three times. VNN1 encodes the Vnn1 protein, whose main function is to inhibit caspase and scavenge reactive oxygen species (Naquet et al., 2014). Vnn1 has been reported to play an important role in tumorigenesis. VNN1 deficient mice developed resistance to oxidative stress, thus inhibiting intestinal inflammation and reducing the incidence of colorectal cancer (Pouyet et al., 2010). FCGRT encodes the α-chain of the neonatal Fc receptor (FcRn), a transporter of immunoglobulin G (IgG) and albumin. FcRn maintains serum IgG and albumin levels in a pH-dependent manner. It also plays a vital role in antigen phagocytosis and presentation of immune complexes (Vidarsson et al., 2006; Patel and Bussel, 2020). Dysregulation of FcRn has been reported to exert effects on the prognosis of non-small cell lung cancer, colorectal cancer, and hepatocellular carcinoma (Dalloneau et al., 2016; Shi et al., 2016). The biological functions of FCGRT in bladder cancer have yet to be elucidated.

Metabolic reprogramming is a hallmark of cancer and an important contributor to cancer progression. The metabolic switch allows the uptake of deregulated nutrients and efficient energy supply to fuel cancer cell growth and division (Martínez-Reyes and Chandel, 2021). In our study, FCGRT was found to alter cancer metabolism by modulating metabolic signaling pathways in both malignant and non-malignant cells within TME. The metabolic changes in neutrophils were able to directly or indirectly influence the TME. For instance, Rice et al. (2018) found that the mitochondrial activity of neutrophils was enhanced in malignant diseases, leading to increased intracellular NADPH levels and ROS production.

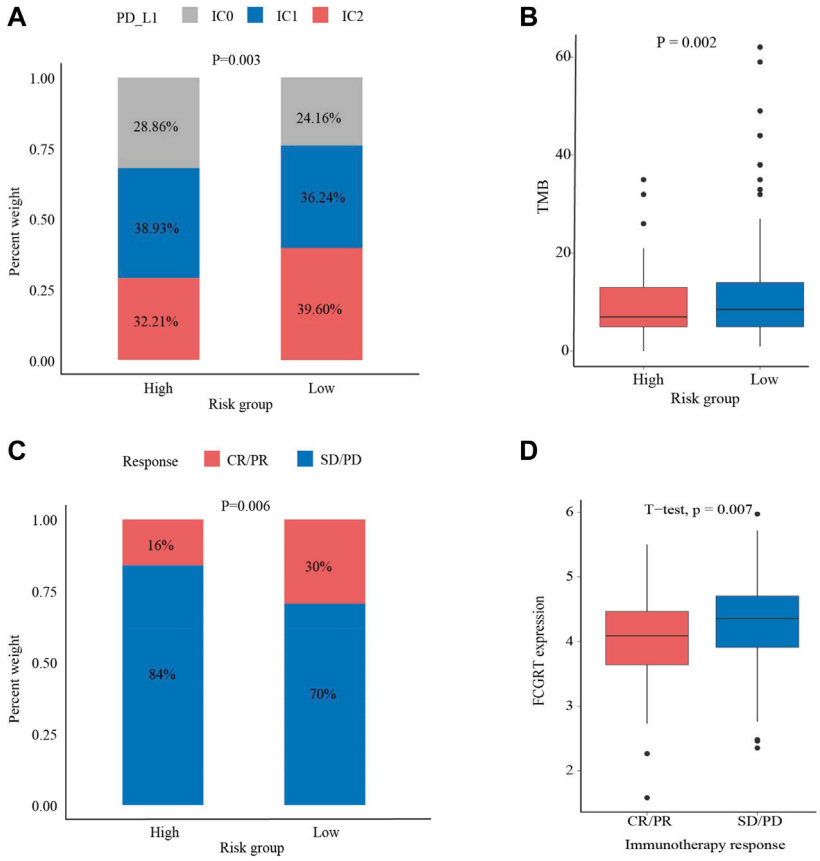

FIGURE 8
The correlation between FCGRT expression and response to immunotherapy **(A,B)** The correlation between FCGRT expression and PD-L1 and TMB level (p = 0.03, p = 0.002) **(C,D)** The correlation between FCGRT expression and immunotherapy sensitivity (p = 0.06, p = 0.007).

The overexpressed ROS hindered T cell activity and created an immunosuppressive environment. In our study, it was observed that FCGRT was correlated with the activation of ROS-related pathways, such as the HIF-1 signaling pathway and oxidative phosphorylation, which might be involved in the complex interaction between neutrophils and TME. Alteration of lipid metabolism in neutrophils also plays an important role in TME remolding. Li et al. found neutrophils at metastatic cancer sites had increased lipid storage, and these accumulated lipids within neutrophils can be transported to metastatic cancer cells *via* a micropinocytosis–lysosome pathway, which subsequently facilitated tumor proliferation and enhanced metastatic environment (Li et al., 2020). The upregulated lipid metabolism mediated by FCGRT might similarly contribute to the development of an immunosuppressive TME.

It is speculated that FCGRT regulates cancer metabolism through the engagement of FcRn with albumin transport (Cadena Castaneda et al., 2020). Albumin is the most abundant protein in the circulation and functions as an endogenous transporter for multiple small molecules such as fatty acids, amino acids, bilirubin, and drugs (Rabbani and Ahn, 2019). Overexpressed FcRn leads to increased albumin recycling, during which the nutrient cargo carried by albumin is released intracellularly and promotes the metabolism and proliferation of cancer cells. These findings were corroborated in human cancer epithelial cells (Larsen et al., 2020). The albumin recycling process was reported to be highly FcRn-dependent and FcRn knockout decreased the metabolic rate of malignant cells *in vitro*, as well as cancer growth *in vivo*. Furthermore, we found that genes related to drug metabolism were also predominantly enriched in FCGRT high group. The underlying mechanism is that FcRn-mediated transcellular recycling mechanism protects albumin-binding drugs from degradation by serum and tissue proteases. The protective role of FcRn extends the circulatory half-life of albumin-binding drugs, and improve their uptake and utilization by target tissues (Yu et al., 2022). New treatment perspectives have been suggested based on the mechanism. Albumin-based drug conjugates were engineered with different affinity for FcRn to fine tune pharmacokinetics, thus achieving an optimal therapeutic profile (Larsen et al., 2018).

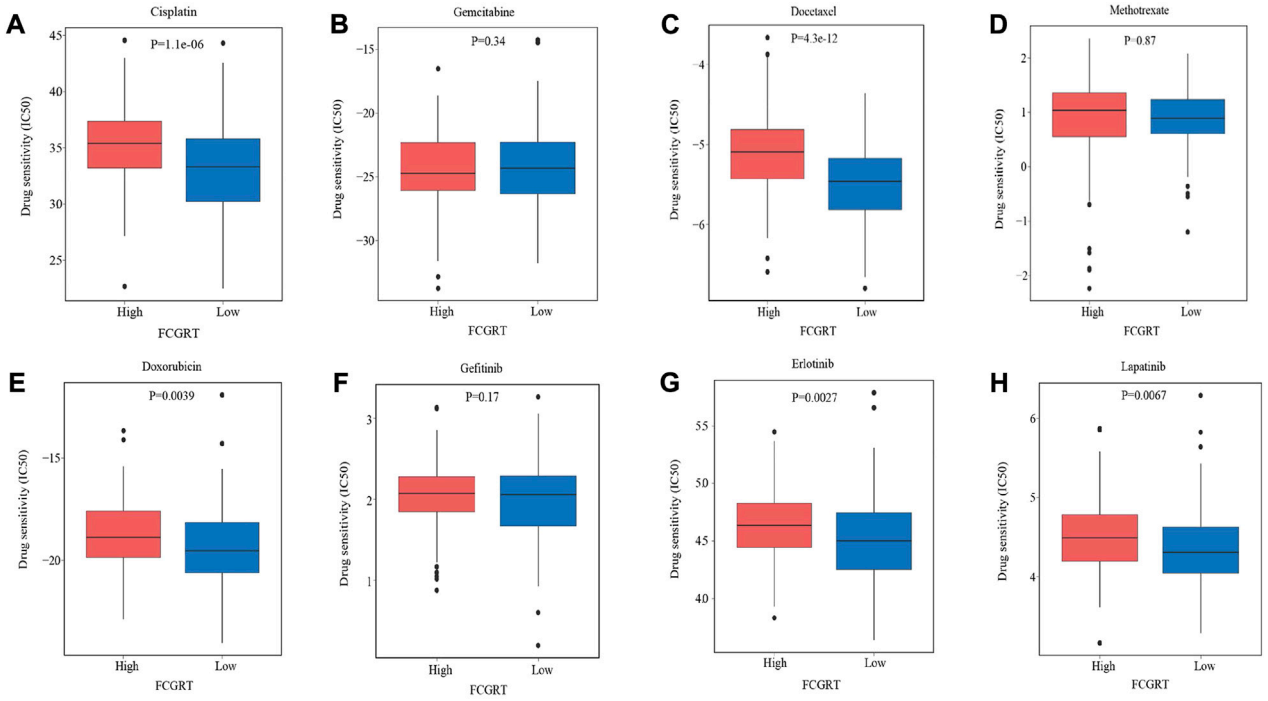

FIGURE 9
The correlation between FCGRT expression and response to chemotherapy and targeted therapy. **(A–H)** Estimated IC50 values of chemotherapy and targeted therapy drugs in FCGRT high and FCGRT low groups.

Despite its participation in cancer metabolic reprogramming, FCGRT also plays a role in cancer immunity (Coffelt et al., 2016). In our study, FCGRT expression was significantly correlated with gene signatures featuring immune regulation, including the chemokine signaling pathway, antigen processing and presentation, and immune cell migration and function. The FcRn-mediated immunosurveillance has been in colorectal cancer (Baker et al., 2013). It was found that FcRn expression within dendritic cells induced IL-12 production and promoted the cross-priming of tumor antigens to CD8 + T cells, thus improving antitumor immunity and inhibiting tumor development. In addition to immune regulation, FcRn expression also affected tumor microenvironment landscapes. Tumors with high expression of FCGRT exhibited increased infiltration by a number of immune cell subtypes, compared to tumors with low expression of FCGRT. This phenomenon indicated the potential role of FCGRT in the identification of an immune-inflamed phenotype (Gerard et al., 2021). Consistent with our study, Castaneda et al. revealed that the proportion of tumor-infiltrating dendritic cells, $CD8^+$ T cells, and NK cells was significantly reduced in FcRn-knockout mice compared to wild-type mice (Castaneda et al., 2018). Although the number of immune activating and immune suppressive cells was both elevated in FCGRT high group, the ratio of $CD8^+$ T cells to Treg cells was decreased, indicating a suppressive TME in general. Furthermore, FCGRT could potentially orchestrate the dysfunction of antitumor immune cells. FCGRT was able to alter the cytotoxic activity of antitumor immune cells, with the enrichment of exhausted $CD8^+$ T cell gene set, unstimulated NK gene set, and naive NKT gene set in FCGRT high group. However, our results were opposite to existing research indicating that FcRn promoted NK cell maturation and interferon γ production (Castaneda et al., 2018). More studies are needed to clarify the role of FCGRT in the development and activation of immune cells.

ICIs have revolutionized the treatment of bladder cancer and extended patient survival to an unprecedented extent. However, not all patients can benefit from immune therapy. We found that FCGRT could serve as a potential biomarker for immunotherapy. Bladder cancer patients with high expression of FCGRT had a lower response rate to ICIs. ICI therapies are designed to reinvigorate the effective antitumor immune response mediated by T cells. Therefore, the functionality of $CD8^+$ T cells determines whether patients are likely to respond to ICI (Waldman et al., 2020). Overexpressed FCGRT altered T cell activation and priming. T cell dysfunction interferes with the development of a robust antitumor response after ICI treatment and weakens the efficacy of immunotherapy. Furthermore, FCGRT expression was found to correlate with a decrease in PD-L1 expression and a low TMB level, which collectively

indicated an unfavorable response to immunotherapy (Shum et al., 2022). PD-L1 expression is the most intuitive predictive biomarker of ICI and has been widely used for patient selection in clinical practice. TMB reflects the level of cancer mutation and the ability to produce neoantigen by malignancies (Chan et al., 2019; Li et al., 2020). The lower the TMB, the less likely that T cells will recognize and eradicate tumor antigens. In addition to immunotherapy, FCGRT was also correlated with high sensitivity to chemotherapy and targeted agents. The alteration of the DNA damage and repair (DDR) pathways mediated by FCGRT may represent an underlying mechanism. Most chemotherapy drugs disrupt DNA integrity or interfere with DNA synthesis to inhibit cancer cell replication. Defects in the DDR pathways make it difficult to detect and repair DNA lesions and improve the therapeutic efficacies of chemotherapy (Goldstein and Kastan, 2015; Reisländer et al., 2020).

There are still some limitations in our study. First, further verification of our conclusions is limited by insufficient data. Clinical samples and prospective studies are warranted for further validation. Second, there is a close link between neutrophil-related genes and tumor microenvironment observed in our research. The underlying mechanism remains unclear and requires investigation in the future. Third, neutrophil-related genes used in our analysis should be more comprehensive and updated to ensure the authenticity of the research.

5 Conclusion

We established a prognostic model that contains five neutrophil-related genes in bladder cancer and proved its possible independent prognostic value. In addition, we found FCGRT-mediated cancer metabolic reprogramming and tumor microenvironment remodeling, which could be used as a novel biomarker for ICIs therapy. Future studies should be conducted to clarify the function of FCGRT in bladder cancer and verify the predictive capacity of the neutrophil-based model in clinical applications.

Data availability statement

The datasets presented in this study can be found in online repositories. The names of the repository/repositories and accession number(s) can be found in the article/Supplementary Material.

Author contributions

RY, XW, and YL conceived and designed the study. WZ, XS and HC performed the bioinformatics analysis and interpretation of the data. XM, YZ and QZ generated the figures and tables. All authors listed have contributed to the article and approved it for publication.

Funding

This work was supported by grants from the National Natural Science Foundation of China (No. 81874044), the Shandong Provincial Natural Science Foundation (No.ZR2020MH236 and No. ZR2019MH050) and the Wu Jieping Medical Foundation (No.320.6750.12129 and No.320.6750.19088–25).

Conflict of interest

The authors declare that the research was conducted in the absence of any commercial or financial relationships that could be construed as a potential conflict of interest.

Publisher's note

Supplementary material

The Supplementary Material for this article can be found online at: https://www.frontiersin.org/articles/10.3389/fphar.2022.1013672/full#supplementary-material

References

Bajbouj, K., Al-Ali, A., Ramakrishnan, R. K., Saber-Ayad, M., and Hamid, Q. (2021). Histone modification in NSCLC: Molecular mechanisms and therapeutic targets. *Int. J. Mol. Sci.* 22 (21), 11701. doi:10.3390/ijms222111701

Baker, K., Rath, T., Flak, M. B., Arthur, J. C., Chen, Z., Glickman, J. N., et al. (2013). Neonatal Fc receptor expression in dendritic cells mediates protective immunity against colorectal cancer. *Immunity* 39 (6), 1095–1107. doi:10.1016/j.immuni.2013.11.003

Bellmunt, J., Valderrama, B. P., Puente, J., Grande, E., Bolós, M. V., Lainez, N., et al. (2022). Recent therapeutic advances in urothelial carcinoma: A paradigm shift in disease management. *Crit. Rev. Oncol. Hematol.* 174, 103683. doi:10.1016/j.critrevonc.2022.103683

Bindea, G., Mlecnik, B., Tosolini, M., Kirilovsky, A., Waldner, M., Obenauf, A. C., et al. (2013). Spatiotemporal dynamics of intratumoral immune cells reveal the immune landscape in human cancer. *Immunity* 39 (4), 782–795. doi:10.1016/j.immuni.2013.10.003

Cadena Castaneda, D., Brachet, G., Goupille, C., Ouldamer, L., and Gouilleux-Gruart, V. (2020). The neonatal Fc receptor in cancer FcRn in cancer. *Cancer Med.* 9 (13), 4736–4742. doi:10.1002/cam4.3067

Calmon, M. F., Rodrigues, R. V., Kaneto, C. M., Moura, R. P., Silva, S. D., Mota, L. D., et al. (2009). Epigenetic silencing of CRABP2 and MX1 in head and neck tumors. *Neoplasia* 11 (12), 1329–1339. doi:10.1593/neo.91110

Castaneda, D. C., Dhommée, C., Baranek, T., Dalloneau, E., Lajoie, L., Valayer, A., et al. (2018). Lack of FcRn impairs natural killer cell development and functions in the tumor microenvironment. *Front. Immunol.* 9, 2259. doi:10.3389/fimmu.2018.02259

Chan, T. A., Yarchoan, M., Jaffee, E., Swanton, C., Quezada, S. A., Stenzinger, A., et al. (2019). Development of tumor mutation burden as an immunotherapy biomarker: Utility for the oncology clinic. *Ann. Oncol.* 30 (1), 44–56. doi:10.1093/annonc/mdy495

Coffelt, S. B., Wellenstein, M. D., and de Visser, K. E. (2016). Neutrophils in cancer: Neutral no more. *Nat. Rev. Cancer* 16 (7), 431–446. doi:10.1038/nrc.2016.52

Dalloneau, E., Baroukh, N., Mavridis, K., Maillet, A., Gueugnon, F., Courty, Y., et al. (2016). Downregulation of the neonatal Fc receptor expression in non-small cell lung cancer tissue is associated with a poor prognosis. *Oncotarget* 7 (34), 54415–54429. doi:10.18632/oncotarget.10074

Eckstein, M., Strissel, P., Strick, R., Weyerer, V., Wirtz, R., Pfannstiel, C., et al. (2020). Cytotoxic T-cell-related gene expression signature predicts improved survival in muscle-invasive urothelial bladder cancer patients after radical cystectomy and adjuvant chemotherapy. *J. Immunother. Cancer* 8 (1), e000162. doi:10.1136/jitc-2019-000162

Gentles, A. J., Newman, A. M., Liu, C. L., Bratman, S. V., Feng, W., Kim, D., et al. (2015). The prognostic landscape of genes and infiltrating immune cells across human cancers. *Nat. Med.* 21 (8), 938–945. doi:10.1038/nm.3909

Gerard, C. L., Delyon, J., Wicky, A., Homicsko, K., Cuendet, M. A., and Michielin, O. (2021). Turning tumors from cold to inflamed to improve immunotherapy response. *Cancer Treat. Rev.* 101, 102227. doi:10.1016/j.ctrv.2021.102227

Goldstein, M., and Kastan, M. B. (2015). The DNA damage response: Implications for tumor responses to radiation and chemotherapy. *Annu. Rev. Med.* 66, 129–143. doi:10.1146/annurev-med-081313-121208

Hedrick, C. C., and Malanchi, I. (2022). Neutrophils in cancer: Heterogeneous and multifaceted. *Nat. Rev. Immunol.* 22 (3), 173–187. doi:10.1038/s41577-021-00571-6

Jaillon, S., Ponzetta, A., Di Mitri, D., Santoni, A., Bonecchi, R., and Mantovani, A. (2020). Neutrophil diversity and plasticity in tumour progression and therapy. *Nat. Rev. Cancer* 20 (9), 485–503. doi:10.1038/s41568-020-0281-y

Kane, A. J., Sughrue, M. E., Rutkowski, M. J., Phillips, J. J., and Parsa, A. T. (2010). EMR-3: A potential mediator of invasive phenotypic variation in glioblastoma and novel therapeutic target. *Neuroreport* 21 (16), 1018–1022. doi:10.1097/WNR.0b013e32833f19f2

Kluth, L. A., Black, P. C., Bochner, B. H., Catto, J., Lerner, S. P., Stenzl, A., et al. (2015). Prognostic and prediction tools in bladder cancer: A comprehensive review of the literature. *Eur. Urol.* 68 (2), 238–253. doi:10.1016/j.eururo.2015.01.032

Larsen, M. T., Mandrup, O. A., Schelde, K. K., Luo, Y., Sørensen, K. D., Dagnæs-Hansen, F, et al. (2020). FcRn overexpression in human cancer drives albumin recycling and cell growth; a mechanistic basis for exploitation in targeted albumin-drug designs. *J. Control. Release* 322, 53–63. doi:10.1016/j.jconrel.2020.03.004

Larsen, M. T., Rawsthorne, H., Schelde, K. K., Dagnæs-Hansen, F., Cameron, J., and Howard, K. A. (2018). Cellular recycling-driven *in vivo* half-life extension using recombinant albumin fusions tuned for neonatal Fc receptor (FcRn). engagement. *J. Control. Release* 287, 132–141. doi:10.1016/j.jconrel.2018.07.023

Li, P., Lu, M., Shi, J., Gong, Z., Hua, L., Li, Q., et al. (2020). Lung mesenchymal cells elicit lipid storage in neutrophils that fuel breast cancer lung metastasis. *Nat. Immunol.* 21 (11), 1444–1455. doi:10.1038/s41590-020-0783-5

Li, R., Han, D., Shi, J., Han, Y., Tan, P., Zhang, R., et al. (2020). Choosing tumor mutational burden wisely for immunotherapy: A hard road to explore. *Biochim. Biophys. Acta. Rev. Cancer* 1874 (2), 188420. doi:10.1016/j.bbcan.2020.188420

Liu, K., Sun, E., Lei, M., Li, L., Gao, J., Nian, X., et al. (2019). BCG-induced formation of neutrophil extracellular traps play an important role in bladder cancer treatment. *Clin. Immunol.* 201, 4–14. doi:10.1016/j.clim.2019.02.005

Liu, K., Zhao, K., Wang, L., and Sun, E. (2018). The prognostic values of tumor-infiltrating neutrophils, lymphocytes and neutrophil/lymphocyte rates in bladder urothelial cancer. *Pathol. Res. Pract.* 214 (8), 1074–1080. doi:10.1016/j.prp.2018.05.010

Markouli, M., Strepkos, D., Basdra, E. K., Papavassiliou, A. G., and Piperi, C. (2021). Prominent role of histone modifications in the regulation of tumor metastasis. *Int. J. Mol. Sci.* 22 (5), 2778. doi:10.3390/ijms22052778

Martínez-Reyes, I., and Chandel, N. S. (2021). Cancer metabolism: Looking forward. *Nat. Rev. Cancer* 21 (10), 669–680. doi:10.1038/s41568-021-00378-6

Matmati, M., Pouwels, W., van Bruggen, R., Jansen, M., Hoek, R. M., Verhoeven, A. J., et al. (2007). The human EGF-TM7 receptor EMR3 is a marker for mature granulocytes. *J. Leukoc. Biol.* 81 (2), 440–448. doi:10.1189/jlb.0406276

Mushinski, J. F., Nguyen, P., Stevens, L. M., Khanna, C., Lee, S., Chung, E. J., et al. (2009). Inhibition of tumor cell motility by the interferon-inducible GTPase MxA. *J. Biol. Chem.* 284 (22), 15206–15214. doi:10.1074/jbc.M806324200

Naquet, P., Pitari, G., Duprè, S., and Galland, F. (2014). Role of the Vnn1 pantetheinase in tissue tolerance to stress. *Biochem. Soc. Trans.* 42 (4), 1094–1100. doi:10.1042/BST20140092

Newman, A. M., Liu, C. L., Green, M. R., Gentles, A. J., Feng, W., Xu, Y., et al. (2015). Robust enumeration of cell subsets from tissue expression profiles. *Nat. Methods* 12 (5), 453–457. doi:10.1038/nmeth.3337

Patel, D. D., and Bussel, J. B ((2020). Neonatal Fc receptor in human immunity: Function and role in therapeutic intervention. *J. Allergy Clin. Immunol.* 146 (3), 467–478. doi:10.1016/j.jaci.2020.07.015

Patel, V. G., Oh, W. K., and Galsky, M. D. (2020). Treatment of muscle-invasive and advanced bladder cancer in 2020. *Ca. Cancer J. Clin.* 70 (5), 404–423. doi:10.3322/caac.21631

Pouyet, L., Roisin-Bouffay, C., Clément, A., Millet, V., Garcia, S., Chasson, L., et al. (2010). Epithelial vanin-1 controls inflammation-driven carcinogenesis in the colitis-associated colon cancer model. *Inflamm. Bowel Dis.* 16 (1), 96–104. doi:10.1002/ibd.21031

Rabbani, G., and Ahn, S. N ((2019). Structure., enzymatic activities., glycation and therapeutic potential of human serum albumin: A natural cargo. *Int. J. Biol. Macromol.* 123, 979–990. doi:10.1016/j.ijbiomac.2018.11.053

Reisländer, T., Groelly, F. J., and Tarsounas, M. (2020). DNA damage and cancer immunotherapy: A sting in the tale. *Mol. Cell.* 80 (1), 21–28. doi:10.1016/j.molcel.2020.07.026

Rice, C. M., Davies, L. C., Subleski, J. J., Maio, N., Gonzalez-Cotto, M., Andrews, C., et al. (2018). Tumour-elicited neutrophils engage mitochondrial metabolism to circumvent nutrient limitations and maintain immune suppression. *Nat. Commun.* 9 (1), 5099. doi:10.1038/s41467-018-07505-2

Rincón, E., Rocha-Gregg, B. L., and Collins, S. R. (2018). A map of gene expression in neutrophil-like cell lines. *BMC Genomics* 19 (1), 573. doi:10.1186/s12864-018-4957-6

Shaul, M. E., and Fridlender, Z. G. (2019). Tumour-associated neutrophils in patients with cancer. *Nat. Rev. Clin. Oncol.* 16 (10), 601–620. doi:10.1038/s41571-019-0222-4

Shi, L., Zhang, W., Zou, F., Mei, L., Wu, G., and Teng, Y. (2016). KLHL21, a novel gene that contributes to the progression of hepatocellular carcinoma. *BMC Cancer* 16 (1), 815. doi:10.1186/s12885-016-2851-7

Shinde-Jadhav, S., Mansure, J. J., Rayes, R. F., Marcq, G., Ayoub, M., Skowronski, R., et al. (2021). Role of neutrophil extracellular traps in radiation resistance of invasive bladder cancer. *Nat. Commun.* 12 (1), 2776. doi:10.1038/s41467-021-23086-z

Shum, B., Larkin, J., and Turajlic, S. (2022). Predictive biomarkers for response to immune checkpoint inhibition. *Semin. Cancer Biol.* 79, 4–17. doi:10.1016/j.semcancer.2021.03.036

Soria, F., Krabbe, L-M., Todenhöfer, T., Dobruch, J., Mitra, A. P., Inman, B. A., et al. (2019). Molecular markers in bladder cancer. *World J. Urol.* 37 (1), 31–40. doi:10.1007/s00345-018-2503-4

Sung, H., Ferlay, J., Siegel, R. L., Laversanne, M., Soerjomataram, I., Jemal, A., et al. (2021). Global cancer statistics 2020: GLOBOCAN estimates of incidence and mortality worldwide for 36 cancers in 185 countries. *Ca. Cancer J. Clin.* 71 (3), 209–249. doi:10.3322/caac.21660

Templeton, A. J., McNamara, M. G., Šeruga, B., Vera-Badillo, F. E., Aneja, P., Ocaña, A., et al. (2014). Prognostic role of neutrophil-to-lymphocyte ratio in solid tumors: A systematic review and meta-analysis. *J. Natl. Cancer Inst.* 106 (6), dju124. doi:10.1093/jnci/dju124

Thompson, D. B., Siref, L. E., Feloney, M. P., Hauke, R. J., and Agrawal, D. K. (2015). Immunological basis in the pathogenesis and treatment of bladder cancer. *Expert Rev. Clin. Immunol.* 11 (2), 265–279. doi:10.1586/1744666X.2015.983082

Tran, L., Xiao, J-F., Agarwal, N., Duex, J. E., and Theodorescu, D. (2021). Advances in bladder cancer biology and therapy. *Nat. Rev. Cancer* 21 (2), 104–121. doi:10.1038/s41568-020-00313-1

Vidarsson, G., Stemerding, A. M., Stapleton, N. M., Spliethoff, S. E., Janssen, H., Rebers, F. E., et al. (2006). FcRn: An IgG receptor on phagocytes with a novel

role in phagocytosis. *Blood* 108 (10), 3573–3579. doi:10.1182/blood-2006-05-024539

Waldman, A. D., Fritz, J. M., and Lenardo, M. J. (2020). A guide to cancer immunotherapy: from T cell basic science to clinical practice. *Nat. Rev. Immunol.* 20 (11), 651–668. doi:10.1038/s41577-020-0306-5

Wang, L., Sfakianos, J. P., Beaumont, K. G., Akturk, G., Horowitz, A., Sebra, R. P., et al. (2021). Myeloid cell-associated resistance to PD-1/PD-L1 blockade in urothelial cancer revealed through bulk and single-cell RNA sequencing. *Clin. Cancer Res.* 27 (15), 4287–4300. doi:10.1158/1078-0432.CCR-20-4574

Wu, Z., Liu, J., Dai, R., and Wu, S. (2021). Current status and future perspectives of immunotherapy in bladder cancer treatment. *Sci. China. Life Sci.* 64 (4), 512–533. doi:10.1007/s11427-020-1768-y

Yu, L., Hua, Z., Luo, X., Zhao, T., and Liu, Y. (2022). Systematic interaction of plasma albumin with the efficacy of chemotherapeutic drugs. *Biochim. Biophys. Acta. Rev. Cancer* 1877 (1), 188655. doi:10.1016/j.bbcan.2021.188655

Zilionis, R., Engblom, C., Pfirschke, C., Savova, V., Zemmour, D., Saatcioglu, H. D., et al. (2019). Viral DNA binding to NLRC3, an inhibitory nucleic acid sensor, unleashes STING, a cyclic dinucleotide receptor that activates type I interferon. *Immunity* 50 (5), 591–599. doi:10.1016/j.immuni.2019.02.009

frontiers | Frontiers in Pharmacology

TYPE Original Research
PUBLISHED 18 November 2022
DOI 10.3389/fphar.2022.1030062

OPEN ACCESS

EDITED BY
Ya Meng,
Zhuhai People's Hospital, China

REVIEWED BY
Heng Sun,
University of Macau, China
Fengjie Guo,
South China University of Technology, China

*CORRESPONDENCE
Lingling Zu,
zulingling@tmu.edu.cn
Song Xu,
xusong198@hotmail.com

†These authors have contributed equally to this work.

SPECIALTY SECTION
This article was submitted to Pharmacology of Anti-Cancer Drugs, a section of the journal Frontiers in Pharmacology

RECEIVED 28 August 2022
ACCEPTED 08 November 2022
PUBLISHED 18 November 2022

CITATION
Zhu Y, Tang Q, Cao W, Zhou N, Jin X, Song Z, Zu L and Xu S (2022), Identification of a novel oxidative stress-related prognostic model in lung adenocarcinoma.
Front. Pharmacol. 13:1030062.
doi: 10.3389/fphar.2022.1030062

Identification of a novel oxidative stress-related prognostic model in lung adenocarcinoma

Yifan Zhu[1,2†], Quanying Tang[1,2†], Weibo Cao[1,2†], Ning Zhou[1,2], Xin Jin[1,2], Zuoqing Song[1,2], Lingling Zu[1,2*] and Song Xu[1,2*]

[1]Department of Lung Cancer Surgery, Tianjin, China, [2]Tianjin Key Laboratory of Lung Cancer Metastasis and Tumor Microenvironment, Lung Cancer Institute, Tianjin Medical University General Hospital, Tianjin, China

Background: Oxidative stress (OxS) participates in a variety of biological processes, and is considered to be related to the occurrence and progression of many tumors; however, the potential diagnostic value of OxS in lung cancer remains unclear.

Methods: The clinicopathological and transcriptome data for lung adenocarcinoma (LUAD) were collected from TCGA and GEO database. LASSO regression was used to construct a prognostic risk model. The prognostic significance of the OxS-related genes was explored using a Kaplan-Meier plotter database. The prediction performance of the risk model was shown in both the TCGA and GSE68465 cohorts. The qRT-PCR was performed to explore the expression of genes. CCK-8, Edu and transwell assays were conducted to analyze the role of *CAT* on cell proliferation migration and invasion in lung cancer. Immune infiltration was evaluated by CIBERSORT and mutational landscape was displayed in the TCGA database. Moreover, the relationship between risk score with drug sensitivity was investigated by pRRophetic.

Results: We identified a prognosis related risk model based on a four OxS gene signature in LUAD, including *CYP2D6*, *FM O 3*, *CAT*, and *GAPDH*. The survival analysis and ROC curve indicated good predictive power of the model in both the TCGA and GEO cohorts. LUAD patients in the high-risk group had a shorter OS compared to the low-risk group. QRT-PCR result showed that the expression of four genes was consistent with previous analysis in cell lines. Moreover, overexpression of *CAT* could decrease the proliferation, invasion and migration of lung cancer cells. The Cox regression analysis showed that the risk score could be used as an independent prognostic factor for OS. LUAD patients in the high-risk score group exhibited a higher tumor mutation burden and risk score were closely related to tumor associated immune cell infiltration, as well as the expression of immune checkpoint molecules. Both the high- and low-risk groups have significant differences in sensitivity to some common chemotherapy drugs, such as Paclitaxel, Docetaxel, and Vinblastine, which may contribute to clinical treatment decisions.

Conclusion: We established a robust OxS-related prognostic model, which may contribute to individualized immunotherapeutic strategies in LUAD.

KEYWORDS
LUAD, oxidative stress, nomogram, immune infiltration, drug response

Introduction

Lung cancer represents one of the most common malignant tumors and the leading cause of cancer-related death in the world (Siegel et al., 2016; Torre et al., 2016; Bade and Dela Cruz, 2020). Moreover, lung adenocarcinoma (LUAD) is the most common histological subtype, accounting for approximately 40% of all lung cancer types (Denisenko et al., 2018). Despite some medical treatments, the treatment of lung adenocarcinoma is not ideal due to metastasis, recurrence, or advanced stage. At present, the treatment of lung adenocarcinoma remains a significant challenge (Torre et al., 2015).

Oxidative stress is a common biochemical state, in which excessive release of reactive oxygen species (ROS) occurs to facilitate an antioxidant defense mechanism. ROS consisting of reactive nonradical species and free radicals (e.g., superoxide anion, hydrogen peroxide, singlet oxygen, *etc.*) (Lü et al., 2010). However, high levels of ROS can cause oxidative damage to proteins, lipids, and DNA (Kirtonia et al., 2020). Moreover, DNA damage plays an important role in initiating tumorigenesis. It has been reported that oxidative stress was involved in the pathogenesis of diabetes, coronary heart disease, cancer and various other diseases[I] (Siegrist and Sies, 2017; Ighodaro, 2018; Klaunig, 2018)[J]. In the progress of tumor research, oxidative stress has been implicated in tumor cell proliferation and migration, promoting the angiogenesis of tumor cells (Sarmiento-Salinas et al., 2021). Moreover, research shows that breast cancer progression is dependent upon oxidative stress-activated stroma (Jezierska-Drutel et al., 2013). Oxidative stress has also been closely associated with a malignant phenotype of prostate cancer cells (Kumar et al., 2008). Studies have shown that exposure to inhalable mineral fiber, particulate matter smaller than 2.5 μm (PM2.5) and cigarette smoke will increase the risk of lung cancer in daily life (Pryor, 1997; Nagai and Toyokuni, 2010). Cigarette smoke can increase the level of ROS and catalyze redox reactions in lung epithelial cells. ROS can also contribute to oxidative stress and lead to both the proliferation and apoptosis of lung epithelial cells (Goldkorn et al., 2014). Moreover, another study suggests that the advanced stage of lung cancer indicates increased levels of oxidative stress (Esme et al., 2008). These studies have demonstrated that there is a close correlation between oxidative stress and LUAD progression.

The potential role of oxidative stress genes on the prognosis of lung adenocarcinoma has not been determined. In the present study, we constructed a prognostic risk score model to analyze the impact of oxidative stress on the prognosis of patients with LUAD and verified its predictive ability in The Cancer Genome Atlas (TCGA) and Gene Expression Omnibus (GEO) cohorts. Furthermore, we classified the patients into two groups and further conducted an analysis of immune cell infiltration, mutational landscape, immune checkpoints, and correlation of the drug response to explore the potential mechanisms in LUAD.

Materials and methods

Data collection

The transcriptome data and corresponding clinicopathological information of LUAD were collected from The Cancer Genome Atlas (TCGA) (https://portal.gdc.cancer.gov/) (Tomczak et al., 2015), comprising 535 LUAD samples and 59 normal tissues. To obtain oxidative stress-related genes accurately, 149 oxidative stress-related genes were contained from Gene Cards (https://www.genecards.org) (Safran et al., 2010) with a relevance score ≥ 16. In addition, the RNA-sequencing dataset with its clinical information downloaded from Gene Expression Omnibus (GEO) (https://www.ncbi.nlm.nih.gov/geo/) (Barrett et al., 2013) were used for validation.

Analysis of differential expressed genes

Comprehensive analysis of oxidative stress-related genes and LUAD transcriptome data from TCGA was conducted with the help of the "limma" R package. The filter criteria were set as |Fold Change|>2, padj <0.05. Finally, 34 genes met the filter conditions. Spearman's correlation analysis was performed to identify the correlation between screened genes.

Construction of an oxidative stress-related risk prognostic model

Survival R package and a univariate Cox regression analysis were used to analyze the association between 34 screened genes and overall survival, respectively. The least absolute shrinkage and selection operator (LASSO) regression was conducted to construct the optimal prognostic risk model. Four OxS-related oxidative stress genes were selected. The risk score model was calculated as follows: risk score = (−0.168∗ expression value of *CYP2D6*) - (0.167 ∗ expression value of *FM O 3*)—(0.059 ∗ expression value of *CAT*) + (0.306 ∗ expression value of *GAPDH*).

Efficacy evaluation

First, The Kaplan Meier plotter database (http://kmplot.com/analysis/) (Lánczky et al., 2016) was conducted to evaluate the association of four genes and overall survival. The samples were separated into high- and low-risk groups based on the median of risk score. The "survminer" and "survival" R Bioconductor packages were used to analyze the overall survival between the two groups using the Kaplan-Meier method with a log-rank test. The receiver operating characteristic curve (ROC) was calculated to analyze the predictive power of the risk model *via* the R "timeROC" package. Both univariate and multivariate Cox regression analysis were also performed to analyze whether the risk score and clinical factors could be independent prognostic factors for LUAD. The results were displayed in forest plots. Finally, a prognostic nomogram based on the clinical characteristics (gender, pathological stage, and age) and risk score was developed to predict the one-, two-, and three-year survival of patients with LUAD through the R "rms" package.

Cell culture

All cell lines were obtained from the American Type Culture Collection (ATCC). BEAS-2B, H1299, and H2030 were cultured in RPMI-1640 medium with 10% fetal bovine serum. All cells were cultured in a humid environment containing with 5% CO_2 at 37°C.

Extraction of RNA and real-time PCR

Total RNAs were obtained from cells by using TRIzol reagent (Invitrogen). Then, cDNA was synthesized by using Prime Script RT Master Mix (TaKaRa, Dalian, China), followed by quantification by TB Green Premix Ex Taq (TaKaRa) on the 7900HT Fast Real-Time PCR System (Applied Biosystems, Foster City, CA, United States ; Thermo Fisher Scientific). The relative gene expression was calculated by using the $2^{-\Delta\Delta CT}$ method. The mRNA levels were normalized by β-actin. The primer sequences were listed in Table 1.

Transfection and overexpression vector

H1299 cells (6×10^5) were seeded on each well of 6-well plates the day before transfection. According to the manufacturer's instructions, the *CAT* overexpressing vector pcDNA-*CAT* (OE-*CAT*) and corresponding negative control (NC) were transfected into H1299 cells by Lipofectamine 2000. After 48 h, cells were harvested for total RNAs and following functional explorations.

Proliferation assays

To evaluate the proliferation of LUAD cells, a Cell counting kit 8 (CCK-8) (Dojindo, Japan) was adopted. In short, cancer cells (5,000 cells/200 μl) were seeded into 96-well plates, and CCK-8 reagent (20 μl) was added into each well. After incubating for 2 h, the absorbance values (450 nm) were detected. For 5-ethynyl-2′-deoxyuridine (Edu) assay, cancer cells were seeded in 96-well plates, incubated with Edu (50 μM) (Sigma) for 2 h, then fixed and permeabilized. The cells were observed analyzed through a fluorescence microscopy.

Transwell migration and invasion assays

For invasion assay, we seeded cells (8×10^4) in 200 μl serum-free medium into the upper chambers coated with matrigel (BD Biosciences, San Diego, CA, United States). Then we added 500 μl medium with 10% FBS into the lower chamber. After 24 h of incubation, the cells invading the matrigel were fixed with 4% paraformaldehyde, stained with 1% crystal violet, and imaged under a light microscope. For migration assay, cells (3×10^4) were seeded into the upper chamber in a similar manner without matrigel.

Implementation of an analysis of the level of immune infiltration

To quantify the proportions of infiltrating immune cells through the transcriptome data profiles from TCGA-LUAD patient cohort, the CIBERSORT algorithm was used to analyze the level of immune cell infiltration. The level of gene expression matrix of tumor-infiltrating immune cells was downloaded from the CIBERSORT database (https://cibersortx.stanford.edu/) (Chen et al., 2018). The CIBERSORT output of infiltrating immune cells proportion were accurate with $p < 0.05$, and only cases with $p < 0.05$ were eligible for further study. The R package "corrplot" was used to evaluate the correlation between immune cells and provide a visual representation.

Analysis of mutational landscapes

The somatic mutation data of the LUAD patients were downloaded from TCGA. The R "maftools" package was obtained to analyze the mutation information. The Tumor Mutation Burden (TMB) considered as the mutation density of tumor genes was calculated as the transformation of total non-synonymous mutations per megabase (Schumacher et al., 2015). The difference in the TMB between the two subgroups was analyzed using a Wilcox test.

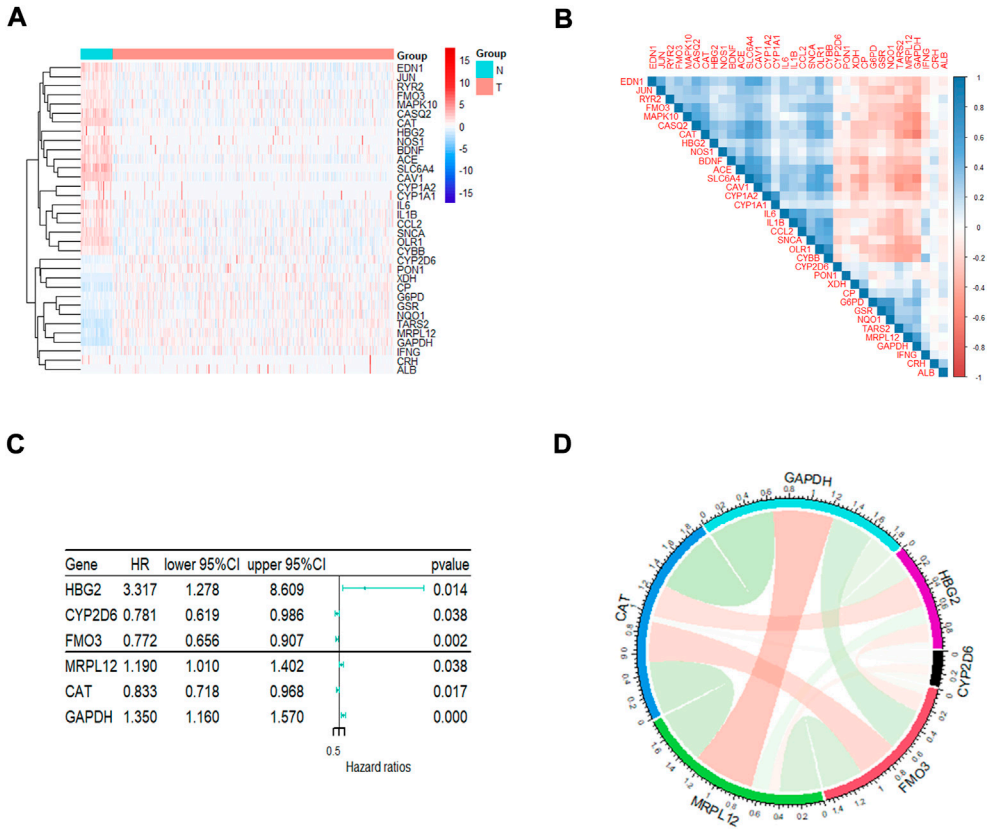

FIGURE 1
The analysis of oxidative stress genes related to prognosis in LUAD. **(A)**The heatmap visualizes the expression of oxidative stress related genes in LUAD. Blue represents low expression while red represents high expression. N represents normal samples and T represents tumor samples. **(B)** Correlation analysis of oxidative stress related genes in LUAD. **(C)** Univariate Cox regression analysis of different oxidative stress genes related to prognosis. **(D)** The correlation of screened genes from regression analysis.

Prediction of chemotherapeutic agents sensitivity

To explore the differences in the chemosensitivity between the low-risk and high-risk groups, The R "pRRophetic" package was used to predict half-maximal inhibitory concentration (IC50) values (Geeleher et al., 2014a; Geeleher et al., 2014b). Various common anticancer drugs and the cell line expression spectrum were downloaded from Genomics of Drug Sensitivity in Cancer (GDSC) (www.cancerrxgene.org/) (Yang et al., 2013). A ridge regression model was constructed to predict the IC50 of chemotherapy drugs.

Statistical analysis

R software (version 4.1.3) and GraphPad Prism 9 were used for statistical analysis. Subgroup differences were analyzed by a Wilcox test. The threshold of statistical significance was set at $p < 0.05$.

Results

Screening of prognosis-related differentially expressed OxS genes in lung adenocarcinoma

A total of 148 OxS genes were included to conduct a differential expression analysis in TCGA-LUAD and the adjacent tissues. The heatmap displayed 34 differentially expressed OxS genes between the normal and tumor tissues, including 13 upregulated and 21 downregulated genes (|Fold Change|>2, padj <0.05) (Figure 1A). A correlation analysis was performed to further explore the intrinsic association between these genes. As shown in Figure 1B, the level of *CAT* expression was most negatively correlated with *GAPDH*, whereas *GSR* expression was most positively correlated with *NQ O 1*. The univariate Cox regression analysis revealed that six out of thirty-four differentially expressed genes were significantly related to OS in LUAD patients. The *HBG2* ($p = 0.014$), *MRPL12* ($p = 0.038$) and *GAPDH* ($p = 0.000$) were considered as risky genes

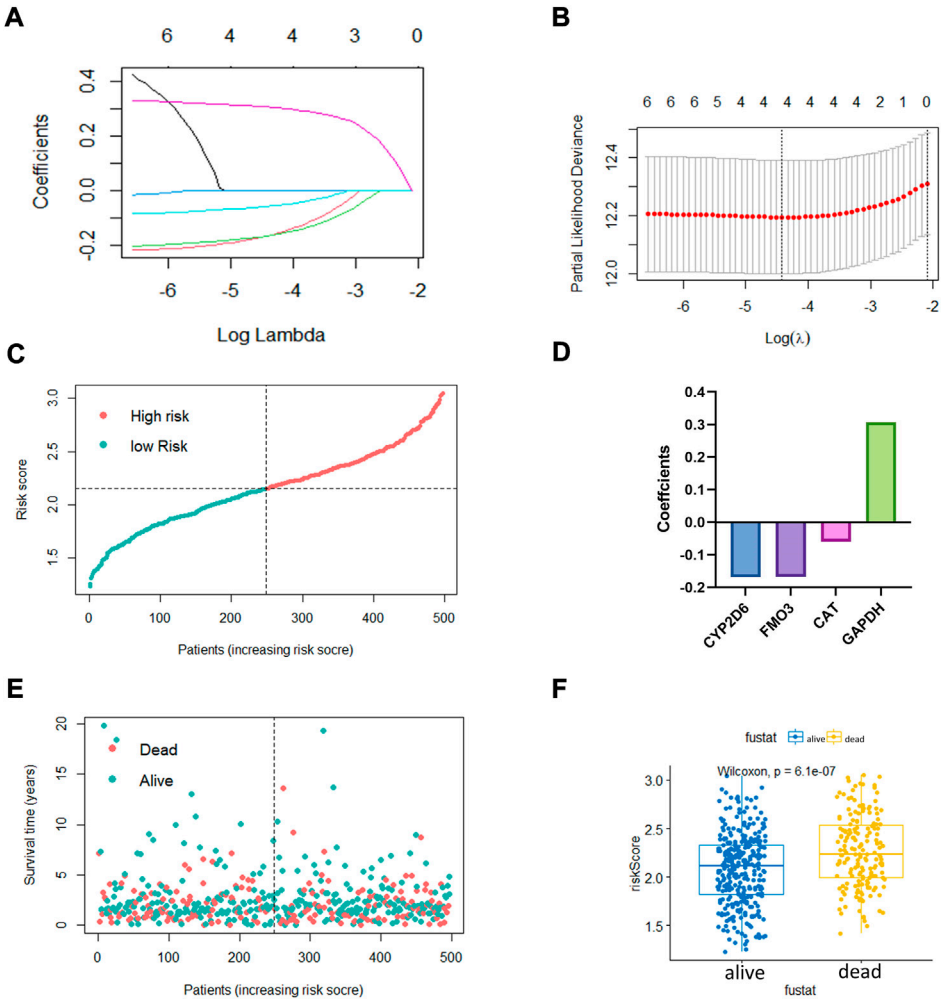

FIGURE 2
The construction of oxidative stress genes based prognostic risk model. **(A,B)** Establishment of model using least absolute shrinkage and selection operator (LASSO) Cox regression analyses. **(C)** Distribution of risk score. **(D)** Coefficients of four genes. **(E,F)** Distribution of survival status and risk score level of alive and dead group.

(HR > 1), whereas the *CYP2D6* ($p = 0.038$), *FM O 3* ($p = 0.002$), and *CAT* ($p = 0.017$) were considered protective genes (HR < 1) (Figure 1C). Chord diagram of Figure 1D showed that among the six genes, the correlation between *GAPDH* and *CAT* was the most significant. The level of *GAPDH* expression was the most likely to be negatively correlated with *CAT*.

Establishment of a prognostic risk score model based on OxS-related genes

The LASSO regression algorithm was conducted for the OxS-related oxidative stress genes with the optimal prognostic power. Four optimal genes, *CYP2D6*, *FM O 3*, *CAT*, and *GAPDH*, were screened as factors to establish the prognostic risk model for LUAD (Figures 2A,B). The bar chart displayed the coefficients analyzed from the LASSO regression (Figure 2D). Moreover, the risk score distribution was accurate as checked in Figure 2C. The risk score level was significantly different between the survival status groups (Figures 2E,F).

To further confirm the prognostic value of the four OxS-related genes in LUAD, the correlation of gene expression with prognosis was investigated respectively in the Kaplan-Meier plotter database. The results showed the expression of *CYP2D6* ($p = 0.012$) and *GAPDH* ($P < 1e\text{-}16$) were negatively correlated with OS, whereas the expression of *FM O 3* ($p = 9.6e\text{-}14$) and *CAT* ($p = 9.4e\text{-}14$) were positively correlated with the OS (Figures 3A–D). Next, the prognostic value of the model was explored in the TCGA and GEO datasets. The risk scores of all LUAD patients in the two cohorts were acquired based on the

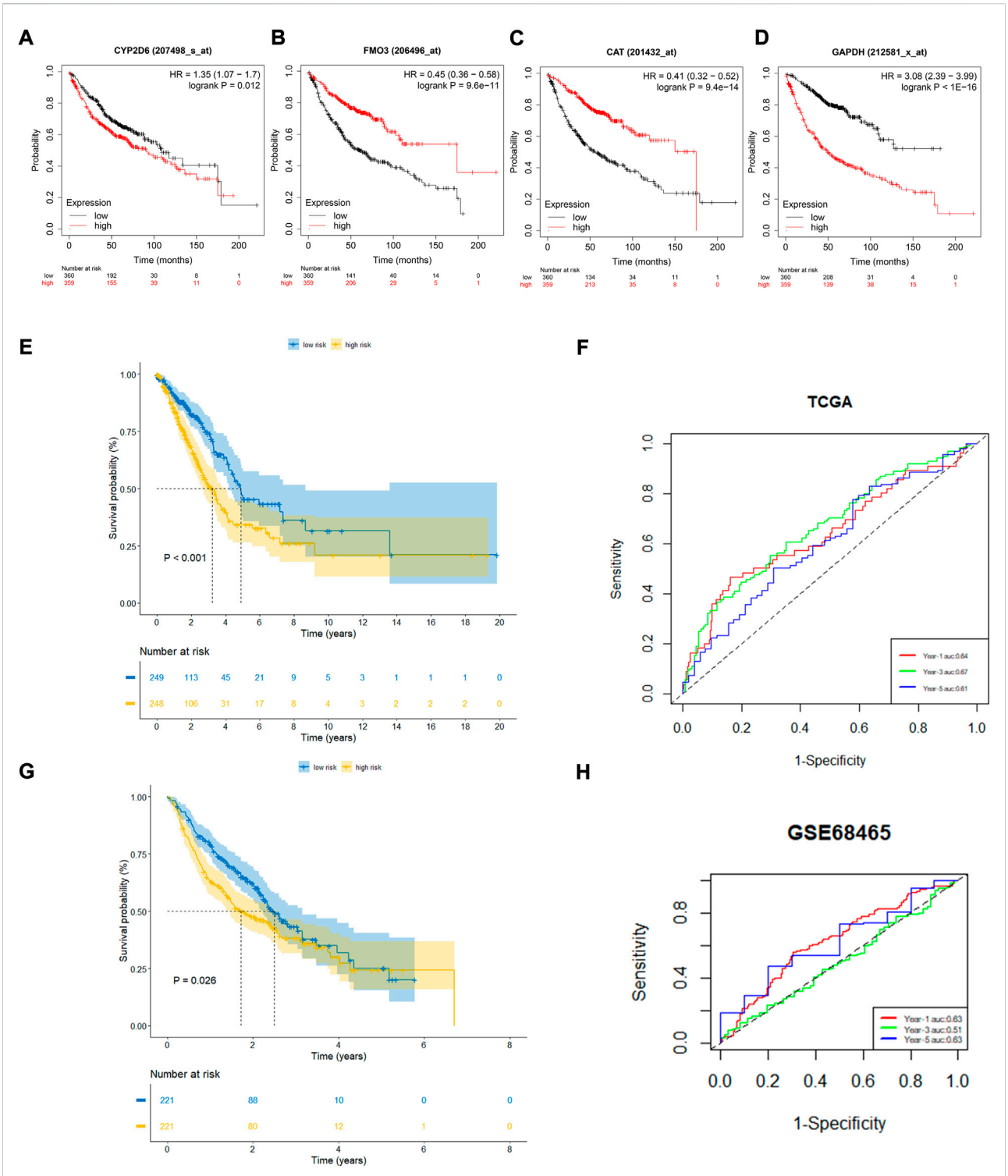

FIGURE 3
The prognostic performance of four genes and risk model. **(A–D)** Kaplan–Meier curves of four filtered genes. **(E,F)** Kaplan–Meier curves displayed that high-risk group had worse prognosis than low-risk group in TCGA cohort with 1,3,5 years AUCs were 0.64,0.67 and 0.61. **(G,H)** Kaplan–Meier curves verified in GEO cohort showed high-risk group had worse prognosis than low-risk group with 1, 3, 5 years AUCs were 0.63, 0.51, and 0.63.

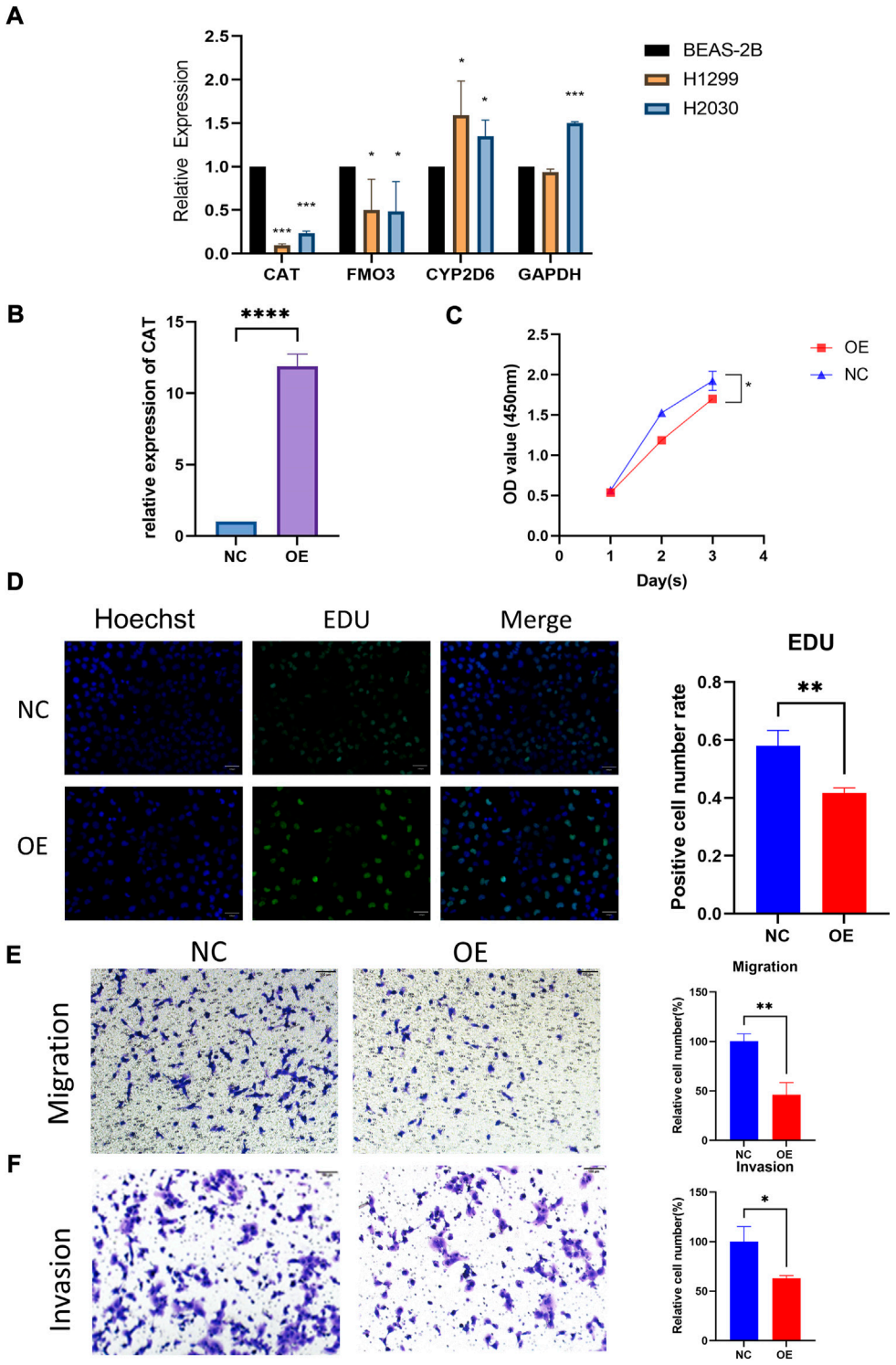

FIGURE 4
Functional verification of CAT. **(A)** Expression levels of four genes in cell lines. **(B)** Construction of CAT overexpression H1299. **(C,D)** CAT inhibited the proliferation function. **(E,F)** CAT inhibited the migration and invasion function. (*$p < 0.05$, **$p < 0.01$, ***$p < 0.001$, ****$p < 0.0001$).

risk calculation formula. Based on the median value of risk score, the LUAD patients in the TCGA cohort were divided into a low-risk group (n = 249) and high-risk group (n = 248). The survival analysis revealed that the patients in the high-risk group exhibited a significantly worse prognosis than the low-risk group (p < 0.001) (Figure 3E). The prognostic value was further verified in the GEO cohort (GSE68465). Compared with the TCGA cohort, the survival analysis in the GSE68465 cohort showed similar results to that of the OS in the high-risk group (n = 221) were obviously shorter than in the low-risk group (n = 221) (Figure 3G). The analysis indicated that the risk score model had good power for predicting the OS of LUAD patients. The AUC at 1, 3, and 5 years achieved 0.64, 0.67, 0.61, and 0.63, 0.51, 0.63, respectively for the TCGA and GSE68465 cohort (Figures 3F,H). Despite the limited 5-year AUC in the GSE68465 cohort, the model had a good ability for predicting patient survival.

Verification of CAT functions in H1299 cell line

The qRT-PCR assay was employed to validate the expression levels of 4 genes in cell lines. The result showed that *CAT* and *FMO 3* expressions were downregulated, whereas *CYP2D6* was upregulated in H1299 and H2030 cell lines compared with BEAS-2B. The expression of *GAPDH* was upregulated in H2030 cell line but similar in H1299 compared with BEAS-2B (Figure 4A). Then we investigated the effect of the aberrant expression of *CAT* on LUAD cells, because which possess the strongest differential expression. A gain-of-function analyses was performed *in vitro* by transfecting a vector harboring *CAT* in H1299 cells. We found that increased *CAT* expression significantly inhibited the proliferation of H1299 cells (Figures 4B,C). The similar results was also observed in Edu assays (Figure 4D). Furthermore, transwell assays with or without Matrigel results demonstrated that ectopic expression of *CAT* remarkably suppressed the invasion and migration of H1299 cells (Figures 4E,F).

Establishment of a risk score-based prognostic nomogram for lung adenocarcinoma

A total of 480 cases with complete clinical information were screened for the univariate and multivariate Cox regression analysis. The univariate Cox regression analysis revealed that the OS of LUAD patients was related to stage (p < 0.001, HR > 1) and risk score (p < 0.001, HR > 1) (Figure 5A). The multivariate Cox regression demonstrated that stage (p < 0.001) and risk score (p < 0.001) could be used as independent prognostic factors for predicting the prognosis of LUAD patients (Figure 5B). Nomogram is a quantitative model for predicting patient clinical outcomes. Based on gender, age, stage, and risk score, a novel prognostic nomogram was constructed to predict the survival of LUAD patients. Each variable had its normalized corresponding point. We calculated the total points of each patient by totaling the points of all variables (Figure 5C). The 1-, 2-, and 3-year survival probabilities of the patients was estimated by drafting a vertical line from the total point axis to the survival axis, which may help clinical workers make clinical decisions.

Differences in the level of immune cell infiltration, mutational landscapes, and immune checkpoints between the high- and low-risk groups

The immune microenvironment of the tumor tissue was composed of fibroblasts, stromal cells, and various immune cells, which influenced the prognosis and treatment in LUAD. To explore the correlation of risk score and level of infiltrating immune cells, CIBERSORT was used as a tool for analyzing the immune cell distribution within the TCGA-LUAD dataset. The landscape of the relative percentage of infiltrating immune cells was displayed in Figure 6A. The correlation between immune cells was analyzed in Figure 6B. All samples were divided into two groups based on the median value of the risk score. The results showed that there was a difference in various infiltrating immune cells between the two groups, including memory B cells (p < 0.0001), resting memory CD4 T cells (p < 0.0001), activated memory CD4 T cells (p < 0.0001), resting NK cells (p < 0.01), activated NK cells (p < 0.05), Monocytes (p < 0.0001), M0 macrophages (p < 0.0001), M1 macrophages (p < 0.05), resting dendritic cells (p < 0.0001), and resting mast cells (p < 0.0001) (Figure 6C). In contrast, there was no statistical significance in the number of naive B cells, plasma cells, CD8 T cells, follicular helper T cells, regulatory T cells, gamma delta T cells, M2 macrophages, activated dendritic cells, activated mast cells, eosinophils and neutrophils between the two groups. The proportion of each immune cell type was provided in Supplementary Table S2.

Moreover, the somatic mutation information of TCGA-LUAD patients was used to explore the correlation between the risk score and mutational landscape. After excluding samples with incomplete mutation information, 451 LUAD patients from the TCGA database were incorporated into the analysis. The samples were divided into a low- and high-risk group based on the median risk score. Detailed mutation information of each gene in all samples was exhibited by a waterfall plot. The top 20 mutated genes were displayed in the plot, whereas the different colors represent different mutation types. Missense mutations were the most common mutation type among the 20 genes shown. Moreover, the mutation frequency

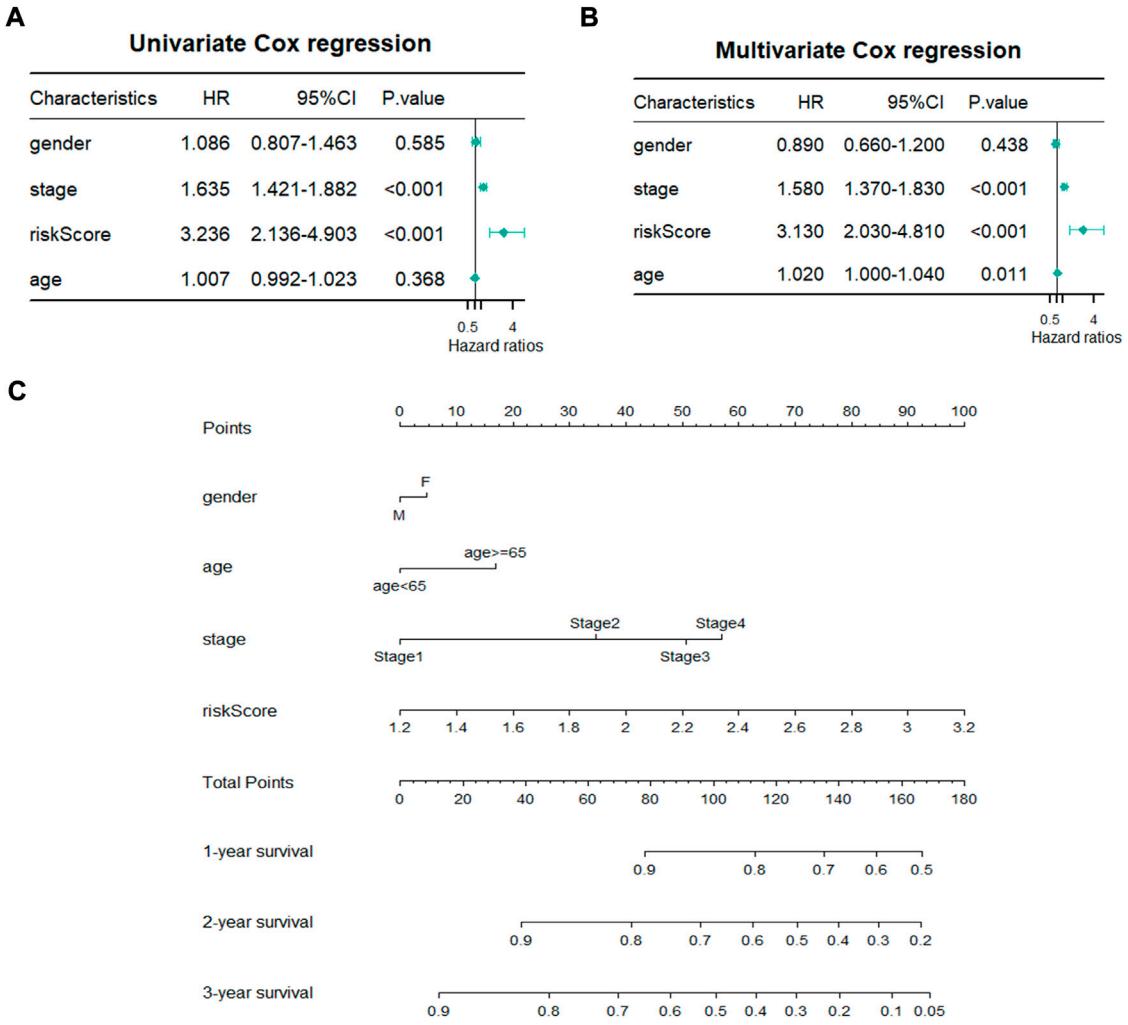

FIGURE 5
Establishment of prognostic nomogram. **(A,B)** Univariate and Multivariate Cox regression analyses of clinicopathological parameters with overall survival. **(C)** A novel prognostic nomogram based on gender, pathological stage, risk score and age.

significantly differed between the low- and high-risk groups in each gene cohort. We found that more mutation events occurred in the high-risk group than in the low-risk group (Figure 7A). The tumor mutation burden (TMB) was visualized in Figure 7B. The TMB in the high-risk group was appreciably higher compared with the low-risk group, indicating the superior effect of immunotherapy. (Figure 7C)

Immune checkpoint molecules are regulatory molecules that play a role in the immune system and play a critical role in maintaining self-tolerance, preventing an autoimmune response, and controlling the timing and intensity of the immune response. The difference in the levels of immune checkpoint expression in the low- and high-risk groups was compared according to the median value. As shown in Figure 8A, the level of TIGIT ($p = 0.05$), CTLA4 ($p < 0.05$), HAVCR2 ($p < 0.05$), IL-10 ($p < 0.0001$), and TGFB1 ($p < 0.01$) differed between the two groups, whereas no statistical difference was observed in the level of LAG3, PDCD1, and CD274 between the two groups. The results suggested that the risk score may be correlated with some immune checkpoints. It may be helpful in the immunotherapy of LUAD. The distribution of immune checkpoint expression levels was also visualized by heatmap in Figure 8B.

Therapeutic potential of the OxS-related risk score in lung adenocarcinoma

We identified some chemotherapeutic drugs and immunosuppressors *via* pRRophetic according to the OxS-related risk score. Lenalidomide ($p < 0.001$), nilotinib ($p <$

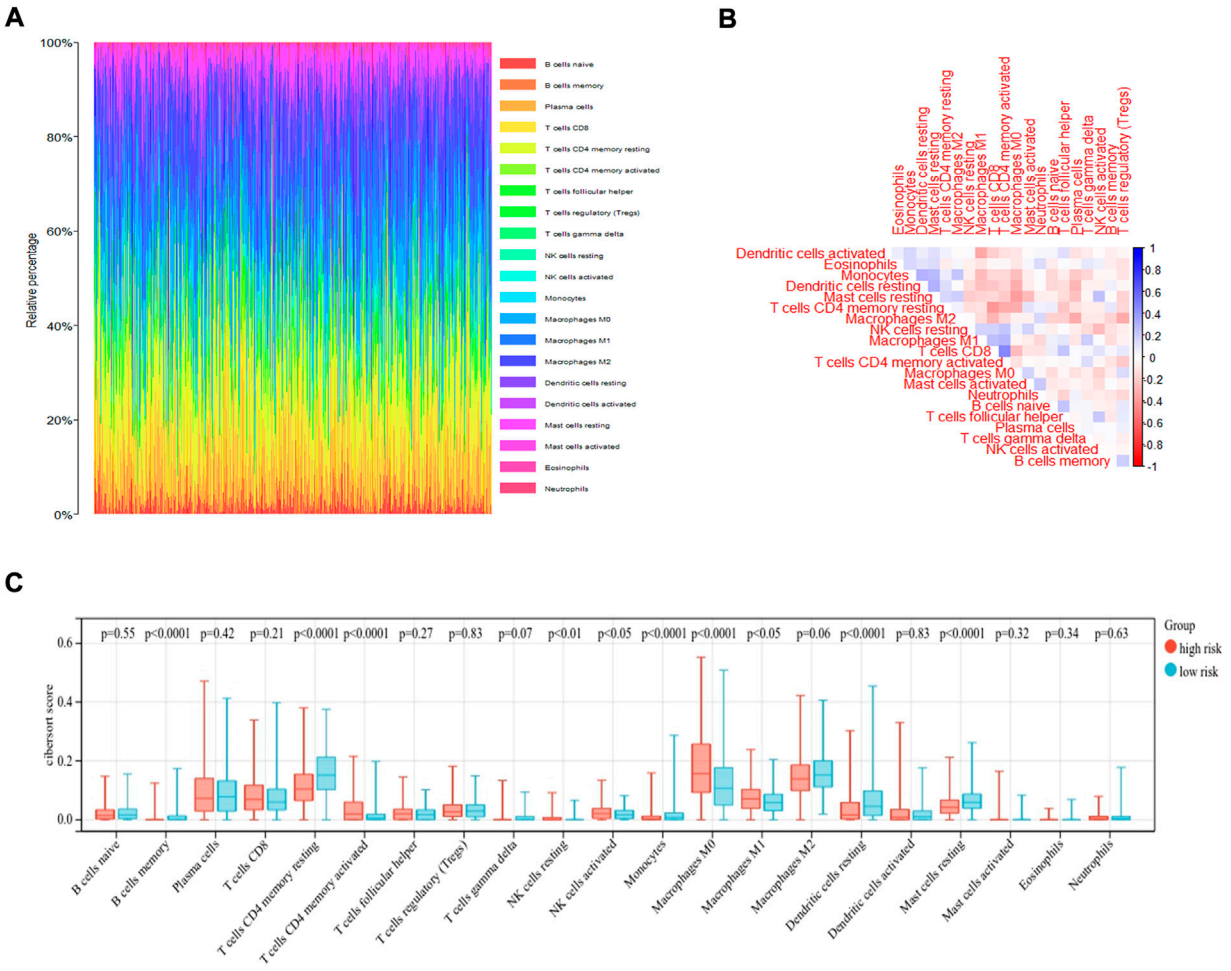

FIGURE 6
CIBERSORT analysis of TCGA-LUAD dataset. **(A)** The bar plot displayed the ratio of different immune infiltrating cells in the TCGA-LUAD datasets based on CIBERSORT algorithm. **(B)**The correlation of immune infiltrating cells. **(C)** Different kinds of immune infiltrating cells are plotted according to risk score level.

0.001), shikonin ($p < 0.001$), methotrexate ($p < 0.001$), displayed lower sensitivity in the high-risk group, whereas epothilone ($p < 0.001$), thapsigargin ($p < 0.001$), rapamycin ($p < 0.001$), vinblastine ($p < 0.001$), elesclomol ($p < 0.001$), docetaxel ($p < 0.001$), parthenolide ($p < 0.001$), and Paclitaxel had higher sensitivity in the high-risk group (Figure 9).

Discussion

As a substantial threat to global public health, lung cancer is associated with a poor prognosis and high mortality (Siegel et al., 2021). Thus, the prognostic gene signatures for the prognosis of LUAD are extremely important for predicting patient survival rate and drug response. Oxidative stress can cause DNA damage and further lead to tumorigenesis and progression. Therefore, the relationship between oxidative stress and its related genes and cancer has attracted substantial attention; however, the relationship between oxidative genes and LUAD has not yet been elucidated. In this study, we constructed a prognostic model based on four oxidative stress genes to predict the overall survival of LUAD patients.

A total of 148 differentially expressed oxidative stress genes were contained in the TCGA database. A univariate Cox regression analysis was used to identify the OxS-related genes and a LASSO regression analysis was conducted to shrink the range to the best. Finally, four oxidative stress genes, including *CYP2D6*, *FM O 3*, *CAT*, and *GAPDH* were identified, which were associated with the prognosis of LUAD patients. The *CYP2D6* gene polymorphisms may enhance oxidative stress and induce oxidative damage (Arafa and

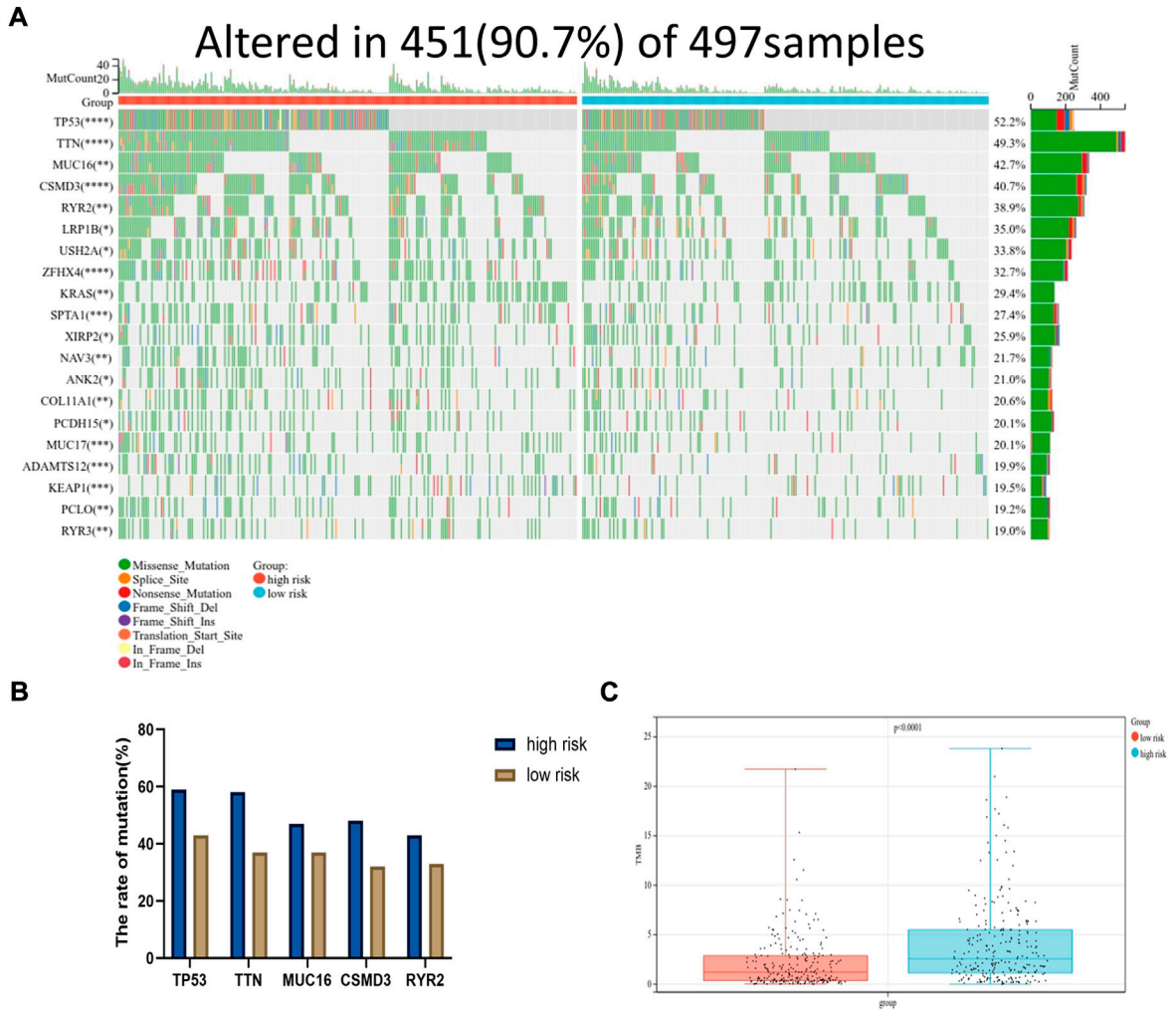

FIGURE 7
Mutational landscape displayed *via* TCGA-LUAD database. **(A)** The waterfall diagram exhibited top 20 genes with highest mutation frequency in LUAD between high and low risk group (*$p < 0.05$, **$p < 0.01$, ***$p < 0.001$, ****$p < 0.0001$). **(B)** The mutation frequency of top five genes. **(C)** The tumor mutation burden of high-risk group was significantly higher than that in low-risk group, $p < 0.0001$.

TABLE 1 Sequence of primers used in this study.

Primer name	Primer sequence (5′-3′)
CYP2D6-F	TAGTGGTGGCTGACCTGTTCTCT
CYP2D6-R	TCGTCGATCTCCTGTTGGACA
CAT-F	CCAGAAGAAAGCGGTCAAGAA
CAT-R	GAGATCCGGACTGCACAAAG
FMO3-F	AATTCGGGCTGTGATATTGC
FMO3-R	TTGAGGAAGGTTCCAAATCG
GAPDH-F	GGAGCGAGATCCCTCCAAAAT
GAPDH-R	GGCTGTTGTCATACTTCTCATGG

Atteia, 2018). Moreover, the *CYP2D6* genotypes can predict Tamoxifen discontinuation and prognosis in patients with breast cancer (He et al., 2020). *FM O 3* is an important oxidative drug metabolizing enzyme, which is Closely related to oxidative stress-responsive transcription factor *NRF2* (Klick and Hines, 2007; Rudraiah et al., 2016). Meanwhile, *FM O 3* has been reported to be investigated as a prognostic marker in hepatocellular carcinoma (Zhu et al., 2021). *CAT* is a key enzyme in the metabolism of H2O2 and play a critical role in the antioxidant defense system of cells (Nadif et al., 2005; Goyal and Basak, 2010; Glorieux and Calderon, 2017). Silenced *CAT* expression increased the

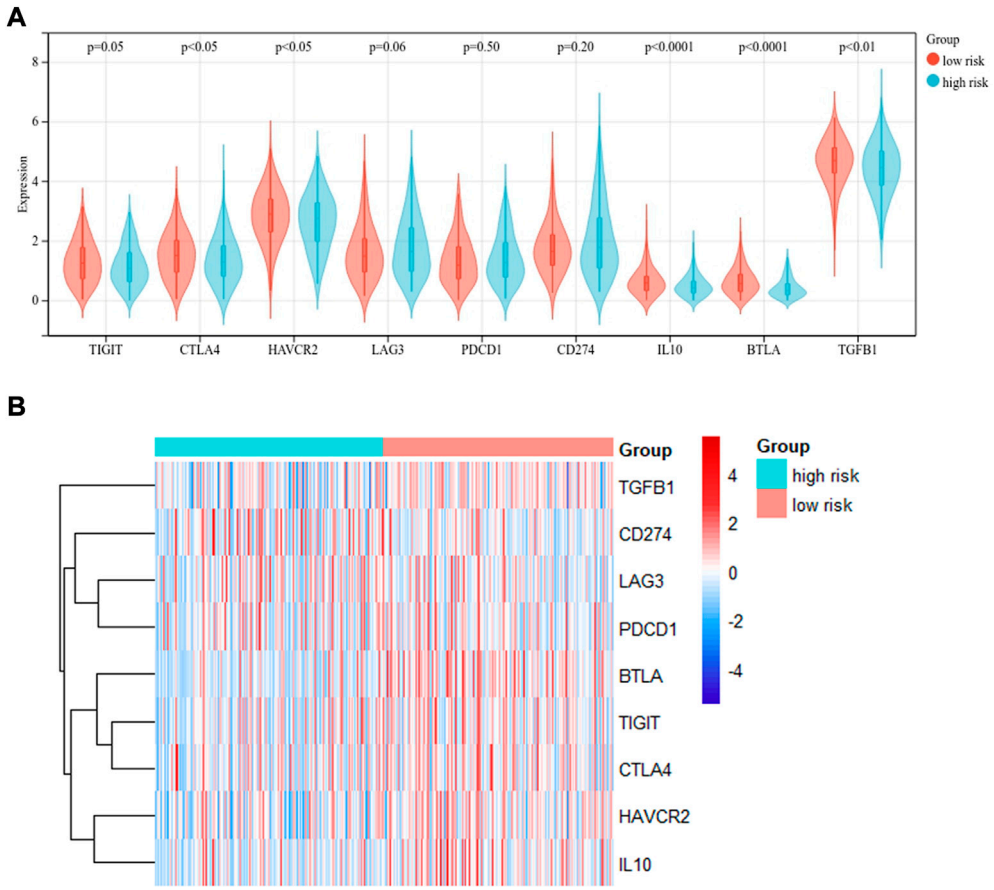

FIGURE 8
Correlation between risk group and immune checkpoints. **(A)** The difference of immune checkpoint expression between the two groups divided by risk score level. **(B)** Heatmap showed the expression of immune checkpoints in two groups.

susceptibility of the cancer cell line BT-20 to oxidative stress (Klingelhoeffer et al., 2012). Moreover, higher *CAT* expression in mesothelioma was associated with a better prognosis (Kahlos et al., 2001). *GAPDH* is a glycolytic enzyme which can mediate cell death under oxidative stress (Nakajima et al., 2009; Nakajima et al., 2017). Previous studies showed that *GAPDH* was involved in apoptosis, the maintenance of DNA integrity, and tumor angiogenesis (Sirover, 2018). Moreover, the level of *GAPDH* expression was up-regulated in human colorectal carcinoma tissues compared with the normal adjacent tissues, and the level of *GAPDH* expression was also increased in colon cancer cell lines (Tang et al., 2012). These results suggest that the four genes may also play an important role in the tumorigenesis and progression of LUAD.

In addition, a novel prognostic model was constructed based on the four screened genes. To the best of our knowledge, our research is the first to build an oxidative stress related prognostic model for LUAD. In addition, the model was confirmed to be an independent prognostic factor for LUAD according to the univariate and multivariate Cox regression. The prognostic value for predicting LUAD patient prognosis was identified with a survival analysis and time ROC analysis. A predictive nomogram based on a signature was constructed to predict the clinical outcomes of LUAD patients.

The proportion of infiltrating immune cells plays a significant role in the response to immunotherapy and cancer progression. Immune regulation is recognized to be associated with the prognosis of patients (Efremova et al., 2018). We verified patients in the low-risk and high-risk groups according to the model. Thus, results showed that patients in the high-risk group had higher NK cell infiltration and a lower level of mast cells than patients in the low-risk group. According to the tumor immunoediting hypothesis (Hellmann et al., 2018), the patients in the high-risk group have higher immunosuppression but lower immunoreactivity than the low-risk group. The number of M0 macrophages in patients in the high-risk group was higher than in the low-risk group. A higher proportion of

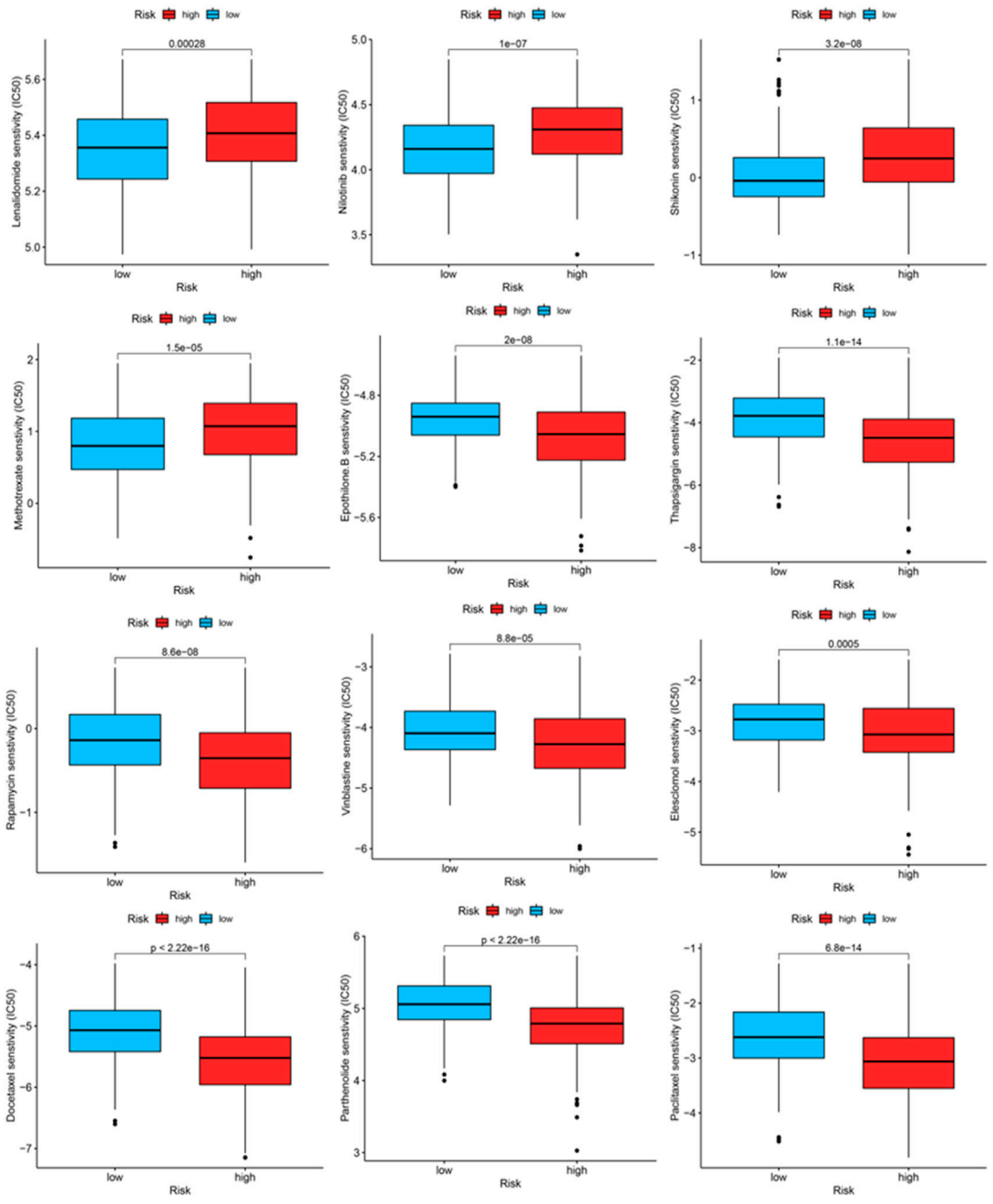

FIGURE 9
The IC50 of chemotherapeutic drugs compared between high-risk and low-risk groups.

M0 macrophages was associated with a worse patient prognosis (Farha et al., 2020). The difference in the infiltrating microenvironment may contribute to cancer progression and lead to a poorer prognosis. The differential expression of immune checkpoints between the two groups suggested the different effects of immunotherapy (Hiam-Galvez et al., 2021). In our study, LUAD patients in the high-risk group were found to exhibit higher levels of TMB. TMB in the tumors was associated with the objective response and may predict the survival of patients according to recent studies (Rizvi et al., 2015; Samstein et al., 2019). The transcriptome data from TCGA were contained to explore the sensitivity of patients to antineoplastic drugs between the two groups. The high-risk group was more sensitive to epothilone, thapsigargin, rapamycin, vinblastine, elesclomol, docetaxel, parthenolide and paclitaxel while displayed lower sensitivity to lenalidomide, nilotinib, shikonin and methotrexate. Our study

revealed the sensitivity of patients to antitumor drugs as verified by risk groups, which may provide a direction for researchers to develop treatment programs with high efficacy.

However, this study has several limitations which must be considered. In our study, the risk model and correlated nomogram were constructed using data from the TCGA and GEO databases which have great robustness. However, caution should be exercised if extrapolating the results of our study to ethnicities other than Asians or Whites. Thus, this study requires further experimental studies.

In conclusion, this study constructed a novel oxidative stress gene-related model comprising *CYP2D6*, *FM O 3*, *CAT*, and *GAPDH* to predict the prognosis of LUAD patients. A significant difference was observed between the high- and low-risk groups in the immune cell infiltration, levels of TMB and immune checkpoint expression. In addition, the model could reveal the sensitivity to chemotherapeutic drugs. Furthermore, the model can help researchers understand the correlation between oxidative stress and LUAD and may also provide novel insight for future anti-tumor immunotherapy.

Data availability statement

Publicly available datasets were analyzed in this study. This data can be found here: The Cancer Genome Atlas https://portal.gdc.cancer.gov/Gene Expression Omnibus https://www.ncbi.nlm.nih.gov/geo/The Kaplan Meier plotter http://kmplot.com/analysis/CIBERSORT https://cibersortx.stanford.edu/GDSC www.cancerrxgene.org/.

Author contributions

YZ, QT, and WC: Conceptualization, methodology, validation, visualization, experimental verification, writing—original draft. NZ: Software, visualization, writing—review and editing. XJ: Validation, writing—review and editing. ZS: Software, validation. LZ and SX: Conceptualization, methodology, supervision.

Funding

The present study was funded by the National Natural Science Foundation of China (82172776), Tianjin Science and Technology Plan Project (19ZXDBSY00060) and (303078100412), Tianjin Key Medical Discipline (Specialty) Construction Project (TJYXZDXK-061B), and Diversified Input Project of Tianjin National Natural Science Foundation (21JCYBJC01770).

Acknowledgments

The authors acknowledge contributions from TCGA, GEO, Kaplan-Meier plotter, GDSC, CIBERSORT dataset for free use.

Conflict of interest

The authors declare that the research was conducted in the absence of any commercial or financial relationships that could be construed as a potential conflict of interest.

Publisher's note

All claims expressed in this article are solely those of the authors and do not necessarily represent those of their affiliated organizations, or those of the publisher, the editors and the reviewers. Any product that may be evaluated in this article, or claim that may be made by its manufacturer, is not guaranteed or endorsed by the publisher.

Supplementary material

The Supplementary Material for this article can be found online at: https://www.frontiersin.org/articles/10.3389/fphar.2022.1030062/full#supplementary-material

References

Arafa, M. H., and Atteia, H. H. (2018). Genetic polymorphisms of cytochrome P450 2D6 (CYP2D6) are associated with long term tramadol treatment-induced oxidative damage and hepatotoxicity. *Toxicol. Appl. Pharmacol.* 346, 37–44. doi:10.1016/j.taap.2018.03.019

Bade, B. C., and Dela Cruz, C. S. (2020). Lung cancer 2020: Epidemiology, etiology, and prevention. *Clin. Chest Med.* 41 (1), 1–24. doi:10.1016/j.ccm.2019.10.001

Barrett, T., Wilhite, S. E., Ledoux, P., Evangelista, C., Kim, I. F., Tomashevsky, M., et al. (2013). NCBI GEO: Archive for functional genomics data sets--update. *Nucleic Acids Res.* 41, D991–D995. doi:10.1093/nar/gks1193

Chen, B., Khodadoust, M. S., Liu, C. L., Newman, A. M., and Alizadeh, A. A. (2018). Profiling tumor infiltrating immune cells with CIBERSORT. *Methods Mol. Biol.* 1711, 243–259. doi:10.1007/978-1-4939-7493-1_12

Denisenko, T. V., Budkevich, I. N., and Zhivotovsky, B. (2018). Cell death-based treatment of lung adenocarcinoma. *Cell Death Dis.* 9 (2), 117. doi:10.1038/s41419-017-0063-y

Efremova, M., Rieder, D., Klepsch, V., Charoentong, P., Finotello, F., Hackl, H., et al. (2018). Targeting immune checkpoints potentiates immunoediting and changes the dynamics of tumor evolution. *Nat. Commun.* 9 (1), 32. doi:10.1038/s41467-017-02424-0

Esme, H., Cemek, M., Sezer, M., Saglam, H., Demir, A., Melek, H., et al. (2008). High levels of oxidative stress in patients with advanced lung cancer. *Respirology* 13 (1), 112–116. doi:10.1111/j.1440-1843.2007.01212.x

Farha, M., Jairath, N. K., Lawrence, T. S., and El Naqa, I. (2020). Characterization of the tumor immune microenvironment identifies M0 macrophage-enriched cluster as a poor prognostic factor in

hepatocellular carcinoma. *JCO Clin. Cancer Inf.* 4, 1002–1013. doi:10.1200/CCI.20.00077

Geeleher, P., Cox, N., and Huang, R. S. (2014). pRRophetic: an R package for prediction of clinical chemotherapeutic response from tumor gene expression levels. *PLoS One* 9 (9), e107468. doi:10.1371/journal.pone.0107468

Geeleher, P., Cox, N. J., and Huang, R. S. (2014). Clinical drug response can be predicted using baseline gene expression levels and *in vitro* drug sensitivity in cell lines. *Genome Biol.* 15 (3), R47. doi:10.1186/gb-2014-15-3-r47

Glorieux, C., and Calderon, P. B. (2017). Catalase, a remarkable enzyme: Targeting the oldest antioxidant enzyme to find a new cancer treatment approach. *Biol. Chem.* 398 (10), 1095–1108. doi:10.1515/hsz-2017-0131

Goldkorn, T., Filosto, S., and Chung, S. (2014). Lung injury and lung cancer caused by cigarette smoke-induced oxidative stress: Molecular mechanisms and therapeutic opportunities involving the ceramide-generating machinery and epidermal growth factor receptor. *Antioxid. Redox Signal.* 21 (15), 2149–2174. doi:10.1089/ars.2013.5469

Goyal, M. M., and Basak, A. (2010). Human catalase: Looking for complete identity. *Protein Cell* 1 (10), 888–897. doi:10.1007/s13238-010-0113-z

He, W., Grassmann, F., Eriksson, M., Eliasson, E., Margolin, S., Thoren, L., et al. (2020). CYP2D6 genotype predicts tamoxifen discontinuation and prognosis in patients with breast cancer. *J. Clin. Oncol.* 38 (6), 548–557. doi:10.1200/JCO.19.01535

Hellmann, M. D., Nathanson, T., Rizvi, H., Creelan, B. C., Sanchez-Vega, F., Ahuja, A., et al. (2018). Genomic features of response to combination immunotherapy in patients with advanced non-small-cell lung cancer. *Cancer Cell* 33 (5), 843–852. e4. doi:10.1016/j.ccell.2018.03.018

Hiam-Galvez, K. J., Allen, B. M., and Spitzer, M. H. (2021). Systemic immunity in cancer. *Nat. Rev. Cancer* 21 (6), 345–359. doi:10.1038/s41568-021-00347-z

Ighodaro, O. M. (2018). Molecular pathways associated with oxidative stress in diabetes mellitus. *Biomed. Pharmacother.* 108, 656–662. doi:10.1016/j.biopha.2018.09.058

Jezierska-Drutel, A., Rosenzweig, S. A., and Neumann, C. A. (2013). Role of oxidative stress and the microenvironment in breast cancer development and progression. *Adv. Cancer Res.* 119, 107–125. doi:10.1016/B978-0-12-407190-2.00003-4

Kahlos, K., Soini, Y., Sormunen, R., KaaRteenaho-Wiik, R., Paakko, P., Linnainmaa, K., et al. (2001). Expression and prognostic significance of catalase in malignant mesothelioma. *Cancer* 91 (7), 1349–1357. doi:10.1002/1097-0142(20010401)91:7<1349:aid-cncr1138>3.0.co;2-d

Kirtonia, A., Sethi, G., and Garg, M. (2020). The multifaceted role of reactive oxygen species in tumorigenesis. *Cell. Mol. Life Sci.* 77 (22), 4459–4483. doi:10.1007/s00018-020-03536-5

Klaunig, J. E. (2018). Oxidative stress and cancer. *Curr. Pharm. Des.* 24 (40), 4771–4778. doi:10.2174/1381612825666190215121712

Klick, D. E., and Hines, R. N. (2007). Mechanisms regulating human FMO3 transcription. *Drug Metab. Rev.* 39 (2-3), 419–442. doi:10.1080/03602530701498612

Klingelhoeffer, C., Kämmerer, U., Koospal, M., Muhling, B., Schneider, M., Kapp, M., et al. (2012). Natural resistance to ascorbic acid induced oxidative stress is mainly mediated by catalase activity in human cancer cells and catalase-silencing sensitizes to oxidative stress. *BMC Complement. Altern. Med.* 12, 61. doi:10.1186/1472-6882-12-61

Kumar, B., Koul, S., Khandrika, L., Meacham, R. B., and Koul, H. K. (2008). Oxidative stress is inherent in prostate cancer cells and is required for aggressive phenotype. *Cancer Res.* 68 (6), 1777–1785. doi:10.1158/0008-5472.CAN-07-5259

Lánczky, A., Nagy, Á., Bottai, G., Munkacsy, G., Szabo, A., Santarpia, L., et al. (2016). miRpower: a web-tool to validate survival-associated miRNAs utilizing expression data from 2178 breast cancer patients. *Breast Cancer Res. Treat.* 160 (3), 439–446. doi:10.1007/s10549-016-4013-7

Lü, J. M., Lin, P. H., Yao, Q., and Chen, C. (2010). Chemical and molecular mechanisms of antioxidants: Experimental approaches and model systems. *J. Cell. Mol. Med.* 14 (4), 840–860. doi:10.1111/j.1582-4934.2009.00897.x

Nadif, R., Mintz, M., Jedlicka, A., Bertrand, J. P., Kleeberger, S. R., and Kauffmann, F. (2005). Association of CAT polymorphisms with catalase activity and exposure to environmental oxidative stimuli. *Free Radic. Res.* 39 (12), 1345–1350. doi:10.1080/10715760500306711

Nagai, H., and Toyokuni, S. (2010). Biopersistent fiber-induced inflammation and carcinogenesis: Lessons learned from asbestos toward safety of fibrous nanomaterials. *Arch. Biochem. Biophys.* 502 (1), 1–7. doi:10.1016/j.abb.2010.06.015

Nakajima, H., Amano, W., Kubo, T., Fukuhara, A., Ihara, H., Azuma, Y. T., et al. (2009). Glyceraldehyde-3-phosphate dehydrogenase aggregate formation participates in oxidative stress-induced cell death. *J. Biol. Chem.* 284 (49), 34331–34341. doi:10.1074/jbc.M109.027698

Nakajima, H., Itakura, M., Kubo, T., Kaneshige, A., Harada, N., Izawa, T., et al. (2017). Glyceraldehyde-3-phosphate dehydrogenase (GAPDH) aggregation causes mitochondrial dysfunction during oxidative stress-induced cell death. *J. Biol. Chem.* 292 (11), 4727–4742. doi:10.1074/jbc.M116.759084

Pryor, W. A. (1997). Cigarette smoke radicals and the role of free radicals in chemical carcinogenicity. *Environ. Health Perspect.* 105, 875–882. doi:10.1289/ehp.97105s4875

Rizvi, N. A., Hellmann, M. D., Snyder, A., Kvistborg, P., Makarov, V., Havel, J. J., et al. (2015). Cancer immunology. Mutational landscape determines sensitivity to PD-1 blockade in non-small cell lung cancer. *Science* 348 (6230), 124–128. doi:10.1126/science.aaa1348

Rudraiah, S., Gu, X., Hines, R. N., and Manautou, J. E. (2016). Oxidative stress-responsive transcription factor NRF2 is not indispensable for the human hepatic Flavin-containing monooxygenase-3 (FMO3) gene expression in HepG2 cells. *Toxicol. Vitro* 31, 54–59. doi:10.1016/j.tiv.2015.11.016

Safran, M., Dalah, I., Alexander, J., Rosen, N., Iny Stein, T., Shmoish, M., et al. (2010). GeneCards version 3: The human gene integrator. *Database (Oxford)* 2010, baq020. doi:10.1093/database/baq020

Samstein, R. M., Lee, C. H., Shoushtari, A. N., Hellmann, M. D., Shen, R., Janjigian, Y. Y., et al. (2019). Tumor mutational load predicts survival after immunotherapy across multiple cancer types. *Nat. Genet.* 51 (2), 202–206. doi:10.1038/s41588-018-0312-8

Sarmiento-Salinas, F. L., Perez-Gonzalez, A., Acosta-Casique, A., Ix-Ballote, A., Diaz, A., Trevino, S., et al. (2021). Reactive oxygen species: Role in carcinogenesis, cancer cell signaling and tumor progression. *Life Sci.* 284, 119942. doi:10.1016/j.lfs.2021.119942

Schumacher, T. N., Kesmir, C., and van Buuren, M. M. (2015). Biomarkers in cancer immunotherapy. *Cancer Cell* 27 (1), 12–14. doi:10.1016/j.ccell.2014.12.004

Siegel, R. L., Miller, K. D., Fuchs, H. E., and Jemal, A. (2021). Cancer statistics, 2017. *Ca. Cancer J. Clin.* 7171 (41), 7–30. doi:10.3322/caac.21387

Siegel, R. L., Miller, K. D., and Jemal, A. (2016). Cancer statistics. *Ca. Cancer J. Clin.* 66 (1), 7–30. doi:10.3322/caac.21332

Siegrist, J., and Sies, H. (2017). Disturbed redox homeostasis in oxidative distress: A molecular link from chronic psychosocial work stress to coronary heart disease? *Circ. Res.* 121 (2), 103–105. doi:10.1161/CIRCRESAHA.117.311182

Sirover, M. A. (2018). Pleiotropic effects of moonlighting glyceraldehyde-3-phosphate dehydrogenase (GAPDH) in cancer progression, invasiveness, and metastases. *Cancer Metastasis Rev.* 37 (4), 665–676. doi:10.1007/s10555-018-9764-7

Tang, Z., Yuan, S., Hu, Y., Zhang, H., Wu, W., Zeng, Z., et al. (2012). Over-expression of GAPDH in human colorectal carcinoma as a preferred target of 3-bromopyruvate propyl ester. *J. Bioenerg. Biomembr.* 44 (1), 117–125. doi:10.1007/s10863-012-9420-9

Tomczak, K., Czerwińska, P., and Wiznerowicz, M. (2015). The cancer Genome Atlas (TCGA): An immeasurable source of knowledge. *Contemp. Oncol.* 19 (1A), A68–A77. doi:10.5114/wo.2014.47136

Torre, L. A., Bray, F., Siegel, R. L., Ferlay, J., Lortet-Tieulent, J., and Jemal, A. (2015). Global cancer statistics. *Ca. Cancer J. Clin.* 65 (2), 87–108. doi:10.3322/caac.21262

Torre, L. A., Siegel, R. L., and Jemal, A. (2016). Lung cancer statistics. *Adv. Exp. Med. Biol.* 893, 1–19. doi:10.1007/978-3-319-24223-1_1

Yang, W., Soares, J., Greninger, P., Edelman, E. J., Lightfoot, H., Forbes, S., et al. (2013). Genomics of drug sensitivity in cancer (GDSC): A resource for therapeutic biomarker discovery in cancer cells. *Nucleic Acids Res.* 41, D955–D961. doi:10.1093/nar/gks1111

Zhu, P., Li, F. F., Zeng, J., Tang, D. G., Chen, W. B., and Guo, C. C. (2021). Integrative analysis of the characteristics of lipid metabolism-related genes as prognostic prediction markers for hepatocellular carcinoma. *Eur. Rev. Med. Pharmacol. Sci.* 25 (1), 116–126. doi:10.26355/eurrev_202101_24355

Frontiers in Pharmacology

Explores the interactions between chemicals and living beings

The most cited journal in its field, which advances access to pharmacological discoveries to prevent and treat human disease.

Discover the latest Research Topics

See more →

Frontiers

Avenue du Tribunal-Fédéral 34
1005 Lausanne, Switzerland
frontiersin.org

Contact us

+41 (0)21 510 17 00
frontiersin.org/about/contact